Nonlinear and Stochastic Methods in Neurosciences

Jonathan Touboul

PhD THESIS

prepared at
INRIA Sophia Antipolis

and presented at the
École Polytechnique
Graduate School of Applied Mathematics

A dissertation submitted in partial fulfillment of the requirements for the degree of

DOCTOR OF MATHEMATICS
Specialized in Neuroscience

Nonlinear and stochastic models in Neuroscience

Jonathan TOUBOUL

Advisor	Pr. Olivier Faugeras	INRIA Sophia Antipolis, France
Reviewers	Pr. Terrence Sejnowski	Salk Institute, San Diego, USA
	Pr. Jean-Christophe Yoccoz	Collège de France, France
	Pr. Marc Yor	Université Pierre et Marie Curie, France
Examiners	Alain Destexhe	UNIC-CNRS, Gif-sur-Yvette, France
	Yves Fregnac	UNIC-CNRS, Gif-sur-Yvette, France
	Wulfram Gerstner	LCN-EPFL, Lausanne, Switzerland
	Claude Viterbo	Ecole Polytechnique, Palaiseau, France

THESE DE DOCTORAT

preparée à
l'INRIA Sophia Antipolis

et présentée à
l'École Polytechnique
École Doctorale de Mathématiques Appliquées.

Thèse présentée en vue d'obtenir le titre de
DOCTEUR EN MATHEMATIQUES
de l'École Polytechnique
Spécialité: Neurosciences

Modèles nonlinéaires et stochastiques en neuroscience

Jonathan TOUBOUL

Directeur:	Pr. Olivier Faugeras	INRIA Sophia Antipolis, France
Rapporteurs	Pr. Terrence Sejnowski	Salk Institute, San Diego, USA
	Pr. Jean-Christophe Yoccoz	Collège de France, France
	Pr. Marc Yor	Université Pierre et Marie Curie, France
Examinateurs	Alain Destexhe	UNIC-CNRS, Gif-sur-Yvette, France
	Yves Fregnac	UNIC-CNRS, Gif-sur-Yvette, France
	Wulfram Gerstner	LCN-EPFL, Lausanne, Switzerland
	Claude Viterbo	Ecole Polytechnique, Palaiseau, France

A Rose,
A ses histoires qui ont éveillé ma curiosité,
A sa modestie, sa morale, qu'elle a si admirablement transmises.

A mon grand-père Yvon
Au brillant mathématicien qu'il aurait été.
Au grand homme qu'il fut;

A mon grand copain.
A son infinie sagesse et à son humanité;
A sa main tendrement posée sur mon épaule;

A Mamie Nelly
A sa générosité sans limite,
A son amour sans borne.

Vous manquez à ma vie.

Abstract

The brain is a very complex system in the strong sense. It features a huge amount of individual cells, in particular the neurons presenting a highly nonlinear dynamics, interconnected in a very intricate fashion, and which receive noisy complex informations. The problem of understanding the function of the brain, the neurons' behavior in response to different kinds of stimuli and the global behavior of macroscopic or mesoscopic populations of neurons has received a lot of attention during the last decades, and a critical amount of biological and computational data is now available and makes the field of mathematical neurosciences very active and exciting.

In this manuscript we will be interested in bringing together advanced mathematical tools and biological problems arising in neuroscience. We will be particularly interested in understanding the role of nonlinearities and stochasticity in the brain, at the level of individual cells and of populations. The study of biological problems will bring into focus new and unsolved mathematical problems we will try to address, and mathematical studies will in turn shed a new light on biological processes in play.

After a quick and selective description of the basic principles of neural science and of the different models of neuronal activity, we will introduce and study a general class of nonlinear bidimensional neuron models described from a mathematical point of view by an hybrid dynamical system. In these systems the membrane potential of a neuron together with an additional variable called the adaptation, has free behavior governed by an ordinary differential equation, and this dynamics is coupled with a spike mechanism described by a discrete dynamical system. An extensive study of these models will be provided in the manuscript, which will lead us to define electrophysiological classes of neurons, i.e. sets of parameters for which the neuron has similar behaviors for different types of stimulations.

We will then deal with the statistics of spike trains for neurons driven by noisy currents. We will show that the problem of characterizing the probability distribution of spike timings can be reduced to the problem of first hitting times of certain stochastic process, and we shall review and develop methods in order to solve this problem.

We will eventually turn to popoulation modelling. The first level of modelization is the network level. At this level, we will propose an event-based description of the network activity for noisy neurons. The network-level description is in general not suitable in order to understand the function of cortical areas or cortical columns, and in general at the level of the cell, the properties of the neurons and of the connectivities are unknown. That is why we will then turn to more mesoscopic models. We first present the derivation of mesoscopic description from first principles, and prove that the equation obtained, called the mean-field equation, is well posed in the mathematical sense. We will then simplify this equation by neglecting the noise, and study the dynamics of periodic solutions for cortical columns models, which can be related

to electroencephalogram signals, with a special focus on the apparition of epileptic activity.

Résumé

Le cerveau est un système très complexe au sens fort. Il est composé d'un nombre immense de cellules, en particulier les neurones, qui présentent une dynamique fortement non-linéaire, interconnecté de façon très complexe, recevant des entrées bruitées et très complexes. Comprendre le fonctionnement du cerveau et le comporement des neurones en réponse à différents types de stimulations et le comportement global de populations macroscopiques ou mésoscopiques de neurones a été l'objet d'intenses recherches depuis les dernières décénies, et une quantité critique de données biologiques et computationnelles est maintenant disponible, faisant du domaine des neurosciences un champ de recherche actif et passionant.

Le but de ce manuscrit est d'utiliser des outils mathématiques avancés afin de résoudre des problèmes biologiques pertinents émergeant dans le domaine de la neuroscience. Nous nous intéresserons particulièrement au rôle des nonlinéarités et aux aspects stochastiques dans le cerveau, tant au niveau de cellules individuelles que de populations neuronales. L'étude théorique de récents problèmes biologiques pose de nouveaux problèmes matématiques non encore résolus que nous cherchons à traiter, et l'étude mathématique de problèmes biologiques nous permettra d'avoir un nouveau regard sur les processus biologiques en jeu.

Après une description rapide et sélective des connaissances en neuroscience et de différents modèles d'activité neuronale, nous introduirons et étudierons une classe générale de modèles de neurones bidimensionnels décrits mathématiquement par un système dynamique hybride. Dans ces sytèmes, le potentiel de membrane d'un neurone est couplé avec une variable additionnelle, dite d'adaptation. La dynamique libre est gouvernée par une équation différentielle ordinaire, et cette dynamique est couplée avec un système dynamique discret modélisant l'émission de potentiels d'action. Une étude extensive de ces modèles est développée dans cette dissertation, et les résultats obtenus nous permettent de définir des classes électrophysiologiques de neurones, c'est-à-dire des jeux de paramètres pour lesquels le système a des comportements similaires en réponse à différents types de stimuli.

Nous nous intéressons ensuite aux statistiques de trains de potentiels d'actions émis par un neurone recevant des entrées bruitées. Nous montrons que caractériser les distributions des temps de spikes peut se ramener à un problème de temps d'atteinte d'une courbe par un processus stochastique. Nous présentons différentes techniques existantes et développons de nouvelles méthodes afin de résoudre ces problèmes.

Enfin, nous nous intéresserons au problème de la modélisation de populations de neurones. Le premier niveau de modélisation est le réseau. A ce niveau de description, nous proposons un modèle événementiel de l'activité du réseau décrite en termes de temps d'impulsions de potentiels d'actions. Ce niveau de description ne permet pas en général de comprendre le fonctionnement d'aires ou de colonnes corticales. De plus, les connectivités et le fonctionnement d'une cellule unique dans un réseau

sont assez mal connues, alors qu'elles forment des structures identifiables à l'échelle d'une population. Pour cette raison nous nous intéressons ensuite aux modélisations mésoscopiques de populations de neurones. Tout d'abord nous présentons la façon de passer d'une description microscopique à une description macroscopique, et démontrons que l'équation ainsi obtenue, appelée équation de champ-moyen, est mathématiquement bien posée. Enfin, nous simplifions ces modèles en négligeant le bruit, et étudions la dynamique des solutions périodiques dans certains modèles de colonnes corticales, qui peut être mis en relation avec les signaux d'électroencéphalogrammes, et nous intéressons particulièrement à l'apparition d'une activité épileptiforme.

Acknowledgments

Questions of science, Science and progress,
Do not speak as loud as my heart.
– Coldplay

First and foremost, I would like to thank my superhero supervisor, Olivier Faugeras. He taught me how to hunt mathematical monsters in biological problems, observe them, stalk them, play with them, cushion their attacks, avoid their traps, solve their enigmas, surprise them, never give up, do whatever is necessary to catch them, to the point of exhaustion, to the bitter end, when Maple had given up weeks before, when the ink is dry, even if you have to dirt your hands, but always keeping fair and reverent: these are sacred monsters who keep the doors of rich and unexplored empires we modestly and respectfully want explore. His amazing energy, creativity, uprightness definitively make him an example for me, as a scientist and as a person.

I would also like to express my deep admiration for Thierry Vieville. For being a great and bright scientist always open to discuss new ideas, for having been able to focus me, define the framework of this dissertation, and find a logic in it. For his modesty, his solidarity, his infinite kindness, and for the good person he is, who gives hope in humanity. For his sense of humor. And mostly for is laugh, this huge, tremendous, loud laugh so reassuring, that shatters fears, worries, mountains.

I would also like to acknowledge the distinguished people of my jury: Terrence Sejnowski, Jean-Christophe Yoccoz, Marc Yor, Alain Destexhe, Yves Fregnac, Wulfram Gerstner and Claude Viterbo. I admire your work and achievements. I am very proud (and anxious) you accepted to review my thesis.

A special thank goes to Bruno Cessac, for his deep scientific views, his sense of humor, his modesty and his great humanity. To François Grimbert for our inflamed discussions about science, mathematics and mathematicians, art, philosophy, love and life, for the music you made me discover, the books you advised me, the unconditional and continuous support you still are. I would like to thank Romain Brette for our scientific collaborations and the afterwork drinks we shared. Thank you to all the Odyssée members for your presence and your support.

I am also indebted to Romain Gary, Milan Kundera, Albert Cohen, Pierre Assouline, Serge Gainsbourg, Michel Berger, Nathan Milstein, Tracy Chapman, Joseph Hassid, Edgard Degas, Bob Dylan, Claude Monet, among others. Without the relief you provide me, my life would be as shaky as a fiddler on the roof.

This work would not have been possible without the everlasting love and support of my family. The infinite attention and support of my mother, our invaluable discussions about life, psychology and mankind, the invaluable support and constant presence of my father, his inspired advice on work, uprightness and our inflamed debates about the world, all this developed my critical mind, my freedom, my curiosity and your love my confidence in life. The wisdom and humanity of my elder

brother have always been examplary to me. The humor, kindness and brightness of my baby brother a constant support. The wisdom, smartness, love and care of my grand mother has always been a reassuring presence along my whole life. Together with those who cannot read these words, you made me the person I am today, and you are the main inspiration of my accomplishments. Though your delicacy, I have to tell you: I love you.

I would eventually like to dedicate this thesis to Claude Brunschwig (X1943 "bis"), a bright student who successfully passed the entrance examination at the École Polytechnique in 1943 though the numerus clausus applied to Jewish people. His mathematical creativity was recognized, and with the support of his classes préparatoires professors he registered new mathematical findings as a Soleau envelope, which unfortunately is now destroyed. He was never able to join the school in Paris. After the examination, he had to hide in the Vercors, was denounced by farmers, arrested, deported in Drancy, and in April 1944 to Auschwitz where he was exterminated. One name, one picture, among six million.

Claude Brunschwig

Without memory, our existence would be barren and opaque,
like a prison cell into which no light penetrates;
like a tomb which rejects the living.
If anything can, it is memory that will save humanity.
For me, hope without memory is like memory without hope...
– Elie Wiesel

Jonathan Touboul.

Contents

List of Figures

List of Tables

Introduction

Neuroscience is undoubtedly a fascinating field of research. It is aimed to understand the nervous system, and in particular the brain and the spinal cord that govern the way we perceive, move, think, remember, learn, speak and feel. This domain is traditionally considered as a branch of biological sciences. However, it recently aroused the interest of other scientific disciplines, including cognitive and Nero-psychology, computer science, physics, and even mathematics. It is agreed that the studies of the brain date back to the Edwin Smith surgical papyrus written in the 17th century BC, where symptoms, diagnosis, and prognosis of two patients wounded in the head are described. Evidence of trepanation dates back to Neolithic times and has been found in various cultures throughout the world. After these pioneering works, the knowledge about the brain structure and function accumulated progressively until the late 1890s. At this time, the invention and the use of the microscope as well as the introduction of Golgi's staining procedure revolutionized our knowledge of the brain. This technique opened the way to the seminal studies of the Spanish histologist and physician Santiago Ramón y Cajal who introduced the neuron doctrine, the hypothesis that the functional unit of the brain is the neuron. These works are the basis of the modern neuroscience theory. Since then, the molecular description of the brain and especially of the neurons has become increasingly precise, and has greatly expanded our understanding of the brain function. Imaging techniques, developed in the second half of the twentieth century, gave access to a huge amount of data, and provided a better understanding of the brain anatomy and function. Today, in the early XXI st century, biology, physics, technology and now mathematics combine in a joint effort to understand neurons and the brain. We are probably in the phase that the American epistemologist Thomas Kuhn calls a scientific revolution, since theoretical findings feed both biological and technical research, which in turn shed light on new theoretical problems.

The present manuscript builds upon these recent findings, and is essentially aimed to better understand different models widely used in computational neuroscience from a mathematical viewpoint. This thesis is also aimed to better understand the effects of noise in these models. It is made of four parts.

Part I: Modelization of Neural activity

The first part of this thesis is devoted to describe the basic principles of the brain functioning, and to introduce the main models used in order to emulate these processes. After a very short description of the brain, its organization and function, we will turn to the description of the nerve cells, which are the elementary units processing the information in the brain. The understanding of the biophysical processes opens the way to model the cell's activity. As any physical system, the nerve cell and the measures are subject to noise. We present the possible origin of variability in the

nervous system and different models of randomness. We then introduce the theory of neuronal excitability: nerve cells can be gathered into classes having the same behavior in response to certain kinds of stimulations. Based upon this phenomenological description, and upon the fact that, as we shall see, neurons communicate by exchanging stereotyped signals called action potentials (or spikes), we eventually introduce phenomenological neuron models aimed to reproduce the input/output relation of nerve cell not taking into account the molecular processes involved.

PART II: BIDIMENSIONAL NONLINEAR NEURON MODELS

Among the wide variety of phenomenological neuron models, two models stand out for their relative simplicity and their ability in reproducing many behaviors observed in cortical neurons, and which are defined by planar nonlinear dynamical systems. We introduce a new class of nonlinear neuron models providing a unified framework in order to study the properties of these two models in particular, and more generally of some nonlinear bidimensional neuron models with adaptation. We first introduce in chapter 2 the class of models and study their essential properties when no spike is emitted (subthreshold regime). The detailed description of the subthreshold dynamics we obtain enables us to understand the origin of the main excitability properties of the neuron in relation with the bifurcations structure of the model. This information leads us to introduce a new model called the *quartic* model, able to reproduce all the possible behaviors for the neurons of this class. In the simulations we perform in this chapter, we observe that such neurons reproduce many spike signatures observed in cortical neurons. Chapter 3 is devoted to the detailed study of the spike patterns and the mathematical mechanisms leading to the emergence of these behaviors. This study is based on the introduction of a discrete-time map governing the spike pattern produced for a given stimulation and a given initial state. A summary of all these results is provided in chapter 4 where we relate the different results we obtained with electrophysiological properties of the neurons. We finally end this section by showing that among these models, the quadratic integrate-and-fire model sensitively depends on the definition of a hard threshold, the cutoff value.

PART III: STATISTICS OF SPIKES TRAINS

These nonlinear effects are very important to understand the neural code. But it is generally agreed that an important aspect of the neural code is the spike variability. Part III is dedicated to the study of the spikes statistics when the neuron is submitted to a random excitation. We begin in chapter 6 by presenting a key theoretical principle, consisting in stating that the problem of describing spike statistics can be expressed as a first-hitting time problem for different stochastic processes. We then review many different techniques of stochastic analysis in order to characterize the probability distribution of spike timings for different classical models. Existing mathematical material does not solve the problem of the spikes statistics for integrate-and-fire neuron with non-instantaneous synaptic integration. Solving this problem is the main focus of chapter 7. To this end, we introduce a new class of stochastic processes, which we call *double integral processes*, corresponding to the set of processes defined as primitive of a Brownian martingale, and we develop a semi-analytical method in order to solve the problem of the first hitting times of these processes to general smooth boundaries.

PART IV: NEURAL POPULATION MODELS

After these studies of single neurons properties, we turn to neural population modeling. As a general remark, a very large number of neurons accounts for the information coding and to a given function, and these sets of neurons present a columnar structure transverse to the brain split into different layers. These systems might be globally apprehended, since structures and functions generally do not appear at the cell level but emerge at different spatial scales.

Because of the complexity of this structuring, realistic neural networks accounting for special functions are in general intractable. We introduce in the first chapter of this part an event-based description of neuronal networks based on modeling the times of the spikes in a network. This model allows to simulate efficiently large sets of spiking neurons in noisy environments. Nevertheless mathematical properties for a large but finite number of neurons are very hard to get. Therefore the other two sections are aimed to develop *mesoscopic* scale descriptions of such networks. Chapter 9 discusses the way to get such a mesoscopic description, called the mean field equation, in noisy networks. We show that these equations are well posed in the mathematical sense, i.e. that there exists a unique solution to the mean field. Chapter 10 is devoted to a preliminary study of a deterministic approximation of the mean field equations corresponding to some classical mesoscopic models of cortical columns, namely Jansen and Rit's and Wendling and Chauvel's models. We focus in particular on the periodic solutions of these systems, and this study gives us a new insight on the origin of the oscillatory activity observed in electroencephalogram recordings and the emergence of epileptiform activity.

Introduction (version française)

La neuroscience est sans aucun doute un champ de recherches fascinant. Son but est de comprendre le système nerveux, et en particulier le cerveau et la moelle épinière, qui gouverne notre façon de percevoir, de se déplacer, de penser, se souvenir, apprendre, parler et ressentir. Ce domaine est traditionnellement considéré comme une branche de la biologie. Néanmoins, elle retient depuis peu de temps l'intérêt de multiples disciplines scientifiques, en particulier la science cognitive, la neuropsychologie, l'informatique, la physique et même les mathématiques. Le premier document retrouvé traitant du cerveau est le papyrus de chirurgie trouvé et déchiffré par l'égyptologue Edwin Smith, écrit au 17eme siècle avant notre ère, où sont décrits symptômes, diagnostics, et pronostics de deux patients blessés à la tête. Les premiers cas de trépanation découverts datent de l'époque Néolithique et ont été retrouvés dans différentes régions du monde et différentes cultures. Après ces travaux, les connaissances sur la structure du cerveau et sur sa fonction se sont progressivement accumulées jusqu'à la fin des années 1890. À cette époque, la découverte et l'usage de la microscopie et de la coloration de Golgi ont révolutionné notre connaissance du cerveau. Cette technique ouvrit la voie au travaux séminaux de histologiste et physicien Santiago Ramón y Cajal qui introduisit la doctrine neuronale, c'est-à-dire l'hypothèse selon laquelle l'unité fonctionnelle du cerveau est le neurone. Cette vision est un principe de base de la neuroscience moderne. Depuis, les descriptions moléculaire du cerveau et des neurones sont devenues de plus en plus précises, et ont grandement accru notre compréhension de leur fonctionnements. Les méthodes d'imagerie développées dans la seconde moitié du XXe siècle nous ont permis d'accéder à un grand nombre de données, et par tant à une meilleure compréhension de l'anatomie et du fonctionnement du cerveau. Aujourd'hui au début du XXIe siècle, la biologie, la physique, la technologie et maintenant les mathématiques convergent dans un effort concerté afin de comprendre les neurones et le cerveau. Nous nous trouvons probablement dans la phase que l'épistémologue américain Thomas Kuhn appelle la révolution scientifique: les découvertes théoriques alimentent à la fois la recherche biologique et technique, ce qui à son tour met en lumière de nouveaux problèmes théoriques.

Ce manuscrit se base sur ces découvertes récentes, et a pour but principal de mieux comprendre d'un point de vue mathématique différents modèles communément utilisés, essentiellement dans des simulations numériques. Cette thèse vise aussi à mieux comprendre les effets du bruit dans ces modèles. Elle est composée de quatre parties.

Partie I: Modélisation de l'activité neuronale

La première partie de cette thèse est consacrée à la description des principes de base du fonctionnement du cerveau, et introduit les modèles principaux pour émuler

ces processus. Après une très courte description du cerveau, de son organisation et de ses fonctions, nous nous intéresserons aux cellules nerveuses qui sont les unités élémentaires traitant les informations dans le cerveau. La compréhension des processus biophysiques ouvre la voie à la modélisation de l'activité de ces cellules. Comme dans tout système physique, les cellules nerveuses et les mesures faites sont sujètes au bruit. Nous présentons rapidement l'origine de la variabilité observée à différents niveaux de l'activité corticale et les différentes façons de modéliser cette composante aléatoire. Nous introduisons ensuite la théorie de l'excitabilité neuronale: les cellules nerveuses peuvent être classifiées en fonction de leur comportement en réponse à différents types de stimulations. En ce basant sur ces observations et sur le fait que les neurones communiquent en échangeant des signaux stéréotypés appelés potentiels d'action (spikes), nous terminons cette partie en présentant des modèles de neurones phénoménologiques ayant pour but de reproduire les relations entrée/sortie des cellules nerveuses ne prenant pas en compte les processus moléculaires impliquées.

Partie II: Modèles nonlinéaires planaires de neurones

Parmi le grande gamme de modèles de neurones phénoménologique, deux modèles semblent sortir du lot pour leur relative simplicité et leur capacité de reproduire de multiples comportements observés dans des neurones. Ces modèles sont définis par des systèmes dynamiques nonlinéaires planaires. Nous introduisons une classe générale de modèles de neurones nonlinéaires constituant un cadre unifié permettant d'étudier les propriétés ce ces deux modèles en particulier, et plus généralement de modèles de neurones nonlinéaires avec adaptation. Nous introduisons d'abord dans le chapitre 2 la classe générale de modèles et étudions leur propriétés principales quand les potentiels d'action ne sont pas émis (régime sous-liminaire). Cette étude détaillée du régime sous-liminaire nous permet de comprendre l'origine des propriétés principales d'excitabilité du neurone en fonction des bifurcations du système. Cette information nous mène à introduire un nouveau modèle appelé *quartique*, capable de reproduire tous les comportements possibles des neurones de cette classe. Les simulations produites dans ce chapitre mènet à la conclusion que de tels modèles reproduisent de multiples signatures de trains de potentiels d'actions observées dans des neurones corticaux. Le chapitre 3 est consacré à l'étude détaillée des types de trains de spikes et des méchanismes mathématiques à l'origine de l'émergence de ces comportements. Cette étude est basée sur l'introduction d'un système dynamique discret qui gouverne la forme du train de spikes produit en réponse à une certaine stimulation et un état initial. Un résumé de ces proprétés est produit au chapitre 4 dans lequel nous mettons en relation les différents résultats mathématiques obtenus avec les propriétés electrophysiologiques des neurones. Nous terminerons cette partie en démontrant que le modèle quadratique dépend très sensible d'un seuil constant, le *cutoff*.

Partie III: Statistiques de trains d'impulsions

Les nonlinéarités modélisées dans la partie précdente sont essentiels à la compréhension du code neuronal. Il est généralement admis qu'une grande partie du codage est également contenu dans la variabilité des trains d'impulsions. La partie III est consacrée à l'étude des statistiques de trains de potentiels d'actions de neurones soumis a des excitations aléatoires. Dans un premier temps, nous présenterons au chapitre 6

un aspect essentiel du problème: la distribution de probabilité des trains d'impulsions peut se ramèner à un problème de premier temps d'atteinte de certains processus à des courbes continues. Nous présenterons différentes techniques d'analyse stochastique afin de caractériser la distribution de probabilité des trains d'impulsion et les appliquerons à quelques modèles classiques de neurones. Les techniques usuelles ne permettent pas de résoudre le problème des statistiques de trains d'impulsions quand l'intégration synaptique n'est pas instantanée. La résolution de ce problème sera l'objet du chapitre 7. Afin de résoudre ce problème, nous introduirons une nouvelle classe de processus stochastiques, les *processus doublement intégrés*, qui correpondent à l'ensemble des processus définis comme la primitive d'une martingale brownienne. Nous développerons dans ce chapitre une méthode semi-analytique afin de résoudre le problème des premiers temps d'atteinte de ces processus à des frontières lisses générales.

PARTIE IV: MODÈLES DE POPULATIONS DE NEURONES

Aprés ces deux études de neurones isolés, nous nous intéresserons à la modélisation de populations de neurones. Un très grand nombre de neurones codent l'information dans le cervau, et ces ensembles de neurones presentent une structure columnaire composée de différentes couches. Ces sytèmes doivent être appréhendés globalement, puisque certaines structures et fonctions n'existent pas au niveau cellulaire mais émergent à difféntes échelles échelles spatiales.
À cause de la complexité de cette structuration, des modèles réalistes de neurones reproduisant certaines fonctions ne sont pas en général traitables mathématiquement. Nous introduirons au chapite 8 une description événementielle de réseau de neurones basée sur la modélisation des instants d'impulsions dans le réseau. Ce modèle nous permettra de simuler efficacement de grands ensembles de neurones à impulsions bruités. Cependant, les propriétés mathématiques de ce réseau pour un grand nombre de neurones sont très difficiles à obtenir. C'est pour cette raison que nous nous interesserons dans les deux dernières parties de ce manuscrit à des descriptions *mésoscopiques* de tels réseaux. Le chapitre 9 traitera de la façon de calculer l'*équation de champ moyen*, une équation mésoscopique représentant le comportement global d'un réseau stochastique. Nous prouvons que ces équations sont bien posées au sens mathématique, c'est à dire qu'il existe une unique solution. Le chapitre 10 est une étude préliminaire de d'approximations déterministes de l'équation de champ moyen correspondant à des modèles classiques de colonnes corticales, les modèles de Jansen et Rit et de Wendling et Chauvel. Nous nous intéresserons principalement aux solutions périodiques de ces systèmes, et ces études projètent une nouvelle lumière sur l'origine de l'activité oscillatoire observée dans des enregistrements d'électroencephalogrammes et sur l'activité épileptiforme.

Part I

Modelization of Neural activity

CHAPTER 1

PRINCIPLES OF NEURAL SCIENCE AND MODELIZATIONS BASICS

Life itself is still beautiful.
– Pontus Alv.

OVERVIEW

Neural science is undoubtedly a fascinating field of research. It is aimed to understand the nervous system, and in particular the brain and the spinal cord that govern the way we perceive, move, think, remember, learn, speak and feel. It processes sensory inputs and recognizes danger, good food, identify potential mates. It controls movements, the voluntary ones (via the motor cortex, the cerebellum, and the basal ganglia) as well as the involuntary ones (nuclei in the brain stem control many involuntary muscle functions such as heart rate and breathing). Evidence strongly suggests that developed brains derive consciousness from the complex interactions between numerous systems within the brain. Almost[1] every animal have either a centralized brain, collections of individual ganglia playing the role of distributed brains or a diffuse nervous system. In this chapter we very roughly introduce several elementary notions of neural science and present the basic function of neurons from a biological and electrophysiological viewpoints. Modeling these processes in order to understand their origin and nature in order to reproduce them efficiently and accurately are the main motivation of the present dissertation.

After describing very briefly the brain and its basic organization, we will be interested in the main cells involved in the brain's information processing: the nerve cells, or neurons. We will describe these cells anatomically, explain its function from a biophysical point of view, characterize the signal they produce and convey, and discuss the electrophysiological basis of these processes. Based on these observations, we will introduce what we will call detailed neuron models, mainly based on a precise description of each process involved in the nerve signal generation. We will then turn to a more functional description of the nerve cells, and introduce classical phenomenological model.

The aim of this chapter is clearly not to give a comprehensive introduction to such a complex structure as the brain, nor of such a passionating field as neurobiology,

[1]Some animals, such as cnidarians and echinoderms do not have a centralized brain, but present instead a decentralized nervous system. Very few primitive animals such as the poriferans (sponge) lack nervous system entirely.

but to provide the reader with the basic concepts we will deal with in the rest of this document. The presentation of the biological background will be therefore highly simplistic, selective and lacunar, but I believe it provides the reader with the minimum of information necessary to appreciate the biological discussions of the theoretical work presented in this dissertation. For more details on the fundamental principles of neural science from a biological point of view, we refer the interested reader to the excellent book of Kandel, Schwartz and Jessell [158] where we got the main information developed here. The reader interested in neuronal modeling is referred to the great books of Koch and colleagues [164, 165], Peter Dayan and Larry Abbott [67]. The reader interested in ionic exchanges in play in the nerve cell to the very interesting book of Bertil Hille [124]. A review of different neuron models viewed as dynamical systems can be found in the excellent book of Izhikevich [146], and phenomenological models of spiking neurons are discussed in depth in [105].

Contents

1.1 BRAIN

1.1.1 General overview

The brain is an unresting assembly of cells that continually receives information, elaborates and perceives it, and makes decision. It is a very complex system. It is composed of an immense number of different cells. Among these cells, the nerve cells, or neurons, are the elementary processing units. Neurons are electrically excitable cells that process and transmit information. There are roughly 100 billion neurons for the human brain ($\approx 10^{11}$ cell bodies), that can be of different types (about forty types of neurons have been identified through the cortex, thousands according to [158]). Besides neurons, the brain is also composed of "supporter" cells, so-called glial (or neuroglial) cells. These cells are divided according to anatomical criteria into (1) neuroglial cells in the brain, further subdivided into oligodentrocytes and astrocytes, and (2) Schwann cells, or neurolemmocytes, in the periphery. Neuroglial cells make up almost one half the volume of the brain and outnumber neurons by about 10 to 1. They play an essential role in the brain function: they provide nutrition and energy, maintain homeostasis (regulates their internal environment), form myelin (electrically-insulating dielectric phospholipid layer that surrounds only the axons of some neurons), participate in signal transmission, ensures structural stabilization of brain tissues, destroy pathogens and remove dead neurons. For years, specialists considered that these cells were not involved in information processing, and this vision seems to be contradicted by some recent studies[2]. The study of these cells and of their influence in the signal processing would be very interesting, but in this dissertation we will concentrate on neuronal cells.

The huge number of nerve cells in the brain is interconnected in a very intricate fashion. In the human brain for instance each neuron is typically connected to 10^4 other. All these cell bodies and connections are packed into a very dense and complex network. To get a grasp of the complexity of the network, in a cubic millimeter of human brain there are more than 10^4 cell bodies and several kilometers of wires. And the high level of structuring of the cerebral cortex makes this system even more complex.

1.1.2 Basic organization of the cerebral cortex

The cortex, superficial part of the encephalon, is mainly composed of grey matter formed by neurons and their unmyelinated fibers. The white matter below the grey matter of the cortex is formed predominantly by myelinated axons interconnecting different regions of the central nervous system. First of all, it has been proved that the grey matter has an horizontal organization in layers (*laminae*) composed of different cell types (see figure 1.1). The number of layers, their cell composition, their thickness and organization are not the same over the whole surface of the cortex. These differences led neuroanatomists to divide the cortex into small regions called

[2] Recent studies tend to prove that astrocytes glial cells interact with neurons and affect their ability to communicate with each other. This suggests that they may influence the information processing. For instance Newman in [205] showed that activated glial cells (i.e. excited by focal injections of certain chemical substances) can inhibit neurons by releasing ATP. He proves for instance in the rat retina using this technique a subsequent reduction of the firing rate of those neurons that displayed spontaneous spike activity.

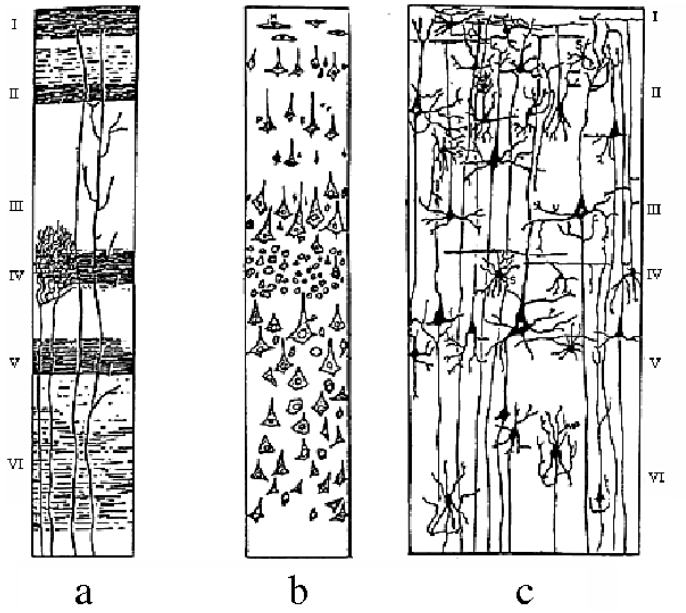

Figure 1.1: Layer organization of the cortex (a) Weigert's coloration shows myelinated fibers (axons) and so the connections inside and between layers, (b) Nissl's coloration only reveals cell bodies (c) Golgi's coloration shows the whole cells (From [209]).

areas (figure 1.2) where those characteristics are homogeneous and that correspond to different functions, e.g., vision or motion. Generally speaking, most of the cortex is made up of six layers of neurons, from layer I at the surface of the cortex to layer VI, deeper, that lies close of the white matter. For humans, its thickness varies from 3 to 6 mm.
More detailed information about cortical structure and function can be found in [113, 156, 158, 214]. The organization of the cortex is not only laminar. It has been observed that neurons tend to be strongly connected in columnar structures perpendicular to the surface of the cortex responding to precise stimulations and having similar activities, called *cortical column*. Several studies provided biological evidence of such small aggregates of about one hundred neurons, 20 up to 50 μm wide, called minicolumns (see e.g. [44, 200]). Larger columnar structures of 300 to 500 μm of diameter displaying similar activities (*macrocolumns*) were studied by Mountcastle in [199].

Let us now zoom further into the brain and describe individual nerve cells.

1.2 Neurons

The information processing in the brain is mainly accomplished through the nerve cells and the connections between them. The neuron's place as the primary functional unit of the nervous system was first recognized in the late 19th century through the work of the Spanish histologist Santiágo Ramon y Cajal. He proposed that neurons were discrete cells acting as metabolically distinct units communicating via specialized circuits and junctions. This vision, known as the neuron doctrine, is one of the central dogma of modern neuroscience. He was the first to provide a suitable descrip-

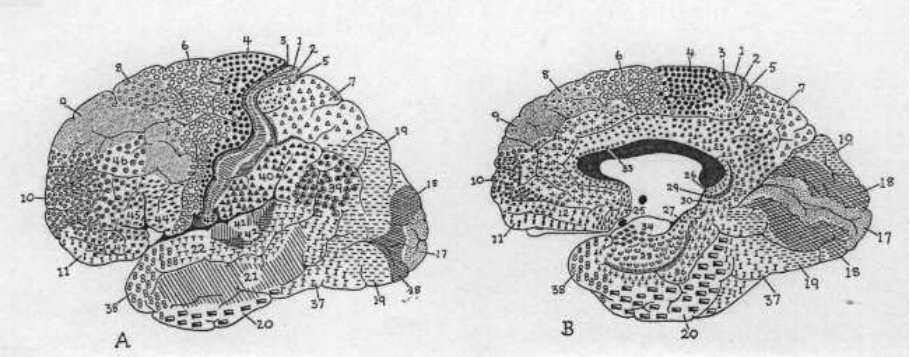

Figure 1.2: In 1909, Brodmann [34] divided the cortex into 52 cytoarchitectonic areas according to the thickness of the cortical layers. For example, layer IV is very thin in the primary motor cortex (area 4) while it is very thick in the primary visual cortex (area 17).

Figure 1.3: The giant axons of the European squid (Loligo vulgaris) were crucial for scientists to understand the action potential (picture: Hans Hillewaert)

tion of the structure nerve cells [219, 220], using Golgi's silver staining method. He showed that all nerve cells share the same basic architecture. Hence the complexity of the brain function depends less on the specialization individual neurons and more on the fact that a great number of these cells form precise and intricate anatomical circuits. The main electrophysiological features of the neurons were obtained by the pioneering works of Hodgkin and Huxley at the same period.

Substantial early knowledge of neuron electrical activity came from experiments on the squid's (see his photo figure 1.3) giant axons. As they are much larger than human neurons, but similar in nature, it was easier to study them with the technology of the first half of the twentieth century. This poor squid suffered pressure, stretch, injections of chemical substances and electrocutions, to record its axon's electrical activity by inserting electrodes into it. The accurate measurements obtained opened the way to the current neural science theory. I solemnly acknowledge the squid 1.3 here for being, to my point of view, a science hero.

1.2.1 Anatomical overview

A typical neuron has four morphologically defined regions: the cell body, dendrites, the axon, and presynaptic terminals. Each of these regions has a distinct role in the communication or generation of signals (see figure 1.4). The cell body (*soma*) is the metabolic center of the cell. It contains the nucleus which stores the genetic

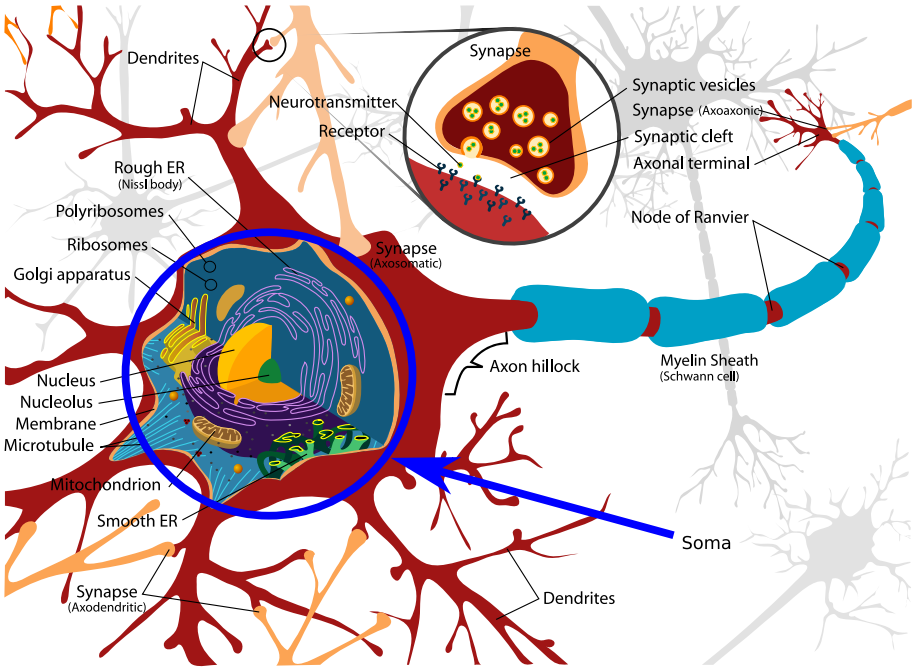

Figure 1.4: Diagram of a typical nerve cell (image: Mariana Ruiz Villarreal, Wikipedia)

information of the cell as well as the endoplasmic reticulum and the whole metabolic apparel for the cell's proteins synthesis. The nucleus ranges from 3 to 18 micrometers in diameter.

The cell body is connected to other nerve cells via cellular extensions called *dendrites*. Dendrites branch out in a tree-like fashion. It is where the majority of input to the neuron occurs. In some few cases, information outflow from dendrites to other neurons can also occur[3].

The information communicated by the nerve cell to other neurons is transmitted by a long tubular structure called the *axon*. An axon can transmit electric signals along distances ranging from 0.1mm to meters. It is a thin structure compared with the cell body. Most neurons have only one axon, but this axon may - and usually will - undergo extensive branching, enabling communication with many target cells. The part of the axon where it emerges from the soma is called the *axon hillock*. Besides being an anatomical structure, the axon hillock is also the part of the neuron that has the greatest density of voltage-dependent sodium channels (see below). This makes it the most easily excited part of the neuron.

Near its ends, the axon divides into branches forming communication sites with other neurons. This structure is referred as the *axon (or presynaptic) terminal*. It contains the *synapses* (see section 1.2.6), specialized structures where neurotransmitter chemicals are released in order to communicate with target neurons. The signal is emitted from the *presynaptic cell* and received by the *postsynaptic cell*. The presynaptic cell transmits signals from the swollen end of its axon. Two communicating

[3]This transmission cannot be held via chemical synapses: there, the backflow of a nerve impulse is impossible since an axon does not possess chemoreceptors and dendrites cannot secrete neurotransmitter chemicals. This unidirectionality of a chemical synapse explains why nerve impulses are conducted only in one direction.

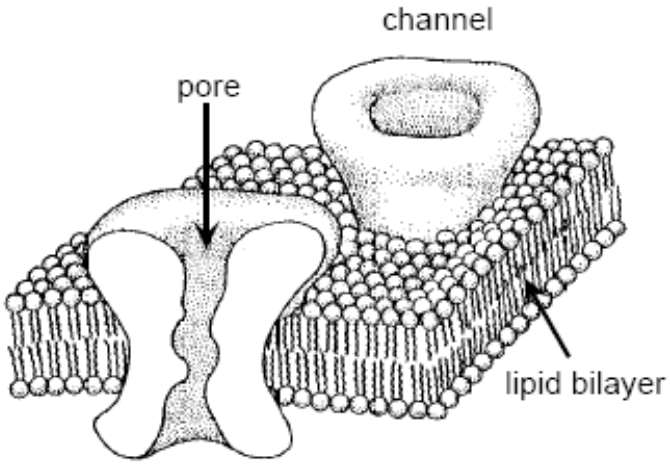

Figure 1.5: Schematic diagram of a section of the nerve cell's membrane with two ion channels embedded in it. The membrane is 3 to 4 nm thick and the ion channels are about 10 nm long. (Adapted in [67] from [124]).

cells are generally not in contact anatomically. The small space between these cells is named the *synaptic cleft*. Most presynaptic terminals end on a postsynaptic neuron's dendrite, but terminals may also end on the soma or less often on the axon of the postsynaptic cell.

Like other cells, neurons are composed and surrounded of a huge number and variety of ions and molecules. A typical cubic micron of cytoplasm might contain, for example, 10^{10} water molecules, 10^8 ions, 10^7 small molecules like amino acids and nucleotides, and 10^5 proteins. Many of these molecules carry charges, either positive or negative. Most of the time there is an excess concentration of negative charge inside the neurons. The nerve cell's membrane is mainly composed of a lipid bilayer 3 to 4 nm thick essentially impermeable to most charged molecules. This bilayer is spanned by highly specialized proteins called *ion channels* (see figure 1.5). These ion channels recognize and select specific ions and conduct them through the membrane. They can be open or closed in response to specific electrical, mechanical or chemical signals. They conduct ions very fast (up to 10^8 ions per second in a single channel) in a very selective way: each type of ion channel allows only one[4] type of ions to pass. Many channels are regulated (or *gated*); they open and close in response to different stimuli: changes in the voltage (*voltage-gated channels*), presence of a chemical transmitter (*ligand-gated channel*) and pressure or stretch (*mechanically gated channels*). Non-gated channels also exist, and are called *resting channels*. The gates can either *activate* (open) or inactivate (close) the channels (see figure 1.6). For a precise description of the structure and function of the ionic channels, we refer to [158, Chapter 6].

1.2.2 The zoo of neurons

Though nerve cell have the same overall organization, many types of nerve cells can distinguished. Eric Kandel in [158, Chapter 2] speaks of at least a thousand of different cells types. Nerve cells can be classified according to different criteria. The

[4] in some rare case few species are selected.

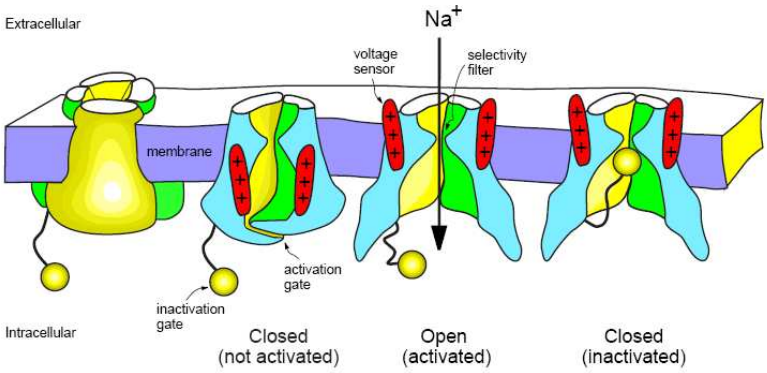

Figure 1.6: Structure of voltage-gated ion channels: voltage sensors open an activation gate and allow selected ions to flow through the channel according to their electrochemical gradients. The inactivation gate blocks the channel. (Taken from [146] where it was modified from [14].)

first classification that can be performed is a structural classification. More precisely, most of neurons can be characterized by their *polarity* (see figure 1.7). They can be one of three main types:

- *Unipolar or pseudounipolar* when the dendrite and axon emerge from same process.
- *Bipolar* when the axon and a single dendrite emerge on opposite ends of the soma.
- *Multipolar* when it has more than two dendrites. In the multipolar cells there exists a further subdivision in function of the length of the synaptic projections. Neurons with long-projecting axonal processes such as the pyramidal cells, Purkinje cells, and anterior horn cells are called *Golgi I* and neurons whose axonal process projects locally such as the granule cell are called *Golgi II*.

Different types of neurons can be distinguished also by the function they play in the nervous system. Neurons conveying informations from tissues and organs to the central nervous system are called *afferent (or sensory) neurons*. The cells transmitting signals from the central nervous system to the effector cells are called *efferent (or motor) neurons*, and the cells connecting neurons within the central nervous system are called *interneurons*.

The action of a neuron on other neurons is also important to understand the role of each individual cell. This role is primarily driven by the type of synapse (see section 1.2.6) and the neurotransmitter used. We distinguish *excitatory* neurons that depolarize their target neurons and *inhibitory* neuron that hyperpolarize their target cell. Nevertheless, this is not a very precise classification, since the action of a presynaptic neuron on a postsynaptic cell does not only depend on the type of neurotransmitter substance released to transmit information, but also the postsynaptic receptor. Eventually *modulatory* neurons evoke more complex effects termed neuromodulation. These neurons use often such neurotransmitters as dopamine, acetylcholine, serotonin.

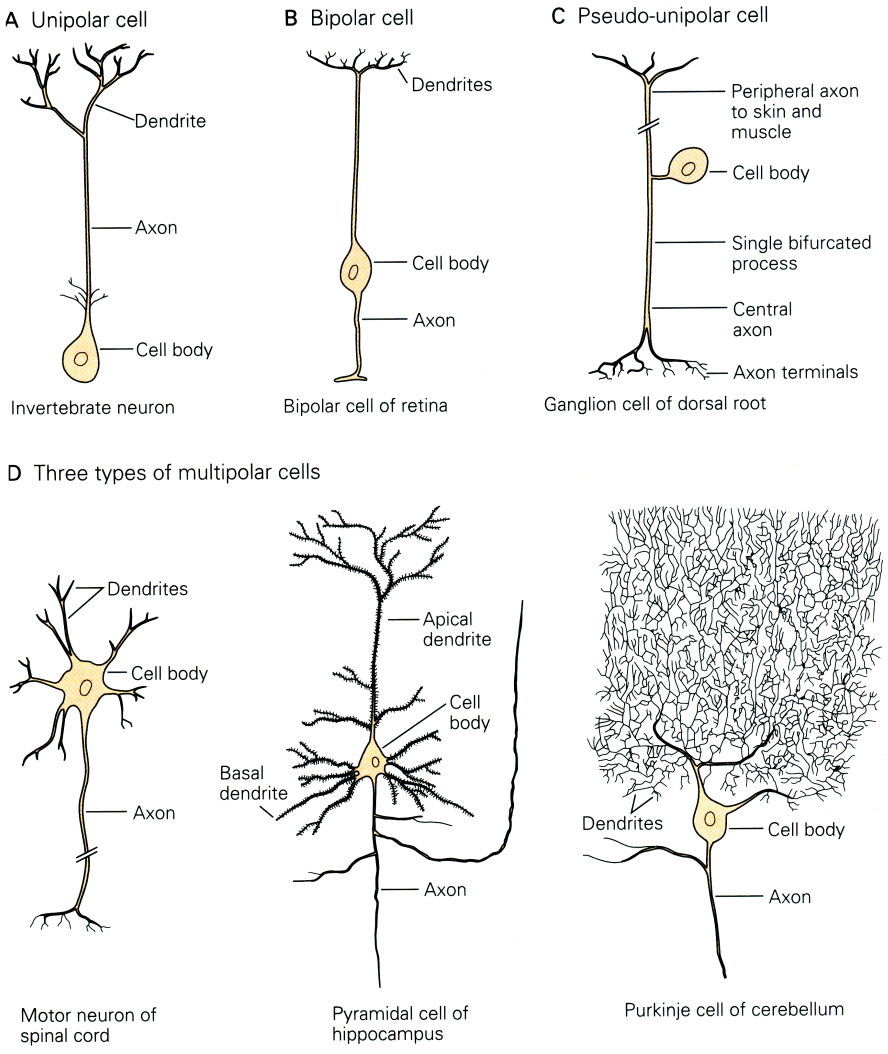

Figure 1.7: Neurons can be classified according to the number of processes that originate from the cell body (their polarity): they can be unipolar, bipolar or multipolar (image taken from [158])

Eventually, another classification, which will be specifically used in this dissertation, distinguishes neurons according to their electrophysiological characteristics, i.e. their spiking signature in response to different kinds of stimulations. This classification will be further studied in section 1.5.

1.2.3 Electrophysiology of neurons

The first thing one notice when penetrating into the cell with an intracellular electrode is the existence of an electrical potential across this membrane (this observation dates back to the late 1930's [53, 127]). The difference of electrical potential between the intracellular and the extracellular potential is an essential measurement of the nerve cell's activity.

Passive properties of nerve cells

The neuron as all cells of the body have passive electrical properties which do not depend sensitively on the neuron's activity, and that affect the cell's electrical signaling: the resting membrane resistance and the membrane capacitance. These characteristics can be acquired by intracellular measurements of the membrane potential in response to current inputs.

Membrane resistance Injecting a negative charge through the an electrode results in most neurons in a subsequent hyperpolarization proportional to the injected current. The slope of this linear relation defines the neuron's input resistance. To compare the membrane properties of neurons of different size, electrophysiologists often use the resistance of a unit area of membrane, the *specific membrane resistance*. This quantity depends on density of resting ion channels and on their conductances.

Membrane capacity The dynamical properties of the input integration when injecting a negative charge in the cell resembles to the one of capacitor. This property is linked with the structure of the the nerve cell's membrane: it is made of two layers of phospholipid molecules, with their polar head facing the intracellular cytoplasm, and the extracellular space, separating the internal and external conducting solutions by a $35-50$ Å thin insulating layer[5]. To understance how a capacitance slows down the voltage response, we need to recall that the voltage across a capacitor V is proportional to the charge Q stored in it:

$$Q = CV$$

In membrane biophysics, the capacitance is usually specified in terms of the *specific membrane capacitance* C_m expressed in microfarad per square centimeter of membrane area. When the voltage across the capacitance changes, a current will flow, and this current is obtain via the charge equation:

$$I_C = C\frac{\mathrm{d}V_m(t)}{\mathrm{d}t}$$

The capacitance depends on the didelectric constant of a medium and on the geometry of the conductors on either side. In a simple capacitor formed by two parallel plates

[5]It is known from elementary physics that whenever a thin insulator is keeping charges apart, it will act like a capacitance.

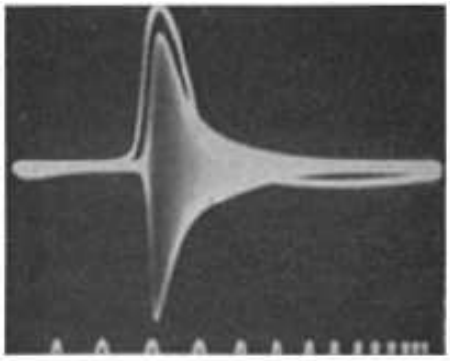

Figure 1.8: Historic oscilloscope record of a net increase of ionic conductance in the membrane of the axon simultaneously to the emission of an action potential by Cole and Curtis [54]. The time marks at the bottom are 1 millisecond apart. The uppermost curve is the action potential.

of area A separated by an insulated of dielectric constant ε_0 and thickness d, the capacitance is:

$$C = \frac{\varepsilon \varepsilon_0 A}{d}$$

where ε is the polarizability of free space universal constant. Cell membranes can be considered as parallel plate capacitors with specific capacitance near $1.0\mu F/cm^2$ (see [52]), which is just slightly higher than a pure lipid bilayer, $0.8\mu F/cm^2$. The high electric capacitance of biological membranes appears to be a direct consequence of their molecular dimensions.

Note that these two properties can also be expressed for the axons and the dendrites, and the quantitative differences between the values in the soma and the process plays a role in the propagation properties of the signal (see [158, chapter 8]).

Active properties of the neurons: Ionic exchanges

Neurons are excitable cells, and their specific properties of generating signals and transmitting them are linked with active properties of the cell. From the electrophysiological point of view, we just saw that the nerve cell's membrane acts like a capacitor and can conduct electrical signals with a given conductivity. We are now interested in the ionic exchanges that drive the cell's activity and that lead to the emission of action potentials.

An important clue about how action potentials are generated came from another experiment performed by Kenneth Cole and Howard Curtis[54]. While recording from the giant axon of the squid, they found that the ion conductance across the membrane increases dramatically during the emission of action potentials (see figure 1.8). This discovery provided the first evidence that the action potential results from changes in the flux of ions through the channels of the membrane. It raised hence a new question: which ions are responsible for the action potential?

A key to this problem was provided by Alan Hodgkin and Bernard Katz. They found in 1949 [129] that the amplitude of the action potential was reduced when the external Na^+ concentration is lowered, indicating that Na^+ influx is responsible for the rising of phase of the action potential. Their data also suggested that the falling

phase of the action potential was caused by a later increase in K^+ permeability. To test this hypothesis, Alan Hodgkin and Andrew Huxley conducted a second series of experiments. They systematically varied the membrane potential of the squid giant axon and measured the resulting changes in the membrane conductance to Na^+ and K^+ (see [128]). It is now understood that four ionic currents are responsible for the electrical activity of the neuron: sodium (Na^+), potassium (K^+), chloride (Cl^-), and calcium (Ca^{2+}). The concentrations of these ions are different on the inside and the outside of a cell. These ionic gradients are the major forces driving neural activity. The extracellular medium has a high concentration of sodium and chloride ions (it is salty medium similar to seawater), and a relatively high concentration of calcium ions. The intracellular medium has high concentrations of potassium and different negatively charged molecules (denote generically A^- for anions) trapped in the intracellular medium (there is no ion channel adapted to send them in the extracellular medium). The flows of sodium and calcium ions appears to be not very significant, at least at rest, while the flows of potassium and chloride ions are quite important. There exist two different kinds of ionic flows through the membrane:

- The *passive redistribution*, linked with the fact that the impermeable anions A^- attract more K^+ into the cell and repel more Cl^- out of the cell, thereby creating concentration gradients.
- The *active transport*, linked with ionic pumps acting on the cell membrane: for example, the Na^+-K^+ pump depicted in figure 1.10 pumps out three Na^+ ions for every two K^+ ions pumped in, thereby maintaining concentration gradients.

Two forces drive each ion species through the membrane channel: the concentration and the electric potential gradients. First, the ions diffuse down the concentration gradient. For example, the K+ ions depicted in figure 1.9.a. diffuse out of the cell because K^+ the internal concentration of potassium is higher than that the external one. While exiting the cell, K^+ ions carry a positive charge and leave a net negative charge inside the cell, thereby producing an outward current. The positive and negative charges accumulate on the opposite sides of the membrane surface, creating an electric potential gradient across the membrane, which we call the *transmembrane potential or membrane voltage*. This potential slows the diffusion of K^+ since these ions are attracted towards the negatively charged interior and repelled from the positively charged exterior of the cell (figure 1.9.b.). At some point an equilibrium is achieved: the concentration gradient and the electric potential gradient exert equal and opposite forces that counterbalance each other, and the net cross-membrane current is zero, as in figure 1.9.c. The value of such an equilibrium potential depends on the ionic species, and it is given by the *Nernst equation* (see e.g. [124]):

$$E_{ion} = \frac{RT}{zF} \log \frac{[Ion]_{out}}{[Ion]_{in}}, \tag{1.1}$$

where $[Ion]_{out}$ and $[Ion]_{in}$ are the ion concentrations outside and inside the cell, respectively; R is the universal gaz constant ($8.315 mJ/(K^\circ \cdot Mol)$), T is the temperature in degrees Kelvin, F is Faraday's constant ($96,480$coulombs$/$Mol) and z is the valence of the ion.

Figure 1.10 shows the different ionic species together with the equilibrium Nernst potential for different ionic species for a typical mammalian neuron.

The Nernst equation gives the equilibrium voltage corresponding to a unique ionic specie only considering the ionic concentrations. It did not take into account the ease

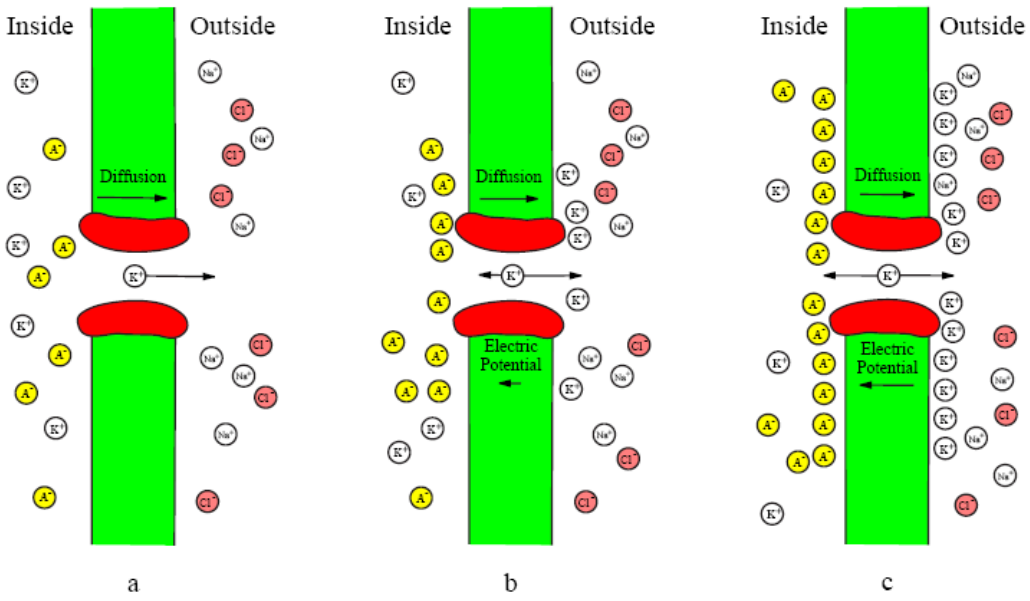

Figure 1.9: Diffusion of K^+ ions through the cell's membrane: (a) creates and electric potential force pointing in the opposite direction, (b) until the diffusion and electrical forces compensate each other (c). The resulting transmembrane potential 1.1 is referred to as the Nernst equilibrium potential for potassium ion (from Izhikevich [146]).

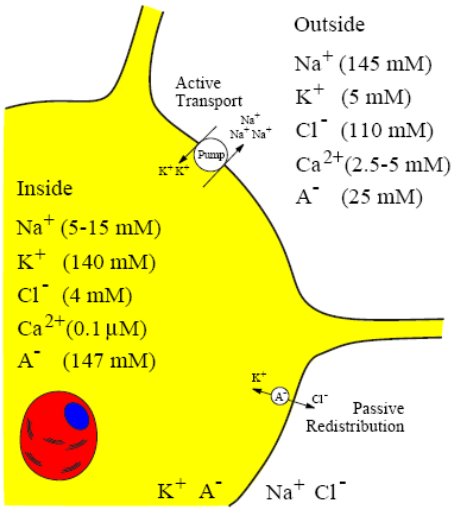

Equilibrium Potentials

$$\mathrm{Na}^+ \quad 62 \log \frac{145}{5} = 90 \text{ mV}$$
$$62 \log \frac{145}{15} = 61 \text{ mV}$$

$$\mathrm{K}^+ \quad 62 \log \frac{5}{140} = -90 \text{ mV}$$

$$\mathrm{Cl}^- \quad -62 \log \frac{110}{4} = -89 \text{ mV}$$

$$\mathrm{Ca}^{2+} \quad 31 \log \frac{2.5}{10^{-4}} = 136 \text{ mV}$$
$$31 \log \frac{5}{10^{-4}} = 146 \text{ mV}$$

Figure 1.10: Ion concentrations and Nernst equilibrium potentials in a typical mammalian neuron at a temperature of $37°C$ (figure taken from [146] where it was adapted from [154]).

with which ions cross the membrane. In terms of electrical current flow, the membrane's conductance provides a convenient measure of how readily the ion crosses the membrane. Another convenient measure is the permeability P of the membrane to a given ion, in velocity unit (cm/s). This quantity measures the rate of solute movement in solution. David Goldman in 1943 published a formula linking of the equilibrium potential, the ionic permeabilities and the intracellular and extracellular ionic concentrations taking into account different ionic species (see [109]):

$$E_m = \frac{RT}{F} \log \left(\frac{P_K [K^+]_{out} + P_{Na} [Na^+]_{out} + P_{Cl} [Cl^-]_{in}}{P_K [K^+]_{in} + P_{Na} [Na^+]_{in} + P_{Cl} [Cl^-]_{out}} \right) \tag{1.2}$$

This equation is known as Goldman, or Goldman-Hodgkin-Katz (GHK) equation. Alan Hodgkin and Bernard Katz used this equation to analyze changes to compute this potential, which is often known as the *reversal potential* (instead of equilibrium potential) because the direction of current flow through the channel switches as the membrane potential passes through this value.

This dynamical equilibrium named the "rest" state is achieved when ionic currents are flowing across the membrane and balance each other so that the net current flowing across the membrane is zero. Maintaining this equilibrium is a major power expenditure for the nervous system. Half the metabolic energy consumed by a mammalian brain is has been estimated to be due to the membrane ionic pumps responsible for the balance of ionic gradients (see [9]), all nerve cell present a quite stable negative potential, ranging from $-70mV$ to $-30mV$. This value is not necessarily fixed and under some condititons where the resting potential dynamically adjusts in function of a network activity (see [67]).

1.2.4 The nerve signal

The signals produced and conveyed by the nerve cell are called *action potentials*, or *spikes*. They are rapid transient nerve electrical impulses with an amplitude of $100mV$ and a duration of about $1ms$ (see figure 1.11). Action potentials are initiated at a specialized trigger region at the origin of the axon, the axon hillock (see section 1.2.1). From this region, the action potential is transported down the axon without failure or distortions at speeds ranging from 1 to 100 meters per second. The amplitude of the action potential travelling along the axon remains almost constant (as we will see in the case of long connections, axons are generally wrapped in a fatty insulating sheath of myelin, which is interrupted at regular intervals by the Ranvier nodes where the action potential is regenerated). The fact that these action potential are highly stereotyped implies that the information conveyed is not in the shape of this signal but rather in the relative times of spike emission and the pathway of the signal through the network.

The course of the action potential can be divided into four parts closely linked with the dynamics of ion channels: the rising phase, the falling phase, the undershoot phase, and the refractory period.

(i) *The spike generation and the rising phase* : A sufficiently strong depolarization of the membrane potential at the axon hillock initiates the action potential. This depolarization is often caused by the injection of extra sodium cations into the cell; these cations can come from a wide variety of sources, such as chemical

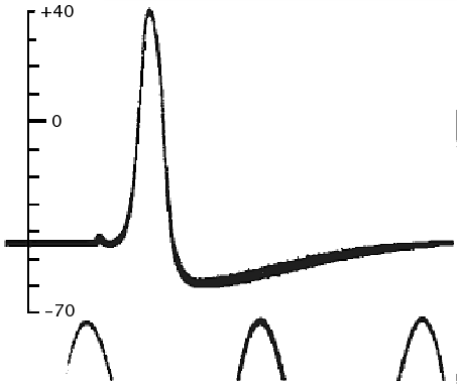

Figure 1.11: First intracellular recording of an action potential obtained in 1939 by Hodgkin and Huxley from the squid giant axon, using glass capillary electrodes filled with sea water. The sinusoid corresponds to a time marker of 500 Hz. The vertical scale indicates the potential in millivolt, the sea water outside being taken as a reference (From [127]).

synapses, sensory neurons or pacemaker potentials. In this phase, the membrane permeability to potassium is low, but much higher than that of other ions, making the resting potential close to E_K.

The depolarization causes the voltage-gated sodium and potassium channels to open, allowing the ions to flow into and out of the axon, respectively. If the depolarization is small, the outward potassium current overwhelms the inward sodium current and the membrane repolarizes back to its normal resting potential around $-70mV$. However, if the depolarization is large enough, the inward sodium current increases more than the outward potassium current and a positive feedback results: the increasing voltage in turn causes even more sodium channels to open, which pushes V still further towards E_{Na}. This positive feedback continues until the sodium channels are fully open and V is close to E_{Na}.

(ii) The *falling phase* : the same raised voltage that opened the sodium channels initially also slowly shuts them off, by stoppering their pores; the sodium channels become inactivated. This lowers the membrane's permeability to sodium, driving the membrane voltage back down. At the same time, the raised voltage opens voltage-sensitive potassium channels; the increase in the membrane's potassium permeability drives back V towards E_K. Combined, these changes in sodium and potassium permeability cause V to drop quickly, repolarizing the membrane and producing the "falling phase" of the action potential.

(iii) The *hyperpolarizing phase* : The raised voltage opened many more potassium channels than usual, and these do not close right away when the membrane returns to its normal resting voltage. The potassium permeability of the membrane is transiently unusually high, driving the membrane voltage V even closer to the potassium equilibrium voltage E_K. Hence, there is a hyperpolarization persisting until the membrane potassium permeability returns to its usual value.

(iv) The *refractory period* : The opening and closing of the sodium and potassium channels during an action potential may leave some of them in a "refractory"

state, in which they are unable to open again until they have recovered. In the absolute refractory period, so many ion channels are refractory that no new action potential can be fired. Significant recovery (desinactivation) requires that the membrane potential remain hyperpolarized for a certain duration. In the relative refractory period, enough channels have recovered that an action potential can be provoked, but only with a stimulus much stronger than usual. These refractory periods ensure that the action potential travels in only one direction along the axon.

Some neurons do not generate action potentials, but instead generate a graded electrical signal, which in turn causes graded neurotransmitter release. Such non-spiking neurons tend to be sensory neurons.

Now that we explained briefly the mechanisms of spike generation, let us present the way the signal propagates along the axons to reach other nerve cells.

1.2.5 Propagation of action potentials

The action potential generated in the soma of the nerve cell propagates as a wave along the axon. Like the soma's membrane, the axon's membrane contains voltage-gated ion channels which allowing propagation of the electrical impulse. These impulses are propagated by charge-carrying ions including the same ionic species as the spike generation, namely the sodium (Na^+), potassium (K^+), chloride (Cl^-), and calcium (Ca^{2+}) ions. The ionic currents flowing towards the intracellular medium at a point on the axon during an action potential spread out along the axon, and depolarize the adjacent sections of its membrane. If sufficiently strong, this depolarization provokes a similar action potential generation in the neighboring membrane patches. This basic mechanism was demonstrated again by Alan Hodgkin in the late 30's: he inhibited by crushing or cooling nerve segments of the squid giant axon and showed that an action potential arriving on one side of the inhibited zone could provoke another action potential on the other side, provided that the inhibited segment was sufficiently short.

Once an action potential has occurred at a patch of membrane, the membrane patch needs time to recover before it can fire again. At the molecular level, this absolute refractory period corresponds to the time required for its ion channels to return to their normal open or closed states. Hence the absolute refractory period ensures that the action potential moves in only one direction along an axon. The currents flowing in due to an action potential spread out in both directions along the axon. However, only the the part of the axon that has not fired yet an action potential can respond: the part that has just fired is unresponsive until the action potential is safely out of range and cannot restimulate that part. Hence the action potential propagates from the axon hillock towards the axonal terminals[6].

The axons of some neurons are ensheathed in myelin regularly interrupted by myelin gaps (Ranvier's nodes). Myelin prevents ions from entering or leaving the axon along myelinated segments. As a general rule, myelination increases the conduction velocity of action potentials and makes them more energy-efficient. The current passively spreads from one Ranvier's node to another. The myelin inhibits

[6]propagation in the opposite direction, known as *antidromic conduction*, exists and is very rare. However, if a laboratory axon is stimulated in its middle, both halves of the axon are unfired, and then two action potentials will be generated, one traveling towards the axon hillock and the other traveling towards the synaptic knobs.

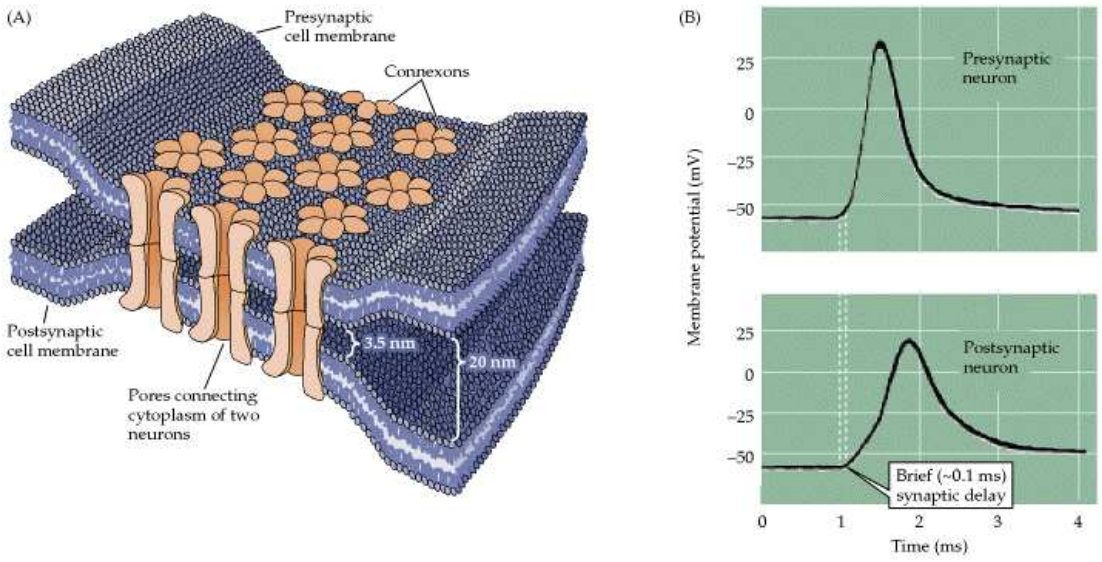

Figure 1.12: Structure and function of gap junctions at electrical synapses. (A) Gap junctions consist of hexameric complexes connecting two similar structure of the pre- and postsynaptic membranes. The pores of the channels connect to one another, creating electrical and chemical continuity between the two cells. (B) Rapid transmission of signals at an electrical synapse in the crayfish (see [102]). An action potential in the presynaptic neuron causes the postsynaptic neuron to be depolarized within a fraction of a millisecond (figure taken from [218]).

charge leakage, and hence when the current reaches another Ranvier node, the depolarization it provokes is sufficient to generate a new action potential at this node; this "hopping" of the action potential from node to node is known as *saltatory conduction*[7], in contrast with the unmyelinated axons where the action potential is continuously transmitted down the axon like a wave.

Now that the signal has been transported from the soma to the axonal terminal, let us describe the way the signal is transmitted to other neurons, in order to close the loop of neuronal processing.

1.2.6 Synaptic Transmission

For communicating with another cell, the neurons make use of one of two basic forms of synaptic transmission: the electrical and the chemical synapses. The strength of the synaptic transmission can be enhanced or reduced, depending of the history of the cellular activity. This *plasticity* of the nerve cells is crucial to memory, learning and other higher brain functions.

The electrical synapse transmission is rapid and stereotyped, and is mainly used to send simple depolarizing signals for systems requiring the fastest possible response. At the location of an electrical synapse, the separation between two neurons is very small ($\approx 3.5nm$). This narrow gap is bridged by the *gap junction channels*, spe-

[7]The mechanism of saltatory conduction was suggested in 1925 by Ralph Lillie in his article [181], the first experimental evidence for saltatory conduction came from Ichiji Tasaki, Taiji Takeuchi and from Andrew Huxley and Robert Stämpfli [138, 250, 251, 252].

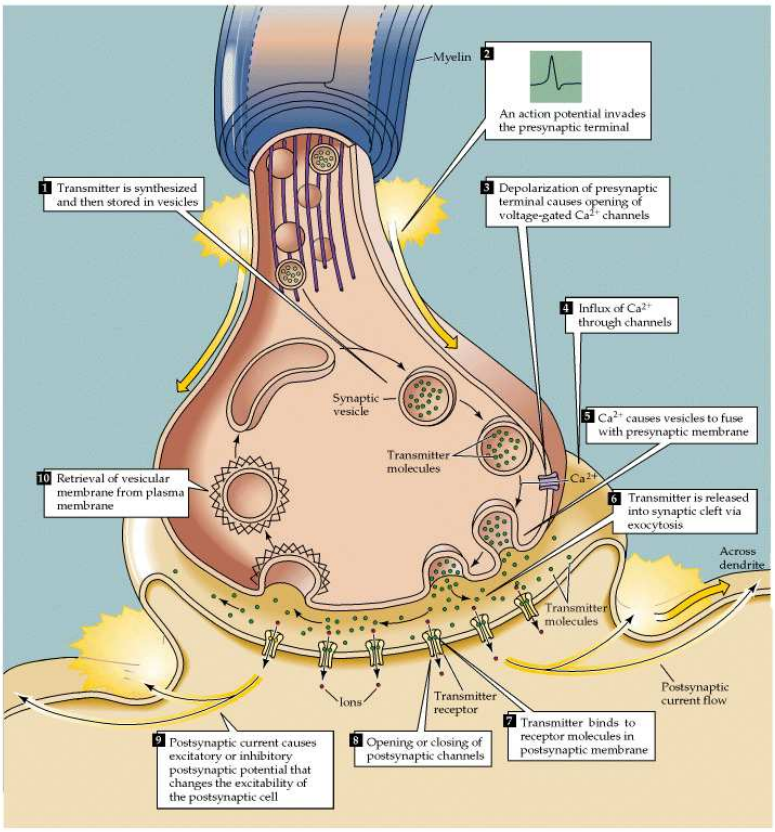

Figure 1.13: Cascade of events involved in the signal transmission at a typical chemical synapse.(from [218]).

cialized protein structures that conduct the flow of ionic current from the presynaptic to the postsynaptic cell (see figure 1.12). Electrical synapses thus work by allowing ionic current to flow passively through the gap junction pores from one neuron to another. The usual source of this current is the potential difference generated locally by the action potential. Without the need for receptors to recognize chemical messengers, signaling at electrical synapses is more rapid than that which occurs across chemical synapses, the predominant kind of junctions between neurons. The relative speed of electrical synapses also allows for many neurons to fire synchronously. Because of the speed of transmission, electrical synapses are found in escape mechanisms and other processes that require quick responses, such as the response to danger of the sea hare Aplysia, which quickly releases large quantities of ink to obscure enemies' vision.

This mechanism of electrical transmission, though rapid, is not the most widely used transmission process between neurons. In most of neural connections, the signal transmission is performed via *chemical synapse*, or *synapse* (without qualifier). Chemical synapses transmit information directionally from a presynaptic cell to a postsynaptic cell and are therefore asymmetric in structure and function. In the case of the chemical synapse, there is no structural continuity between pre- and postsynaptic neurons. The region separating these two cells, called the *synaptic cleft*, is usually wider than the mean adjacent intercellular space, and ranges between 20 and 40nm. The chemical synaptic transmission is based on the release by the presynaptic

neuron of *neurotransmitter*, a chemical substance that binds to specific receptors on the postsynaptic cell membrane. To this purpose, the presynaptic terminals contain discrete collections of synaptic vesicles, each of which filled with several thousand of transmitter molecules. During the discharge of a presynaptic action potential, Ca^{2+} enters the presynaptic terminal through voltage-gated Ca^{2+} channels at the active zone. The rise of Ca^{2+} concentration causes the vesicles to fuse with the presynaptic membrane and thereby release their neurotransmitter into the synaptic cleft (*exocytosis*). The neurotransmitter molecules then diffuse across the synaptic cleft and bind to their receptors on the postsynaptic cell membrane. This in turn activates the receptors, leading to the opening or closing of ion channels. The resulting flux alters the membrane conductance and potential of the postsynaptic cell (see figure 1.13).

These several steps account for the synaptic delay at chemical synapses, which can be as short as 0.3ms, but that often lasts several milliseconds. Hence it lacks the speed of electrical transmission. Nevertheless, it has the important property of amplifying the signal and hence even a small presynaptic nerve terminal generating a weak current can release thousands of transmitter molecules that can depolarize even a large postsynaptic cell.

When the receptors of the postsynaptic cell bind neurotransmitter molecules, they respond by opening nearby ion channels, causing ions to flow in or out and changing the local transmembrane potential of the cell. The resulting change in voltage is called a *postsynaptic potential*. The result of this process can be excitatory in the case of depolarizing currents (this is the more general case), or inhibitory in the case of hyperpolarizing currents. The excitatory or inhibitory nature of a synapse depends on the types of ion channel conduct the postsynaptic current displays, which in turn is a function of both the type of receptors and the type of neurotransmitter employed at the synapse. If a signal is transmitted at an excitatory synapse, then the depolarization of the cell can be strong enough so that an action potential can be initiated in the postsynaptic cell. If the depolarization induced by the excitatory postsynaptic potential is not be sufficient for an action potential initiation, then the effect of the depolarization will be last for some time, and will be progressively attenuated. Therefore, if the neuron receives other signals from the same or other neurons, the postsynaptic potentials (PSP) they provoke will be summed. This phenomenon is known as the *synaptic integration*.

All these phenomena can be modeled independently, and result in what we call the *detailed neuron models*

1.3 Electrophysiological Modelization of the Neuronal Activity

In the previous section, we described from a biological point of view the basic mechanisms in play inside the neurons and the transmission mechanisms between neurons. In this section, we present physical and mathematical models for each of these process. The models built upon these considerations will be called *detailed neuron models* since they will be based on a detailed description of the neuron and of each structure's dynamics. We try to keep the presentation intuitive and try to make explicit all the simplifications and their biological origins. This section is only devoted to present models of the neuronal activity itself. Modelizations of synaptic inputs will be presented later.

From a biophysical point of view, action potentials are the result of currents that

pass through ion channels in the cell's membrane. In their extensive series of experiments on the giant axon of the squid, Hodgkin and Huxley succeeded in measuring these currents and described their dynamics in terms of differential equations.

1.3.1 Models of ionic currents

The total current flowing across the membrane through all of its ion channels is called the membrane current of the neuron. By convention, the membrane current is defined as positive when positive ions leave the neuron and negative when positive ions enter the neuron. The total membrane current is determined by summing currents due to all of the different types of channels within the cell membrane, including voltage-dependent and synaptic channels. We label the different types of channels in a cell membrane with an index i. As discussed in the last section, the current carried by a set of channels of type i with reversal (Nernst) potential E_i, vanishes when the membrane potential satisfies $V = E_i$. For many types of channels, the current increases or decreases approximately linearly when the membrane potential deviates from this value. The difference $(V - E_i)$ is called the *driving force*, and the membrane current per unit area due to the type i channels is written as $g_i(V - E_i)$ in this linear approximation, where the factor g_i is the conductance per unit area related to the channel. Summing over the different types of channels, we obtain the total membrane current:

$$I_m = \sum_i g_i (V - E_i)$$

In the linear model, it is easy to compute the *resting potential* of the neuron, i.e. the membrane potential corresponding to a null total ionic current. This current reads, considering the 4 ionic species introduced:

$$V_{rest} = \frac{g_{Na} E_{Na} + g_{Ca} E_{Ca} + g_{Cl} E_{Cl} + g_K E_K}{g_{Na} + g_{Ca} + g_{Cl} + g_K}$$

This quite simplistic model is the most commonly used to described ionic currents, and is also chosen in this dissertation. It is valid for small changes of the voltage.

More precise models of voltage-ionic currents relations take into account the ion permeability and the selectivity of membranes. This formalism know as the Goldman-Hodgkin-Katz (GHK) formulation, was developed by Goldman in [109] and used by Hodgkin and Katz [129]. The GHK equations involve the membrane permeability to ions, a variable that quantifies the membrane's ability to let ions flow in and out the cell (see [124, Chapter 14]). The GHK current equation says that the current carried by ion S is equal to the related membrane's permeability P_S multiplied by a nonlinear function of the voltage:

$$I_S = P_S z_S \frac{V F^2}{RT} \frac{[S]_{in} - [S]_{out} \exp(-z_S F E/RT)}{1 - \exp(-z_S F E/RT)} \tag{1.3}$$

With this model one can derive of the reversal potential equation (1.2) that we used to explain the spike mechanism. For more details on the GHK equation and its derivation, we refer to [124, Chapter 14].

1.3.2 Models of gated ionic channels

As described in section 1.2.1, many ion channels are voltage-gated and their properties depend on the membrane potential. Gates can *activate* or *inactivate* the channel

(i.e. open or close it respectively, see figure 1.6). To model their function, Hodgkin and Huxley introduced two variables: the probability m of an activation gate to be in the open state, and the probability h of an inactivation gate to be in the open state. These variables are probabilities, hence real numbers in $[0,1]$. When channels are partially open, $m \in (0,1)$, when the channels are completely activated, $m = 1$, and when it is completely deactivated, $m = 0$. The proportion of open channels in a large population is hence given by:

$$p = m^a h^b; \tag{1.4}$$

where a (resp. b) is the number of activation (resp. inactivation) gates per channel. Some channels do not have inactivation gates ($b = 0$), hence $p = m^a$. Such channels do not inactivate, and they result in persistent currents. In contrast, channels that do inactivate result in transient currents.

The dynamics of the activation variable m is classically described by a general first-order differential equation:

$$\frac{\mathrm{d}m}{\mathrm{d}t} = \frac{m_\infty(V) - m}{\tau(V)} \tag{1.5}$$

where $m_\infty(V)$ is called the *steady-state activation function*, and $\tau(V)$ the *activation time constant*. These two functions can be measured experimentally. The activation function has a sigmoidal shape and the time constant a unimodal shape (see figure 1.14).

The dynamics of the inactivation variable h can also be described by the first-order differential equation

$$\frac{\mathrm{d}h}{\mathrm{d}t} = \frac{h_\infty(V) - h}{\tau(V)} \tag{1.6}$$

Here again we call where $h_\infty(V)$ is called the *steady-state inactivation function*, and $\tau(V)$ the *inactivation time constant*. For the inactivation function, h_∞ is an inverted sigmoidal function (decreasing, tends to 1 at $-\infty$ and to 0 at $+\infty$, see figure 1.14).

1.3.3 The Hodgkin-Huxley model and its reductions

The original Hodgkin-Huxley model

The original Hodgkin-Huxley model is a very classical and widely used detailed neuron model. Though we do not study this model in depth, it is an important model and will be referred to in discussions for being a reference model.

Using pioneering experimental techniques of that time, Hodgkin and Huxley [128] determined that the squid axon curries three major currents: voltage-gated persistent K^+ current with four activation gates, voltage-gated transient Na^+ current with three activation gates and one inactivation gate, and Ohmic leak current, I_L, which is carried mostly by chloride ions Cl^-.

The basic electrical relation between the membrane potential and the currents read:

$$C\frac{\mathrm{d}V}{\mathrm{d}t} = I(t) - I_K - I_{Na} - I_L,$$

This equation, considering the linear model of $I-V$ relations, the model of voltage-gated channels we just introduced and considering the maximal conductance for each ionic specie instead of the real conductance, can be written as follows:

ion	E_{ion} (mV)	$\bar{g_{ion}}$ (mS/cm^2)
Na	115	120
K	-12	36
L	10.6	0.3

Table 1.1: Parameters of Hodgkin-Huxley model: (shifted) Nernst potentials and maximal conductances. The membrane capacity is $C = 1\mu F/cm^2$. The voltage scale is shifted so that the resting potential is 0 (i.e. shifted by approximately $+65mV$)

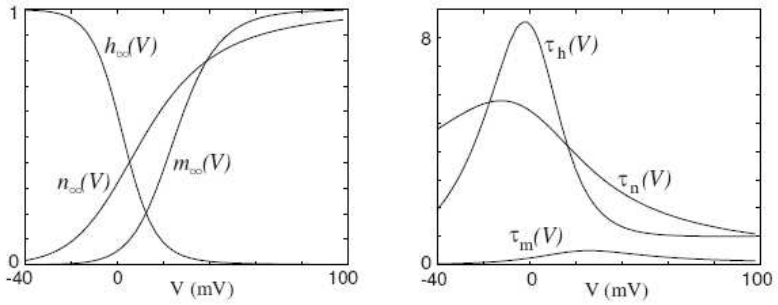

Figure 1.14: Steady state (in)activation functions (left) and time constants (right) in the Hodgkin-Huxley model.

$$\begin{cases} C\dot{V} &= I(t) - \bar{g_K} n^4 (V - E_K) - \bar{g_{Na}} m^3 h (V - E_{Na}) - \bar{g_L}(V - E_L) \\ \dot{n} &= \alpha_n(V)(1-n) - \beta_n(V) n \\ \dot{m} &= \alpha_m(V)(1-m) - \beta_m(V) m \\ \dot{h} &= \alpha_h(V)(1-h) - \beta_h(V) h \end{cases} \tag{1.7}$$

In this equation, the we denoted $\dot{x}$ the derivative dx/dt for a variable x. The functions α_i and β_i result of instantiations of the steady-state activation and inactivation functions and of the time constant functions. The equations are presented this way for historical reasons. The related steady-state (in)activation functions of the variable x simply reads $x_\infty = \alpha_x/(\alpha_x + \beta_x)$ and its time constant $\tau_x = 1/(\alpha_x + \beta_x)$. The functions α_x and β_x classically chosen are:

$$\begin{cases} \alpha_n(V) = 0.01 \frac{10-V}{\exp(\frac{10-V}{10})-1} & \beta_n(V)) = 0.125 \exp\left(-\frac{V}{80}\right) \\ \alpha_m(V) = 0.01 \frac{25-V}{\exp(\frac{25-V}{10})-1} & \beta_m(V)) = 4 \exp\left(-\frac{V}{18}\right) \\ \alpha_h(V) = 0.07 \exp\left(-\frac{V}{80}\right) & \beta_h(V)) = \frac{1}{\exp(\frac{30-V}{10})+1} \end{cases} \tag{1.8}$$

In the original model proposed by Hodgkin and Huxley, these functions and constant are set as in table 1.1.

The related steady state (in)activation function and time constants are plotted in figure 1.14.

This model is widely used in the neuroscience community. It is quite precise, and has the advantage of being based on the main biophysical principles it emulates. It is now quite well understood from a dynamical systems point of view. Its bifurcations have been identified numerically, and this model presents a very interesting bifurcation portrait (see e.g. [47]) including an incredible zoology of bifurcations and even

chaos. It is able to generate spikes, which are very similar to intracellular recordings, presenting the four phases described in section 1.2.4, bursts, and different other electrophysiological signals, when varying its parameters. Its main drawback is its high complexity and dimensionality that prevent from analytical studies and efficient simulations. The literature about Hodgkin-Huxley model is huge, and this model is still very actively used in the top neuroscience research. Many variants of this model have been proposed (new ion channels considered, different dynamics – [105, Chapter 2.3] – introduction of additional biophysical parameters such as the temperature –see e.g. [93]–).

Many reductions of these models have been proposed in order to be mathematically tractable or more efficient computationally. These reduced models include the famous Fitzhugh–Nagumo and Morris–Lecar models. These two models are bidimensional approximations of the original Hodgkin–Huxley model based on quantitative observations (the m variable, which is the fastest, is here considered as instantaneous, i.e. simply equal to its asymptotic value $m_\infty(V)$, the time constants of h and n are almost the same, and the graphs of the functions $n_\infty(V)$ and $m_\infty(V)$ are very similar, therefore n and $1-h$ are identified, ...). These two-dimensional models are way more tractable. One of their main advantage is the low dimensionality allowing one to perform a phase plane analysis. This type of models have been extensively studied, from a mathematical and simulation points of view. We will not present here the equations and the results obtained by analyzing these models, and refer to [47, 105, 146, 164].

1.3.4 Models of spike propagation

The models we presented in this section considered only punctual neurons. It is based on the assumption that the membrane potential is constant all along the neuron. Models taking into account the spatial extension of the axon or models of dendrites have been also developed in order to emulate the signal propagation along the axons. These models involve in general reaction-diffusion partial differential equations and models of dendritic tree structures (the interested reader is referred to [67, 105] and mostly to [164]).

1.3.5 Models of synapses

The synaptic signal and its integration will be of particular importance in the study of neuronal networks and noise integration. We will always consider in this dissertation that the contributions of different incoming spikes or input current are linearly summed. More precisely, we consider an incoming impulse (Dirac pulse) will generate a typical postsynaptic pulse (PSP) of current or conductivity. The current or conductance at the level of the postsynaptic cell is considered as the convolution of the incoming signal (spike train or continuous firing rate) with the PSP. Different models of PSPs will be considered (see figure 1.15):

- *Instantaneous postsynaptic current (conductance) :* the impulse response of the synapse is a Dirac pulse of current (conductance). This model is mainly used in chapter 6.

- *Exponentially decaying postsynaptic current (conductance):* the inputs received at a given synapse generate an exponentially decaying synaptic current (conductance) of type $\exp(-t/\tau)\mathbb{1}_{t\geq 0}$. Chapter 7 builds upon this model.

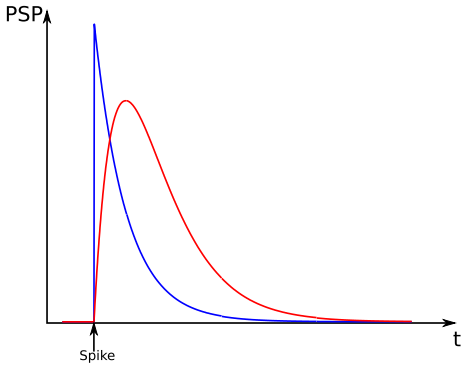

Figure 1.15: Typical postsynaptic (current or conductance) pulses with the same time constant. Blue: exponentially decaying PSP and Red: second-order PSP.

- *Second-order postsynaptic current (conductance) pulse :* the impulse response is the solution of a second order linear differential equation, taking into account both the rise time and the decay time of real PSPs. This model introduced by Rotterdam et al [275] and is of type $\alpha\beta t e^{-\beta t}\mathbb{1}_{t\geq 0}$. These functions have been successfully applied to neural mass models and will be used in chapters 8, 9 and 10.
- *General postsynaptic current (conductance) pulse :*In [105, section 4.1.3], the authors consider general postsynaptic pulses $\alpha(t)$, and will be used in chapter 8.

1.4 NOISE IN NEURONS

In vivo recordings of neuronal activity are characterized by their high variability. Different studies of the spikes trains of individual neurons indicate that the firing patterns seem to be random. The origin of the irregularity in the electrical activity of cortical neurons in vivo has been widely studied and has received no satisfactory answer so far. Nevertheless it is commonly admitted that a) part of this variability can be considered as noise [235, 239], and b) that a large part of the noise experienced by a cortical neuron is due to the intensive and random excitation of synaptic sites.

We describe some of the biological evidence that supports these statements and propose mathematical models of the synaptic noise.

1.4.1 Sources of variability

It is generally agreed that a large part of the noise experienced by a cortical neuron is due to the intensive and random excitation of synaptic sites.

It has been observed from *in vivo* recordings of cortical neurons in awake [43] and anesthetized animals [69] that a spontaneous activity exists and that the related spike process can be considered as Poisson. This Poisson model of independent synaptic inputs, or rather its diffusion limit approximation, is the model we will mainly use is this dissertation.

The origin of irregularities is still poorly known. Gerstner and Kistler in [105] discuss this question at length. They obtain an interesting classification, and show

that we can distinguish between intrinsic noise sources that generates stochastic behavior at the level of the neuronal dynamics and extrinsic sources arising from network effects and synaptic transmission. We briefly summarize the main points:

- A permanent noise source is the thermal noise linked with discrete nature of electric charge carriers. Fluctuations linked with this phenomenon are however of minor importance compared to other noise sources in neurons.
- The finite number of ion channels is another noise source.Most of the ion channel have only two states: they are open or closed. The electrical conductivity of a patch of membrane is proportional to the number of open ion channels. The conductivity therefore fluctuates and so does the potential[8]
- Noise is also due to signal transmission and network effects (extrinsic noise): synaptic transmission failures, randomness of excitatory and inhibitory connections, for instance, and global networks effects (see for instance [36]) where random excitatory/inhibitory connectivity can produce highly irregular spikes trains even in the absence of noise.

To account for the variability in spike trains, many models have been proposed. Some are based on random point processes, mainly input dependent renewal systems (see [105]). These models are quite hard to handle mathematically and often lack of biological plausibility, and therefore will not be used in the rest of the dissertation. We will be particularly interested in this thesis in diffusion approximations of noisy spike trains, and chapters 6, 7 and 8 build upon these models.

1.4.2 Point processes

The simplest point process used in order to model spike train is a non-homogeneous Poisson processes. This process has the property of being forgetful, which is an advantage from the mathematical point of view, but a great drawback for modeling spike trains which do not reflect this absence of memory. For instance, refractory period and intrinsically bursting cells cannot be taken into account in a inhomogeneous Poisson process. Given an instantaneous firing rate $r(t)$, the inhomogeneous Poisson process with intensity $r(t)$ is a random distribution of tops (discrete events) modeling the spike time sequence $(T_n)_{n\geq 0}$. Of all renewal processes sharing the same mean firing rate $\int_0^t r(s)\,ds$, the Poisson process is the one which has the maximum Shannon entropy, and for this reason if no other information is known about a spike train, Poissonian model minimize artificial correlations. But if spike coding in concerned, it has to be noted that no information is embedded in its precise spike times: conditionally on the fact that there are N spikes in a given interval, the times of the spikes are uniformly distributed.

Intracellular spike trains recordings present many differences with Poisson spike trains. In particular, spikes cannot be fired arbitrarily fast because of the cell's refractoriness[9], wether it has a strictly positive probability for Poisson processes. Other models, for instance from the class of "simple modulated renewal processes" [221] such as Gamma processes, can be used. They are more biologically plausible (see e.g. [286] and references herein).

[8]There exists models taking into account the finite number of ion channel, and that they can reproduce the observed variability in some cases(see for instance [50]).

[9]Note that the refractory period prevents from modeling spike trains with unidimensional Markov processes.

1.4.3 Diffusion approximation

In term of neuron models we concentrate on several classes of integrate-and-fire spiking neuron models because they bring together a relative mathematical simplicity and a great power for reproducing many observed neuronal activities [141]. In this field, Knight [163], pioneered the study of the effect of noise with a simplified model in which the threshold was drawn randomly after each spike. Gerstner [105] extended these results and studied both slow noise models, in which either the threshold or the reset is drawn randomly after each spike, and fast escape rate noise models. In the context of synchrony in neuronal networks, Abbott *et al* [1] studied a phase noise model. However, none of these models can represent in a realistic way the synaptic noise as experienced by cortical neurons.

We concentrate on the effect of synaptic currents. Synaptic currents can be described by a simple system of ordinary differential equations (see for instance [68]). We study the impact of noise originating from realistic synaptic models on the dynamics of the firing probability of a spiking neuron.

We only explore two levels of complexity for the synaptic currents, 1) instantaneous (described by delta function) synaptic currents, and 2) synaptic currents described by an instantaneous jump followed by an exponential decay. The dynamics of the firing probability of a neuron receiving a bombardment of spikes through such synaptic currents is studied in the framework of the diffusion approximation (in the neuronal context, see [270]). This approximation is justified when a large number of spikes arrive through synapses that are weak compared to the magnitude of the firing threshold, which is the relevant situation in the cortex. In the diffusion approximation, the random component in the synaptic currents can be treated as a Brownian motion in the case of instantaneous synapses. On the other hand, when synapses have a finite temporal response, as in the more realistic models, synaptic noise has a finite correlation time and thus becomes "colored" noise. Thanks to the diffusion approximation, the dynamics of the firing probability can be studied in the framework of the stochastic calculus theory (see for instance [160]).

Many mathematical descriptions of the synaptic current I^{syn} have been proposed (see Destexhe *et al* [68] or [105]). We consider two types of increasingly complex synaptic current models:

(i) Instantaneous synapses: if we neglect the synaptic integration, considering that the synaptic time constants are small with respect to the membrane interaction, the post-synaptic input can be described by a Brownian motion, which is the diffusion approximation of a rescaled sum of Poisson processes. For this we assume that the synaptic inputs are spikes arriving at N synapses $i \in \{1, \ldots, N\}$, each with a synaptic efficiency ω_i, at the spikes times t_i^k. The input synaptic current can be written:

$$dI_t^{\text{syn}} = \sum_{i=1}^{N} \omega_i \sum_k \delta(t - t_i^k) \stackrel{\text{def}}{=} \sum_{i=1}^{N} \omega_i dS_i(t), \tag{1.9}$$

where the $S_i(t)$s are point processes representing the spikes trains arriving in each synapse.

Neurons are connected to thousand of neurons (in general, $N \approx 10^3 - 10^4$). If we assume that the synaptic input spikes times follow a probability law with mean μ_i and variance σ_i^2 (for instance Poisson processes, $\sigma_i^2 = \mu_i$) and are pairwise

independent[10], I^{syn} is the sum of N independent Poisson processes, of mean $\omega_i\mu_i$ and of variance $\omega_i^2\mu_i$. We assume that the ω_is are such that there exist μ, σ in $(0,\infty)$ such that[11]:

$$\begin{cases} \sum_{i=1}^{N} \omega_i\mu_i \underset{N\to\infty}{\longrightarrow} \mu \\ \sum_{i=1}^{N} \omega_i^2\mu_i \underset{N\to\infty}{\longrightarrow} \sigma^2 \end{cases}$$

By Donsker's theorem [23]

$$\sum_{i=1}^{N} \omega_i \Big(S_i(t) - \mu_i t \Big) \xrightarrow{\mathscr{L}} \sigma W_t \tag{1.10}$$

where $(W_t)_{t\geq 0}$ is a standard Brownian motion (see Appendix C for a definition), and the symbol $\xrightarrow{\mathscr{L}}$ indicates that the process on the lefthand side converges in law to the process on the righthand side when $N \to \infty$.

The diffusion approximation consists in approximating the synaptic jump process (1.9) by the continuous process:

$$I_t^{\text{syn}} = \mu t + \sigma W_t \tag{1.11}$$

(ii) Exponentially decaying synaptic current: because the postsynaptic interaction has a finite integration time, say τ_s, the following equation arises naturally

$$\tau_s dI_t^{\text{syn}} = -I_t^{\text{syn}} dt + \sum_{i=1}^{N} \omega_i \sum_k \delta(t - t_i^k) \tag{1.12}$$

Note that we have assumed that τ_s was the same for all synapses and neglected the rise time of the synaptic current. The second assumption is justified on the ground that the rise time of a synapse is typically very short compared to the relaxation time.

A diffusion approximation similar to the one in the previous paragraph yields the following diffusion approximation of the synaptic noise with exponential decay:

$$\tau_s dI_t^{\text{syn}} = (-I_t^{\text{syn}} + \mu)\, dt + \sigma dW_t \tag{1.13}$$

(iii) More realistic models of the synaptic current I^{syn} introduce a dependency on the membrane potential. A classical model is the *transmitter*-activated ion channels. The current that passes through the ion channels depends on a synaptic conductivity $g_s(t)$ and on the difference between the actual value of the membrane potential and the reversal potential V_{rev}: $I^{\text{syn}}(V,t) = g_s(t)(V - V_{\text{rev}})$. The synaptic conductivity g_s accounts for the noise, either instantaneous or not. A diffusion approximation similar to the one above yields the following representations for the synaptic current:

(a) For instantaneous synaptic conductivities:

$$dI_t^{\text{syn}} = (\lambda_g \sqrt{N} dt + \mu_g \sqrt{N} dW_t)\,(V(t) - V_{\text{rev}}). \tag{1.14}$$

[10]The independence hypothesis is a key hypothesis and is quite difficult to justify biologically. Nevertheless, the same result would hold under very technical and strong conditions on the decorrelation of the process. It is a very intricate theory and we will not deal with it here.

[11]In general this condition can be achieved by a rescaling and a change of time applied to the process

(b) For synaptic conductivities with exponential decay:

$$\begin{cases} dI_t^{\text{syn}} = g_s(t)(V(t) - V_{\text{rev}}) \\ \tau_s dg_s(t) = (-g_s(t) + \lambda_g\sqrt{N})\,dt + \mu_g\sqrt{N}dW_t. \end{cases} \tag{1.15}$$

1.4.4 Validations of the models

Along with proposed models for random spike trains comes the need for theoretical and mathematical tools to confront the models to experiments. There are many tools to quantify the likelyhood of a given model.

- *Trial-averaged firing rate.*
- *Inter-spike interval histogram*
- *Interval maps:* two-dimensional of all couples $(T_n, T_{n+1} - T_n)$ over successive trials. It combining trial-averaged firing rates (projection on the abscissa), ISI histograms (projection on the ordinates) and supplementary statistical information (see [221]).
- *Fano factor:* scalar estimator equal to the empirical variance of the spike train divided by its empirical expectation over multiple trials. Poisson process always has a Fano factor equal to 1. For general point processes, Fano factors has no simple expressions. For renewal processes, it appears to be constant depending on the statistics of the process (see [286]). In real neurons, and for instance for ganglion cells, the spike trains Fano factor is not constant. and depends on the average firing rate (see figure 1.16).

1.5 Spike patterns and neuronal excitability

In this section we now turn to more phenomenological models, based on spike times description. Spikes are the elementary unit of the neural code, and therefore the neural code can be considered binary (all-or-none). We have seen that neurons are excitable systems, in the sense that they are typically at rest but can fire spikes in response to certain forms of stimulation. The evoked firing pattern, in relation to the type of stimulation, characterize the cell's computational properties. From this point of view, the cell can either simply sum (integrate) the inputs or respond to some precise types of stimulation (resonators), and fire precise spike patterns.

These characteristics will be fundamental throughout the dissertation. Indeed, chapters 2, 3 and 4 are aimed to reproduce spike patterns, excitability and substhreshold behavior with simple formal models, and chapters 6 and 7 to reproduce spike statistics, upon which is built up chapter 8.

1.5.1 Excitability

Alan Hodgkin in 1948 [126] studied the spiking behavior of excitable membranes in response to the injection of steps of currents of various amplitudes. His experiments are illustrated in figure 1.17 using recordings of rat neocortical and brainstem neurons. When the injected current amplitude is small, the neurons are quiescent. When it becomes larger, the nerve cell fires spike trains, and depending on the average frequency of these spike trains, Hodgkin identified two major classes of excitability:

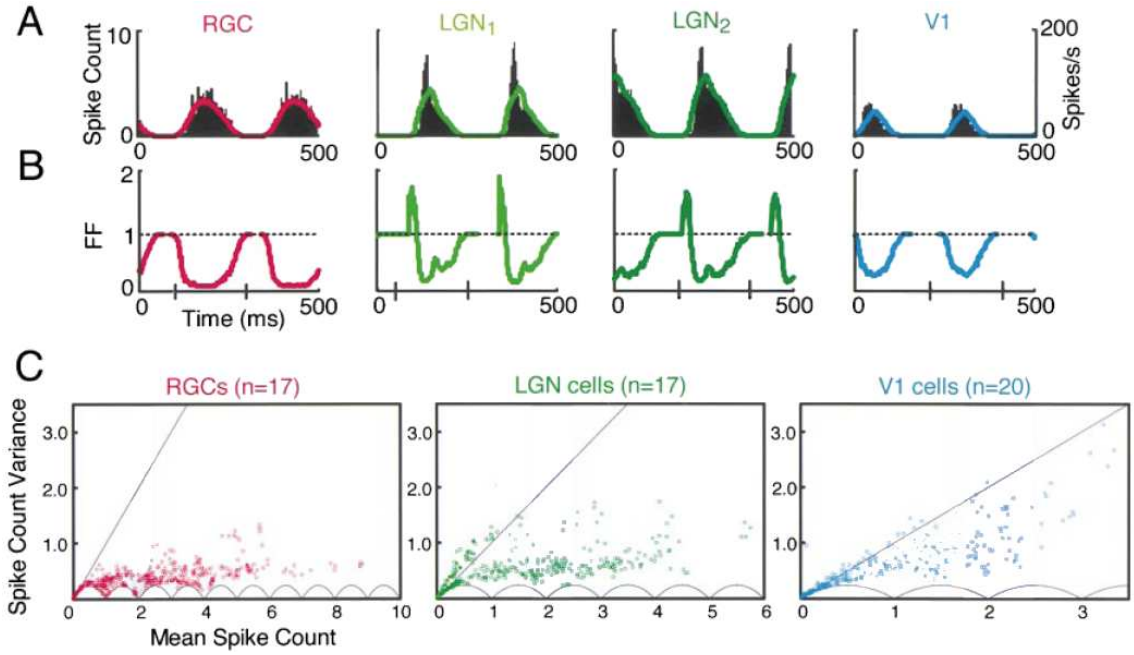

Figure 1.16: Fano factors in the cat visual system, responding to a drifting grating. (A) Mean spike count (firing rate) of different cat visual cells, using binning windows of 50 ms. (B) Corresponding Fano factors (FF) calculated from the same 50 ms intervals. The clear anti-correlation between spiking activity and Fano factor reveals that spikes are relatively more regular at high firing rates. The high FF of LGN cells is attributable to spike bursts. (C) Mean spike count versus variance, for all 50 ms intervals and all measured cells from each area. The scalloped curve at the bottom is a theoretical lower bound for the spike count, due to the fact that it can only take integer values. From [159, 286].

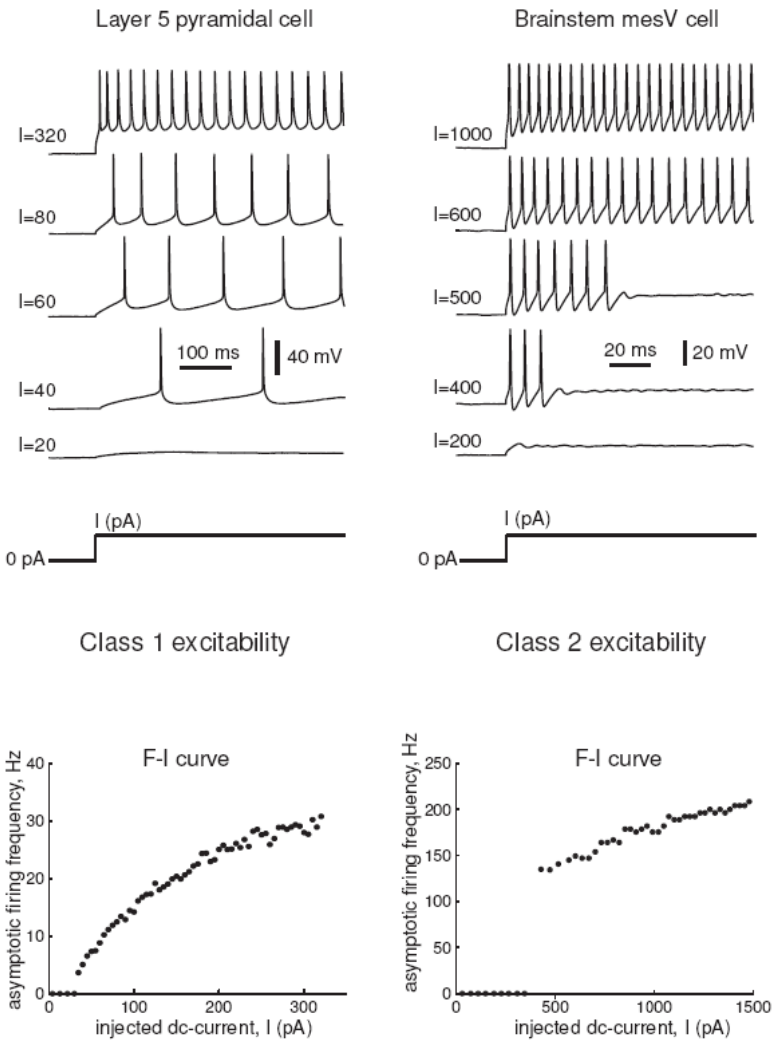

Figure 1.17: (Top) Typical responses of membrane potentials of two neurons to steps of DC-current of various magnitudes. (Bottom) Related frequency-current ($F-I$) curves qualitatively different (recordings of layer 5 pyramidal neurons of the rat's primary visual cortex (left) and mesV neuron from rat brainstem (right)). From Izhikevich 2007 [145]

- *Class 1 excitability*: action potentials can be generated with arbitrarily low frequency, depending on the strength of the applied current.
- *Class 2 excitability*: action potentials are generated in a certain frequency band that is relatively insensitive to changes in the strength of the applied current.

Class 1 neurons, sometimes called type I neurons, fire with a frequency that may vary smoothly over a broad range, starting from 0 Hz to high firing rates as high as 100Hz or even higher. In contrast, the frequency band of class 2 excitable neurons is quite limited, typically ranging from 150 to 200 Hz, but it can vary from neuron to neuron. The qualitative distinction between the classes noticed by Hodgkin is that the frequency-current relation starts from zero and continuously increases for Class 1 neurons, and is discontinuous for class 2 neurons. Obviously, the two classes of excitability have different neuro-computational properties. Class 1 excitable neurons can smoothly encode the amplitude of the stimulation it gets into the frequency of their spiking output, and class 2 neurons act as threshold elements reporting when the strength of input is above a certain value.

1.5.2 Frequency preference and resonance

Some neurons simply integrate the input they get and fire a spike if the inputs where high enough or received consecutively fast. This type of neuron is named integrator. This type of neuron responds to high-frequency inputs, and therefore acts as a coincidence detector because it is most sensitive to the pulses arriving simultaneously.

Some neurons react to pulses when received at a certain frequency, and are named resonators (e.g. mesV neuron). These behaviors have been observed in many in-vitro recordings (see [141, 143] and references herein). The same selectivity exists in vivo as shown by Bryant and Segundo [40]: bursts having a precise frequency added to a noisy signal are detected.

Subthreshold PSP oscillations can explain this behavior. Such behaviors have been observed in many cortical cells [5, 6, 10, 22, 157, 183, 184, 186, 187, 188]. Assume that a presynaptic pulse evokes an (exponentially decaying) oscillatory postsynaptic behavior. The effect of the second pulse depends on its timing relative to the first pulse: if the interval between the pulses is near the natural period, the second pulse arrives during the rising phase of oscillation and increases the amplitude of oscillation further. In this case the effects of the pulses add up. If the interval between pulses is near half the natural period the second pulse arrives during the falling phase of oscillation, and it leads to decrease the oscillations amplitude.

1.5.3 Thresholds and action potentials

As we will see in section 1.6, a common model of spike emission consists in considering that neurons have firing thresholds: when their membrane potential reaches a given threshold, the neuron fires. Great efforts have been made to determine such thresholds experimentally. Unfortunately, the concept of firing threshold is not well defined, in experimental studies as well as in models. Most of the time, the membrane potential value that separates subthreshold depolarizations from action potentials (if accurately detected) depends on the prior activity of the neuron. For example, if a neuron having transient Na^+ current just fired an action potential, the current is partially inactivated, and a subsequent depolarization above the firing threshold might

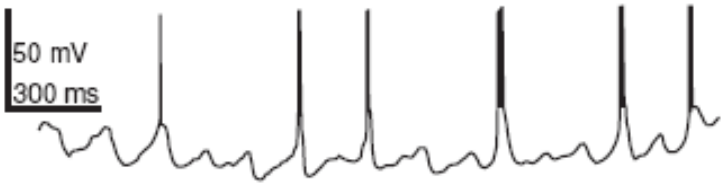

Figure 1.18: Slow subthreshold oscillation of membrane potential of cat thalamocortical neuron evoked by slow hyperpolarization (modified from Roy et al. 1984).

not evoke another action potential. Conversely, if the neuron was briefly hyperpolarized and then released from hyperpolarization, it could fire a rebound post-inhibitory spike.

1.5.4 Spike latency

An interesting neuronal property is the latency-to-first-spike. A barely superthreshold stimulation can evoke action potentials with a significant delay, which could be as large as a second in some cortical neurons. Usually, such a delay is attributed to slow charging of the dendritic tree or to the action of the A-current, which is a voltage-gated transient K+ current with fast activation and slow inactivation. The current activates quickly in response to a depolarization and prevents the neuron from immediate firing. With time, however, the A-current inactivates and eventually allows firing. We see that the existence of long spike latencies is an innate neurocomputational property of integrators. It is still not clear how or when the brain is using it. Two most plausible hypotheses are 1) Neurons encode the strength of input into spiking latency. 2) Neuronal responses become less sensitive to noise, since only prolong inputs can cause spikes. Interestingly, resonators do not exhibit long latencies

1.5.5 Subthreshold oscillation

Interactions between fast and slow conductances can result in low-frequency subthreshold oscillation of membrane potential, such as the one in figure 1.18, The oscillation is caused by the interplay between activation and inactivation of the slow Ca^{2+} current and inward h-current. Subtreshold oscillations are discussed further in chapter 2.

1.5.6 Firing patterns of cortical neurons

Cortical neurons exhibit numerous firing patterns, i.e. characteristic trains of action potentials in response to stimulation by current injections (usually depolarizing pulses). Three main notions will be discussed in order to distinguish different spike patterns (see figure 1.19):

- *Tonic and phasic spiking:* Tonically spiking cells fire continuous trains of action potentials for the duration of the depolarizing pulse of injected current (see figure 1.19-B/D). On the contrary, phasically spiking cells respond to a sustained

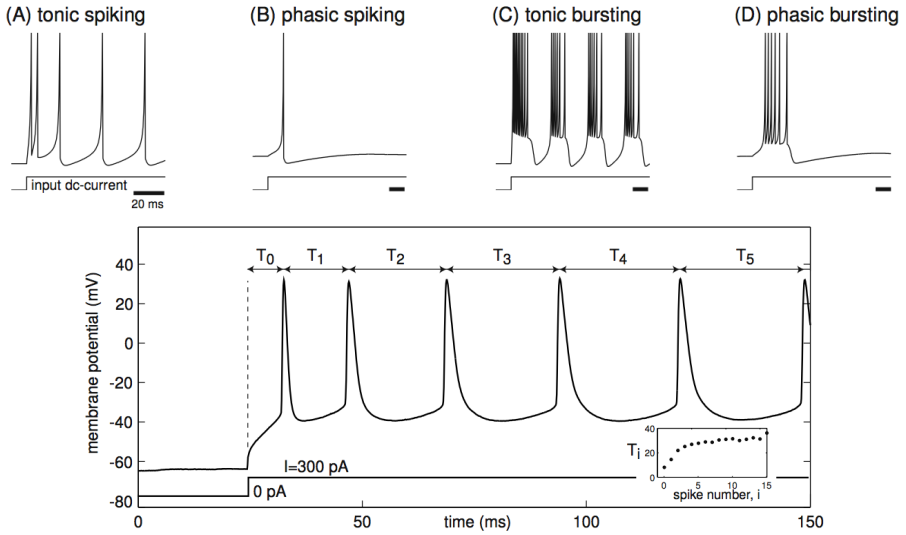

Figure 1.19: Various firing behaviors in response to a sustained depolarizing pulse. Upper panel. Phasic patterns (B,D), tonic patterns (A,C), spiking patterns (A,B) and bursting patterns (C,D). Lower panel. Accommodation of the discharge pattern: interspike intervals increase (From [145]).

depolarizing current pulse with a very brief train of action potentials followed by no further firing (see figure 1.19-A/C).

- *Bursting:* Sometimes neurons use rapid clusters of two or more action potentials, called *bursts*, as basic signaling events instead of simple spikes (see figure 1.19-C/D).

- *Accommodation:* Neurons sometimes show spike frequency adaptation, i.e. a decrease of firing frequency in response to a sustained depolarizing pulse. They are said to be *accommodating* (see figure 1.19). In contrast, non-accommodating neurons keep a constant discharge frequency to such current injections.

As explained in [145], cortical neurons exhibit six major discharge patterns.

- *Regular spiking (RS)* is a tonic spiking with possible adapting frequency that present a stationary firing rate in response to a sustained depolarizing pulse. This firing pattern is the most spread among excitatory neurons (see figure 1.20).

- *Chattering (CH)* corresponds to high frequency bursts with a relatively short interburst period. This behavior has mainly been observed in layer III Purkinje cell but also concerns excitatory cells in layers II and IV (see figure 1.20).

- *Intrinsically bursting (IB)* neurons respond with bursts of action potential at the beginning of a strong depolarizing injection, followed by tonic spiking. The main representatives of this firing pattern are found among layer V PCs (see figure 1.21).

- *Fast spiking (FS)* is a high frequency tonic spiking with little adaptation, observed in inhibitory cells (mostly basket and chandelier cells). Fast spiking cells show irregular spiking when injected with weak currents (see figure 1.22).

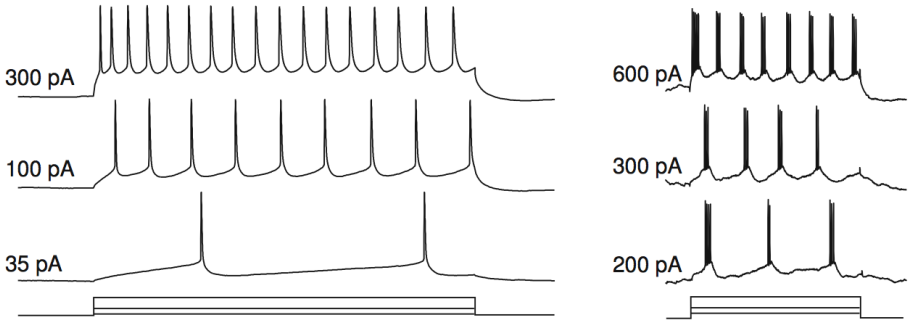

Figure 1.20: Regular spiking (left) and chattering (right) in response to sustained depolarizing pulses of various amplitudes (shown at the bottom of the recordings) (From [145]).

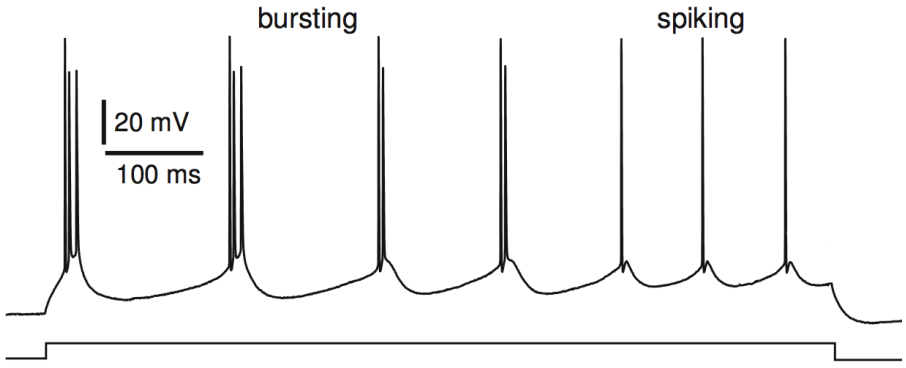

Figure 1.21: Intrinsic bursting in response to a sustained depolarizing pulse. Initial bursting is followed by tonic spiking (From [145]).

- *Low-threshold spiking (LTS)* neurons have a tonic firing pattern with strong accommodation. Their name comes from their tendency to exhibit post inhibitory rebounds (spontaneous emission of spikes consecutive to an hyperpolarizing current injection). They can show low frequency firing and phasic responses to weak stimulations (see figure 1.22). LTS neurons are inhibitory interneurons (mostly Martinotti, double bouquet and bitufted cells).

- *Late spiking (LS)* neurons respond to a depolarizing pulse with a slow increase of membrane potential followed, after a delay possibly as long as one second, by low frequency tonic spiking. Late spiking mainly concerns neurogliaform inhibitory interneurons (see figure 1.22).

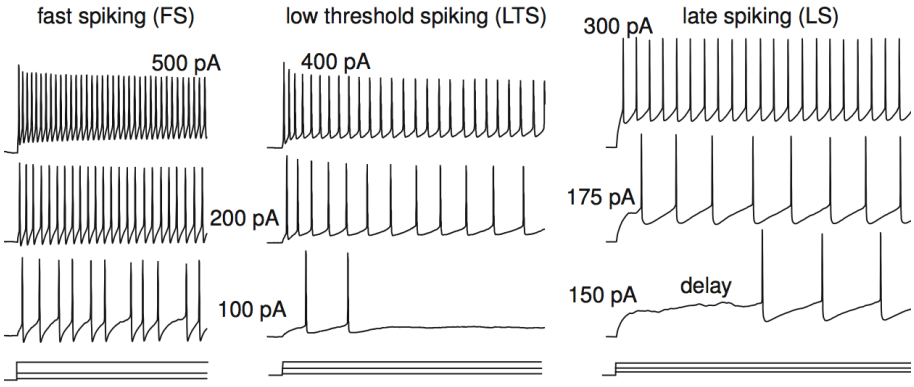

Figure 1.22: Fast spiking (left), low-threshold spiking (center) and late spiking (right) in response to sustained depolarizing pulses of various amplitudes (From [145]).

It appears from the above description that excitatory and inhibitory cells can both be divided into three electrophysiological classes (RS, CH and IB for excitatory neurons, and FS, LTS and LS for inhibitory interneurons). Actually, the firing patterns displayed by inhibitory cells are way more diversified and an alternative classification has been proposed for them.
In [194], the authors propose the following electrophysiological classes and subclasses to characterize interneurons firing patterns (see figure 1.23).

- *Non-accommodating (NAC)* neurons show tonic firing without spike frequency adaptation in response to a wide range of depolarizing current injections. Many FS and LS neurons exhibit this behavior. This class of discharge patterns has three subclasses: *c* (classic discharge), *b* (discharge with initial burst) and *d* (discharge with initial delay).

- *Accommodating (AC)* neurons fire tonically with spike adaptation. Hence they do not reach as high discharge frequencies as NAC cells do. While FS and LS interneurons can exhibit this behavior, most cells of this type are LTS neurons. This class admits the same subclasses as NAC discharges (c,b and d).

- *Stuttering (STUT)* can be displayed by some FS and LS cells. It consists in the firing of high frequency clusters of spikes (which are not bursts) separated by unpredictable periods of quiescence. The three subclasses c, b and d are also represented in stuttering patterns.

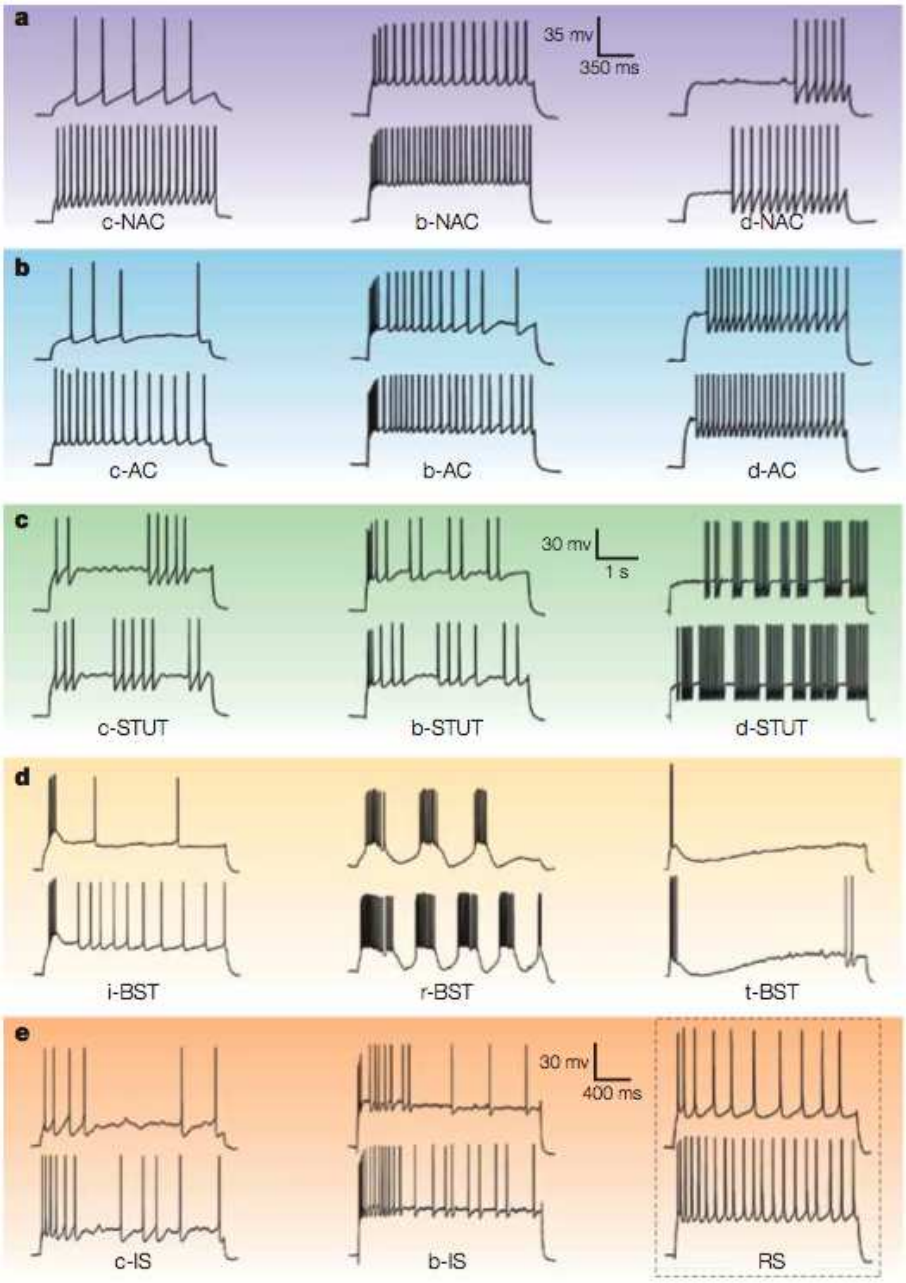

Figure 1.23: The five electrophysiological classes of interneurons (top to bottom) with their subclasses (left to right, see text). In the dashed-lined square at the bottom right corner of the table, examples of regular spiking from excitatory cells are shown for comparison (From [194]).

- *Bursting (BST):* Large basket cells are the only interneurons using bursting (BST) as their main signaling event. They fire bursts of spikes after a slow depolarizing wave, followed by strong slow hyperpolarization. This class has three subclasses: *i* (initial burst followed by regular spike emissions) , *r* (repetitive bursting) and *t* (transient, i.e. phasic burst).

- *Irregular spiking (IS)* cells fire single spikes, in a random fashion, and show strong accommodation. c and b subclasses are represented among irregular firing patterns.

1.6 PHENOMENOLOGICAL NEURON MODELS

The models presented in section 1.3 are based on a precise description of the neuronal basis of spike emission and are able to reproduce a wide class of neuronal behaviors, but are quite complex to handle mathematically and numerically. The aim of this section is to present simpler models aimed to reproduce the "pertinent information" of a neural code: the spike times. *Phenomenological neuron models* consist in modeling the times of emission of the action potential rather than the precise value of the membrane potential for any time.

1.6.1 Linear integrate-and-fire neuron models

Integrate-and-fire (IF) models are based on the assumption that a spike is emitted as soon a cell's membrane potential reaches a certain potential *threshold*. These models were first investigated by Lapicque [171, 172] who introduced those models before any substantial knowledge on the impulse generation mechanisms was acquired. These models have been widely studied and they keep very popular for their simplicity and their ability to reproduce many neuronal behaviors [148, 163, 243, 244, 270]. The simplest integrate-and-fire model passively integrates the input. When the membrane potential reaches a threshold, a spike is emitted and the membrane potential is reset. From a biophysical point of view, the existence of a threshold is not clear. Platkiewitz and Brette currently try to define a threshold in a precise model such as the Hodgkin and Huxley model, and they showed that a certain separatrix curve in the phase plane can be considered as a spike threshold. We will see that we can get rid of this threshold by considering nonlinear models.

The Perfect Integrate-and-Fire model

The perfect integrate-and-fire model is the simplest model of this class. In this model, the membrane potential basically integrates the input current, fires when it reaches a constant threshold value θ and is subsequently reset a fixed value V_{reset}.

$$\begin{cases} C\frac{dV}{dt} & = I(t) \\ V(t_0^-) & = \theta \quad \Rightarrow V(t_0) = V_{reset} \quad \bigoplus \quad \text{spike emitted} \end{cases} \tag{1.16}$$

This model is highly simplistic and unrealistic. Assume that the membrane potential is reset at time t_0. The next spike time for a general input current $I(\cdot)$ is given by

$$t_1 \stackrel{\text{def}}{=} \inf\{t > t_0, V_{reset} + \int_{t_0}^{t} I(s)\,ds \geq \theta)\}.$$

For a constant positive input current I, spikes are emitted at regular intervals of time, at a frequency $I/(C(\theta - V_{reset}))$, and therefore has type I excitability. Nevertheless, the fact that the input–frequency relation is linear is quite unrealistic. Moreover, we observe that second arbitrary small positive input current elicit spikes and spike trains generated by a constant input are perfectly regular.

The Leaky Integrate-and-Fire neuron

Incorporating the leak resistance of the membrane yields to the famous leaky integrate-and-fire model. The standard equation governing the membrane potential of a LIF neuron is given by:

$$C\frac{\mathrm{d}V}{\mathrm{d}t} + \frac{V}{R} = I(t) \tag{1.17}$$

If the membrane potential reaches a threshold value θ at time t_0 (i.e. $V(t_0^-) = \theta$) then a spike is emitted and the membrane potential is instantaneously reset to a constant value ($V(t_0) = V_{reset}$).

In its general version, the leaky integrate-and-fire model may incorporate an absolute refractory period. In this case, if V reaches θ at time t_0, the dynamics of V is frozen during a period of time Δ^{abs}. The classical integration (1.17) starts afresh at time $t_0 + \Delta^{\mathrm{abs}}$ with the new initial condition V_{reset}.

This equation is linear, the related Green's function reads $e^{-t/RC}$, and $V(t)$ is determined in a closed form in function of the input current $I(t)$. For constant inputs one can readily prove that the neuron will spike only for inputs greater than $(\theta - V_{reset})/R$, and in that case, the time of the first spike reads:

$$T_{th} = -\tau_m \log\left(1 - \frac{\theta - V_{reset}}{RI}\right)$$

which gives the input-spike frequency relation. In the case where an absolute refractory is considered, the spike frequency f satisfies for subthreshold inputs:

$$f = \frac{1}{\Delta^{\mathrm{abs}} - \tau_m \log\left(1 - \frac{\theta - V_{reset}}{RI}\right)}$$

In that case again, the neuron has type I excitability. This input–frequency is more realistic than the one of the perfect integrate-and-fire. Indeed, for currents below I_{th} no spike is triggered, at $I = I_{th}$, the slope of the f–I curve is infinite. For large currents, the firing rate saturates to the inverse of the refractory period, which means that the neuron spikes almost immediately after the refractory period. In the case where there is no refractory period, the frequency is unbounded, and has a linear asymptote of slope $\frac{1}{V_{th}C}$ (identical to the slope of the nonleaky unit).

Adaptation

In order to better account for the adaptation, Wehmeier and colleagues [279] introduced a time dependent shunting conductance g_{adapt} with reversal potential equal to the resting potential set at zero. Each spike increases the conductance by a fixed amount G_{spike}, and between the spikes, g_{adapt} decreases exponentially with a time constant τ_{adapt}. Such a variable emulates both the absolute and the relative refractory

periods, and is referred in general as an *adaptation parameter*:

$$\begin{cases} C\frac{\mathrm{d}V}{\mathrm{d}t} = -\frac{V}{R} - g_{adapt}V + I \\ \tau_{adapt}\frac{\mathrm{d}g_{adapt}}{\mathrm{d}t} = -g_{adapt} \end{cases}$$

When V reaches the threshold θ at time t^*, a spike is generated and subsequently: g_{adapt} is increased by a fixed value G_{spike} (i.e. $g_{adapt}(t^*) = g_{adapt}(t^{*-}) + G_{spike}$) and V is reset to a constant value V_{reset}.

Time-dependent threshold

An alternative to these models is to consider a varying voltage threshold (see e.g. [45, 130]). A usual way to take it into account is to consider the threshold function $\theta(1+\alpha e^{-(t-t')/\tau_{adapt}})$.

Resonate-and-fire neuron

The simplest model presenting type II excitability is called the resonate-and-fire (or Young) model (see [92, 287]). It is a two-dimensional extension of the integrate-and-fire model incorporating a second variable often interpreted as accounting for the low threshold persistant potassium current. Let W denote the magnitude of this current. The equation of the linear resonate-and-fire model reads:

$$\begin{cases} C\frac{\mathrm{d}V}{\mathrm{d}t} = I - g_{leak}(V - V_{leak}) - W \\ \dot{W} = (V - V_{1/2}) \end{cases}$$

In this model again, when the potential reaches a threshold, a spike is elicited and both the variables V and W are reset to constant values.

Random variability is often added to the parameters of these models (reset voltage, threshold, ...) in order to reproduce the variability observed in intracellular recordings. Nevertheless, all these models fail in reproducing some behaviors which are fundamentally nonlinear. This is what motivated some authors to introduce and study nonlinear integrate and fire neurons.

1.6.2 The nonlinear integrate-and-fire neuron models

Unidimensional models

These models were developed mainly to take into account the nonlinearities observed in the spike generation mechanisms. The most general *nonlinear* unidimensional integrate-and-fire model is governed by the equation:

$$\tau_m \frac{dV}{dt} = F(V) + G(V)I \tag{1.18}$$

As before, when the solution of this equation reaches the threshold θ, V is reset to a fixed value V_{reset} and a spike is emitted. $G(\cdot)$ can be interpreted as a voltage-dependant input resistance and $-F(V)/(V - V_{\text{rest}})$ correspond to a voltage-dependant decay constant. The simplest of these models features a quadratic nonlinearity [37, 174, 175] given by the equation (1.19):

$$\frac{dV}{dt} = V^2 + I \tag{1.19}$$

This equation can blow up in finite time, i.e. the solution of this equation diverges to infinite for a finite time value. This explosion time is often considered as the spike time. Indeed, the solution of this equation with initial condition $V(t_0) = V_0$ reads:

$$V(t) = -\sqrt{A}\tan\left(-(t-t_0)\sqrt{A} - \arctan\left(\frac{V_0}{\sqrt{A}}\right)\right)$$

and since the tangent function diverges when its argument is $k\frac{\pi}{2}$ for $k \in \mathbb{Z}$.

Notice that $\dot{x} = b + x^2$ is a topological normal form for the saddle-node bifurcation as discussed in appendix A. The properties of the bifurcation will drive the properties of the system when considering constant inputs. The right-hand side of the model is strictly greater than b, and hence if $b > 0$, the neuron will fire a periodic train of action potentials with a period

$$T = \frac{1}{\sqrt{b}}(\mathrm{Arctan}\frac{\theta}{\sqrt{\mathrm{b}}} - \mathrm{Arctan}\frac{\mathrm{V_{reset}}}{\sqrt{\mathrm{b}}})$$

where θ is the spike threshold which can be possibly infinite. Hence the frequency scales as $\sqrt{b}$, as in the typical class 1 excitable systems. When $b < 0$, the system presents two equilibria, one of which being stable and corresponding to the neuron's resting state, and the other unstable and corresponding to the spike threshold. Unlike its linear predecessor, the quadratic integrate-and-fire neuron is a genuine integrator. It exhibits saddle-node bifurcation, it has a soft threshold, and it generates spikes with latencies, like many mammalian cells do. Besides, the model is canonical as proved by Ermentrout and Kopell [82] in the sense that the entire class of neuronal models near saddle-node on invariant circle bifurcation can be transformed into this model by a piecewise continuous change of variables

Nicolas Fourcaud-Trocmé and colleagues [95] proposed a similar model based on a modelization of the dynamic of the sodium activation variable which yields the exponential integrate-and-fire neuron, as an approximation of conductance based models, and show that this model reproduces the dynamics of simple conductance-based models and also intrinsic neuronal properties. The equation of the membrane potential in that case reads:

$$C\frac{du}{dt} = -g_l(u - E_l) + g_l\Delta_t e^{\frac{u-V_t}{\Delta_t}} + I \tag{1.20}$$

Romain Brette studied in [32] the general integrate-and-fire models. In this paper he models the spike map (i.e. the map giving the next interspike interval in function of the current one) and finds that, under conditions satisfied in particular by the periodically and aperiodically driven leaky integrator as well as some of its variants, the spike map is increasing on its range, which leaves no room for chaotic behavior, derives a rigorous expression of the Lyapunov exponent, and analyzes the periodically driven perfect integrator. He shows that the restriction of the phase map to its range is always conjugate to a rotation, and provides an explicit expression of the invariant measure.

Some of these models, complemented with adaptation, are presented in the next sections, together with a precise subthreshold potential and spikes mathematical studies.

Bidimensional Nonlinear IF models

Bidimensional nonlinear neuron models feature both the nonlinearity of the spike generation and a additional recovery variable. This type of phenomenological models

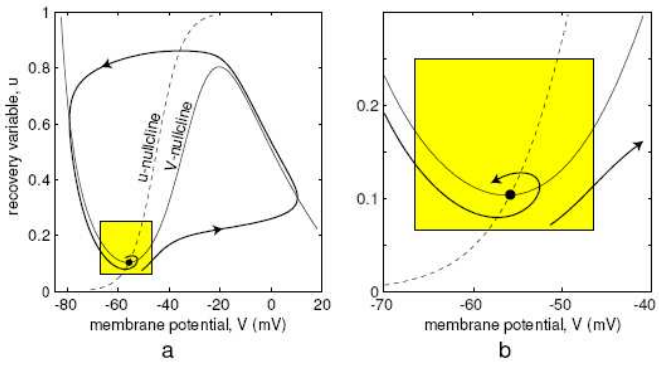

Figure 1.24: Phase portrait for a model having a potential variable V and a recovery variable u. The principle of the approximation is to focus on the dynamics around the fixed point (from [145]).

will be discussed in depth in the following chapter.

One of these models is quite extensively studied by Eugene Izhikevich in his book [146]. This model is called the quadratic integrate-and-fire model (or Izhikevich' model). In this book Izhikevich explains how to derive these equations from more detailed neuron models. The principle of his derivation consist in considering that the decision for spiking or not is made at the resting state, and fully depends on the shape of the nullclines around this point (see figure 1.24). To model the subthreshold behavior of such neurons and the initial segment of the up-stroke of an action potential, the principle is to consider only a small neighborhood of the rest state confined to the shaded square in figure 1.24, since the rest of the phase space is considered to encode only the peak and the down-stroke of the action potential. Since the shape of the action potential is stereotyped, it is less important than the subthreshold dynamics leading to this action potential, then we can retain detailed information about the left knee and its neighborhood and simplify the vector field outside the neighborhood.

Quadratic Adaptive Integrate-and-fire (Izhikevich') model Eugene Izhikevich [141] proposed a model combining both Latham's quadratic nonlinearity and an adaptation variable. Because of the quadratic term, the membrane potential variable can escape to infinity in finite time. This corresponds to the upstroke corresponding to the firing of an action potential. The modeling of the downstroke is quite sharp: it is considered as an instantaneous reset for the membrane potential variable V, while the adaptation variable w is augmented by a fixed amount w_{reset} modeling the spike-triggered adaptation. Appropriate rescalings lead to the more classical minimal quadratic model:

$$\begin{cases} \dot{v} &= v^2 - w + I \\ \dot{w} &= a(bv - w) \end{cases}$$

This model can be also derived via the analysis of I–V relationships. This point of view allows one to derive the parameters of the simple model using instantaneous (peak) and steady-state I-V relations. More precisely, let us write the system in the

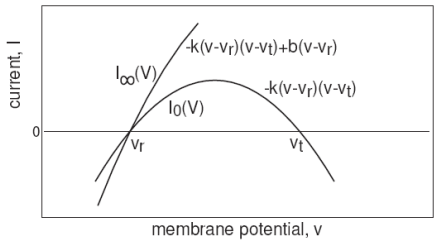

Figure 1.25: The relationship between the parameters of the simple model and instantaneous and steady state *I–V* relations, $I_0(V)$ and $I_\infty(V)$

following equivalent form:

$$\begin{cases} C\dot{v} = k(v-v_r)(v-v_t) - w + I & \text{if } v \geq v_{peak} \text{ then} \\ u = a\{b(v-v+r) - w\} & v \leftarrow c;\ u \leftarrow u+d \end{cases}$$

where v is the membrane potential, w is the recovery current, and C is the membrane capacitance. The quadratic polynomial $k(v-v_r)(v-v_t)$ approximates the subthreshold part of the instantaneous *I–V* relation $I_0(V)$. Here, v_r is the resting membrane potential, and v_t is the instantaneous threshold potential, as in Fig. 1.25. That is, instantaneous depolarizations above v_t result in spike response. The polynomial $k(v-v_r)(v-v_t)+b(v-v_r)$ approximates the subthreshold part of the steady-state *I–V* relation $I_1(V)$. When $b<0$, its maximum approximates the rheobase current of the neuron, i.e., the minimal amplitude of a DC-current needed to fire a cell. Its derivative with respect to v at $v=v_r$, i.e., $b-k(v_r-v_t)$s, corresponds to the resting input conductance, which is the inverse of the input resistance. Knowing both the rheobase and the input resistance of a neuron, one could determine the parameters k and b.

This model nevertheless loses the good property of having a soft threshold, as discussed in chapter 5.

Adaptive exponential integrate-and-fire model Following the ideas of Izhikevich, Romain Brette and Wulfram Gerstner [30] used the exponential nonlinearity proposed by Fourcaud-Trocme and collaborators [95] together with an adaptation variable. This model is interesting because its parameters can be easily related to physiological quantities, and the model has been successfully fit to a biophysical model of a regular spiking pyramidal cell and to real recordings of pyramidal cells [51, 155].

1.7 CONCLUSION

In this chapter we briefly presented the functioning of nerve cells and the overall structure of the brain. Related to these phenomena, we presented some models to emulate the processes in play, from detailed models emulating the behaviors of each component of the nerve cell to the phenomenological models aimed to reproduce globally the behavior of nerve cells. We also discussed the origin of noise and different types of modelizations for noisy synaptic inputs. Phenomenological models such as the adaptive nonlinear models will be studied in depth in part II, the statistics of action potentials in part III and population models in part IV.

Part II

Bidimensional Nonlinear Neuron Models

This part is dedicated to the study of nonlinear bidimensional neuron models, which from a mathematical point of view are hybrid dynamical systems, i.e. whose dynamics is defined by a continuous-time dynamical system modelling the subthreshold behavior of the neuron, coupled with a discrete dynamical system corresponding the spike emission. The subthreshold dynamics is studied in chapter 2, the spike dynamics related with the discrete dynamical system in chapter 3 and all these results are reviewed in chapter 4 in which we provide an electrophysiological-class description of the model, i.e. a partition of the parameter space corresponding to different neurological behaviors.

CHAPTER 2

SUBTHRESHOLD DYNAMICS OF BIDIMENSIONAL NONLINEAR INTEGRATE-AND-FIRE NEURONS

Desperation is a necessary ingredient to learning anything or creating anything.
If you ain't desperate at some point, you ain't interesting.
– Jim Carrey

OVERVIEW

In this chapter we define a new class of bidimensional integrate-and-fire neuron models being computationally efficient and biologically plausible, i.e., able to reproduce a wide range of behaviors observed in in vivo or in vitro recordings of cortical neurons. This class includes, for instance, two models widely used in computational neuroscience, the Izhikevich' quadratic integrate-and-fire model and the Brette–Gerstner's adaptive exponential models we introduced in section 1.6.2. These models are hybrid dynamical systems defined both by a continuous dynamics, the subthreshold behavior, and a discrete dynamics, the spike and reset process. This chapter is devoted to the study of the subthreshold system. We provide the full local subthreshold bifurcation diagram of the members of this class and show that they all present the same bifurcations: an Andronov-Hopf bifurcation manifold, a saddle-node bifurcation manifold, a Bogdanov-Takens bifurcation, and possibly a Bautin bifurcation, i.e., all codimension two local bifurcations in a two-dimensional phase space except the cusp. Among other global bifurcations, this system shows a saddle homoclinic bifurcation curve. We show how this bifurcation diagram generates the most prominent cortical neuron behaviors. This very general study will lead us to introduce a new neuron model, the *quartic model*, able to reproduce all the behaviors of the Izhikevich and Brette-Gerstner models and also self-sustained subthreshold oscillations, which are of great interest in neuroscience and that the two classical models cannot reproduce. This work was published in SIAM Journal on Applied Mathematics [255], and is the first part of the full study of this class of models. The next chapter will be devoted to the study of the spiking mechanism and will provide a better understanding of the spike patterns generated. The full study of these models will eventually lead us to define electrophysiological classes of neurons, i.e. sets of parameters for which the model behaves the same way in response to different kinds of stimulations. We deal with classifying the models with respect to their electrophysiological class in chapter

4.

Contents

INTRODUCTION

During the past few years, in the neurocomputing community, the problem of finding a computationally simple and biologically realistic model of neuron has been widely studied, in order to be able to compare experimental recordings with numerical simulations of large-scale brain models. The key problem is to find a model of neuron realizing a compromise between its simulation efficiency and its ability to reproduce what is observed at the cell level, often considering in-vitro experiments [144, 165, 225].

Among the numerous neuron models, from the detailed Hodgkin–Huxley model [128] still considered as the reference, but unfortunately computationally intractable when considering neuronal networks, down to the simplest integrate-and-fire model [105] very effective computationally, but unrealistically simple and unable to reproduce many behaviors observed, two models seem to stand out [144]: the adaptive quadratic (Izhikevich [141] and related models such as the theta model with adaptation [80, 123]) and exponential (Brette and Gerstner [30]) neuron models. These two models are computationally almost as efficient as the integrate-and-fire model. The Brette–Gerstner model involves an exponential function, which needs to be tabulated if we want the algorithm to be efficient. They are also biologically plausible, and reproduce several important neuronal regimes with a good adequacy with biological data, especially in high-conductance states, typical of cortical in vivo activity. Nevertheless, they fail in reproducing deterministic self-sustained subthreshold oscillations, a behavior of particular interest in cortical neurons for the precision and robustness of spike generation patterns, for instance in the inferior olive nucleus [22, 186, 187], in the stellate cells of the entorhinal cortex [5, 6, 157], and in the dorsal root ganglia (DRG) [10, 183, 184]. Some models have been introduced to study from a theoretical point of view the currents involved in the generation of self-sustained subthreshold oscillations [284], but the model failed in reproducing lots of other neuronal behaviors.

The aim of this chapter is to define and study a general class of neuron models, containing the Izhikevich and Brette–Gerstner models, from a dynamical systems point of view. We characterize the local bifurcations of these models and show how their bifurcations are linked with different biological behaviors observed in the cortex. This formal study will lead us to define a new model of neuron, whose behaviors include those of the Izhikevich–Brette–Gerstner (IBG) models but also self-sustained subthreshold oscillations.

In the first section, we introduce a general class of nonlinear neuron models which contains the IBG models. We study the fixed-point bifurcation diagram of the elements of this class, and show that they present the same local bifurcation diagram, with a saddle-node bifurcation curve, an Andronov–Hopf bifurcation curve, a Bogdanov–Takens bifurcation point, and possibly a Bautin bifurcation, i.e., all codimension two bifurcations in dimension two except the cusp. This analysis is applied in the second section to the Izhikevich and the Brette–Gerstner models. We derive their bifurcation diagrams and prove that none of them shows the Bautin bifurcation. In the third section, we introduce a new simple model—the *quartic model*—presenting, in addition to common properties of the dynamical system of this class, a Bautin bifurcation, which can produce self-sustained oscillations. Last, the fourth section is dedicated to numerical experiments. We show that the quartic model is able to reproduce some of the prominent features of biological spiking neurons. We

give qualitative interpretations of those different neuronal regimes from the dynamical systems point of view, in order to give a grasp of how the bifurcations generate biologically plausible behaviors. We also show that the new quartic model, presenting supercritical Hopf bifurcations, is able to reproduce the oscillatory/spiking behavior presented, for instance, in the DRG. Finally, we show that numerical simulation results of the quartic model show a good agreement with biological intracellular recordings in the DRG.

2.1 Bifurcation analysis of a class of nonlinear neuron models

In this section we introduce a large class of formal neurons which are able to reproduce a wide range of neuronal behaviors observed in cortical neurons. This class of models is inspired by the review made by Izhikevich [144]. He found that the quadratic adaptive integrate-and-fire model was able to simulate efficiently a lot of interesting behaviors. Brette and Gerstner [30] defined a similar model of neuron which presented a good adequacy between simulations and biological recordings.

We generalize these models, and define a new class of neuron models, wide but specific enough to keep the diversity of behaviors of the IBG models.

2.1.1 The general class of nonlinear models

In this chapter, we are interested in neurons defined by a dynamical system of the type

$$\begin{cases} \frac{\mathrm{d}v}{\mathrm{d}t} = F(v) - w + I, \\ \frac{\mathrm{d}w}{\mathrm{d}t} = a(bv - w), \end{cases}$$

where a, b, and I are real parameters and F is a real function.[1]

In this equation, v represents the membrane potential of the neuron, w is the adaptation variable, I represents the input intensity of the neuron, $1/a$ is the characteristic time of the adaptation variable, and b accounts for the interaction between the membrane potential and the adaptation variable.[2]

This equation is a very general model of neuron. For instance when F is a polynomial of degree three, we obtain a FitzHugh–Nagumo model, when F is a polynomial of degree two the Izhikevich neuron model [141], and when F is an exponential function the Brette–Gerstner model [30]. However, in contrast with continuous models like the FitzHugh–Nagumo model [105], the two latter cases diverge when spiking, and an external reset mechanism is used after a spike is emitted.

In this chapter, we want this class of models to have common properties with the IBG neuron models. To this purpose, let us make some assumptions on the function F. The first assumption is a regularity assumption.

Assumption 2.1.1. F is at least three times continuously differentiable.

[1] The same study can be done for a parameter-dependent function. More precisely, let $E \subset \mathbb{R}^n$ be a parameter space (for a given n) and $F : E \times \mathbb{R} \to \mathbb{R}$ a parameter-dependent real function. All the properties shown in this section are valid for any fixed value of the parameter p. Further p-bifurcations studies can be done for specific $F(p,\cdot)$. The first equation can be derived from the general I-V relation in neuronal models: $C\frac{\mathrm{d}V}{\mathrm{d}t} = I - I_0(V) - g(V - E_K)$, where $I_0(V)$ is the instantaneous I-V curve.

[2] See, for instance, section 2.2.2, where the parameters of the initial equation (2.26) are related to biological constants and where we proceed to a dimensionless reduction.

A second assumption is necessary to ensure us that the system would have the same number of fixed points as the IBG models.

Assumption 2.1.2. The function F is strictly convex.

Definition 2.1.1 (convex neuron model)**.** We consider the two-dimensional model defined by the equations

$$\begin{cases} \frac{dv}{dt} = F(v) - w + I, \\ \frac{dw}{dt} = a(bv - w), \end{cases} \tag{2.1}$$

where F satisfies Assumptions 2.1.1 and 2.1.2 and characterizes the passive properties of the membrane potential.

Many neurons of this class blow up in finite time. These neurons are the ones we are interested in.

Remark 1. Note that all the neurons of this class do not blow up in finite time. For instance if $F(v) = v\log(v)$, it will not. For F functions such that $F(v) = (v^{1+\alpha})R(v)$ for some $\alpha > 0$, where $\lim_{v\to\infty} R(v) > 0$ (possibly ∞), the dynamical system will possibly blow up in finite time. We prove this property in chapter 3, and we will further prove that if $F(v) = (v^{2-\alpha})R(v)$ for some $\alpha > 0$ where $R(v)$ tends to a finite limit, the adaptation value at the explosion time of v also blows up whereas if $F(v) = (v^{2+\alpha})R(v)$ for some $\alpha > 0$, where $\lim_{v\to\infty} R(v) > 0$ (possibly ∞), then the adaptation at the explosion times of the spike will have finite limits.

If the solution blows up at time t^* or reaches a finite cutoff value, a spike is emitted, and subsequently we have the following reset process:

$$\begin{cases} v(t^*) = v_r, \\ w(t^*) = w(t^{*-}) + d, \end{cases} \tag{2.2}$$

where v_r is the reset membrane potential and $d > 0$ a real parameter. Equations (2.1) and (2.2), together with initial conditions (v_0, w_0), give us the existence and uniqueness of a solution on $\mathbb{R}^+$.

The two parameters v_r and d are important to understand the repetitive spiking properties of the system, and will be studied in depth in chapter 3. In the present chapter we focus on the bifurcations of the subthreshold dynamical system with respect to (a, b, I), in order to characterize the behavior of the neuron before spiking (and blowing up).

2.1.2 Fixed points of the system

To understand the qualitative behavior of the dynamical system defined by (2.1) before the blow up (i.e., between two spikes), we begin by studying the fixed points and analyze their stability. The linear stability of a fixed point is governed by the Jacobian matrix of the system, which we define in the following proposition.

Proposition 2.1.1. The Jacobian of the dynamical system (2.1) can be written

$$L := v \mapsto \begin{pmatrix} F'(v) & -1 \\ ab & -a \end{pmatrix}. \tag{2.3}$$

The fixed points of the system satisfy the equations

$$\begin{cases} F(v) - bv + I = 0, \\ bv = w. \end{cases} \tag{2.4}$$

Let $G_b(v) := F(v) - bv$. From 2.1.1 and 2.1.2, we know that the function G_b is strictly convex and has the same regularity as F. To have the same behavior as the IBG models, we want the system to have the same number of fixed points. To this purpose, it is necessary that G_b has a minimum for all $b > 0$. Otherwise, the *convex* function G_b would have no more than one fixed point, since a fixed point of the system is the intersection of an horizontal curve and G_b.

This means for the function F that $\inf_{x\in\mathbb{R}} F'(x) \leq 0$ and $\sup_{x\in\mathbb{R}} F'(x) = +\infty$. Using the monotony property of F', we write Assumption 2.1.3.

Assumption 2.1.3.

$$\begin{cases} \lim\limits_{x\to-\infty} F'(x) \leq 0, \\ \lim\limits_{x\to+\infty} F'(x) = +\infty. \end{cases}$$

Assumptions 2.1.1, 2.1.2, and 2.1.3 ensure us that for all $b \in \mathbb{R}_+^*$, G_b has a unique minimum, denoted $m(b)$, which is reached. Let $v^*(b)$ be the point where this minimum is reached.

This point is the solution of the equation

$$F'(v^*(b)) = b. \tag{2.5}$$

Proposition 2.1.2. The point $v^*(b)$ and the value $m(b)$ are continuously differentiable with respect to b.

Proof. We know that F' is a bijection. The point $v^*(b)$ is defined implicitly by the equation $H(b,v) = 0$, where $H(b,v) = F'(v) - b$. H is a C^1-diffeomorphism with respect to b, and the differential with respect to b never vanishes. The implicit function theorem (see, for instance, [84, Annex C.6]) ensures us that $v^*(b)$ solution of $H(b,v^*(b)) = 0$ is continuously differentiable with respect to b, and so does $m(b) = F(v^*(b)) - bv^*(b)$. □

Theorem 2.1.3. *The parameter curve defined by* $\{(I,b);\ I = -m(b)\}$ *separates three behaviors of the system (see Figure* 2.1*):*

(i) *If* $I > -m(b)$*, then the system has no fixed point.*

(ii) *If* $I = -m(b)$*, then the system has a unique fixed point,* $(v^*(b), w^*(b))$*, which is nonhyperbolic. It is unstable if* $b > a$*.*

(iii) *If* $I < -m(b)$*, then the dynamical system has two fixed points* $(v_-(I,b), v_+(I,b))$ *such that*

$$v_-(I,b) < v^*(b) < v_+(I,b).$$

The fixed point $v_+(I,b)$ *is a saddle fixed point, and the stability of the fixed point* $v_-(I,b)$ *depends on* I *and on the sign of* $(b-a)$*:*

(a) *If* $b < a$*, the fixed point* $v_-(I,b)$ *is attractive.*

(b) *If* $b > a$*, there is a unique smooth curve* $I^*(a,b)$ *defined by the implicit equation* $F'(v_-(I^*(a,b),b)) = a$*. This curve reads* $I^*(a,b) = bv^*(a) - F(v^*(a))$*, where* $v^*(a)$ *is the unique solution of* $F'(v^*(a)) = a$*.*

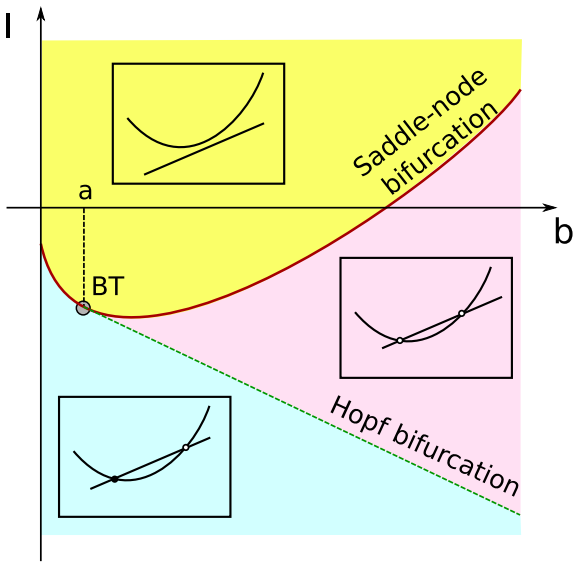

Figure 2.1: Number of fixed points and their stability in the plane (I,b) for the exponential adaptive model.

(b.1) *If $I < I^*(a,b)$, the fixed point is attractive.*
(b.2) *If $I > I^*(a,b)$, the fixed point is repulsive.*

Proof.

(i) We have $F(v) - bv \geq m(b)$ by definition of $m(b)$. If $I > -m(b)$, then for all $v \in \mathbb{R}$ we have $F(v) - bv + I > 0$ and the system has no fixed point.

(ii) Let $I = -m(b)$. We have already seen that G_b is strictly convex and continuously differentiable and for $b > 0$ reaches its unique minimum at the point $v^*(b)$. This point is such that $G_b(v^*(b)) = m(b)$, and so it is the only point satisfying $F(v^*(b)) - bv^*(b) - m(b) = 0$.

Furthermore, this point satisfies $F'(v^*(b)) = b$. The Jacobian of the system at this point reads

$$L(v^*(b)) = \begin{pmatrix} b & -1 \\ ab & -a \end{pmatrix}.$$

Its determinant is 0, and so the fixed point is nonhyperbolic (0 is eigenvalue of the Jacobian matrix). The trace of this matrix is $b - a$. So the fixed point $v^*(b)$ is attractive when $b > a$ and repulsive when $b > a$. The case $a = b$, $I = -m(b)$ is a degenerate case which we will study more precisely in section 2.1.3.

(iii) Let $I < -m(b)$. By the strict convexity assumption, Assumption 2.1.2, of the function G together with Assumption 2.1.3, we know that there are only two intersections of the curve G to a level $-I$ higher than its minimum. These two intersections define our two fixed points. At the point v^* the function is strictly lower than $-I$, and so the two solutions satisfy $v_-(I,b) < v^*(b) < v_+(I,b)$.

Let us now study the stability of these two fixed points. To this end, we have to characterize the eigenvalues of the Jacobian matrix of the system at these points.

We can see from formula (2.3) and the convexity assumption, Assumption 2.1.2, that the Jacobian determinant, equal to $-aF'(v)+ab$, is a decreasing function of v and vanishes at $v^*(b)$, and so $\det(L(v_+(I,b)))<0$ and the fixed point is a saddle point (the Jacobian matrix has a positive and a negative eigenvalue).

For the other fixed point $v_-(I,b)$, the determinant of the Jacobian matrix is strictly positive. So the stability of the fixed point depends on the trace of the Jacobian. This trace reads $F'\big(v_-(I,b)\big)-a$.

(a) When $b<a$, we have a stable fixed point. Indeed, the function F' is an increasing function equal to b at $v^*(b)$, and so $\mathrm{Trace}\big(L(v_-(I,b))\big)\leq F'(v^*(b))-a=b-a<0$ and the fixed point is attractive.

(b) If $b>a$, then the type of dynamics around the fixed point v_- depends on the input current (parameter I). Indeed, the trace reads

$$T(I,b,a):=F'\big(v_-(I,b)\big)-a,$$

which is continuous and continuously differentiable with respect to I and b, and which is defined for $I<-m(b)$. We have

$$\begin{cases}\lim\limits_{I\to -m(b)} T(I,b,a)=b-a>0,\\ \lim\limits_{I\to-\infty} T(I,b,a)=\lim\limits_{x\to-\infty}F'(x)-a<0.\end{cases}$$

So there exists a curve $I^*(a,b)$ defined by $T(I,b,a)=0$ and such that

- for $I^*(b)<I<-m(b)$, the fixed point $v_-(I,b)$ is repulsive;
- for $I<I^*(b)$, the fixed point v_- is attractive.

To compute the equation of this curve, we use the fact that point $v_-(I^*(b),b)$ is such that $F'(v_-(I^*(b),b))=a$. We know from the properties of F that there is a unique point $v^*(a)$ satisfying this equation. Since $F'(v^*(b))=b$, $a<b$, and F' is increasing, the condition $a<b$ implies that $v^*(a)<v^*(b)$.

The associated input current satisfies fixed points equation $F(v^*(a))-bv^*(a)+I^*(a,b)=0$, or equivalently

$$I^*(a,b)=bv^*(a)-F(v^*(a)).$$

The point $I=I^*(a,b)$ will be studied in detail in the next section, since it is a bifurcation point of the system.

□

Figure 2.1 represents the different zones enumerated in Theorem 2.1.3 and their stability in the parameter plane (I,b).

Remark 2. In this proof, we used the fact that F' is invertible on $[0,\infty)$. Assumption 2.1.3 is the weakest possible to ensure that this will be the case and that F has a unique minimum.

2.1.3 Bifurcations of the system

In the study of the fixed points and their stability, we identified two bifurcation curves where the stability of the fixed points changes. The first curve $I = -m(b)$ corresponds to a saddle-node bifurcation and the curve $I = I^*(a,b)$ to an Andronov–Hopf bifurcation. These two curves meet in a specific point, $b = a$ and $I = -m(a)$. This point has a double 0 eigenvalue (a nilpotent Jacobian matrix), and we show that it is a Bogdanov–Takens bifurcation point.

Let us show that the system undergoes these bifurcations with no other assumption than 2.1.1, 2.1.2, and 2.1.3 on F. We also prove that the system can undergo only one other codimension two bifurcation, a Bautin bifurcation, and that there is no other bifurcation of codimension two or three.

Saddle-node bifurcation curve

In this section we characterize the behavior of the dynamical system along the curve of equation $I = -m(b)$, and we prove the following theorem.

Theorem 2.1.4. *The dynamical system* (2.1) *undergoes a saddle-node bifurcation along the parameter curve:*

$$(SN) : \{(b,I)\ ;\ I = -m(b)\}, \tag{2.6}$$

when $F''(v^*(b)) \neq 0$.

Proof. We derive the normal form of the system at this bifurcation point. Following the works of Guckenheimer and Holmes [118] and Kuznetsov [167], we check the genericity conditions to ensure that the normal form at the bifurcation point will have the expected form (see appendix A).

Let $b \in \mathbb{R}^+$ and $I = -m(b)$. Let $v^*(b)$ be the unique fixed point of the system for these parameters. The point $v^*(b)$ is the unique solution of $F'(v^*(b)) = b$. At this point, the Jacobian matrix (2.3) reads

$$L(v^*(b)) = \begin{pmatrix} b & -1 \\ ab & -a \end{pmatrix}.$$

This matrix has two eigenvalues 0 and $b-a$. The pairs of right eigenvalues and right eigenvectors are

$$0, U := \begin{pmatrix} 1/b \\ 1 \end{pmatrix} \quad \text{and} \quad b-a, \begin{pmatrix} 1/a \\ 1 \end{pmatrix}.$$

Its pairs of left eigenvalues and left eigenvectors are

$$0, V := (-a, 1) \quad \text{and} \quad b-a, (-b, 1).$$

Let $f_{b,I}$ be the vector field

$$f_{b,I}(v,w) = \begin{pmatrix} F(v) - w + I \\ a(bv - w) \end{pmatrix}.$$

The vector field satisfies

$$\begin{aligned} V\left(\frac{\partial}{\partial I} f_{b,I}(v^*(b), w^*(b))\right) &= (-a,1) \cdot \begin{pmatrix} 1 \\ 0 \end{pmatrix} \\ &= -a < 0. \end{aligned}$$

So the coefficient of the normal form corresponding to the Taylor expansion along the parameter I does not vanish.

Finally, let us show that the quadratic terms of the Taylor expansion in the normal form does not vanish. With our notations, this condition reads

$$V\left(D_x^2 f_{b,-m(b)}(v^*(b),w^*(b))(U,U)\right) \neq 0.$$

This property is satisfied in our framework. Indeed,

$$\begin{aligned} V\left(D_x^2 f_{b,-m(b)}(v^*(b),w^*(b))(U,U)\right) &= V\left(\begin{pmatrix} U_1^2\frac{\partial^2 f_1}{\partial v^2}+2U_1U_2\frac{\partial^2 f_1}{\partial v\partial w}+U_2^2\frac{\partial^2 f_1}{\partial w^2} \\ U_1^2\frac{\partial^2 f_2}{\partial v^2}+2U_1U_2\frac{\partial^2 f_2}{\partial v\partial w}+U_2^2\frac{\partial^2 f_2}{\partial w^2}\end{pmatrix}\right) \\ &= V\left(\begin{pmatrix}\frac{1}{b^2}F''(v^*)\\ 0\end{pmatrix}\right) \\ &= (-a,1)\cdot\begin{pmatrix}\frac{1}{b^2}F''(v^*)\\ 0\end{pmatrix} \\ &= -\frac{a}{b^2}F''(v^*) < 0. \end{aligned}$$

So the system undergoes a saddle-node bifurcation along the manifold $I = -m(b)$. □

Remark 3. Note that $F''(v^*(b))$ can vanish only countably many times since F is strictly convex.

Andronov–Hopf bifurcation curve

In this section we consider the behavior of the dynamical system along the parameter curve $I = I^*(b)$, and we consider the fixed point v_-.

Theorem 2.1.5. *Let $b > a$, $v^*(a)$ be the unique point such that $F'(v^*(a)) = a$ and $A(a,b)$ be defined by the formula*

$$A(a,b) := F'''(v^*(a)) + \frac{1}{b-a}\left(F''(v^*(a))\right)^2. \tag{2.7}$$

If $F''(v^*(a)) \neq 0$ and $A(a,b) \neq 0$, then the system undergoes an Andronov–Hopf bifurcation at the point $v^*(a)$, along the parameter line

$$(AH) := \left\{(b,I)\ ;\ b > a \text{ and } I = bv^*(a) - F(v^*(a))\right\}. \tag{2.8}$$

This bifurcation is subcritical if $A(a,b) > 0$ and supercritical if $A(a,b) < 0$.

Proof. The Jacobian matrix at the point $v^*(a)$ reads

$$L(v^*(a)) = \begin{pmatrix} a & -1 \\ ab & -a \end{pmatrix}.$$

Its trace is 0 and its determinant is $a(b-a) > 0$, and so the matrix at this point has a pair of pure imaginary eigenvalues $(i\omega, -i\omega)$, where $\omega = \sqrt{a(b-a)}$. Along the curve of equilibria when I varies, the eigenvalues are complex conjugates with real part $\mu(I) = \frac{1}{2}\mathrm{Tr}\big(L(v_-(I,b))\big)$ which vanishes at $I = I^*(a,b)$.

We recall that from Proposition 2.1.2, this trace varies smoothly with I. Indeed, $v_-(b,I)$ satisfies $F(v_-(I,b))-bv_-(I,b)+I=0$ and is differentiable with respect to I. We have

$$\frac{\partial v_-(I,b)}{\partial I}(F'(v_-(I,b))-b)=-1.$$

At the point $v_-(I^*(b),b)=v^*(a)$, we have $F'(v^*(a))=a<b$, and so for I close to this equilibrium point, we have

$$\frac{\partial v_-(I,b)}{\partial I}>0.$$

Now let us check that the transversality condition of an Andronov–Hopf bifurcation is satisfied (see [118, Theorem 3.4.2]). There are two conditions to be satisfied: the transversality condition $\frac{\mathrm{d}\mu(I)}{\mathrm{d}I}\neq 0$ and the nondegeneracy condition $l_1\neq 0$, where l_1 is the first Lyapunov coefficient at the bifurcation point.

First of all, we prove that the transversality condition is satisfied:

$$\begin{aligned}\mu(I)&=\frac{1}{2}\mathrm{Tr}(L(v_-(I,b)))\\&=\frac{1}{2}(F'(v_-(I,b))-a),\\\frac{\mathrm{d}\mu(I)}{\mathrm{d}I}&=\frac{1}{2}F''(v_-(I,b))\frac{\mathrm{d}v_-(I,b)}{\mathrm{d}I}\\&>0.\end{aligned}$$

Let us now write the normal form at this point. To this purpose, we change variables:

$$\begin{cases}v-v^*(a)=x,\\w-w_a=ax+\omega y.\end{cases}$$

The (x,y) equation reads

$$\begin{cases}\dot{x}=-\omega y+(F(x+v^*(a))-ax-w_a)=:-\omega y+f(x),\\\dot{y}=\omega x+\frac{a}{\omega}(ax-F(x+v^*(a))+w_a-I)=:\omega x+g(x).\end{cases}\tag{2.9}$$

According to Guckenheimer in [118], we state that the Lyapunov coefficient of the system at this point has the same sign as B, where B is defined by

$$B:=\frac{1}{16}[f_{xxx}+f_{xyy}+g_{xxy}+g_{yyy}]+\frac{1}{16\omega}[f_{xy}(f_{xx}+f_{yy})-g_{xy}(g_{xx}+g_{yy})-f_{xx}g_{xx}+f_{yy}g_{yy}].$$

Replacing f and g by the expressions found in (2.9), we obtain the expression of A:

$$\begin{aligned}B&=\frac{1}{16}F'''(v^*(a))+\frac{a}{16\omega^2}(F''(v^*(a)))^2\\&=\frac{1}{16}F'''(v^*(a))+\frac{1}{16(b-a)}(F''(v^*(a)))^2\\&=\frac{1}{16}A(a,b).\end{aligned}$$

Hence when $A(a,b)\neq 0$, the system undergoes an Andronov–Hopf bifurcation. When $A(a,b)>0$, the bifurcation is subcritical and the periodic orbits generated by the Hopf bifurcation are repelling, and when $A(a,b)<0$, the bifurcation is supercritical and the periodic orbits are attractive (the formula of A has also been introduced by Izhikevich in [146, eq. (15), p. 213]). □

Remark 4. The case $A(a,b)=0$ is not treated in the theorem and is a little bit more intricate. We fully treat it in section 2.1.3 and show that a Bautin (generalized Hopf) bifurcation can occur if the A-coefficient vanishes. Since the third derivative is a priori unconstrained, this case can occur, and we prove in section 2.3 that this is the case for a simple (quartic) model.

Bogdanov–Takens bifurcation

We have seen in the study that this formal model presents an interesting point in the parameter space, corresponding to the intersection of the saddle-node bifurcation curve and the Andronov–Hopf bifurcation curve. At this point, we show that the system undergoes a Bogdanov–Takens bifurcation.

Theorem 2.1.6. *Let F be a real function satisfying Assumptions* 2.1.1*,* 2.1.2*, and* 2.1.3*. Let $a\in\mathbb{R}_+^*$ and $b=a$, and let $v^*(a)$ be the only point such that $F'(v^*(a))=a$. Assume again that $F''(v^*(a))\neq 0$.*

Then at this point and with these parameters, the dynamical system (2.1) *undergoes a subcritical Bogdanov–Takens bifurcation of normal form:*

$$\begin{cases}\dot\eta_1=\eta_2,\\ \dot\eta_2=\left(\frac{8F''(v^*(a))\,aI_1}{(a+b_1)^3}\right)-\left(\frac{2(2b_1\,a+I_1F''(v^*(a)))}{(a+b_1)^2}\right)\eta_1+\eta_1^2+\eta_1\eta_2+\mathcal{O}(\|\eta\|^3),\end{cases}\tag{2.10}$$

where $b_1:=b-a$ and $I_1=I+m(a)$.

Proof. The Jacobian matrix (2.3) at this point reads

$$L(v^*(a))=\begin{pmatrix}a & -1\\ a^2 & -a\end{pmatrix}.$$

This matrix is nonzero and has two 0 eigenvalues (its determinant and trace are 0). The matrix $Q:=\left(\begin{smallmatrix}a & 1\\ a^2 & -a\end{smallmatrix}\right)$ is the passage matrix to the Jordan form of the Jacobian matrix:

$$Q^{-1}\cdot L(v^*(a))\cdot Q=\begin{pmatrix}0 & 1\\ 0 & 0\end{pmatrix}.$$

To prove that the system undergoes a Bogdanov–Takens bifurcation, we show that the normal form reads

$$\begin{cases}\dot\eta_1=\eta_2,\\ \dot\eta_2=\beta_1+\beta_2\eta_1+\eta_1^2+\sigma\eta_1\eta_2+\mathcal{O}(\|\eta\|^3)\end{cases}\tag{2.11}$$

with $\sigma=\pm1$. The proof of this theorem consists of (i) proving that the system undergoes a Bogdanov–Takens bifurcation, (ii) finding a closed-form expression for the variables β_1 and β_2, and (iii) proving that $\sigma=1$.

First of all, let us prove that the normal form can be written in the form of (2.11). This is equivalent to showing some transversality conditions on the system (see, for instance, [167, Theorem 8.4]).

To this end, we center the equation at this point and write the system in the coordinates given by the Jordan form of the matrix. Let $\left(\begin{smallmatrix}y_1\\ y_2\end{smallmatrix}\right)=Q^{-1}\left(\begin{smallmatrix}v-v^*(a)\\ w-w_a\end{smallmatrix}\right)$ at the point $b=a+b_1$, $I=-m(a)+I_1$. We get

$$\begin{cases}\dot y_1=y_2+\frac{b_1}{a}(ay_1+y_2),\\ \dot y_2=F(ay_1+y_2+v^*(a))-w_a-m(a)+I_1-a^2y_1-ay_2-b_1(ay_1+y_2).\end{cases}\tag{2.12}$$

Let us denote $v_1 = ay_1 + y_2$. The Taylor expansion on the second equation gives us

$$\begin{aligned}
\dot{y}_2 &= F(v_1 + v^*(a)) - w_a - m(a) + I_1 - a^2 y_1 - a y_2 - b_1(a y_1 + y_2) \\
&= F(v^*(a)) + F'(v^*(a))v_1 + \frac{1}{2}F''(v^*(a))v_1^2 - w_a - m(a) \\
&+ I_1 - a^2 y_1 - a y_2 - b_1(a y_1 + y_2) + \mathscr{O}(\|v_1\|^3) \\
&= (F(v^*(a)) - w_a - m(a)) + I_1 + (F'(v^*(a)) - a)v_1 - b_1 v_1 + \frac{1}{2}F''(v^*(a))v_1^2 \\
&+ \mathscr{O}(\|v_1\|^3) \\
&= I_1 - b_1(a y_1 + y_2) + \frac{1}{2}F''(v^*(a))(a y_1 + y_2)^2 + \mathscr{O}(\|y\|^3). \qquad (2.13)
\end{aligned}$$

Let us denote for the sake of clarity $\alpha = (b_1, I_1)$ and write (2.12) as

$$\begin{cases} \dot{y}_1 = y_2 + a_{00}(\alpha) + a_{10}(\alpha) y_1 + a_{01}(\alpha) y_2, \\ \dot{y}_2 = b_{00}(\alpha) + b_{10}(\alpha) y_1 + b_{01}(\alpha) y_2 + \frac{1}{2} b_{20}(\alpha) y_1^2 + b_{11}(\alpha) y_1 y_2 + \frac{1}{2} b_{02}(\alpha) y_2^2 + \mathscr{O}(\|y\|^3). \end{cases} \qquad (2.14)$$

From (2.12) and (2.13), it is straightforward to identify the expressions for the coefficients $a_{ij}(\alpha)$ and $b_{ij}(\alpha)$.

Let us now use the change of variables:

$$\begin{cases} u_1 = y_1, \\ u_2 = y_2 + \frac{b_1}{a}(a y_1 + y_2). \end{cases}$$

The dynamical system governing (u_1, u_2) reads

$$\begin{cases} \dot{u}_1 = u_2, \\ \dot{u}_2 = (1 + \frac{b_1}{a}) - b_1 a u_1 + \frac{1}{2}\frac{a^3 F''(v^*(a))}{a + b_1} u_1^2 + \frac{a^2 F''(v^*(a))}{a + b_1} u_1 u_2 + \frac{1}{2}\frac{a F''(v^*(a))}{a + b_1} u_2^2. \end{cases}$$

The transversality conditions of a Bogdanov–Takens bifurcation [118, 167] can easily be verified from this expression:

(BT.1) The Jacobian matrix is not 0.

(BT.2) With the notations of (2.14), we have $a_{20} = 0$ and $b_{11}(0) = aF''(v^*(a)) > 0$, and so $a_{20}(0) + b_{11}(0) = aF''(v^*(a)) > 0$.

(BT.3) $b_{20} = a^2 F''(v^*(a)) > 0$.

(BT.4) We show that the map

$$\left(x := \begin{pmatrix} y_1 \\ y_2 \end{pmatrix}, \alpha := \begin{pmatrix} I_1 \\ b_1 \end{pmatrix}\right) \mapsto \Big[f(x,\alpha), \mathrm{Tr}\big(D_x f(x,\alpha)\big), \mathrm{Det}\big(Dx f(x,\alpha)\big) \Big]$$

is regular at the point of interest.

From the two first assumptions, we know that the system can be put in the form of (2.11). Guckenheimer in [118] proves that this condition can be reduced to the nondegeneracy of the differential with respect to (I_1, b_1) of the vector $\binom{\beta_1}{\beta_2}$ of (2.11).

In our case, we can compute these variables β_1 and β_2 following the calculation steps of [167], and we get

$$\begin{cases} \beta_1 = \frac{8F''(v^*(a))\,a I_1}{(a+b_1)^3}, \\ \beta_2 = -\frac{2(2b_1 a + I_1 F''(v^*(a)))}{(a+b_1)^2}. \end{cases} \tag{2.15}$$

Hence the differential of the vector $\binom{\beta_1}{\beta_2}$ with respect to the parameters (I_1, b_1) at the point $(0,0)$ reads

$$D_\alpha \beta|_{(0,0)} = \begin{pmatrix} \frac{8F''(v^*(a))}{a^2} & 0 \\ -2\frac{F''(v^*(a))}{a^2} & -4/a \end{pmatrix}.$$

This matrix has a nonzero determinant if and only if $F''(v^*(a)) \neq 0$.

Therefore we have proved the existence of a Bogdanov–Takens bifurcation under the condition $F''(v^*(a)) \neq 0$.

Let us now show that $\sigma = 1$. Indeed, this coefficient is given by the sign of $b_{20}(0)\big(a_{20}(0) + b_{11}(0)\big)$ which in our case is equal to $a^3 F''(v^*(a))^2 > 0$, and so the bifurcation is always of the type (2.10) (generation of an unstable limit cycle) for all the members of our class of models. □

The existence of a Bogdanov–Takens bifurcation point implies the existence of a smooth curve corresponding to a saddle homoclinic bifurcation in the system (see [167, Lemma 8.7]).

Corollary 2.1.7. There is a unique smooth curve (P) corresponding to a saddle homoclinic bifurcation in the system (2.1) originating at the parameter point $b = a$ and $I = -m(a)$ defined by the implicit equation:

$$(P) := \left\{ I = -m(a) - \frac{12}{25F''(v^*(a))}(b-a)^2;\ b > a \right\}. \tag{2.16}$$

Moreover, for (b, I) in a neighborhood of $(a, -m(a))$, the system has a unique and hyperbolic unstable cycle for parameter values inside the region bounded by the Hopf bifurcation curve and the homoclinic bifurcation curve (P), and it has no cycle outside this region.

Proof. As noticed, from the Bogdanov–Takens bifurcation point, we have the existence of this saddle homoclinic bifurcation curve. Let us now compute the equation of this curve in the neighborhood of the Bogdanov–Takens point. To this purpose we use the normal form we derived in Theorem 2.1.6 and use the local characterization given, for instance, in [167, Lemma 8.7] for the saddle homoclinic curve:

$$(P) := \left\{ (\beta_1, \beta_2)\ ;\ \beta_1 = -\frac{6}{25}\beta_2^2 + o(\beta_2^2),\ \beta_2 < 0 \right\}.$$

Using the expressions (2.15) yields

$$(P) := \left\{ \begin{array}{l} (I = -m(a) + I_1,\, b = a + b_1)\,; \\ \dfrac{8F''(v^*(a))aI_1}{(a+b_1)^3} = \dfrac{24}{25}\dfrac{(2b_1 a + I_1 F''(v^*(a)))^2}{(a+b_1)^4} + o(|b_1| + |I_1|) \\ \text{and } b_1 > -\dfrac{I_1 F''(v^*(a))}{2a} \end{array} \right\}.$$

We can solve this equation. There are two solutions but only one satisfying $I_1 = 0$ when $b_1 = 0$. This solution is the curve of saddle homoclinic bifurcations, and reads:

$$(P) := \left\{ \begin{array}{l} I = -m(a) + I_1,\, b = a + b_1)\,; \\ I_1 = \dfrac{\left(-\frac{25}{6}a - \frac{37}{6}b_1 + \frac{5}{6}\sqrt{25a^2 + 74b_1 a + 49{b_1}^2}\right)a}{F''(v^*(a))} + o(|b_1| + |I_1|) \\ \text{and } b_1 > -\dfrac{I_1 F''(v^*(a))}{2a} \end{array} \right\}.$$

which is equivalent to formula (2.16) □

Bautin bifurcation

In the study of the Andronov–Hopf bifurcation, we showed that the sub- or supercritical type of bifurcation depended on the variable $A(a,b)$ defined by (2.7). If this variable changes sign when b varies, then the stability of the limit cycle along Hopf bifurcation changes stability. This can occur if the point $v^*(a)$ satisfies the following condition.

Assumption 2.1.4. For $v^*(a)$ such that $F'(v^*(a)) = a$, we have

$$F'''(v^*(a)) < 0.$$

Indeed, if this happens, the type of Andronov–Hopf bifurcation changes, since we have

$$\begin{cases} \lim\limits_{b \to a^-} A(a,b) = +\infty, \\ \lim\limits_{b \to +\infty} A(a,b) = F'''(v^*(a)) < 0. \end{cases}$$

In this case the first Lyapunov exponent vanishes for

$$b = a - \frac{(F''(v^*(a)))^2}{F'''(v^*(a))}.$$

At this point, the system has the characteristics of a Bautin (generalized Hopf) bifurcation. Nevertheless, we still have to check two nondegeneracy conditions to ensure that the system actually undergoes a Bautin bifurcation:

(BGH.1) The second Lyapunov coefficient of the dynamical system l_2 does not vanish at this equilibrium point.

(BGH.2) Let $l_1(I,b)$ be the first Lyapunov exponent of this system and $\mu(I,b)$ the real part of the eigenvalues of the Jacobian matrix. The map

$$(I,b) \mapsto (\mu(I,b), l_1(I,b))$$

is regular at this point.

In this case the system would be locally topologically equivalent to the normal form:

$$\begin{cases} \dot{y}_1 = \beta_1 y_1 - y_2 + \beta_2 y_1 (y_1^2 + y_2^2) + \sigma y_1 (y_1^2 + y_2^2)^2, \\ \dot{y}_2 = \beta_1 y_2 - y_1 + \beta_2 y_2 (y_1^2 + y_2^2) + \sigma y_2 (y_1^2 + y_2^2)^2. \end{cases}$$

We reduce the problem to the point that checking the two conditions of a BGH bifurcation becomes straightforward.

Let $(v^*(a), w_a)$ be the point where the system undergoes the Bautin bifurcation (when it exists). Since we already computed the eigenvalues and eigenvectors of the Jacobian matrix along the Andronov–Hopf bifurcation curve, we can use it to reduce the problem. The basis where we express the system is given by

$$\begin{cases} Q := \begin{pmatrix} \frac{1}{b} & \frac{\omega}{ab} \\ 1 & 0 \end{pmatrix}, \\ \binom{x}{y} := Q^{-1} \binom{v - v^*(a)}{w - w_a}. \end{cases}$$

Let us write the dynamical equations satisfied by (x,y):

$$\begin{cases} \dot{x} = \omega y, \\ \dot{y} = \frac{ab}{\omega} \left(F\left(v^*(a) + \frac{1}{b}x + \frac{\omega}{ab}y\right) - w_a - x + I_a - ay \right). \end{cases}$$

To ensure that we have a Bautin bifurcation at this point we will need to perform a Taylor expansion up to the fifth order, and so we need to make the following assumption.

Assumption 2.1.5. The function F is six times continuously differentiable at $(v^*(a), w_a)$.

First, let us denote $v_1(x,y) = \frac{1}{b}x + \frac{\omega}{ab}y$; the Taylor expansion reads

$$\begin{aligned} \dot{y} = {} & \frac{ab}{\omega}\left(F(v^*(a)) - w_a + I\right) + \frac{ab}{\omega}\left[F'(v^*(a))v_1(x,y) - ay\right] + \frac{1}{2}\frac{ab}{\omega}\left[F''(v^*(a))v_1(x,y)^2\right] \\ & + \frac{1}{6}\frac{ab}{\omega}F'''(v^*(a))v_1(x,y)^3 + \frac{1}{4!}\frac{ab}{\omega}F^{(4)}(v^*(a))v_1(x,y)^4 \\ & + \frac{1}{5!}\frac{ab}{\omega}F^{(5)}(v^*(a))v_1(x,y)^5 + \mathscr{O}\left(\left\|\binom{x}{y}\right\|^6\right). \end{aligned}$$

This expression, together with the complex left and right eigenvectors of the Jacobian matrix, allows us to compute the first and second Lyapunov coefficients and to check the existence of a Bautin bifurcation.

Nevertheless, we cannot push the computation any further at this level of generality, but, for a given function F presenting a change in the sign of $A(a,b)$, this can easily be done through the use of a symbolic computation package. In the following proof we show that the quartic model undergoes a Bautin bifurcation.

Proof. To prove that the quartic model undergoes a Bautin bifurcation at the point

$$\begin{cases} b = \frac{5}{2}a, \\ I = -3\left(\frac{a}{4}\right)^{4/3}(2a-1), \\ v^*(a) = -\left(\frac{a}{4}\right)^{1/3}. \end{cases} \tag{2.17}$$

we compute the first and second lyapunov exponents and prove that the conditions given to characterize Bautin bifurcations are satisfied.

The first Lyapunov exponent: Using a suitable affine change of coordinates having for origin the point (2.17), we can readily write the dynamical system in the form:

$$\begin{cases} \dot{x} = \omega y, \\ \dot{y} = \frac{ab}{\omega}\left(6v^*(a)^2 v_1(x,y)^2 + 4v^*(a)v_1(x,y)^3 + v_1(x,y)^4\right) \\ \quad = \frac{1}{2}F_2\left(\binom{x}{y},\binom{x}{y}\right) + \frac{1}{6}F_3\left(\binom{x}{y},\binom{x}{y},\binom{x}{y}\right) + \frac{1}{24}F_3\left(\binom{x}{y},\binom{x}{y},\binom{x}{y},\binom{x}{y}\right), \end{cases} \tag{2.18}$$

where $v_1(x,y) = \frac{1}{b}x + \frac{\omega}{ab}y$. Let us denote $F_2(X,Y)$, $F_3(X,Y,Z)$, and $F_4(X,Y,Z,T)$ the multilinear symmetric vector functions of (2.18) ($X,Y,Z,T \in \mathbb{R}^2$):

$$\begin{cases} F_2\left(\binom{x}{y},\binom{z}{t}\right) = \binom{0}{12\frac{ab}{\omega}v^*(a)^2 v_1(x,y)v_1(z,t)}, \\ \dots \end{cases}$$

To compute the two first Lyapunov exponents of the system, we follow Kuznetsov's method [167]. In this method we need to compute some specific right and left complex eigenvectors, which can be chosen in our case to be

$$\begin{cases} p = \begin{pmatrix} \frac{1}{-i\sqrt{ab-a^2}+a} \\ 1 \end{pmatrix}, \\ q = \begin{pmatrix} \frac{1}{2}\frac{(i\sqrt{a(b-a)}+a)b}{b-a-i\sqrt{a(b-a)}} \\ 1/2\,\frac{(i\sqrt{a(b-a)}+a)^2}{a(b-a-i\sqrt{a(b-a)})} \end{pmatrix}. \end{cases} \tag{2.19}$$

We now put the system in a complex form letting $z = x + iy$.

We can now compute the complex Taylor coefficients g_{ij}:

$$\begin{cases} g_{20} = \langle p, F_2(q,q)\rangle, \\ g_{11} = \langle p, F_2(q,\overline{q})\rangle, \\ g_{02} = \langle p, F_2(\overline{q},\overline{q})\rangle, \\ \\ g_{30} = \langle p, F_3(q,q,q)\rangle, \\ g_{21} = \langle p, F_3(q,q,\overline{q})\rangle, \\ g_{12} = \langle p, F_3(\overline{q},\overline{q},\overline{q})\rangle, \\ g_{03} = \langle p, F_3(\overline{q},\overline{q},\overline{q})\rangle, \\ \dots \end{cases} \tag{2.20}$$

So the Taylor coefficients (2.20) read

$$\begin{cases} g_{20} = 12\frac{ab}{\omega}v^*(a)^2 v_1\left(\frac{1}{2}\frac{(i\sqrt{a(b-a)}+a)b}{b-a-i\sqrt{a(b-a)}}, \frac{1}{2}\frac{(i\sqrt{a(b-a)}+a)^2}{a(b-a-i\sqrt{a(b-a)})}\right)^2, \\ g_{11} = 12\frac{ab}{\omega}v^*(a)^2 v_1(q)v_1(\bar{q}), \\ g_{02} = 12\frac{ab}{\omega}v^*(a)^2 v_1(\bar{q})v_1(\bar{q}), \\ \\ \dots \end{cases} \tag{2.21}$$

Now let $S(I,b) := F'(v_-(I,b))$ be the value of the derivative of the function F, defined around the bifurcation point we are interested in.

The Jacobian matrix in the neighborhood of the point (2.17) reads

$$L(v) = \begin{pmatrix} S(I,b) & 1 \\ ab & -a \end{pmatrix}.$$

Let us denote $\alpha = \binom{I}{b}$ the parameter vector and $\lambda(\alpha) = \mu(\alpha) \pm i\omega(\alpha)$ the eigenvalues of the Jacobian matrix. We have

$$\begin{cases} \mu(\alpha) = \frac{1}{2}(S(\alpha) - a), \\ \omega(\alpha) = \frac{1}{2}\sqrt{-(S(\alpha)-a)^2 + 4ab}. \end{cases}$$

With these notations, let $c_1(\alpha)$ be the complex defined by

$$c_1(\alpha) = \frac{g_{20}g_{11}(2\lambda + \bar{\lambda})}{2|\lambda|^2} + \frac{|g_{11}|^2}{\lambda} + \frac{|g_{02}|^2}{2(2\lambda - \bar{\lambda})} + \frac{g_{21}}{2}$$

(in this formula we omit the dependence in α of λ for the sake of clarity).

The first Lyapunov exponent $l_1(\alpha)$ eventually reads

$$\boxed{l_1(\alpha) = \frac{Re(c_1(\alpha))}{\omega(\alpha)} - \frac{\mu(\alpha)}{\omega(\alpha)^2}\mathrm{Im}(c_1(\alpha))} \tag{2.22}$$

The second Lyapunov exponent : The method to compute the second Lyapunov exponent is the same as the one we described in the previous section. The expression is given by the following formula:

$$\begin{aligned} 2l_2(0) = {} & \frac{1}{\omega(0)}\mathrm{Re}[g_{32}] \\ & + \frac{1}{\omega(0)^2}\mathrm{Im}\left[g_{20}\bar{g_{31}} - g_{11}(4g_{31} + 3\bar{g_{22}}) - \frac{1}{3}g_{02}(g_{40} + \bar{g_{13}}) - g_{30}g_{12}\right] \\ & + \frac{1}{\omega(0)^3}\left\{\mathrm{Re}\left[g_{20}\left(\bar{g_{11}}(3g_{12} - \bar{g_{30}}) + g_{02}(\bar{g_{12}} - 1/3g_{30}) + \frac{1}{3}\bar{g_{02}}g_{03}\right)\right.\right. \\ & \left.\left. + g_{11}\left(\bar{g_{02}}\left(\frac{5}{3}\bar{g_{30}} + 3g_{12}\right) + \frac{1}{3}g_{02}\bar{g_{03}} - 4g_{11}g_{30}\right)\right] \right. \\ & \left. + 3\,\mathrm{Im}[g_{20}g_{11}]\,\mathrm{Im}[g_{21}]\right\} \\ & + \frac{1}{\omega(0)^4}\left\{\mathrm{Im}\left[g_{11}\bar{g_{02}}\left(\bar{g_{20}}^2 - 3\bar{g_{20}}g_{11} - 4g_{11}^2\right)\right]\right. \\ & \left. + \mathrm{Im}[g_{20}g_{11}]\left(3\,\mathrm{Re}(g_{20}g_{11}) - 2|g_{02}|^2\right)\right\}. \end{aligned}$$

This expression is quite intricate in our case. Nevertheless, we have a closed-form expression depending on the parameter a, vanishing for two values of the parameter a. We evaluate numerically this second Lyapunov exponent. We get the following expression:

$$\begin{aligned} l_2(a) \approx & -0.003165\,a^{-\frac{28}{3}} - 0.1898\,a^{-\frac{22}{3}} + 0.3194\,a^{-16/3} \\ & - 0.05392\,a^{-\frac{25}{3}} + 0.1400\,a^{-\frac{19}{3}} - 0.3880\,a^{-7/3} + 0.5530\,a^{-10/3} \\ & + 0.7450\,a^{-13/3}. \end{aligned} \tag{2.23}$$

We can see that this numerical exponent vanishes only for two values of the parameter a which are

$$\{0.5304, 2.385\}.$$

The expression of the determinant of the matrix $D_{I,b}\,(\mu(I,b), l_1(I,b))$ is even more involved, and so we do not reproduce it here (it would take pages to write down its numerical expression!). Nevertheless, we proceed exactly as we did for the second Lyapunov exponent and obtain again the rigorous result that this determinant never vanishes for all $a > 0$. □

2.1.4 Conclusion: The full bifurcation diagram

We now summarize the results obtained in this section in the two following theorems.

Theorem 2.1.8. *Let us consider the formal dynamical system*

$$\begin{cases} \dot{v} = F(v) - w + I, \\ \dot{w} = a(bv - w), \end{cases} \tag{2.24}$$

where a is a fixed real, b and I bifurcation parameters, and $F : \mathbb{R} \mapsto \mathbb{R}$ a real function. If the function F satisfies the assumptions that

(A.1) *the function F is three times continuously differentiable,*

(A.2) *F is strictly convex, and*

(A.3) *F' satisfies the conditions*

$$\begin{cases} \lim\limits_{x \to -\infty} F'(x) \leq 0, \\ \lim\limits_{x \to \infty} F'(x) = \infty, \end{cases}$$

then the dynamical system (2.24) *shows the following bifurcations:*

(B1) *A saddle-node bifurcation curve:*

$$(SN) : \{(b,I)\ ;\ I = -m(b)\},$$

where $m(b)$ is the minimum of the function $F(v) - bv$ (if the second derivative of F does not vanish at this point).

(B2) *An Andronov–Hopf bifurcation line:*

$$(AH) := \left\{(b,I)\ ;\ b > a \ \textit{and}\ \ I = bv^*(a) - F(v^*(a))\right\},$$

where $v^*(a)$ is the unique solution of $F'(v^*(a)) = a$ (if $F''(v^*(a)) \neq 0$). This type of Andronov–Hopf bifurcation is given by the sign of the variable

$$A(a,b) = F'''(v^*(a)) + \frac{1}{b-a} F''(v^*(a))^2.$$

If $A(a,b) > 0$, then the bifurcation is subcritical, and if $A(a,b) < 0$, then the bifurcation is supercritical.

(B3) *A Bogdanov–Takens bifurcation point at the point $b = a$ and $I = -m(a)$ if $F''(v^*(a)) \neq 0$.*

(B4) *A saddle homoclinic bifurcation curve characterized in the neighborhood of the Bogdanov–Takens point by*

$$(P) := \left\{ I = -m(a) - \frac{12}{25F''(v^*(a))}(b-a)^2;\ b > a \right\}.$$

Theorem 2.1.9. *Consider the system* (2.1)*, where a is a given real number, b and I are real bifurcation parameters, and $F : E \times \mathbb{R} \mapsto \mathbb{R}$ is a function satisfying the following assumptions:*

(A.5) *The function F is six times continuously differentiable.*

(A.2) *F is strictly convex.*

(A.3) *F' satisfies the conditions*

$$\begin{cases} \lim\limits_{x \to -\infty} F'(x) \leq 0, \\ \lim\limits_{x \to \infty} F'(x) = \infty. \end{cases}$$

(A.4) *Let $v^*(a)$ be the unique real such that $F'(v^*(a)) = a$. We have*

$$F'''(v^*(a)) < 0.$$

Furthermore, consider the following conditions:

(BGH.1) *The second Lyapunov coefficient of the dynamical system $l_2(v^*(a)) \neq 0$.*

(BGH.2) *Let $l_1(v)$ denote the first Lyapunov exponent and $\lambda(I,b) = \mu(I,b) \pm i\omega(I,b)$ the eigenvalues of the Jacobian matrix in the neighborhood of the point of interest. The map $(I,b) \to (\mu(I,b), l_1(I,b))$ is regular at this point.*

Having these, the system undergoes a Bautin bifurcation at the point $v^*(a)$ for the parameters $b = a - \frac{F''(v^*(a))^2}{F'''(v^*(a))}$ and $I = bv^*(a) - F(v^*(a))$.

Remark 5. Theorem (2.1.8) enumerates some of the bifurcations that any dynamical system of the class (2.1) will always undergo. Together with Theorem 2.1.9, they summarize all the local bifurcations the system can undergo, and no other fixed-point bifurcation is possible. In section 2.3 we introduce a model actually showing all these local bifurcations.

2.2 Applications: Izhikevich and Brette–Gerstner models

In this section we show that the neuron models proposed by Izhikevich in [141] and Brette and Gerstner in [30] are part of the class studied in section 2.1. Using the results of the latter section, we derive their bifurcation diagram and obtain that they show exactly the same types of bifurcations.

2.2.1 Adaptive quadratic IF model

We produce here a complete description of the bifurcation diagram of the adaptive quadratic integrate-and-fire model proposed by Izhikevich in [141] and [146, Chapter 8]. We use here the dimensionless equivalent version of this model with the fewest parameters:

$$\begin{cases} \dot{v} = v^2 - w + I, \\ \dot{w} = a(bv - w). \end{cases} \tag{2.25}$$

Equation (2.25) is clearly a particular case of (2.1) with

$$F(v) = v^2.$$

F is clearly strictly convex and C^∞. $F'(v) = 2v$, and so it also satisfies Assumption 2.1.3. Furthermore, the second derivative never vanishes, and so the system undergoes the three bifurcations stated in Theorem 2.1.8.

(Izh.B1) A saddle-node bifurcation curve defined by

$$\left\{ (b,I)\ ;\ I = \frac{b^2}{4} \right\}.$$

For $(I,b) \in \mathbb{R}^2$, the fixed point is given by $(v^*(b) = \frac{1}{2}b,\ w^*(b) = \frac{1}{2}b^2)$.

For $I < \frac{b^2}{4}$, the fixed point(s) are

$$v_\pm(b,I) = \frac{1}{2}\left(b \pm \sqrt{b^2 - 4I}\right).$$

(Izh.B2) An Andronov–Hopf bifurcation line:

$$\left\{ (I,b)\ ;\ b > a \text{ and } I = \frac{a}{2}\left(b - \frac{a}{2}\right) \right\},$$

whose type is given by the sign of the variable

$$A(a,b) = \frac{4}{b-a}.$$

This value is always strictly positive, and so the bifurcation is always subcritical.

(Izh.B3) A Bogdanov–Takens bifurcation point for $b = a$ and $I = \frac{a^2}{4}$, $v^*(a) = \frac{a}{2}$.

(Izh.B4) A saddle homoclinic bifurcation curve satisfying the quadratic equation near the Bogdanov–Takens point:

$$(P) := \left\{ I = \frac{a^2}{4} - \frac{6}{25}(b-a)^2;\ b > a \right\}.$$

Figure 2.2 represents the fixed points of this dynamical system, and their stability, together with the bifurcation curves.

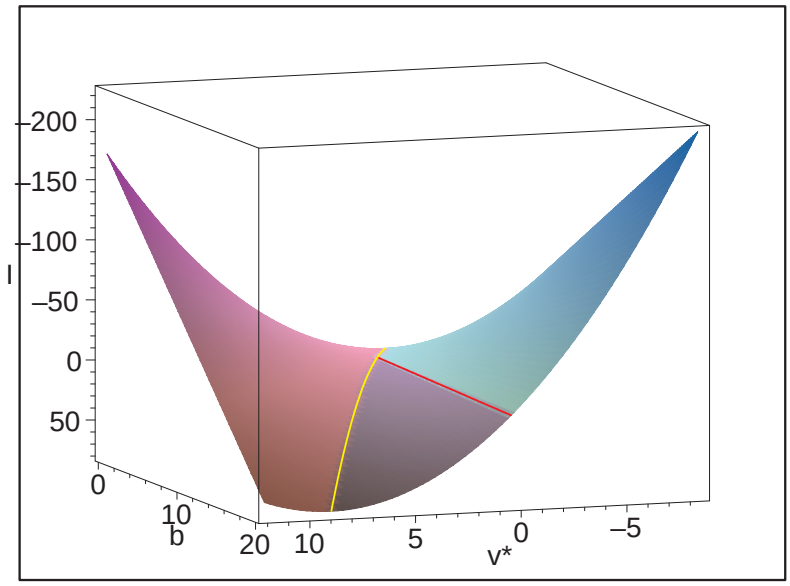

Figure 2.2: Representation of the v fixed point with respect to the parameters I and b in the Izhikevich model. The reddish component is the surface of saddle fixed points, the purplish one corresponds to the repulsive fixed points, and the greenish/bluish one corresponds to the attractive fixed points The yellow curve corresponds to a saddle-node bifurcation and the red one to an Andronov–Hopf bifurcation.

2.2.2 Adaptive exponential IF model

In this section we study the bifurcation diagram of the adaptive exponential neuron. This model has been introduced by Brette and Gerstner in [30]. This model, inspired by the Izhikevich adaptive quadratic model, can be fitted to biological values, takes into account the adaptation phenomenon, and is able to reproduce many behaviors observed in cortical neurons. The bifurcation analysis we derived in section 2.1 allows us to understand how the parameters of the model can affect the behavior of this neuron. We show that this model is part of the general class studied in section 2.1, and we obtain the fixed-point bifurcation diagram of the model.

Reduction of the original model

This original model is based on biological constants and is expressed with a lot of parameters. We first reduce this model to a simpler form with the fewest number of parameters.

The basic equations proposed in the original paper [30] read

$$\begin{cases} C\frac{\mathrm{d}V}{\mathrm{d}t} = -g_L(V-E_L) + g_L\Delta_T \exp\left(\frac{V-V_T}{\Delta_T}\right) \\ \qquad\qquad -g_e(t)(V-E_e) - g_i(t)(V-E_i) - W + I_m, \\ \tau_W \frac{\mathrm{d}W}{\mathrm{d}t} = \kappa(V-E_L) - W. \end{cases} \tag{2.26}$$

First, we do not assume that the reversal potential of the w equation is the same as the leakage potential E_L, and we write the equation for the adaptation variable by

$$\tau_W \frac{\mathrm{d}W}{\mathrm{d}t} = a(V-\bar{V}) - W.$$

Next we assume that $g_e(\cdot)$ and $g_i(\cdot)$ are constant (in the original paper it was assumed that the two conductances were null).

After some straightforward algebra, we eventually get the following dimensionless equation equivalent to (2.26):

$$\begin{cases} \dot{v} = -v + e^v - w + I, \\ \dot{w} = a(bv - w), \end{cases} \tag{2.27}$$

where we denoted

$$\begin{cases} \tilde{g} := g_L + g_e + g_i, \\ \tau_m := \frac{C}{\tilde{g}}, \\ B := \frac{\kappa}{\tilde{g}} \left(\frac{E_L}{\Delta_T} + \log(\frac{g_L}{\tilde{g}} e^{-V_T/\Delta_T}) \right), \\ v(\tau) := \frac{V(\tau\tau_m)}{\Delta_T} + \log\left(\frac{g_L}{\tilde{g}} e^{-V_T/\Delta_T} \right), \\ w(\tau) := \frac{W(\tau\tau_m)}{\tilde{g}\Delta_T} + B, \\ a := \frac{\tau_m}{\tau_W}, \\ b := \frac{\kappa}{\tilde{g}}, \\ I := \frac{I_m + g_L E_L + g_e E_e + g_i E_i}{\tilde{g}\Delta_T} + \log(\frac{g_l}{\tilde{g}} e^{-V_T/\Delta_T}) + B \end{cases} \tag{2.28}$$

and where the dot denotes the derivative with respect to τ.

The differential equations and the parameters have a physiological interpretation. The first equation is the membrane equation, which states that the capacitive current through the membrane (C is the membrane capacitance) is the sum of the injected current I and of the ionic currents. The first term is the leak current (g_L is the leak conductance and E_L is the leak reversal potential), the membrane time constant is $\tau_m = C/g_L$. The second (exponential) term approximates the sodium current, responsible for the generation of action potentials [95]. The approximation results from neglecting the inactivation of the sodium channel and assuming that activation is infinitely fast (which is reasonable). Because activation curves are typically Boltzmann functions [12], the approximated current is exponential near spike initiation. The voltage threshold V_T is the maximum voltage that can be reached without generating a spike (without adaptation), and the slope factor Δ_T quantifies the sharpness of spikes. In the limit of zero slope factor, the model becomes an integrate-and-fire model with a fixed threshold V_T. Quantitatively, it is proportional to the slope constant k in the activation function of the sodium current. The second variable w is an adaptation current with time constant τ_w, which includes both spike-triggered adaptation, through the reset $w \to w + d$, and subthreshold adaptation, through the coupling (variable b). It may model ionic channels (e.g. potassium) or a dendritic compartment. Quantitatively, the coupling variable b can result from a linearization of the dynamics of a ionic channel, or from the axial conductance in the case of a dendritic compartment. We generally assume $b > 0$ in this chapter, although the analysis also applies for $b < 0$ when $|b|$ is not too large.

Remark 6. These expressions confirm the qualitative interpretation of the parameters a, b, and I of the model (2.1). Indeed, $a = \frac{\tau_m}{\tau_w}$ accounts for the time scale of the adaptation (with the membrane time scale as reference), and the parameter $b = \frac{\kappa}{\tilde{g}}$ is proportional to the interaction between the membrane potential and the adaptation

variable and inversely proportional to the total conductivity of the membrane potential. Eventually, I is an affine function of the input current I_m and models the input current of the neurons.

Bifurcation diagram

From (2.27) we can clearly see that the Brette–Gerstner model is included in the formal class studied in the present chapter with

$$F(v) = e^v - v.$$

This function satisfies Assumptions 2.1.1, 2.1.2, and 2.1.3. Furthermore, its second order derivative never vanishes.

Theorem 2.1.8 shows that the system undergoes the following bifurcations:

(BG.B1) A saddle-node bifurcation curve defined by

$$\{(b,I)\,;\, I = (1+b)(1-\log(1+b))\}.$$

So $v^*(b) = \log(1+b)$. For $I \leq (1+b)(1-\log(1+b))$, the system has the fixed points

$$\begin{cases} v_-(I,b) := -W_0\left(-\frac{1}{1+b}e^{\frac{I}{1+b}}\right) + \frac{I}{1+b}, \\ v_+(I,b) := -W_{-1}\left(-\frac{1}{1+b}e^{\frac{I}{1+b}}\right) + \frac{I}{1+b}, \end{cases} \tag{2.29}$$

where W_0 is the principal branch of Lambert's W function[3] and W_{-1} the real branch of Lambert's W function such that $W_{-1}(x) \leq -1$, defined for $-e^{-1} \leq x < 1$.

(BG.B2) An Andronov–Hopf bifurcation line for

$$\{(b,I)\,;\, b > a \text{ and } I = I^*(a,b) = (1+b)\log(1+a) - (1+a)\}$$

at the equilibrium point $(v^*(a) = \log(1+a),\, w_a = bv^*(a))$. This type of Andronov–Hopf bifurcation is given by the sign of the variable

$$A(a,b) = F'''(v^*(a)) + \frac{1}{b-a}F''(v^*(a))^2 = (1+a) + \frac{4}{b-a}(1+a)^2 > 0.$$

So the bifurcation is always subcritical, and there is not any Bautin bifurcation.

(BG.B3) A Bogdanov–Takens bifurcation point at the point $b = a$ and $I = \log(1+a)$.

(BG.B4) A saddle homoclinic bifurcation curve satisfying, near the Bogdanov–Takens point, the equation

$$(P) := \left\{ I = (1+a)(\log(1+a)-1) - \frac{12}{25(1+a)}(b-a)^2;\, b > a \right\}.$$

In Figure 2.3 we represent the fixed points of the exponential model and their stability, together with the bifurcation curves, in the space (I,b,v).

[3]The Lambert W function is the inverse function of $x \mapsto xe^x$.

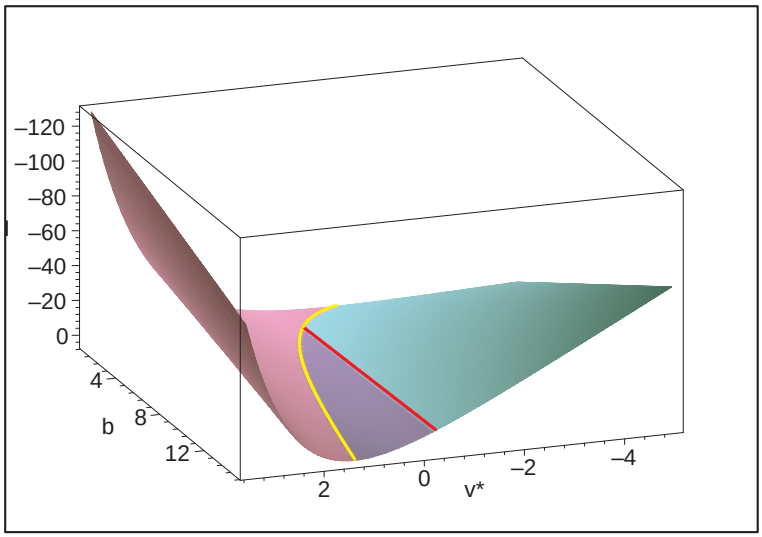

Figure 2.3: Representation of the v fixed point of the Brette–Gerstner model with respect to the parameters I and b. The reddish/pinkish component is the surface of saddle fixed points, the purplish one corresponds to the repulsive fixed points, and the bluish/greenish one corresponds to the attractive fixed points The yellow curve corresponds to a saddle-node bifurcation and the red one to an Andronov–Hopf bifurcation.

2.3 THE RICHER QUARTIC MODEL

In this section, we introduce a new specific model having a richer bifurcation diagram than the two models studied in section 2.2. It is as simple as the two previous models from the mathematical and computational points of view. To this end, we define a model which is part of the class studied in section 2.1 by specifying the function F.

2.3.1 The quartic model: Definition and bifurcation map

Let $a > 0$ be a fixed real and $\alpha > a$. We instantiate the model (2.1) with the function F a quartic polynomial:

$$F(v) = v^4 + 2av.$$

Remark 7. The choice of the function F here is just an example where all the formulas are rather simple. Exactly the same analysis can be done with any F function satisfying $F'''(v^*(a)) < 0$ and the transversality conditions given in Theorem 2.1.9. This would be the case, for instance, for any quartic polynomial $F(v) = v^4 + \alpha v$ for $\alpha > a$.

The function F satisfies Assumptions 2.1.1, 2.1.2, and 2.1.5. $F'(v) = 4v^3 + 2a$ satisfies Assumption 2.1.3.

Nevertheless, we have to bear in mind that the second order derivative vanishes at $v = 0$:

$$\begin{cases} \dot{v} = v^4 + 2av - w + I, \\ \dot{w} = a(bv - w). \end{cases} \tag{2.30}$$

Theorem 2.1.8 shows that the quartic model undergoes the following bifurcations:

(B1) A saddle-node bifurcation curve defined by

$$(SN) := \left\{ (b,I)\ ;\ I = 3\left(\frac{b-2a}{4}\right)^{(4/3)} \right\}.$$

Proof. Indeed, the function G reads $G(v) = v^4 + (2a-b)v$ and reaches its minimum at the point $v = (\frac{b-2a}{4})^{(1/3)}$. So the minimum of G is $m(b) = -3(\frac{b-2a}{4})^{(4/3)}$. □

The point $v^*(b)$ is $(\frac{b-2a}{4})^{(1/3)}$, and we have closed-form expressions (but rather complicated) for the two fixed points for $I < 3(\frac{b-2a}{4})^{(4/3)}$ since the quartic equation is solvable in radicals. The closed form expression can be obtained using a symbolic computation package like Maple using the command

```
S:=allvalues( solve( x^4 + (2*a - b) * x + I0 = 0,x));
```

(B2) An Andronov–Hopf bifurcation curve for $b > a$ along the straight line

$$(AH) := \left\{ (I,b)\ ;\ b > a \text{ and } I = -\left(\frac{a}{4}\right)^{1/3} b - \left(\frac{a}{4}\right)^{4/3} \right\}.$$

The fixed point where the system undergoes this bifurcation is $v^*(a) = -(\frac{a}{4})^{1/3}$. The kind of Andronov–Hopf bifurcation we have is governed by the sign of

$$\alpha = -24\left(\frac{a}{4}\right)^{1/3} + \frac{144}{b-a}\left(\frac{a}{4}\right)^{4/3}.$$

Finally, the type of bifurcation changes when b varies.

- When $b < \frac{5}{2}a$, then $\alpha > 0$, hence $l_1 > 0$, and the Andronov–Hopf bifurcation is subcritical.
- When $b > \frac{5}{2}a$, then $\alpha < 0$, hence $l_1 < 0$, and the Andronov–Hopf bifurcation is supercritical.

We prove below that the change in the type of Hopf bifurcation is obtained via a Bautin bifurcation.

(B3) A Bogdanov–Takens bifurcation point is located at $b = a$ and $I = -3(\frac{a}{4})^{(4/3)}$.

(B4) A saddle homoclinic bifurcation curve satisfying, near the Bogdanov–Takens point, the equation

$$(P) := \left\{ I = -7\left(\frac{a}{4}\right)^{\frac{4}{3}} - \frac{1}{25}\left(\frac{4}{3}\right)^{\frac{2}{3}}(b-a)^2;\ b > a \right\}.$$

(B5) A Bautin bifurcation at the point $\left(b = \frac{5}{2}a, I = -3(\frac{a}{4})^{4/3}(2a-1)\right)$ and a saddle node bifurcation of periodic orbits coming along (see section 2.3.2).

Figure 2.4 represents the bifurcation curves and the fixed point of the quartic model in the space (I,b,v).

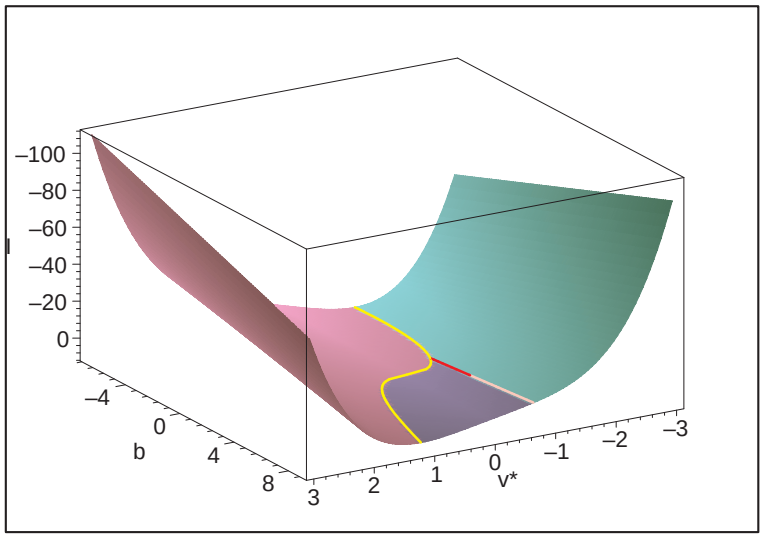

Figure 2.4: v fixed points and their stability in function of I and b. The reddish/pinkish component is the surface of saddle fixed points, the purplish one corresponds to the repulsive fixed points, and the bluish/greenish one corresponds to the attractive fixed points. The yellow curve corresponds to a saddle-node bifurcation, the red curve to a subcritical Andronov–Hopf bifurcation, and the greyish one to the supercritical Andronov–Hopf bifurcation. The intersection point between the yellow and the red curve is the Bogdanov–Takens bifurcation point, and the intersection point of the red and greyish curves is the Bautin bifurcation point.

2.3.2 The Bautin bifurcation

As we have seen in the last section, at the point

$$\begin{cases} v^*(a) = -\left(\frac{a}{4}\right)^{1/3}, \\ I = -3\left(\frac{a}{4}\right)^{4/3}(2a-1), \\ b = \frac{5}{2}a \end{cases} \tag{2.31}$$

the Jacobian matrix of the system has a pair of purely conjugate imaginary eigenvalues and a vanishing first Lyapunov exponent.

The proof that the quartic model undergoes a Bautin bifurcation at this point is provided in section 2.1.3. We prove that the system actually undergoes a Bautin bifurcation except for two particular values of the parameter a. With this same method we obtain a closed-form expression for the second Lyapunov exponent. We show that this second Lyapunov exponent vanishes for two values of a, whose expressions are complicated. These calculations are rigorous, but nevertheless, the interested reader can find numerical expressions of this exponent to get a grasp on its behavior in the appendix (see (2.23)) and of the two numerical values of a such that $l_2(a)$ vanishes.

Things are even more involved when we are interested in the regularity of the map $(I,b) \mapsto (\mu(I,b), l_1(I,b))$. Nevertheless, we obtain that this determinant never vanishes.

Eventually, for all a different from the critical values where the second Lyapunov exponent vanishes, the system undergoes a Bautin bifurcation.

Note finally that the Bautin bifurcation point separates two branches of sub- and supercritical Hopf bifurcations. For nearby parameter values, the system has two

coexisting limit cycles, an attractive one and a repelling one, which collide and disappear via a saddle-node bifurcation of periodic orbits.

2.4 Electrophysiological classes

In the previous sections we emphasized the fact that the class of models we defined in section 2.1 was able to reproduce the behaviors observed by Izhikevich in [144]. In this section, first we show that the quartic model indeed reproduces the behaviors observed by Izhikevich and which correspond to cortical neuron behaviors observed experimentally. We also produce some simulations of self-sustained subthreshold oscillations which occur only when the dynamical system has attracting periodic orbits, which is not the case in the other usual models of this class.

Izhikevich in [144] explains the main features we obtain in numerical simulations from the neurocomputational point of view. In chapter 4, we comment on these same features from the dynamical systems point of view mainly for the adaptive exponential model for its physiological relevance in that its parameters can be easily related to physiological quantities. By study different quantities of the model as a dynamical system, we will be able to define electrophyisiological classes, i.e. sets of parameters where the model responds qualitatively the same way to different current inputs.

2.4.1 Simulation results

Simulation results for the quartic model introduced in section 2.3 are provided here. In the simulated model, the spike is not represented by the blow up of the potential membrane v, but we consider that the neuron emits a spike when its membrane potential crosses a constant threshold. Note that the numerical simulations are very robust with respect to the choice of the threshold, if taken large enough, since the underlying equation blows up in finite time, and the adaptation variable converges. This issue is specifically discussed in chapter 5 and in the paper [256]. This is also the case for the exponential model, but not for the quadratic model (see discussions herein).

Let θ be our threshold. The simulated model considered in this section is the solution of the equations

$$\begin{cases} \dot{v} = v^4 + 2av - w + I, \\ \dot{w} = a(bv - w) \end{cases} \tag{2.32}$$

together with the spike-and-reset condition

$$\text{If } v(t^-) > \theta \Rightarrow \begin{cases} v(t) = v_r, \\ w(t) = w(t^-) + d. \end{cases} \tag{2.33}$$

Simulations have been done using an Euler numerical scheme, with a time step ranging from 10^{-1} to 10^{-2} depending on the precision needed, and with time intervals ranging from 10 to 500. This method is very efficient numerically and remains precise. Other integration methods could be used, and the qualitative results we obtained do not depend on the integration scheme, as soon as the time step is small enough.

Remark 8. Note that we did not reproduce the last three behaviors presented by Izhikevich in [144, *Figs.* 1.(R)*,* 1.(S)*, and* 1.(T)]. Indeed, these behaviors are not in the scope of the present chapter and do not correspond to the model we studied.

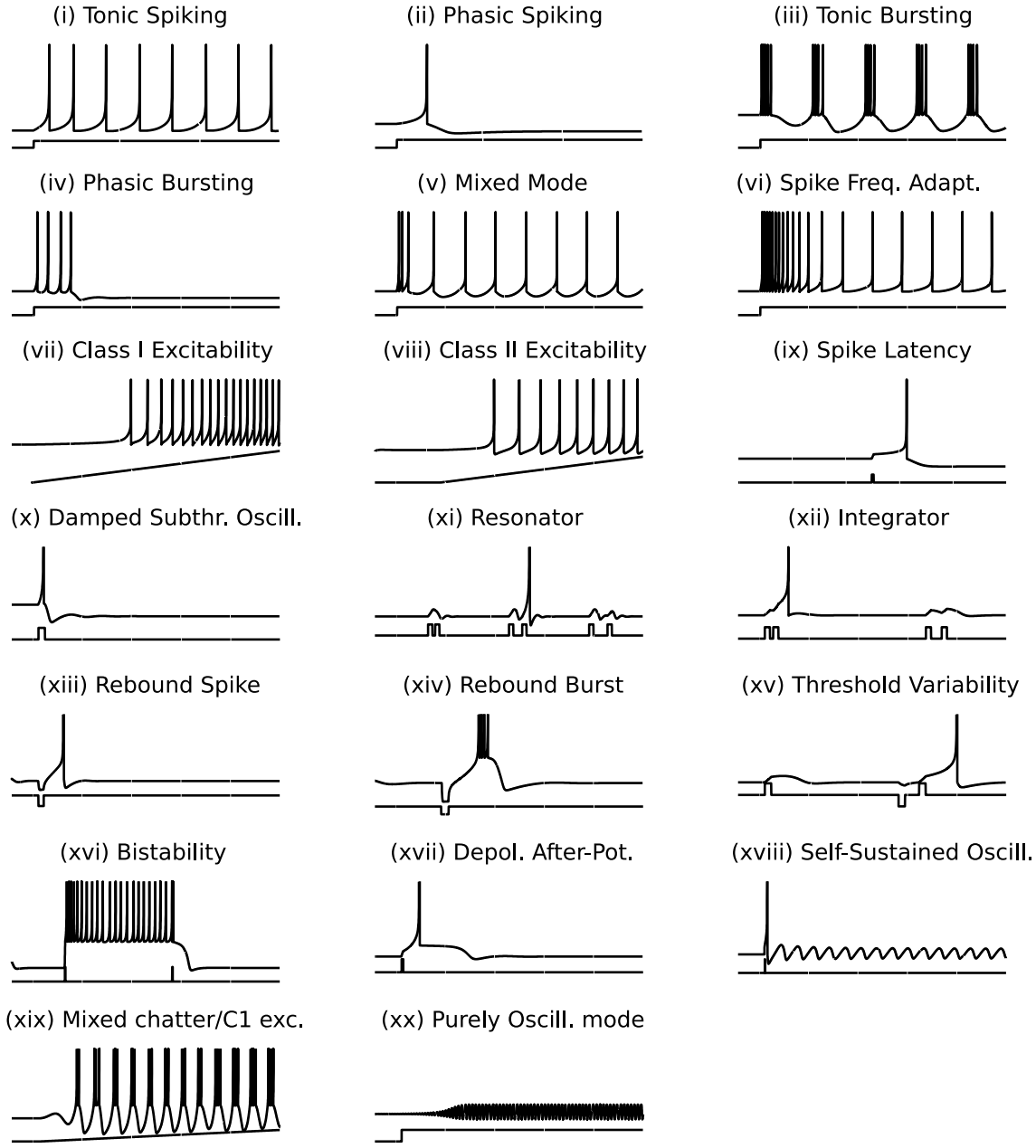

Figure 2.5: Different remarkable neurocomputational interesting behaviors of the neuron model (2.32) with the reset condition (2.33) for different choices of the parameters (a, b, I, v_r, d). The higher curve represents the membrane potential v and the lower one the input current I (see table 2.1) for the numerical values of each simulations).

(i) Tonic Spiking	(ii) Phasic Spiking	(iii) Tonic Bursting
$a=1$; $b=0.49$; $v_r=0$; $I(t)=1.561_{t>1}(t)$; $d=1$; $T=10$; $dt=0.01$; $\theta=10$;	$a=1$; $b=0.76$; $v_r=0.2$; $I=0.371_{t>1}(t)$; $d=1$; $T=10$; $dt=0.01$; $\theta=10$;	$a=0.15$; $b=1.68$; $v_r=(-2a+b)^{\frac{1}{3}}$; $I=4.671_{t>1}(t)$; $d=1$; $T=30$; $dt=0.01$; $\theta=10$;
(iv) Phasic Bursting	(v) Mixed Mode	(vi) Spike Freq. Adaptation
a =1.58; b =1.70; $v_r=-\frac{a}{4}^{\frac{1}{3}}$; $I(t)$ =0.731$_{t>1}(t)$; $d=0.01$; T =50; dt =0.01; θ =10.	a =0.07; b =0.32; v_r =0; $I(t)$ =3.841$_{t>1}(t)$; $d=1.50$; T =50; dt =0.01; θ =10.	a =0.02; b =0.74; v_r =0; $I(t)$ =4.331$_{t>1}(t)$; $d=0.36$; T =50; dt =0.01; θ =10.
(vii) Class 1 Excitability	(viii) Class 2 Excitability	(ix) Spike Latency
a =4; b =0.67; v_r =−1.3; $I(t)=-0.1+0.23t$; $d=1$; T =30; dt =0.01; θ =10.	a =1; b =1.09; v_r =−1.2; $I(t)$ =0.06t; $d=5$; T =50; dt =0.01; θ =20.	a =0.02; b =0.42; v_r =0; $I(t)$ =5$\delta_{7.5}(t)$; $d=1$; T =15; dt =0.01; θ =10.
(x) Damped Subthr. Oscill.	(xi) Resonator	(xii) Integrator
a =2.58; b =4.16; v_r =0.1; $I(t)$ =2$\delta_2(t)$; $d=0.05$; T =20; dt =0.01; θ =10.	a =5.00; b =7.88; v_r =−1.28; $I(t)$ =$\delta_{6,6.8,15,16.5,24,26}(t)$; $d=0.5$; T =30; dt =0.01; θ =10.	a =1.00; b =1.10; v_r =−0.97; $I(t)$ =$\delta_{2.5,3.3,17.5,19}(t)$; $d=0.5$; T =25; dt =0.01; θ =10.
(xiii) Rebound Spike	(xiv) Rebound Burst	(xv) Threshold variability
a =1; b =2; v_r =−0.63; $I(t)=-0.48-5\delta_{2.5}(t)$; $d=1$; T =50; dt =0.1; θ =10.	a =1; b =2; v_r =1.3; $I(t)=-0.48-30\delta_{6.5}(t)$; $d=1$; T =20; dt =0.01; θ =10.	a =1; b =1.23; v_r =−0.91; $I(t)$ =$\delta_{2,16.5}-\delta_{15}$; $d=1$; T =20; dt =0.01; θ =10.
(xvi) Bistability	(xvii) Depol. after-pot	(xviii) Self-sustained oscill.
a =1; b =1.2; v_r =0.8; $I(t)=-0.47+20*(\delta_{10}-\delta_{30})$; $d=0.5$; T =50; dt =0.01; θ =10.	a =1; b =1.5; v_r =0.06; $I(t)$ =2δ_3; $d=0.01$; T =30; dt =0.01; θ =10.	a =1; b =2.5; v_r =−0.63; $I(t)=-0.475+10*\delta_{10}$; $d=1$; T =100; dt =0.01; θ =10.
(xix) Mixed Chatter/ C^1 exc.	(xx) Purely oscill.	
a =0.89; b =3.65; v_r =1.12; $I(t)$ =0.07t; $d=1$; T =50; dt =0.01; θ =10.	a =1; b =2.6; v_r =−0.63; $I(t)=-0.471_{t>1}$; $d=1$; T =500; dt =0.01; θ =10.	

Table 2.1: Simulation parameters to produce figure 2.5.

More precisely, in the study of the general model (2.1), we considered for phenomenological reasons $a>0$, modelling the leak of the adaptation variable: the adaptation would converge to its rest value if it was not influenced by the membrane potential v. If we considered $a<0$, this adaptation variable would diverge exponentially from this rest value if it was not controlled by the membrane potential v. The inhibition-induced behaviors [144, *Figs.* 1.(S) *and* 1.(T)] require a to be strictly negative, and so we will not comment on these behaviors any further.

Similarly, the accommodation behavior presented by Izhikevich in [144, *Fig.* 1.(R)] is a limit case when w is very slow and the adaptation efficiency b very high. Mathematically speaking, it corresponds to a case where $a\to 0$ and $ab\to\lambda\neq 0$. This case is not taken into account in our study and amounts to replacing (2.1) by an equation of the type

$$\begin{cases}\frac{\mathrm{d}v}{\mathrm{d}t}=F(v)-w+I,\\ \frac{\mathrm{d}w}{\mathrm{d}t}=ab(v-v_0),\end{cases}\tag{2.34}$$

and the study of this equation is not in the scope of the present chapter.

In table 2.1, we provide the numerical values used to obtain the simulations of figure 2.5. In this table, the $\delta_u(t)$ function is defined by

$$\delta_{u_1,\dots,u_N}(t)=\begin{cases}1 & \textit{if } t\in\bigcup_{k\in\{1,\dots,N\}}[u_k,u_k+0.3],\\ 0 & \textit{else}.\end{cases}$$

The simulated behaviors we obtained in Figure 2.5 have been obtained playing with the bifurcation parameters in the phase plane. The way the parameters were set was based on a qualitative reasoning on the phase plane and the bifurcation diagram

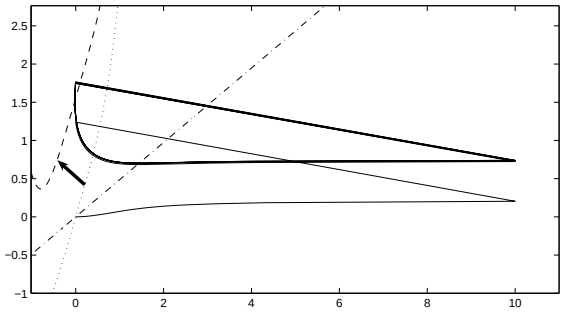

Figure 2.6: Tonic spiking: phase plane trajectory. The dotted curve is the v nullcline at the initial time. It is shifted to the dashed one when applying a constant input current. The new dynamical system has no fixed point and spikes regularly. We can see the spiking cycle appearing.

in a way we describe in chapter 4. The simulations presented in the figure 2.5 are done with the quartic model.

2.4.2 Bifurcations and neuronal dynamics

In this section we link the neuronal behaviors shown in Figure 2.5 with the bifurcations of the system. We are first interested in behaviors generated by applied current steps to the neuron. These behaviors consist in studying the effect of the initial condition on the dynamics, as we will see in the following chapters.

- (i), (iii), (v), (vi) *Tonic behaviors* : Tonic behaviors correspond to a sustained destabilization of the resting voltage. In the four cases we discuss here, the voltage of a neuron is at rest for a given value of input current I. Then a current step is applied to the neuron and subsequently, the neuron emits an infinite sequence of spikes (as long as the current step is applied). This behavior hence can correspond to destabilizing on a permanent basis the resting state, which can be achieved either by crossing the saddle-node or the Andronov-Hopf bifurcation, or to be permanently reset outside the attraction basin of the fixed point. When the system does not returns to the attraction basin of the resting state, two cases can occur depending on the parameters: either the system has a stable limit cycle (it is the case when the system undergoes a Bautin bifurcation). In this case, the destabilization can result in the generation of self-sustained subthreshold oscillations, as in the case (xx). If there is no stable limit cycle nor stable non-spiking trajectory, then the neuron will emit infinitely many spikes, as in the cases cited. The different spike patterns observed are a result of the interplay between the subthreshold dynamics and the reset process. It will be studied further in chapter 3. The phase plane orbits give a grasp on the phenomena occurring. We observe that the case of tonic regular spiking is linked with the existence of what we will call a *limit spiking cycle*, i.e. a trajectory including spikes similar to a cycle containing a spike point ($v = \infty$, or $v =$ threshold in the numerical case). In that case the adaptation variable w converges to an attracting stable value w_{spike}. This value satisfies the relation $w_s(t_{\text{spike}}) + b = w_{\text{spike}}$,

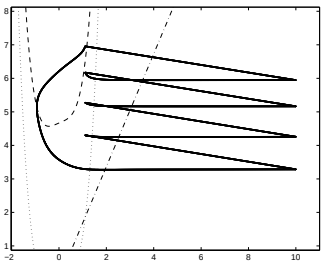

(a) Phase plane of the tonic bursting (without the transient phase)

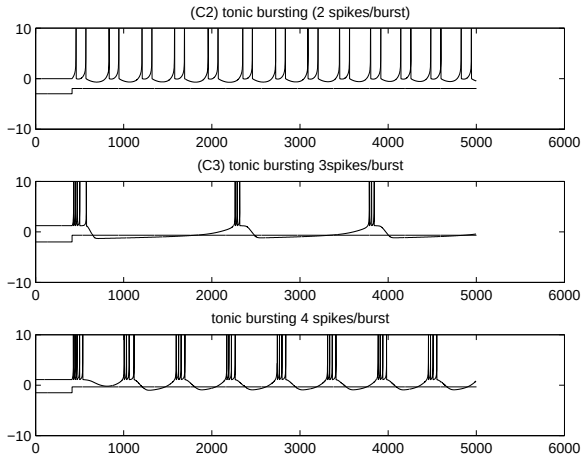

(b) Controlling the number of spikes per burst

Figure 2.7: Tonic bursting: phase plane trajectory. The dotted curve is the v nullcline at the initial time. It is shifted to the dashed one when applying a constant input current. The new dynamical system has no fixed point. We can see the multiple spike limit cycle here.

where $w_s(\cdot)$ is solution of (2.32) with the initial conditions

$$\begin{cases} v(0) = v_r, \\ w(0) = w_{\text{spike}} \end{cases}$$

and where t_{spike} denotes the time of the spike.

The mixed mode (v) and the spike frequency adaptation (vi) are particular cases of tonic spiking differing by the way they converge to this spiking limit cycle. While in the spike frequency adaptation the convergence is smooth, in the mixed mode the convergence happens quite fast, the system sends a burst of few spikes before converging to the spiking cycle.

The case of the tonic bursting is induced by the same mechanism. Nevertheless, in that case (see figure 2.7(a)) the generalized cycle towards which the trajectory converges contains few (≥ 2) spikes. It is interesting to note that in that case if we consider the reset locations, they form a cycle, with at least a point in the zone $\{(v,w); w > F(v) + I\}$. So the system emits quickly a precise number of spikes and then crosses the v nullcline. At this point, the membrane potential decays before spiking. We can see numerically that the system converges to a stable *bursting cycle* (see Figure 2.7(a)) Interestingly enough, the two-dimensional system is able to reproduce the diagrams presented by Izhikevich in [142] in an (at least) three-dimensional space, because of the singularity of the model (explosion or threshold/reinitialization). If the system was regular, this behavior would not have been possible because it would have contradicted the Cauchy–Lipschitz theorem of existence and uniqueness of a solution.

Note that we can choose exactly the number of spikes per burst by changing

the adaptation parameter d and that the bursting can be of parabolic or square-wave type as defined in Hoppensteadt and Izhikevich [133] (see Figure 2.7(b)).

These tonic behaviors will be studied further in section 3.

- (ii), (iv) *Phasic behaviors*: In these behaviors the current step applied is not high enough to destroy all the stable subthreshold orbits (fixed points or limit cycles). In that case there exists a subthreshold orbit, and the system will fall after emitting a finite number of spikes in the attraction basin of this stable trajectory. If the "initial condition" of the system, i.e. the previous stable fixed point, is inside the attraction basin of the new fixed point, then no spike will be emitted. If it is outside this attraction bass in, then the neuron will elicit spikes. If the trajectory goes back in the attraction basin of the stable fixed point, then we will have a return to equilibrium after the emission of few spikes. This is what we call a phasic behavior. These behaviors will be also studied a little bit more in depth in chapter 3.

- (vii)/(viii) *Excitability types*: The excitability properties of these types of neurons will be discussed in chapter 4. These behaviors are linked with the way the equilibrium loses stability, i.e. either via saddle-node bifurcation (type I) or via Andronov-Hopf bifurcation (type II excitability), and on the parameters of the model.

All the other behaviors are generated using current pulses, and are linked with the local behavior around the destabilized fixed point. These behaviors will mainly be studied in the chapter 4. It corresponds to the integration of perturbations at the stable equilibrium point.

- (ix)/(xvii) *Spike latency / DAP*: It is a particular case of phasic spiking when the equilibrium v^* or the reset point v_r is near a point such that $F(v) = F'(v) = 0$. The membrane potential dynamics is very slow around this point. In the spike latency behavior, the initial point is close to this point, which generates the observed latency. In our case, it is around the minimum of the function F (see Figure 2.9(ix)). In the depolarized after-potential (DAP) case, the reset occurs near this point, which is also in the attraction basin of the stable fixed point.

- (x), (xi), (xii), (xv) *Damped subthreshold oscillations, resonator and integrator, threshold variability* are linked with the imaginary part of the eigenvalues of the Jacobian matrix at the fixed point. When this imaginary part is non null, then a perturbation will result in damped subthreshold oscillations, and multiple excitations will respond stronger to particular frequency inputs (resonator). The oscillations around the fixed point also generate the threshold variability behavior. When this imaginary part is null, the neuron will be an integrator: since it returns monotonously to equilibrium, the more two excitations are close the more it will depolarize the neuron.

- (xiii)/(xiv) *Rebound spike or burst*: These behaviors are linked with the topology of the attraction basin of the fixed point as discussed in chapter 4

- (xvi) *Bistability*: The bistability behavior (Figure 2.8) is quite interesting since it presents two stable trajectories: the stable fixed point (stable for the subthreshold dynamics) and a stable tonic spiking trajectory (stable from the spikes point of view).

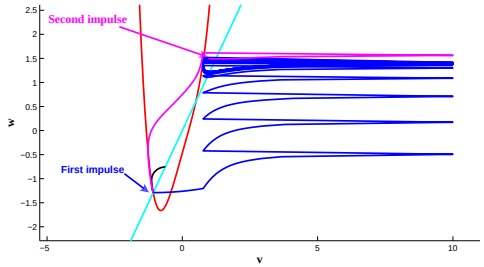

(a) Bistability: return to equilibrium via the same impulse

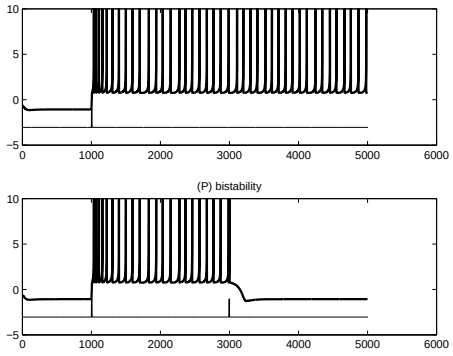

(b) Bistability

Figure 2.8: Bistability phenomenon: The first impulse induces a self-sustained tonic spiking behavior while the system has a stable fixed point. The second impulse perturbs this regular spiking behavior, and the system falls in the attraction basin of the stable fixed point.

- (xviii)/(xx) *Self-sustained subthreshold oscillations and purely oscillating mode*: They are linked with the supercritical Hopf bifurcation and its stable periodic orbit. These two behaviors cannot be obtained in the IBG models since the Hopf bifurcations are always subcritical.

2.4.3 Self-sustained subthreshold oscillations in cortical neurons

In this study we gave a set of sufficient conditions to obtain an IBG-like model of neuron. In this framework we proposed a model that displays a Bautin bifurcation the IBG neurons lack; as a consequence our model can produce subthreshold oscillations. In this section, we explain from a biological point of view the origin and the role of those oscillations and reproduce in vivo recordings.

In the IBG models, the Andronov–Hopf bifurcation is always subcritical. The only oscillations created in these models are damped (see Figure 2.10(a)) and correspond in the phase plane to the convergence to a fixed point where the Jacobian matrix has complex eigenvalues. Our quartic model undergoes supercritical Andronov–Hopf bifurcations, and so there are attracting periodic solutions. This means that the neurons can show self-sustained subthreshold oscillations (Figures 2.10(b) and 2.10(c)), which is of particular importance in neuroscience.

Most biological neurons show a sharp transition from silence to a spiking behavior, which is reproduced in all the models of class (2.1). However, experimental studies suggest that some neurons may experience a regime of small oscillations [184]. These subthreshold oscillations can facilitate the generation of spike oscillations when the membrane gets depolarized or hyperpolarized [186, 187]. They also play an important role in shaping specific forms of rhythmic activity that are vulnerable to the noise in the network dynamics.

For instance, the inferior olive nucleus, a part of the brain that sends sensory information to the cerebellum, is composed of neurons able to support oscillations around the rest potential. It has been shown by Llinás and Yarom [186, 187] that the

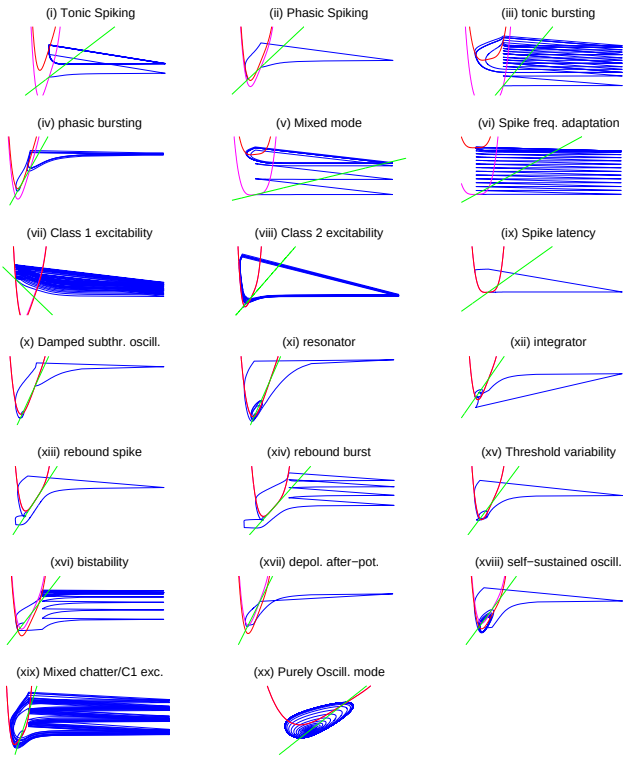

Figure 2.9: Phase diagrams corresponding to the behaviors presented in Figure 2.5.

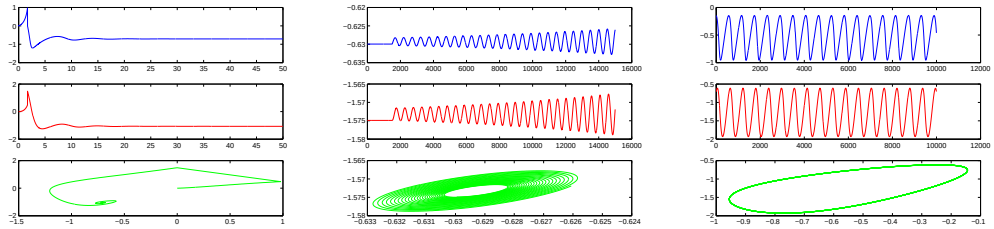

(a) Damped oscillations (b) Transient phase towards the self-sustained oscillations (c) Self-sustained oscillations (stationary state)

Figure 2.10: The quartic model shows damped subthreshold oscillations like the IBG models (Figure 2.10(a)): the trajectory collapses to a fixed point (parameters: $a = 1$, $b = 1.5$, $I = 0.1$, $T_{max} = 100$, $dt = 0.01$). The upper (blue) curve represents the solution in v, the middle (red) one w, and the lower one (green) the trajectory in the plane (v,w). Self-sustained subthreshold oscillations of the quartic model (Figures 2.10(b) and 2.10(c)): the trajectory is attracted towards a limit cycle (parameters: $a = 1$, $b = 5/2$, $I = -3(a/4)^{4/3}(2a-1)$, $T_{max} = 150000$, $dt = 0.01$, $I = (-3(a/4)^{4/3}(2a-1)+0.001)$.

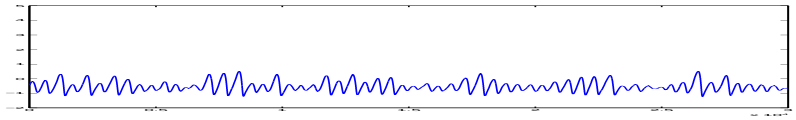

(a) Without spiking

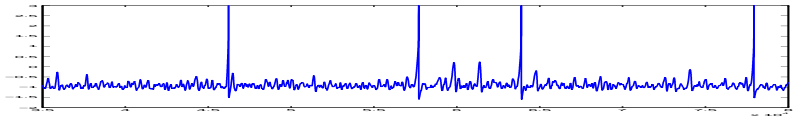

(b) With intermittent spiking

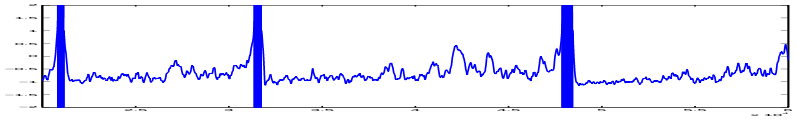

(c) With intermittent bursting

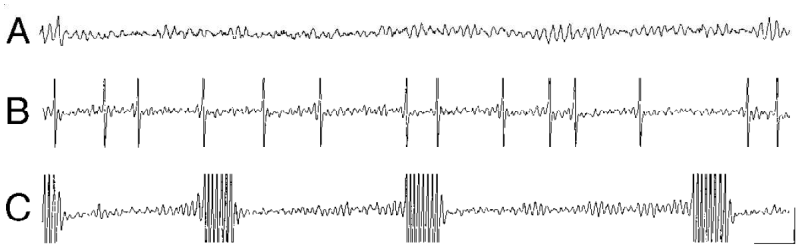

(d) Biological recordings

Figure 2.11: Subthreshold membrane oscillations, qualitatively reproducing the recordings from [183] in DRG neurons. Traces illustrate (2.11(a)) oscillations without spiking, (2.11(b)) oscillations with intermittent spiking, and (2.11(c)) oscillations with intermittent bursting (in the figures, spikes are truncated). The noisy input is an Ornstein–Ulhenbeck process. The biological recordings 2.11(d) are reproduced from [183, *Fig.* 1*J* and used with permission.

precision and robustness of these oscillations are important for the precision and the robustness of spike generation patterns. The quartic model is able to reproduce the main features of the inferior olive neuron dynamics:

i. autonomous subthreshold periodic and regular oscillations (see intracellular recordings of inferior olive neurons in brain stem slices in [187]),

ii. rhythmic generation of action potentials.

The robust subthreshold oscillations shown by in vivo recordings [22, 184, 187] correspond in our quartic model to the stable limit cycle coming from the supercritical Hopf bifurcation. The oscillations generated by this cycle are stable, and they have a definite amplitude and frequency. This oscillation occurs at the same time as the rhythmic spike generation in the presence of noisy or varying input. Note that other neuron models such as those studied above, even if they do not undergo a supercritical Hopf bifurcation, can also exhibit oscillations in the presence of noise, for instance near a subcritical Hopf bifurcation. Nevertheless, these oscillations do not have the regularity in the amplitude and the frequency linked with the presence of

an attracting limit cycle. The results we obtain simulating the quartic model are very similar to those obtained by in vivo recordings (see Figure 2.11).

But the inferior olive neurons are not the only neurons to present subthreshold membrane potential oscillations. For instance, stellate cells in the enthorhinal cortex demonstrate theta frequency subthreshold oscillations [5, 6, 157], linked with the persistent Na^+ current I_{NaP}.

We now conclude this section on the specific example of subthreshold self-sustained oscillations given by the dorsal root ganglia (DRG) neuron. This neuron presents subthreshold membrane potential oscillations coupled with repetitive spike discharge or burst, for instance in the case of a nerve injury [10, 183]. Figure 2.11(d) shows biological in vivo intracellular recordings performed by Liu et al. [183] from a DRG neuron of an adult male rat. The recorded membrane potentials exhibit high frequency subthreshold oscillation in the presence of noise, combined with a repetitive spiking or bursting. These behaviors can be reproduced by the quartic model, as we can see in Figure 2.11, around a point where the system undergoes a supercritical Hopf bifurcation.[4]

Conclusion

In this chapter we defined a general class of neuron models able to reproduce a wide range of neuronal behaviors observed in experiments on cortical neurons. This class includes the Izhikevich and the Brette–Gerstner models, which are widely used. We derived the bifurcation diagram of the neurons of this class and proved that they all undergo the same types of bifurcations: a saddle-node bifurcation curve, an Andronov–Hopf bifurcation curve, and a codimension two Bogdanov–Takens bifurcation. We proved that there was only one other possible fixed-point bifurcation, a Bautin bifurcation. Then using those theoretical results we proved that the Izhikevich and the Brette–Gerstner models had the same bifurcation diagram.

This theoretical study allows us to search for interesting models in this class of neurons. Indeed, Theorem 2.1.8 ensures us that the bifurcation diagram will present at least the bifurcations stated. This information is of great interest if we want to control the subthreshold behavior of the neuron of interest.

Following these ideas, we introduced a new neuron model of our global class undergoing the Bautin bifurcation. This model, called the *quartic model*, is computationally and mathematically as simple as the IBG models and able to reproduce some cortical neuron behaviors which the IBG models cannot reproduce.

This study focused on the subthreshold properties of this class of neurons. The adaptative reset of the model is of great interest and is a key parameter in the repetitive spiking properties of the neuron. Its mathematical study is very rich. A new insight of its properties is given in chapter 3. This study also allows us to define new electrophysiological classes of neuron, i.e. sets of parameters for which the neuron has the same qualitative behaviors in response to different stimulations. These results are provided for the general model and in the particular case of the adaptive exponential model [30] in chapter 4, were we explain the origin of different behaviors observed in the neuron.

[4] The amplitude and frequency of the subthreshold oscillations can be controlled choosing a point on the supercritical Hopf bifurcation curve.

CHAPTER 3

SPIKING DYNAMICS OF BIDIMENSIONAL INTEGRATE-AND-FIRE NEURONS

Craziness is like heaven.
– Jimi Hendrix

ABSTRACT

The class of non-linear integrate and fire neuron models introduced in the previous chapter are hybrid dynamical systems combining differential equations and discrete resets, which generate complex dynamics. The dynamical properties of the subthreshold system has studied in chapter 2. This previous study does not account for the spiking properties of the model. We study in this chapter the spike patterns produced by these models. These patterns of activity are the result of an interplay between the continuous subthreshold dynamics and the reset process. Interestingly, the reset induces in bidimensional models behaviors only observed in higher dimensional continuous systems such as bursting and chaos.

This is why in the first section we study in depth the subthreshold dynamical system, and characterize its main dynamical properties. We then introduce a suitable framework in order to study the spike dynamics through the use of a discrete map, called the adaptation map. The relationship between spiking behavior and dynamical properties of the map is then investigated. We show in particular that the system can exhibit a transition to chaos via a cascade of period adding including chaotic transitions, which was previously observed in Hodgkin-Huxley models and in Purkinje cells.

This work was done in collaboration with Romain Brette, has been published as a research report [259] and is still in preparation for publication.

Contents

3.1 Introduction

As stated in chapter 2, finding a computationally simple and biologically realistic model of neuron has been a great endeavor in computational neuroscience, the main interest being to be able to obtain mathematically tractable models in order to understand the nature of the nerve cell activity, and computationaly simple in order to be able to compare experimental recordings with large scale brain models. The class of nonlinear bidimensional spiking neuron models with adaptation defined in section 2 and also studied for instance in [30, 144, 255] seems to present the advantages of being mathematically tractable, efficiently implemented, and able to reproduce a large number of electrophysiological signatures such as bursting or regular spiking. These models emulate the membrane potential of the nerve cell v together with an adaptation variable w, and distinguishes between to phases of the neuronal activity: the *subthreshold* behavior corresponding to the input integration at the level of the cell, and the emission of action potentials (spikes). The subthreshold dynamics is governed by the following ordinary differential equation:

$$\begin{cases} \frac{dv}{dt} = F(v) - w + I \\ \frac{dw}{dt} = a(bv - w) \end{cases} \tag{3.1}$$

where a, b are real parameters accounting respectively for the time constant ratio between the adaptation variable and the membrane potential and to the coupling strength between these two variables, I is a real parameter modeling a DC-input current in the neuron, and F is a real function accounting for the leak and spike initiation currents. Following [255], we assume F to be regular (at least three times continuously differentiable), strictly convex, and its derivative to have a negative limit at $-\infty$ and an infinite limit at $+\infty$. In order to ensure that the neuron will elicit spikes, we add the following assumption:

Assumption 3.1.1. There exists $\varepsilon > 0$ such that $F(v)$ grows faster than $v^{1+\varepsilon}$ when $v \to \infty$ (i.e. there exists $\alpha > 0$ such that $F(v)/v^{1+\varepsilon} \geq \alpha$ when $v \to +\infty$).

We prove in section 3.2.4 that the membrane potential blows up in finite time in these cases. Among these models, the *quadratic adaptive* model [144] corresponds to the case where $F(v) = v^2$, and has been recently used by Eugene Izhikevich and coworkers [147] in very large scale simulations of neural networks. The *adaptive exponential* model [30] corresponds to the case where $F(v) = e^v - v$, is based on an electrophysiological description of the sodium current responsible for the generation of action potentials following the work of [95], has the interest that its parameters can be related to electrophysiological quantities, and has been successfully fit to intracellular recordings of pyramidal cells [51, 155]. The *quartic* model [255] corresponds to the case where $F(v) = v^4 + 2av$ and has the advantage of being able to reproduce all the behaviors featured by the other two and also self-sustained subthreshold oscillations which are of particular interest to model certain nerve cells.

As we proved in [256] and in chapter 5, in the case of the quadratic adaptive model (or when the function F diverges slower than v^2 when $v \to \infty$, i.e. when there exists $V_F > 0$ such that $F(v)/v^2$ is bounded for $v \geq V_F$), the adaptation variable blows up at the same time as the membrane potential. In these cases one is led to introduce a hard threshold, the cutoff value θ, which has no biophysical interpretation. A spike is emitted at the time t^* when the membrane potential v reaches a cutoff value θ, and the membrane potential is instantaneously reset to a constant value v_r and the

adaptation variable is updated to $w(t^*)+d$ where $w(t^*)$ is the value of the adaptation variable at the time of the spike and $d>0$ is the spike-triggered adaptation parameter. The spiking properties are highly sensitive to changes in this cutoff parameter (see chapter 5), and therefore constitutes a new bifurcation parameter which artificially adds complexity to the model.

In this chapter, we are interested in models for which the adaptation variable does not blow up. In this case, spikes are emitted when the membrane potential blows up. Therefore we shall consider models with an F function satisfying the following assumption:

Assumption 3.1.2. There exists $\varepsilon>0$ such that F grows faster than $v^{2+\varepsilon}$ when $v\to\infty$ (i.e. there exists $\alpha>0$ such that $F(v)/v^{2+\varepsilon}\geq\alpha$ when $v\to\infty$).

In these cases as proved in [256] (see also section 3.2.4), the membrane potential blows up in finite time and at this explosion time the adaptation variable will converge to a finite value. A spike is emitted at the time t^* when the membrane potential blows up. At this time, the adaptation variable converges to the value

$$w(t^{*-}) \stackrel{\text{def}}{=} \left(\lim_{t\to t^*} w(t)\right).$$

At spike time, the membrane potential is reset to a constant value v_r and the adaptation variable is incremented by a positive quantity, the spike-triggered adaptation parameter:

$$v(t) \xrightarrow[t\to t^*]{} \infty \implies \begin{cases} v(t^*) = v_r \\ w(t^*) = w(t^{*-}) + d \end{cases} \tag{3.2}$$

In these models, the reset mechanism makes the value of the adaptation variable at the time of the spike critical. Indeed, when a spike is emitted at time t^*, the new initial condition of the system (3.1) is $(v_r, w(t^*)+d)$. Therefore, this value governs the subsequent evolution of the membrane potential, and hence the spike pattern produced.

These models are *hybrid* dynamical systems, in the sense that they are defined by both a continuous and a discrete dynamical system. This structure make these models very interesting. Indeed the addition of the reset to the bidimensional continuous dynamical systems makes possible behaviors which cannot appear in autonomous bidimensional nonlinear ordinary differential equations, such as bursting and chaos (see [30, 141, 255] and figure 2.5). In this chapter we will rigorously study from a mathematical point of view these different behaviors, in order to understand their origin and to get insights about the related parameter ranges.

To this end, we precisely study in section 3.2 the orbits of equation (3.1) in the phase plane (v,w) in order to characterize the value of the adaptation variable at the time of the spike. We will be particularly interested in the attraction basins of the subthreshold attractors (SA), i.e. non spiking (bounded) attractors of the models. We will also introduce an essential tool to study the spike patterns, the adaptation map Φ. We will show that the properties of this map are closely linked with the dynamical properties of the subthreshold system. Section 3.3 will be devoted to the case where the subthreshold system has no fixed point. In that case, the neuron will fire whatever its initial condition. Therefore the study of the iterations of the map Φ will allow us to discriminate between different modes of tonic spiking. Section 3.4 is devoted to the case where there exist non-spiking (subthreshold) orbits. In this case,

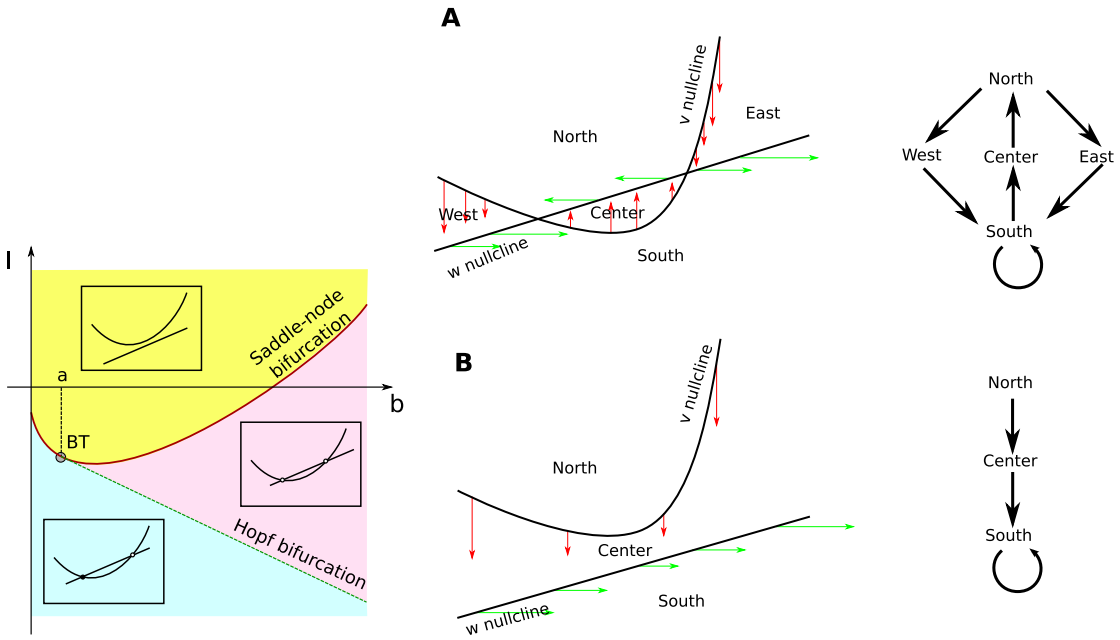

(a) Fixed Points and Stability

(b) Nullclines and symbolic dynamics

Figure 3.1: (a): Number of fixed points and their stability in the plane (I, b) for the exponential adaptive model. (b): Nullclines of the dynamical system (horizontal axis: v; vertical axis: w). A. The nullclines intersect in two points, and divide the phase space into 5 regions. The potential V increases below the V-nullcline, w increases below the w-nullcline. The direction of the flow along each boundary gives the possible transitions between regions (right). Spiking can only occur in the South region. B. The nullclines do not intersect. All trajectories must enter the South region and spike.

depending on the initial condition, the system can either fire infinitely many spikes (tonic spiking) or finitely many spikes (phasic spiking). In the last section 3.5 we comment these results from a neurocomputational viewpoint.

3.2 Detailed study of the subthreshold dynamics

In order to study the spike dynamics, we first need to understand the underlying continuous dynamical system defined by the differential equations. We shall call *subthreshold orbits* the orbits that do not spike (i.e., bounded orbits for positive time). Among these orbits, we will be particularly interested in the *subthreshold attractors* (SA), which are the non spiking (bounded) attractors of the subthreshold system. Since the subthreshold system is a bidimensional continuous dynamical system, these SAs are either fixed points or limit cycles.

3.2.1 Subthreshold Attractors

The number and stability of fixed points were studied in [255], and this study accounts for many excitability properties of these models, as described in [258]. The basic local bifurcation structure is given in figure 3.1(a). The parameter a is a scal-

ing parameter, and as a function of b and I the set of fixed points has the following structure: let us denote $v^*(x)$ the unique solution, when it exists, of the equation $F'(v^*(x)) = x$, and by $F'_{-\infty}$ the limit of $F'(x)$ for $x \to -\infty$. This value can be either finite (but nonpositive) or equal to $-\infty$. Note that because of the strict convexity assumption, if there exists a solution, it is unique. Furthermore, $v^*(x)$ is defined for any $x \in (F'_{-\infty}, \infty)$. For x in this interval, we denote $m(x) = F(v^*(x)) - xv^*(x)$ the unique minimum of the application $t \mapsto F(t) - xt$. We have:

i. If $I > -m(b)$, the system has no fixed point.

ii. If $I = -m(b)$, the system has a unique fixed point, $(v^*(b), w^*(b))$, which is nonhyperbolic. It is unstable if $b > a$. Along this curve in the parameter space (I,b), the system undergoes a saddle-node bifurcation provided that $F''(v^*(b)) \neq 0$.

iii. If $I < -m(b)$, then the dynamical system has two fixed points $(v_-(I,b), v_+(I,b))$ such that

$$v_-(I,b) < v^*(b) < v_+(I,b).$$

The fixed point $v_+(I,b)$ is a saddle fixed point, and the stability of the fixed point $v_-(I,b)$ depends on I and on the sign of $(b-a)$:

(a) If $b < a$, the fixed point $v_-(I,b)$ is attractive.

(b) If $b > a$, it depends on the input current I with respect to the value $I_H(a,b) = bv^*(a) - F(v^*(a))$.

(c) At the point $b = a$ and $I = -m(a)$, the system undergoes a Bogdanov-Takens bifurcation provided that $F''(v_a) \neq 0$. Therefore, from this point, there is a saddle homoclinic bifurcation curve characterized in the neighborhood of the Bogdanov–Takens point by

$$(P) \stackrel{\text{def}}{=} \left\{ (I, b \geq a)\, ; I_{Sh} = -m(a) + -\frac{12}{25}\frac{(b-a)^2}{F''(v^*(a))} + o(|\,(b-a)^2\,|) \right\}. \tag{3.3}$$

(c.1) If $I < I_H(a,b)$, the fixed point $v_-(I,b)$ is attractive.

(c.2) If $I > I_H(a,b)$, the fixed point $v_-(I,b)$ is repulsive.

(c.3) On the parameter line given by

$$(AH) \stackrel{\text{def}}{=} \left\{ (b,I)\ ;\ b > a \ \text{ and } \ I = I_H(a,b) = bv^*(a) - F(v^*(a)) \right\},$$

the system undergoes an Andronov Hopf bifurcation, whose type is given by the sign of the variable

$$A(a,b) = F'''(v^*(a)) + \frac{1}{b-a}F''(v^*(a))^2.$$

If $A(a,b) > 0$, then the bifurcation is subcritical, and if $A(a,b) < 0$, then the bifurcation is supercritical. If furthermore we have $F'''(v^*(a)) < 0$ and some technical conditions fulfilled, then the system undergoes a Bautin bifurcation at the point $v^*(a)$ for $b = a - \frac{F''(v^*(a))^2}{F'''(v^*(a))}$ and $I = bv^*(a) - F(v^*(a))$.

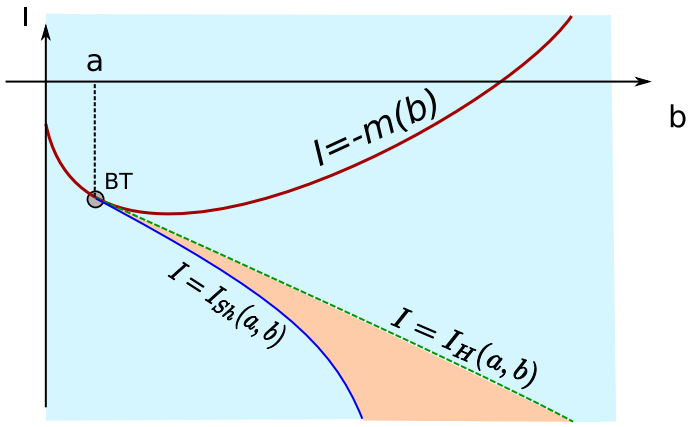

Figure 3.2: Unstable limit cycles in the case where there is no Bautin bifurcation. The system has no periodic orbit in the blue zone, and a unique unstable periodic orbit in the orange zone. For a fixed $b > a$, the family appears via Hopf bifurcation at $I = I_H$ and disappears via saddle-homoclinic bifurcation at $I = I_{Sh}$. BT is the Bogdanov-Takens bifurcation point.

Let us now discuss the number and stability of periodic orbits. First of all, when the subthreshold system has no fixed point, it is clear that no limit cycle can exist, because in planar systems, the existence of a cycle implies the existence of at least one fixed point inside the cycle. In the case where the Hopf bifurcation is always subcritical the system will present unstable cycles originating from the Hopf bifurcation for $b > a$, which will collide with the saddle fixed-point manifold and disappear via saddle-homoclinic bifurcation around the Bogdanov-Takens bifurcation (see figure 3.2). For input currents between the current value corresponding to the Hopf and the saddle-homoclinic bifurcation, there exists an unstable cycle in the system. The saddle-homoclinic bifurcation curve can then be continued, and it either remains finite for all $b > a$, or tend to $-\infty$, in which case cycles would exist for any I smaller than the current associated with the Hopf bifurcation. Because of the structure of the vector field presented in figure 3.1(b).A., cycles necessarily contains the fixed point v_-, and do not include the fixed point v_+, because the intersection of the South zone and the set $\{v \geq v_+\}$ is stable and therefore no trajectory can escape from this zone. At a subcritical Hopf bifurcation, cycles appear around the fixed point v_-, and inflate when decreasing the input current until reaching the saddle fixed point v_+.

In the cases where the system undergoes a Bautin bifurcation, the structure of the limit cycles is slightly more complex. Indeed, in addition to the subcritical Bogdanov-Takens bifurcation, the system undergoes a Bautin bifurcation. Locally around this point, a family of stable limit cycles and family of unstable ones coexist, collide and disappear via a fold (saddle-node) bifurcation of limit cycles. We numerically computed these two curves in the case of the quartic model using the MatCont toolbox [71, 72] and present the results in figure 3.3. We observe that for $b < a$, there is no limit cycle (zone (0)).

I. For $a < b < b_{CLC}$, there is one family of limit cycles, starting from Hopf bifurcation and disappearing via saddle-homoclinic bifurcation.

II. For $b_{CLC} < b < b_{GH}$ the family of limit cycles undergoes two folds of limit cycles. There are two branches of unstable limit cycles and a branch of stable

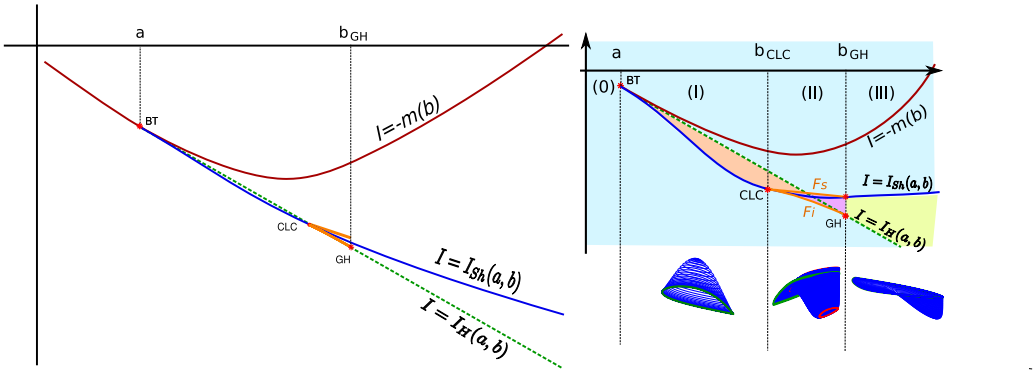

(a) Bifurcation Diagram (generated with MatCont) (b) Zoom and Limit Cycles

Figure 3.3: Limit cycles in the case where a Bautin bifurcation exist. The saddle-node of limit cycles presents a singular point corresponding to a cusp of limit cycles. From this point emerge two branches of saddle-node of limit cycles. The lower branch of folds of limit cycles connects to the Bautin point, while the upper branch connects with the saddle-homoclinic bifurcation. (a) The orange curve represents the fold of limit cycles, the singular point CLC corresponds to a cusp of limit cycles. In the blue region there is no limit cycle. Zone (0) : No cycle. Zone (I): There exists a unique family of limit cycles in the orange zone, starting from Hopf bifurcation and disappearing via saddle-homoclinic bifurcation. Zone (II) the family of limit cycles undergoes two folds of limit cycles. There are two branches of unstable limit cycles and a branch of stable limit cycles. The family appears via subcritical Hopf bifurcation and disappears via saddle-homoclinic bifurcation. In zone (III) there is a unique family of stable limit cycles in the yellow zone for inputs between the saddle-homoclinic and the supercritical Hopf bifurcation, disappearing via saddle-homoclinic bifurcation. (b) Families of limit cycles in each case. Green cycle = saddle-homoclinic orbit, red cycle= fold of limit cycle.

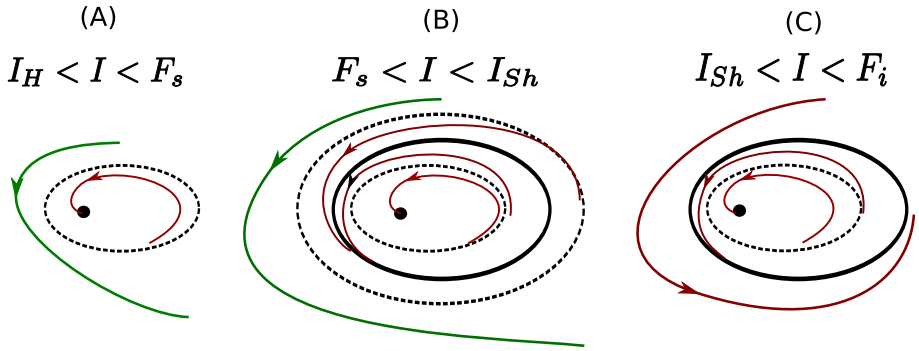

Figure 3.4: Families of limit cycles in zone (II) of the diagram corresponding to $b_{CLC} < b < b_{GH}$. Dashed cycles correspond to unstable periodic orbits, plain cycles to stable periodic orbit, the black dot symbolizes the fixed point. Red orbits are those attracted by the stable limit cycles or fixed point, and green orbits the other ones.

limit cycles. One of the branches of unstable limit cycles disappears via saddle-homoclinic bifurcation.

III. For $b > b_{GH}$ there is a unique family of stable limit cycles in the green zone emerging from a supercritical Hopf bifurcation and disappearing via saddle-homoclinic bifurcation.

In zones (0),(I) and (III) the structure of limit cycles is quite simple. Case (II) is more complex and needs some attention (see figure 3.4). In this case, the Bautin bifurcation generates a fold of limit cycles bifurcation in its neighborhood. We observe numerically that the curve of fold of limit cycles has a singular point where the system undergoes a cusp of limit cycles. Between the Bautin bifurcation point and the cusp of limit cycles point, the curve of folds of limit cycles can be parameterized as the graph of a function of b: $\{(I,b);\, I = F_i(b)\}$. The second branch of fold of limit cycles branching to the first one at the cusp point disappears via saddle-homoclinic bifurcation. It can also be characterized as the graph of a function of b: $\{(I,b);\, I = F_s(b)\}$. For $I_H < I < F_s$ there is a unique unstable limit cycle around the stable fixed point. For $F_s < I < I_{Sh}$ there are three limit cycles, two unstable limit cycles circle a stable limit cycle. For $I_{Sh} < I < F_i$ there are two limit cycles: an unstable around the fixed point, circled by a stable one. Therefore, in that case, the system presents self-sustained subthreshold oscillations before the Bautin bifurcation. Note eventually that zone (II) is relatively small in the parameter space.

The presence of periodic orbits shapes the structure of the stable manifold of the saddle-fixed point. We describe now the topology of this stable manifold and the shape of the attraction basins of the possible subthreshold attractors.

3.2.2 Stable manifold and attraction basins

We are now interested in the structure of the attraction basins of SAs. A point (v,w) belongs to the attraction basin of a SA if and only if the system (3.1) starting from this point converges towards this attractor. The topology of this set is governed by the subthreshold dynamics, and the problem of identifying in a closed form the attraction basin of the SAs is very hard to handle formally. Nevertheless in our particular case, the structure of these attraction basins can be characterized because the system has

the property that the shape of this attraction basin is closely related to the structure of the stable manifold of the saddle fixed point (SMSFP).

The first order expansion of the SMSFP around the saddle fixed point is given by the eigenvalues and eigenvectors of the Jacobian matrix at this point. The SMSFP is composed of two submanifolds: one of them is locally contained in the zone $v \geq v_+$ which we denote Γ^+ and the other in the zone $v \leq v_+$ and will be denoted Γ^-. In all the cases, the submanifold Γ^+ is fully above the v-nullcline (i.e. $w \geq F(v) + I$), because of the direction of the eigenvectors of the Jacobian matrix at this point and of the shape of the vector field. This submanifold stays in the North zone described in figure 3.1(b) and this curve is the graph of an increasing function of v. The shape of the submanifold Γ^- locally in the zone $v \leq v_+$ and below the v-nullcline, depends on finer properties of the vector field, as we discuss in the sequel and in section 3.2.3.

Subcritical case:

We are first interested in the case where the system presents a unique repulsive periodic orbit. The description of the shape of the SMSFP is based on qualitative arguments including Cauchy–Lipschitz and Poincaré–Bendixon theorems. Since this orbit is a trajectory of the dynamical system, no solution can cross it because of the Cauchy-Lipschitz theorem. The attraction basin of the stable fixed point will therefore be delineated by the periodic orbit: any trajectory having its initial condition inside this closed orbit will necessarily converge to the fixed point because of the Poincaré-Bendixon theorem, and no solution starting outside this zone can converge towards this fixed point because it cannot cross the periodic orbit. Therefore, the attraction basin of the stable fixed point is the zone in the phase plane delineated by the unstable limit cycle. In that case, the submanifold Γ^- winds around this cycle. Indeed, this submanifold can be computed using the backward equation related to (3.1). If it is an unbounded orbit, this stable manifold will split the phase plane into two zones, one of which containing the unstable limit cycle and the stable fixed point. Any trajectory starting in the zone containing the stable fixed point will either converge to the fixed point if it is inside the attraction basin of this fixed point delineated by the unstable periodic orbit, or will be trapped inside this zone and will not enter inside the periodic orbit. In the latter case, this trajectory cannot diverge because of the structure of the trajectories and the shape of Γ^+. The Poincaré-Bendixon theorem would imply that there exists a stable fixed point or a stable periodic orbit in this zone which is not the case. Therefore the shape Γ^- will necessarily be bounded, and because of Poincaré-Bendixon's theorem, it will either converge to a fixed point or to a periodic orbit. Since there is no stable fixed point reachable by the stable manifold (the stable fixed point is repulsive for the backwards dynamics, and is trapped in the limit cycle), this orbit will converge to the limit cycle (see figure 3.5(a)).

In the cases where there is no unstable limit cycle around the SA (i.e. for $b < a$, or $b > a$ and $I < I_{Sh}$), the attraction basin of the SA will be unbounded, and its shape will be deduced from the shape of the SMSFP.

For the submanifold Γ^-, several cases can occur, depending on the limit of the derivative of F at $-\infty$, which we denote $F'_{-\infty}$.

- The stable manifold of the saddle fixed point can cross both nullclines (see figure 3.5(b)). As proved in [258], this will be the case when $F'_{-\infty} > -\infty$ and if $b \geq \frac{(F'_{-\infty}+a)^2}{4a}$,
- It can cross the w-nullcline (which will always be the case when $a < -F'_{-\infty}$) but

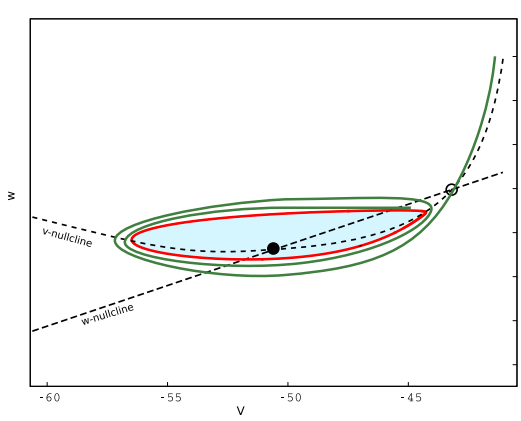

(a) Stable Manifold and limit cycle

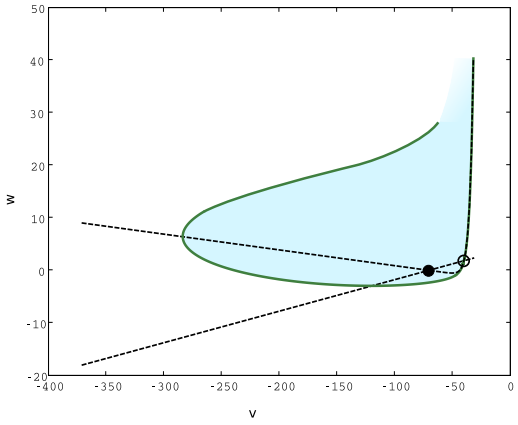

(b) Fixed point, separatrix crosses both nullcline

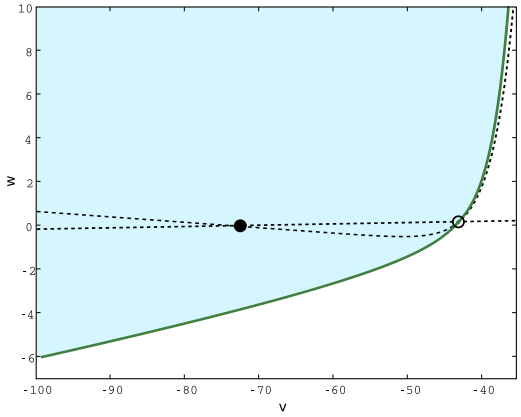

(c) Fixed point, separatrix crosses no nullcline

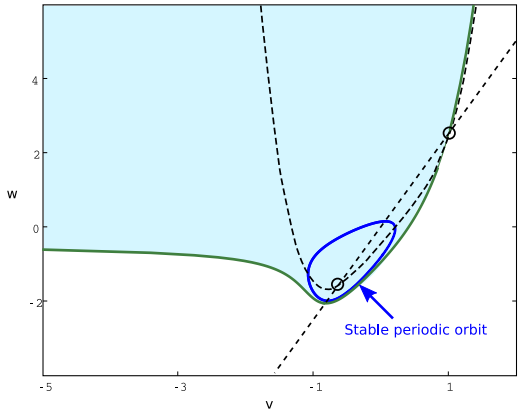

(d) Periodic orbit, separatrix crosses the w-nullcline

Figure 3.5: Representation of the attraction basin and the stable manifold of the saddle fixed point in different cases. (a): A repulsive limit cycle (red curve) exists around the stable fixed point (black circle), the SMSFP (green line) converges towards the cycle, and the attraction basin (blue zone) is bounded. The black dashed lines corresponds to the nullclines. (b): Case where the separatrix crosses both nullclines (same color code), in the case of the adaptive exponential model with original parameters except $a = 2g_L$ and $\tau_m = \tau_w$; (c): Case where the stable manifold crosses no nullcline: it is the graph of an increasing function of v which delineates the attraction basin of the stable fixed point (case of the dimensioned adaptive exponential model with the original parameters except $a = 2g_L$ and $\tau_w = \tau_m/3$); (d): Case where the stable manifold only crosses the w-nullcline. It was represented in the case where the stable trajectory is a periodic orbit (quartic model, $a = 1$, $b = 2.51 > b_{GH}$, $I = -0.5$).

not the v-nullcline. In this case, the SMSFP is the graph of a function of v, that will be decreasing before it crosses the nullcline and increasing after this point (see figure 3.5(d)),

- It can cross no nullcline, and in this case the separatrix is the graph of an increasing function of v (see figure 3.5(c)). This case never occurs when $F'_{-\infty} = -\infty$.

In these cases, the SMSFP is unbounded, and splits the phase plane into two connected components, one of which containing the SA. This component is the attraction basin of the SA.

Hence we conclude that the attraction bassin of the stable fixed point is either bounded and delineated by the unstable limit cycle, or unbounded and delineated by the stable manifold of the saddle fixed point.

Bautin case

This dichotomy also applies in the case where the system undergoes a Bautin bifurcation: if the SA (fixed point or stable periodic orbit) is circled by an unstable limit cycle, then the attraction basin of the SA will be delineated by this cycle, and if not, the attraction basin will be delineated by the SMSFP.

Consider for instance the case of figures 3.3 and 3.4. Using the notations of figure 3.3 we can prove that:

- When there is no fixed point, the system has no SA and there is no saddle fixed point.
- For $b < a$ and $I < -m(b)$, the system has a unique stable fixed point whose attraction basin is unbounded and delineated by the SMSFP.
- For $a < b < b_{CLC}$, the case is very similar to the subcritical case and the behavior depends on the input current:
  - If $I_H < I < -m(b)$ the system has no SA and two unstable fixed points. This case is treated in section 3.2.3.
  - If $I_{Sh} < I < I_H$ where I_{Sh} is the value of the current at the saddle-homoclinic bifurcation, the system has a unique SA which is a stable fixed point, circled by an unstable limit cycle. This periodic orbit delineates the attraction basin of the stable fixed point and the SMSFP winds around it
  - If $I < I_{Sh}$ the system has a unique stable fixed point whose attraction basin is unbounded and delineated by the SMSFP.
- For $b_{CLC} < b < b_{GH}$, we have:
  - For $I_{SN} < I < \max(I_H, F_s)$ there are two unstable fixed points and no periodic orbit, hence no SA.
  - For $\max(I_H, F_s) < I < F_s$, the system has a unique SA which is a stable fixed point, circled by an unstable limit cycle. This periodic orbit delineates the attraction basin of the stable fixed point and the SMSFP winds around it (case of figure 3.5(a)).

  - For $F_s < I < I_{Sh}$ the system has two SAs: a fixed point and a stable limit cycle (see figure 3.4(B)). The stable fixed point is circled by an unstable limit cycle which delineates its attraction basin. The stable periodic orbit is contained in a ring delineated by two unstable limit cycles. This ring is the attraction basin of the stable limit cycle. The submanifold Γ^- of the SMSFP winds around the exterior unstable limit cycle.
  - For $I_{Sh} < I < F_i$ the system has a stable fixed point whose attraction basin is delineated by an unstable periodic orbit circling around it (see figure 3.4(C)). Around this cycle there is a stable limit cycle, whose attraction basin is an unbounded zone with one hole delineated by the unstable limit cycle and the SMSFP which is unbounded.
  - For $I < F_i$ the system has a stable fixed point whose attraction basin is unbounded and delineated by the SMSFP.

- In the case $b > b_{GH}$, we have:
  - if $I_{Sh} < I < -m(b)$ the system has no SA and two unstable fixed points.
  - if $I_H < I < I_{Sh}$ the system has two unstable fixed points and a stable periodic orbit whose attraction basin is unbounded and delineated by the SMSFP.
  - if $I < I_H$ the system has a stable fixed point with an unbounded separatrix.

3.2.3 Heteroclinic orbits

In the case where there are two unstable fixed points, one of which is repulsive and the other saddle, then the component Γ^+ of the SMSFP is the graph of an increasing function of v for $v \geq v_+$ and stays above the v-nullcline. The submanifold Γ^- will connect to the repulsive fixed point, for the same reasons as mentioned in the case of the presence of an unstable limit cycle. Indeed, if we consider the backward equation starting in the neighborhood of the saddle fixed point, the repulsive fixed point of the forward dynamics becomes attractive, and it is the unique bounded trajectory possible. The stable manifold when considering the backward equation will either converge to the fixed point, or will diverge, according to Poincaré-Bendixon's theorem. But assuming that it is unbounded leads to a contradiction: if it was unbounded, it would separate two zones of the phase plane (see figure 3.5), one of which containing the unstable fixed point. A trajectory having its initial condition in this zone will be trapped in it for all $t > 0$. But in this zone, the trajectory will be bounded because of the structure of the vector field, but there is neither fixed point nor stable periodic orbit. Therefore Poincaré-Bendixon's theorem leads to a contradiction, and the stable manifold necessarily connects to the repulsive fixed point. This connection can be one of two types (see figure 3.6): a monotonous connection in the case where the eigenvalues of the Jacobian matrix of the repulsive fixed point are real, and an oscillating connection when the eigenvalues have a non-null imaginary part. This branch of stable manifold is therefore a heteroclinic orbit, connecting a repulsive equilibrium to a saddle equilibrium. It is structurally stable, and disappears at the Hopf bifurcation. In the case where the Hopf bifurcation is subcritical, the heteroclinic orbit connecting the repulsive fixed point and the saddle fixed point converts into a heteroclinic orbit connecting the saddle fixed point with the repulsive limit cycle and we are in the case of figure 3.5(a). In the case where the Hopf bifurcation is supercritical (after the Bautin bifurcation) the heteroclinic orbit will simply disappear. By continuity, the SMSFP will be, after the bifurcation, of type 3.5(b).

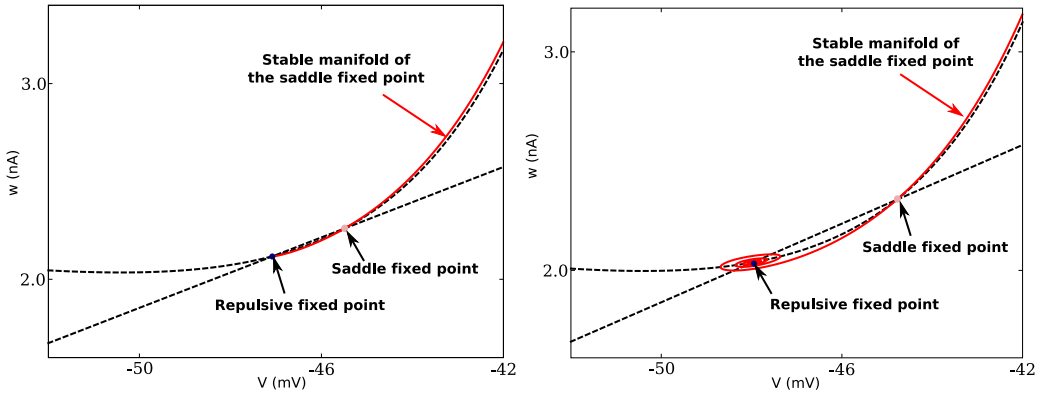

(a) Monotonous connection to equilibrium (b) Oscillatory connection to equilibrium

Figure 3.6: Stable manifold of the saddle fixed point in the case of two unstable equilibria. Dashed black curves are the nullclines of the system and the red curve is the stable manifold.

3.2.4 Symbolic dynamics and spiking regions

This detailed description of the subthreshold dynamics allows us to get a better insight of the dynamics and to make the diagram 3.1(b) more precise. Indeed, we are now able to provide a Markov partition of the phase plane (see fig.3.7).

- In the case $I > -m(b)$, there is no SA, and the phase plane is partitioned into the *up zone* above the v-nullcline, i.e. defined by $\{(v,w); w \geq F(v)+I\}$, the *center zone* between the two nullclines and the spiking zone below the w-nullcline $\{(v,w);\ w \leq bv\}$. We observe that any trajectory having its initial condition in the up zone enters in finite time the center zone. Indeed, while the orbit is in the up zone, the derivative of the adaptation variable is strictly inferior to $-d(F(v)+I, bv)$ the distance between the two nullclines. In the center zone, w is decreasing and v is increasing. Because of the vector field along the v-nullcline, we observe that the orbit cannot go back to the up zone. Since in this zone w is a decreasing function of v and the boundary bv an increasing function, it will enter in finite time the spiking zone. In this spiking zone defined by $w \leq bv$, the trajectory is trapped, and the membrane potential blows up in finite time.

- In the case where there are SAs, we reviewed the different shapes of the related attraction basins. These regions correspond to what we call the *rest* region, in the sense that any orbit starting inside this zone will never fire. This zone is stable under the dynamics, and does not communicate with the other zones (see figures 3.7(b), 3.7(c) and 3.7(d)). We define here again the spiking zone below both the w-nullcline and the SMSFP. This zone is also stable under the dynamics. The *right* zone is the zone above the w-nullcline and below the SMSFP. In this zone, for any initial condition below the v-nullcline, v is increasing and w decreasing. Therefore, the derivative of v increases, and the orbit will enter the spiking zone in finite time, since the orbit is a non-increasing function of v and the boundary is strictly increasing. If the initial condition is in the right zone below the SMSFP and above the v-nullcline, both v and w will be decreasing and therefore the orbit cannot stay above the v-nullcline indefinitely, because of the

presence of the unstable manifold of the saddle fixed point, and therefore will be in the right zone below the v nullcline after a finite time, and therefore in the spiking zone in finite time. The *up* zone is the rest of the phase plane. In this zone, orbits do not stay indefinitely, and cannot enter either the rest zone or the right zone, hence enter in finite time the spiking zone.

- In the cases where are two unstable fixed points and no stable limit cycles (Figures 3.7(e) and 3.7(f)), there is no SA except from the SMSFP. We define the *up* zone above both the w-nullcline and the SMSFP, the right zone the zone between the SMSFP and the w-nullcline and the *spiking* zone below both the w-nullcline and the SMSFP. In the spiking zone, as we will see, the system will fire. For any initial condition in the right zone, since the orbit will not cross the SMSFP, it will necessarily enter the spiking zone in finite time.

This is very important in terms of spikes. Indeed, we can prove that for any initial condition in the spiking region, the membrane potential v will blow up in finite time, and therefore a spike will be emitted. Indeed, let (v_0, w_0) be a given initial condition in the bottom region at time t_0. According to the shape of the vector field, as presented in our Markov partition, the whole trajectory will be trapped in this zone. But in this zone, we always have $w \leq v$ and therefore for all $t \geq t_0$ we have $w(t) \leq b\,v(t)$. According to Gronwall's theorem, the membrane potential at time $t \geq t_S$ will be greater than or equal to the solution of:

$$\begin{cases} \dot{\tilde{v}} & = F(\tilde{v}) - b\,\tilde{v} + I \\ \tilde{v}(t_S) & = v(t_S) \end{cases}$$

which blows up in finite time by the virtue of assumption 3.1.1.

Therefore any trajectory entering the bottom region will spike, and furthermore any trajectory having its initial condition outside the rest region will enter the bottom region in finite time, and elicit a spike. As we have seen, the dynamics of the reset after a spike depends on the value of the adaptation variable at the times of the spikes, which we describe in the following section.

3.2.5 Behavior of the adaptation variable at spike times

In the spiking zone, we saw that the membrane potential blew up in finite time. This zone does not intersect the v-nullcline. Therefore, in this zone, the orbit (v, w) with initial condition (v_0, w_0) at time t_0 inside the spiking zone can be written as the graph of a function of v for all $t \geq t_0$, i.e. $w(t) = W(v(t))$ where the function W is the solution of the differential equation:

$$\begin{cases} \frac{\mathrm{d}W}{\mathrm{d}v} = \frac{a(bv-w)}{F(v)-w+I} \\ W(v_0) = w_0 \end{cases} \tag{3.4}$$

Proof. Let $\delta(t) = W(v(t)) - w(t)$. We have $\delta(t_0) = 0$ and furthermore, since the value of $F(v) - w + I > 0$, $\frac{\mathrm{d}\delta}{\mathrm{d}t} = \frac{\mathrm{d}W}{\mathrm{d}v}\frac{\mathrm{d}v}{\mathrm{d}t} - \frac{\mathrm{d}w}{\mathrm{d}t} = 0$, and hence $\delta(t) \equiv 0$. □

To study the value of the adaptation variable at the explosion time of the membrane potential, we simply study the limit of the equation of the orbits when $v \to \infty$. Here we prove that this value is finite under assumption 3.1.2, and that if $F(v)/v^2$ is asymptotically bounded, the adaptation value tends to infinity. This theorem justifies the introduction of this assumption.

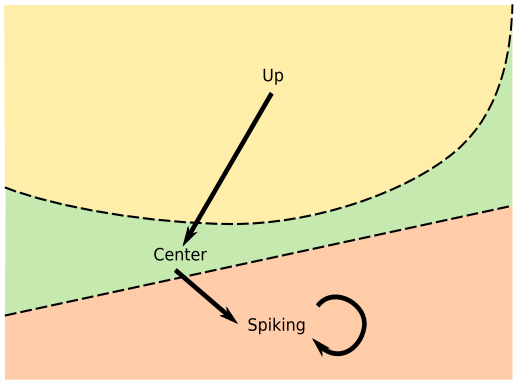

(a) No fixed point case

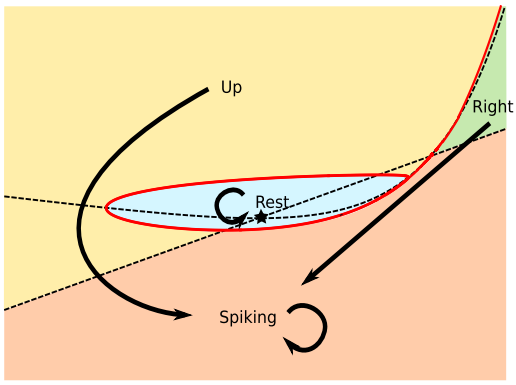

(b) Unstable limit cycle

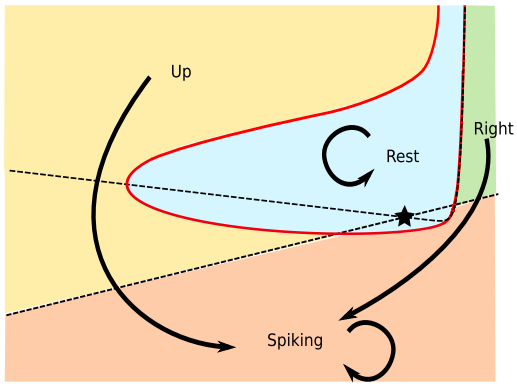

(c) Unbounded attraction basin crossing both nullclines

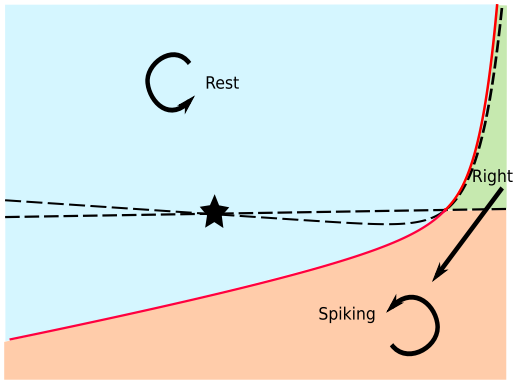

(d) Unbounded attraction basin crossing no nullcline

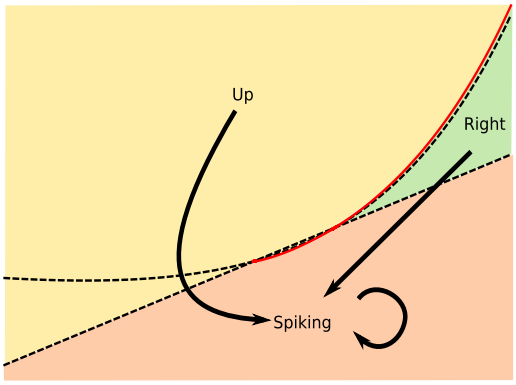

(e) Monotonous heteroclinic orbit

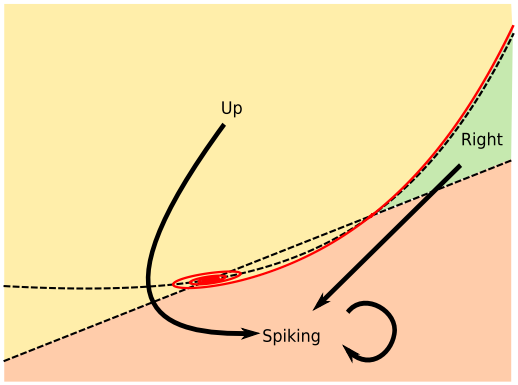

(f) Oscillatory heteroclinic orbit

Figure 3.7: Markov partition of the dynamics: the bottom region is a stable region where each trajectory starting from the up or right region will end up in finite time. The rest region composed of the attraction basin of the possible stable trajectory is an isolated region.

Theorem 3.2.1. *Under assumption 3.1.2, the adaptation variable is finite at the times of the spikes. If $F(v)/v^2$ is bounded when $v \to \infty$, the adaptation variable at the times of the spikes tends to infinity.*

Proof. In section 3.2.4, we proved that all the orbits of the system that are not in the attraction basin of the (possible) stable fixed point enter after a finite time the *spiking zone* where they are trapped. This spiking zone is fully included in the half space $\{w < bv\}$, and in this zone the membrane potential blows up in finite time.

The value of the adaptation variable at the time of the spike can therefore be computed using the orbital equation (3.4). We consider $(v(t), w(t))$ an orbit of the differential system (3.1) such that the membrane potential blows up at time t^*. Let $(v_1 = v(t_1), w_1 = w(t_1))$ be a point of the orbit inside the spiking zone. We recall that in the spiking zone, we have $w(t) \leq bv(t)$ and $w(t)$ is non-decreasing. Hence we have

$$\frac{\mathrm{d}W}{\mathrm{d}v} \leq \frac{a(bv - w_1)}{F(v) - bv + I} \tag{3.5}$$

and therefore

$$W(v) \leq w_1 + \int_{v_1}^{v} \frac{a(bu - w_1)}{F(u) - bu + I}\, du$$

If F satisfies assumption 3.1.2, this integral converges when $v \to \infty$. Therefore, $W(v)$ (resp. $w(t)$) is an upperbounded nondecreasing function of v (resp. time), and therefore has a finite value when $v \to \infty$ (resp. $t \to t^*$).

In the case where $F(v)/v^2$ is bounded, this integral does not converge. Using the same technique, we lowerbound this value:

$$\frac{\mathrm{d}W}{\mathrm{d}v} \geq \frac{a(b - W)}{F(v) - w_1 + I}. \tag{3.6}$$

Gronwall's theorem [117] ensures us that the solution of equation (3.4) will be lowerbounded for $v \geq v_1$ by the solution of the linear ordinary differential equation:

$$\begin{cases} \frac{\mathrm{d}z}{\mathrm{d}v} = \frac{a(b-z)}{F(v) - w_1 + I} \\ z(v_1) = w_1 \end{cases} \tag{3.7}$$

that reads:

$$z(v) = \left(\int_{v_1}^{v} \frac{abu}{F(u) - w_1 + I} e^{-g(u)}\, du + w_1 \right) e^{g(v)}$$

where $g(v) = \int_{v_1}^{v} -\frac{a\,du}{F(u) - w_1 + I}$. Because of assumption 3.1.1, the integrand is integrable, and the function g has a finite limit $g(\infty)$ when $v \to \infty$. The exponential terms will hence converge when $v \to \infty$. But the integral involved in the particular solution diverges in the case where $F(v)$ grows slower than v^2, since the integrand is equivalent when $u \to \infty$ to

$$\frac{abu}{F(u)} e^{-g(\infty)}$$

When $F(u)$ grows slower than v^2 there exists $\alpha > 0$ such that $F(v) \leq \alpha v^2$ asymptotically and therefore the solution of the linear differential equation (3.7) tends to infinity when $v \to \infty$ faster than a logarithmic function of v, and so does $W(v)$, and hence $w(t)$ blows up at the time when $v(t)$ blows up. In the case where $F(v)$ grows slower than $v^{2-\varepsilon}$, the solution of the differential equation diverges faster than v^{ε}. □

We conclude that in the case of the quadratic adaptive model, the adaptation variable blows up at the explosion time of the membrane potential variable v, and in the case of the quartic and exponential models, the adaptation variable remains bounded.

For the quadratic model, and models such that the nonlinear function $F(v)$ grows slower than a quadratic function when $v \to \infty$, the system can only be defined using a cutoff value for the spikes. The value of the adaptation variable at the cutoff θ will be given by $W(\theta)$, and therefore will heavily depend on the cutoff value, in a very sensitive way as discussed in [256].

In the quartic and exponential models, and for any model such that $F(v)$ grows faster than $v^{2+\varepsilon}$ for a given $\varepsilon > 0$, the adaptation variable converges, and hence the model can be defined with an infinite threshold.

In these cases, for technical reasons we will use a transformed version of the orbital equation (3.4) obtained by changing variables. For (v_0, w_0) in the spiking zone, we consider $u = (v - v_0 + 1)^{-\varepsilon/2}$ where $\varepsilon > 0$ is given by assumption 3.1.2. When $v(t)$ blows up, $u(t)$ tends to zero, and the orbit in the plane (v,u) satisfies the equation:

$$\begin{cases} \frac{d\tilde{W}}{du} = -\frac{2a(bu^{-2/\varepsilon} - \tilde{W} + \beta)}{\varepsilon u^{1+2/\varepsilon}(F(u^{-2/\varepsilon} + v_0 - 1) - \tilde{W} + I)} \stackrel{\text{def}}{=} g(u, \tilde{W}) \\ \tilde{W}(1) = w_0 \end{cases} \tag{3.8}$$

where $\beta = b(v_0 - 1)$

As we can see in equation (3.1), at the times where the membrane potential blows up and since the adaptation variable remains bounded, the derivative of the adaptation variable tends to infinity when v blows up. For this reason, accurate numerical simulations are quite hard to perform. But since in the phase plane the orbit has a regular equation, an accurate algorithm based on the simulation of the orbital equation as soon as the orbit enters the spiking zone provides a precise and stable evaluation of the adaptation value at the time of the spike using standard simulation algorithms (Runge-Kutta, Euler, ...). This method was implemented in order to produce our numerical simulations.

3.2.6 Existence and uniqueness of a solution

We first discuss the well-posedness of these equations. Mathematically, the problem is well-posed if the system defined by equations (3.1) and (3.2) together with an initial condition (v_0, w_0) at time t_0 has a unique solution defined for all $t \geq t_0$. The precise study we just performed gives us a better understanding of the dynamics of the subthreshold system. In particular, we saw that the solutions of the subthreshold equation (3.1) blew up in finite time, and under assumption 3.1.2, the adaptation variable at these times has a finite value. The solutions of the subthreshold equations are hence not defined for all time. The reset condition is therefore essential to have a forward solution to the problem defined for all $t \geq t_0$. The reset condition is sufficient for the problem to be well posed, as we prove in the following:

Proposition 3.2.2. The equations (3.1) and (3.2), together with initial conditions (v_0, w_0) at time t_0 have a unique solution defined for $t \geq t_0$.

Proof. Because of the regularity assumption on F, Cauchy-Lipschitz theorem of existence and uniqueness of solution applies for equation (3.1) up to the explosion time. If the solution of (3.1) does not blow up in finite time, we have existence and uniqueness of solutions for the problem. If the solution blows up at time t^*, then we are reset to

a unique point, defined by the reset condition (3.2), and we are again in the case we already treated starting from $(v_r, w(t^*)+d)$ at time t^*. We can apply this mechanism again provided since the value of $w(t^*)$ is finite. Furthermore, to be able to prove the existence and uniqueness of solution for all $t \geq t_0$, we need to ensure that the interspike interval does not tend to 0 (i.e. spikes do not accumulate at a given time). The spike time decreases when the value of the adaptation on the reset line decreases. Therefore we have to ensure that the adaptation value at the times of the spike do not tend to $-\infty$. But for w_0 in the spiking zone, the value of the adaptation variable is increasing all along the trajectory and therefore the new adaptation value after a spike is emitted will be greater than the former value plus d, and hence it is impossible that this reset value tends to $-\infty$. We conclude that the interspike interval has a lower bound on this trajectory, and between two spike times, there is a unique solution. Therefore we have existence and uniqueness of a solution starting from (v_0, w_0) which is defined for all $t \geq t_0$. □

Another interesting question from the mathematical and neural coding points of view would be to solve the related Cauchy problem. This problem consists in proving that there exists a unique solution defined for all $t \in \mathbb{R}$. The Cauchy problem was addressed by Romain Brette in [33] in the case of spiking models defined by a one dimensional ODE with a finite spiking threshold and a reset condition. He found that the reset introduced a countable and ordered set of backward solutions for a given initial condition, and that this structure of solutions had important implications in terms of neural coding. The case of the system given by (3.1) and (3.2) can be treated in the same fashion as done in [33] and one obtains the same results as Brette in [33]. It is done in appendix D.

3.2.7 The adaptation map

Now that we are ensured that there exists a unique solution to the forward problem given by equations (3.1) and (3.2), we are interested in characterizing the spike patterns fired by a neuron of this type. These patterns are governed by the initial condition of the system after each spike, and this is why we now introduce an essential element of our work, a discrete map called the adaptation map.

Definition 3.2.1 (The adaptation map)**.** We denote by $\mathscr{D}$ the domain of adaptation values w_0 such that the solution of (3.1) with initial condition (v_r, w_0) blows up in finite time. Let $w_0 \in \mathscr{D}$, and denote $(v(t), w(t))$ the solution of (3.1) with initial condition (v_r, w_0) and t^* the blowing time of v. The adaptation map Φ is the unique function such that

$$\Phi(w_0) = w(t^*) + d$$

The adaptation map gives the next reset location of a spiking orbit with initial condition on the *reset line* $v = v_r$. If we are interested in the spike patterns generated from an initial condition (v_0, w_0) where $v_0 \neq v_r$, the analysis will be valid after the first spike is emitted. More precisely, if (v_0, w_0) is in the attraction basin of a bounded trajectory or on the stable manifold of the saddle fixed point, then it will not elicit a spike. If it is not, then it will fire in finite time and be reset on the line $v = v_r$ at a given value w_1. From this point, the study of the iterations of the map Φ will be valid.

Moreover, assume that in the dynamical system defined by (3.1) starting from the initial condition (v_r, w_0) is in a tonic spiking behavior (i.e. fires infinitely many spikes). Then let $(t_n)_{n\geq 0}$ be the sequence of spike times, and define the sequence of adaptation

reset points by $w_n \stackrel{\text{def}}{=} w(t_n) = w(t_n^-) + d$. The adaptation map of this dynamical system is the function Φ such that

$$\Phi(w_n) = w_{n+1}$$

Hence we will be able to apply techniques of nonlinear analysis of iterations of maps to study the spiking location sequences and the spiking times.

For these reasons, we will be interested in the sequel in the dynamics of the iterations of the map Φ which corresponds to a trajectory starting from an initial condition on the reset line. The intersections of the nullclines with the reset lines are of particular interest in the study of Φ. We define:

$$\begin{cases} w^* & = F(v_r) + I \\ w^{**} & = bv_r \end{cases} \tag{3.9}$$

Both points depend on the reset voltage v_r. Interestingly enough, besides v_r, the point w^* only depends on the input current and the nonlinearity, while the point w^{**} only depends on the parameter b. The figure Fig.3.8 represents bundles of trajectories for $w_0 < w^*$ or $w_0 > w^*$ in the case where the nullclines do not intersect. It illustrates the qualitative distinctions linked with the relative location of w with respect to w^*.

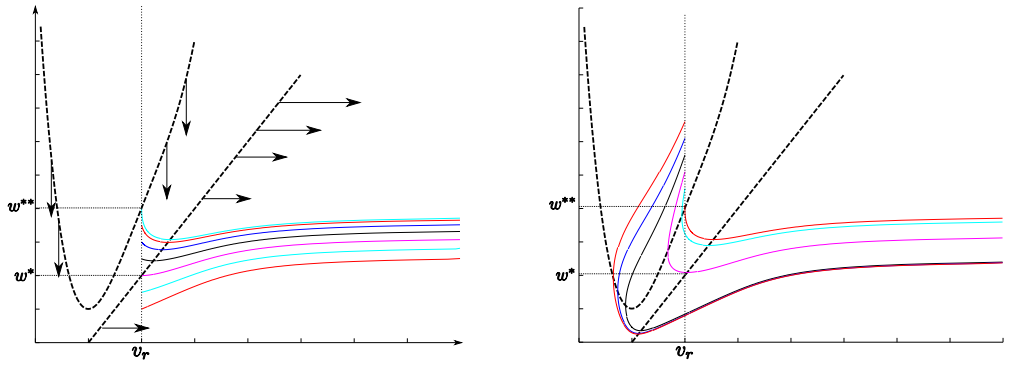

(a) Phase plane for $w_0 < w^*$ (b) Phase plane for $w_0 > w^*$

Figure 3.8: Phase plane and trajectories for the quartic model in the no-fixed point case. The trajectories starting from $w < w^{**}$ have an increasing w all along the trajectory, which is not the case for $w > w^{**}$. For $w > w^*$, we observe that the trajectory turns around the point (v_r, w^*) and crosses again the line $v = v_r$ before spiking.

The sequence of interspike intervals is the image of the orbit under Φ by the application $\mathscr{T} : w \in \mathscr{D} \mapsto t^*(w)$, where $t^*(w)$ is the spike time if the membrane potential starts at (v_r, w) at time $t = 0$. Although this map is not always injective, the spike patterns are qualitatively governed by the adaptation map.

Now that we introduced the main framework of our study, we will study more precisely the properties of the adaptation map Φ and its links with the spike patterns produced. The different spike patterns are linked with the topology of the domain $\mathscr{D}$ and with properties of the map Φ. We chose here to present our results in function of the subthreshold dynamical properties, since it will make our mathematical analysis clearer. We will summarize the different regions of parameters for which a given spike pattern is produced in section 3.5.2.

3.3 NO FIXED POINT CASE

In this section we consider the case where there is no fixed point in for the sub-threshold dynamical system. This case corresponds to the case where $I > -m(b)$. In that case the system has neither stable fixed point nor limit cycle, and hence no bounded trajectory, and the neuron will fire whatever its initial condition, which means that the definition domain $\mathscr{D}$ of the adaptation map Φ is $\mathbb{R}$.

3.3.1 Description of the adaptation map

We prove the following theorem.

Theorem 3.3.1. *In the case $I > -m(b)$ and under the condition 3.1.2, the adaptation map satisfies the following properties (see figure Fig.3.9):*

- *It is increasing on $(-\infty, w^*]$ and decreasing on $[w^*, \infty)$,*
- *For all $w < w^{**}$ we have $\Phi(w) \geq w + d \geq w$,*
- *Φ is regular (at least continuously differentiable),*
- *It is concave for $w < w^*$,*
- *It has a unique fixed point in $\mathbb{R}$,*
- *It has a horizontal asymptote (plateau) when $w \to +\infty$*

This theorem is important to understand the main properties of the *adaptation sequence* $(w_n)_{n\geq 0}$ starting from a given initial condition $w_0 \in \mathscr{D}$ defined by:

$$w_{n+1} = \Phi(w_n) \qquad n \geq 0 \tag{3.10}$$

These properties would be straightforward if we had a spiking threshold, the only technical intricacy is the fact that the spike occurs when the membrane potential blows up.

Proof. The proof of this theorem is mainly based on a characterization of the orbits in the phase plane, given by equations (3.4) and (3.8). Using these equations, the orbit of the system with initial condition (v_r, w_0) in the spiking zone (i.e. $w_0 \leq w^*$) can be written as:

$$\tilde{W}(u; w_0) = w_0 - \int_u^1 g(s, \tilde{W}(s, w_0))\, ds. \tag{3.11}$$

We have in particular

$$\Phi(w_0) = \lim_{u \to 0} \tilde{W}(u, w_0) + d. \tag{3.12}$$

- *Monotony:* Let $w_1(0) < w_2(0) \leq w^*$. The orbits $(v_1(t), w_1(t))$ having initial condition $(v_r, w_1(0))$ at time $t = 0$ and $(v_2(t), w_2(t))$ having initial condition $(v_r, w_2(0))$ at time $t = 0$ will never cross because of Cauchy-Lipschitz theorem. Since they both are in the center or in the spiking zone of diagram 3.7(a), they satisfy equation (3.4) and since they do not cross, we will always have $\tilde{W}_1(v) \leq \tilde{W}_2(v)$, and thus $\Phi(w_1(0)) \leq \Phi(w_2(0))$.

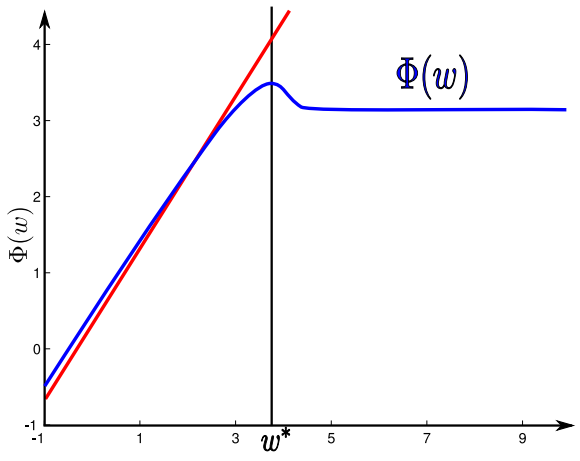

Figure 3.9: The adaptation map Φ in the case of the quartic model for $I > -m(b)$ (no-fixed point). The blue line corresponds to the map Φ, the red line to the identity map and the black line localizes w^*. We represent on this diagram the main properties of Φ stated in theorem 3.3.1 (w^{**} is smaller than -1 in this case and does not appear in this plot.)

Let us now assume that $w^* \leq w_1(0) < w_2(0)$. In that case, the initial condition is in the up zone of diagram 3.7(a). In this zone, we have seen that both variables v and w decrease. The orbit enters in finite time the center zone where v increases and w keeps decreasing. The orbits will therefore cross one time the reset line before spiking. This reset line is a Jordan section, and Jordan's theorem (see for instance [74, Chap. 9, appendix, p. 246]) implies that the solutions are always ordered on this section, and the order of the adaptation value at the two new crossing positions w_1^1 and w_2^1 is inverted, i.e. $w_2^1 < w_1^1$. By application of the previous case, we obtain

$$\Phi(w_1(0)) = \Phi(w_1^1) \geq \Phi(w_2^1) = \Phi(w_2(0)).$$

We conclude that the map Φ is increasing on $(-\infty, w^*]$ and decreasing on $[w^*, \infty)$.

- *Behavior for $w < w^{**}$:* If $w < w^{**}$, then w will increase all along the trajectory, and hence for all t smaller than the spike time t_s, we have $w(t) \geq w$ and therefore $w(t_s) \geq w$ and hence $\Phi(w) \geq w + d$.

- *Regularity:* The regularity of Φ for $w < w^*$ comes from the theorem of regularity of the solution of an ordinary differential equation with respect to its initial condition. Since in the region $w < w^*$ (center and spiking regions of diagram 3.7(a)) the value of $F(v) - w + I$ never vanishes, the orbit starting from the initial condition (v_r, w_0) satisfies equations (3.4) in the plane (v, w) and equation (3.8) in the plane (u, w). In order to apply the regularity theorem with respect to the initial condition, we consider here equation (3.8) and check the regularity conditions.

  The function g is C^∞ with respect to its two variables on $(0, 1] \times \mathbb{R}$. We prove that it is regular at the point $u = 0$. First, the map g tends to 0 when $u \to 0$ because of condition 3.1.2, since it is equivalent when $u \to 0$ to $-2ab/(\varepsilon u^{1+4/\varepsilon} F(u^{-2/\varepsilon} + v_r -$

1)) which tends to 0 ($F(u^{-2/\varepsilon}+v_r-1)\leq \alpha u^{-4/\varepsilon-2}$). Furthermore it is Lipschitz on $[0,1]$ with respect to $\tilde{W}$ since the partial derivative of this function reads:

$$\frac{\partial g}{\partial \tilde{W}} = \frac{2a}{\varepsilon u^{1+2/\varepsilon}} \frac{(F(u^{-2/\varepsilon}+v_r-1)-b(u^{-2/\varepsilon}+v_r-1)+I)}{(F(u^{-2/\varepsilon}+v_r-1)-\tilde{W}+I)^2}$$

This derivative is therefore positive, and because of assumption 3.1.2 tends to zero when $u\to 0^+$. Therefore, this function can be extended as a continuously differentiable function in the neighborhood of 0 and using the theorem of Cauchy-Lipschitz with parameters, we conclude that the map $\tilde{W}$ is continuous with respect to the initial condition.

We can obtain even more regularity, provided that we prove that the map g has limits for its partial derivatives of higher order. The higher order partial derivatives of g with respect to $\tilde{W}$ will converge to zero when $u\to 0^+$ using the same argument, and by induction, we can prove that this is true for all the derivatives with respect to $\tilde{W}$ at $u=0^+$. The partial derivative with respect to u are slightly more intricate in the general case, but in the case of the quartic and exponential model, we can readily prove that g is C^∞ in $(u,\tilde{W})$ and therefore the theorem of Cauchy-Lipschitz with parameters implies that the map $\tilde{W}(\cdot,\cdot)$ and $\Phi(\cdot)$ are C^∞.

For $w\geq w^*$, the orbit will turn around the point (v_r,w^*). Hence Φ is the composition of the application giving the first crossing location of the orbit with the curve $\{v=v_r\}$ and Φ for $w<w^*$. The second is continuously differentiable or even more regular because of the latter argument, and the first one is C^∞ because of the standard theory of Poincaré applications (Cauchy-Lipschitz theorem with parameters for the system 3.1).

- *Concavity:* As already stated, for $w<w^*$, the solution of equation (3.1) will never cross the v nullcline, and the equation of the orbits in the phase plane $(u,\tilde{W})$ is given by equation (3.8), whose solution can be formally written using equation (3.11). We have:

$$\begin{cases} \frac{\partial g}{\partial \tilde{W}} &= \frac{2a}{\varepsilon u^{1+2/\varepsilon}} \frac{F(u^{-2/\varepsilon}+v_r-1)-b(u^{-2/\varepsilon}+v_r-1)+I}{(F(u^{-2/\varepsilon}+v_r-1)-\tilde{W}+I)^2} > 0 \\ \frac{\partial^2 g}{\partial \tilde{W}^2} &= \frac{4ab}{\varepsilon u^{1+2/\varepsilon}} \frac{F(u^{-2/\varepsilon}+v_r-1)-b(u^{-2/\varepsilon}+v_r-1)+I}{(F(u^{-2/\varepsilon}+v_r-1)-\tilde{W}+I)^3} > 0 \end{cases} \tag{3.13}$$

using the fact that $F(v)-w+I>0$ and $w<bv$. Because of (3.8) the following formula for the second derivative of Φ with respect to w_0.

$$\frac{\partial^2 \tilde{W}}{\partial w_0^2} = -\int_u^1 \frac{\partial^2 g}{\partial \tilde{W}^2}\left(\frac{\partial \tilde{W}}{\partial w_0}\right)^2 + \frac{\partial g}{\partial \tilde{W}}\frac{\partial^2 \tilde{W}}{\partial w_0^2},$$

Because of the second inequality (3.13) we have $\frac{\partial^2 \tilde{W}}{\partial w_0^2} \leq -\int_u^1 \frac{\partial g}{\partial \tilde{W}}\frac{\partial^2 \tilde{W}}{\partial w_0^2}$, and furthermore $\frac{\partial^2 \tilde{W}}{\partial w_0^2}(1,w_0)=0$. Thus using Gronwall's theorem we obtain the convexity of the function $\tilde{W}(u,\cdot)$ for all u.

The adaptation map Φ is defined by

$$\Phi(\cdot) = \lim_{u\to 0} \tilde{W}(u,\cdot) + d$$

Since g is at least C^2 in the second variable, so is the flow (Cauchy-Lipschitz theorem with parameters) and hence Φ has the same convexity property for $w < w^*$.

- *Existence and uniqueness of fixed point:* Since $\Phi(w) \geq w + d$ for all $w < w^{**}$ and $\Phi(w)$ is a non-increasing function for $w > w^*$, we have existence of at least one fixed point. If $\Phi(w^*) < w^*$, then there exists a fixed point $w_{fp} \leq w^*$. Because of the concavity property of Φ, there is no other fixed point in $(-\infty, w^*)$, and since Φ is decreasing on (w^*, ∞), it has no fixed point for $w > w^*$. If $\Phi(w^*) > w^*$, the map Φ has no fixed point for $w \leq w^*$ because of the concavity of Φ and has a unique fixed point for $w > w^*$ since Φ is non-increasing for $w > w^*$.

- *Horizontal asymptote (plateau) :* The principle of the proof is to show that there exists a solution whose membrane potential diverges to $-\infty$ when integrating the backward equation (i.e. changing t by $-t$), so that the solution separates the phase plane into two subdomains, and the orbits are trapped in one of the two domains. In the zone above this solution, the map Φ will be decreasing and lowerbounded, hence will converge when $w \to +\infty$.

  To prove the existence of such a solution, we search for an invariant subspace of the phase plane for the backwards dynamics (i.e for the dynamical system $(v_b(t) = v(-t), w_b(t) = w(-t))$) below the v-nullcline $\mathscr{N}$ (i.e. included in the center or spiking zones).

  It is sufficient to consider domains bounded by two lines, of type:

$$\mathscr{B} \stackrel{\text{def}}{=} \{(v,w) \mid v \leq v_0, w \leq w_0 + \alpha(v - v_0)\}$$

  where the real parameters α, v_0, w_0 are free.

  We show that we can find real parameters (v_0, w_0, α) such that this domain is invariant by the backwards dynamics and does not cross $\mathscr{N}$. We will search for non positive values of α.

  First of all, for the boundary $\{v = v_0, w \leq w_0\}$, we want $\frac{\mathrm{d}v_b}{\mathrm{d}t} \leq 0$, which only means $w_b \leq w^*(v_0) = F(v_0) + I$.

  Now we have to characterize both v_0 , w_0 and α such that the vector field is flowing out of the affine boundary $\mathscr{B}$. This means that $\langle \binom{\dot{v}}{\dot{w}} | \binom{\alpha}{-1} \rangle \leq 0$ where $\langle \cdot | \cdot \rangle$ denotes the Euclidean dot product. This condition simply reads $\alpha\dot{v} - \dot{w} \leq 0$ and has to be fulfilled on each point of the boundary, which is equivalent to:

$$\begin{cases} H_\alpha(v) & \stackrel{\text{def}}{=} \alpha(F(v) - w + I) - a(bv - w) \leq 0 \text{ with} \\ w & = w_0 + \alpha(v - v_0) \end{cases} \tag{3.14}$$

  We first fix α and v_0 so that $\mathscr{B}$ is fully included in the center or spiking zones. This condition is achieved by taking $v_0 < v^*(0)$, the value where F achieves its minimum, and $\lim_{v \to -\infty} F'(v) < \alpha < F'(v_0) < 0$. Because of the convexity assumption and the fact that the limit of the derivative of F at $-\infty$ is strictly negative, there exists $F_{\min}$ such that for all $v \in \mathbb{R}$ we have $F(v) \geq F_{\min}$. We have on the boundary of the domain:

$$\begin{aligned} H_\alpha(v) &\leq \alpha(F_{\min} - w + I) - a(bv - w) \\ &\leq \alpha(F_{\min} - \alpha(v - v_0) - w_0 + I) - a(b(v - v_0) - \alpha(v - v_0) + bv_0 - w_0) \\ &\leq (v - v_0)\{-\alpha^2 - ab + \alpha a\} + \{-\alpha w_0 + \alpha I + \alpha F_{\min} - abv_0 + aw_0\} \end{aligned}$$

Therefore the lefthand term of condition (3.14) is bounded by an affine function of v. The slope coefficient is negative. Therefore a sufficient condition for (3.14) to be satisfied is that the second term is negative. This affine term reads:

$$(a-\alpha)w_0 + \alpha I + \alpha F_{\min} - a\,b\,v_0$$

and hence involves a term proportional to w_0 with a positive coefficient, and w_0 is the last free parameter of the boundary. Choosing a large negative value for w_0 solves the problem.

We have defined a domain $\mathscr{B}$ on the boundary of which the vector field flows outwards, and hence the backward equation's vector field flows inwards this zone. Therefore, $\mathscr{B}$ is flow invariant for the backward solution, and every solution having its initial condition in this zone does not cross the nullcline, hence goes to infinity with a speed lowerbounded by the minimal distance between le nullcline and $\mathscr{B}$.

We have proved that there is an orbit such that the membrane potential of the backward solution goes to $-\infty$, and whose forward solution spikes (since the initial condition in the spiking zone). This solution necessarily crosses the line $\{v = v_r\}$; denote w_L the value of w at this intersection. This solution splits the phase space in two subspaces which do not communicate: every orbit starting in one of the two subspaces will stay in this subspace by application of Cauchy-Lipschitz theorem. Hence for all $w > w^*$, $\Phi(w) \geq \Phi(w_L)$, hence Φ is decreasing and lowerbounded, hence converges to a finite value when $w \to +\infty$ and its graph presents an horizontal asymptote.

□

We characterized the shape of the adaptation map in the case where the subthreshold system has no fixed point. In this case, the spiking will necessarily be of *tonic* type, i.e. the neuron will fire infinitely many spikes (this will be the case whenever $\Phi(\mathscr{D}) \subset \mathscr{D}$). Since the system has a tonic spiking behavior, the study of the adaptation sequence of iterations of Φ provides a good way to understand the different tonic spiking patterns observed in these models.

3.3.2 Regular spiking

As observed numerically in the previous chapter, and as we can see in figure 3.10, the regular spiking is linked with the presence in the hybrid system of a generalized limit cycle, the *regular spiking limit cycle*, virtually containing one point having an infinite value of the membrane potential. From a mathematical point of view, this property simply corresponds to the convergence of the adaptation sequence (3.10). Indeed, if this sequence converges, then the frequency of the spikes will also converge[1].

Since we do not have closed form expressions for the map Φ, we provide here sufficient conditions on the dynamics of Φ leading to a regular spiking behavior.

[1]If the adaptation sequence does not converge, the only way for the neuron to fire spikes regularly corresponds to the case where the sequence jumps between points corresponding to the same spike time. This occurs when the ISI map $\mathscr{T}$ is not one-to-one. In that particular case, there is necessarily a point lower than w^* which corresponds to a sharp after-potential and the a point greater than w^* corresponding to a broad after potential, and the sequence will then be considered as a regular bursting from a biophysical point of view as well as from our mathematical point of view.

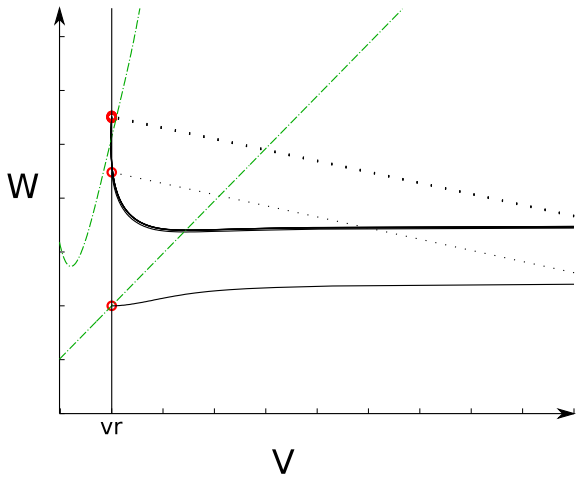

Figure 3.10: Spiking generalized limit cycle, case of the quartic model. In the simulation, we have cut the trajectories to a given threshold. Threshold has been taken large enough to ensure we simulate the intrinsic system. Green dotted curves represent the nullclines, the red circles the sequence of reset positions, the solid black curves the orbit of the solution of the differential equation and the dotted lines the reset.

Theorem 3.3.2. *Assume that* $\Phi(w^*) \leq w^*$. *Then the adaptation sequence* (3.10) *converges for any initial condition.*

Proof. First of all we note that the interval $(-\infty, w^*]$ is stable under Φ. Indeed, Φ is increasing on this interval, therefore for all $w \in (-\infty, w^*]$, $\Phi(w) \leq \Phi(w^*) \leq w^*$. Similarly, we necessarily have $w^{**} < w^*$, since theorem 3.3.1 ensures us that for all $w < w^{**}$ we have $\Phi(w) > w$, and the interval $[w^{**}, w^*]$ is invariant under Φ since $w^{**} \leq \Phi(w^{**}) \leq \Phi(w^*) \leq w^*$. Therefore, the fixed point of Φ is contained in this interval.

Moreover Φ maps the interval $[w^*, \infty)$ on the interval $(-\infty, \Phi(w^*)]$ since Φ is decreasing on this interval, and therefore for all $w \in [w^*, \infty)$, we have $\Phi(w) \leq \Phi(w^*) \leq w^*$. Therefore, is is sufficient to prove that the sequence of iterates of Φ converges on $(-\infty, w^*]$.

For $w_0 \in [w^{**}, w^*]$, the sequence $(w_n)_{n\geq 0}$ is a monotonous sequence (since Φ is increasing on this interval) in a compact set, and hence will necessarily converge to the unique fixed point of Φ.

If $w_0 < w^{**}$ then $\Phi(w_n) \geq w_n + d$ while $w_n \leq w^{**}$ and hence there exists an index N such that $w^{**} \leq w_N \leq w^*$, and the previous result applies and gives us the convergence of the sequence.

We conclude therefore that for any initial condition $w \leq w^*$ the sequence converges to the unique fixed point of Φ, and since Φ maps the interval $[w^*, \infty)$ on $(-\infty, w^*]$, for any initial condition in this interval, the sequence (3.10) will converge to the fixed point of Φ. □

The following theorem provides a sufficient condition on the map Φ to get regular spiking or bursts of period two.

Theorem 3.3.3. *Assume that* $\Phi(w^*) \geq w^*$ *and* $\Phi^2(w^*) \geq w^*$. *Then the adaptation sequence either converges to the fixed point of* Φ *or to a period two cycle.*

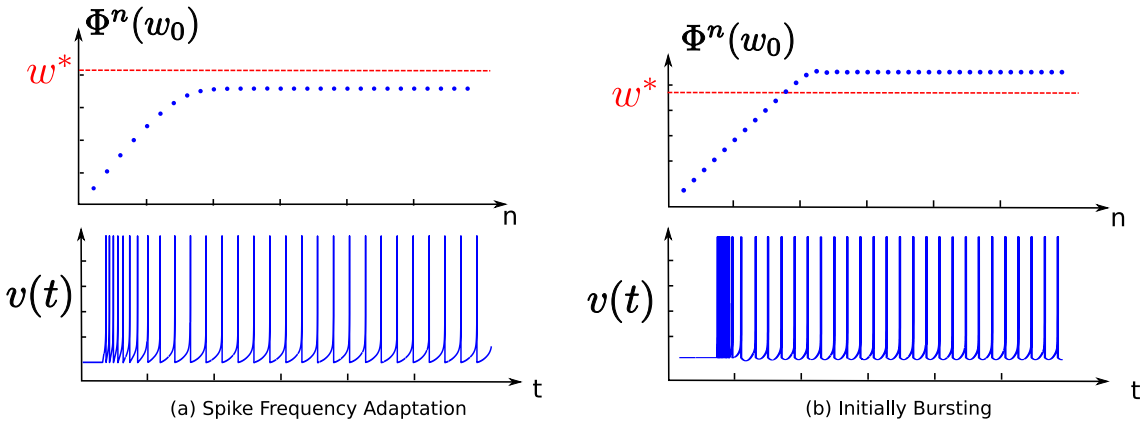

Figure 3.11: Regular spiking. The different transient phases (initially bursting, spike frequency adaptation) are linked with the relative position of the fixed point with respect to w^*.

Proof. Let w_0 be a given initial condition for the sequence (3.10). Necessarily this sequence (w_n) will enter the interval $[w^*, \Phi(w^*)]$ after a finite number of iterations. Indeed, assume that $w_0 < w^*$. Since there is no fixed point in $(-\infty, w^*)$, Φ is increasing and $\Phi(w) \geq w$ in this interval, the sequence cannot be upperbounded by w^*. Hence there will be an integer p such that $\Phi^p(w_0) \leq w^*$ and $\Phi^{p+1}(w_0) \geq w^*$. Then because of the monotony of Φ on $(-\infty, w^*)$ we have $\Phi^{p+1}(w_0) \leq \Phi(w^*)$. Thus $w_{p+1} \in [w^*, \Phi(w^*)]$. If $w_0 > w^*$, because of the monotony of Φ on (w^*, ∞) we have $\Phi(w_0) \leq \Phi(w^*)$ and hence the sequence will enter the interval $[w^*, \Phi(w^*)]$ after a finite number of iterations.

Moreover, the interval $[w^*, \Phi(w^*)]$ is stable under Φ, since Φ is decreasing on this interval, and

$$\Phi([w^*, \Phi(w^*)]) = [\Phi^2(w^*), \Phi(w^*)] \subset [w^*, \Phi(w^*)].$$

Let $w \in [w^*, \Phi(w^*)]$ and $w_n = \Phi^n(w)$ the related adaptation sequence. Since Φ^2 is increasing on this invariant bounded interval, the sequences (w_{2n}) and (w_{2n+1}) are monotonous and both converge to a fixed point of Φ^2, hence (w_n) either converges to a fixed point of Φ or to a periodic orbit of period two depending on the stability of the fixed point. □

We have identified two simple sufficient conditions on Φ to obtain a regular spiking behavior. These criteria are not directly related to the parameters of the model, but they will be useful in order to describe mathematically the dependency with respect to the parameters as done in section 3.3.4. They can also be used in numerical simulations to compute the zones of parameters corresponding to this regular spiking behavior, as we do in section 3.5.2.

This analysis accounts for the stationary spiking behavior as well as for the transient phase, i.e. before the convergence of the sequence. In the spike patterns analysis, we generally distinguish between two types of regular spiking: the spike frequency adaptation that corresponds to the case where the spike frequency smoothly converges to its stationary value, and initial bursting mode (or mixed mode) where the neuron transiently fires a burst before spiking regularly. From the biological point of view, the distinction between these behaviors is not so clear, and we can continuously go from one behavior to the other. Mathematically, the difference between

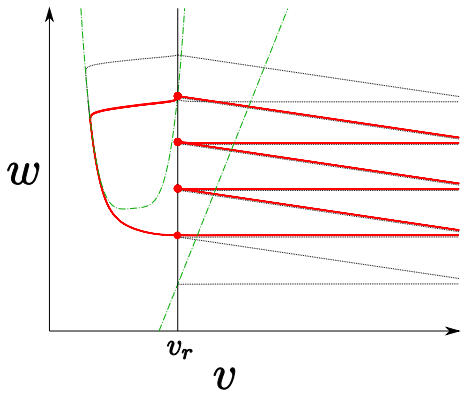

Figure 3.12: Bursting generalized limit cycle. Trajectories are cut to a given threshold high enough to approximate the behavior of the system with explosion. The red curve corresponds to the bursting limit cycle, and the red circles the reset locations on this cycle. The black trajectory is the transient phase, and the green dotted curves correspond to the nullclines of the system.

these two behaviors corresponds to the value of the fixed point of the adaptation map. Indeed, assume that the fixed point of the map Φ is smaller than w^*. In this case, when the sequence will converge towards the fixed point, the value of the adaptation sequence will always be smaller than w^*, and the orbit will present a sharp after potential. The interspike interval in this zone is quite smooth and therefore the convergence towards the fixed point will result in the smooth adaptation of the spike frequency. If the fixed point is greater than w^*, when we apply a current step to the system, it will fire spikes with a sharp after-potential before converging to the fixed point where the system will present a broad after potential, therefore the system will present a typical transient phase corresponding to the initial bursting mode.

We conclude that if the neuron satisfies theorem 3.3.2, it will be in an adapting mode, and if not, it will be in an initial bursting mode. This criterion predicts the results numerically obtained by Naud and collaborators [203], as discussed in more details in section 3.5.2.

3.3.3 Tonic Bursting

As observed numerically in the previous chapter and as we can see in figure 3.12, the bursting activity is linked with the existence of a generalized limit cycle of the hybrid system, the *bursting limit cycle*, virtually containing a few points having an infinite membrane potential. The regular bursting behavior, whatever the transient behavior, is related to the presence of such a cycle, and this cycle corresponds exactly to periodic orbits for the adaptation map Φ.

We can provide a condition for having cycles of any period. Indeed, one of the simplest application of Sarkovskii's theorem (see e.g. [70]) is that if there exists a periodic point of period 3, then there exist periodic points of any period, hence bursts with any number of spikes per burst. Theorem 3.3.4 provides a simple criterion on Φ to have a period 3 cycle.

Theorem 3.3.4 (Cycles of any period)**.** *Let* $w_1 \stackrel{\text{def}}{=} \min\{\Phi^{-1}(w^*)\}$. *Assume that:*

$$\begin{cases} \Phi(w^*) > w^* \\ \Phi^2(w^*) < w_1 \\ \Phi^3(w^*) > w^* \end{cases} \tag{3.15}$$

Then there exists a non-trivial period 3 cycle, hence the reset process has cycles of any period.

Proof. The only thing to prove is that there exists a point $x \in \mathbb{R}$ such that

$$\begin{cases} \Phi^3(x) = x \\ \Phi(x) \neq x \end{cases}$$

We know that there exists a unique fixed point of Φ, which we denote w_{fp} and which lies in the interval $[w^*, \Phi(w^*)]$. Here we prove that there exists another solution of $\Phi^3(x) = x$. Indeed, let us describe the function Φ^3:

- It is increasing on $(-\infty, w_2)$ where $w_2 = \min\{\Phi^{-2}(w^*)\}$, and $\Phi^3(w) > w$ on this interval by concavity

- decreasing on (w_2, w_1) and $\Phi^3(w_1) = \Phi^2(w^*) < w_1$ hence the curve crosses once the curve $y = x$, at a point strictly lower than w^*.

Hence we proved that there exists a period 3 cycle. Sarkovskii's theorem (see e.g. [70]) ensures us that there are cycles of any period for the map Φ . □

Remark 9. This theorem gives us a simple condition on Φ to get period 3 cycles. This implies that the system has periodic points of any period, but also that it has an uncountable number of non asymptotically periodic points, which is referred as chaos in the paper of Li and Yorke [180]. Nevertheless this property can be rather defined as *topological* chaos, and does not correspond to the usual definition of chaos in mathematics and in neuroscience where it is understood as sensitive dependency on the initial condition.

Simple sufficient conditions such as the ones given in theorem 3.3.4 in the case of periodic points of period three can be provided to for cycles of any given period. The difficulty is to prove that these conditions are satisfied, since we have no closed form expression for the map Φ, and in this case numerical simulation is helpful. As we will see in section 3.3.4, the system will undergo a period-adding bifurcation structure with respect to the reset value of the membrane potential, and therefore bursts of many periods will be observed.

3.3.4 Dependency on the parameters

We have seen that in the case where the subthreshold dynamics has no fixed point, the spike patterns produced can correspond to tonic spiking or tonic bursting depending on the parameters of the system. The question we address in this section is to characterize the dependency of the spike patterns with respect to the parameters of the model, and the bifurcations from one behavior to the other.

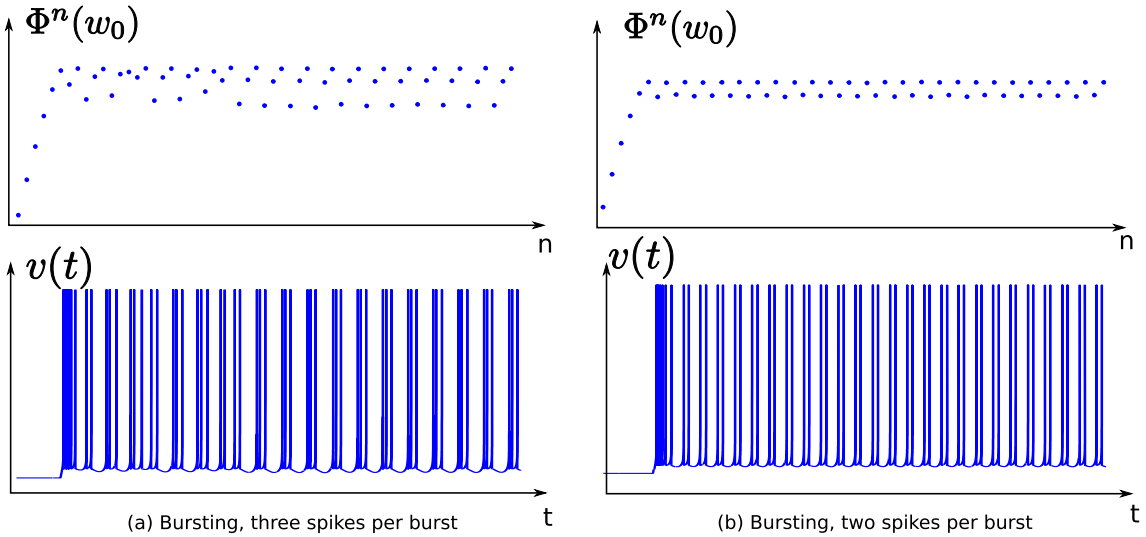

(a) Bursting, three spikes per burst

(b) Bursting, two spikes per burst

Figure 3.13: Bursting in the quartic model: bursts with different number of spike per bursts and related periodic orbit of Φ.

Bifurcations with respect to the spike-triggered adaptation parameter

The parameter having the simplest effect on the dynamics is the spike-triggered adaptation parameter d: it simply shifts vertically (i.e. along the y-axis) the adaptation map, and does not modify its shape. This simple behavior allows us to understand qualitatively the changes in the behavior of the adaptation sequence.

First of all, note that the unique fixed point of the map Φ is an increasing function of the spike-triggered adaptation d. We denote it $w_{fp}(d)$.

If the adaptation map is globally contracting (i.e. $\max_{v\in\mathbb{R}}|\Phi'(v)|<1$), we will not observe bifurcations in the parameter d, and the sequence will always converge to the unique fixed point.

If the map is not globally contracting, bifurcations can appear with respect to the parameter d. Denote by $\mathscr{I}_1$ the set of $w\in\mathbb{R}$ such that $|\Phi'(w)|>1$. This set is a bounded closed set included in $[w^*,\infty)$, because of the convexity property of Φ and the presence of the plateau. Indeed, if $w_{fp}<w^*$, then since Φ is increasing we would have $0<\Phi'(w_{fp})<1$. Furthermore, because of the plateau region, we have $\Phi'(w_{fp}(d))\to 0$ when $d\to\infty$. As stated, since the shape of Φ does not depend on d, neither does $\mathscr{I}_1$.

If $w_{fp}(0)>\max\{\mathscr{I}_1\}$, then the fixed point of the system is always stable for all $d>0$ and there is no bifurcation in d.

If $w_{fp}(0)\in\mathscr{I}_1$, we denote by $d_1=\inf\{d>0; w_{fp}(d)\notin\mathscr{I}_1\}$. The fixed point will be unstable and the neuron will be bursting or chaotically spiking while $d<d_1$, and for $d>d_1$, the fixed point becomes stable and the neuron will fire regularly. At the point where $d=d_1$, the fixed point has a multiplier equal to -1 because of the negativity and continuity of the derivative, and the map undergoes a non-generic doubling bifurcation. The transversality condition (see e.g. [167, section 4.5]) is never satisfied since we have $\frac{\partial\Phi}{\partial d}\equiv 1$ (see equation (3.12)) and hence $\frac{\partial^2\Phi}{\partial w\partial d}\equiv 0$.

If $w_{fp}(0)<\min\{\mathscr{I}_1\}$, we similarly define $d_1=\inf\{d>0, w_{fp}(d)\in\mathscr{I}_1\}$ and $d_2=\sup\{d\geq d_1, w_{fp}(d)\in\mathscr{I}_1\}$. The system will undergo a degenerate period doubling bifurcation at the point $w_{fp}(d_1)$ for $d=d_1$ and a period doubling bifurcation at the point $w_{fp}(d_2)$ for $d=d_2$. For $d\in(d_1,d_2)$, the system does not have a stable fixed point. It can emit

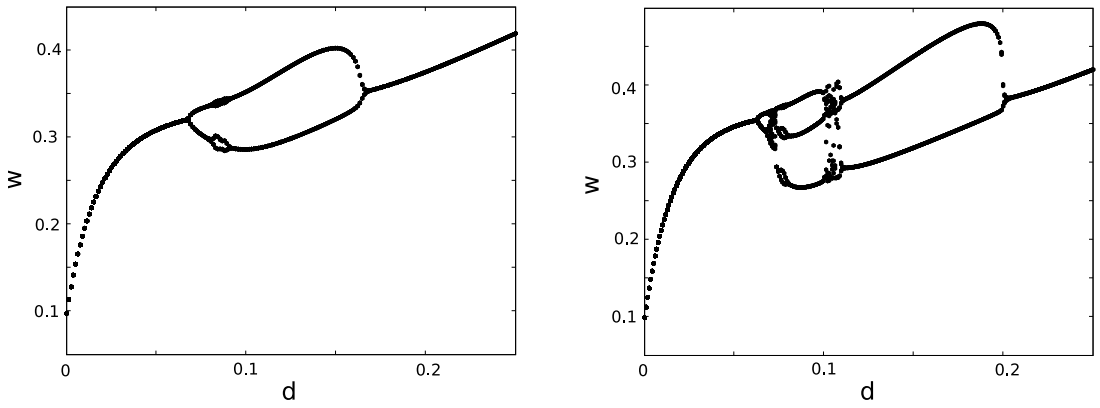

(a) $v_r = -48.2mV$ (b) $v_r = -47.7mV$

Figure 3.14: Orbits under Φ for different initial conditions, varying the spike-triggered adaptation parameter d, in the case of the dimensioned Adaptive Exponential model. We can observe that for d small enough the system converges towards the fixed point of Φ. When increasing d, as described in the text, the fixed point loses stability via a period doubling bifurcation and a cycle of period 2 appears. In the case (a) the system presents another period doubling bifurcation for $d \approx 0.8$, and then returns to equilibrium via an inverted period doubling bifurcation. In the second simulation for a larger value of v_r , the system involves chaotic spiking patterns.

bursts, or even have a chaotic behavior in this zone (see figure 3.14).

Stabilization by the input current

The input current is a very interesting parameter, since it can be related to a biophysical value that can be controlled in *in vitro* experiments. Moreover, the set of input currents such that the system has no fixed point has a very simple shape, corresponding to the semi-infinite interval $(-m(b),\infty)$.

Interestingly, we prove that increasing the input current has a stabilizing effect on the behavior of the neuron: we prove in theorem 3.3.5 that for I large enough the adaptation sequence always converges to a fixed point.

Theorem 3.3.5. *Let the parameters a, b, v_r, d be fixed. There exists I_s such that for all $I > I_s$ all orbits under Φ converges.*

Proof. The proof of this theorem is based on the changes induced by increasing the current around the point (v_r, w^*). We prove that increasing I enough will make the system satisfy the hypothesis of theorem 3.3.2.

The point w^* depends on I, and therefore we denote it $w^*(I)$ in this proof for the sake of clarity. We change variables and consider $\hat{w} = w - I$. The change of variables maps w^* to $\hat{w}^* = F(v_r)$. The equations satisfied by $(v,\hat{w})$ are readily deduced from the original system, the new adaptation map can be written as:

$$\hat{\Phi}(\hat{w}) = \Phi(\hat{w} + I) - I,$$

and the condition of theorem 3.3.2 simply reads $\hat{\Phi}(\hat{w}^*) \leq \hat{w}^*$.

The equation of the trajectory in the phase plane $(v,\hat{w})$ for any initial condition in the spiking zone can be parametrized as a function of v: $\hat{w}(t) = \hat{W}(v(t), v_0, w_0, I)$, where $\hat{W}$ satisfies the equation:

$$\begin{cases} \frac{\partial \hat{W}}{\partial v} = \frac{a(bv-\hat{W})}{F(v)-\hat{W}} - \frac{aI}{F(v)-\hat{W}} \stackrel{\text{def}}{=} \hat{g}(v,\hat{W},I) \\ \hat{W}(v_0,v_0,w_0,I) = w_0 \end{cases}$$

Let $I_0 > -m(b)$ a fixed current, $\delta > 0$ a given real and $\Delta = d+1$ where d is the spike-triggered adaptation parameter. Because of the shape of the vector field, the trajectories with initial condition (v_r, w^*) can be parameterized as a function of v with a singularity at $v = v_r$. We consider the trajectories on the interval $[v_r, v_r+\delta]$, and we prove that the infimum of the variable $\hat{W}$ with initial condition $(v_r, \hat{w}^*)$, for $I \geq I_0$ and $v \in [v_r, v_r+\delta]$ is smaller than $F(v_r) - \Delta$.

To this end, let us characterize the orbits starting from this point $(v_r, \hat{w}^*)$ as a function of the input current I. First of all, it is clear using Gronwall's theorem that $I \mapsto \hat{W}(v, v_r, \hat{w}^*, I)$ is decreasing. Therefore we have $\hat{W}(v_r+\frac{\delta}{2}, v_r, \hat{w}^*, I) \leq \hat{W}(v_r+\frac{\delta}{2}, v_r, \hat{w}^*, I_0) \stackrel{\text{def}}{=} \hat{w}_0$ and hence $\hat{W}(v_r+\delta, v_r, \hat{w}^*, I) \leq \hat{W}(v_r+\delta, v_r+\frac{\delta}{2}, \hat{w}_0, I)$.

Assume now that the infimum of $\hat{W}$ for all $v \in [v_r+\frac{\delta}{2}, v_r+\delta]$ is greater than $F(v_r)-\Delta$. We have:

$$\hat{g}(v,\hat{W},I) - \hat{g}(v,\hat{W},I_0) = -\frac{a(I-I_0)}{F(v)-\hat{W}}$$

and hence:

$$\begin{aligned} \hat{W} &\geq F(v_r) - \Delta \\ F(v) &\leq \max_{v \in [v_r, vr+\delta]} F(v) \\ F(v) - \hat{W} &\leq \max_{v \in [v_r, vr+\delta]} F(v) - F(v_r) + \Delta \\ \frac{1}{F(v)-\hat{W}} &\geq \frac{1}{\max_{v \in [v_r, vr+\delta]} F(v) - F(v_r) + \Delta} \\ -\frac{a(I-I_0)}{F(v)-\hat{W}} &\leq -\frac{a(I-I_0)}{\max_{v \in [v_r, vr+\delta]} F(v) - F(v_r) + \Delta} \end{aligned}$$

which is constant and strictly negative. Therefore, using Gronwall's theorem, we have

$$\hat{W}(v_r+\delta, v_r, \hat{w}^*, I) - \hat{W}(v_r+\delta, v_r, \hat{w}^*, I_0) \leq -\frac{a(I-I_0)\delta}{\max_{v \in [v_r, vr+\delta]} F(v) - F(v_r) - \Delta}$$

Therefore there exists I_1 such that for all $I > I_1$, we have $\min_{v \in [v_r, v_r+\delta]} \hat{W}(v) < F(v_r) - \Delta$. This contradicts the assumption that the infimum of $\hat{W}$ for all $v \in [v_r+\frac{\delta}{2}, v_r+\delta]$ is greater than $F(v_r)-\Delta$. Hence there exists I_1 such that for all $I > I_1$, we have $\min_{v \in [v_r, v_r+\delta]} \hat{W}(v) < F(v_r) - \Delta$, which means in particular $\min_v W(v) < F(v_r) + I - \Delta$. This minimal value is reached when the trajectory crosses the w-nullcline, and denote by v_1 the value of the variable v at this crossing time. We have, for all $I > I_1$:

$$\begin{aligned}\Phi(w^*(I)) &= \lim_{v\to\infty} W(v) + d \\ &= W(v_1) + \int_{v_1}^{\infty} \frac{a(bv - W)}{F(v) - W + I}\, dv + d\end{aligned}$$

Moreover, we have $W(v) \geq bv_r$ for all v and $W(v) \leq bv$ for $v \geq v_1$. Therefore, we have:

$$\int_{v_1}^{\infty} \frac{a(bv - W)}{F(v) - W + I}\, dv \leq \int_{v_1}^{\infty} \frac{ab(v - v_r)}{F(v) - bv + I}\, dv.$$

The integrand is positive between v_r and v_1, hence we have in particular:

$$\begin{aligned}\Phi(w^*(I)) &\leq F(v_r) + I - \Delta + d + \int_{v_r}^{\infty} \frac{ab(v - v_r)}{F(v) - bv + I}\, dv \\ &= F(v_r) + I - 1 + \int_{v_r}^{\infty} \frac{ab(v - v_r)}{F(v) - bv + I}\, dv\end{aligned}$$

The integrand tends to zero when $I \to \infty$ and is bounded by an integrable function (for instance the same function with $I = I_0$), hence by Lebesgue's theorem tends to 0 when $I \to \infty$. Therefore, there exists $I_s > I_0$ such that for all $I > I_s$, the integral is strictly smaller than 1, and therefore:

$$\Phi(w^*(I)) \leq F(v_r) + I = w^*(I).$$

Hence theorem 3.3.2 applies, which ends the proof. □

Therefore, we can see that increasing the input current has a stabilizing effect on the dynamics. We present in figure 3.15 some numerical results illustrating this stabilization effect in the case of the exponential integrate-and-fire model. We observe for two different values of v_r that the system undergoes bifurcations with respect to the input current, sometimes involving chaotic spiking, but above a given value of the input current, the system spikes regularly, and the adaptation sequence converges towards its fixed point. Moreover, we have seen in the proof that when $I \geq I_s$, theorem 3.3.2 applies. Hence for I large enough, the system will present a spike frequency adaptation transient phase. Decreasing it will make the system switch to the case where there are two fixed points treated in section 3.4.

Cascade of period adding bifurcations and chaos with respect to v_r

Another parameter preserving the number of fixed point is the reset value of membrane potential v_r. The dependency of the adaptation map with respect to this parameter is very intricate. The effect of increasing the reset value sharpens the adaptation map, and therefore can destabilize the possible stable fixed point or stable cycles. This qualitative observation is confirmed by numerical simulations. In the case of the exponential model, for v_r small enough, the adaptation map is smooth, because the slope of the exponential function for small v values tends to zero. But in the case of the quartic model, decreasing v_r also sharpens F because of the fast divergence of the quartic function.

We provide in figure 3.16 a graph of the stationary adaptation sequence (i.e. removing the transient phase) as a function of the reset voltage v_r corresponding to the

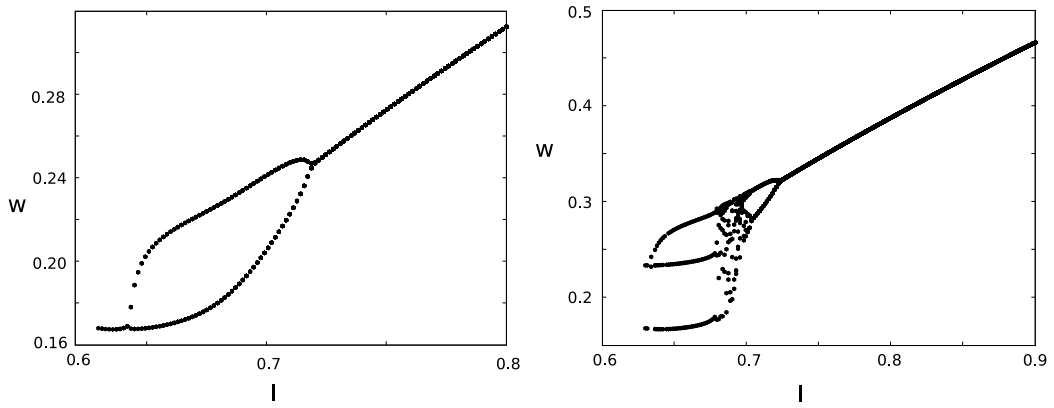

(a) $d = 0.1nA$ (b) $d = 0.5nA$

Figure 3.15: Orbits under Φ when varying the input current I in the case of the dimensioned Adaptive Exponential model. (a): Small v_r, the dynamics only presents a loss of stability via period doubling and then returns to equilibrium. (b): greater value of v_r: a period two cycle appears at the saddle-node current, immediately followed by a period 3 cycle, then via period-adding bifurcation the system returns to a period two cycle, and then by period doubling bifurcation to regular spiking. The transition from period three to period two shows a chaotic behavior.

quartic model. A similar diagram was given in the case of the adaptive exponential model in [258]. We observe that the system present sharp transitions from rest (regular spiking) to cycles of period two (bursts with two spikes per burst) via a period doubling bifurcation, and from cycles of period n to cycles of period $n+1$ for $n \geq 2$ via period adding bifurcations involving chaotic spiking regions.

3.3.5 Multistability

In section 3.3.2, we gave a sufficient condition on the map Φ for the convergence of the sequence (3.10) to the fixed point of Φ whatever the initial condition, which implies that the fixed point of Φ is stable and that its attraction basin is equal to $\mathbb{R}$. Nevertheless, in the case where the map Φ is not globally contracting, multistable behaviors could appear, corresponding to the coexistence of stable spiking orbits.

The study of periodic orbits is quite intricate in general systems, and this study in our case is even more complex since we do not have a closed form for the map Φ. We nevertheless observe numerically that cases of this type do not seem to occur: the stationary behavior of the adaptation sequence is the same whatever the initial condition.

3.4 Existence of fixed points

In the case where $I < -m(b)$, the system has two fixed points, one of which is always a saddle fixed point. We already studied in section 3.2 the stable manifold of this saddle fixed point (SMSFP) and explained in the cases where there exist SAs (fixed points or periodic orbit) how this manifold shaped the related attraction basin.

This stable manifold is essential for characterizing the definition domain and the

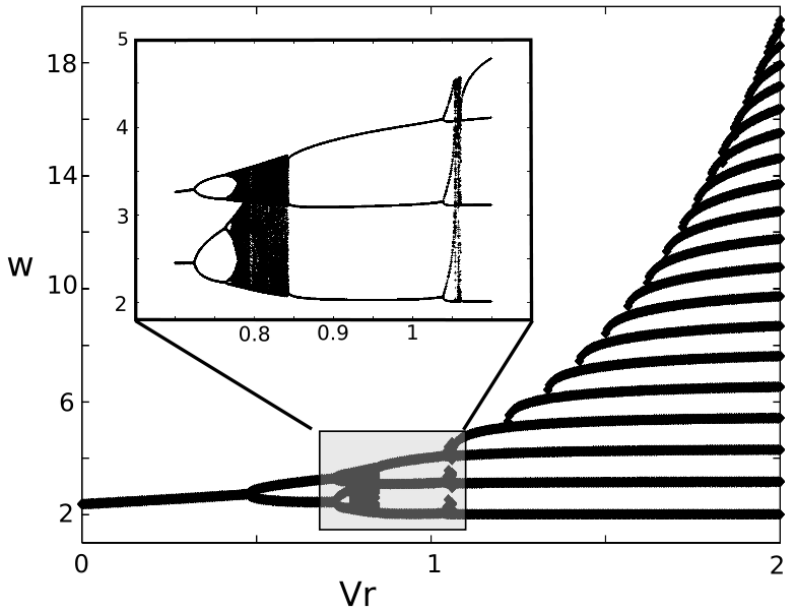

Figure 3.16: The period adding bifurcation cascade in the adaptation sequence for the quartic model, $a = 0.03$, $b = 0.7$, $d = 1.15$, and $v_r \in [0,2]$, and a zoom on the transitions from period 2 to period 3 and period 3 to period 4. The same phenomenon appears in the adaptive exponential model, see [258].

the dynamics of Φ. The map Φ will only be defined for values of w such that (v_r, w) is neither in the attraction basin of the possible SA nor on the SMSFP. We will study different cases in function of the topology of the intersection of the reset line with these sets, and mainly distinguish the cases where there is no intersection, finitely or countably many intersections or a continuous uncountable set of intersections.

3.4.1 Unconditional tonic behaviors

We are first interested in the cases where the reset line $\{v = v_r\}$ neither crosses the SMSFP nor the attraction basin of the possible SA. We know that the SMSFP is the graph of an unbounded increasing function of v for $v \geq v_+$ where v_+ is the greatest fixed point of the system. The cases where the SMSFP do not cross the reset line necessarily correspond to the cases where the stable manifold is included in a half plane $\{v \geq v_{\min}\}$. This corresponds to the cases where:

- the subthreshold system has two unstable fixed points and no stable limit cycle (Figs. 3.6(a) and 3.6(b)).
- an unstable limit cycle circles the stable fixed point (Fig. 3.5(a))
- the stable manifold crosses both nullclines (Fig. 3.5(b)).

In these cases, for all $v_r \leq v_{\min}$, the reset line does not intersect the SMSFP nor any possible attraction basin. Therefore, the adaptation map Φ is defined on $\mathbb{R}$ and the proof of theorem 3.3.1 readily extends to this case. Hence in these cases Φ is a regular map increasing and concave on $(-\infty, w^*]$ and decreasing on $[w^*, \infty)$, having a unique fixed point, a horizontal asymptote at infinity and such that $\Phi(w) \geq w + d$ for all $w \leq$

w^{**}. Since the map Φ is defined on $\mathbb{R}$ (and therefore $\Phi(\mathscr{D}) \subset \mathscr{D}$), if the neuron fires a spike, then it will fire infinitely many spikes. In that case, the map satisfies the same properties as when the subthreshold system has no fixed point, and theorems 3.3.2, 3.3.3 and 3.3.4 apply.

3.4.2 Phasic behaviors

In this section, we consider the cases where the reset line intersects the attraction basin $\mathscr{B}$ of SA and denote by $\mathscr{C}$ the SMSFP. The set of adaptation values on the reset line that do not lead the system to fire is given by:

$$\mathscr{A} = \{w \in \mathbb{R}\,;\, (v_r, w) \in \mathscr{B} \text{ or } (v_r, w) \in \mathscr{C}\}\,.$$

The definition domain of the adaptation map in this case is

$$\mathscr{D} = \mathbb{R} \setminus \mathscr{A},$$

the set of initial conditions corresponding to a phasic spiking (i.e. emission of a finite number of spikes) is given by

$$P = \bigcup_{n=0}^{\infty} \Phi^{-n}(\mathscr{A})$$

and the complement of this set corresponds to the tonic spiking cases.

To study further the behavior of the system in this case, we discuss different cases depending on the shape of the stable manifold and the position of v_r with respect to the fixed point v_+. Interestingly, the shape of the stable manifold only depends on the parameters of the subthreshold system.

3.4.3 The stable manifold Γ^- does not cross the v-nullcline

We first consider the case where the manifold Γ^- does not cross the v-nullcline. We distinguish two cases depending on wether $v_r \leq v_+$ or not.

Proposition 3.4.1. If the manifold Γ^- does not cross the v-nullcline and $v_r > v_+$, the manifold Γ^+ separating the spiking and non-spiking regions is the graph of an increasing function of v, and is above the two nullclines. The definition domain $\mathscr{D}$ of the adaptation map Φ is an open interval $(-\infty, w_{\max}(v_r))$ with $w_{\max}(v_r) > w^* (> w^{**})$. We denote $\Phi(w_{\max}(v_r)^-) \overset{\text{def}}{=} \lim_{w \to w_{\max}(v_r)} \Phi(w)$ the left limit of Φ at the point $w_{\max}(v_r)$. We have:

- If $\Phi(w_{\max}(v_r)^-) > w_{\max}(v_r)$ the system fires finitely many spikes whatever the initial condition in $\mathscr{D}$,
- If $\Phi(w_{\max}(v_r)^-) < w_{\max}(v_r)$ and $\Phi(w^*) < w_{\max}(v_r)$ the system fires infinitely many spikes whatever the initial condition in $\mathscr{D}$,
- Else, the system will either fire finitely or inifinitely many spikes depending on the initial condition.

Proof. First of all, we note that Φ satisfies the same properties on $\mathscr{D}$ as the one given in theorem 3.3.1. The shape of the domain $\mathscr{D}$ is readily deduced from the shape of the separatrix.

- In the case where $\Phi(w_{\max}(v_r)^-) > w_{\max}(v_r)$ (see figure 3.18(d)) there exists a real $\varepsilon > 0$ such that $\Phi(w) - w \geq \varepsilon$ for all $w \in \mathscr{D}$. Indeed, because of the monotony of Φ on $(w^*, w_{\max}(v_r))$ we have for all w in this interval $\Phi(w) \geq \Phi(w_{\max}(v_r)^-) > w_{\max}(v_r) \geq w$ and because of the convexity property of Φ and the fact that $\Phi(w) \geq w + d$ for all $w \leq w^{**}$, the distance between Φ and the identity map is lower-bounded. Hence $\Phi(w) \geq w + \varepsilon$, and there exists $N > 0$ such that $\Phi^N(w) \geq w_{\max}(v_r)$, thus the system has a phasic spiking behavior (see figure 3.18(g)).

- In the case where $\Phi(w_{\max}(v_r)^-) < w_{\max}(v_r)$ and $\Phi(w^*) < w_{\max}(v_r)$ (see figure 3.18(c)), then we have $\Phi(\mathscr{D}) \subset \mathscr{D}$, since the maximum of the map Φ is reached at w^*, and therefore the system will fire infinitely many spikes. Depending on the properties of the map Φ and of its fixed point, the system can either spike regularly (when the fixed point is stable), generate bursting or chaotic spike patterns. Figure 3.18(g) corresponds to this case when the fixed point is stable and generates a regular spiking behavior.

- In the case where $\Phi(w^*) \geq w_{\max}(v_r)$, we do not have $\Phi(\mathscr{D}) \subset \mathscr{D}$. In this case, $\mathscr{D}$ can be split into two different sets that can have quite intricate shapes: a set of values of the adaptation variable where the neuron fires finite many spikes and a set where the neuron fires infinitely many spikes. To study these sets, we define

$$P_1 = \{w \in \mathscr{D} \,;\, \Phi(w) \geq w_{\max}(v_r)\}$$

  This set corresponds to the set of adaptation values w such that $\Phi(w) \notin \mathscr{D}$ and hence that will fire one spike and then return to a subthreshold stable orbit. We then define recursively the set $P_{n+1} = \Phi^{-1}(P_n)$ of initial conditions such that the neuron will fire exactly $n+1$ spikes before being attracted by the stable subthreshold orbit. The set of phasic spiking initial conditions is therefore defined by

$$P = \bigcup_{n=1}^{\infty} P_n,$$

  and the set of tonic spiking is $\mathscr{D} \setminus P$. In figure 3.17 we represented the construction of these two sets until T_3, and we observe the complexity of the set we will obtain. If the fixed point is stable, both the tonic spiking and the phasic spiking sets will be a countable union of non-empty intervals, and the adaptation sequence will jump from one interval to the other until reaching the attraction basin of the fixed point of Φ, where they keep trapped. If the fixed point is unstable, the tonic spiking set will be countable, defined by the union of the consecutive reciprocal images of the unstable fixed point under Φ . Therefore the neuron will not present cycles. In this case, the behavior of Φ strongly depends on the initial condition.

□

Proposition 3.4.2. If $v_r \leq v_+$ and Γ^- does not cross the v-nullcline, the definition domain $\mathscr{D}$ is an open interval $(-\infty, w_{\max}(v_r))$ with $w_{\max}(v_r) \leq w^*$. The neuron fires infinitely many spikes if and only if $\Phi(w_{\max}(v_r)^-) \leq w_{\max}(v_r)$. In this case the neuron is in a regular spiking mode with spike frequency adaptation.

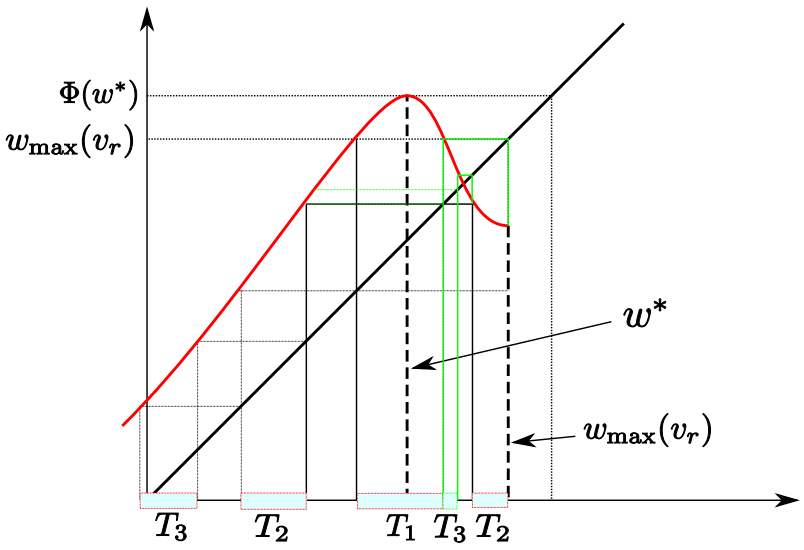

Figure 3.17: Construction of the phasic spiking set in the case of an unbounded separatrix when $\Phi(w^*) > w_{\max}$, for three iterations. The red curve is the map Φ and the black line the first bissector. The green construction line correspond to the contribution of the set T_2 for $w > w^*$ to T_3.

Proof. If $v_r \leq v_+$ and Γ^- does not cross the v-nullcline, it is clear that the definition domain $\mathscr{D}$ of the adaptation map Φ an open interval $(-\infty, w_{\max}(v_r))$ where $w_{\max}(v_r) \leq w^*$ is the value of the adaptation variable at the intersection point of the reset line with Γ^-. The maximal value of Φ on its definition domain is given by $\Phi(w_{\max}(v_r)^-)$.

- if $\Phi(w_{\max}(v_r)^-) \leq w_{\max}(v_r)$, then we have $\Phi(\mathscr{D}) \subset \mathscr{D}$ and hence the system is always in a regular spiking mode if it fires one spike. Moreover, the proof of theorem 3.3.2 readily extends to the present case and therefore the system will be in a regular spiking mode with spike frequency adaptation.

- If $\Phi(w_{\max}(v_r)^-) > w_{\max}$, because of the convexity property (which can be proved in exactly the same way as in theorem 3.3.1), there exists $\varepsilon > 0$ such that $\Phi(w) - w \geq \varepsilon$ and therefore the system will return to rest after firing finitely many spikes.

□

In the case where Γ^- intersects no nullcline (e.g. in the case of figure 3.18(a)), we will have $w_{\max}(v_r) \leq w^{**}$ and hence $\Phi(w_{\max}(v_r)^-) \geq w_{\max}(v_r) + d$, hence the system will always be in a phasic spiking mode. In the tonic spiking cases of propositions 3.4.1 and 3.4.2 the system presents a bistable behavior: a stable subthreshold behavior and a stable spiking one coexist.

The stable manifold Γ^- crosses the v-nullcline

If the stable manifold crosses the v-nullcline as in figure 3.5(b), then there exists $v_{\min} \leq v_-$ such that the SMSFP is included in the half plane $\{v \geq v_{\min}\}$. For each $v \leq v_{\min}$, we have $\mathscr{D} = \mathbb{R}$ and the results of section 3.4.1 apply. For $v \geq v_{\min}$, the spiking behavior of the system satisfies the following:

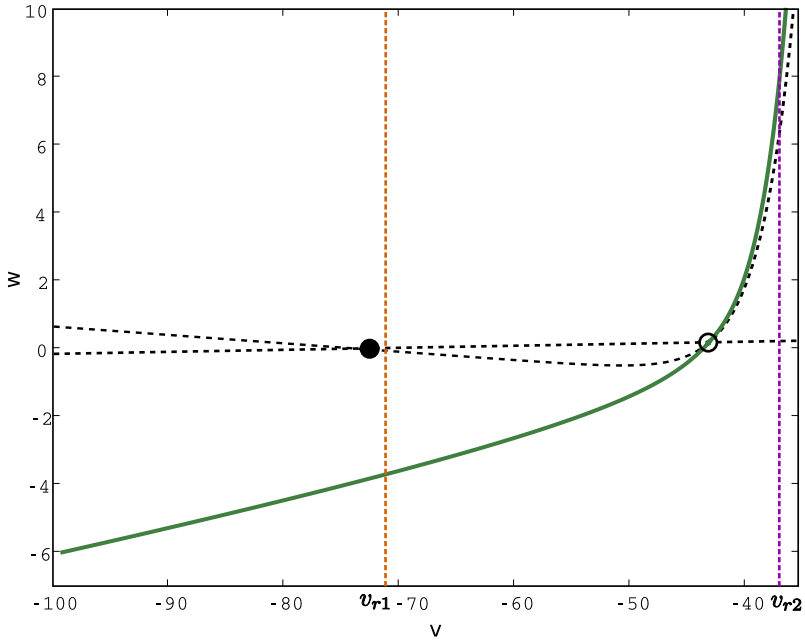

(a) Unbounded separatrix crossing no nullcline

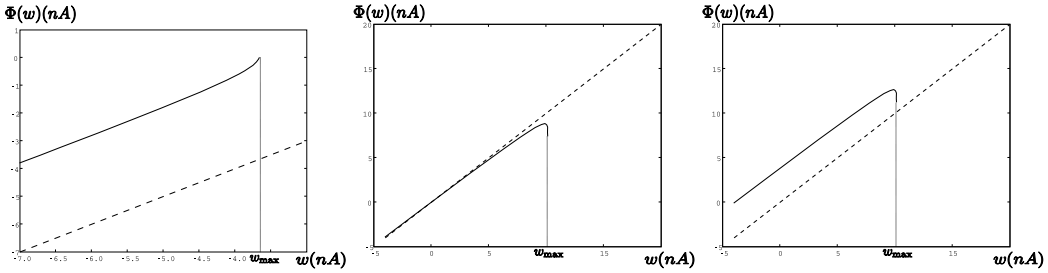

(b) Adaptation map for $v_r = v_{r1}$ (c) Adaptation map for $v_r = v_{r2}$ and $d = d_1$ (d) Adaptation map for $v_r = v_{r2}$ and $d = d_2$

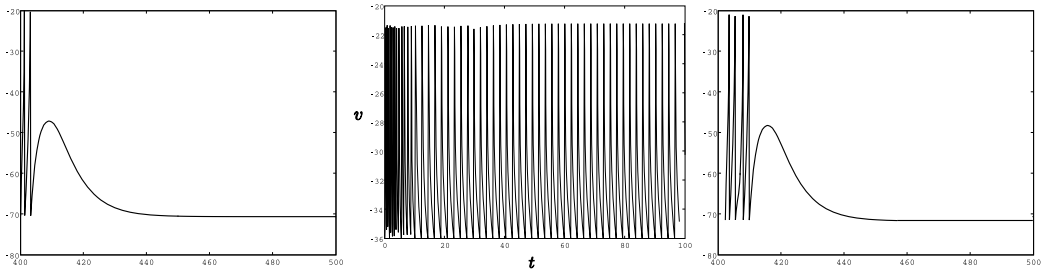

(e) Trace of v for $v = v_{r1}$ (f) Trace of v for $v = v_{r2}$ and $d = d_1$ (g) Trace of v for $v = v_{r2}$ and $d = d_2$

Figure 3.18: Case of an unbounded separatrix: unconditional phasic behavior for $v < v_-$. In the case $v > v_+$, the behavior can either be phasic or tonic depending on the parameters of the system. It can also depend on the initial condition. Case of the adaptive exponential model, original parameters, $a = .2g_L$ and $\tau_w = \tau_m/3$, $d_1 = 0.01nA$ and $d_2 = 3nA$. We chose $v_{r1} = -70.6mV$ (value of the original model) and $v_{r2} = -36mV$ which is unrealistically high for biological applications, and results in very fast spiking behaviors as in the case of figure (f).

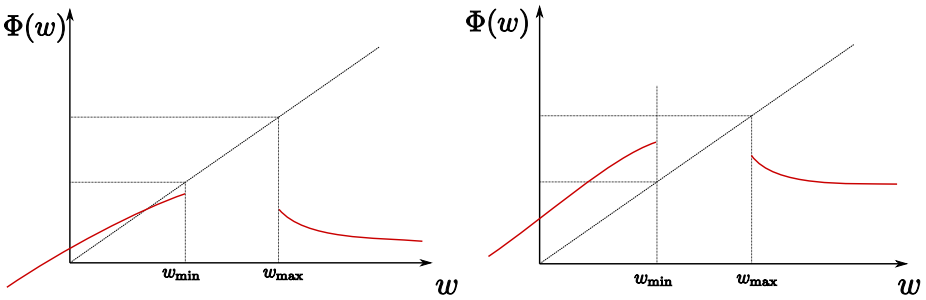

(a) Tonic spiking case

(b) Phasic spiking case

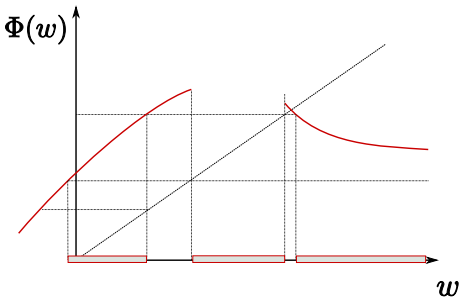

(c) Dependency on initial condition

Figure 3.19: Case where the SMSFP crosses the v-nullcline, in the case of the quartic model, $a = 1$, $b = 2.5$, $I = -0.5$, $v_r = 0$ and different values of d. (a): Tonic spiking mode, the adaptation sequence converges towards the fixed point of Φ. (b): Phasic spiking mode: for any initial condition the adaptation sequence will enter the zone $[w_{\min}, w_{\max}]$ and the neuron stops firing. (c): the spiking behavior is tonic or phasic depending on the initial condition. The blue boxes represent the zones of initial conditions related to a phasic behavior with zero or one spikes emitted.

Proposition 3.4.3. For $v \geq v_{\min}$, the reset line intersects the attraction basin on a bounded interval $(w_{\min}(v_r), w_{\max}(v_r))$ and the definition domain of the adaptation map is the union of two semi-infinite intervals:

$$\mathscr{D} = (-\infty, w_{\min}(v_r)) \cup (w_{\max}(v_r), \infty) \stackrel{\text{def}}{=} \mathscr{I}_1 \cup \mathscr{I}_2.$$

The spiking pattern satisfies the following classification (see figure 3.19):

- If $\sup_{w \in \mathscr{I}_1} \Phi(w) \in [w_{\min}(v_r), w_{\max}(v_r)]$, the system fires finitely many spikes
- If $\sup_{w \in \mathscr{I}_1} \Phi(w) < w_{\min}(v_r)$, the system fires infinitely many spikes. If $v_r \leq v_+$, the system presents regular spiking with spike frequency adaptation.
- If $\sup_{w \in \mathscr{I}_1} \Phi(w) > w_{\max}(v_r)$, the system fires finitely or infinitely many spikes depending on the initial condition.

Proof. The shape of the domain $\mathscr{D}$ is a direct consequence of the assumption on Γ^-. First of all, we note that any orbit starting from (v_r, w) with $w \in \mathscr{I}_2$ will cross the reset line on $\mathscr{I}_1$ after a finite time, and therefore we have $\Phi(\mathscr{I}_2) \subset \Phi(\mathscr{I}_1)$.

- If $\sup_{w \in \mathscr{I}_1} \Phi(w) \in [w_{\min}(v_r), w_{\max}(v_r)]$ (see figure 3.19(a)), then there exists $\varepsilon > 0$ such that $\sup_{w \in \mathscr{I}_1} \Phi(w) - w \geq \varepsilon$ and therefore any orbit will exit $\mathscr{D}$ and enter the

subthreshold orbits set after firing few spikes. For any initial condition $w \in \mathscr{I}_2$ we have $\Phi(w) \subset \Phi(\mathscr{I}_1)$ and therefore either $\Phi(w)$ is in the attraction basin of the subthreshold equilibrium, or it is in $\mathscr{I}_1$ and the above analysis applies and the system is in a phasic spiking mode.

- If $\sup_{w\in\mathscr{I}_1} \Phi(w) < w_{\min}(v_r)$ (see figure 3.19(b)), then necessarily $\Phi(\mathscr{I}_1) \subset \mathscr{I}_1$ and the map Φ has a fixed point in $\mathscr{I}_1$. Furthermore, we have $\Phi(\mathscr{D}) \subset \mathscr{I}_1$ and therefore the system will be in a tonic spiking behavior. If $v_r \leq v_+$, we have $w_{\min} < w^*$, the fixed point is attracting and for any initial condition the adaptation sequences converge to this fixed point (see proof of theorem 3.3.2). Moreover in that case the transient phase is characterized by spike frequency adaptation.

  If $v_r > v_+$, the type of tonic spiking depends on the properties of the map, the system is in a regular spiking mode with initial bursting, a bursting mode or a chaotic spiking mode.

- If $\sup_{w\in\mathscr{I}_1} \Phi(w) > w_{\max}(v_r)$ (see figure 3.19(c)), then there exists an interval $J \subset \mathscr{D}$ such that all the trajectory with initial condition (v_r, w) with $w \in J$ will stop firing after one spike. We can build the phasic and the tonic subspaces of $\mathscr{D}$ recursively as done in the previous case. The shape of this set can be quite complex, and the behavior of the adaptation sequence depends on the initial condition on this set.

□

Bounded attraction basin

In the case where the attraction basin of the SA is delineated by a periodic orbit, we denote by $v_{\min}$ the minimal value of the membrane voltage on the cycle and by $v_{\max}$ its maximal value. The behavior of the system for $v_r \in (v_{\min}, v_{\max})$ is very complex. Indeed, the reset line will cross the attraction basin on an interval of values for the adaptation $(w_{\min}, w_{\max})$, but since the stable manifold spirals around the orbit and converges to it, there is a countable sequence of intersection points of the reset line with the stable manifold: $(m_i, i \in \mathbb{N})$ converging to $w_{\min}$ and $(M_i, i \in \mathbb{N})$ converging to $w_{\max}$. At each of these points the map Φ is undefined and there is a jump of the values of the map Φ. Hence the definition domain of the map Φ has a complex shape, and Φ an intricate discontinuous dynamics on it.

For $v_r > v_{\max}$ the reset line will cross the stable manifold on a finite set of adaptation values, and at these points the map Φ is undefined and has a unique discontinuity, case we now generalize and study.

3.4.4 Case $\mathscr{D} = \mathbb{R} \setminus \mathscr{A}$ where $\mathscr{A}$ is a finite or countable set

The case where the reset line crosses the SMSFP but not any attraction basin of SA is more intricate (see figure 3.20). It corresponds to the cases where:

- the subthreshold system has two unstable fixed points and no stable limit cycle, and $v_r \geq v_{\min}$ (cases of Figures 3.6(a) and 3.6(b)). When the stable manifold oscillates around the fixed point, there is a countably many intersection points.

- the subthreshold system has a stable fixed point and an unstable periodic orbit. In that case let us denote by $v_{p,\max}$ (respectively $v_{p,\min}$) the maximal (respectively

minimal) value of the variable v or the periodic orbit. The line $\{v = v_r\}$ crosses the SMSFP but not the attraction basin when $v_{\min} \leq v_r < v_{p,\min}$ or $v_r \geq v_{p,\max}$.

In these two cases, the reset line $\{v = v_r\}$ has finitely many intersections with the stable manifold (except if $v_r = v_-$), and we denote by $\mathscr{A}$ the set of intersection points. The map Φ is defined on $\mathbb{R} \setminus \mathscr{A}$. This set is a finite union of open intervals. On each interval, the map Φ satisfies the properties given in theorem 3.3.1 for the same reasons as the ones given in the related proof. At the intersection points of the reset line with the SMSFP, the shape of the orbits of the differential system (3.1) changes, and this implies that at these points the map Φ is discontinuous.

If $v_r > v_+$ then the map Φ will have a unique discontinuity point where the map is undefined (see figure 3.20(e)). For $v_{\min} < v_r < v_-$ it will have an odd number of such points (figures 3.20(c) and 3.20(d)) and for $v_r > v_-$, an even number. In the case where the Jacobian matrix has complex eigenvalues at the equilibrium v_-, the Poincaré map will have an infinite countable set of discontinuity points for $v_r = v_-$. The dynamics of Φ in this region of parameters will therefore be very complex. It can have multiple fixed points, no fixed point, and the map is discontinuous.

The set of adaptation values such that the system stops firing after a finite number of spikes emitted (phasic spiking regime) is given by:

$$\bigcup_{n=0}^{\infty} \Phi^{-n}(\mathscr{A})$$

It is the set of initial conditions such that the orbits are exactly on the SMSFP after a finite number of iterations.

Therefore, the topology and the dynamics of Φ on these sets is quite complex. The related spiking sequence is also extremely complex in these cases:

- If the map Φ has not fixed point, regular spiking is impossible, and the system will either present bursts or irregular spiking.
- If there is a unique fixed point, then regular spiking and bursts can coexist depending on the initial condition on the reset line.
- The case where there are many fixed points (see figure 3.20(d)) is even more complex. In this case the system could have different regular spiking frequencies, depending on the initial condition. In this case of multiple attractors, the system could switch between these attractors, be chaotic, present hysteresis and its sensitivity increases.

3.5 DISCUSSION

3.5.1 Physiological relevance

The first two-dimensional spiking neuron model with diverging spiking dynamics was introduced by Izhikevich [141], who showed that these models could qualitatively reproduce many different electrophysiological features of real neurons, such as spike-frequency adaptation, bursting, resonance, rebound spiking... A variation of that model, the adaptive exponential integrate-and-fire model [30], includes an exponential spike initiation current [95], which is a realistic approximation of the sodium

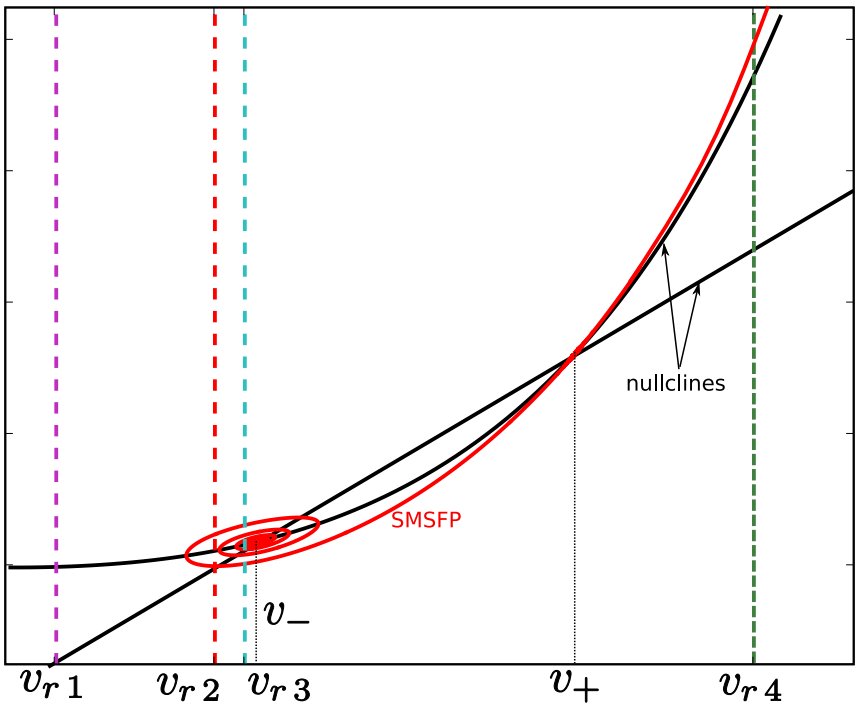

(a) Nullclines and different reset locations v_{r1}, v_{r2}, v_{r3}, v_{r4} corresponding to different qualitative behaviors for the map Φ.

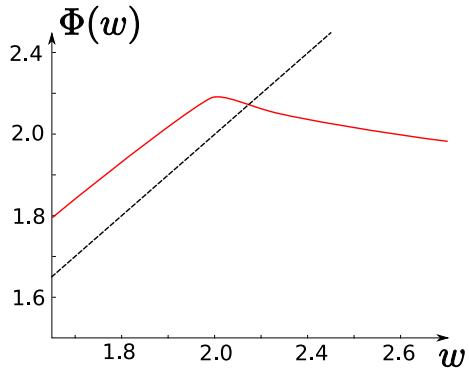

(b) $v_r = v_{r1}$: Φ is continuous

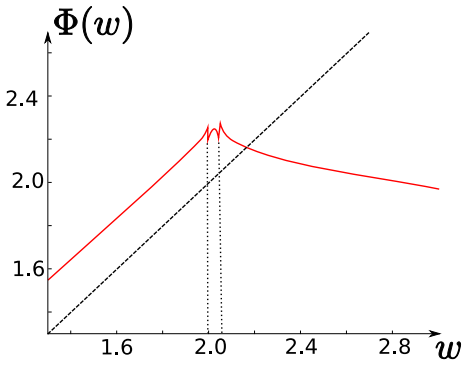

(c) $v_r = v_{r2}$: 2 discontinuity points

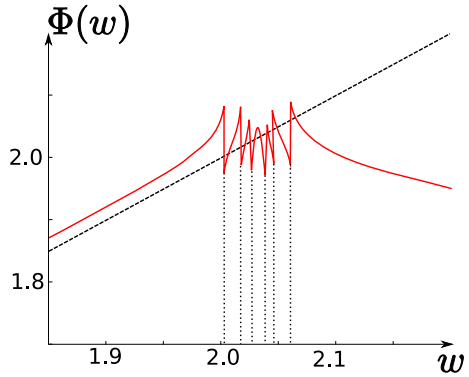

(d) $v_r = v_{r3}$: 6 discontinuity points, 7 fixed points

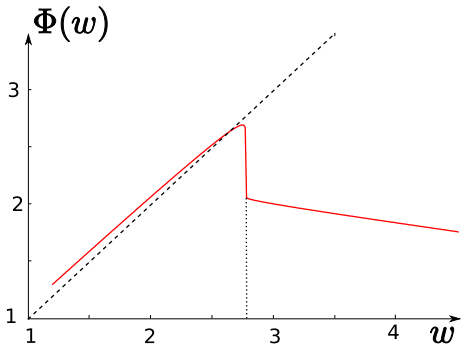

(e) $v_r = v_{r4}$: 1 discontinuity point

Figure 3.20: Case of two unstable fixed points for the classical adaptive exponential model. Phase plane and graph of the map Φ for different values of v_r, for the same set of parameters.

current (whose activation function is a Boltzmann function). That model (and variants) is able to quantitatively predict the responses of real neurons to injected currents in terms of spike times, with a millisecond precision [16, 51, 155]. The quartic model [255] is another variant which can exhibit sustained subthreshold oscillations. Thus, a mathematical analysis of those models has direct biological relevance. That analysis was first addressed in [255, 258], mainly in terms of subthreshold dynamics. Here we studied the patterns of spikes, which correspond to orbits under the adaptation map.

Dynamical properties of that map can be related to electrophysiological features of the neuron model. When the differential system has a stable fixed point, orbits are generally finite, i.e., a finite number of spikes are emitted, which is called *phasic spiking* (one spike) or *phasic bursting* (several spikes). In some situations, typically when the reset value is high, finite and infinite orbits can coexist, i.e., the system is bistable.

When the differential system has no stable fixed point, orbits are infinite, an infinite number of spikes are emitted, which is called *tonic spiking*. This is the most interesting aspect of the dynamics, where we must look at the properties of the adaptation map. When orbits converge to a fixed point of that map, spikes become regularly spaced, which corresponds electrophysiologically to the *regular spiking* behavior. Thus, theorem 3.3.2 provides conditions under which the neuron model has a regular spiking behavior. Periodic orbits translate to repeating spike patterns, which corresponds electrophysiologically to the *bursting* behavior, where the period is the number of spikes per burst. The existence of fixed points or periodic orbits depends in a complex way on the parameters. In particular, a period-adding bifurcation structure appears when increasing the reset parameter. It is particularly interesting to see that these two-dimensional models can exhibit chaos, whose electrophysiological signature is irregular spiking. Chaos has been observed in higher dimensional continuous neuron models such as the Hodgkin-Huxley model and variants [91, 121, 226]. It has also been observed in real neurons in vitro, such as the Purkinje cell [83, 135, 185, 193], where period doubling was observed in experiments when increasing the temperature with a fixed input current.

3.5.2 Classifications

In [258], the authors defined electrophysiological classes for the subthreshold dynamics in the case of the adaptive exponential model[2]. These classes are sets of parameters such that the neuron has the same qualitative behavior in response to different levels of input currents. We know that when I is smaller than $-m(b)$ the neuron will be in a phasic spiking behavior and when I is large enough, it will fire regularly. Classes are therefore distinguished depending on what is happening between these two stages, and three cases are possible:

0. The neuron always fires regularly (no transition).

1. The neuron first bursts then fires regularly (1 transition, see e.g. figure 3.15(b)).

2. The neuron fires regularly, then bursts, then fires regularly again (2 transitions, see e.g. figure 3.15(a)).

[2] their classification readily generalizes to the whole class of models we study here

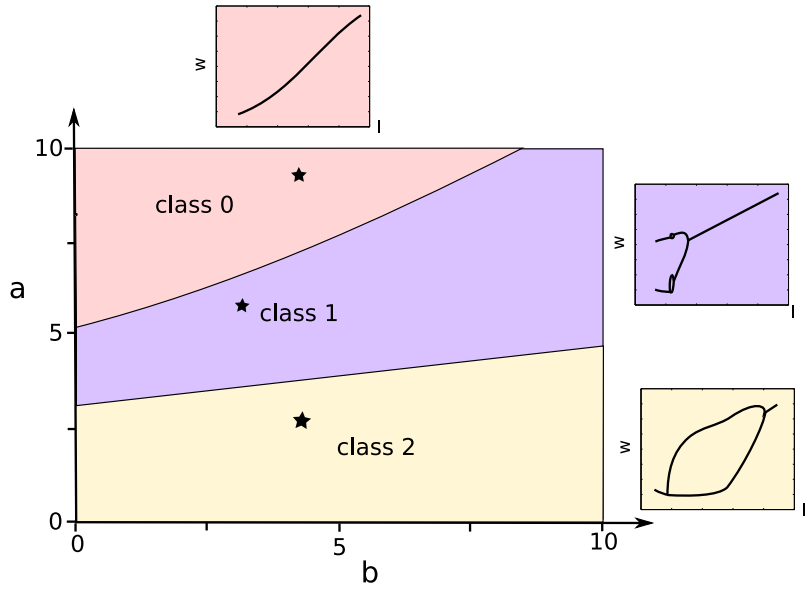

Figure 3.21: Electrophysiological classes for the quartic model with $d = 10$ and $v_r = 1$, as a function of the parameters a and b. Class 2 dissapears when d is small enough. Both classes 1 and 2 disappear when v_r is close to the minimum of F (or small enough in the case of the exponential model). Sample members of these classes have been represented in the small figures around the classification figure: we represented the adaptation sequence after a given elapsed time, as a function of the input current. Parameters are marked with stars: class 0: $a = 8.5$, $b = 4.5$, class 1: $a = 6$, $b = 3.2$, and class 2: $a = 2.5$, $b = 4.5$.

Classes 0 and 1 are observed in general whatever v_r and d for given values of a and b. Class 2 exists less often, and is generally observed for large values of the spike triggered adaptation d. We numerically compute the transitions between regular spiking and bursting. In Figure 3.21 we represented the number of transitions (i.e. the class of neuron) as a function of the parameters a and b for different pairs (v_r, d).

Let us now be more specific and define zones of parameters corresponding to a unique given behavior. The criteria for regular spiking given in theorems 3.3.2 and 3.3.3 rely on some very simple properties of the map Φ. We apply here the results of these theorems in order to define sets of parameters corresponding to different classes of behaviors: regular spiking with spike frequency adaptation, regular spiking with initial bursting, burst of period two, and a class of burst of unspecified period and chaotic spiking. The case where theorem 3.3.2 applies corresponds to the case of regular spiking with spike frequency adaptation. In the case where theorem 3.3.3 applies, we check the stability of the fixed point of Φ by computing the related multiplier: if it is smaller than one in absolute value, the system is in a regular spiking mode with intial bursting, and if not, the neuron fires bursts of period two. Eventually, in the cases where none of the theorems applies, the system is necessarily in a bursting or chaotic mode.

We have seen that when I is high enough or when d is high enough, the neuron fires regularly. Figure 3.22(c) helps us specify the parameter sets related to regular spiking (with initial bursting or spike frequency adaptation) and bursting. We observe in figure 3.22(c) that the input current has a stabilizing effect on the whole

dynamics: we simulated a case where the map Φ is not globally contracting for input currents close to $-m(b)$. When increasing the current, we observe that the map becomes globally contracting when the input current is high enough, which results in a regular spiking behavior. Therefore the electrophysiological class depends on d.

Another pair of interesting parameters is the pair of reset parameters (v_r, d). The influence of these two parameters was numerically studied by Naud and collaborators in the case of the dimensioned adaptive exponential model (see [203]) for a current value twice the value of the saddle-node bifurcation current. They numerically simulated the spike trains and classified them as chaotic spiking, bursting, regular spiking with spike frequency adaptation and initial bursting. The mathematical criteria we have presented predict these zones, as shown on figure 3.22.

3.5.3 Perspectives

In this chapter we studied the spike patterns produced by neurons in the class of models introduced in [255] in the case where the spike is emitted when the membrane potential blows up. We introduced a discrete map called the adaptation map, which is a generalization of the usual Poincaré applications in dynamical systems corresponding to the case where the Poincaré section is set a infinity.The rigorous mathematical study of this map allowed us to distinguish between the different spike patterns fired, and to derive simple criteria to characterize different spiking regimes of the neuron. These criteria can be easily applied in order to derive classes of parameters corresponding to different kinds of behaviors. We also proved that the system presented bifurcations as a function of the reset value of the membrane potential.

This study of a hybrid dynamical system opens the way to the study of different spiking models, such as bidimensional compartment models or bidimensional spiking models with or without explosion. In particular, this study readily applies to the case of Izhikevich' quadratic integrate-and-fire model which is a bidimensional nonlinear spiking neuron model where spikes are emitted when the membrane potential reaches a finite threshold. This framework may also be interesting in other fields of applied mathematics, and in particular in mathematical biology, ecology, economy and generally in any nonlinear system where discrete events occur depending on the state of the variables of the system.

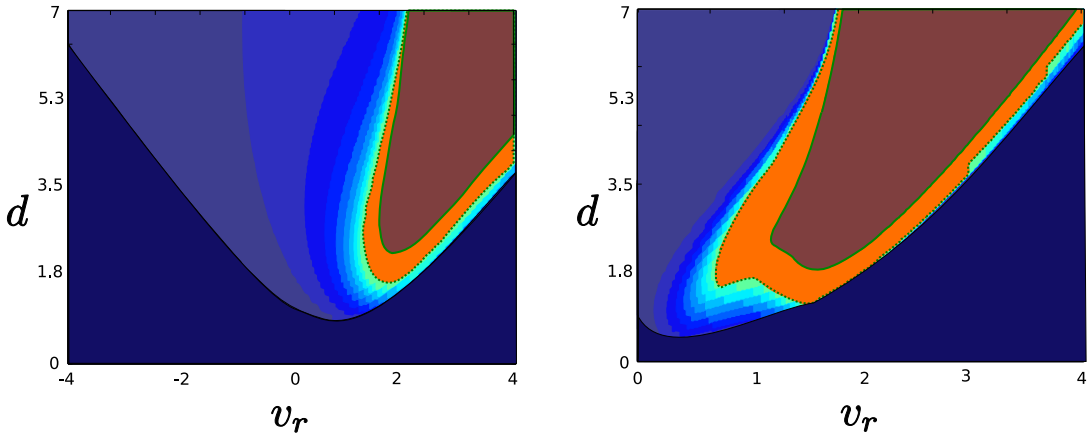

(a) Exponential Model

(b) Quartic Model

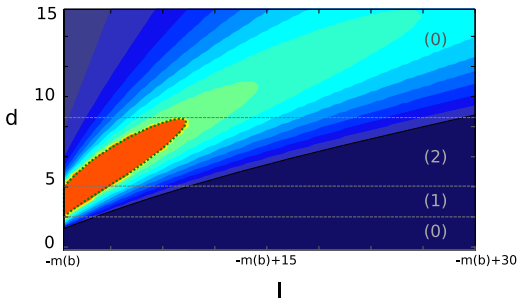

(c) Quartic Model

Figure 3.22: Parameter zones corresponding to different spiking behaviors. (a): Reduced adaptive exponential model with $a = 1$, $b = 2$ and $I = 3$. (b): Quartic model, $a = 1$, $b = 2$, $I = -m(b) + 2$. (c): $a = 1$, $b = 1$, $v_r = 1.5$. Regular spiking is indicated in blue. The dark blue zone corresponds to spike frequency adaptation, and the other blue regions correspond to initial bursting. The color intensity is proportional to the multiplier of the fixed point: the smaller the multiplier the darker the region. The separatrix we obtain in figure (a) is very close to the one found numerically by Naud and collaborators in [203]. Bursts and chaotic spiking are indicated in red/orange. The orange region corresponds to bursts with two spikes per burst (according to theorem 3.3.3). The green dotted line corresponds to the period doubling bifurcation. The brown zone corresponds to burst and chaos and the green solid line corresponds the initiation of the cascade of period doubling at the transition from period two to period three. In (c) the electrophysiological classes are represented as a function of d.

CHAPTER 4

APPLICATION: DEFINING ELECTROPHYSIOLOGICAL CLASSES

ABSTRACT

In the last two sections we discussed the mathematical properties of a class of neuron models and explained briefly the reasons why they were able to reproduce the diversity of electrophysiological features displayed by real neurons while keeping a simple model, for simulation and analysis purposes. Among these models, the adaptive exponential integrate-and-fire model is physiologically relevant in that its parameters can be easily related to physiological quantities. The interaction of the differential equations with the reset results in a rich and complex dynamical structure. In this chapter we relate the subthreshold features of the model to the dynamical properties of the differential system and the spike patterns to the properties of a Poincaré map defined by the sequence of spikes. We build upon the results obtained in the chapters 2 and 3 an electrophysiological class description for the models of this class, i.e. the sets of parameters where the model responds qualitatively the same way to different current inputs. We are particularly interested in the Adaptive Exponential Model, for which we provide the closed-form equations in the parameter space of the separatrix we obtain between electrophysiological classes. This work is a collaboration with Romain Brette to be published in Biological Cybernetics [258].

Contents

4.1 Introduction

As reviewed in the previous two chapters, several authors recently studied two-variable spiking models [30, 144, 254] which, despite their simplicity, can reproduce a large number of electrophysiological signatures such as bursting or regular spiking. Different sets of parameter values correspond to different electrophysiological classes.

All these two-dimensional models are qualitatively similar, and we will be in this chapter especially interested in the adaptive exponential integrate-and-fire model (AdEx, [30]) because its parameters can be easily related to physiological quantities, and the model has been successfully fit to a biophysical model of a regular spiking pyramidal cell and to real recordings of pyramidal cells [51, 155]. As already introduced, this model is described by two variables, the membrane potential V and an adaptation current w, whose dynamics are governed by the following differential equations:

$$\begin{cases} C\frac{\mathrm{d}V}{\mathrm{d}t} & = -g_L(V-E_L)+g_L\Delta_T \exp\left(\frac{V-V_T}{\Delta_T}\right) \\ & \quad -w+I \\ \tau_w\frac{\mathrm{d}w}{\mathrm{d}t} & = b(V-E_L)-w \end{cases} \tag{4.1}$$

When the membrane potential V is high enough, the trajectory quickly diverges because of the exponential term. This divergence to infinity models the spike (the shape of the action potential is ignored, as in the standard integrate-and-fire model). For displaying or simulation purposes, spikes are usually cut to some finite value (e.g. 0 mV). When a spike occurs, the membrane potential is instantaneously reset to some value V_r and the adaptation current is increased:

$$\begin{cases} V & \to V_r \\ w & \to w+d \end{cases} \tag{4.2}$$

Remark 10. The spike-triggered adaptation parameter denoted by d corresponds to the parameter denoted by b in the original article of Brette and Gerstner [30], and the parameter b of (4.1) corresponds to the parameter a of the original paper. We choose here to keep the same notations as in the previous chapters in order for the dissertation for the sake of consistency.

Although the differential system is only two-dimensional, the reset makes the resulting dynamical hybrid system very rich, as discussed in chapter 3.

The differential equations and the parameters have a physiological interpretation. The first equation is the membrane equation, which states that the capacitive current through the membrane (C is the membrane capacitance) is the sum of the injected current I and of the ionic currents. The first term is the leak current (g_L is the leak conductance and E_L is the leak reversal potential), the membrane time constant is $\tau_m = C/g_L$. The second (exponential) term approximates the sodium current, responsible for the generation of action potentials [95]. The approximation results from neglecting the inactivation of the sodium channel and assuming that activation is infinitely fast (which is reasonable). Because activation curves are typically Boltzmann functions [12], the approximated current is exponential near spike initiation. The voltage threshold V_T is the maximum voltage that can be reached without generating a spike (without adaptation), and the slope factor Δ_T quantifies the sharpness of spikes. In the limit of zero slope factor, the model becomes an integrate-and-fire

model with a fixed threshold V_T. Quantitatively, it is proportional to the slope constant k in the activation function of the sodium current. The second variable w is an adaptation current with time constant τ_w, which includes both spike-triggered adaptation, through the reset $w \to w+d$, and subthreshold adaptation, through the coupling (variable b). It may model ionic channels (e.g. potassium) or a dendritic compartment. Quantitatively, the coupling variable b can result from a linearization of the dynamics of a ionic channel, or from the axial conductance in the case of a dendritic compartment. We generally assume $b > 0$ in this chapter, although the analysis also applies for $b < 0$ when $|b|$ is not too large.

The interaction of the differential equations with the reset results in a rich dynamical structure. There are 9 parameters plus the injected current I, but these can be reduced to 4 variables plus the current I by changes of variables (e.g. setting V_T as the reference potential, Δ_T as the voltage unit, τ_m as the time unit, etc.). Thus, the electrophysiological class of the model, defined loosely here as the set of qualitative behaviors for different values of I, is parametrized in a 4-dimensional space. In this chapter, we will make this definition more precise by explaining different electrophysiological signatures in terms of dynamics of the model. Because we are dealing with a hybrid dynamical system, we shall study here two distinct dynamical aspects of the model: the subthreshold dynamics, defined by the differential equations (section 4.2), and the spiking dynamics, defined the sequence of resets (section 4.4). The former case was addressed in chapter 2 in a more general setting: we apply these results in order to derive new specific results, in particular about oscillations, attraction basins and rebound properties, that are interesting from a biological point of view. In the latter case, we will see that the spike patterns of the model correspond to orbits under a Poincaré map, which we shall call the *adaptation map* Φ. Interestingly, we find that this map can have chaotic dynamics under certain circumstances, as studied in chapter 3.

All simulations shown in this chapter were done with the Brian software [112] The code is available on ModelDB at the following URL:
`http://senselab.med.yale.edu/modeldb/ShowModel.asp?model=114242`.

4.2 SUBTHRESHOLD BEHAVIOR

The equations of the AdExp model can be written in dimensionless units by expressing time in units of the membrane time constant $\tau_m = C/g_L$, voltage in units of the slope factor Δ_T and with reference potential V_T, and rewriting both the adaptation variable w and the input current I in voltage units. We already did this transformation in the chapter 2, but write it down here again for the sake of completeness, and for keeping interpreting a little bit more the results obtained.

We obtain the following equivalent model:

$$\begin{cases} \frac{d\bar{V}}{dt} = -\bar{V} + e^{\bar{V}} - \bar{w} + \bar{I} \\ \bar{\tau_w} \frac{d\bar{w}}{dt} = \bar{b}\bar{V} - \bar{w} \end{cases} \tag{4.3}$$

and when a spike is triggered:

$$\begin{cases} \bar{V} & \to \bar{V_r} \\ \bar{w} & \to \bar{w} + \bar{d} \end{cases} \tag{4.4}$$

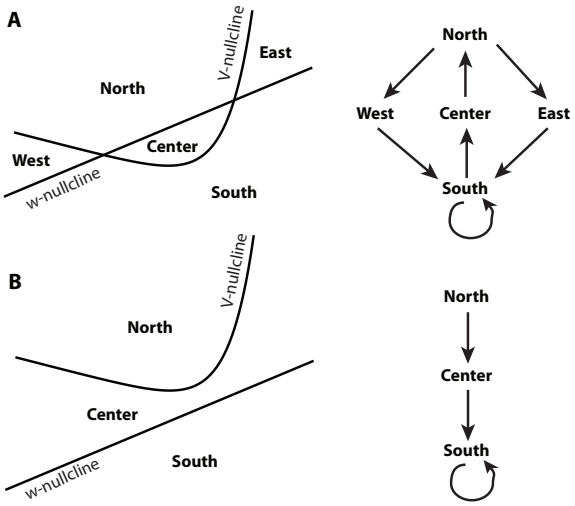

Figure 4.1: Nullclines of the dynamical system (horizontal axis: V; vertical axis: w). A. The nullclines intersect in two points, and divide the phase space into 5 regions. The potential V increases below the V-nullcline, w increases below the w-nullcline. The direction of the flow along each boundary gives the possible transitions between regions (right). Spiking can only occur in the South region. B. The nullclines do not intersect. All trajectories must enter the South region and spike.

where

$$\begin{cases} \bar{\tau_w} & := \frac{\tau_w}{\tau_m} = \frac{g_L \tau_w}{C} \\ \bar{b} & := \frac{b}{g_L} \\ \bar{I} & := \frac{I}{g_L \Delta_T} + (1 + \frac{b}{g_L}) \frac{E_L - V_T}{\Delta_T} \\ \bar{t} & := \frac{t}{\tau_m} \\ \bar{d} & := \frac{d}{g_L \Delta_T} \\ \bar{V_r} & := \frac{V_r - V_T}{\Delta_T} \\ \bar{V}(\bar{t}) & := \frac{V(t) - V_T}{\Delta_T} \\ \bar{w}(\bar{r}) & := \frac{w(t) + b(E_L - V_T)}{g_L \Delta_T} \end{cases} \tag{4.5}$$

Thus, as already mentioned in 2 only two parameters characterize the subthreshold dynamics: the ratio of time constants τ_w/τ_m and the ratio of conductances b/g_L (note: b can be seen as the stationary adaptation conductance), and the rescaled model belongs to the class studied in this chapter with $F(v) = e^v - v$, i.e., F is convex, three times continuously differentiable, has a negative derivative at $-\infty$ and an infinite derivative at $+\infty$. Therefore it has the same bifurcation structure, which is related as we develop here to electrophysiological properties, excitability type, rheobase current, voltage threshold, I-V curve. Besides, we give quantitative conditions for the occurrence of oscillations, along with a formula for their frequency. Finally, we examine the rebound properties of the model, in relationship with the attraction basin of the stable fixed point.

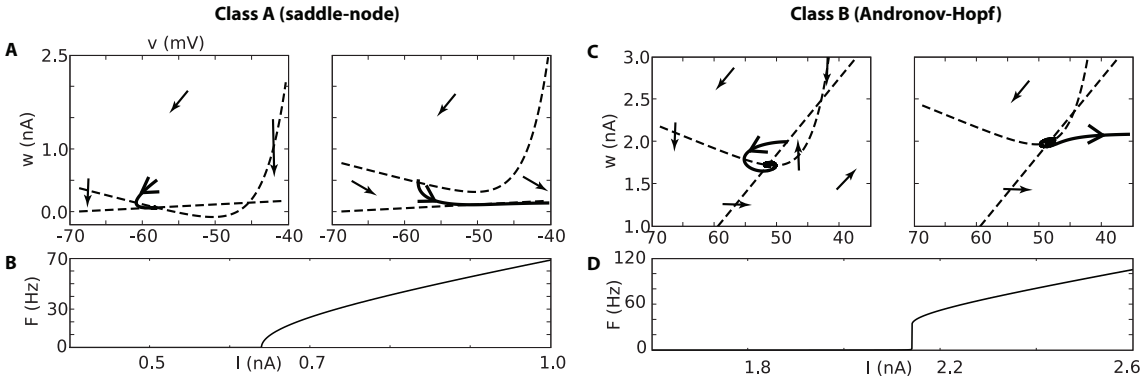

Figure 4.2: Excitability types. A,B. Type I: $\frac{b}{g_L} < \frac{\tau_m}{\tau_w}$ (here: $b = .2g_L,\ \tau_m = 3\tau_w$). When I is increased, the resting point disappears through a saddle-node bifurcation: the two fixed points merge and disappear. The current-frequency curve is continuous (B). C,D. Type II: $\frac{b}{g_L} > \frac{\tau_m}{\tau_w}$ (here: $b = 3g_L,\ \tau_m = .5\tau_w$). When I is increased, the resting point becomes unstable through an Andronov-Hopf bifurcation: the stable fixed point becomes unstable. The current-frequency curve is discontinuous, there is a non-zero minimum frequency (D).

4.2.1 Excitability

The dynamics in the phase plane (V,w) are partly determined by the number and nature of fixed points, which are the intersections of the two nullclines (Fig. 4.1):

$$\begin{aligned} w &= F(v)+I \quad \textit{(V-nullcline)} \\ w &= bv \quad \textit{(w-nullcline)} \end{aligned}$$

and that read in the original parameters for the AdExp model:

$$\begin{aligned} w &= -g_L(V-E_L)+g_L\Delta_T \exp\left(\frac{V-V_T}{\Delta_T}\right)+I \quad \textit{(V-nullcline)} \\ w &= b(V-E_L) \quad \textit{(w-nullcline)} \end{aligned}$$

Because the membrane current (first equation) is a convex function of the membrane potential V, there can be no more than two fixed points. When the input current I increases, the V-nullcline goes up and the number of fixed points goes from two to zero, while the trajectories go from resting to spiking. The excitability properties of the model depend on how the transition to spiking occurs, that is, on the bifurcation structure.

Excitability types

When I is very negative, there are two fixed points, one of which is stable (the resting potential). It appears that, when increasing I, two different situations can occur depending on ratio b/a, more precisely in the AdExp model, depending on the quantity $\frac{b\tau_w}{C} = \frac{b}{g_L}\frac{\tau_w}{\tau_m}$ (ratio of conductances times ratio of time constants).

If $b < a$ ($\frac{b}{g_L} < \frac{\tau_m}{\tau_w}$), then the system undergoes a saddle-node bifurcation when I is increased, i.e., the stable and unstable fixed points merge and disappear at the point $I = -m(b) = F(v^*(b))$. When the fixed points disappear, the vector field is almost null

around the former fixed point (the *ghost* of the fixed point). Since the vector field can be arbitrarily small close to the bifurcation, the trajectory can be trapped for an arbitrarily long time in the ghost of the fixed point, so that the firing rate can be arbitrary small when I is close to the bifurcation point (threshold). This property also explains the phenomenon of spike latency. This fact generally implies that the model has type I excitability, that is, the current-frequency curve is continuous (Fig. 4.2), but type II excitability may occur if the reset V_r is high (so that trajectories do not enter the ghost zone). However, we note that this latter case corresponds to bistable spiking before the bifurcation (4.4.3).

If $b > a$ (i.e. $\frac{b}{g_L} > \frac{\tau_m}{\tau_w}$), then the system undergoes a subcritical Andronov-Hopf bifurcation before the saddle-node one, meaning that the stable fixed point first becomes unstable before merging with the other fixed point. This fact implies generally that the model has type II excitability, that is, the current-frequency curve is discontinuous at threshold, the firing rate suddenly jumps from zero to a finite value when the bifurcation point is crossed (Fig. 4.2). It is however possible to have type I excitability in very specific cases, when the trajectory resets close to the stable manifold of the saddle fixed point.

In the following, we shall refer to the first case as class A and to the second one as class B. As noted above, excitability types I and II are related but not identical to classes A and B (for example, the model may belong to class A but have no well-defined excitability type when it is bistable).

For the limit case $b = a$ (i.e. $\frac{b}{g_L} = \frac{\tau_m}{\tau_w}$), the system undergoes a Bogdanov-Takens bifurcation. It has codimension two, i.e. it appears when simultaneously varying the two parameters $\bar{b}$ and $\bar{I}$. At this point, the family of unstable periodic orbits generated around the Andronov-Hopf bifurcation collides with the saddle fixed point and disappears via a saddle-homoclinic bifurcation. There is no other bifurcation in this model (as well as in Izhikevich model [144]). Other similar models such as the quartic model may also undergo a Bautin bifurcation, associated with stable oscillations (see chapter 2).

As already discussed, the system can have zero, one or two fixed points depending on the input current. When it has two fixed points, we denote by $x_+ < x_-$ the two fixed points for the general model and by V_+ and V_- in the AdExp model. The fixed points in the case of the original AdExp model are deduced from the expressions given in section 2.2.2 using the Lambert function W:

$$\begin{cases} V_- := E_L + \frac{I}{g_L+b} - \Delta_T W_0\left(-\frac{1}{1+b/g_L} e^{\frac{I}{\Delta_T(g_L+b)} + \frac{E_L-V_T}{\Delta_T}}\right) \\ V_+ := E_L + \frac{I}{g_L+b} - \Delta_T W_{-1}\left(-\frac{1}{1+b/g_L} e^{\frac{I}{\Delta_T(g_L+b)} + \frac{E_L-V_T}{\Delta_T}}\right) \end{cases} \tag{4.6}$$

where W_0 is the principal branch of the Lambert function and W_{-1} the real branch of the Lambert function such that $W_{-1}(x) \leq -1$, defined for $-e^{-1} \leq x < 1$.

The fixed point x_+, or V_+, is always a saddle fixed point (hence unstable), i.e. its Jacobian matrix has an eigenvalue with positive real part and an eigenvalue with negative real part. The fixed point V_- is stable if the model has class A parameters, otherwise it depends on the current I, as we discuss below.

Rheobase current

The rheobase current is the minimum constant current required to elicit a spike. This electrophysiological definition could be ambiguous because it depends on the initial

condition. If we consider that the current is slowly increased until a spike is elicited, then it corresponds to the first point when the stable fixed point becomes unstable, which depends on the parameter class (note that this is true only when the Andronov-Hopf bifurcation is subcritical).

For class A ($b < a$), it corresponds to the saddle-node bifurcation point:

$$I_{\rm rh}^A = -m(b) \tag{4.7}$$

which is obtained by calculating the intersection of the nullclines when these are tangent. It corresponds in the AdExp model for class A ($\frac{b}{g_L}\frac{\tau_w}{\tau_m} < 1$) to the curve:

$$I_{\rm rh}^A = (g_L + b)\Big[V_T - E_L - \Delta_T + \Delta_T \log\left(1 + \frac{b}{g_L}\right)\Big]. \tag{4.8}$$

For class B parameters ($b > a$), it corresponds to the Andronov-Hopf bifurcation point:

$$I_{\rm rh}^B = bv^*(a) - F(v^*(a)) \tag{4.9}$$

that reads for the AdExp model in the case $\frac{b}{g_L}\frac{\tau_w}{\tau_m} > 1$ to the curve:

$$I_{\rm rh}^B = (g_L + b)\Big[V_T - E_L - \Delta_T + \Delta_T \log(1 + \frac{\tau_m}{\tau_w})\Big] + \Delta_T g_L(\frac{b}{g_L} - \frac{\tau_m}{\tau_w}) \tag{4.10}$$

It is important to note that the saddle-node bifurcation also occurs in the class B case at the point $I_{SN} = I_{rh}^I$ ($> I_{\rm rh}^B$; for class B we use I_{SN} instead of I_{rh}^I to avoid ambiguities).

Voltage threshold for slow inputs

For a parametrized input $I_b(t)$, the threshold is the minimum value of the parameter b for which a spike is elicited. For example, the rheobase current is the threshold constant current. However, the notion of a spike threshold for neurons is often described as a *voltage threshold*, although the voltage is not a stimulation parameter (thus, it implicitly refers to an integrate-and-fire model). It is nevertheless possible to define a meaningful voltage threshold for the case of constant current inputs as follows: the voltage threshold is the maximum stationary voltage V for subthreshold constant current inputs ($I \leq I_{\rm rh}$). For the exponential integrate-and-fire model [95], this is simply V_T. For the present model, it corresponds to the voltage V_- at the first bifurcation point, when the stable fixed point becomes unstable.

Not surprisingly, its value depends on the excitability type. In the general case, for class A parameters ($b < a$), the voltage threshold is

$$V_{\rm threshold}^{\rm slow} = v^*(b),$$

which reads for the AdExp model in the case $b/g_L < \tau_m/\tau_w$

$$V_{\rm threshold}^{\rm slow} = V_T + \Delta_T \log(1 + b/g_L)$$

and for class B parameters ($b > a$)

$$V_{\rm threshold}^{\rm slow} = v^*(a)$$

and for the AdExp model for $b/g_L < \tau_m/\tau_w$

$$V_{\rm threshold}^{\rm slow} = V_T + \Delta_T \log(1 + \tau_m/\tau_w)$$

Interestingly, the threshold for class A parameters depends on the ratio of conductances (b), while the threshold for class B parameters on the ratio of time constants (a).

Voltage threshold for fast inputs

For short current pulses ($I = q\delta(t)$, where q is the total charge and $\delta(t)$ is the Dirac function), the voltage threshold is different, but the same definition may be used: it is the maximum voltage V that can be reached without triggering a spike. Injecting short current pulses amounts to instantaneously changing the membrane potential V, i.e., in the phase space (V,w), to moving along an horizontal line. If, by doing so, the point (V,w) exits the attraction basin of the stable fixed point, then a spike is triggered. Therefore, the threshold is a curve in the phase space, defined as the boundary of the attraction basin of the stable fixed point (for which we have unfortunately no analytical expression, although it can be computed numerically). Therefore the model displays *threshold variability*: the voltage threshold depends on the value of the adaptation variable w, i.e., on the previous inputs. The boundary of the attraction basin of the stable fixed point is either the stable manifold of the saddle fixed point (separatrix) or a limit cycle.

4.2.2 I-V curve

The I-V curve of a neuron is the relationship between the opposite of the (constant) injected current and the stationary membrane potential (it may also be defined for non-constant input currents, see e.g. [16]). Experimentally, this curve can be measured with a voltage-clamp recording. We obtain a simple expression by calculating I at the intersection of the nullclines:

$$I(v) = bv - F(v)$$

that can be written for the AdExp model in the form:

$$I(V) = (b+g_L)(V-E_L) - g_L\Delta_T \exp\left(\frac{V-V_T}{\Delta_T}\right)$$

Thus, far from threshold, the $I-V$ curve is linear and its slope is the leak conductance plus the adaptation conductance.

4.2.3 Oscillations

Because of the coupling between the two variables V and w, there can be oscillations near the resting potential. For the AdExp model or the Izhikevich' model, only damped oscillations exist, and self-sustained oscillations are not possible, except via Bautin bifurcation that exists for instance in the quartic model. Oscillations occur when the eigenvalues associated with the stable fixed point are complex; when they are real, solutions converge (locally) exponentially to the stable fixed point.

Because of the nature of the bifurcations, near the rheobase current (section 4.2.1), the model is non-oscillating if it has class A parameters ($b < a$, or $b/g_L < \tau_m/\tau_w$) and oscillating if it has class B parameters. Far from threshold, these properties can change. In this section we give explicit expressions for the parameter zones corresponding to both regimes.

The parameter zones depend on the excitability types, on the finiteness of $F'_{-\infty} \stackrel{\text{def}}{=} \lim_{v\to-\infty} F'(v)$, the ratio $a = \tau_w/\tau_m$ and the following condition:

$$b < \frac{(F'_{-\infty}+a)^2}{4a} \tag{4.11}$$

translated for the AdExp model in:

$$\frac{b}{g_L} < \frac{\tau_m}{4\tau_w}\left(1-\frac{\tau_w}{\tau_m}\right)^2 \tag{4.12}$$

These results are summarized in Fig. 4.3.

Identification of the oscillating regions

Oscillations around a stable equilibrium appear only when the systems has a stable fixed point, i.e. if $I < -m(b)$ for $b < a$ and $I < bv^*(a) - F(v^*(a))$ for $b > a$. Furthermore, the system will oscillate around the stable equilibrium v_- if and only if the imaginary part of the eigenvalues of the Jacobian matrix of the system at this point is non-null. This condition can be written at the stable equilibrium v_- via the discriminant δ defined by:

$$\delta = \big(F'(v_-)+a\big)^2 - 4ab.$$

The system will oscillate around the stable fixed point v_- if and only if $\delta < 0$. To invert this inequality, we compute the zones where we have

$$(x+a)^2 - 4ab < 0 \tag{4.13}$$

and check that a solution v_- exists. There exists a v_- such that $F'(v_-) = x$ if and only if $F'_{-\infty} := \lim_{u\to-\infty} F'(u) < x < F'(v^*(b)) = b$, since $v_- < v^*(b)$ and F' is increasing.

The solution of (4.13) is $x \in \{x_-, x_+\}$ where

$$x_\pm = -a \pm 2\sqrt{ab}$$

First of all we are interested in the apparition of oscillations in the class A case. We know that when the input current I is close to the rheobase current I^I_{rh} given by (4.7), the system returns monotonously to the resting potential. The system begins to oscillate when there exist solutions to the equation $F'(v_-) = x_+$. It is straightforward to check that x_+ is always lower than b, since this condition is equivalent to the condition $(a-b)^2 \geq 0$, which is always true.

If $F'_{-\infty} = -\infty$, as it is the case in the quadratic and quartic models, the condition $x_+ > F'_{-\infty}$ is trivial and always satisfied. If $F'_{-\infty} > -\infty$, then this condition can be written:

$$\{(a,b)\ ;\ a < -F'_{-\infty} \text{ or } 0 > F'_{-\infty} > -a \text{ and } b > \frac{(F'_{-\infty}+a)^2}{4a}\}$$

In this zone, oscillations occur when the current I is below I_+, where:

$$I_+^- = bv^*(x_+) - F(v^*(x_+))$$

Hence it appears for class A parameters. After the Bogdanov-Takens point, the equilibrium associated with x_+ is unstable, hence does not give rise to damped subthreshold oscillations.

In the case where $F'_{-\infty} > -\infty$ and $F'_{-\infty} > -a$, we always have $\frac{(F'_{-\infty}+a)^2}{4a} < a$. When $b = a$, we have $x_+ = a$ and hence $I_+ = I_v^-(v^*(a))$, which is the current at the Bogdanov-Takens

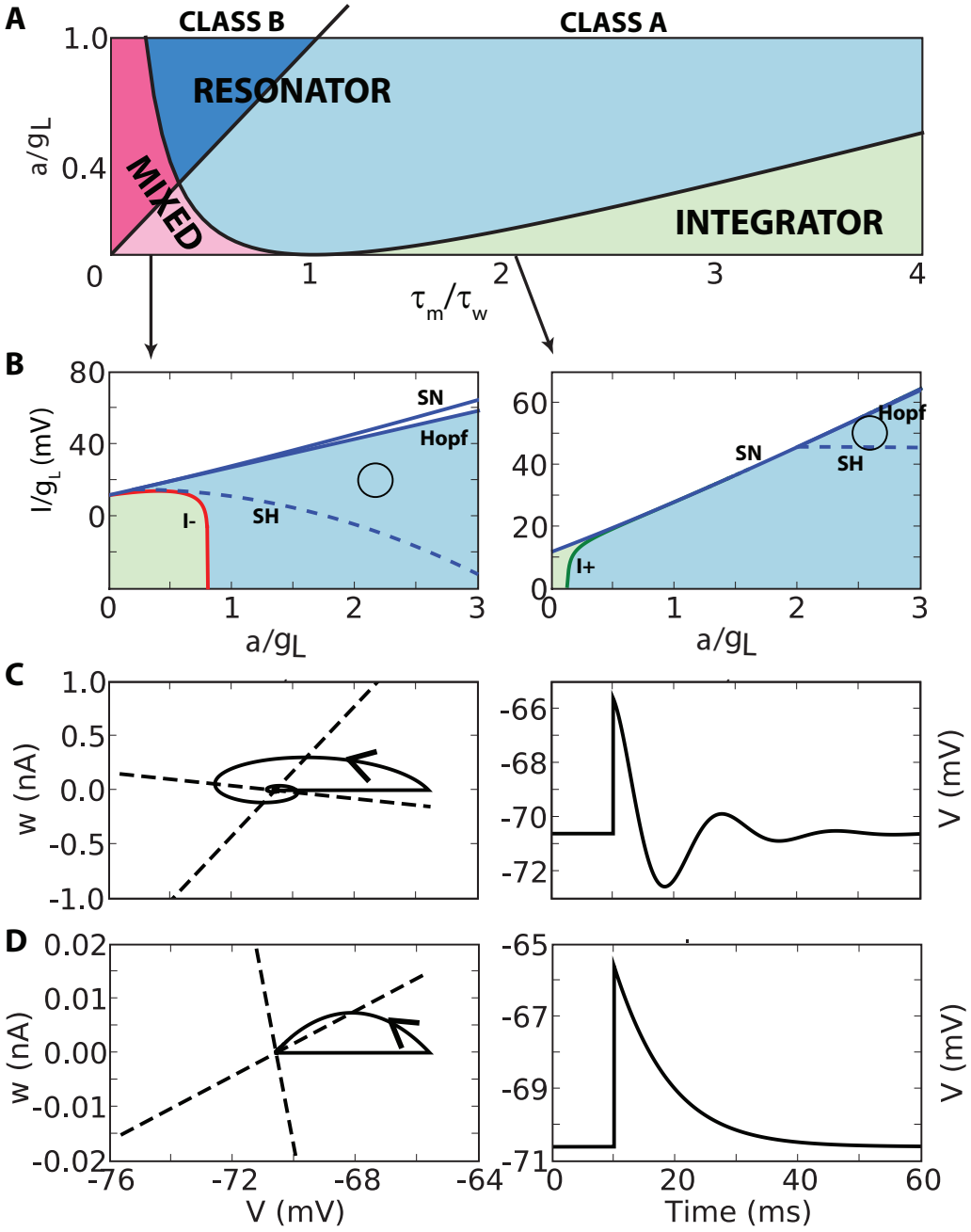

Figure 4.3: Oscillations. A. Behavior of the model as a function of a/g_L and τ_m/τ_w. Light (dark) colors indicate class A (class B) parameters. Blue: resonator mode (oscillations for any or almost any I). Green: integrator mode (oscillations for any I). Pink: mixed mode (resonator if I is large enough, otherwise integrator). B. Behavior of the model as a function of a/g_L and I/g_L for $\tau_m = .2\tau_w$ (left) and $\tau_m = 2\tau_w$ (right). White: spiking; blue: oscillations; green: no oscillation. Spiking occurs when I is above the saddle-node curve (SN) in the class A regime, and above the Hopf curve (Hopf) in the class B regime. A repulsive limit cycle (circle) exists when I is above the saddle-homoclinic curve (SH; only for class B). Oscillations occur when $I_- < I < I_+$ (on the left, $I_+ \geq I_{SN}$; on the right, $I_- = -\infty$). C,D. Response of the system to a short current pulse (Dirac) near the resting point, in the resonator regime (C; $a = 10g_L$, $\tau_m = \tau_w$) and in the integrator regime (D; $a = .1g_L$, $\tau_m = 2\tau_w$). Left: response in the phase space (V, w); right: voltage response in time.

bifurcation point. This result was predictable since around the saddle node bifurcation the system does not oscillate around the fixed point and around the Andronov-Hopf bifurcation the system does oscillate, and these two curves meet at the Bogdanov-Takens point. Furthermore, after the Bogdanov-Takens point, the equilibrium associated with x_+ is no more stable, hence damped subthreshold oscillations associated with this separatrix only appear for class A parameters.

The oscillations possibly disappear when a solution to $F'(v_-) = x_-$ exists. Since $x_- = -a - 2\sqrt{ab} < 0$, the condition $x_- < b$ is always satisfied. The condition $x_- > F'_{-\infty}$ is always satisfied when $F'_{-\infty} = -\infty$. If $F'_{-\infty} > -\infty$, then the condition $x_- > F'_{-\infty}$ is equivalent to the set of conditions

$$a < -F'_{-\infty} \qquad \text{and} \qquad b < \frac{(a+F'_{-\infty})^2}{4a}.$$

In these cases, oscillations disappear when $\bar{I} < \bar{I_-}$, where:

$$\bar{I_-} = bv^*(x_-) - F(v^*(x_-))$$

In the case of the AdExp model with the original parameters, the expression of $I_\pm$ reads:

$$I_\pm = (g_L + a)\Delta_T \log\left(\frac{g_L\tau_w - C \pm 2\sqrt{aC\tau_w}}{g_L\tau_w}\right) - \Delta_T \frac{g_L\tau_w - C \pm 2\sqrt{aC\tau_w}}{\tau_w} - (g_L + a)(E_L - V_T) \quad (4.14)$$

Hence there are two qualitatively different cases.

First of all, if $F'_{-\infty} = -\infty$, then the currents $I_\pm$ exist whatever the parameters of the model.

1. For class A parameters, the neuron oscillates around its stable equilibrium if and only if $I_- < I < I_+$.
2. For class B parameters, the neuron oscillates around the stable equilibrium if and only if $I_- < I < I^B_{rh}$.

If $F'_{-\infty} > -\infty$, then the behavior of the system depends on the parameters a and b and on the inequality

$$b > \frac{(F'_{-\infty} + a)^2}{4a} \quad (4.15)$$

1. For class A parameters, we have:
   (a) if $a < -F'_{-\infty}$, then I_+ always exists. If condition (4.15) is satisfied, then I_- does not exist and the system oscillates for $I < I_+$. If condition (4.15) is not satisfied, both I_+ and I_- are defined, and the system oscillates for $I_- < I < I_+$.
   (b) if $a > -F'_{-\infty}$, then I_- is undefined and I_+ only exists when condition (4.15) is satisfied. Hence if condition (4.15) is satisfied, the system oscillates for $I < I_+$ else it never oscillates.
2. For class B parameters, only the existence of I_- is important. When I_- is defined, then the system oscillates for any $I > I_-$. If I_- is not defined, the system always oscillates. In the class B regime, note that condition (4.15) is always satisfied. Hence we have:

(a) if $a < -F'_{-\infty}$ and condition (4.15) is not satisfied then I_- exists and the system oscillates for any subthreshold current greater than I_-.

(b) else it oscillates for any subthreshold current.

When the system oscillates, the oscillation (angular) frequency is given by $\bar{\omega} = -\delta$. If $F'_{-\infty} = -\infty$, then the frequency of the oscillations is bounded. If $F'_{-\infty} > -\infty$, then in the low-voltage approximation (far from $v_- << 0$), reads:

$$\bar{\omega} \approx 4ab - (F'_{-\infty} + a)^2$$

When the system oscillates, the time constant of the decay is the inverse of the opposite of the real part of the eigenvalues, which is $\frac{2}{a - F'(v_-)}$.

It becomes infinitely fast in the low voltage approximation if $F'_{-\infty} = -\infty$, else converges to

$$\frac{2}{a - F'_{-\infty}}$$

Oscillations for class A parameters in the AdExp model

Three cases appear:

- If inequality (4.12) is false, then the model oscillates when $I < I_+$, where the formula for I_+ is given in Appendix 4.2.3. In practice, we observe that I_+ is very close to the rheobase current, so that the model almost always oscillates below threshold.

- If inequality (4.12) is true and $\tau_m > \tau_w$, then the model never oscillates near the fixed point.

- If inequality (4.12) is true and $\tau_m < \tau_w$, then the model oscillates when $I_- < I < I_+$, where the formula for I_- is given in Appendix 4.2.3.

Oscillations for class B in the AdExp model

Two cases appear:

- If inequality (4.12) is false, then the model always oscillates near the fixed point, for any subthreshold input current I.

- If inequality (4.12) is true, then the model oscillates only when $I > I_-$.

We call the occurrence of oscillations the *resonator* regime and their absence the *integrator* regime (see 4.2.4). The model is called a resonator when it is always (for all I) or almost always (for $I < I_+$) in the resonator regime, i.e., when inequality (4.12) is false; it is called an integrator when it never oscillates, i.e., when $\tau_m > \tau_w$ and inequality (4.12) is true; it is said to be in a mixed mode when it oscillates only above some value I_- (see Fig. 4.3).

Frequency of oscillations in the AdExp model

When the model oscillates, the frequency of the oscillations is:

$$F = \frac{\omega}{2\pi} = \frac{2b}{\pi g_L \tau_w} - \frac{2}{\pi \tau_m}\left(e^{\frac{V_- - V_T}{\Delta_T}} - 1 + \frac{\tau_m}{\tau_w}\right)^2, \tag{4.16}$$

which can be approximated far from threshold ($V_- \ll V_T$) as follows:

$$F = \frac{\omega}{2\pi} \approx \frac{2b}{\pi g_L \tau_w} - \frac{2}{\pi \tau_m}\left(1 - \frac{\tau_m}{\tau_w}\right)^2. \tag{4.17}$$

4.2.4 Input integration

The way the model integrates its inputs derives from the results above.

Resonator vs. integrator

On the temporal axis, the integration mode can be defined locally (for a small input $I(t)$) as

$$V(t) = V_0 + (K \star I)(t)$$

where the kernel K is the linear impulse response of the model around V_0, and $K \star I$ is a convolution. This impulse response is determined by the eigenvalues of the stable fixed point. When these are complex, the kernel K oscillates (with an exponential decay), as discussed in section 4.2.3 (see Fig. 4.3C). In that case the model acts as a *resonator*: two inputs are most efficient when separated by the characteristic oscillation period of the model (given by eq. 4.16). The membrane time constant is $-1/\lambda$, where λ is the real part of the eigenvalues, that reads:

$$\tau = \frac{2}{a - F'(v_-)}.$$

Far from threshold ($v \ll -1$), this time constant tends to 0 when $F'_{-\infty} = -\infty$, else it tends to:

$$\tau \approx \frac{2}{a - F'_{-\infty}},$$

or, for the AdExp model in the case $V \ll V_T$:

$$\tau = 2\frac{\tau_m \tau_w}{\tau_m + \tau_w}$$

When the eigenvalues are real, the kernel K is a sum of two exponential functions, and the model acts as an integrator. In that case there are two time constants, given by the real part of the eigenvalues. It is interesting to note that there is a parameter region where both integration modes can exist, depending on the (stationary) input current I: oscillations arise only when the model is sufficiently depolarized ($I > I_-$).

Adaptation

There are two sorts of adaptation in the model: threshold adaptation and voltage adaptation. The former one comes from the orientation of the separatrix in the (V,w) plane, as we discussed in section 4.2.1. The latter one derives from the fact that in the integrator mode (no oscillation), the model kernel K is a sum of two exponential functions. If the slower one is negative, then the response to a step shows an overshoot (as in Fig. 4.4D for a negative current step), which is a form of adaptation (the voltage response is initially strong, then decays). That overshoot in the AdExp model can be seen when there is no oscillation and $\tau_m < \tau_w$ (see section 4.3), i.e., in the *mixed mode* shown in pink in Fig. 4.3, when the input current is low ($I < I_-$).

4.2.5 The attraction basin of the stable fixed point

Limit cycle

The existence of a repulsive limit cycle arises for class B parameters from the Andronov-Hopf bifurcation. The saddle-node and Andronov-Hopf bifurcations collide via a Bogdanov-Takens bifurcation. In the neighborhood of this bifurcation, the family of limit cycles disappears via a saddle-homoclinic bifurcation. The normal form of the Bogdanov-Takens bifurcation gives us a local approximation of this saddle-homoclinic bifurcation curve around the point in parameter space given by (4.18) (see [254]), and the full saddle-homoclinic curve can be computed numerically using a continuation algorithm. The current I above which a limit cycle exists is locally approximated at the second order around the Bogdanov-Takens point $b = a$, $I = I_{BT} \stackrel{\text{def}}{=} -m(a)$ by the following expression:

$$I_{\text{cycle}} = I_{BT} - \frac{12}{25}\frac{(b-a)^2}{aF''(v^*(a))} + o\left((b-a)^2\right), \tag{4.18}$$

for $b > a$, which has the expression for the AdExp model:

$$I_{\text{cycle}} = I_{BT} - \frac{12}{25}\frac{\Delta_T \tau_w^2}{C(\tau_m+\tau_w)}(b - \frac{C}{\tau_w})^2 + o(b_1^2) \tag{4.19}$$

for $b > \frac{C}{\tau_w}$, where I_{BT} is the rheobase current at the Bogdanov-Takens bifurcation:

$$I_{BT} = (g_L + \frac{C}{\tau_w})\left[V_T - E_L - \Delta_T + \Delta_T \log\left(1 + \frac{C}{g_L \tau_w}\right)\right]$$

Below the threshold current I_{cycle}, there is no limit cycle (see next section). Above the I_{cycle}, there is a family of limit cycles, which are repulsive in the case of the AdExp model or the quadratic adaptive model, and that depend on the location of the parameters with respect to the Bautin bifurcation in the cases where it exists, circling anti-clockwise around the stable fixed point (see Fig. 4.3B and 4.4A); the saddle fixed point is outside that cycle. Interestingly, it appears that one can exit the attraction basin of the stable fixed point (and thus generate a spike) not only by increasing V, but also by decreasing V or w (or increasing w). This phenomenon is sometimes called *rebound*, and we discuss it further in section 4.2.6.

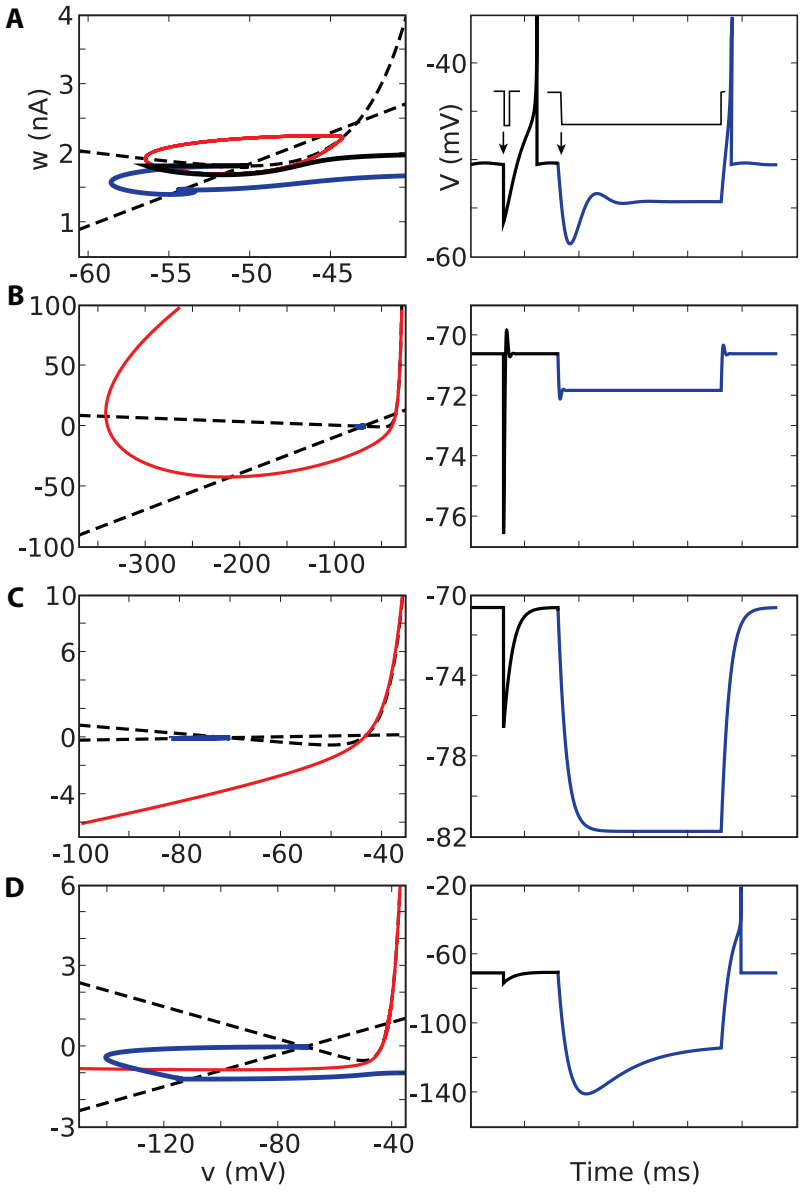

Figure 4.4: The attraction basin of the stable fixed point and rebound properties. Left column: the dashed lines represent the nullclines, each panel corresponds to a different set of parameter values; the red line delimits the attraction basin of the stable fixed point; the black line is the trajectory of the model in response to a short negative current pulse, while the blue line is the trajectory in response to a long negative current step. Right column: voltage response of the model to the a short pulse (black) and to a long step (blue). A. Class B resonator ($a = 3g_L,\ \tau_w = 2\tau_m$) close to the rheobase current. A repulsive limit cycle appears. Trajectories can escape the attraction basin and spike with fast or slow hyperpolarization. B. Class A resonator ($a = 10g_L,\ \tau_m = 12\tau_w$). The separatrix crosses both nullclines (for both branches, V and w go to $+\infty$). In theory trajectories can escape the attraction basin with hyperpolarization, but one would need to reach unrealistically low voltages (< -200 mV). C. Integrator ($a = .2g_L, \tau_m = 3\tau_w$). The separatrix does not cross the nullclines. No rebound is possible. D. Class B mixed mode ($a = g_L,\ \tau_w = 10\tau_m$). The separatrix crosses the w-nullcline. Rebound is possible with long hyperpolarization (short hyperpolarization can also induce rebounds, but with unrealistically low voltages).

Separatrix

Some information about the stable manifold of the saddle fixed point can be obtained from the nullclines (when these intersect). The nullclines cut the plane in 5 connected zones, which we call North, South, West, East and Center, as shown in figure 4.1. The stable manifold consists in two trajectories which converge to the saddle fixed point. Near the saddle point, these two trajectories must lie in the North and South zone, or in the Center and East zones.

First we remark that all the trajectories starting from the East zone must spike. Indeed, in that region, V increases and w decreases, until it crosses the w-nullcline horizontally and enters the South zone. From that point, V keeps on increasing and w increases, which implies that the trajectory can only remain in the South zone or enter the East zone. However, the direction of the vector fields along the border does not allow crossing from South to East. Therefore, the trajectory will remain in the South zone and will spike. It follows that no part of the stable manifold can be in the East zone. Therefore it has to be locally in the North and South zones. By following the manifold from the saddle point to the North, we can see that V and w increase and, since the manifold cannot enter the East zone, it remains in the North zone and goes to infinity. In practice, it is in fact very close (but slightly to the left) of the V-nullcline, as shown in Fig. 4.4.

By following the manifold from the saddle point to the South, we can see that it has the same orientation as in the North zone, as long as it remains in the South zone. It may however cross the w-nullcline (Fig. 4.4D), and possibly the V-nullcline again (Fig. 4.4B).

For class A regime, or class B when $I < I_{\text{cycle}}$, there is no limit cycle. In that case the stable manifold of the saddle fixed point is an unbounded separatrix, i.e., it delimits the attraction basin of the stable fixed point. From the position of the nullclines, it appears that the stable manifold must cross the saddle fixed point from above both nullclines (North) to below both nullclines (South). It follows that the side above the nullclines is the graph of an increasing function of V (see Fig. 4.4). As for the other part of the manifold, several cases can occur: it may cross the w-nullcline, both nullclines or none. We can show that if condition (4.11) is false, then both nullclines are crossed, and if $\tau_m < \tau_w$, then at least the w-nullcline is crossed. These conditions cover all parameter regions except the zone where the model is always an integrator (no oscillations); in particular, it includes class B parameters. The position of the separatrix has important implications for the rebound property (section 4.2.6).

To understand whether the stable manifold can cross the w-nullcline and possibly the V-nullcline, we study the asymptotic behavior of the solutions when $t \to -\infty$. The idea is the following: if the manifold goes to $-\infty$ (for V), then the derivative of the nonlinear term vanishes tends to its limit $F'_{-\infty}$ which can either be finite, or $-\infty$. In the following we shall assume that the manifold does not cross the V-nullcline. In that case, the voltage $V(t)$ of the manifold, seen as a solution of the system, goes to $-\infty$ as $t \to -\infty$, and we will look for possible contradictions.

If we have $F'_{-\infty} = -\infty$, the trajectories are asymptotically horizontal and hence will necessarily cross the w-nullcline, but not necessarily the v-nullcline. In the case where $F'_{-\infty} > -\infty$, the approximated dynamics can be solved analytically. Asymptotically, the differential equations satisfied by a given solution (v, w) of the rescaled model can be approximated by:

$$\begin{cases} \dot{v} &= F'_{-\infty} v - w + I \\ \dot{w} &= a(bv - w) \end{cases} \tag{4.20}$$

When $t \to -\infty$, the solutions of the linear system either spiral around the fixed point (complex eigenvalues) or align asymptotically to the direction of eigenvector associated to the smallest negative eigenvalue of the matrix L governing the dynamics of the linear system (4.20):

$$L = \begin{pmatrix} F'_{-\infty} & -1 \\ ab & -a \end{pmatrix}$$

If the eigenvalues of this matrix are complex, i.e., when $b > \frac{(a+F'_{-\infty})^2}{4a}$, then the solutions spiral around the fixed point. Therefore the trajectories cross the V-nullcline, which contradicts our initial hypothesis. Thus when $b > \frac{(a+F'_{-\infty})^2}{4a}$ (resonator regime), the stable manifold crosses both nullclines.

If the eigenvalues are real, the trajectories of the linear system align asymptotically to the direction of the lower eigenvalue

$$\lambda_- = -\frac{1}{2}(a - F'_{-\infty} + \sqrt{(F'_{-\infty} + a)^2 - 4ab})$$

This eigenvalue is always strictly negative hence solutions will diverge when $t \to -\infty$. The eigenvector associated with this eigenvalue is:

$$\begin{pmatrix} \frac{2}{a+F'_{-\infty}+\sqrt{(F'_{-\infty}+a)^2-4ab}} \\ 1 \end{pmatrix}$$

The slope of that eigenvector is always inferior to $F'_{-\infty}$, so that (linearized) trajectories do not cross the V-nullcline. However they can cross the w-nullcline when the slope of the eigenvector is smaller than b, i.e.:

$$\frac{a + F'_{-\infty} + \sqrt{(F'_{-\infty} + a)^2 - 4ab}}{2} < b$$

and this condition is satisfied when $b > \frac{1}{2}(a + F'_{-\infty})$. Assuming $\bar{a} > 0$, the inequality is always true if $\bar{\tau_w} > -F'_{-\infty}$; when when $\bar{\tau_w} < -F'_{-\infty}$, the inequality is never true given that the eigenvalues are real ($b > \frac{(a+F'_{-\infty})^2}{4a}$).

In summary, the stable manifold crosses both nullclines when $b > \frac{1}{2}(a + F'_{-\infty})$(resonator regime), and it crosses at least the w-nullcline when $\bar{\tau_w} > -F'_{-\infty}$ or $F'_{-\infty} = -\infty$.

4.2.6 Rebound

The term *rebound* refers to the property that a spike can be triggered by hyperpolarizing the membrane. This can be done either by sending a short negative current pulse, which amounts to moving the state vector (V, w) horizontally to the left, or by slowly hyperpolarizing the membrane with a long negative current step (or ramp) and releasing it, which amounts to moving the state vector along the w-nullcline.

For class A parameters, there is no limit cycle and there is an unbounded separatrix. If $\tau_m < \tau_w$ or if condition (4.11) is false, then the separatrix crosses the w-nullcline. It follows that both types of rebounds are possible. Otherwise the model is in the integrator regime, and the the separatrix may not cross the w-nullcline. In

that case it is only possible to trigger a spike by increasing the voltage: there is no rebound.

For class B parameters, there is either a repulsive limit cycle which circles the stable fixed point when the input current is close enough to the rheobase current ($I > I_{\text{cycle}}$), or the separatrix crosses both the w-nullcline and the v-nullcline. In both cases, it is possible to exit the attraction basin of the stable fixed point and thus trigger a spike by changing any variable in any direction. Therefore, both types of rebound are possible. Note that with short current pulses, a more negative voltage must be reached in order to trigger a spike.

4.2.7 After-potential

After a spike, the state vector resets to a certain point in the state space. The subsequent trajectory is determined by this initial state. We will discuss the spike sequences in more details in section 4.4, but here we simply note that if the state vector is reset above the V-nullcline, then the membrane potential V will first decrease then increase (broad after-potential, or after-potential hyperpolarization); if the state vector is reset below the V-nullcline, V will increase (sharp after-potential).

The depolarizing after potential (figure 2.5.(xvii).) is linked with the position of the reset in the oscillatory case. In that case, if the neuron elicits a spike and is reset in the attraction basin of the stable fixed point, then the return to equilibrium will present oscillations around the fixed point. If the reset occurs on a point of a converging trajectory for which the voltage is increasing, the return to equilibrium will be characterized by a depolarizing afterpotential, i.e. the voltage will increase before returning to equilibrium.

4.3 Overshoot

As discussed in section 4.2.4, the response of the neuron to a current step can present an overshoot when the coefficient of the slower exponential term is negative. In this section we show that in the low-voltage approximation ($V \ll V_T$), there is an overshoot if and only if $\tau_m < \tau_w$ and there is no oscillation, thus, in the mixed mode regime (Fig. 4.3).

Indeed, in the low voltage approximation, the dynamics is linear and is governed by the operator:

$$L = \begin{pmatrix} -1 & -1 \\ \frac{\bar{a}}{\tau_w} & -\frac{1}{\tau_w} \end{pmatrix}$$

which can be diagonalized. The overshoot appears only when the eigenvalues are real. In this case, the voltage response to a short pulse (Dirac) is a sum of two exponential functions $v(t) = \alpha e^{-t/\tau_1} + \beta exp^{-t/\tau_2}$ (we set the resting potential to 0) where $\frac{-1}{\tau_1}$ and $\frac{-1}{\tau_2}$ are the two real eigenvalues of L. The coefficient of the slower exponential term is

$$\frac{\varepsilon}{2\delta}(\sqrt{\delta}(1-\bar{\tau_w}) + \delta)$$

with $\delta = (1-\bar{\tau_w})^2 - 4\bar{a}\bar{\tau_w}$. We now write the negativity condition of this coefficient:

$$\sqrt{\delta}(1-\bar{\tau_w}) + \delta < 0 \Leftrightarrow 1 - \bar{\tau_w} < -\sqrt{\delta}$$

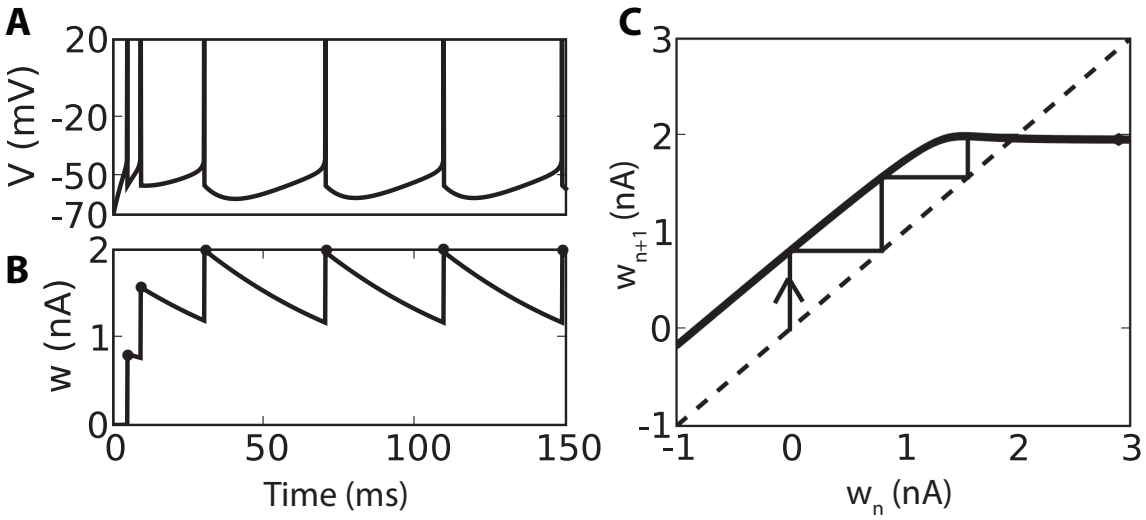

Figure 4.5: The adaptation map. A, B. Response of a class A model to a suprathreshold constant input (A: membrane potential V; B: adaptation variable w). The value of w after each spike defines a sequence (w_n). C. The adaptation map Φ maps the value of the adaptation variable from one spike to the next. The sequence (w_n) is the orbit of w_0 under Φ.

A necessary condition for this inequality to be satisfied is $\bar{\tau_w} > 1$. In this case, the condition reads:

$$(1-\bar{\tau_w})^2 > \delta = (1-\bar{\tau_w})^2 - 4\bar{a}\bar{\tau_w}$$

which is always true since $\bar{a}\bar{\tau_w} > 0$. Hence the overshoot appears in the low voltage approximation (far from threshold) when $\bar{\tau_w} > 1$, i.e., when $\tau_m < \tau_w$.

4.4 SPIKE PATTERNS

In the previous section, we analyzed the subthreshold dynamics of the model and found a rich structure, with the two parameters b and a, i.e. b/g_L and τ_m/τ_w for the AdExp model, controlling excitability, oscillations and rebound properties. Here we turn to the patterns of spikes, such as regular spiking, tonic/phasic bursting or irregular spiking, and explain them in terms of dynamics. Compared to the previous section, two additional parameters play an important role: the reset value V_r and the spike-triggered adaptation parameter d.

To study the spike sequences, use the Poincaré map (or adaptation map) introduced in chapter 3 which transforms the continuous time dynamics of the system into the discrete time dynamics of that map.

4.4.1 The adaptation map

In this section we recall the definition of this map and present some of its main features in the specific case of the AdExp model. v

We recall that after a spike emission, the potential V is always reset to the same value V_r, therefore the trajectory is entirely determined by the value of the adaptation variable w at spike time: the sequence of values (w_n), $w_n = t_n$ ($t_n =$ time of spike number n) uniquely determines the trajectory after the first spike. The adaptation function Φ

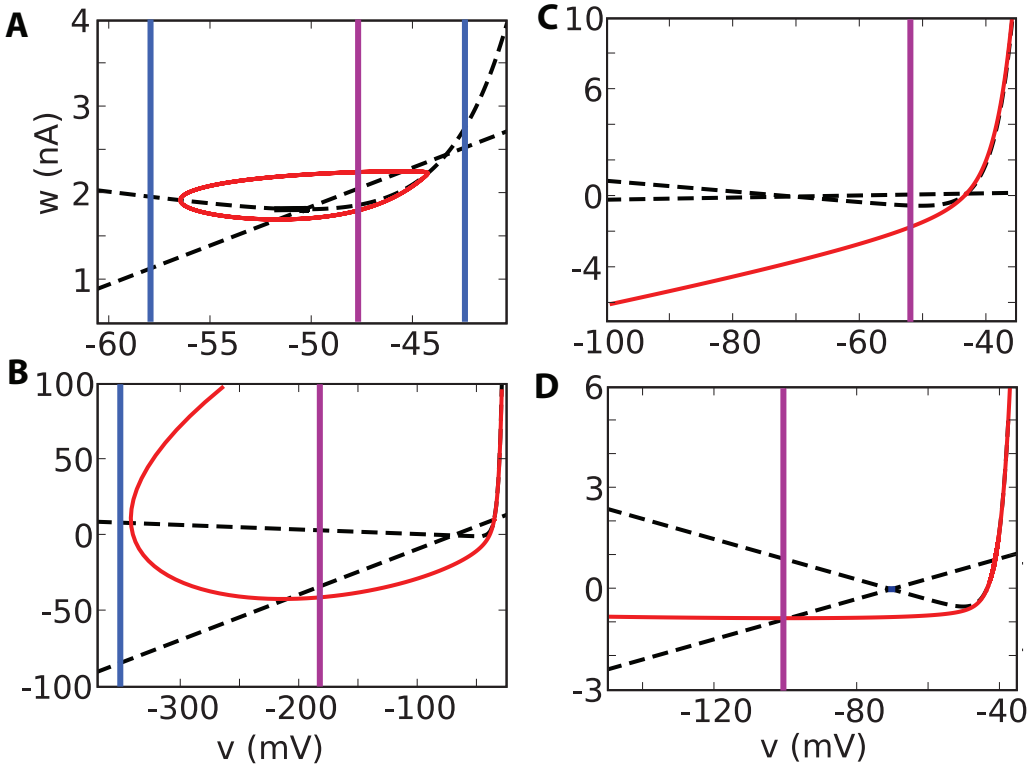

Figure 4.6: The spiking domain $\mathscr{D}$ for the same cases as in Fig. 4.4, when the nullclines (dashed lines) intersect. The attraction basin of the stable fixed point is bounded by the red curve. The blue and purple vertical lines indicate the reset line $V = V_r$. When that line is outside the attraction basin (blue), then $\mathscr{D} = \mathbb{R}$ and the model is bistable (tonic/resting). When the line intersects the attraction basin (purple), then $\mathscr{D}$ is an interval or the union of two intervals. In that case, the model is generally phasic (C,D) but may be bistable (A,B). In practice, with realistic values of d (spike-triggered adaptation), bistability essentially occurs when there is a limit cycle (A).

mapping w_n to w_{n+1} introduced in chapter 3 will therefore be used to characterize the spikes. We define again $\mathscr{D}$ as the domain of the adaptation variable w such that the solution of (4.1) with initial condition (V_r, w) spikes (blows up in finite time). Then the adaptation map Φ is

$$\Phi : \begin{cases} \mathscr{D} \mapsto \mathbb{R} \\ w_0 \mapsto w_\infty + d \end{cases} \tag{4.21}$$

where w_∞ is the value of w at divergence time (spike time) for the trajectory starting from (V_r, w_0), as illustrated in Fig. 4.5. The sequence (w_n) is the orbit of w_0 under Φ, as shown in Fig. 4.5C. Note that this sequence may be finite if for some n, $w_n \notin \mathscr{D}$. The property that the sequence is infinite (resp. finite) is called *tonic spiking* (resp. *phasic spiking*). The spike patterns are determined by the dynamical properties of Φ (fixed points, periodic orbits, etc.), as we show in next section. First, we examine the spiking domain $\mathscr{D}$.

When there is no stable fixed point, i.e., when I is above the rheobase current (section 4.2.1), either $I_{\rm rh}^A$ or $I_{\rm rh}^B$ depending on the excitability type, then any trajectory spikes, except that starting at a countable number of points in the case $I_{\rm rh}^B < I <$

$I_{\rm rh}^A$: the unstable fixed points or the intersections of the line $V = V_r$ with the stable manifold of the saddle fixed point.($\mathscr{D} = \mathbb{R} \setminus \{\text{these points}\}$. When there is a stable fixed point, all trajectories starting inside the attraction basin of that fixed point will not spike. The spiking domain $\mathscr{D}$ is then the complementary of the intersection of the reset line $V = V_r$ with the attraction basin of the stable fixed point (up to a projection onto the w axis), as shown in Fig. 4.6. We previously found (4.2.5) that the attraction basin of the stable fixed point is either a limit cycle or the stable manifold of the saddle fixed point. In the latter case, it may have a minimum voltage (resonator) or not (integrator or mixed). Fig. 4.6 shows how these different cases determine the spiking domain $\mathscr{D}$. We summarize these findings below, and describe the adaptation map Φ.

We first define two special values w^* and w^{**} as follows: the reset line $V = V_r$ intersects the V-nullcline and w-nullcline at the points (V_r, w^*) and (V_r, w^{**}), respectively, where

$$\begin{cases} w^* & = -g_L(V_r - E_L) + g_L \Delta_T \exp\left(\frac{V_r - V_T}{\Delta_T}\right) + I \\ w^{**} & = b(V_r - E_L) \end{cases}$$

Nearby spiking trajectories starting on the reset line $V = V_r$ above w^* (i.e., above the V-nullcline) may spike only after half a turn (since V initially decreases), or possibly an odd number of half-turns, which implies that the vertical order of the trajectories is reversed at spike time: Φ is locally decreasing above w^*. Spiking trajectories starting below w^* spike either directly or after an even number of half-turns, so that Φ is locally increasing below w^*. It follows that the sequences (w_n) are bounded.

We now describe the map Φ and the spiking domain $\mathscr{D}$ for the two excitability types, depending on the input current I.

1. Class A:

   (a) (subthreshold) if $I < I_{rh}^A$, then there is a stable fixed point and no limit cycle (see section 4.2.5). If the separatrix has no lower bound (typically: integrator or mixed regime), then the domain $\mathscr{D}$ is an interval $(-\infty, w_{\max})$ where $w_{\max}$ is the value of the adaptation variable on the separatrix for $V = V_r$. The map Φ is continuous on that set. We note that if $V_- < V_r < V_+$, then there can only be phasing spiking: indeed, $w_{n+1} > w_n + b$ for all n, therefore at some point the orbit exits $\mathscr{D}$.

   When the separatrix has a lower voltage bound $V_{\min}$ (typically: resonator), then there are two cases. If $V_r < V_{\min}$, then $\mathscr{D} = \mathbb{R}$ and Φ has the same properties as in case 1b. If $V_r > V_{\min}$, then $\mathscr{D} = (-\infty, w_{\min}) \cup (w_{\max}, +\infty)$. Besides, $\Phi((w_{\max}, +\infty)) \subset \Phi((-\infty, w_{\min}))$.

   (b) (suprathreshold) if $I > I_{rh}^A$, all trajectories spike. Therefore, $\mathscr{D} = \mathbb{R}$. The adaptation map is concave for $w < w^*$, regular, has a unique fixed point and an a horizontal asymptote when $w \to +\infty$.

2. Class B:

   (a) (subthreshold) if $I < I_{\rm cycle}$, then there is a stable fixed point and no limit cycle, so that the situation is similar to case 1b.

   (b) (subthreshold) if $I_{\rm cycle} < I < I_{rh}^B$, then there is a stable fixed point and a repulsive limit cycle bounding the attraction basin of the stable fixed point. Let $V_{\max}$ and $V_{\min}$ be the two extremal voltage values of the limit cycle. For $V_r < V_{\min}$ or $V_r > V_{\max}$, $\mathscr{D} = \mathbb{R}$ and Φ has the same properties as in case 1b.

(c) (suprathreshold) if $I_{rh}^B < I < I_{SN}$, then there are two unstable fixed points and no limit cycle, hence all trajectories spike. Therefore $\mathscr{D} = \mathbb{R}$. When $V_r \in (V_-, V_+)$, the adaptation map is discontinuous at some point $w_{\max} < w^*$, and $\Phi(w_{\max}) < \Phi(w_{\max}^-)$ (when trajectories start circling around the fixed point). Thus Φ is locally but not globally increasing on $(-\infty, w^*)$. The map Φ also has a horizontal asymptote when $w \to +\infty$.

(d) (suprathreshold) if $I > I_{SN}$, then $\mathscr{D} = \mathbb{R}$ and Φ has the same properties as in case 1b (class A).

Tonic spiking occurs for any initial w_0 if $\mathscr{D} = \mathbb{R}$ (in particular, in the suprathreshold regime). In other cases, spiking is generally phasic but there can be tonic spiking if the set $\bigcap_{n=0}^{\infty} \Phi^n(\mathscr{D})$ is not empty. When it occurs, the model is bistable.

The sequence $(w_n)_{n\geq 0}$ of values of the adaptation variable at spike times is the orbit of w_0 under Φ: $w_n = \Phi^n(w_0)$. Since there is a mapping from w to the interspike interval, the properties of Φ determine the spike patterns. In the following, we examine the relationship between the adaptation map Φ and the spike patterns.

4.4.2 Tonic Spiking

Regular Spiking

Regular spiking means that interspike intervals are regular, possibly after a transient period of shorter intervals. For the adaptation variable, it means that the sequence (w_n) converges, i.e., Φ has a stable fixed point. This situation is shown in Fig. 4.5. For low initial values of the adaptation variable, Φ is increasing and $\Phi(w) > w$, so that the sequence (w_n) is increasing, implying that the duration of interspike intervals decreases (this implication is true for $w < w^*$, i.e., before the maximum of Φ).

The shape of after-potentials (broad or sharp) depends, as we previously saw, on whether (V_r, w) is above or below the V-nullcline, i.e., whether $w > w^*$ or $w < w^*$. Asymptotically, the condition for broad resets is thus $w_{\text{fp}} > w^*$, where w_{fp} is the fixed point of Φ. Given the properties of Φ, this means $\Phi(w^*) > w^*$. Since the parameter d (spike-triggered adaptation) shifts the curve of Φ vertically, there is a minimum d above which resets are (at least asymptotically) broad.

When Φ is continuous (cases 2d and 1b), it always has a fixed point (since $\Phi(w) > w + d$ for low w and Φ converges to a finite limit when $w \to +\infty$), but that fixed point may not be stable. That property depends on all parameter values; in particular, the fixed point is an attraction basin when d or I is large enough (for large d, the fixed point is on the plateau of Φ, which implies broad resets). If the fixed point is not stable, then the sequence (w_n) may converge to a periodic orbit or be irregular.

Bursting

A bursting response is a sequence of shortly spaced spikes, separated by longer intervals. For the adaptation variable w, it corresponds to a periodic orbit, where the period equals the number of spikes per burst. For the adaptation map, p-periodic orbits are associated with stable fixed points of Φ^p. This situation is illustrated in Fig. 4.7. Typically, bursting occurs for large reset values V_r: the first spike resets the trajectory to a high voltage value, which induces a fast spike, and the adaptation builds up after each spike, until the trajectory is reset above the V-nullcline (after the peak of Φ at w^*). At that point $dV/dt < 0$ and the trajectory must turn in phase space before

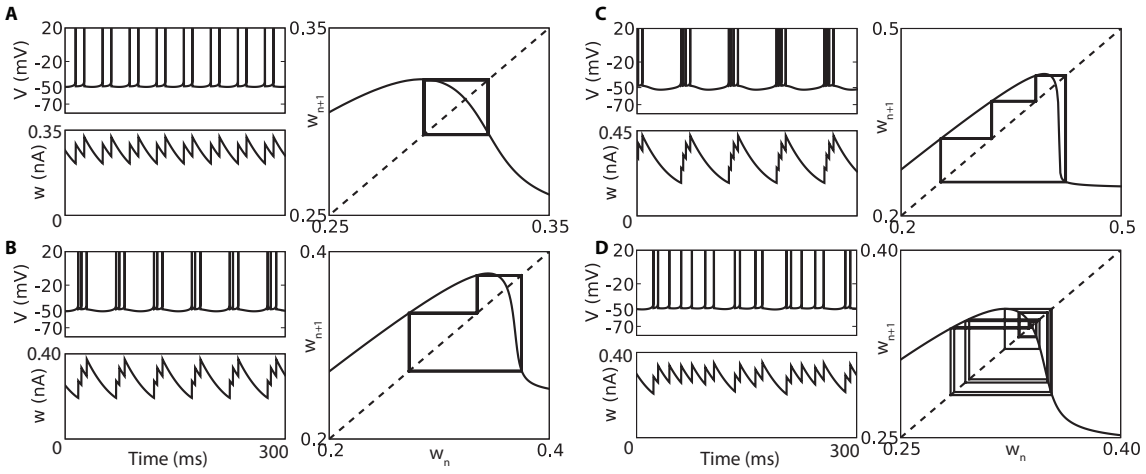

Figure 4.7: Bursting and chaos. Each panel shows a sample response (V and w) from the model, with different values of V_r (parameters: $C = 281$ pF, $g_L = 30$ nS, $E_L = -70.6$ mV, $V_T = -50.4$ mV, $\Delta_T = 2$ mV, $\tau_w = 40$ ms, $b = 4$ nS, $d = 0.08$ nA, $I = .8$ nA). A burst with n spikes corresponds to an n-periodic orbit under Φ. The last spike of each burst occurs in the decreasing part of Φ, inducing a slower trajectory. A. Bursting with 2 spikes ($V_r = -48.5$ mV). B. Bursting with 3 spikes ($V_r = -47.7$ mV). C. Bursting with 4 spikes ($V_r = -47.2$ mV). D. Chaotic spiking ($V_r = -48$ mV).

it spikes, producing a long interspike interval. Thus, the number of spikes per burst increases when V_r increases (since w^* increases with V_r) and when d decreases. Thus the bifurcation diagram with respect to V_r (Fig. 4.8) shows a period adding structure. Interestingly, when zooming on a transition from n to $n+1$ spikes, a period doubling structure appears, revealing chaotic orbits.

Chaotic spiking

The period doubling structure shown in Fig. 4.8B implies that orbits are chaotic for some parameter values. A sample response of the model for one of those values is shown in Fig. 4.7D. It results in irregular, unpredictable firing, in response to a constant input current.

4.4.3 Phasic spiking

Phasic spiking or (bursting) can occur in subthreshold regimes ($I < I_{\rm rh}^A$ for class A parameters, $I < I_{\rm rh}^B$ for class B), when there is a stable fixed point and $\mathscr{D} \neq \mathbb{R}$. In that case, the system needs to be destabilized (e.g. a short current pulse, which may be positive or negative, as explained section 4.2.6). The situation depends on the properties of the attraction basin of the stable fixed point, and can be understood from Fig. 4.6.

We can distinguish two cases:

1. If $\mathscr{D} = (-\infty, w_{\min})$ (C,D: integrator or mixed regime), then when $V_- < V_r < V_+$ there can only be phasic spiking, otherwise tonic spiking is possible. Indeed, if $V_- < V_r < V_+$, then the sequence (w_n) is such that $w_{n+1} > w_n + d$, so that it must exit $\mathscr{D}$ in finite time.

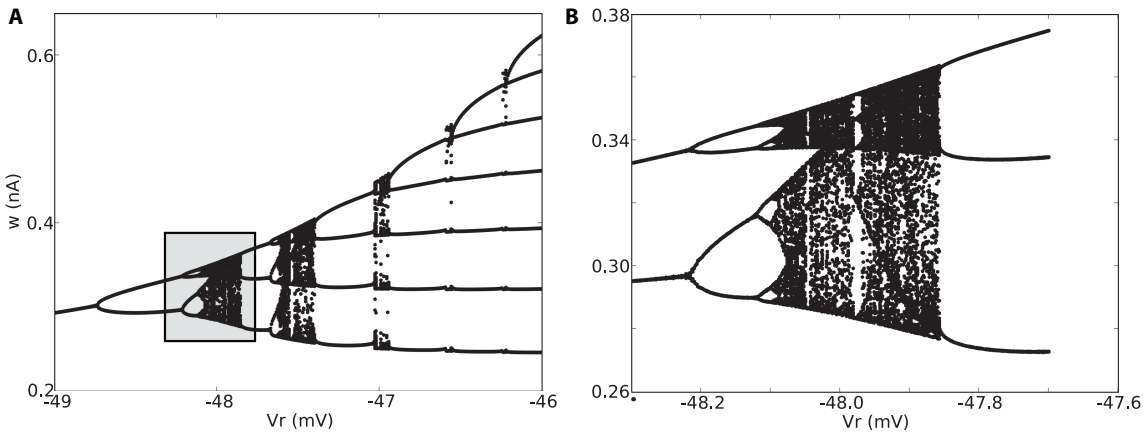

Figure 4.8: Bifurcation structure with increasing V_r (same parameters as in Fig. 4.7). A. Bifurcation diagram showing a period adding structure (orbits under the adaptation map Φ with varying values for V_r). Fixed points indicate regular spiking, periodic orbits indicate bursting, dense orbits indicate chaos. B. Zoom on the bifurcation diagram A (as indicated by the shaded box), showing a period doubling structure.

2. If $\mathscr{D} = (-\infty, w_{\min}) \cup (w_{\max}, +\infty)$ (A,B: resonator or mixed regime), then there can only be phasic spiking $\Phi(w_{\min}) > w_{\max}$, otherwise tonic spiking is possible.

When tonic spiking (or bursting) is possible, then the model is bistable (it can be turned on or off with current pulses).

4.5 Discussion

The adaptive exponential integrate-and-fire model [30] is able to reproduce many electrophysiological features seen in real neurons, with only two variables and four free parameters. Besides, its parameters have a direct physiological interpretation. In the framework of this model, we can define an *electrophysiological class* as a set of dynamical properties for different values of the input I (for given parameter values). In this chapter, we tried to provide a classification of the parameter space as complete as possible, which is summarized for subthreshold dynamics in Fig. 4.3. The subthreshold dynamics depends only on the ratio of time constants (τ_m/τ_w) and on the ratio of conductances (b/g_L), but is already non-trivial. The model can have excitability type I or II depending whether it leaves the resting state through a saddle-node or an Andronov-Hopf bifurcation. It may act as an oscillator or an integrator depending on the eigenvalues associated to the resting point. It may spike in response to hyperpolarizing currents (rebound), depending on the properties of the attraction basin of the stable fixed point, which is bounded by either a limit cycle or a separatrix.

The spiking dynamics is even more rich, as it also depends on the reset parameters d and V_r. We related the spike patterns with orbits under a discrete Poincaré map Φ, and found a rich bifurcation structure including even chaos. Regular spiking corresponds to a stable fixed point of Φ, bursting corresponds to periodic orbits under Φ and irregular spiking corresponds to chaotic orbits under Φ.

Most of the results shown in this chapter generalize to two-dimensional spiking models in which the first (membrane) equation is $dV/dt = F(V) + I - w$, where F is a smooth convex function whose derivative is negative at $-\infty$ and infinite at $+\infty$ (in particular, Izhikevich model and the quartic model have these properties). We are

currently working on the mathematical proofs of these results in that more general setting and on a more complete picture of the spiking dynamics [258]. This work will provide both a dynamical system understanding of the the spiking properties of the model and analytical methods to relate the parameter values with electrophysiological classes. Another interesting line of research is the investigation of the responses of such bidimensional models to time-varying inputs, as was done in [32] for one-dimensional integrate-and-fire models.

CHAPTER 5

SENSITIVITY TO THE CUTOFF VALUE IN THE QUADRATIC ADAPTIVE INTEGRATE-AND-FIRE MODEL

OVERVIEW

As already discussed, the quadratic adaptive integrate-and-fire model [141, 145] is recognized as very interesting for its computational efficiency and its ability to reproduce many behaviors observed in cortical neurons. For this reason it is currently widely used, in particular for large scale simulations of neural networks. This model is part of the general class of models studied in chapter 2: it emulates the dynamics of the membrane potential of a neuron together with an adaptation variable. The subthreshold dynamics is governed by a two-parameter differential equation, and a spike is emitted when the membrane potential variable reaches a given cutoff value. Subsequently the membrane potential is reset, and the adaptation variable is added a fixed value called the spike-triggered adaptation parameter. We show in this chapter that when the system does not converge to a resting state, both variables of the subthreshold dynamical system blow up in finite time. The cutoff is therefore essential for the model to be well defined and simulated. The divergence of the adaptation variable makes the system very sensitive to the cutoff: changing this parameter dramatically changes the spike patterns produced. Furthermore from a computational viewpoint, the fact that the adaptation variable blows up and the very sharp slope it has when the spike is emitted implies that the time step of the numerical simulation needs to be very small (or adaptive) in order to catch an accurate value of the adaptation at the time of the spike. It is not the case for the similar quartic [255] and exponential [30] models whose adaptation variable does not blow up in finite time, and which are therefore very robust to changes in the cutoff value.

Contents

5.1 INTRODUCTION

During the past few years, in the neuro-computing community, the problem of finding a computationally simple and biologically realistic model of neuron has been widely studied, in order to be able to compare experimental recordings with numerical simulations of large-scale brain models. The key problem is to find a model of neuron realizing a compromise between its simulation efficiency and its ability to reproduce what is observed at the cell level, often considering in-vitro experiments [144, 165, 225]. Among the variety of computational neuron models, nonlinear spiking models with adaptation have recently been studied by several authors [30, 144, 255] and seem to stand out. They are relatively simple, i.e. mathematically tractable, efficiently implemented, and able to reproduce a large number of electrophysiological signatures such as bursting or regular spiking. These models satisfy the equations:

$$\begin{cases} \frac{dv}{dt} &= F(v) - w + I \\ \frac{dw}{dt} &= a(b - w) \end{cases} \tag{5.1}$$

where a and b are non-negative parameters and $F(v)$ is a regular strictly convex function satisfying assumption:

Assumption 5.1.1. There exists $\varepsilon > 0$ and $\alpha > 0$ for which $F(v) \geq \alpha v^{1+\varepsilon}$ when $v \to \infty$ (we will say that F grows faster than $v^{1+\varepsilon}$ when $v \to \infty$).

A spike is emitted at the time t^* when the membrane potential v reaches a cutoff value θ. At this time, the membrane potential is reset to a constant value c and the adaptation variable is updated to $w(t^*) + d$ where $w(t^*)$ is the value of the adaptation variable at the time of the spike and $d > 0$ is the spike-triggered adaptation parameter.

For these models we prove in section 5.2 that the membrane potential blows up in finite time. Among these models, the *quadratic adaptive* model [144] corresponds to the case where $F(v) = v^2$, and has been recently used by Eugene Izhikevich and coworkers [147] in very large scale simulations of neural networks. The *adaptive exponential* model [30] corresponds to the case where $F(v) = e^v$, has the interest that its parameters can be related to electrophysiological quantities, and has been successfully fit to intracellular recordings of pyramidal cells [51, 155]. The *quartic* model [255] corresponds to the case where $F(v) = v^4 + 2av$ and has the advantage to of being able to reproduce all the behaviors featured by the other two and also self-sustained subthreshold oscillations which are of particular interest to model certain nerve cells.

In these models, the reset mechanism makes critical the value of the adaptation variable at the time of the spike. Indeed, when a spike is emitted at time t^*, the new initial condition of the system (5.1) is $(c, w(t^*) + d)$. Therefore, this value governs the subsequent evolution of the membrane potential, and hence the spike pattern produced. For instance in [258, 259], the authors show that the sequence of reset locations after each spike time shapes the spiking signature of the neuron.

Hence characterizing the reset location of the adaptation variable is essential to characterize the spiking properties of these models. To this end, we precisely study in this chapter the orbits of equation (5.1) in the phase plane (v, w) in order to characterize the value of the adaptation variable at the time of the spike. We prove in section 5.2 that the adaptation variable diverges when $v \to \infty$ in the case of the quadratic model and converges in the cases of the exponential and of the quartic model, and

study in section 5.3 the consequences of this fact on the spiking signatures and on numerical simulation methods.

5.2 ADAPTATION VARIABLE AT THE TIMES OF THE SPIKES

As we can see in equation (5.1), the greater the membrane potential the greater the derivative of the adaptation variable. When the membrane potential blows up, the adaptation variable may either remain bounded or blow up, depending on the shape of the divergence of v. When this divergence is not fast enough, the adaptation variable simultaneously blows up.

We prove here that for the models satisfying assumption 5.1.1 the membrane potential blows up in finite time. We also prove that for quadratic adaptive model[1] the adaptation variable blows up at the same time as a logarithmic function of v, whereas if there exists $\varepsilon > 0$ such that $F(v)$ grows faster than $v^{2+\varepsilon}$ when $v \to \infty$, then the adaptation variable remains bounded when $v \to \infty$.

In [255], we have seen that there exists possibly one stable fixed point for system 5.1, which corresponds to a resting state. In [259], we prove that all the orbits of the system that do not converge to this stable fixed point will be trapped after a finite time in a zone fully included in the half space $\{w < bv\}$ called the *spiking zone*[2]. Denote t_0 a time such that the orbit is inside the spiking zone. In this zone, we have

$$\frac{\mathrm{d}v}{\mathrm{d}t} \geq F(v) - bv + I$$

It is simple to prove that the solution of the equation

$$\begin{cases} \frac{\mathrm{d}u}{\mathrm{d}t} = F(u) - bu + I \\ u(t_0) = v(t_0) \end{cases}$$

blows up in finite time under the assumption 5.1.1[3]. Using Gronwall's theorem [117] we conclude that $v(t) \geq u(t)$ and hence v blows up in finite time.

To prove the divergence of the adaptation variable when the membrane potential blows up in the case of the quartic model, we study the orbit of a solution $(v(t), w(t))$ of the differential system (5.1) such that the membrane potential blows up at time t^*, and characterize the behavior of $w(t)$ in function of $v(t)$. In the spiking zone, we have seen that $w(t) \leq bv(t)$ and therefore $F(v) - w + I \geq F(v) - bv + I$ which tends to infinity when v tends to infinity. Since $v(t)$ blows up there exists a time $t_1 \in [t_0, t^*)$ such that we will have $F(v(t)) - w(t) + I \geq k > 0$ for all $t \in [t_1, t^*)$. We denote $(v_1 := v(t_1), w_1 := w(t_1))$. After time t_1, because of this inequality, the trajectory in the phase plane can be

[1] We can prove more generally that when $F(v)/v^2$ tends to a finite constant (possibly 0), the adaptation variable will blow up when the membrane potential blows up

[2] In the case where the subthreshold system has no fixed point this property can be derived from the shape of the vector field in the phase plane, as well as in the case where the initial condition (v, w) is such that v is greater than the largest v-value of the fixed points (the biggest solution of $F(v) - bv + I = 0$) and $w \leq bv$: in this case the vector field on the line $w = bv$ implies that the trajectory keeps trapped in this zone. In the case where there exist fixed points, the proof is slightly more complex and involves the description of the stable manifold of the saddle fixed point.

[3] For the quadratic model we can get analytic expressions of the solutions involving the tangent function, and therefore can derive an upperbound of the explosion time.

written as the graph of a function $W(v)$ that satisfies the equation:

$$\begin{cases} \frac{dW}{dv} = \frac{a(b-W)}{F(v)-W+I} \\ W(v_1) = w_1 \end{cases} \tag{5.2}$$

(i.e. $w(t) = W(v(t))$ for $t \in [t_1, t^*)$). Since $w(t)$ is increasing for $t \in [t_1, t^*)$, we necessarily have:

$$\frac{dW}{dv} \geq \frac{a(b-W)}{F(v)-w_1+I} \tag{5.3}$$

Therefore Gronwall's theorem [117] ensures us that the solution of equation (5.2) will be lowerbounded for $v \geq v_1$ by the solution of the linear ordinary differential equation:

$$\begin{cases} \frac{dz}{dv} = \frac{a(b-z)}{F(v)-w_1+I} \\ z(v_1) = w_1 \end{cases} \tag{5.4}$$

that reads:

$$z(v) = \left(\int_{v_1}^{v} \frac{abu}{F(u)-w_1+I} e^{-g(u)}\, du + w_1 \right) e^{g(v)}$$

where $g(v) = -\int_{v_1}^{v} \frac{a\,du}{F(u)-w_1+I}$. Because of assumption 5.1.1, the integrand is integrable, and the function g has a finite limit $g(\infty)$ when $v \to \infty$. The exponential terms will hence converge when $v \to \infty$. But the integral involved in the particular solution diverges in the quadratic case[4], since the integrand is equivalent when $u \to \infty$ to

$$\frac{ab}{u} e^{-g(\infty)}$$

Hence the solution of the linear differential equation (5.4) tends to infinity when $v \to \infty$ faster than a logarithmic function of v, and so does $W(v)$, and hence $w(t)$ blows up at the time when $v(t)$ blows up.

Let us now upperbound the adaptation variable on the orbits of the system. Using the same notations, since $w_1 \leq w(t) \leq bv(t)$ for $t \in [t_1, t^*)$, we have:

$$\frac{dW}{dv} \leq \frac{a(bv-w_1)}{F(v)-bv+I} \tag{5.5}$$

and hence

$$W(v) \leq w_1 + \int_{v_1}^{v} \frac{a(bu-w_1)}{F(u)-bu+I}\, du$$

In the case where $F(u) = u^2$ this integral is bounded by a logarithmic function of v and in the case where $F(u)$ grows faster than $u^{2+\varepsilon}$, this integral converges when $v \to \infty$. Furthermore, since W is an increasing upperbounded function, it converges when $v \to \infty$.

We therefore conclude that in the case of the quadratic adaptive model, the adaptation variable blows up at the explosion time of the membrane potential variable v and this divergence is logarithmic in v, and in the case of the quartic and exponential models, the adaptation variable converges. The value of the adaptation variable at the cutoff θ is simply given by $W(\theta)$, that depends on the parameters of the system and of the initial condition. In the case of the quadratic model it is an unbounded increasing function of θ , and in the quartic and exponential models, a converging function of θ.

[4] or when $F(v)$ grows slower than v^2,

5.3 Consequences

The divergence of the adaptation variable at the times of the spikes significantly impacts the theoretical, qualitative and computational analysis of the model.

We have seen that changing the cutoff value resulted in changing the value of the adaptation variable at the times of the spikes. Let (v_0, w_0) be an initial condition for the system (5.1). If the neuron fires, its membrane potential will reach the cutoff value θ at a given time. Since the membrane potential blows up in finite time, the time of the first spike emitted will not be very sensitive to changes in the cutoff value provided it is high enough. But the after-spike reset location $(c, W(\theta)+d)$ will significantly change when varying θ. The whole subsequent evolution of the system is therefore affected, as soon as the second spike is emitted. Thus the spike pattern produced depends on the cutoff value.

In the case of the quartic and exponential models, the adaptation variable converges when the cutoff tends to infinity. Therefore, the model defined by (5.1) with an infinite cutoff value is mathematically well defined. In that case, a spike is emitted when the membrane potential blows up and subsequently we reset the membrane potential to a fixed value c and add to the value of adaptation variable at the explosion time the spike-triggered adaptation parameter. We call this system the *intrinsic* system. The behavior of the system and the spike patterns it produces can be mathematically studied (see [258, 259]). Interestingly, these intrinsic spike patterns undergo bifurcations with respect to the parameters of the model. When considering a finite cutoff, the model (or the numerical simulation) will approximate these intrinsic behaviors provided that the cutoff threshold is high enough. The sensitivity to the cutoff in these cases will hence be very limited except in very small regions of the parameter space around the bifurcations of the intrinsic system. Unfortunately, for the quadratic model, no intrinsic behavior can be defined because of the divergence of the adaptation variable: the behaviors it produces will depend on the choice of the threshold.

First of all, we have seen that the dependency of this reset location in the quadratic model is a logarithmic function of θ, which makes the variations of the reset value in function of the cutoff unbounded but quite slow. Small changes in the cutoff slightly impact the value of the reset adaptation variable. For instance if we consider the firing rate of a neuron in the case where the system has no fixed point, increasing the cutoff value results in the case of the quadratic model in a a slow continuous decrease of the firing rate of the neuron that tends to zero as the cutoff increases, whereas the firing rate converges for the quartic model to the related intrinsic firing rate (see figure 5.1.(g)).

When considering the spike patterns produced, the effects of changes in the cutoff value for the quadratic model are much more dramatic. Indeed, the sequence of adaptation values at the times of spikes shapes the spike pattern produced: for instance, regular spiking corresponds to the convergence of this sequence, and bursting to cycles in this sequence. These properties are very sensitive to changes in the parameters of the model: bifurcations between different spike patterns, and even chaos appear when the model's parameters vary (see [204, 258, 259]). In the case of the quadratic model, we have seen that these adaptation values strongly depend on the cutoff. Therefore, since the dependency on the cutoff is unbounded, from a given initial condition and for fixed values of the parameters, increasing the cutoff may result in crossing many bifurcation lines, and hence in producing many different behaviors. We present in figure 5.1 a graph showing that bifurcations and chaos occur with re-

spect to the cutoff value, in the usual range of simulation parameters. For instance, a period doubling bifurcation appears when varying the cutoff value (in figure 5.1(e) we give a graph of the stationary reset values in function of the threshold θ), that results in abruptly switching from a regular spiking behavior to a bursting behavior (figures 5.1(a) and 5.1(b)). More complex bifurcation structures involving chaotic patterns also appear, and in this case, infinitesimal changes in the cutoff value result in dramatic changes in the behavior. This raises the question of the meaning of the cutoff value in these ranges of parameters (see figure 5.1(f)). Changing the cutoff in that case makes the system switch between chaotic spiking, bursts with 8, 4 and eventually 2 spikes, for the cutoff values considered. And this behavior will not be observed only for very particular values of the parameters of the system. Depending on the extension of the interval where the cutoff value varies, quite a large set of parameters will present bifurcations in the nature of the emitted spike train.

Because of this sensitivity, the cutoff value and the different parameters of the model have to be very carefully evaluated in order to quantitatively fit datasets. In this context the meaning of the threshold and therefore the problem of its accurate evaluation has to be specifically addressed in the case of the quadratic model, since it has no clear biophysical interpretation.

Eventually, from the numerical viewpoint, the unboundedness of the adaptation variable and of its time derivative at the explosion times of the membrane potential makes the accurate computation of this value very difficult. In particular, the time step necessary to accurately estimate this value has to be very small (or to be adaptive as a function of the value of the membrane potential variable) in order to obtain the right spike pattern. These remarks relativize the statement that this model can be efficiently simulated since very accurate methods have to be implemented in order to correctly evaluate the adaptation variable at the time of the spike.

These remarks do not apply for the models where the adaptation variable converges at the times of the spikes. In these cases, the system has intrinsic properties that make the times of the spike and the adaptation variable at these times robust to the choice of the cutoff value provided it is big enough and the numerical simulations less sensitive to the choice of the time step.

CONCLUSION

In this chapter we proved that the adaptation variable of the adaptive quadratic model blew up at the times of the spikes whereas it converged for the quartic and the adaptive exponential models. This property has some important implications that are discussed in the chapter. From a theoretical point of view, we showed that the nature of the spike patterns produced undergoes bifurcations with respect to the cutoff value, and this made the system very sensitive to this parameter: small changes in the value of this parameter can deeply affect the nature of the spiking pattern. From a quantitative viewpoint, it raises the question of how to evaluate this threshold in order to fit datasets, and from a numerical viewpoint, it has implications on the efficiency of the simulation algorithms to use. The convergence of this value for models having a faster blow up at the times of the spike, such as the quartic or the exponential adaptive models, implies that the system presents intrinsic spiking properties which can be mathematically studied, efficiently simulated and robust to changes in the cutoff value.

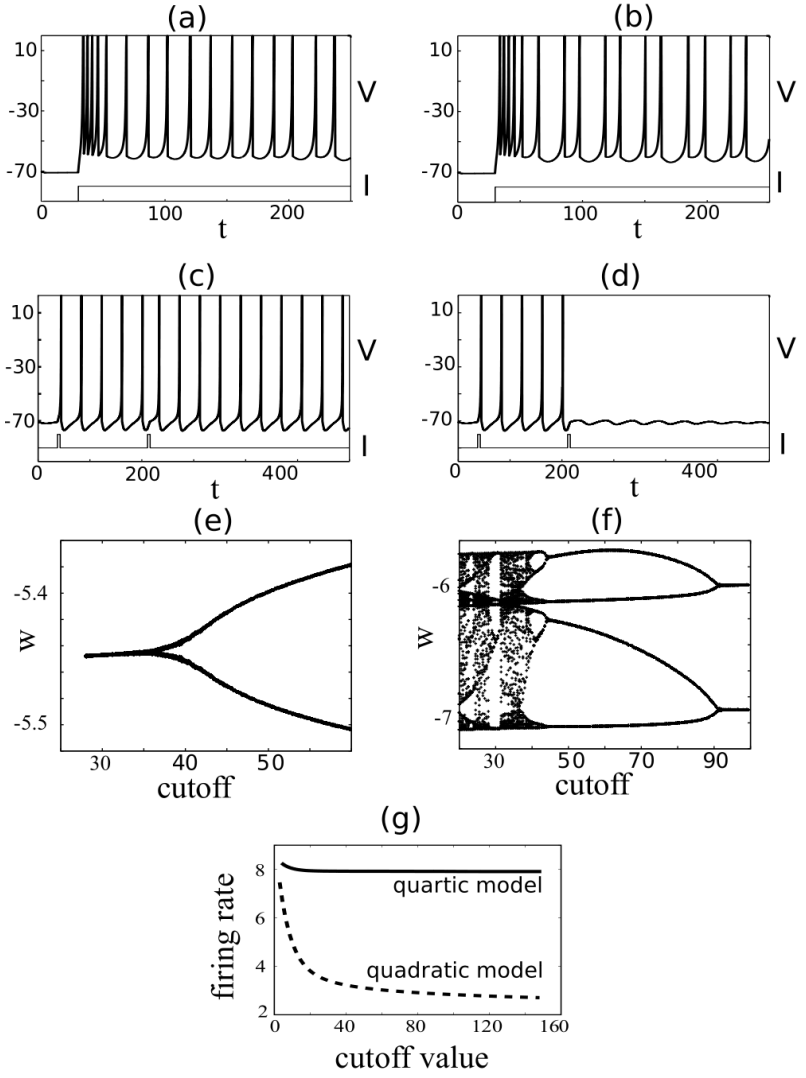

Figure 5.1: Sensitivity of the spike patterns with respect to the cutoff value for the quadratic model, for different set of parameters. Parameters used: $(A) = \{a = 0.02; b = 0.19; c = -60; d = 1.419\}$; $(B) = \{a = 0.1; b = 0.26; c = -60; d = 0;\}$, $(C) = \{a = 0.02, b = 0.19, c = -57.7, d = 1.15\}$. For figure (a) and (b) the parameters used are (A) with cutoff of 36 and 38 respectively: a small increase of the cutoff results in a sharp transition from spiking to bursting, linked with a period doubling bifurcation for the adaptation value at the reset represented in figure (e). Figures (c) and (d) corresponds to the parameters (B) with cutoffs value 32.9 and 33 respectively. Changing the cutoff results in two very different global behaviors. Fig. (e) and (f) represent the stationary sequence of reset values as functions of the threshold θ. Figure (f) corresponds to the set of parameters (C) for cutoff values ranging from 20 to 100: an intricate bifurcation structure appears. Figure (g) shows the convergence of the firing rate to the intrinsic firing rate in the case of the quartic model, while the firing rate of the quadratic model regularly decreases to 0.

Part III

Statistics of Spikes Trains

This part is dedicated to the study of the spike statistic under the diffusion approximation of the noise. In chapter 6 we show how the problem of describing spike statistics can be expressed as a first-hitting time problem for different stochastic processes, and review many different techniques in order to characterize the probability distribution of spike timings. One of the problem which is unsolved by usual techniques is the problem of the statistics of integrate-and-fire neuron models when considering a non-instantaneous synaptic integration. Solving this problem is the main focus of chapter 7. We introduce a class of processes, which we call *double integral processes*, corresponding to the set of processes defined as primitive of a Brownian martingale, and develop a semi-analytical method in order to solve the problem of the first hitting times of these processes to general smooth boundaries. An approximation formula is provided together with the related convergence rate.

CHAPTER 6

THE STATISTICS OF SPIKE TRAINS FOR STOCHASTIC INTEGRATE-AND-FIRE NEURON MODELS

Si j'avais été mieux au fait de la guerre littéraire,
j'aurais mis mon gilet pare-balles en velours côtelé.
– Pierre Assouline.

ABSTRACT

We discuss the statistics of spikes trains for different types of integrate-and-fire neurons and different types of synaptic noise models. In contrast with the usual approaches in neuroscience, mainly based on statistical physics methods such as the Fokker-Planck equation or the mean-field theory, we chose the point of the view of the stochastic calculus theory to characterize neurons in noisy environments. We present seven stochastic calculus techniques that can be used to find the probability distributions attached to the spikes trains. We illustrate the power of these techniques for five types of widely used neuron models. Despite the fact that these techniques are mathematically intricate we believe that they can be useful for answering questions in neuroscience that naturally arise from the variability of neuronal activity. For each technique we indicate its range of applicability and its limitations. This work was done together with Olivier Faugeras, and the main results presented in this chapter were published in the Journal of Physiology, Paris [260]. In this chapter we nevertheless bring some new results: we present, extend and apply Brunel's method to different kinds of neuron models, provide a new insight of Durbin's method and extend its application domain, and discuss the problem of noisy synaptic conductances.

Contents

6.1 Introduction

During the past forty years, modelling and understanding the effects of noise in cortical neurons has been a central and difficult endeavor in neuroscience. Many approaches have been used in order to characterize the spikes trains, most of them borrowed from statistical physics. At the level of the cell, the effects of noise have been studied first by Gerstein and Mandelbrot [103] who proposed random walk models to emulate the stochastic activity of a neuron, and Stein [243] who first modeled and simulated the neuronal variability. Knight [163] in 1972 introduced and studied the first noisy integrate-and-fire neuron model. His work has been generalized by Gerstner [105]. Brunel and colleagues used the Fokker-Planck equation to characterize the effect of noise at the level of the cell [37, 38] and of the network [35, 36]. Samuelides and his colleagues used the meanfield and large deviations framework to characterize large sets of randomly connected neurons driven by noise [233]. In the present chapter we adopt the point of view of the theory of stochastic calculus in an attempt to characterize the stochastic properties of neuron models and the statistics of the spikes trains they generate. We illustrate these techniques with five types of widely used neuron models.

The techniques are mathematically quite intricate. Nevertheless, we believe that they can be useful for answering questions in neuroscience that naturally arise from the variability of neuronal activity. For instance, they can give access to the probability distribution of the spikes trains, while other methods only give partial informations on this distribution. Moreover, the use of stochastic calculus methods enables us to get rid of such technical hypotheses as the stationarity of the process, the sparsity of the networks or the time scales approximations, which are generally required. It is for instance applied in chapter 8 to propose an event-based modelization of stochastic neuron networks and a very efficient way to simulate stochastic spiking neuron models. Moreover, characterizing the law of the ISI gives very important informations to fit and validate models. For each technique presented we indicate its range of applicability and its limitations.

In section 1.4.3, we discussed the origin of the variability in cortical neurons and their mathematical modelling, and justified the use of the Brownian motion through the use of a diffusion approximation. In this chapter we first present different classical mathematical models, which differ in their intrinsic dynamics or in the noise models used. We then present few important stochastic methods for computing spikes trains statistics, and apply them to the different types of neurons we consider, and eventually compare the accuracy and the efficiency of these methods.

6.2 Neuron Models

In this chapter, a *stochastic neuron model* is defined by (i) a membrane potential dynamics and (ii) a synaptic dynamics. The neuron emits a spike when its membrane potential reaches a, possibly time-varying, threshold function $\theta(t)$. We are interested in characterizing the sequence $\{t_i\}$, $i = 1, \cdots$, $t_i > 0$, $t_{i+1} > t_i$ when the neuron emits spikes. We present four simple models of spiking neurons submitted to noisy synaptic input, discuss their biological relevance and perform a basic stochastic analysis of the spikes times. In detail, a neuron model is defined by an equation:

$$\tau_m dV_t = f(t,V_t)\,dt + I_e(t)\,dt + dI^{\text{syn}}(V_t,t) \tag{6.1}$$

where $f(t,v)$ governs the free membrane potential dynamics, $I_e(t)$ is the injected or ex-

ternal current and the deterministic term of synaptic integration, and I_t^{syn} represents the noisy synaptic inputs due to background synaptic activity.

In the following sections, we review different models of neuronal dynamics in which the synaptic current can be described by one of the models discussed in section 1.4.3.

6.2.1 Model I: The noisy leaky integrate-and-fire model with instantaneous synaptic current

The simplest model we consider is the integrate and fire where the membrane potential V follows the following stochastic differential equation:

$$\begin{cases} \tau_m dV_t = (V_{\text{rest}} - V_t + I_e(t))\, dt + \sigma dW_t \\ V_0 = 0 \end{cases} \tag{6.2}$$

where τ_m is the time constant of the membrane, V_{rest} the rest potential and W_t a Brownian process representing the synaptic input. This equation is the Ornstein-Uhlenbeck equation. The neuron emits a spike each time its membrane potential reaches a threshold θ or a threshold function $\theta(t)$. When a spike is emitted, the membrane potential is reinitialized to the initial value, e.g. 0.

This is the simplest continuous noisy spiking model. The leaky integrate-and-fire neuron was first introduced by Lapicque [171] in a discussion on membrane polarizability. It idealizes the neuron as a capacitor in parallel with a resistor and driven by a current I_e (see e.g. [105]).

The noisy integrate-and-fire neuron with instantaneous synaptic current (6.2) has recently received a lot of attention to investigate the nature of the neural code [41, 195, 234, 269]. As shown in section 1.4.3, equation (1.11), it can be seen as the diffusion approximation of Stein's model [103, 242] where the synaptic inputs are considered as Poisson processes.

It is one of the few neuronal models for which analytical calculations can be performed. Indeed, equation (6.2) can be solved in closed form:

$$V_t = V_{\text{rest}}(1 - e^{-\frac{t}{\tau_m}}) + \frac{1}{\tau_m}\int_0^t e^{\frac{s-t}{\tau_m}} I_e(s)\, ds + \frac{\sigma}{\tau_m}\int_0^t e^{\frac{s-t}{\tau_m}} dW_s \tag{6.3}$$

The stochastic process V_t is Gauss-Markov. It is the sum of a deterministic part and the product of e^{-t/τ_m} with the random process $\int_0^t e^{s/\tau_m} dW_s$ defined by a stochastic integral (see appendix C). Thanks to a change of time scale through the Dubins-Schwarz' theorem C.1.6, it can be turned into a Brownian motion. It is easy to show that it is a centered Gauss-Markov process with covariance function $\rho(t) = \frac{\tau_m}{2}\left(e^{2\frac{t}{\tau_m}} - 1\right)$. This function is used in the application of the Dubins-Schwarz' theorem to change the time scale to obtain a Brownian motion: $\int_0^t e^{s/\tau_m} dW_s \overset{\mathscr{L}}{=} W_{\rho(t)}$.

The spiking condition of this neuron, $V_t = \theta(t)$, can be written in terms of this simpler stochastic process:

$$\int_0^t e^{\frac{s}{\tau_m}} dW_s = W_{\rho(t)} = \frac{\tau_m}{\sigma}\left[(\theta(t) - V_{\text{rest}})\, e^{\frac{t}{\tau_m}} + V_{\text{rest}} - \frac{1}{\tau_m}\int_0^t s\, e^{\frac{s}{\tau_m}} I_e(s)\, ds\right] \overset{\text{def}}{=} a(t) \tag{6.4}$$

In order to fulfill our program we are thus naturally led to study the first hitting time of the Brownian motion $W_{\rho(t)}$ to the curved boundary $a(t)$.

6.2.2 Model II: The noisy leaky integrate-and-fire model with exponentially decaying synaptic current

We modify the model of section 6.2.1 to include an exponentially decaying synaptic current as described in section 1.4.3, equation (1.13):

$$\begin{cases} \tau_m dV_t &= (V_{\text{rest}} - V_t)dt + I_e(t)dt + I_t^{\text{syn}}dt \\ \tau_s dI_t^{\text{syn}} &= -I_t^{\text{syn}}dt + \sigma dW_t \end{cases}$$

This model is a more precise description of the synaptic current and is still simple enough to be analyzed mathematically. Nevertheless, its analytical study is quite challenging and only a few results are available.

We integrate this system of two stochastic differential equations in closed form (see section 7.2.1 for the calculations). The synaptic current is simply an Ornstein-Uhlenbeck process and reads:

$$I_t^{\text{syn}} = I_0^{\text{syn}} e^{-\frac{t}{\tau_s}} + \frac{\sigma}{\tau_s}\int_0^t e^{\frac{s-t}{\tau_s}} dW_s,$$

where I_0^{syn} is a given random variable, and the membrane potential reads:

$$V_t = V_{\text{rest}}(1-e^{-\frac{t}{\tau_m}}) + \tfrac{1}{\tau_m}\textstyle\int_0^t e^{\frac{s-t}{\tau_m}} I_e(s)\,ds + \\ \dfrac{I_0^{\text{syn}}}{1-\frac{\tau_m}{\tau_s}}(e^{-\frac{t}{\tau_s}} - e^{-\frac{t}{\tau_m}}) + \dfrac{\sigma}{\tau_m\tau_s} e^{-\frac{t}{\tau_m}} \displaystyle\int_0^t e^{\frac{s}{\alpha}} \left(\int_0^s e^{\frac{u}{\tau_s}} dW_u \right) ds$$

where $\frac{1}{\alpha} = \frac{1}{\tau_m} - \frac{1}{\tau_s}$. Therefore, the membrane potential is the sum of a deterministic process and a function of the non-Markov Gaussian differentiable process[1] X_t defined by:

$$X_t = \int_0^t e^{s/\alpha} \left(\int_0^s e^{u/\tau_s} dW_u \right) ds \tag{6.5}$$

The spiking condition can be written:

$$X_t = -\frac{\alpha\tau_s}{\sigma} I_0^{\text{syn}}(e^{\frac{t}{\alpha}} - 1) + \frac{\tau_m\tau_s}{\sigma}\left[(\theta - V_{\text{rest}})e^{\frac{t}{\tau_m}} + V_{\text{rest}} - \frac{1}{\tau_m}\int_0^t e^{\frac{s}{\tau_m}} I_e(s)\,ds \right]. \tag{6.6}$$

Studying the spikes sequence of the LIF model with exponentially decaying synaptic currents amounts to studying the first hitting time of the process X_t defined by (6.5) to a continuous deterministic boundary. This non-Markov process will lead us in section 7.2.1 to introduce a general class of processes which we call the *double integral process* (DIP), defined by:

$$X_t \overset{\text{def}}{=} \int_0^t g(s)M_s ds = \int_0^t g(s)\left(\int_0^s f(u)dW_u \right) ds \tag{6.7}$$

for some real measurable functions f and g.

We already noted that the process X_t was non Markovian. We show in chapter 7 that the two-dimensional process (X_t, M_t) is a Gaussian Markov process, and furthermore, conditionally to M_s, that the increments $(X_t - X_s, M_t - M_s)$ are independent of the σ-field $\mathscr{F}_s$ (see appendix C for the definitions of these terms).

[1] The proof that X_t is non-Markov is given in chapter 7.

For a given t, the random variable $Y_t \stackrel{\text{def}}{=} (X_t, M_t)$ is a Gaussian two-dimensional variable of parameters:

$$\left\{ \begin{array}{ll} \mathbb{E}(Y_t) & = (0,0) \\ \mathbb{E}[Y_t^T \cdot Y_t] & = \left(\begin{array}{cc} \rho_X(t) & C_{(X,M)}(t) \\ C_{(X,M)}(t) & \rho_M(t) \end{array} \right) \end{array} \right. \tag{6.8}$$

where the functions $\rho_X(t)$, $C_{(X,M)}(t)$ and $\rho_M(t)$ are defined by:

$$\left\{ \begin{array}{ll} \rho_M(t) & \stackrel{\text{def}}{=} \int_0^t f(s)^2 ds \\ \rho_X(t) & \stackrel{\text{def}}{=} 2\int_0^t g(s) \left(\int_0^s g(u)\rho_M(u)du \right) ds \\ C_{(X,M)}(t) & \stackrel{\text{def}}{=} \int_0^t g(s)\rho_M(s)ds \end{array} \right. \tag{6.9}$$

It can be checked that the Markov process $(Y_t)_t$ transition measure (see Appendix C.1.2 for a definition) has a Gaussian density w.r.t. Lebesgue's measure ds:

$$\mathscr{N}\left(\left(\begin{array}{l} x_s + m_s \int_s^t g(u)du \\ m_s \end{array} \right), \tilde{C}(s,t) \right) \tag{6.10}$$

where the correlation matrix $\tilde{C}(s,t)$ reads:

$$\tilde{C}(s,t) = \left(\begin{array}{ll} 2\int_s^t g(u) \left(\int_s^u g(v) \int_s^v f(w)^2 \, dw \, dv \right) du & \int_s^t g(u) \left(\int_s^u f(v)^2 dv \right) du \\ \int_s^t g(u) \left(\int_s^u f(v)^2 dv \right) du & \int_s^t f(u)^2 du \end{array} \right) \tag{6.11}$$

We now define the simplest non trivial double integral process, which turns out to be of great interest for the study of the spike train statistics of the present model of neuron: the *Integrated Wiener Process* (IWP) where the functions f and g are identically equal to 1:

$$X_t \stackrel{\text{def}}{=} \int_0^t W_s \, ds \tag{6.12}$$

The transition measure of the process (X_t, W_t) can be written:

$$\begin{aligned} \mathbb{P}\Big[X_{t+s} \in du, W_{t+s} \in dv \Big| X_s = x, W_s = y \Big] &\stackrel{\text{def}}{=} p_t(uv; x,y)du\,dv = \\ &\frac{\sqrt{3}}{\pi t^2} \exp\Big[-\frac{6}{t^3}(u-x-ty)^2 + \frac{6}{t^2}(u-x-ty)(v-y) - \frac{2}{t}(v-y)^2 \Big] du\,dv \end{aligned} \tag{6.13}$$

6.2.3 Model III: The noisy nonlinear integrate-and-fire neuron with instantaneous synaptic current

The models studied so far are linear and cannot be used to model nonlinear behaviors of neurons. For instance, it is known that many neuron models such as the $I_{Na,P}, I_K$ current model (with a persistent Na^+ current with instantaneous activation kinetics and a slower persistent K^+ current, see [146, Chapt. 4] for a good review) or the Hodgkin-Huxley model present an Andronov-Hopf bifurcation. To model the behavior of such neurons in the vicinity of these bifurcations, Ermentrout and Kopell in [82] and Izhikevich in [146] proposed the following one-dimensional model:

$$\left\{ \begin{array}{l} dV_t = (V_t^2 + I_e(t))dt + \sigma dW_t \\ V_0 = V_{\text{reset}} \end{array} \right. \tag{6.14}$$

together with the spiking condition:

$$V(t^-) \geq \theta \Rightarrow V(t) = V_{\text{reset}} \text{ and a spike is emitted.}$$

Note that in the analytical model it can be useful to take $\theta = \infty$ and in this case, the problem is an explosion time problem and not a boundary crossing problem. Other types of nonlinearities can generate other possibly interesting bifurcations. This is an area of active research.

This model can be generalized to more complex nonlinearities:

$$\begin{cases} dV_t = (F(V_t) + I_e(t))dt + \sigma dW_t \\ V_0 = V_{\text{reset}} \end{cases} \tag{6.15}$$

The quadratic model has been studied analytically for constant inputs. The nonlinear stochastic differential equation is quite intricate to analyze in general. We review some of its main properties. First, without spiking mechanism, the process blows up almost surely in finite time, hence the neuron will fire almost surely in finite time. Secondly, there exists a weak solution up to the explosion time but the law of the process is unknown apart from the fact that is not Gaussian. Its transition density is unknown so far. Usual approaches like the Fokker-Planck equation (see appendix C.1.2) fail in finding this law as we show next.

If the external current is constant, the infinitesimal generator of the process (6.14) is defined by $\mathscr{L} \stackrel{\text{def}}{=} \frac{1}{2}\sigma^2\partial_x^2 + (x^2 + I_e)\partial_x$ (see appendix C.1.2). Its transition probability density $p(t, x_0, x)$ is formally solution of the Fokker-Planck equation:

$$\frac{\partial p}{\partial t}(t, x_0, x) = \mathscr{L}^* p(t, x_0, x) \tag{6.16}$$

$$= \frac{1}{2}\sigma^2\partial_y^2 p(t, x_0, x) - \partial_x\left[(x^2 + I_e)p(t, x_0, x)\right]. \tag{6.17}$$

A formal solution is provided by Heun's triconfluent function h_t (see [230] and Maple10® documentation). The solution can be written $p(t, x_0, x) = f_1(x)\, f_2(t)$ where:

$$\begin{cases} f_1(x) & = \alpha_1 h_t\left(-\left(\frac{3}{2}\right)^{2/3} \frac{c_1}{\sigma^{2/3}}, -3, \frac{I_e \sqrt[3]{12}}{\sigma^{4/3}}, -\sqrt[3]{\frac{2}{3\sigma^2}}x\right) \\ & \quad + \beta_1 e^{-\frac{2x(3I_e + x^2)}{3\sigma^2}} h_t\left(-\left(\frac{3}{2}\right)^{2/3} \frac{c_1}{\sigma^{2/3}}, 3, \frac{Ie \sqrt[3]{12}}{\sigma^{4/3}}, 1/3\sqrt[3]{\frac{2}{3\sigma^2}}\right) \\ f_2(t) & = \alpha_2 e^{\frac{c_1}{2\tau}t} \end{cases}$$

where α_1, β_1, β_2 and c_1 are real constants depending on the initial condition x_0. Unfortunately Heun's triconfluent function is a very fast-diverging function which is not integrable on $\mathbb{R}$. Hence the function $p(t, x_0, x) = f_1(x)\, f_2(t)$ is not a transition probability density: there is no solution of the Fokker-Planck equation for this process.

Another way of characterizing its law is to use the generalized Girsanov formula (see theorem C.1.7 or [160]). More precisely, let S denote the first explosion time of the process V_t, and Γ be a Borelian subset of $\mathbb{R}$. We have for any $t < T$:

$$\mathbb{P}[V_t \in \Gamma, S > T] = \mathbb{E}\left[\exp\left(\int_0^T (W_s^2 + I_e)dW_s - \frac{1}{2}\int_0^T (W_s^2 + I_e)^2 ds\right) \mathbb{1}_{W_t \in \Gamma}\right] \tag{6.18}$$

This formula characterizes the law of the process between two spikes, but unfortunately does not yield a usable form of the transition probability. This difficulty is

intrinsic to the problem which blows up in finite time. Nevertheless we show in section 6.3.5 that we can characterize the statistics of the spikes trains for this model of neuron.

6.2.4 Model IV: Nonlinear integrate-and-fire models with decaying synaptic current

The previous model is a special case in a larger class of nonlinear models defined by the two equations

$$\begin{cases} \tau_m dV_t = (f(V_t) + I_e(t))dt + I_{\text{syn}}(t)dt \\ dI_{\text{syn}}(t) = -I_{\text{syn}}(t)dt + \sigma dW_t \end{cases} \tag{6.19}$$

together with the spiking condition:

$$V(t^-) \geq \theta \Rightarrow V(t) = V_{\text{reset}} \text{ and a spike is emitted.}$$

f is a non-linear function, for instance a quadratic function $f(v) = v^2$ ([146], contains an exponential function $f(v) = e^v - v$ ([30]), or a quartic function $f(v) = v^4$ ([254]).

As expected from the previous discussion very little can be obtained analytically, since the model combines the difficulties of the last two models: as in the LIF model with exponentially decaying synaptic current of section 6.2.2, the membrane potential is non Markovian and, as in the quadratic IF model, it blows up in finite time almost surely.

Despite these negative remarks, we can write down the corresponding Kolmogorov (Fokker-Planck) equation. Let $p(t, v_0, i_0, v, i_s)$ be the transition probability density of the full process (6.19) and assume that the input current $I_e(t)$ is constant. The Kolmogorov (Fokker-Planck) equation for this model reads:

$$\tau_m \partial_t p + \partial_v\{(f(v) + I_e + i_s)p\} + \frac{\tau_m}{\tau_s}\partial_{i_s}\{-i_s p\} = \frac{\sigma^2 \tau_m}{2\tau_s^2}\partial_{i_s}^2 p, \tag{6.20}$$

where we have omitted the dependence in the variables for the sake of clarity.

6.2.5 Model V: Leaky integrate-and-fire neuron with instantaneous synaptic conductances

We consider the leaky integrate-and-fire neuron with instantaneous synaptic conductivities. According to equation (1.14) in section 1.4.3, the membrane potential satisfies the equation:

$$dV_t = (-\lambda(V_t - V_{\text{rest}}) + I_e(t))\,dt + \sigma(V_t - V_{\text{rev}})dW_t, \tag{6.21}$$

which we can write by a simple change of origin for V and a subsequent modification of I_e:

$$dV_t = (-\lambda V_t + I_e(t))\,dt + \sigma V_t dW_t$$

This equation is a linear non-homogeneous stochastic differential equation which can be solved in closed form. The homogeneous solution is seen to be:

$$X_t = \exp\left(-(\lambda + \frac{\sigma^2}{2})t + \sigma W_t\right),$$

and the solution is:

$$V_t = V_0 X_t + \int_0^t I_e(s) X_{t-s}\, ds \tag{6.22}$$

Studying the spikes sequence of the LIF model with instantaneous synaptic conductivities amounts once again to studying the first hitting time of the process V_t defined by (6.22). This process is quite difficult to study in its general formulation since the noise and the input current are mixed.

Finally, we can consider a model of neuron having both noisy synaptic conductances and noisy current. In the most general case of this model, the equation of the membrane potential reads:

$$dV_t = \left(-\lambda(t)(V_t - V_{\text{rest}}) + I_e(t)\right) dt + \left(\sigma_g(t)(V_t - V_{\text{rev}}) + \sigma_I(t) dW_t\right), \tag{6.23}$$

which can also be solved in closed form:

$$V_t = X_t \left[V_0 + \int_0^t X_u^{-1} \left\{ I_e(u) - \sigma_g(u)\sigma_I(u) \right\} du + \int_0^t X_u^{-1} \sigma_I(u) dW_u \right]$$

where

$$X_u \stackrel{\text{def}}{=} \exp\left[\int_0^t \left(-\lambda(u) - \frac{1}{2}\sigma_g^2(u) \right) du + \int_0^t \sigma_g(u) dW_u \right]$$

6.3 STOCHASTIC APPROACH FOR THE STATISTIC OF SPIKE TRAINS

In this section we characterize the spikes trains statistics of the five types of neurons defined in the first part of this chapter.

We have seen that the problem was equivalent to the first hitting time problem, also called the first passage time, for stochastic processes (see equations (6.4) and (6.6)). The information we would like to obtain is the probability density function of the spikes times, which contains all the information on the statistics of the spikes trains (mean, variance, higher order moments, when they exist).

First passage time problems for one-dimensional diffusion processes through time-dependent boundary have received a lot of attention over the last three decades. Unfortunately, the evaluation of the first passage time pdf through a constant or time dependent boundary is in general an arduous task which has still not received a satisfactory solution. Analytic results are scarce and fragmentary, even if closed form solutions exist for some very particular cases. A review of the different methods to compute first hitting times of stochastic processes is given in the introductory section of chapter 7.

In two or higher dimensions, the problem is even more complex and results can hardly be found. For the *simplest* two dimensional process, the Integrated Wiener Process (IWP) defined in (6.12), people like McKean [197] Goldman [110], Lachal [168, 169, 170] solved the problem for a constant boundary with stochastic calculus methods. Lefebvre used the Kolmogorov (Fokker-Planck) equation to find in some special cases closed-form solutions [108]. Generalizations of these formulas to other boundaries and other kinds of processes are simply not available. We have recently proposed a formula for approximating these hitting times for general Double Integral Processes (DIP) and general boundaries [262].

We focus on analytical or partially analytical methods. The main goal is to compute the probability distribution of the spikes times. When this is not possible one

can be satisfied to obtain some statistics of the spikes trains, such as the mean firing rate [37, 38, 94].

Table 6.1 shows in its left column different methods we emphasize in this chapter together with their possible use for solving the problem for the neuron models presented in section 6.2. The letter "Y" indicates that the method can be applied to completely solve the problem, i.e. to get the pdf of the hitting time in an analytical or computational way for general boundaries, the letter "N" that it cannot. Question marks "?" are used for open problems that have no known solution, and the $\sim$ symbols are used for problem that are partially solved by the method. This symbol is used for instance if the method only provides statistics on the law of the hitting time (expectation, standard deviation, ...) or only provides the law for some specific inputs. The bold face indicates the problems we provide solutions for in this dissertation, including negative results. The star, "*", is used if the result is new, to our knowledge.

Methods \ Models	I	II	III	IV	V
Volterra (Durbin)	**Y**	**N***	**?**	**?**	$\sim^*$
Feynman-Kac	$\sim$	?	**N**	?	**N**
Martingales	$\sim$	$\sim$	?	?	$\sim^*$
Brunel *etal*	$\sim$	$\sim$	$\sim$	$\sim$	$\sim^*$
Girsanov's approach*	**Y***	**Y***	?	?	Y^*

Table 6.1: Analytical and semi-analytical methods which can be applied to find spike statistics for different models. The symbols used in the table are explained in the text.

6.3.1 The Volterra Method

This method consists in finding a Volterra integral equation satisfied by the probability density function p of the first hitting time τ of a stochastic process $(X_t)_{t\geq 0}$ to a curved boundary. It has been applied by Plesser to the leaky integrate-and-fire neuron in [215] to find the pdf of the first hitting time of a leaky IF neuron driven by a general input current.

In this section we first describe the method and generalize Plesser's result to the problem of an IF neuron modeled as a continuous one dimensional Gauss-Markov process $(X_t)_{t\geq 0}$ where the spiking condition is given by a smooth curved boundary denoted by $a(t)$. We then apply this to the models I and II.

Gauss-Markov processes

By Doob's theorem [75], we know that there exist a Brownian motion W, a non-zero real function g and a non-decreasing real function h such that :

$$\forall t \geq 0 \quad X_t = g(t)\, W_{h(t)},$$

and hence the transition probability density function $q(t,x|s,y)$ of this process can be

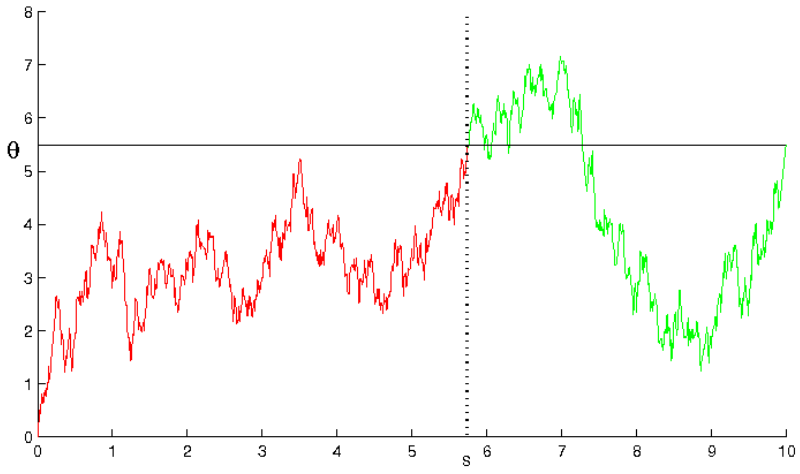

Figure 6.1: Principle of the Volterra's method: conditioning the transition probability density by the location of the first hitting time s of the curve θ.

written using that of the standard Brownian motion (see appendix C):

$$q(t,x|s,y) = \frac{1}{\sqrt{2\pi(h(t)-h(s))}} \exp\left(-\frac{\left(\frac{x}{g(t)}-\frac{y}{g(s)}\right)^2}{2(h(t)-h(s))}\right) \tag{6.24}$$

The smoothness of the functions h and g determines that of the covariance function of the process. Indeed we have, for $s \leq t$:

$$\mathbb{E}\left[X_t X_s\right] = g(t)g(s)h(s)$$

We assume that this autocorrelation function is continuously differentiable with respect to s and t, which is the case for most of the processes encountered in practice. Let $x_0 < a(0)$ the starting point at $t = 0$ of the process (X_t). By the strong Markov property (see Appendix C for the definition) of X_t, conditioning on the first hitting time s of the process to a (see figure 6.1), we can write:

$$\begin{aligned} q(t,a(t)|0,x_0) &= \int_0^t \mathbb{P}(t,a(t),\tau \in ds|0,x_0) \qquad (6.25)\\ &= \int_0^t q(t,a(t)|s,a(s))p(s)ds \\ &= \int_0^t \frac{1}{\sqrt{2\pi(h(t)-h(s))}} \exp\left(-\frac{\left(\frac{a(t)}{g(t)}-\frac{a(s)}{g(s)}\right)^2}{2(h(t)-h(s))}\right) p(s)\,ds \qquad (6.26) \end{aligned}$$

This equation is a weakly singular Volterra equation of the first kind with a square root singularity at $s = t$ since we have:

$$\begin{cases} h(t)-h(s) \underset{s\to t}{\sim} h'(t)(t-s) \\ \dfrac{\left(\frac{a(t)}{g(t)}-\frac{a(s)}{g(s)}\right)^2}{2(h(t)-h(s))} \underset{s\to t}{\sim} \dfrac{\left(\left[\frac{a}{g}\right]'(t)\right)^2}{h'(t)}(t-s) \end{cases}$$

Hence the Volterra equation can be solved: we have existence and uniqueness of a solution (see e.g. [182]) which is necessarily the pdf we are looking for.

Different algorithms can be used to numerically solve this problem. They are reviewed for instance in Linz' book [182]. We have used in our simulations a two points block-by-block method which amounts to solving a linear system. This method appears to be computationally very efficient and rather robust.

Other Volterra equations have been proposed, for instance in [42] or [73]. The equation proposed in [73] is a second-kind Volterra equation which can be deduced straightforwardly from (6.26). The formula proposed by Buonocore in [42] is slightly different, and has the advantage of removing the singularity of the kernel in the Volterra equation.

Note that this approach can be applied to any other kind of neuron model which has a Markovian membrane potential dynamics. Nevertheless the main difficulty is to find the transition probability density of the underlying process and to check if the singularity of its transition kernel is integrable or not. For instance the transition probability density of the quadratic integrate-and-fire neuron is not known and the Fokker-Planck's theorem C.1.12 cannot be applied (see section 6.2.3).

LIF neuron with instantaneous synaptic currents

The previous method applies directly to the LIF neuron with instantaneous synaptic conductances (model I) since we have seen in section 6.2.1 that the membrane potential of such a neuron is governed by a Gauss-Markov process (an Ornstein-Uhlenbeck process). Consider the Gauss-Markov process

$$U_t \stackrel{\text{def}}{=} \int_0^t e^{\frac{s-t}{\tau_m}} dW_s.$$

it has the covariance function:

$$\mathbb{E}(U_t U_s) = \frac{\tau_m}{2} e^{-(t+s)} \left(e^{\frac{2s}{\tau_m}} - 1 \right) \quad 0 \leq s \leq t$$

With the notations of the last section, we have:

$$\begin{cases} g(t) = e^{-t} \\ h(t) = \frac{\tau_m}{2} \left(e^{\frac{2t}{\tau_m}} - 1 \right) \end{cases}$$

The associated Volterra kernel is weakly singular, hence the method described in the last section applies directly.

Indeed, according to equation (6.3), the membrane potential of such a neuron can be written:

$$V_t = V_{\text{rest}}(1 - e^{-\frac{t}{\tau_m}}) + \frac{1}{\tau_m} \int_0^t e^{\frac{s-t}{\tau_m}} I_e(s)\, ds + \frac{\sigma}{\tau_m} U_t$$

and hence the spiking condition reads:

$$U_t = a(t) \stackrel{\text{def}}{=} \frac{\tau_m}{\sigma} \left\{ \theta(t) - V_{\text{rest}}(1 - e^{-\frac{t}{\tau_m}}) - \frac{1}{\tau_m} \int_0^t e^{\frac{s-t}{\tau_m}} I_e(s)\, ds \right\},$$

where $\theta(t)$ is a time varying threshold.

The block-by-block algorithm of [182] for computing the solution of a weakly singular Volterra equation can be applied to compute the probability distribution of the spikes for any input current and any (autonomous) threshold function. This method

is very general and converges very fast towards the expected solution. The mid-point approximation can also be used, and its precision is $\mathcal{O}(\sqrt{k})$ where k is the mesh step used for the integral approximation. Nevertheless the observed convergence order is higher. For the block-by-block method, the precision of the algorithm cannot be computed easily since the kernel is not Lipschitz continuous. Nevertheless, it is commonly accepted that it has a higher precision than the mid-point method. These two quadrature methods amount to solving a linear system, which can be implemented in a very efficient way. On a an Intel®Core 2 CPU 6700 2.66GHz, it takes less than 0.02 seconds for around for a time step of 0.01 on the interval $[0,5]$.

Figure 6.2 shows some examples of the pdfs associated to various inputs. When the variance is high the law of the first hitting time of the LIF neuron converges to that of the standard Brownian motion. In the small variance case, the behavior of the first hitting time depends on the existence of a spike in the deterministic case ($\sigma = 0$). When there is no deterministic spike, an interesting phenomenon appears:

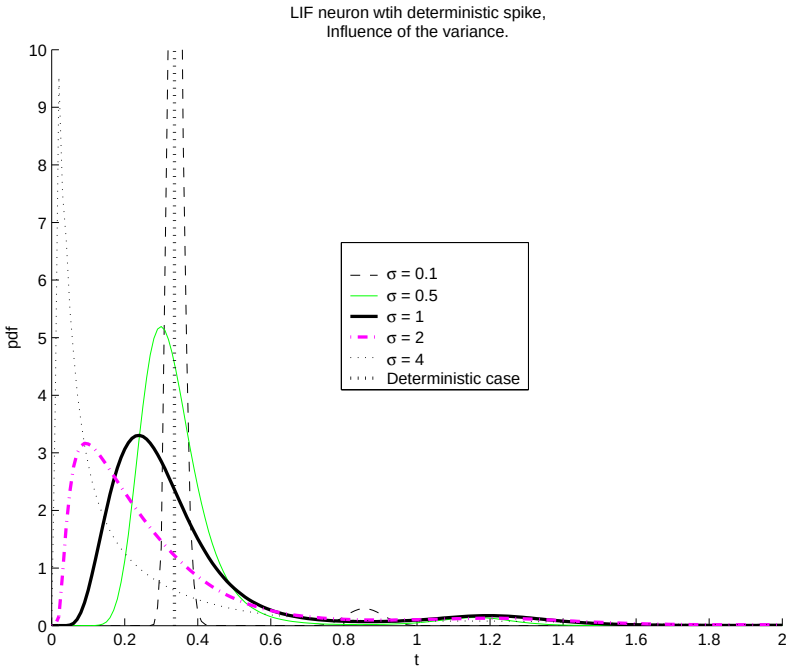

Figure 6.2: Influence of the noise standard deviation for the LIF neuron with instantaneous synaptic currents: case where a spike is emitted in when there is no noise: the pdf of the first hitting time ranges from a Dirac distribution located at the deterministic spike time in the small variance case, to the distribution of the Brownian motion first hitting time in the large variance case. [$I_e(t) = 2 + 2sin(2\pi t)$, $\tau_m = 1$, $\theta = 1$, $V_r = 0$]

the probability distribution of the spike is very diffuse over $\mathbb{R}$ and vanishes slowly, see figure 6.3.

Exponentially decaying synaptic currents

The problem becomes more difficult for two-dimensional processes such as the ones arising with the linear or nonlinear neuron models with exponentially decaying synaptic currents. In this section we derive the equation satisfied by the probability density

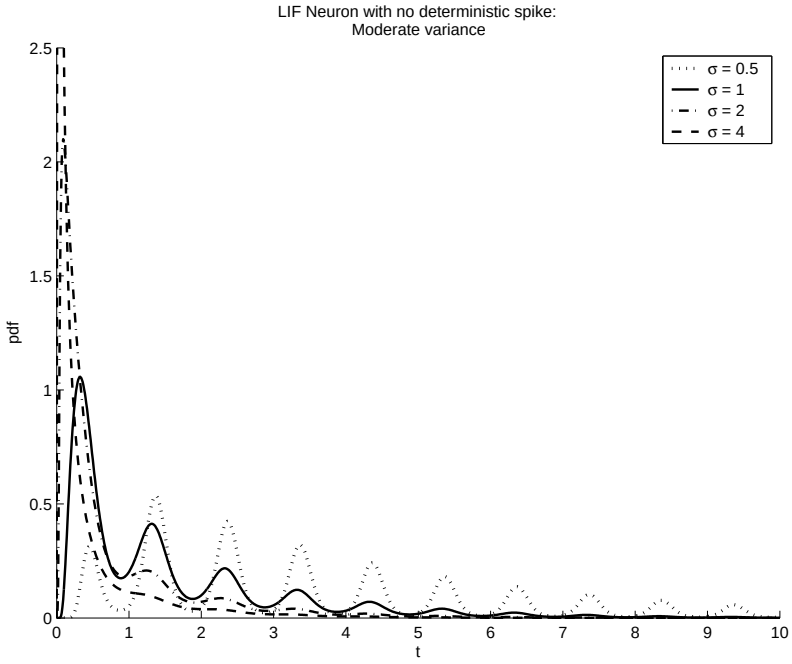

(a) Influence of the noise standard deviation for the LIF neuron with instantaneous synaptic currents when no spike is emitted in the deterministic case. Case of a moderate variance. Same neuronal parameters as in Fig.6.2 but $I_e(t) = 0.5 + sin(2\pi t)$

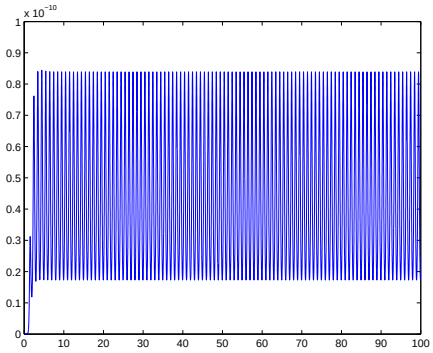

(b) No deterministic spike emitted and very small standard deviation: The distribution is almost uniform, hence the spike time contains very little information

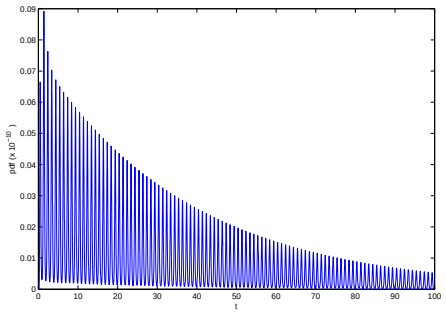

(c) No deterministic spike emitted and small standard deviation: the pdf very slowly decays (standard deviation slightly greater than case (b)).

Figure 6.3: Different simulations with Volterra's method of the pdf of the hitting time of the LIF neuron with instantaneous synaptic currents,when no spike is emitted in the deterministic case (see text).

of the first hitting time for the LIF model with exponentially decaying synaptic currents, model II, show that this equation is not well-posed and that classical methods for solving the resulting integral equations fail.

The main difficulty is that the stochastic term X_t defined in (6.5) of the membrane potential V_t of the neuron is non-Markovian, but the pair $(X_t, I_t^{\text{syn}})_{t\geq 0}$ is. As usual we denote by τ the first hitting time of the process X_t to a curved boundary $a(t)$. We prove in [262] that the pair $(\tau, I_\tau^{\text{syn}})$ has a density p with respect to Lebesgue's measure:

$$p(t,x;0,x_0,y_0)\,dt\,dx = \mathbb{P}\left(\tau \in dt,\, I_\tau^{\text{syn}} \in dx \middle| V_0 = x_0, I_0^{\text{syn}} = y_0\right)$$

We use an adapted version of the Markov argument of section 6.3.1 to obtain the following integral equation:

$$\mathbb{P}\left(X_t \geq a(t) \middle| X_0 = x_0, I_0^{\text{syn}} = I_0\right) = \int_0^t \int_{\mathbb{R}} \mathbb{P}\left(X_t \geq a(t) \middle| X_s = a(s), I_s^{\text{syn}} = y\right) p(s,y;0,x_0,I_0)\,ds\,dy \quad (6.27)$$

This equation is a Fredholm integral equation with respect to y and a Volterra equation of type I with respect to s. The kernel, noted $K(t,z;s,y)$, is equal to

$$\mathbb{P}\left(X_t \geq a(t) \middle| X_s = a(s), I_s^{\text{syn}} = y\right).$$

The term on the lefthand side of the equation, noted $g(t,z)$, is equal to

$$\mathbb{P}\left(X_t \geq a(t) \middle| X_0 = x_0, I_0^{\text{syn}} = I_0\right).$$

With these notations, equation (6.27) can be rewritten as

$$g(t,z) = \int_0^t \int_{\mathbb{R}} K(t,z;s,y) p(s,y;0,x_0,I_0)\,dy\,ds \quad (6.28)$$

Expressions for g and K can be deduced from the law of the underlying two-dimensional process and the results of section 6.2.2. The process X_t is a Gaussian process of mean $x_0 + I_0 \int_0^t g(u)du$ of variance $\rho_X(t)$ given by (6.9).

Since g can be written:

$$\begin{aligned} g(t,z) &= \mathbb{P}\left(X_t \geq a(t) \middle| X_0 = x_0, I_{\text{syn}}(0) = I_0\right) \\ &= \frac{1}{2}\left(\text{erf}\left(\frac{a(t) - x_0 - I_0\tau_s(e^{t/\tau_s} - 1)}{\sqrt{2\pi\rho_X(t)}}\right) - 1\right) \end{aligned}$$

it is regular for all values of (t,z).
The kernel K can be written:

$$\begin{aligned} K(t,z;s,y) &\stackrel{\text{def}}{=} \mathbb{P}\left(X_t \geq a(t) \middle| X_s = a(s), I_{\text{syn}}(s) = y\right) \\ &= \frac{1}{2\pi\sqrt{D(s,t)}} \exp\left(-\frac{1}{2}(X(t,y) - \mu(s,t,z))^T C(s,t)^{-1}(X(t,y) - \mu(s,t,z))\right), \end{aligned}$$

where

$$\begin{cases} D(s,t) = \det(C(s,t)) \\ \mu(s,t,z) = \begin{pmatrix} a(s) + z\int_s^t g(u)\,du \\ z \end{pmatrix} \\ X(t,y) = \begin{pmatrix} a(t) \\ y \end{pmatrix} \end{cases},$$

and $C(s,t)$ is the cross-correlation matrix (6.8).

The general theory for finding solutions to such an integral equation relies on the regularity and integrability of g and K and on the reduction to an integral equation of the second type. The reduction to the second type can be achieved formally by taking the partial derivative of both sides of (6.28) with respect to the variable t. Reordering the terms this yields

$$g_t(t,z) - \int_{\mathbb{R}} K(t,z;t,y)p(t,y;0,x_0,I_0)dy = \int_0^t \int_{\mathbb{R}} K_t(t,z;s,y)p(s,y;0,x_0,I_0)dyds$$

Because $K(t,z;t,y) = \delta(y-z)$ (δ is the Dirac delta function), this can be rewritten as

$$g_t(t,z) - p(t,z;0,x_0,I_0) = \int_0^t \int_{\mathbb{R}} K_t(t,z;s,y)p(s,y;0,x_0,I_0)dyds$$

A Taylor expansion at $s=t$ shows that K_t is singular of order $(t-s)^{-3}$ and hence does not satisfy the integrability conditions that are necessary for this equation to be well-posed.

Nonlinear Models III and IV

The membrane potential for models III and IV is non-Gaussian and hence the previous method cannot be applied directly. For the model IV, the method would probably fail for the same reason as for Model II. For the model III, the only problem is to get an expression of the transition probability density involved in equation (6.25). As already discussed in 6.2.3, the transition probability density is very hard to characterize, probably because of the explosion of the process. Generally speaking when the process is non Gaussian, provided that the transition density is known, one has to check that the kernel of the Volterra's equation is $\mathbb{L}^2$, and that the affine term deduced from the transition probability density is continuous. Because of the singularities of the solutions of these equations (that blow up in finite time with positive probability), these integrability and regularity conditions are not guaranteed.

Noisy synaptic conductances (Model V)

We wrote in section 6.2.5 the solution of the equation of the membrane potential with noisy synaptic conductances. It is a non-Gaussian Markov process, hence the framework developed so far cannot apply directly. Nevertheless we can solve in closed form the problem in the case of a constant specific "equilibrium" current $I_e(t) \equiv V_{rest} - V_{rev}$. In this case, the membrane potential starting at V_{reset} at $t=0$ reads:

$$V_t = V_{rev} + (V_{reset} - V_{rev}) \exp\left(-(\lambda + \frac{\sigma^2}{2})t + \sigma W_t\right)$$

Therefore the spike time probability distribution has the law of the first hitting time of the Brownian motion to the boundary

$$\frac{1}{\sigma}\log\left(\frac{\theta - V_{rev}}{V_{reset} - V_{rev}}\right) + \frac{1}{\sigma}\left(\lambda + \frac{\sigma^2}{2}\right)t \tag{6.29}$$

and therefore could be computed via Volterra's method. Nevertheless as we can see the boundary here is affine and hence we can use the Martingale's approach described later in section 6.3.4 to obtain a closed form expression for the probability density function.

6.3.2 Durbin's Method

The problem of the first hitting time of the Brownian motion to a general boundary has also been studied by Durbin [76, 78]. His formula involves the product of two terms, one of which being very hard to compute numerically and to characterize formally. He uses this integral equation to deduce a series approximation of the pdf and proves convergence under the restriction that the boundary considered is concave or convex (see appendix [253] for a detailed explanation of the original proof of Durbin's formula).

We show that Durbin's complex formula is a consequence of the simpler Volterra's formula, that the algorithm propose by Durbin is valid whatever the boundary considered (with no convexity restriction), and that this method is way less efficient than the one proposed in Volterra's section.

Let us first state Durbin's theorem in the most general case.

Theorem 6.3.1. *Consider a Gauss-Markov process Y of mean 0[2] and covariance function $\rho(s,t)$, and let $a(t)$ be the general boundary considered. Assume that*

1. *The boundary function $a(t)$ is continuous in $[0,t)$ and left differentiable at t.*
2. *The covariance function $\rho(s,u)$ is positive definite and has continuous first order partial derivatives on the set : $\{(s,t); 0 \leq s \leq u \leq t\}$[3]*
3. *The variance of the increment $Y_t - Y_s$ satisfies the condition:*

$$\lim_{s \nearrow t} \frac{1}{t-s} \mathbb{E}\left[(Y_t - Y_s)^2\right] = \lambda_t \tag{6.30}$$

where $0 < \lambda_t < \infty$ [4]

Then the first passage density of Y_t to the boundary $a(t)$ is given by:

$$p(t) = b(t)\, f(t) \tag{6.31}$$

where $b(t)$ is the limit, when it exists, defined by:

$$b(t) \stackrel{\text{def}}{=} \lim_{s \nearrow t} \frac{1}{t-s} \mathbb{E}\left[\mathbb{1}_{\tau_a(Y) \geq s}(a(s) - Y_s) | Y_t = a(t)\right] \tag{6.32}$$

and f is the density of Y on the boundary, i.e.:

$$f(t) \stackrel{\text{def}}{=} \frac{1}{\sqrt{2\pi\rho(t,t)}} e^{-\frac{a(t)^2}{2\rho(t,t)}}$$

Durbin's formula is equivalent to the following Volterra's equation:

$$\left(\frac{a(t)}{t} - a'(t)\right) q(t, a(t)|0,0) = p(t) + \int_0^t p(s) \left(\frac{a(t)-a(s)}{t-s} - a'(t)\right) q(t-s, a(t)|0, a(s))\, ds,$$

[2] if it is not the case, we only have to substract the mean function $m(t) := \mathbb{E}[Y_t]$ to the process Y_t and study the process $Y_t - m(t)$ instead of Y_t crossing the boundary $a(t) - m(t)$ instead of $a(t)$.

[3] where appropriate left (resp. right) derivatives are taken at s=t (resp. $s = 0$) and $u = t$

[4] Note that since $\mathbb{E}\left[(Y_t - Y_s)^2\right] = \rho(t,t) - 2\rho(s,t) + \rho(s,s)$, (6.30) is equivalent to the requirement: $\lim_{s \nearrow t}\left[\frac{\partial \rho(s,t)}{\partial s} - \frac{\partial \rho(s,t)}{\partial t}\right] = \lambda_t$

We perform the proof in the case of the Brownian motion for the sake of compactness of expressions, but the proof is exactly similar in the general case of a Gauss-Markov process (or can be deduced from the present one using Doob's representation theorem for Gauss-Markov processes).

We have:

$$\begin{aligned} b(t) &= \lim_{s \nearrow t} \frac{1}{t-s} \mathbb{E}\left[\mathbb{1}_{\tau_a \geq s} (a(s) - Y_s) | Y_t = a(t)\right] \\ &= \lim_{s \nearrow t} \frac{1}{t-s} \mathbb{E}\left[(a(s) - Y_s) | Y_t = a(t)\right] - \lim_{s \nearrow t} \frac{1}{t-s} \mathbb{E}\left[\mathbb{1}_{\tau_a < s} (a(s) - Y_s) | Y_t = a(t)\right] \qquad (6.33) \\ &\stackrel{\text{def}}{=} E_1 + E_2 \end{aligned}$$

Then we know that the conditional expectation of Y_s knowing Y_t is $\frac{s}{t} Y_t$ for the Brownian motion.

So the first term of (6.33) simply reads:

$$\mathbb{E}\left[Y_s | Y_t = a(t)\right] = \frac{s}{t} a(t) = a(t) + \frac{s-t}{t} a(t)$$

Hence we get:

$$\begin{aligned} b(t) &= \lim_{s \nearrow t} \left(\frac{a(s) - a(t)}{t-s} + \frac{a(t)}{t} \right) + E_2 \\ &= \frac{a(t)}{t} - a'(t) + E_2 \end{aligned}$$

Conditioning on the first hitting time u of the process Y to the barrier $a(t)$, we obtain the following expression for the term E_2:

$$\begin{aligned} E_2 &= \lim_{s \nearrow t} \frac{1}{t-s} \mathbb{E}\left[\mathbb{1}_{\tau_a < s} (a(s) - Y_s) | Y_t = a(t)\right] \\ &= \lim_{s \nearrow t} \int_0^s \frac{1}{t-s} \mathbb{E}\left[(a(s) - Y_s) | Y_u = a(u),\ Y_t = a(t)\right] \frac{p(u)}{q(t, a(t) | 0, 0)} du. \end{aligned}$$

Using the strong Markov property of Y and the properties of the conditional expectation, recalling that the regression coefficient of Y_s on Y_t given $Y_u = a(u)$ is given by $\frac{s-u}{t-u}$, we have

$$\begin{aligned} \mathbb{E}\left[Y_s | Y_t = a(t),\ Y_u = a(u)\right] &= a(u) + \frac{s-u}{t-u} \left(a(t) - a(u)\right). \\ &= a(t) + \frac{s-t}{t-u} \left(a(t) - a(u)\right) \end{aligned}$$

So we get:

$$\begin{aligned} \lim_{s \nearrow t} \mathbb{E}\left[a(s) - Y_s | Y_t = a(t),\ Y_u = a(u)\right] &= \lim_{s \nearrow t} \frac{a(s) - a(t)}{t-s} + \frac{a(t) - a(u)}{t-u} \\ &= \frac{a(t) - a(u)}{t-u} - a'(t) \end{aligned}$$

So eventually the following formula for E_2 holds:

$$E_2 = \int_0^t \left(\frac{a(t)-a(u)}{t-u} - a'(t) \right) p(u) \frac{q(t-u, a(t)|0, a(u))}{q(t, a(t)|0, 0)} \, du$$

So finally, using the formula (6.31), we have the fixed point equation searched:

$$p(t) = \left(\frac{a(t)}{t} - a'(t) \right) q(t, a(t)|0, 0) + \int_0^t \left(\frac{a(t)-a(u)}{t-u} - a'(t) \right) p(u) q(t-u, a(t)|0, a(u)) \, du \tag{6.34}$$

Hence we have equivalence between Durbin's formulation (6.32) and the Volterra's equation (6.34).

This equation is a straightforward consequence of Volterra's equation (6.26), as proved by David Williams in the appendix of [78].

Durbin provides an algorithm to compute the solution of his equation. This approximation method consist in truncating the following series expansion:

$$p(t) = \sum_{j=1}^{\infty} (-1)^{j-1} q_j(t)$$

where

$$q_j(t) = \int_0^t \int_0^{t_1} \cdots \int_0^{t_{j-2}} \left[\frac{a(t_{j-1})}{t_{j-1}} - a'(t_{j-1}) \right] \times \prod_{i=1}^{j-1} \left[\frac{a(t_{i-1}) - a(t_i)}{t_{i-1} - t_i} - a'(t_{i-1}) \right] f(t_{j-1}, \cdots, t_1, t) \, dt_{j-1} \cdots dt_1 \quad (t_0 = t)$$

He shows in [78] that this series converges, under the condition that the boundary $a(\cdot)$ is convex or concave, using the fact that its remainder tends to zero. This representation of the solution, from the viewpoint of Volterra's theory, is very well known: it is simply the iterated kernels formula for the equation (6.34). It is very classical, and is valid whenever the kernel of the Volterra's equation is continuous. The principle is to consider this equation as a fixed point equation on a functional space: p is a fixed point of the functional:

$$\mathscr{L} : f \mapsto \left(\frac{a(t)}{t} - a'(t) \right) q(t, a(t)|0, 0) - \int_0^t \left(\frac{a(t)-a(s)}{t-s} - a'(t) \right) p(s) q(t-s, a(t)|0, a(s)) \, du$$

and building an iterative approximation via the iteration of the operator $\mathscr{L}$ (also known as Picard's method when the operator is contracting). Here the kernel of the Volterra's equation reads:

$$K(s,t) = \left(\frac{a(t)-a(s)}{t-s} - a'(t) \right) q(t-s, a(t)|0, a(s)).$$

It is clearly continuous, since the only possible discontinuity is on the line $s = t$, but on this line we have, when a is C^2,

$$\left(\frac{a(t)-a(s)}{t-s} - a'(t) \right) \sim (t-s) a''(t)$$

$$q(t-s, a(t)|0, a(s)) \sim \frac{1}{\sqrt{2\pi(t-s)}}$$

and therefore the kernel is continuous on the line $t = s$. Furthermore, the affine term in the equation, $(\frac{a(t)}{t} - a'(t))q(t,a(t)|0,0)$, is also continuous. Indeed, the only possible discontinuity would be at $t = 0$, but since we assumed that $a(0) > 0$, this function is continuous at $t = 0$ and is 0 at this point. Hence there exists a unique fixed point for the functional equation (6.34) in the set of continuous functions, and this solution can be computed with the resolvent kernel, which is the limit given in the theorem (these results are quite classical, see for instance [39, 182]).

We provide here a sketch of the proof, details can be found for instance in [182, Theorem 3.1].

We have seen that the kernel and the affine terms of the equation are continuous on $\mathbb{R}^+$. Therefore they are bounded on any bounded interval. We consider the solution of this equation on a time interval $[0,T]$, and denote by Q and K two positive constants such that:

$$\begin{cases} \left| \left(\frac{a(t)}{t} - a'(t) \right) q(t,a(t)|0,0) \right| \leq Q \\ |K(s,t)| \leq K \end{cases}$$

We consider for a given initial condition f the iterated kernels:

$$\begin{cases} f_0 & = f \\ f_{n+1} & = \mathscr{L} f_n \end{cases}$$

and we introduce $\varphi_n := f_n - f_{n-1}$ the difference between two consecutive iterates ($\varphi_0 = f$). We obtain the equation:

$$\varphi_n = \int_0^t K(s,t)\varphi_{n-1}(s)\,ds$$

We then prove easily that $|\varphi_n(t)| \leq Q\frac{(Kt)^n}{n!}$ for any given t in $[0,T]$. Therefore the series converges and we denote by $\varphi \stackrel{\text{def}}{=} \sum_{n=0}^{\infty} \varphi_n$. Since this series converges absolutely, we can readily prove that this function φ satisfies the fixed point equation. Hence we have existence of a fixed point and convergence of the iterates to a fixed point. To prove the uniqueness of solution, we proceed exactly the same way using a *reductio ad absurdum*, assuming that there exist two fixed points and showing that in reality these two fixed point are identical (this involves exactly the same estimations as for proving the existence of a fixed point).

We hence proved that Durbin's equation was a direct consequence of Volterra's equation (6.26), but to derive this equation we further need to assume that the boundary has a Lipschitz derivative. Nevertheless, with Volterra's point of view we do not need to assume that the boundary has to be convex or concave: it can be any regular boundary function. The formula provided by Durbin is way more complex than the intuitive Volterra's equation. Its application domain is a little bit more restricted, and eventually the algorithm proposed by Durbin to compute the pdf of the hitting time is very inefficient compared to the method proposed in section 6.3.1. Indeed, it involves successive integrals on spaces of increasing dimensions, which is very heavy to implement numerically.

6.3.3 The Feynman-Kac's Method

Feynman-Kac's formula (see appendix C.1.2) gives a representation of the Laplace transform of the first hitting time of a stochastic process. This technique partially solves problems I and III for constant inputs and constant boundaries, and are very difficult to generalize to other models or types of boundaries.

Leaky Integrate-and-fire neuron with constant external current and instantaneous synaptic currents

We consider a leaky integrate-and-fire neuron with constant current input I_e and instantaneous synaptic white noise current. Let $W \overset{\text{def}}{=} (W_t)_{t\geq 0}$ be a standard Brownian motion. Thanks to a change of origin of V_t in equation (6.2), the associated membrane potential process is an Ornstein-Ulhenbeck (OU) process $V \overset{\text{def}}{=} (V_t)_{t\geq 0}$ with parameter $\lambda \in \mathbb{R}$, solution of the linear SDE:

$$\begin{cases} dV_t = -\lambda V_t dt + dW_t \\ V_0 = x \in \mathbb{R} \end{cases} \tag{6.35}$$

The process V_t is a diffusion process with infinitesimal generator denoted by $\mathscr{L}$, given by (see appendix C.1):

$$\mathscr{L} f(x) = \frac{1}{2}\frac{\partial^2 f}{\partial x^2}(x) - \lambda x \frac{\partial f}{\partial x}(x), \quad x \in \mathbb{R} \tag{6.36}$$

This equation is central to the theory of Hermite's functions, see [260, appendix B]. The properties of the first hitting time of the OU process have been widely studied. For instance, in [4], the authors give three representations of the probability density of these processes, and in [224] we find an explicit expression of the moments of those hitting times.

Let $a \in \mathbb{R}$ be a given fixed real number and denote by τ_a the first passage time of the process V_t to the constant a.

The Laplace transform of τ_a can be computed as follows [29, 237].

Proposition 6.3.2. For $x < a$ the Laplace transform of τ_a is given by

$$\mathbb{E}_x\left[e^{-\alpha\tau_a}\right] = \frac{\mathscr{H}_{-\alpha/\lambda}(-x\sqrt{\lambda})}{\mathscr{H}_{-\alpha/\lambda}(-a\sqrt{\lambda})} = \frac{e^{\lambda x^2/2}\mathscr{D}_{-\alpha/\lambda}(-x\sqrt{2\lambda})}{e^{\lambda a^2/2}\mathscr{D}_{-\alpha/\lambda}(-a\sqrt{\lambda})} \tag{6.37}$$

where $\mathscr{H}_\nu$ stands for the Hermite function and $\mathscr{D}_{-\alpha/\lambda}$ for the parabolic cylinder functions respectively (see Lebedev [177, chapter 10] for a detailed study of these functions).

Proof. We use the hitting time characterization given by the Feynman-Kac equations, obtained in section 6.4. The Laplace transform of the first passage time is given by theorem C.1.9 as the unique solution of the boundary value problem:

$$\begin{cases} \mathscr{L}u(x) & = \alpha u(x), \text{ for } x < a \\ u(a) & = 1 \\ \lim\limits_{x\to-\infty} u(x) & = 0 \end{cases} \tag{6.38}$$

The theory of parabolic equations applies since the coefficients of the diffusion operator $\mathscr{L}$ are $\mathscr{C}^\infty$. This is a singular value problem since the interval is not bounded. Nevertheless one can prove that the solution can be written (see theorem C.1.10):

$$\mathbb{E}_x\left[e^{-\alpha\tau_a}\right] = \frac{\psi_\alpha(x)}{\psi_\alpha(a)}$$

where $\psi_\alpha(\cdot)$ is, up to some multiplicative constant, the unique increasing positive solution of the equation $\mathscr{L}u = \alpha u$ which is, up to a change of variable, the equation

for the Hermite's functions, see [260, appendix B]. The two fundamental solutions of this linear differential equations are $\mathscr{H}_{-\alpha/\lambda}(x\sqrt{\lambda})$ and $\mathscr{H}_{-\alpha/\lambda}(-x\sqrt{\lambda})$. The function ψ_α is up to a positive constant the one that is increasing. With the series expansion of the Hermite's functions, it is clear that $\psi_\alpha(x) = \mathscr{H}_{-\alpha/\lambda}(-x\sqrt{\lambda})$. This proves the first equality in (6.37). The second equality relies on the relation between $\mathscr{H}_\nu$ and $\mathscr{D}_\nu$.

□

From this characterization, we can compute all the moments of the law of τ_a by differentiating the Laplace transform at 0. This provides the first three moments which are used later to validate some of our numerical techniques, see [224] for a proof of this:

Theorem 6.3.3. *Let us define* $\alpha \stackrel{\text{def}}{=} \frac{\mu}{\sigma}$ *and* $\beta \stackrel{\text{def}}{=} \frac{\sigma}{\theta\sqrt{\tau}}$ *and the three following functions:*

$$\Phi_1(z) \stackrel{\text{def}}{=} \frac{1}{2}\sum_{n=1}^{\infty}\left(\frac{2}{\beta}\right)^n \frac{1}{n!}\Gamma(\frac{n}{2})(z-\alpha)^n$$
$$\Phi_2(z) \stackrel{\text{def}}{=} \frac{1}{2}\sum_{n=1}^{\infty}\left(\frac{2}{\beta}\right)^n \frac{1}{n!}\Gamma(\frac{n}{2})\left(\Psi(\frac{n}{2})-\Psi(1)\right)(z-\alpha)^n$$
$$\Phi_1(z) \stackrel{\text{def}}{=} \frac{3}{8}\sum_{n=1}^{\infty}\left(\frac{2}{\beta}\right)^n \frac{1}{n!}\Gamma(\frac{n}{2})(z-\alpha)^n\rho_n^{(3)}$$

where Γ *is the gamma function,* $\Psi(z) = \frac{\Gamma'(z)}{\Gamma(z)}$ *is the digamma function, and*

$$\rho_n^{(3)} = \left(\Psi(\frac{n}{2})-\Psi(1)\right)2 + \left(\Psi'(\frac{n}{2})-\Psi'(1)\right)$$

If τ_θ *is the hitting time of an OU process starting at 0 to the barrier* θ*, we have:*

$$\mathbb{E}[\tau_\theta] = \tau(\Phi_1(1)-\Phi_1(0))$$
$$\mathbb{E}[\tau_\theta^2] = \tau^2(2\Phi_1(1)^2 - \Phi_2(1) - 2\Phi_1(1)\Phi_1(0) + \Phi_2(0))$$
$$\mathbb{E}[\tau_\theta^3] = \tau^3\left\{6\Phi_1(1)^3 - 6\Phi_1(1)\Phi_2(1) + \Phi_3(1)\right.$$
$$\left. -6(\Phi_1(1)^2 - 3\Phi_2(1))\Phi_1(0) + 3\Phi_1(1)\Phi_2(0) - \Phi_3(0)\right\}$$

Quadratic Integrate-and-fire neuron

The Feynman-Kac method relies heavily on the very strong assumption that there exists a solution satisfying the limit condition $\lim_{x\to-\infty} u(x) = 0$. This assumption is in effect satisfied only in very few cases. Furthermore, this method can only be applied to autonomous systems, and hence cannot be applied to neuron models with deterministic time-dependent synaptic inputs. For instance we show here that it cannot be applied to the one-dimensional quadratic integrate-and-fire neuron defined in section 6.2.3, even in the simple case of a constant external current.

Assume that the membrane potential of the neuron satisfies the stochastic differential equation:

$$dX_t = f(X_t)dt + \sigma dW_t$$

The infinitesimal operator of the associated semigroup $\mathscr{L}$ is givenby:

$$\mathscr{L}h(x) = \frac{1}{2}\sigma^2\frac{d^2h}{dx^2}(x) + f(x)\frac{\mathrm{d}h}{\mathrm{d}x}(x), \quad x\in\mathbb{R} \tag{6.39}$$

Let u_λ be the Laplace transform of the first hitting time τ_a to a constant a:

$$u_\lambda(x) = \mathbb{E}\left(e^{-\lambda\tau_a}\middle| X_0 = x\right)$$

u_λ is a solution, when it exists, of the Feynman-Kac differential equation (C.11), which in the case of the quadratic integrate-and-fire neuron can be written:

$$\begin{cases} \frac{1}{2}\sigma^2\frac{d^2u_\lambda(x)}{dx^2} + (x^2+I_e)\frac{\mathrm{d}u_\lambda(x)}{\mathrm{d}x} - \lambda u_\lambda(x) = 0 \\ u_\lambda(a) = 1 \\ u_\lambda(x) \underset{x\to-\infty}{\longrightarrow} 0 \end{cases} \tag{6.40}$$

This ordinary differential equation is a triconfluent Heun equation with boundary conditions (see e.g. [230, Prop.1.3.6] and Maple ®documentation). As in section 6.2.3 we denote by h_t the triconfluent Heun function. We have

$$u_\lambda(x) = \alpha h_t\left(\frac{-3^{2/3}\lambda}{\sqrt[3]{a}}, 3, \frac{b\sqrt[3]{3}}{a^{2/3}}, \frac{-x}{\sqrt[3]{3a}}\right) + \beta h_t\left(\frac{-3^{2/3}\lambda}{\sqrt[3]{a}}, -3, \frac{b\sqrt[3]{3}}{a^{2/3}}, \frac{x}{\sqrt[3]{3a}}\right) e^{-1/3\frac{x\left(3b+x^2\right)}{a}} \tag{6.41}$$

It can be verified again that the triconfluent Heun function $h_t(\alpha,3,\beta,x)$ diverges very fast when $|x|\to\infty$. Hence there is no solution to the boundary problem (6.40).

For the same type of reasons it appears that Feynmann-Kac's method fails in finding the Laplace transform of the spike probability distribution in the case of Model V. In that case, the solution of the differential equation involves Kummer's functions, that are also fast diverging.

6.3.4 Martingale Methods

This method consists in finding a martingale related to the membrane potential process. The optimal stopping theorem applied at the first hitting time gives a functional related to the law of the first hitting time. If this functional is not trivial, we can get interesting informations on the law of the first hitting time (in general its Laplace transform). This method is applied classically to characterize the Laplace transform of the first hitting times of the Brownian motion to a constant boundary, for instance in [160].

The most general ways for finding martingales related to processes is to use an associated partial differential equation linked with the infinitesimal generator of the process. Nevertheless, this method is quite particular and can be applied only to very particular cases. One of the simplest example illustrating this technique is the problem of the first hitting time of the Brownian motion to a constant boundary (see e.g. [160, pages 79–81]). Indeed, as straightforward application of Itô's theorem, it is well known that the process $e^{\theta B_t - \frac{\theta^2}{2}t}$ is a martingale for all θ. Let us denote by τ_a the first hitting time of the Brownian motion with the constant a. It is clear that this hitting time is almost surely finite. Furthermore, it is clear that $e^{\theta B_{t\wedge\tau_a} - \frac{\theta^2}{2}t\wedge\tau_a}$ is a bounded martingale so a uniformly integrable martingale, hence the optional sampling theorem C.1.1 applies, hence we have for any $t>0$

$$\mathbb{E}\left[e^{\theta B_{t\wedge\tau_a} - \frac{\theta^2}{2}t\wedge\tau_a}\right] = 1$$

Eventually, letting $t \to \infty$ and using Lebesgue's theorem, we obtain the Laplace transform of τ_a:

$$\mathbb{E}\left[e^{-\frac{\theta^2}{2}\tau_a}\right] = e^{-\theta a}$$

which is known as the Laplace transform of the inverse normal distribution, whose probability density reads:

$$p(t) = \frac{|a|}{\sqrt{2\pi t^3}} e^{-a^2/2t} \quad t > 0$$

An alternative method, based on the properties of the Brownian motion, can be used to compute this density. This method is based on the the reflection principle for the Brownian motion, which is the consequence of the Markov and the time-inversion properties of the Brownian motion. We have:

$$\begin{aligned}
\mathbb{P}[\tau_a < t] &= \mathbb{P}[\tau_a < t; B_t > a] + \mathbb{P}[\tau_a < t; B_t < a] \\
&= \mathbb{P}[B_t > a] + \mathbb{P}[\tau_a < t; B_t < a] \\
&= \mathbb{P}[B_t > a] + \mathbb{E}\left[\mathbb{1}_{\tau_a < t}\mathbb{P}\left[B_t < a \middle| \mathscr{F}_{\tau_a}\right]\right] \\
&= \mathbb{P}[B_t > a] + \mathbb{E}\left[\mathbb{1}_{\tau_a < t}\mathbb{P}\left[B_{t-\tau_a+\tau_a} - B_{\tau_a} < 0 \middle| \mathscr{F}_{\tau_a}\right]\right] \\
&= \mathbb{P}[B_t > a] + \mathbb{E}\left[\mathbb{1}_{\tau_a < t}\mathbb{P}\left[\widetilde{B}_{t-\tau_a} < 0 \middle| \mathscr{F}_{\tau_a}\right]\right] \quad \text{(Strong Markov property)} \\
&= \mathbb{P}[B_t > a] + \frac{1}{2}\mathbb{P}[\tau_a < t]
\end{aligned}$$

Therefore the repartition function of τ_a reads

$$\mathbb{P}[\tau_a < t] = \sqrt{\frac{2}{\pi}} \int_{a/\sqrt{t}}^{\infty} e^{-x^2/2} dx$$

and differentiating w.r.t. t we get the probability density function of τ_a:

$$p(t) = \frac{|a|}{\sqrt{2\pi t^3}} e^{-a^2/2t} \quad t > 0.$$

Exponentially decaying synaptic currents

A more interesting example of this technique is provided by Lachal in [168] who solved the problem for the perfect integrator neuron without deterministic input current and with exponential synaptic conductances[5]:

$$\begin{cases} dV_t &= I^{\text{syn}}(t)dt \\ \tau_s dI^{\text{syn}}(t) &= -I^{\text{syn}}(t)dt + \sigma dW_t \end{cases} \tag{6.42}$$

This method involve quite intricate calculations, which can be interesting from a mathematical point of view. We nevertheless omit them in this dissertation, since this technique is very specific, involves some art in the calculations and cannot be easily generalized to other neuron models or other boundaries. The interested reader can find the details of the proof in [168].

[5]This model cannot be considered as a biological case by itself but can be seen as a limit case of the model of section 6.2.2 in the small τ_s or large τ_m limits

Model V for constant equilibrium inputs

This technique can be used to compute the spike statistics of Model V in the case of constant equilibrium inputs $I_e \equiv V_{rest} - V_{rev}$ (we call the input *equilibrium inputs* since this level of constant input because it amounts to equalizing V_{rev} and $V_{rest} + I_e$). Indeed, as already proved in section 6.3.1, the law of the spike times in that case is equal to the law of the first hitting time of the Brownian motion to an affine boundary.

To generalize the result just obtained for constant boundaries to affine boundaries, we use Girsanov's theorem C.1.7, or more precisely the simpler Cameron Martin's theorem. It states that the process $X_t := W_t - \gamma t$ is a Brownian motion under the probability measure $\mathbb{Q}_\gamma$ having the density with respect to the initial probability density $\mathbb{P}$:

$$\mathbb{Q}_\gamma|_{\mathscr{F}_t} = e^{\gamma U_t - \frac{\gamma^2}{2}t}\mathbb{P}|_{\mathscr{F}_t}$$

where U_t is the canonical process. Furthermore, we have:

$$\begin{aligned}\tau_{at+b} &= \inf\{t > 0, W_t = at + b\} \\ &= \inf\{t > 0, W_t - at = b\}\end{aligned}$$

Hence τ_{at+b} under $\mathbb{P}$ has the same law as τ_b under $\mathbb{Q}_{-a}$, and hence we have:

$$\mathbb{P}(\tau_{at+b} \in dt) = e^{-ab-\frac{a^2}{2}t}\frac{|b|}{\sqrt{2\pi t^3}}e^{-b^2/2t} = \frac{|b|}{\sqrt{2\pi t^3}}e^{-\frac{1}{2t}(at+b)^2}$$

With the boundary found for the problem of leaky integrate-and-fire neuron with noisy synaptic conductances obtained in equation (6.29), we have:

$$\begin{cases} a &= \frac{1}{\sigma}\left(\lambda + \frac{\sigma^2}{2}\right) \\ b &= \frac{1}{\sigma}\log\left(\frac{\theta - V_{rev}}{V_r - V_{rev}}\right) \end{cases}$$

It is interesting to note that these two coefficients are positive, and therefore the probability that this neuron at this level of excitation does not spike is strictly positive and reads:

$$1 - e^{-2\frac{(\lambda+\frac{\sigma^2}{2})\log\left(\frac{\theta - V_{rev}}{V_r - V_{rev}}\right)}{\sigma^2}}$$

6.3.5 Brunel's Method

Nicolas Brunel and his collaborators developed a method to compute the stationary mean firing rate of integrate-and-fire neurons, based on the Fokker-Planck equation [37, 94]. This method is the only one to provide partial informations for nonlinear integrate-and-fire neuron with instantaneous or exponentially decaying synaptic currents. It is based on a careful description of the boundary conditions for the Fokker-Planck equation, that can be solved in the case of instantaneous synapses, giving access to the stationary probability distribution of the membrane potential, from which in turns we can derive the mean firing rate. He treated the cases of the leaky integrate-and-fire models with instantaneous or exponentially decaying synaptic currents, and the case of the quadratic integrate-and-fire model with an infinite threshold and a reset at $-\infty$.

In the case of exponentially decaying synaptic currents, regular and singular perturbation methods give access to approximations of the mean firing rate in the limits

of short and large correlation time. Analytical expressions can be found. Nevertheless, it can be quite difficult to use, and is only valid for the *free dynamics* of the neuron (i.e. without any deterministic time-dependent inputs, $I_e = constant$) and in the limit of the stationnary state (i.e. when $t \to \infty$).

The method consists in

1. Computing the stationary distribution of the membrane potential using the Fokker-Planck equation (C.18).

2. Using the fact that the stationary firing rate of the neuron is the full probability flux of the stationary probability at the threshold θ.

It has been applied successfully to the LIF neuron with instantaneous synaptic current. In this case the stationary distribution can be computed in closed form (see [36]) and hence also the stationary firing rate ν_0:

$$\frac{1}{\nu_0} = \tau_m \sqrt{\pi} \int_{\frac{V_r-\mu}{\sigma}}^{\frac{\theta-\mu}{\sigma}} e^{s^2} (1 + \mathrm{erf}(s))\, ds \tag{6.43}$$

Nonlinear IF with instantaneous synaptic currents

In this section we apply Brunel's method to the one-dimensional nonlinear models with instantaneous synaptic currents (Model III) and compute in closed form the stationary firing rate of the neuron for general nonlinear function, and apply this formula to the quadratic and quartic nonlinearities. The membrane potential of the nonlinear IF neuron with instantaneous noisy current satisfies the equation:

$$\tau_m dV_t = (\mu + F(V_t))\, dt + \sigma dW_t$$

where $F(v)$ is a convex function. In the case of the quadratic IF, $F(v) = v^2$, in the case of the quartic model $F(v) = v^4 + av$) and in the case of the exponential model $F(v) = e^v - v$.

The related transition probability density satisfies the associated Fokker-Planck equation C.18:

$$\tau_m \frac{\partial P(t,x)}{\partial t} = \frac{\sigma^2}{2} \frac{\partial^2 P(t,x)}{\partial x^2} - \frac{\partial}{\partial x}\big((\mu + F(x))P(t,x)\big)$$

Hence the stationary transition P_0 is a solution of the ordinary differential equation:

$$\frac{\sigma^2}{2} \frac{\mathrm{d}^2 P_0(x)}{\mathrm{d}x^2} - \frac{\mathrm{d}}{\mathrm{d}x}\big((\mu + F(x))P_0(x)\big) = 0$$

This equation is a linear differential equation and can be solved in closed form. Let us denote by $g(\cdot)$ a primitive of $\frac{2}{\sigma^2}(F(x) + \mu)$. The general solution of this equation reads:

$$P_0(x) = \left(\alpha \int_0^x e^{-g(y)}\, dy + \beta \right) e^{g(x)}. \tag{6.44}$$

where α and β are constants defined by the initial (or boundary conditions) , which are governed by the continuity of the probability density and the continuity of the probability flow at the reset potential V_r:

1. $P_0(\theta) = 0$

2. $P_0(V_r^+) - P_0(V_r^-) = 0$ (continuity at the reset potential)
3. $\frac{dP_0}{dV}(V_r^+) - \frac{dP_0}{dV}(V_r^-) = \frac{dP_0}{dV}(\theta)$: conservation of the "probability flux": the current flowing out at the threshold is reinjected at the reset.

The firing rate of the neuron is equal to the probability voltage flux J_V through the boundary θ. This flux is defined by the relation $\partial_t P + \partial_V J_V = 0$ and hence reads in the stationary limit:

$$J_V = \frac{\mu + F(V)}{\tau_m} P_0 - \frac{\sigma^2}{2\tau_m} \frac{dP_0}{dV}.$$

Therefore the the stationary firing rate ν_0 is linked with the derivative of the stationary probability density function via the relation:

$$\frac{\partial P_0}{\partial V}(\theta) = -2\nu_0 \frac{\tau_m}{\sigma^2}$$

Equation (6.44) together with these boundary conditions defines a unique solution. Indeed, the function p_0 can be written in the form:

$$P_0(x) = \begin{cases} \alpha_1 e^{g(x)} + \beta_1 e^{g(x)} \int_{V_r}^{x} e^{-g(y)}\, dy & x \in (-\infty, V_r) \\ \alpha_2 e^{g(x)} + \beta_2 e^{g(x)} \int_{\theta}^{x} e^{-g(y)}\, dy & x \in (V_r, \theta) \end{cases}$$

The boundary conditions together with the normalization condition $\int_{-\infty}^{\theta} p_0(x)\, dx = 1$ give a unique solution.

In detail the solution is defined up to the multiplicative constant (β_2):

$$\begin{cases} \alpha_2 = 0 \\ \alpha_1 = \beta_2 \int_{\theta}^{V_r} e^{-g(y)}\, dy \\ \beta_1 = 0 \end{cases} \tag{6.45}$$

And the normalization condition $\int_{-\infty}^{\theta} p_0(x)\, dx = 1$ yields:

$$\beta_2 = \frac{1}{\int_{\theta}^{V_r} e^{-g(y)}\, dy \int_{-\infty}^{V_r} e^{g(x)}\, dx + \int_{\theta}^{V_r} \int_{\theta}^{x} e^{g(x)-g(y)}\, dy dx}$$

The stationary probability density P_0 is plotted in figure 6.4 for the quadratic and quartic cases.

We can obtain the stationary firing rate of the noisy quadratic integrate-and-fire with threshold:

$$\begin{aligned} \nu_0 &= -\frac{\sigma^2}{2\tau_m} \left. \frac{dP_0(x)}{dx} \right|_{x=\theta} \\ &= \frac{\sigma^2}{2\tau_m} \beta_2 \end{aligned} \tag{6.46}$$

which can be rewritten in terms of the parameters of the system:

$$\nu_0 = \frac{\sigma^2}{2\tau_m} \frac{1}{\int_{\theta}^{V_r} e^{-g(y)}\, dy \int_{-\infty}^{V_r} e^{g(x)}\, dx + \int_{\theta}^{V_r} \int_{\theta}^{x} e^{g(x)-g(y)}\, dy dx} \tag{6.47}$$

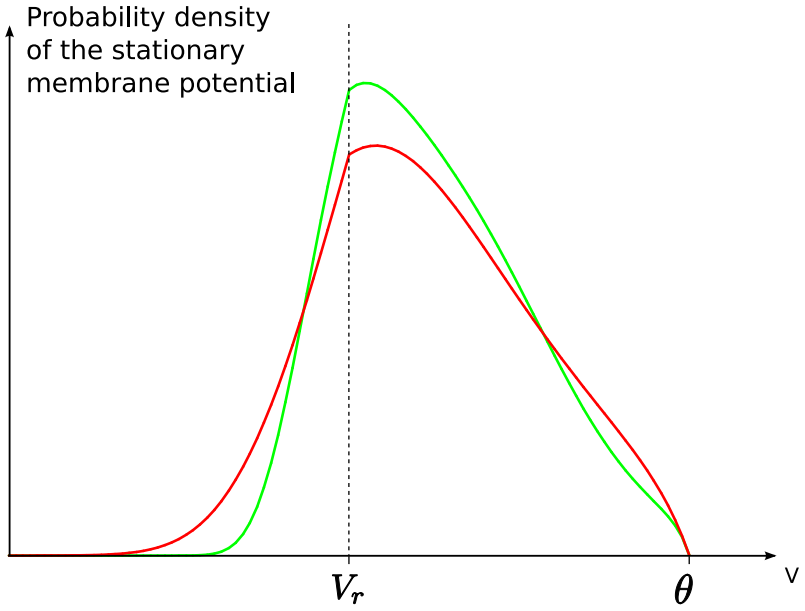

Figure 6.4: Stationary distributions of the membrane potential for the quadratic (red line) and quartic (green line) neuron models. We observe that even if they do not have the same probability distribution, they almost have the same slope at $V = \theta$ and hence their stationary mean firing rate are similar

The same technique can be used when the spike condition is when the solution blows up and the reset is at $-\infty$. In this case, the threshold is $\theta = \infty$ and the reset $V_r = -\infty$. We lose the equation $p_0(\theta) = 0$ but the fact that the solution has to be integrable provides a new constraint. This way we obtain the stationary distribution $p_{0,\infty}$ of the quadratic IF model with infinite spike threshold:

$$P_{0,\infty}(x) = \frac{2\nu_{0,\infty}\tau_m}{\sigma^2}\int_x^\infty e^{g(x)-g(y)}\,dy$$

and the stationary firing rate is given by the normalization condition:

$$\nu_{0,\infty} = \frac{\sigma^2}{2\tau_m}\left[\int_{-\infty}^\infty e^{g(x)}\int_x^\infty e^{-g(y)}\,dy\,dx\right]^{-1}.$$

Taking into account exponentially decaying current

Using a perturbation technique together with the Fokker-Planck framework, Nicolas Brunel and colleagues in [37, 94] obtained expansion of this firing rate in the case of colored noise , i.e. in the case of exponentially decaying synaptic currents with time constant τ_s, in the linear and nonlinear cases (models II and IV). More precisely, the membrane potential in this case is solution of the equation:

$$\begin{cases} \tau_m dV_t = F(V_t)dt + I_t^{\text{syn}}dt \\ \tau_s dI_t^{\text{syn}} = -I_t^{\text{syn}}dt + \sqrt{\tau_m}\sigma dW_t \end{cases}$$

where $F(\cdot)$ can be linear (model II) or nonlinear (model IV). The associated Fokker-Planck equation reads:

$$\tau_m \partial_t P(t,V,I^{\text{syn}}) + \partial_V[(F(V)+I^{\text{syn}})P] + \frac{\tau_m}{\tau_s}\partial_{I^{\text{syn}}}[-I^{\text{syn}}P] = \frac{\sigma^2\tau_m^2}{2\tau_s^2}\partial^2_{I^{\text{syn}}}P,$$

where $P(t,V,I^{\text{syn}})$ is the transition probability density of the process (V,I^{syn}) at time t. This equation can be written in terms of the probability fluxes of V and w, which we denote J_V and $J_{I^{\text{syn}}}$, defined by:

$$J_V(t,V,I^{\text{syn}}) = \frac{1}{\tau_m}(F(V)+I^{\text{syn}})P(V,I^{\text{syn}},t)$$
$$J_{I^{\text{syn}}}(t,V,I^{\text{syn}}) = \frac{1}{\tau_s}(-\frac{\tau_m}{\tau_s}\frac{\sigma^2}{2}\partial_{I^{\text{syn}}}P - I^{\text{syn}}P)$$

and yields the continuity equation:

$$\tau_m \partial_t P(t,V,I^{\text{syn}}) + \partial_V J_V(t,V,I^{\text{syn}}) + \partial_{I^{\text{syn}}} J_{I^{\text{syn}}}(t,V,I^{\text{syn}}) = 0$$

Even in the stationary case ($t \to \infty$), the equation cannot be solved in a closed form. But one can get rid of this obstruction by considering that the time scales of the membrane potential and of the synaptic integration are separable. When the ratio τ_s/τ_m tends to zero (*short correlation limit*), the solution is the same as the one given for the white noise case. When this ratio tends to infinity (*large correlation limit*), an exact solution can be also provided. the first order correction to the short correlation limit in the case of the leaky integrate and fire neuron is $O(\sqrt{\tau_s/\tau_m})$, and for the quadratic integrate and fire is of order $O(\tau_s/\tau_m)$, which makes a qualitative difference between the two models. This difference is linked with the boundary conditions chosen by Brunel and Latham [37] who do not consider a finite spiking threshold (the neuron fires if its membrane potential tends to $+\infty$ and is reset at $-\infty$). In the long correlation limit, the correction is in $O(\tau_m/\tau_s)$. By combining these two limit cases, Brunel and Latham [37] derive an approximation of the firing rate over the whole range of values of τ_s/τ_m in the suprathreshold regime, i.e. in the case where the current is sufficient to make the neuron spike in the absence of noise. This expression is not valid in the subthreshold case.

In order to solve the Fokker-Planck equation or its flux version in these cases, we have to fix boundary conditions. These conditions are different in the case when the intrinsic neuronal dynamics is linear or nonlinear. Let us first treat the case of the Model II (or the Model IV case where there exists a finite voltage threshold value for the spike emission). In this case, the boundary conditions are quite complex. Brunel and Latham's derivation in [37] proceeds from biophysical considerations. First of all, the equations for the reset are quite similar as in the white noise case:

$$J_V(\theta,I^{\text{syn}}) = \nu(I^{\text{syn}})$$
$$J_V(V_r^+,I^{\text{syn}}) - J_V(V_r^-,I^{\text{syn}}) = \nu(I^{\text{syn}})$$

where $\nu(I^{\text{syn}})$ is the instantaneous firing rate of the neuron at current I^{syn}. The total firing rate of the neuron is $\int_{\mathbb{R}} \nu(I^{\text{syn}})\,dI^{\text{syn}}$. By definition of the flux and in particular since is cannot be negative at $V=\theta$ for every I^{syn}, we have $P(\theta,I^{\text{syn}})=0$ if $I^{\text{syn}}+F(\theta)<0$, implying in this case that the flux is null for these values of current. On the other hand, $P(\theta,I^{\text{syn}})$ is positive for $I^{\text{syn}}+F(\theta)>0$ when the neuron fires. Eventually, the boundary condition for P read:

$$(I^{\text{syn}} + F(\theta))P(\theta, I^{\text{syn}}) = \nu(I^{\text{syn}})\tau_m$$
$$(I^{\text{syn}} + F(\theta))\left\{P(V_r^+, I^{\text{syn}}) - P(V_r^-, I^{\text{syn}})\right\} = \nu(I^{\text{syn}})\tau_m$$

For the boundary conditions on the current variable I^{syn}, the authors note that the only location where the neuron can escape the phase plane is through $V = \theta$, and hence the flux through I^{syn} must go to zero for large $|I^{\text{syn}}|$. Therefore the boundary conditions on I^{syn} read:

$$\lim_{I^{\text{syn}} \to \pm\infty} J_{I^{\text{syn}}}(V, I^{\text{syn}}) = 0$$

which is implied for instance by:

$$\lim_{I^{\text{syn}} \to \pm\infty} \frac{\partial P}{\partial I^{\text{syn}}} = 0$$
$$\lim_{I^{\text{syn}} \to \pm\infty} I^{\text{syn}} P = 0$$

In the small τ_s/τ_m limit, the two dimensional Fokker-Planck equation can be solved using singular perturbations techniques. In that limit, the variance of I^{syn} becomes proportional to $\sigma\sqrt{\tau_s/\tau_m}$. The parameter $\sqrt{\tau_s/\tau_m}$ is the small parameter in which the Fokker-Planck equation is expanded. To integrate the equations, Fourcaud and Brunel [94] develop very skillful calculations and finally obtain analytical formulations for the correcting terms of the stationary mean firing rate. Up to the first order in $\sqrt{\tau_s/\tau_m}$, the firing rate reads:

$$\nu = \nu_0 - \sqrt{\frac{\tau_s}{\tau_m}} \frac{\alpha}{2\tau_m\sqrt{\pi}} \frac{\psi(\frac{\theta-\mu}{\sigma}) - \psi(\frac{V_r-\mu}{\sigma})}{\left(\int_{\frac{V_r-\mu}{\sigma}}^{\frac{\theta-\mu}{\sigma}} \psi(s)\, ds\right)^2}$$

where $\psi(s) = e^{s^2}(1 + \text{erf}(s))$ and $\alpha = \sqrt{2}|\zeta(1/2)|$ and $\zeta(\cdot)$ is the Riemann zeta function (see e.g. [3]). They observe that up to the first order, the firing rate can be written as:

$$\nu = \left(\tau_m\sqrt{\pi} \int_{\frac{V_r-\mu}{\sigma} + \frac{\alpha}{2}\sqrt{\tau_s}\tau_m}^{\frac{\theta-\mu}{\sigma} + \frac{\alpha}{2}\sqrt{\tau_s}\tau_m} \psi(s)\, ds\right)^{-1}$$

Hence the effect of the synaptic integration can be seen as introducing an effective threshold $\theta + \sigma\frac{\alpha}{2}\sqrt{\tau_s}\tau_m$ and an effective reset potential $V_r + \sigma\frac{\alpha}{2}\sqrt{\tau_s}\tau_m$.

In the nonlinear case, the approach is more elegant. Considering that a spike is emitted when the membrane potential goes to infinity and is reset at $-\infty$. Brunel and Latham [37] develop the same type of calculations as in the previous case, but get rid of the complexity of solving the differential equation with the boundary condition, turning it into limit conditions. We do not present here their calculations since it is only technical calculations typical of singular or nonsingular perturbation theory, and only provide their results for their great interest since they are the only analytical information available for Model IV.

In the long correlation time limit $\tau_s/\tau_m \to 0$, the zeroth order approximation is the one given by ν_0 computed in equation 6.47. The first order correction is null, and the second order corrective coefficient is:

$$\nu_{2s} = \nu_0 \frac{\tau_m \nu_0}{\sigma^2} \int_{\mathbb{R}} dv \int_v^{\infty} \exp(\psi(v) - \psi(u))(h(u) - h(v) - 4F'(u))$$

where $\psi(v) = \int_0^v 2F(u)/\sigma^2\, du$ and h is a solution of $h'(v) = -3F''(v) - 4F'(v)\psi'(v)$.

In the long correlation time limit ($\tau_s/\tau_m \to \infty$), the strategy for solving the Fokker-Planck equations is the same, and the calculations are simpler in this case. The stationary firing rate for the quadratic model reads up to the first order in τ_m/τ_s:

$$\nu = \frac{\sqrt{\mu}}{\pi\tau_m} - \frac{\tau_m}{\tau_s}\frac{\sigma^2}{16\pi\tau_m\mu^{3/2}}$$

These two limits can then be put together to find an approximation of the mean firing rate whatever the ratio τ_s/τ_m. The authors obtained a good agreements with numerical simulations of the solutions of the Fokker-Planck equation.

Noisy synaptic conductances

For Model V, this approach also applies, but the derivation of the stationary transition density is a little bit more complex. In the case of equation (6.23) with constant external current I_e, the Fokker-Planck equation reads:

$$\partial_t p = \frac{\sigma_g^2}{2}\partial_x^2\{(x-V_g)^2 p(x)\} + \lambda\,\partial_x\{(x-V_I)p(x)\}$$

with $V_g = V_{\text{rev}} - \frac{\sigma_I}{\sigma_g}$ and $V_I = V_{\text{rest}} + \frac{I_e}{\lambda}$.

When considering the stationary problem, we end up with the following differential equation to solve, with α a real parameter to be set considering the boundary conditions:

$$\frac{\sigma_g^2}{2}\partial_x\{(x-V_g)^2 p(x)\} + \lambda(x-V_I)p(x) = \alpha$$

which we write in the form:

$$\partial_x F(x) + \frac{2\lambda}{\sigma_g^2}\frac{(x-V_I)}{(x-V_g)^2}F(x) = \alpha$$

where $F(x) = (x-V_g)^2 p(x)$. This equation is well posed for $x < V_g$ and $x > V_g$ but not considering intervals containing V_g. For $x > V_g$ or $x < V_g$ the solution can be written in the form:

$$p = \frac{e^{-h(x)}}{(x-V_g)^2}\left(\alpha\int_{V_r}^{x} e^{h(y)}dy + \beta\right)$$

where h is a primitive of $\frac{2\lambda}{\sigma_g^2}\frac{(x-V_I)}{(x-V_g)^2}$, for instance for $x > V_g$:

$$\frac{2\lambda}{\sigma_g^2}\left\{\log(x-V_g) - \frac{V_g-V_I}{x-V_g}\right\},$$

and for $x < V_g$:

$$\frac{2\lambda}{\sigma_g^2}\left\{-\log(V_g-x) - \frac{V_g-V_I}{x-V_g}\right\}.$$

We consider $V_g < V_I$ and $V_g < V_r$, which is the most plausible case if we consider a null synaptic current, because of the numerical values of the reversal potentials of the main ionic species involved in the spike generation (see chapter 1). We integrate this equation with the boundary conditions in three steps: first for $x < V_g$ (with the constants α_1 and β_1), then for $V_g < x < V_r$ (constants α_2 and β_2) and for $V_r < x < \theta$

(constants α_3 and β_3). We know that the solution is 0 for $x > \theta$. We consider first the case $x < V_r$, and we observed that necessarily $\alpha_3 = 0$ to keep the finite and integrable density at $x = V_r$, and that $\beta_3 = 0$ for the probability to have a finite integral. Therefore, the stationary probability density is identically null for $x < V_g$. For $V_r < x < \theta$, the condition $p(\theta) = 0$ gives the condition on the coefficients $\beta_3 = -\alpha_3 \int_{V_r}^{\theta} \exp(h(y))\, dy$. Hence on this interval the solution reads:

$$p(x) = \alpha_3 \frac{e^{-h(x)}}{(x-V_g)^2} \int_{\theta}^{x} e^{h(y)} dy.$$

The continuity condition for $V = V_r$ gives us β_2 in function of α_3:

$$\beta_2 = \alpha_3 \int_{\theta}^{V_r} e^{h(y)}\, dy$$

and the jump condition for $x = V_r$ corresponds to $\frac{\alpha_3}{(\theta - V_g)^2}$ fixes the coefficient β_2 in function of α_3:

$$\alpha 2 = \alpha_3 \left(1 - \left(\frac{V_r - V_g}{\theta - V_g}\right)^2\right)$$

Therefore we obtain a closed form of the whole solution, scaled linearly by a parameter α_3 which has to be set to comply with the normalization condition, hence that reads:

$$\alpha_3 = \left(\int_{V_g}^{V_r} \frac{e^{-h(x)}}{(x-V_g)^2} \left(\left(1 - \left(\frac{V_r - V_g}{\theta - V_g}\right)^2\right) \int_{V_r}^{x} e^{h(y)}\, dy + \int_{\theta}^{V_r} e^{h(y)}\, dy \right) dx + \int_{V_r}^{\theta} \frac{e^{-h(x)}}{(x-V_g)^2} \int_{\theta}^{x} e^{h(y)}\, dy \right)^{-1}.$$

This coefficient gives us the stationary mean firing rate for this model:

$$\nu = \frac{\alpha_3}{(\theta - V_g)^2}$$

6.3.6 Girsanov's method

Closed-form formulas can be obtained for simple processes and some classes of boundaries, as we have seen in section 6.3.4. For instance, the first hitting time of the Brownian motion to affine boundaries has a closed-form expression. It is known that piecewise affine functions are dense in the set of continuous functions. The principle of what we call Girsanov's method is to build upon this property an approximation of the law of the first hitting time of more complex processes to general boundaries.

This technique was developed for the Brownian motion by Wang and Potzelberger in the late 90's, and then extended by Borovkov and colleagues[27, 210, 217, 278]. It was recently extendend to general one-dimensional diffusion processes [277] such as the Ornstein-Uhlenbeck processes (LIF neuron) or the nonlinear integrate-and-fire neurons.

The principle of the method is illustrated in figure 6.5. It consists first in generalizing the formula obtained for the affine boundary for the Brownian motion to piecewise affine boundaries. This step is rather simple and is performed using the Markov property of the Brownian motion. More precisely, let $a(t)$ be a continuous piecewise linear boundary, with possible breaks on the points of the partition

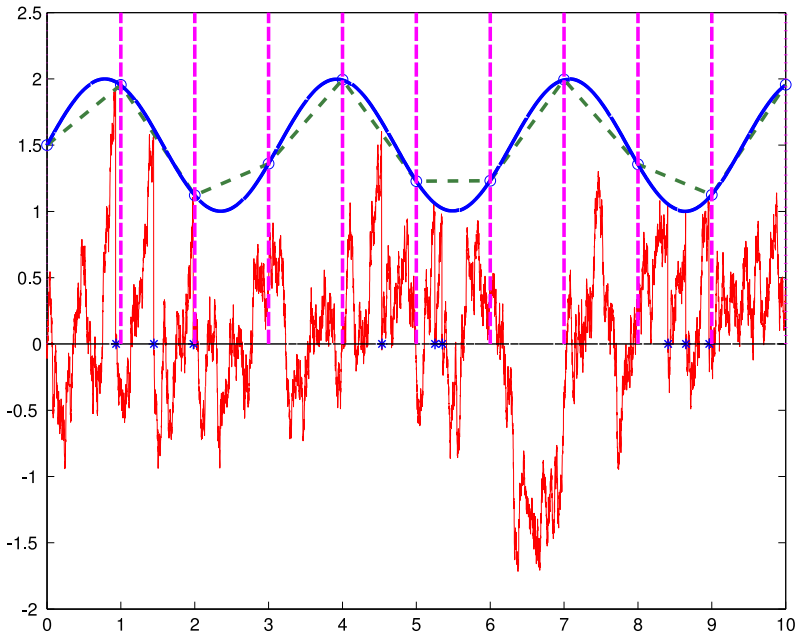

Figure 6.5: The principle of Girsanov's approximation method for the Ornstein-Uhlenbeck process: a change of time is performed to change the Gauss Markov process into a Brownian motion and the resulting boundary is approximated by a piecewise affine function.

$0 = t_0 < t_1 < \ldots < t_n \overset{\text{def}}{=} t$ (i.e. a is affine on the intervals $[t_j, t_{j+1}]$ for $j = 0 \ldots n-1$), and τ_a be the first hitting time of the Brownian motion to the boundary a, then

$$\mathbb{P}(\tau_a \leq t) = 1 - \mathbb{E}(g(W(t_1), \ldots, W(t_n), a))$$

where

$$g(x1, \ldots, x_n, a) = \prod_{j=1}^{n} \mathbb{1}_{x_j < a_j} \left(\exp\left[-\frac{2(a_{j-1} - x_{j-1})(a_j - x_j)}{t_j - t_{j-1}} \right] \right),$$

where $a_j = a(t_j)$. This equation can be easily interpreted: the probability that the Brownian motion has not crossed the affine boundary prior to time t is equal to the probability that it did not cross the boundary between time t and t_{n-1} conditionally to the fact that it did not cross the boundary prior to t_{n-1} times the probability that the process did not cross the boundary prior to time t_{n-1}. Markov's property for the Brownian motion yields the formula.

Using this formula, the approximation principle of the first hitting time of the Brownian motion to curved boundaries consists in defining a partition of a time interval $[0, T]$. On this partition, the crossing probability of the Brownian motion with the general boundary is approximated by the one of the Brownian motion with an affine approximation of the boundary on this partition, formula which is given by the first step. When the boundary is regular enough (continuously differentiable with a Lipschitz derivative), then this approximation is proved to converge.

The speed of convergence was widely studied and the first explicit bound of the approximation was provided by Borovkov and Novikov [27] eight years after the description of this algorithm. Under some regularity conditions on the boundary, the approximation is proved to converge in $O(\varepsilon)$ where ε is the step of the partition.

This technique was finally complemented in 2007 for general diffusion processes with piecewise continuous boundaries [277]. This applies for instance for the Ornstein-Ulhenbeck process, providing an alternative solution to the ones proposed previously. Hence one of the main advantage of this technique is to provide a closed-form solution for the approximation of the hitting time we search together with a rate of convergence. Furthermore, whereas all other methods fail to extend to Model III, this method can be extended to these models, as we show in chapter 7.

One of the main drawbacks of this technique is that it involves the computation on an expectation over $\mathbb{R}^n$ where n is the number of points in the partition. Increasing the precision of the approximation means increasing this n. The expectation involved in the formula can be computed as an integral on $\mathbb{R}^n$ weighted by the multidimensional probability of the Brownian motion at the times of the partition. To compute this integral, we could use Gaussian integration algorithms (see e.g. [245]). Nevertheless, the most efficient method when n increases is to use a Monte-Carlo algorithm to compute the expectation. This method consists in approximating the expectation by an empirical expectation. More precisely, let $(t_1,\dots,t_n)$ be a partition of $[0,t]$. The method consists in drawing N samples $(x_1^k,\dots,x_n^k)_{k=1\dots N}$ by drawing in the law of the process $(W_{t_1},\dots,W_{t_n})$ and computing $1-\frac{1}{N}\sum k=1^N g(x_1^k,\dots,x_n^k,a)$. The standard error given by this estimator can be deduced by the work of Niederreiter [206] and is given by

$$\sqrt{\frac{\sum_{k=1}^N g(x_1^k,\dots,x_n^k,a)-\frac{1}{N}\sum_{k=1}^N g(x_1^k,\dots,x_n^k,a)}{N(N-1)}}$$

This method can apply to Models I, III and V with instantaneous synaptic currents or conductances since they are all solutions of diffusion equations.

We extend this method in chapter 7 to the cases of exponentially decaying synaptic currents, developping a new semi-analytical technique to characterize the pdf of the first hitting time of this type of processes with integrated noise, which we will call Double Integral Processes.

6.3.7 Monte-Carlo Simulation method

Description of the algorithm

The Monte-Carlo simulation method is a widely used method in many fields of applications. It is a numerical algorithm based on repeated computation of random or pseudo-random numbers. Since it is model-free, it can be used even when no analytical or exact mathematical result are available.

To approximate of the pdf of the first hitting time of a given stochastic process to a general boundary, Monte-Carlo method consists in simulating a large number N of independent time-discretized paths of the process. In details, let us denote by V_t the process under consideration and $\overline{V}_t$ its time discretization, by $a(\cdot)$ the boundary and by τ_a the first hitting time of the process V_t to this boundary. The simulation of the path stops at a time $\overline{\tau}_a$ supposedly approximating τ_a. For each path $\overline{V}$, up to time $\overline{\tau}_a$, the discrete time stochastic process $\overline{V}$ is numerically simulated for instance using an Euler scheme.

At each time step, either the simulation stops if the process is considered to have crossed the threshold, or proceeds:

- if $\overline{V}_{(k+1)\delta} \geq a((k+1)\,\delta)$ then $\overline{\tau}_a = (k+1)\delta$ and the simulation of the path is stopped.

- if $\bar{V}_{(k+1)\delta} < a((k+1)\delta)$, the simplest algorithm would continue the simulation of the path. Nevertheless, the approximation of τ_a we get using this technique is of very poor accuracy. It has been proved [108] that this approximation is of order $\sqrt{\delta}$.

To improve the accuracy of the algorithm, an interesting idea (see [108]) is to compute the probability that the continuous time process conditioned on taking the value $\bar{V}_{k\delta}$ at time $k\delta$ and $\bar{V}_{(k+1)\delta}$ at time $(k+1)\delta$ hits the constant boundary $a(\cdot)$ for $t \in (k\delta,(k+1)\delta)$. When δ is small enough and the function a smooth enough, the boundary can be considered as constant equal to $a(k\delta)$, and the process V_t as a Brownian motion. Therefore the probability to compute is approximated by the probability $p(\delta,\bar{V}_{k\delta},\bar{V}_{(k+1)\delta})$ of a Brownian bridge with intensity δ (i.e. a Brownian motion conditioned to take the value $\bar{V}_{k\delta}$ at time 0 and $\bar{V}_{(k+1)\delta}$ at time δ) to hit the constant $a(k\delta)$. This probability is easy to compute and its value is:

$$p(\delta,x,y) = \exp\left(-2\frac{(a-x)(a-y)}{\sigma^2\delta}\right).$$

In this case we thus consider that the probability to cross the frontier between times $k\delta$ and $(k+1)\delta$ is equal to this value. To simulate our hitting time, we can for instance simulate a Bernoulli random variable of parameter $p(\delta,\bar{V}_{k\delta},\bar{V}_{(k+1)\delta})$:

- If this random variable is equal to 1 then we set $\bar{\tau}_a = (k+1)\delta$ and we stop the simulation.
- If this random variable is equal to 0 then the simulation proceeds.

This new simulation algorithm has a first order accuracy (see for instance the works of Gobet [108]). Nevertheless, the rate of convergence of $\bar{\tau}_a$ towards τ_a is still an open problem. This problem amounts to characterizing the convergence of such quantities as $\mathbb{P}(\bar{\tau}_a \leq t)$ towards $\mathbb{P}(\tau_a \leq t)$, even for simple models such as Model I.

Lastly, these simulations necessitate a huge number of simulated sample path in order to get a good accuracy. Therefore, these algorithms are very time consuming, but they offer the advantage to be applicable for any model and any boundary provided some loose conditions are satisfied. Another advantage is that these algorithms are highly parallelizable. This means that provided that one can generate in parallel independent sets of random (or pseudo-random) numbers, each trajectory can be computed independently. This is why we implemented for our applications for general models a parallel Monte-Carlo algorithm on GPU (see chapter 8).

Numerical results

For model I, Volterra, Durbin, Girsanov and Monte-Carlo simulation apply. When the input current is deterministic, the membrane potential is the realization of an Ornstein-Uhlenbeck process, and the moments can be expressed using the analytical expressions of theorem 6.3.3. A comparison of the theoretical value with the numerical simulation is provided in table 6.2.

All the methods presented are known to converge to the real pdf, hence if the simulation is accurate enough, all the methods can have an arbitrary precision. Nevertheless, the simulation parameters were chosen according the computation time required by the numerical method. As expected, in this simulation, Volterra's method is the most accurate, and computationally the most efficient for the simulations we

method	$\mathbb{E}\left[T\right]$	$\mathbb{E}\left[T^2\right]$	$\mathbb{E}\left[T^3\right]$
theoretical values	1.9319289	7.1356162	40.0830265
Durbin, 30 terms, $T_{max} = 10^{36}$, step = 10^{-2}	1.9292822	7.1269290	39.8541918
Monte-Carlo, 10^6 realizations, step = 10^{-2}	1.876826	6.413294	31.013929
Volterra, step = 0.02	1.9319291	7.1356167	40.0830298

Table 6.2: Values of the first 3 moments of the OU process and the empirical values, for the parameters: $\theta = \sigma = 2$, $V_{\text{rest}} = \tau_m = 1$, $I_e = 0$, see equation (6.2). The theoretical values are obtained using the formulas of theorem 6.3.3 by truncating the series Φ_i up to a high order.

performed. The parameters in Volterra's method have been chosen to get a good accuracy, but still the computation time is under half a second. Monte-Carlo simulations have been done using the enhanced algorithm presented. Though having a quite good convergence rate, it appears to be very sharp even for a huge number of trials (it is known to converge as $1/\sqrt{N}$ where N is the number of trials), as we can see in the values of the expectation, and very computationally inefficient (the simulation took 1h47m for a very low precision, while Volterra's method takes 0.02s for a high precision, on a Intel Core2 CPU 6700 @ 2.66GHz)

In Figure 6.6 we compare three of the methods available to compute the spike statistics of Model I driven by periodic inputs: Durbin's method, Volterra's method and a Monte-Carlo simulation. Durbin's and Volterra's results are indistinguishable. The simulation times are very high for both Monte-Carlo and Durbin's methods (around a minute for both, the Monte-Carlo simulation runs 10^6 sample paths and Durbin's method 800 sample points and 9 terms of the series). Volterra's method is very efficient and for 10^4 sample points, lasts less than $0.02s$. We also see from the enlargement in the figure that the Monte-Carlo simulation does not have the expected regularity even at this level of precision.

CONCLUSION

In this chapter we studied different types of integrate-and-fire neuron models from the point of view of the stochastic calculus. We showed that characterizing the spikes times of a neuron was equivalent to solving a first hitting time problem for a stochastic process to a given continuous curve. We then presented different methods which can be applied in order to solve such problems. One of them, the Feynman-Kac method, is very restrictive, since it can only be applied to stationary boundaries (this is also the case of the Fokker-Planck equation formalism). A classical method, Durbin's method, was extended, and proved to be equivalent to Volterra's method. We also presented the recent Girsanov's method upon which the next chapter builds up in order to compute the distribution of the spikes times for the LIF neuron with exponentially decaying synaptic conductances. In this case, the only available and partial result is Brunel's who computed the stationary firing rate of this neuron model [38].

Nevertheless for the nonlinear models of types III and IV the stochastic calcu-

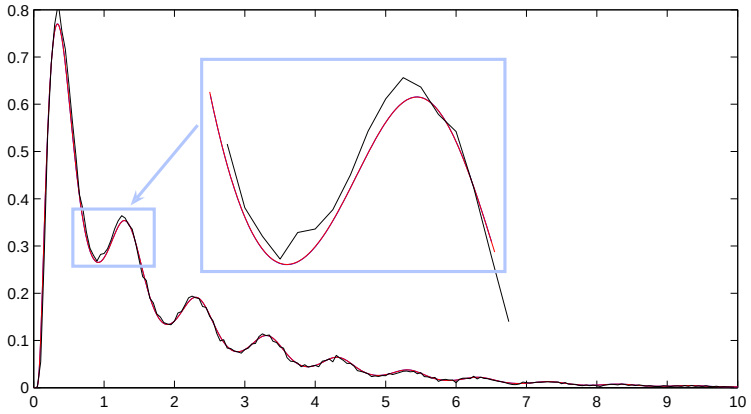

Figure 6.6: Graphical comparison with Monte-Carlo simulation and Durbin's simulations

lus methods still fail to provide the complete statistical information about the spikes and one has to resort to the Fokker-Planck approximate formalism. Studying more complex and biologically plausible mechanisms such as STDP in this framework is another interesting perspective of the present study. This work was presented at the NeuroComp conference in Pont-à-Mousson [86], at the first computational neuroscience day in Gif-sur-Yvette, and at the Probability and Biology Seminar of Paris VI University. It is published as a review paper in the Journal of Physiology, Paris [260].

Chapter 7

First hitting times of Double Integral Processes to curved boundaries

Az men ken nit iberhar'n dos shlechteh,
ken men dos guteh nit derleben.
– Yiddish proverb

ABSTRACT

In the previous chapter we presented the relationship between the problem of characterizing the statistics of spikes for integrate-and-fire neuron models and the problem of first hitting times of stochastic processes. We showed that stochastic calculus methods can be successfully applied to derive the probability distribution of the interspike interval. We nevertheless observed that no method applied to the case of exponentially decaying synaptic currents. This problem is linked with the fact that the membrane potential process involves a non-Markovian process which we called a Double Integral Process. In this section we generalize this problem to a wider class of stochastic processes and provide a way to approximate the law of this hitting time. More generally, the problem of finding the probability distribution of the first hitting time of Double Integral Processes (DIPs) such as the Integrated Wiener Process (IWP) has been an important and difficult endeavor in stochastic calculus. It has applications in many fields of physics (first exit time of a particle in a noisy force field) or in biology and neuroscience (spike time distribution of an integrate-and-fire neuron with exponentially decaying synaptic current). The only results available are Brunel's *et al* approximation of the stationary mean crossing time and the distribution of the first hitting time of the IWP to a constant boundary. We generalize these results and find an analytical formula for the first hitting time of the IWP to a continuous piecewise cubic boundary. We use this formula to approximate the law of the first hitting time of a general DIP to a smooth curved boundary, and we provide an estimation of the convergence of this method. The accuracy of the approximation is computed in the general case for the IWP and the effective calculation of the crossing probability can be carried out through a Monte-Carlo method. These results are the fruit of a collaboration with Olivier Faugeras, and they are published in Advances in Applied Probablity [262].

Contents

7.1 Introduction

First passage time problems for one-dimensional diffusion processes through a time-dependent boundary have received a lot of attention over the last three decades. Unfortunately, the evaluation of the first passage time probability distribution function (pdf) through a constant or time dependent boundary is in general an arduous task which has still not received a satisfactory solution. Analytical results are scarce and fragmentary, even if closed form solutions exist for some very particular cases. Since no analytical method seem to solve the problem, one is led either to the study of the asymptotic behavior of this function and of its moments (see e.g. [207, 208]), or to the use of somewhat *ad-hoc* numerical procedures yielding approximate evaluations of the first passage time distributions. Such procedures can be classified as follows: (i) those that are based on probabilistic approaches (see e.g. [42, 73, 76, 77, 90, 152, 153, 179, 211, 212, 223, 224, 238]), and (ii) purely numerical methods, such as the widely used Monte-Carlo method which applies without any restriction, but whose results are generally too coarse (for numerical methods, see e.g. [11, 88, 107, 162]).

In two and higher dimensions, the problem is even more complex and results can hardly be found. For the simplest Double Integral Process (DIP), the Integrated Wiener Process (IWP) defined in (7.10), McKean [197] Goldman [110], Lachal [168, 169, 170] found the probability distribution of the first hitting time to a constant boundary using stochastic calculus methods. Lefebvre used the Kolmogorov (Fokker-Planck) equation to find in some special cases closed-form solutions [178]. Generalizations of these formulas to other boundaries and other kinds of processes are simply not available. In the present chapter, we propose a closed-form solution for the first hitting time of the IWP to a piecewise cubic function, and apply this formula to find an approximation of the first hitting time of a DIP to any smooth curved boundary. We also provide an estimation of the rate of convergence of this approximation.

In the first section, we introduce a motivation of this study, define the Double Integral Process and prove the main properties which will be useful for us in the rest of the chapter. In the second section, we study the first hitting times of the IWP and provide a closed-form formula for the first hitting time of this process to a piecewise cubic function. In the third section, we introduce the approximation method of the first hitting time of the IWP to any smooth curved boundary, and find the rate of convergence of this method. Finally in the last section we provide an approximation formula for the first hitting time of a general DIP to a curved boundary. The fifth section describes briefly a numerical Monte-Carlo algorithm which can be used to compute the probability repartition function efficiently.

7.2 The Double Integral Process

In this section we introduce the Double Integral Process (DIP) and prove some useful properties. But before the mathematical study of the problem, we motivate this theoretical work by a specific problem arising in neuroscience: the distribution of the spike times for an integrate-and-fire neuron with exponentially decaying synaptic currents.

7.2.1 Motivation

The definition of the DIP and the study of its first hitting times of curved boundaries has been motivated by numerous physical and biological problems. For instance a problem arising in neuroscience is to characterize the probability distribution of the spike (action potentials) times in presence of synaptic noise (see [105] for an introduction of the neuronal modelization of spiking neurons and [261] for review of the problem of spike time distribution).

A classical neuron model (Models I and II of chapter 6) is the leaky integrate-and-fire model, where the membrane potential $V(t)$ of a neural cell integrates external inputs and the noise at the synapses, and emits a spike when the membrane potential reaches a deterministic threshold function $\theta(t)$ (which is constant in general). We recall here for the sake of completeness some of the main features of this model in order to make clear the motivations of the further developments. There is a clear overlap with section 6.2.2, but we believe that fixing notations and recalling the problem makes this chapter more clear.

In this model, the membrane potential is solution of the equation:

$$\tau_m dV(t) = \big(-(V(t) - V_{\text{rest}}) + I_e(t) \big)\, dt + dI_s(t) \tag{7.1}$$

In this equation τ_m is the characteristic time of integration of the membrane potential, V_{rest} is the rest potential of the neuron, I_e represents deterministic external inputs and I_s the noisy synaptic inputs (see for instance [86, 105, 261]). The simplest model of synaptic noise is a standard Brownian motion, if we neglect the integration time of the synapse. Nevertheless, real post-synaptic currents have a very short rise time and a larger decay time.

If we take into account the decay time of the synapse τ_s, then the synaptic current is solution of the stochastic differential equation:

$$\tau_s dI_s(t) = -I_s(t)dt + \sigma dW_t$$

We can integrate this system of stochastic differential equations as follows. The equation governing the membrane potential yields

$$V(t) = V_{\text{rest}}(1 - e^{-\frac{t}{\tau_m}}) + \tfrac{1}{\tau_m}\textstyle\int_0^t e^{\frac{s-t}{\tau_m}} I_e(s)\, ds + \tfrac{1}{\tau_m}\int_0^t e^{\frac{s-t}{\tau_m}} I_s(s)\, ds,$$

and the synaptic current equation can be integrated as

$$I_s(t) = I_s(0)e^{-\frac{t}{\tau_s}} + \frac{\sigma}{\tau_s}\int_0^t e^{\frac{s-t}{\tau_s}} dW_s,$$

where $I_s(0)$ is a given random variable. We define $\frac{1}{\alpha} = \frac{1}{\tau_m} - \frac{1}{\tau_s}$. Replacing in the first equation $I_s(t)$ by its value in the second equation we obtain

$$V(t) = V_{\text{rest}}(1 - e^{-\frac{t}{\tau_m}}) + \tfrac{1}{\tau_m}\textstyle\int_0^t e^{\frac{s-t}{\tau_m}} I_e(s)\, ds + \\ \frac{I_s(0)}{1 - \frac{\tau_m}{\tau_s}}(e^{-\frac{t}{\tau_s}} - e^{-\frac{t}{\tau_m}}) + \frac{\sigma}{\tau_m \tau_s} e^{-\frac{t}{\tau_m}} \int_0^t e^{\frac{s}{\alpha}} \left(\int_0^s e^{\frac{s'}{\tau_s}} dW_{s'} \right) ds$$

The time of the spike emission is the first hitting time of $V(t)$ to the threshold $\theta(t)$, so the first hitting time of the stochastic process, which is a particular case of what we will call in the sequel Double Integral Process (DIP)

$$X_t = \int_0^t e^{\frac{s}{\alpha}} \left(\int_0^s e^{\frac{s'}{\tau_s}} dW_{s'} \right) ds \tag{7.2}$$

to the deterministic curved boundary

$$a(t) = \theta(t) - \left(V_{\text{rest}} \left(1 - e^{-\frac{t}{\tau_m}} \right) + \frac{1}{\tau_m} \int_0^t e^{\frac{s-t}{\tau_m}} I_e(s)\, ds + \frac{I_s(0)}{1-\frac{\tau_m}{\tau_s}} \left(e^{-\frac{t}{\tau_s}} - e^{-\frac{t}{\tau_m}} \right) \right).$$

7.2.2 Definition and main properties of DIPs

In this section, we define a class of stochastic processes including the process (7.2), and prove some useful properties of these processes.

Definition 7.2.1 (DIP)**.** Let $f \in \mathbb{L}^2(\mathbb{R})$ and $g \in \mathbb{L}^1(\mathbb{R})$. Let M_t be the martingale defined by $M_t := \int_0^t f(s) dW_s$.

The *double integral process (DIP)* associated to the functions f and g is defined for all t by:

$$X_t = \int_0^t g(s) M_s ds = \int_0^t g(s) \left(\int_0^s f(u) dW_u \right) ds \tag{7.3}$$

Proposition 7.2.1. The two-dimensional process (X_t, M_t) is a Gaussian Markov process.

Proof. First of all, note that if $\mathscr{F}_t^X$ (resp. $\mathscr{F}_t^M$) defines the canonical filtration associated to the process X (resp. M) then it is clear that $\forall t \geq 0$, $\mathscr{F}_t^X \subset \mathscr{F}_t^M$. Hence the filtration associated to the pair $(X_t, M_t)_{t \geq 0}$ is simply $(\mathscr{F}_t^M)_{t \geq 0}$, which we denote in the sequel $(\mathscr{F}_t)_{t \geq 0}$

It is also clear that M is a martingale, and satisfies the Markov property. Let $s \leq t$. We have:

$$\begin{aligned} X_t &= \int_0^t g(u) M_u du \\ &= \int_0^s g(u) M_u du + \int_s^t g(u) M_u du \end{aligned}$$

$$X_t = X_s + \int_s^t g(u)(M_u - M_s) du + M_s \int_s^t g(u) du \tag{7.4}$$

Conditionally to M_s, the process $\int_s^t g(u)(M_u - M_s) du$ is independent of $\mathscr{F}_s^M$ so the law of X_t knowing (X_s, M_s) is independent of the sigma-algebra $(\mathscr{F}_t)$, and so is M, so eventually the pair (X, M) is Markov.

The pair is clearly a Gaussian process since its two components are. Indeed, M is Gaussian as the limit of the Riemann sums of Brownian increments, which are Gaussian, and X is also the limit of Riemann sums of a Gaussian process, namely M, with the weights given by g.

□

Remark 11. In the proof of proposition 7.2.1, we proved also that conditionally to M_s, the increments $(X_t - X_s, M_t - M_s)$ are independent of the σ-field $\mathscr{F}_s$.

Proposition 7.2.2. For each value of $t \geq 0$, the random variable $Y_t := (X_t, M_t)$ is a two-dimensional Gaussian variable of parameters:

$$\begin{cases} \mathbb{E}[Y_t] & = (0,0) \\ \mathbb{E}\left[Y_t^T \cdot Y_t\right] & = \begin{pmatrix} \rho_X(0,t) & C_{(X,M)}(0,t) \\ C_{(X,M)}(0,t) & \rho_M(0,t) \end{pmatrix} \end{cases} \tag{7.5}$$

where the functions $\rho_X(s,t)$, $C_{(X,M)}(s,t)$ and $\rho_M(s,t)$ are defined by:

$$\begin{cases} \rho_M(s,t) & = \int_s^t f(u)^2 du \\ \rho_X(s,t) & = 2\int_s^t g(u)\left(\int_s^u g(v)\rho_M(s,v)dv\right)du \\ C_{(X,M)}(s,t) & = \int_s^t g(u)\rho_M(s,u)du \end{cases} \tag{7.6}$$

The transition measure of the Markov process $(Y_t)_t$ has a Gaussian density w.r.t. Lebesgue's measure:

$$\mathscr{N}\left(\begin{pmatrix} x_s + m_s\int_s^t g(u)du \\ m_s \end{pmatrix}, \tilde{C}(s,t)\right) \tag{7.7}$$

where the correlation matrix $\tilde{C}(s,t)$ reads:

$$\tilde{C}(s,t) = \begin{pmatrix} \rho_X(s,t) & C_{(X,M)}(s,t) \\ C_{(X,M)}(s,t) & \rho_M(s,t)du \end{pmatrix} \tag{7.8}$$

Proof. The calculations are essentially straightforward. To compute the transition density function, we use the equation (7.4) and write:

$$\begin{pmatrix} X_t \\ M_t \end{pmatrix} = \begin{pmatrix} X_s + M_s\int_s^t g(u)du \\ M_s \end{pmatrix} + \begin{pmatrix} \int_s^t g(u)(M_u - M_s)du \\ M_t - M_s \end{pmatrix} \tag{7.9}$$

The first term in the sum in the righthand side of (7.9) is $\mathscr{F}_s$ measurable. Given $X_s = x_s$ and $M_s = m_s$, it is equal to

$$\begin{pmatrix} x_s + m_s\int_s^t g(u)du \\ m_s \end{pmatrix}$$

The second term is independent of $\mathscr{F}_s$ and is Gaussian.

Eventually, the process Y_t knowing $Y_s = (x_s, m_s)$ has the same law as the Gaussian process:

$$\mathscr{N}\left(\begin{pmatrix} x_s + m_s\int_s^t g(u)du \\ m_s \end{pmatrix}, \tilde{C}(s,t)\right)$$

□

Definition 7.2.2 (IWP)**.** The *Integrated Wiener Process* is a special case of the DIP where the functions f and g are identically equal to 1 :

$$X_t = \int_0^t W_s\, ds \quad M_s = W_s \tag{7.10}$$

From proposition 7.2.2, we know that its transition measure reads:

$$\mathbb{P}\Big[X_{t+s}\in du, W_{t+s}\in dv \Big| X_s = x, W_s = y\Big] \overset{\text{def}}{=} p_t(uv;x,y)du\,dv =$$
$$\frac{\sqrt{3}}{\pi t^2}\exp\Big[-\frac{6}{t^3}(u-x-ty)^2+\frac{6}{t^2}(u-x-ty)(v-y)-\frac{2}{t}(v-y)^2\Big]du\,dv \quad (7.11)$$

Lemma 7.2.3. Let $(X_t)_{t\geq 0}$ be a DIP defined by (7.3). Assume that $f(s)\neq 0$ for all $s\geq 0$. The study of the hitting times of the DIP X is equivalent to the study of the simpler process:

$$\tilde{X}_t = \int_0^t \tilde{g}(s)W_s ds,$$

where $\tilde{g}$ is defined in the proof.

Proof. Let $(M_t)_t$ be the martingale defined by:

$$M_t = \int_0^t f(s)dW_s$$

Dubins-Schwarz' theorem[1] ensures us that there exists a Brownian motion $(W_t)_t$ such that almost surely

$$M_t = W_{\langle M\rangle_t}$$

We note

$$\Phi(t) = \langle M\rangle_t = \int_0^t f^2(s)ds$$

Φ is continuous and since we assumed that $f(s)\neq 0$ for all $s\geq 0$, strictly increasing, so it is a bijection. Its derivative $\Phi'(t)$ exists and is nonzero for all $t\geq 0$. We use the change of variable $u=\Phi(s)$. We have:

$$\begin{aligned} X_t &= \int_0^t g(s)M_s\,ds \\ &\overset{\mathscr{L}}{=} \int_0^t g(s)W_{\Phi(s)}ds \\ &= \int_0^{\Phi^{-1}(t)} \frac{g(\Phi^{-1}(u))}{\Phi'\big(\Phi^{-1}(u)\big)}W_u\,du \end{aligned}$$

Hence the hitting time of a general DIP can be deduced from the hitting time of the process $\tilde{X}_t = X_{\Phi(t)}$ which is of type $\int_0^t \tilde{g}(s)W_s ds$, where $\tilde{g}(t)=\frac{g(\Phi^{-1}(t))}{\Phi'(\Phi^{-1}(t))}$ □

7.3 First hitting time of the integrated Wiener process

We consider the special case $(W_t)_{t\geq 0}$, a standard Brownian motion. We are interested in the first hitting time to a curved boundary $a(t)$ of the stochastic process:

$$X_t = \int_0^t W_s ds \quad (7.12)$$

[1] Even though $\langle M\rangle_\infty \neq \infty$ because of our hypothesis on f, see [160].

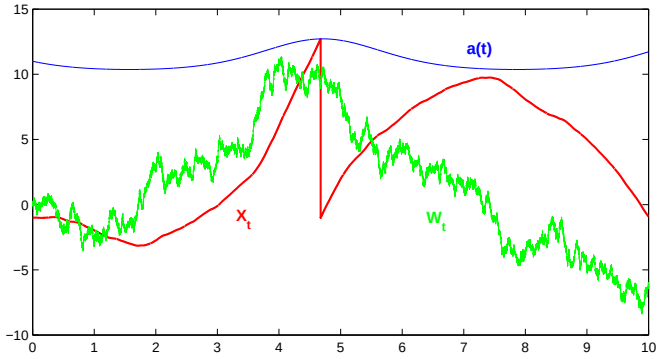

Figure 7.1: A sample path of the process $U_t = (X_t, W_t)$ where X is a standard IWP and W a standard Brownian motion, and a boundary curve $a(t)$. The IWP X_t is reset to 0 when it crosses the boundary.

This problem has been widely studied and has received no satisfactory solution so far. One of the main difficulties comes from the fact that the process is non Markov, so we have to refer to the underlying Wiener process. Classical approaches based on Volterra equations or Durbin's method, work for the Brownian motion, but fail in providing a solution to this problem (see for instance [261] for a review). To achieve the program of characterizing those hitting times, we first recall existing results on the first hitting times to constant boundaries, generalize them to cubic and piecewise cubic boundaries, to end with the approximation formula for general boundaries.

7.3.1 First hitting time to a constant boundary

Lachal in [169] studies this problem in the case where the boundary is a constant. More precisely, in this section we study the process $U_t = (X_t + x + ty, W_t + y)$ where X_t is the standard IWP. We denote by

$$\tau_a = \inf\left\{t > 0\ ;\ X_t + x + ty = a\right\}$$

the first passage time at a of the first component of the bidimensional Markov process U_t. The work of Lachal [169] follows the work of McKean [197], where the joint law of the process (τ_a, W_{τ_a}) is computed in the case $x = a$. The result is:

$$\begin{aligned}\mathbb{P}\left[\tau_a \in dt\ ;\ |W_{\tau_a}| \in dz \middle| U_0 = (a,y)\right] &\overset{\text{def}}{=} \mathbb{P}_{(a,y)}(\tau_a \in dt;\ |W_{\tau_a}| \in dz) \\ &= \frac{3z}{\pi\sqrt{2}t^2} e^{-(2/t)(y^2 - |y|z + z^2)} \left(\int_0^{4|y|z/t} e^{-3\theta/2} \frac{d\theta}{\sqrt{\pi\theta}}\right) \mathbb{1}_{[0,+\infty)}(z) dz dt \quad (7.13)\end{aligned}$$

We denote this density by $m^a(t,y,z)$.

Later, Goldman in [110] computed the distribution of the random variable τ_a in the case where $x < a$ and $y \leq 0$ and obtained the formula:

$$\mathbb{P}\Big[\tau_a \in dt \big| U_0 = (x,y)\Big] = dt\Big[\sqrt{\frac{3}{8\pi t^3}}\big(\frac{3(a-x)}{t} - y\big)e^{-3(a-x-ty)^2/(2t^3)} + \int_0^{+\infty} z dz \int_0^t \int_0^{\infty} \mathbb{P}\Big[\tau_0 \in ds\ ;\ |W_{\tau_0}| \in d\mu \big| U_0 = (0,z)\Big] q_{t-s}(x,y;a,z)\Big] \quad (7.14)$$

where $q_t(x,y;u,v) = p_t(x,y;u,v) - p_t(x,y;u,-v)$.

Lastly, Lachal in [169] extended all these results and gave the joint distribution of the pair (τ_a, W_{τ_a}) in all cases. The quite complex formula reads:

$$\mathbb{P}_{(x,y)}\left[\tau_a \in dt\ ;\ W_{\tau_a} \in dz\right] = |z|\Big[p_t(x,y;a,z) - \int_0^t \int_0^{+\infty} m^0(s,-|z|,\mu) p_{t-s}(x,y;a,-\varepsilon\mu)\, d\mu\, ds\Big] \mathbb{1}_A(z) dz dt \quad (7.15)$$

where $A = [0,\infty)$ if $x < a$, $A = (-\infty, 0]$ if $x > a$, $\varepsilon = \text{sign}(a-x)$ and $m^0(s,-|z|,\mu)$ is given by McKean's formula (7.13). We denote this density by $l^a_{x,y}(t,z)$.

7.3.2 First Hitting time to a cubic boundary

The problem we address now is the question of finding similar formulae for more general boundaries. For the Brownian motion itself, few results are available. A formula has been found for a linear boundary using Girsanov's theorem, for a quadratic boundary using the Laplace transform characterization (see [116]). Lastly, the method of images has been shown to provide closed form results in very particular cases (see [213] for a review). The difficulty for finding closed-form characterizations of the first hitting time of the Brownian motion incited people to look for approximations. Monte-Carlo simulation is often used. Even if it can be used with no restriction, it is often considered too coarse and computationally inefficient. Furthermore, it is purely numerical and global, and does not provide any analytical information on the hitting time. For these reason, other semi-analytical methods of approximation have been developed to provide analytical approximations [63, 76, 77, 217, 277], sometimes together with error estimations [27, 210].

The problem is even more complex for the first hitting time of the integrated Wiener process.

In this section we apply Girsanov's theorem to transform the problem of finding a closed-form expression of the first hitting time of the IWP to a cubic function to the problem discussed in the previous section that has been solved by McKean, Goldman and Lachal [110, 169, 197]. More precisely, we prove that under a certain probability, the process $W_t + \frac{\beta}{2}t^2 + \alpha t + x$ is a Wiener process. Under this probability, the process $X_t + \frac{\beta}{6}t^3 + \frac{\alpha}{2}t^2 + tx + y$ has the law of an IWP. Hence the knowledge of the probability density function (pdf) of the first hitting time of the IWP to a constant will give us, using Girsanov's theorem, the pdf of the hitting time of the IWP to the cubic

$$t \mapsto \frac{\beta}{6}t^3 + \frac{\alpha}{2}t^2 + bt + a.$$

For the sake of generality we compute the new probability starting at a general time s at the point (x,y). The index $\{s,(x,y)\}$ denotes in the following the conditioning on the event $(X_s = x, W_s = y)$.

Theorem 7.3.1. *The process $W_t + \alpha(t-s) + \frac{\beta}{2}(t-s)^2 + y$, $0 \le s \le t$ is a Wiener process starting at y at time s, under the probability:*

$$\mathbb{P}^{\alpha,\beta}_{s,(x,y)}\Big|_{\mathscr{F}_{s,t}} = D^{\alpha,\beta}_{s,(x,y)}(t)\,\mathbb{P}_{s,(x,y)}\Big|_{\mathscr{F}_{s,t}} \tag{7.16}$$

where:

$$D^{\alpha,\beta}_{s,(x,y)}(t) = \exp\Big(-\frac{1}{6}\beta^2(t^3-s^3) - \frac{1}{2}\alpha\beta(t^2-s^2) - \frac{1}{2}\alpha^2(t-s) \\ -(\alpha+t\beta)W_t + (\alpha+s\beta)y + \beta(X_t - x)\Big) \tag{7.17}$$

Proof. We consider the full process $U^{\alpha,\beta}_t = (X^{\alpha,\beta}_t, W^{\alpha,\beta}_t) = (X_t + x + yt + \frac{\alpha}{2}(t-s)^2 + \frac{\beta}{6}(t-s)^3, W_t + y + \alpha(t-s) + \frac{\beta}{2}(t-s)^2) = (X^{\alpha,\beta}_t, W^{\alpha,\beta}_t)$. This is a diffusion process satisfying the two-dimensional stochastic differential equation:

$$\begin{cases} dX^{\alpha,\beta}_t &= W^{\alpha,\beta}_t\,dt \\ dW^{\alpha,\beta}_t &= (\alpha + (t-s)\beta)\,dt + dW_t \end{cases} \tag{7.18}$$

to be solved for $t \ge s \ge 0$, with initial conditions $U^{\alpha,\beta}_s = (x,y)$.

We want $W^{\alpha,\beta}_t$ to be a Brownian motion under a new probability. This is a straightforward application of Girsanov's theorem (or the particular case of Cameron-Martin's formula). We define

$$L^{\alpha,\beta}_t := -\int_s^t (\alpha + \beta h)dW_h,\ 0 \le s \le t$$

This is a martingale for $\mathscr{F}_{s,t}$ satisfying $\langle L^{\alpha,\beta}, L^{\alpha,\beta}\rangle_t = \int_s^t (\alpha+\beta h)^2\,dh$, therefore $\mathbb{E}[\exp\{\frac{1}{2}\langle L^{\alpha,\beta}, L^{\alpha,\beta}\rangle_t\}] < \infty$, $0 \le s \le t < \infty$. We conclude from Novikov's criterion that $W_t - \langle W, L^{\alpha,\beta}\rangle_t = W^{\alpha,\beta}_t$ is a Brownian motion under a new probability, noted $\mathbb{P}^{\alpha,\beta}_{s,(x,y)}$.

The Radon-Nicodym derivative $D^{\alpha,\beta}_{s,(x,y)}(t)$ of this new probability with respect to the initial probability $\mathbb{P}_{s,(x,y)}$ is given by Girsanov's theorem and is equal to

$$\exp\left(L^{\alpha,\beta}_t - \frac{1}{2}\left\langle L^{\alpha,\beta}, L^{\alpha,\beta}\right\rangle_t\right).$$

This can be written

$$\begin{aligned} D^{\alpha,\beta}_{s,(x,y)}(t) &= \frac{d\mathbb{P}^{\alpha,\beta}}{d\mathbb{P}}\Big|_{\mathscr{F}_{s,t}} \\ &= \exp\Big(-\frac{1}{2}\int_s^t (\alpha+h\beta)^2 dh + \int_s^t (\alpha+h\beta)dW_h\Big) \\ &= \exp\Big(-\frac{1}{2}\big(\alpha^2(t-s) + \alpha\beta(t^2-s^2) + \frac{1}{3}\beta^2(t^3-s^3)\big) \\ &\quad -\alpha(W_t - y) - \beta(tW_t - sy) + \beta(X_t - x)\Big) \end{aligned}$$

using Ito's formula for the process tW_t. Hence we obtain a formula equivalent to (7.17). □

Remark 12. In this proof we have seen that the IWP comes from the stochastic integration of the function $\alpha+\beta t$ with respect to the Brownian density. If we had chosen a polynomial of degree greater than 1, the integration by parts would have produced higher-order integrals of the Brownian motion that we do not want to deal with since we have no knowledge of their first hitting time. This is the reason why we study in the sequel the first hitting time of the IWP to cubic boundaries and why we cannot go further. This method does not generalize to polynomial boundaries of degree larger than three. Anyway we show that this is sufficient to approximate the probability distribution of the first hitting time of the IWP and of other DIP to general curved boundaries, precisely by approximating these boundaries with piecewise-cubic polynomials.

We note

$$d^{\alpha,\beta}(s,x,y;t,u,v) = \exp\Big(-\frac{1}{6}\beta^2(t^3-s^3) - \frac{1}{2}\alpha\beta(t^2-s^2) - \frac{1}{2}\alpha^2(t-s) \\ -(\alpha+t\beta)v + (\alpha+s\beta)y + \beta(u-x)\Big) \quad (7.19)$$

the probability density function of the new probability w.r.t. the initial one.

Theorem 7.3.2. *Let τ_C be the first hitting time of the standard IWP to the cubic curve C of equation*

$$C(t-s) = a + b(t-s) + \frac{\alpha}{2}(t-s)^2 + \frac{\beta}{6}(t-s)^3. \quad t \geq s$$

Under the reference probability $\mathbb{P}$, the law of the random variable (τ_C, W_{τ_C}) satisfies the equation:

$$\mathbb{P}_{s,(x,y)}(\tau_C \in dt, W_{\tau_C} \in dz) = d^{-\alpha,-\beta}(s,x,y-b;t,a,z-b-\alpha(t-s)-\frac{\beta}{2}(t-s)^2) \\ \times \mathbb{P}_{s,(x,y-b)}(\tau_a \in dt, W_{\tau_a} + b + \alpha(\tau_a - s) + \frac{\beta}{2}(\tau_a - s)^2 \in dz) \quad (7.20)$$

The second term of the righthand side is given by Lachal's formula (7.15) *if $a \neq x$ or by McKean's formula* (7.13) *if $a = x$.*

Proof. Let $\Gamma \subset \mathbb{R}$ be a measurable set and $t \geq s \geq 0$. We have by the change of probability formula:

$$\begin{aligned}
\mathbb{P}^{\alpha,\beta}_{s,(x,y)}(\tau_a \leq t, W_{\tau_a} \in \Gamma) &= \mathbb{E}_{s,(x,y)}\left[\mathbb{1}_{s\leq\tau_a\leq t, W_{\tau_a}\in\Gamma} D^{\alpha,\beta}_{s,(x,y)}(t)\right] \\
&= \mathbb{E}_{s,(x,y)}\left[\mathbb{1}_{s\leq\tau_a\leq t, W_{\tau_a}\in\Gamma}\mathbb{E}_{s,(x,y)}\left(D^{\alpha,\beta}_{s,(x,y)}(t)\middle|\mathscr{F}_{s\vee\tau_a, t\wedge\tau_a}\right)\right] \\
&= \mathbb{E}_{s,(x,y)}\left[\mathbb{1}_{s\leq\tau_a\leq t, W_{\tau_a}\in\Gamma} D^{\alpha,\beta}_{s,(x,y)}(t\wedge\tau_a)\right] \\
&= \mathbb{E}_{s,(x,y)}\left[\mathbb{1}_{s\leq\tau_a\leq t, W_{\tau_a}\in\Gamma} D^{\alpha,\beta}_{s,(x,y)}(\tau_a)\right] \\
&= \int_\Gamma\int_s^t D^{\alpha,\beta}_{s,(x,y)}(t')\mathbb{P}_{s,(x,y)}\left(\tau_a \in dt' \,;\, W_{\tau_a}\in dz\right)
\end{aligned}$$

In going from the second to the third equation we used the fact that, according to Girsanov's theorem, $D^{\alpha,\beta}_{s,(x,y)}(t)$ is a martingale.

If $x \neq a$, the last probability is given by Lachal's formula (7.15) and gives the density of the hitting time of (τ_a, W_{τ_a}) under the new probability $\mathbb{P}^{\alpha,\beta}_{s,(x,y)}$:

$$D^{\alpha,\beta}_{s,(x,y)}(t)|z|\Big[p_t(x,y;a,z) - \int_0^t \int_0^{+\infty} \mathbb{P}_{(0,-|z|)}\{\tau_0 \in ds';\, W_{\tau_0} \in d\mu\}\, p_{t-s'}(x,y;a,-\varepsilon\mu)\Big]\, \mathbb{1}_A(z)$$

where $A = [0,\infty)$ if $x < a$ and $A = (-\infty, 0]$ if $x > a$, $\varepsilon = \text{sign}(a-x)$ and $\mathbb{P}_{(0,-|z|)}$ is given by McKean's formula (7.13).

We are interested in the probability density under $\mathbb{P}$ of the first hitting time of the curve $C(t-s)$. This hitting time reads:

$$\begin{aligned}
\tau_C &= \inf\Big\{t > s,\, X_t = C(t-s) \;\Big|\; X_s = x, W_s = y\Big\} \\
&= \inf\Big\{t > s,\, X_t - \frac{\beta}{6}(t-s)^3 - \frac{\alpha}{2}(t-s)^2 = a \;\Big|\; \\
&\quad X_s = x, W_s = y - b\Big\} \\
&= \inf\Big\{t > s,\, X_t^{-\alpha,-\beta} = a \;\Big|\; X_s^{-\alpha,-\beta} = x, W_s^{-\alpha,-\beta} = y - b\Big\}
\end{aligned}$$

Hence τ_C under $\mathbb{P}_{s,x,y}$ has the same law as τ_a under $\mathbb{P}^{-\alpha,-\beta}_{s,x,y-b}$. The corresponding location of $W_{\tau_a}^{-\alpha,-\beta}$ is $W_{\tau_a} + b + \alpha(t-s) + \frac{\beta}{2}(t-s)^2$.

So eventually the law of τ_C, W_{τ_C} under $\mathbb{P}$ reads:

$$\begin{aligned}
\mathbb{P}_{s,(x,y)}(\tau_C \in dt, W_{\tau_C} \in dz) &= d^{-\alpha,-\beta}(s,x,y-b\,;\,t,a,z-b-\alpha(\tau_a - s) - \frac{\beta}{2}(\tau_a - s)^2) \\
&\quad \times \mathbb{P}_{s,(x,y-b)}(\tau_a \in dt, W_{\tau_a} + b + \alpha(\tau_a - s) + \frac{\beta}{2}(\tau_a - s)^2 \in dz)
\end{aligned}$$

which is exactly (7.20).

If $x \neq a$, this formula reads:

$$\begin{aligned}
\mathbb{P}_{s,(x,y)}(\tau_C \in dt, W_{\tau_C} \in dz) &= d^{-\alpha,-\beta}(s,x,y-b\,;\,t,a,z-b-\alpha(t-s) - \frac{\beta}{2}(t-s)^2) \\
&\quad \times l^a_{x,y-b}(t-s, z-b-\alpha(t-s) - \frac{\beta}{2}(t-s)^2)\, dt\, dz \quad (7.21)
\end{aligned}$$

where $l^\alpha_{x,y}$ is Lachal's density (7.15).

If $x = a$ the same calculus using McKean's formula (7.13) gives us the formula of the hitting time probability density using the same method:

$$\begin{aligned}
\mathbb{P}_{s,(x,y)}(\tau_C \in dt, W_{\tau_C} \in dz) &= d^{-\alpha,-\beta}(s,x,y-b\,;\,t,a,z-b-\alpha(t-s) - \frac{\beta}{2}(t-s)^2) \\
&\quad \times m(t-s, y-b, z-b-\alpha(t-s) - \frac{\beta}{2}(t-s)^2)\, dt\, dz \quad (7.22)
\end{aligned}$$

□

7.4 APPROXIMATION OF THE FIRST HITTING TIME OF THE IWP TO A GENERAL BOUNDARY

In this section we provide the formula of the first hitting time of the IWP to a piecewise cubic function and use it to compute an approximation formula of the law of the first hitting time of the IWP to a general smooth curved boundary. We also provide the convergence rate of this approximation. This approach in inspired the works [27, 210, 217, 277] on the first hitting time of the Brownian motion to a general boundary. In [217, 277], the authors use the formula of the first hitting time of the Brownian motion to an affine boundary to derive an approximation of the first hitting time of the Brownian motion to a curved boundary, approximated by a piecewise affine boundary. The rate of approximation is computed in [27]. This approach is here applied to our problem for the IWP. Here the boundary is approximated by a cubic spline, for which we compute an explicit formula for the pdf of the first hitting time of the IWP. We then compute the convergence speed to the first hitting time of the IWP to a general boundary of the first hitting time of a cubic spline approximation.

7.4.1 First hitting time to a continuous piecewise cubic function

In this section we consider the first hitting time of an IWP to a continuous piecewise cubic function $C(t)$ defined on the interval $[0,T]$:

$$C(t) = \sum_{i=0}^{n-1} \left(a_i + b_i(t-t_i) + \frac{\alpha_i}{2}(t-t_i)^2 + \frac{\beta_i}{6}(t-t_i)^3 \right) \mathbb{1}_{[t_i,t_{i+1})}(t) \tag{7.23}$$

The coefficients $\{(a_i,b_i,\alpha_i,\beta_i),\ i=1\dots n\}$ are constant on each interval $[t_i,t_{i+1})$, $i=1,\cdots,n-1$. The continuity assumption [1] requires that

$$\forall i \in \{1,\dots,n-1\}\ \ a_{i+1} = a_i + b_i(t_{i+1}-t_i) + \frac{\alpha_i}{2}(t_{i+1}-t_i)^2 + \frac{\beta_i}{6}(t_{i+1}-t_i)^3$$

We denote by $(U_t)_{t\geq 0}$ the two-dimensional process $(X_t,W_t)_{t\geq 0}$ and assume that the starting point U_0 is fixed:

$$X_0 = x, W_0 = y$$

We recall that the process $(U_t)_t$ is strongly Markovian with transition density (7.11). We denote by τ_C^s the first hitting time of the process $(X_t)_{t\geq s}$ to the curve C before the time T:

$$\tau_C^s := \inf\{t > s;\ X_t = C(t)\}$$

Let us fix $t \in [0,T[$, and note p the index of the bin containing t (i.e. $t \in [t_p,t_{p+1})$). The principle of the proof is to use the strong Markov property of $(U_t)_t$ to express $\mathbb{P}(\tau_C^0 \geq t | U_0)$ recursively as an integral of a product of $p+1$ terms. p of these terms are related to the results of section 7.3.2 and their analytical expression is obtained from Theorem 7.3.2, see Fig. 7.2.

[1] This continuity assumption is not essential. Nevertheless we limit ourselves to a continuous boundary because it is sufficient to find good approximations of the first hitting time pdf with continuous functions, since we prove in theorem 7.4.2 that for Lipschitz continuous boundaries there exists a density for the first hitting time. If the boundary was not continuous, then the density function of the first hitting times would have atoms at the points of discontinuity of the boundary. This could be handled at the cost of an unnecessary increase in technical difficulty.

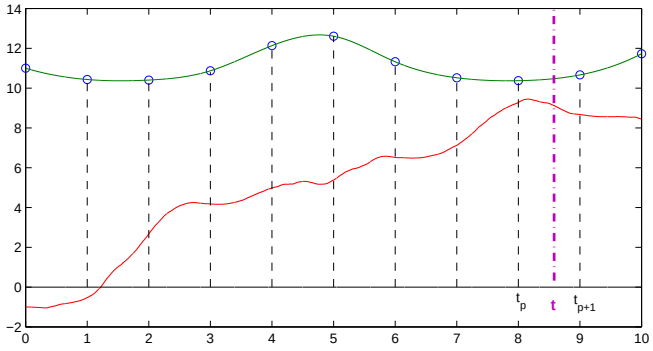

Figure 7.2: Principle of the proof of theorem 7.4.1: probability that the first hitting time is greater than $t \in [t_p, t_{p+1})$.

We know that τ_C^s is a stopping time under the filtration associated to U, which is strongly Markovian. The event $\{U_{t_1} = u_1, \tau_C^0 \geq t_1, U_0\}$ is in $\mathscr{F}^{U_{t_1}}$ therefore $\mathbb{P}\left(\tau_C^0 \geq t \middle| U_{t_1} = u_1, \tau_C^0 \geq t_1, U_0\right) = \mathbb{P}\left(\tau_C^{t_1} \geq t \middle| U_{t_1} = u_1\right)$. It follows that

$$\begin{aligned}\mathbb{P}\left(\tau_C^0 \geq t \middle| U_0\right) &= \int^{(2)} \mathbb{P}\left(\tau_C^0 \geq t \middle| U_{t_1} = u_1, \tau_C^0 \geq t_1, U_0\right) \mathbb{P}\left(U_{t_1} \in du_1,\ \tau_C^0 \geq t_1 \middle| U_0\right) \\ &= \int^{(2)} \mathbb{P}\left(\tau_C^{t_1} \geq t \middle| U_{t_1} = u_1\right) \mathbb{P}\left(U_{t_1} \in du_1,\ \tau_C^0 \geq t_1 \middle| U_0\right)\end{aligned}$$

The first term in this integral is similar to the lefthand side of the equation. By an immediate recursion we get:

$$\begin{aligned}\mathbb{P}\left(\tau_C^0 \geq t \middle| U_0\right) = \int^{(4)} & \mathbb{P}\left(\tau_C^{t_2} \geq t \middle| U_{t_2} = u_2\right) \\ & \times \mathbb{P}\left(U_{t_2} \in du_2,\ \tau_C^{t_1} \geq t_2 | U_{t_1} = u_1\right) \\ & \times \mathbb{P}\left(U_{t_1} \in du_1,\ \tau_C^0 \geq t_1 \middle| U_0\right) \\ & \cdots \\ = \int^{(2p)} & \mathbb{P}\left(\tau_C^{t_p} \geq t \middle| U_{t_p} = u_p\right) \\ & \times \mathbb{P}\left(U_{t_p} \in du_p,\ \tau_C^{t_{p-1}} \geq t_p | U_{t_{p-1}} = u_{p-1}\right) \\ & \times \mathbb{P}\left(U_{t_{p-1}} \in du_{p-1},\ \tau_C^{t_{p-2}} \geq t_{p-1} | U_{t_{p-2}} = u_{p-2}\right) \\ & \times \ldots \\ & \times \mathbb{P}\left(U_{t_1} \in du_1,\ \tau_C^0 \geq t_1 \middle| U_0\right) \qquad (7.24)\end{aligned}$$

where $\int^{(N)}$ denotes an integral on $\mathbb{R}^N$. Note that the integration variables $(u_i)_{\{i=1,\ldots p\}}$ are two-dimensional.

The terms in the product (7.24) are of the same kind. Their expression is given by theorem 7.4.1.

Indeed, since

$$\{U_{t_k} \in du_k,\ \tau_C^{t_{k-1}} \geq t_k\} = \{U_{t_k} \in du_k\} \setminus \left\{U_{t_k} \in du_k,\ \tau_C^{t_{k-1}} < t_k\right\},$$

where $\setminus$ is the set difference, we have

$$\begin{aligned}
&\mathbb{P}\left(U_{t_k} \in du_k,\ \tau_C^{t_{k-1}} \geq t_k | U_{t_{k-1}} = u_{k-1}\right) \\
&\quad = \mathbb{P}\left(U_{t_k} \in du_k | U_{t_{k-1}} = u_{k-1}\right) - \mathbb{P}\left(U_{t_k} \in du_k,\ \tau_C^{t_{k-1}} \leq t_k | U_{t_{k-1}} = u_{k-1}\right) \\
&\quad = \mathbb{P}\left(U_{t_k} \in du_k | U_{t_{k-1}} = u_{k-1}\right) - \int_{t_{k-1}}^{t_k} \mathbb{P}\left(U_{t_k} \in du_k, \tau_C^{t_{k-1}} \in ds | U_{t_{k-1}} = u_{k-1}\right) \\
&\quad = \mathbb{P}\left(U_{t_k} \in du_k | U_{t_{k-1}} = u_{k-1}\right) \\
&\qquad - \int_{t_{k-1}}^{t_k} \int_{\mathbb{R}} \mathbb{P}\left(U_{t_k} \in du_k | \tau_C^{t_{k-1}} = s,\ W_s = y,\ U_{t_{k-1}} = u_{k-1}\right) \\
&\qquad \times \mathbb{P}\left(\tau_C^{t_{k-1}} \in ds,\ W_s \in dy \,\middle|\, U_{t_{k-1}} = u_{k-1}\right) \\
&\quad = \Big(p_{t_k - t_{k-1}}(u_k; u_{k-1}) \\
&\qquad - \int_{t_{k-1}}^{t_k} \int_{\mathbb{R}} p_{t_k - s}(u_k; C(s), y) \mathbb{P}\left(\tau_C^{t_{k-1}} \in ds,\ W_s \in dy \,\middle|\, U_{t_{k-1}} = u_{k-1}\right)\Big) du_k
\end{aligned}$$

where $p_t(x, y; u, v)$ is the transition density function (7.11) of the process U. The curve C on the interval $[t_{k-1}, t_k)$ is a fixed cubic function; The hitting time of the IWP starting at u_{k-1} to C has a known density computed in section 7.3.2 and the term we are interested in can be deduced from the expression we derived previously.

Hence we have proved the following theorem:

Theorem 7.4.1. *The law of the first hitting time of the IWP to a continuous piecewise cubic boundary is given by the formula:*

$$\begin{aligned}
\mathbb{P}\left(\tau_C^0 \geq t \,\middle|\, U_0\right) = \int^{(2p)} \mathbb{P}\left(\tau_C^{t_p} \geq t | U_{t_p} = u_p\right) \prod_{k=1}^{p} \Bigg(& p_{t_k - t_{k-1}}(u_k; u_{k-1}) \\
& - \int_{t_{k-1}}^{t_k} \int_{\mathbb{R}} p_{t_k - s}(u_k; C(s), y) \mathbb{P}\left(\tau_C^{t_{k-1}} \in ds,\ W_s \in dy \,\middle|\, U_{t_{k-1}}\right) \Bigg) du_k
\end{aligned} \tag{7.25}$$

7.4.2 Approximation of the first hitting time to a general boundary

In this section we derive an approximation of the first hitting time before a given time T of the IWP to a general smooth boundary using the results of the previous section.

Let $f : \mathbb{R} \mapsto \mathbb{R}$ be a continuously differentiable function. Let also $T > 0$ and

$$0 = t_0 < t_1 < \ldots < t_n = T$$

be a partition, noted π, of the interval $[0, T]$. We denote by $\delta(\pi)$ the mesh step defined as:

$$\delta(\pi) = \max\{t_{i+1} - t_i,\ i = 0 \ldots n-1\}$$

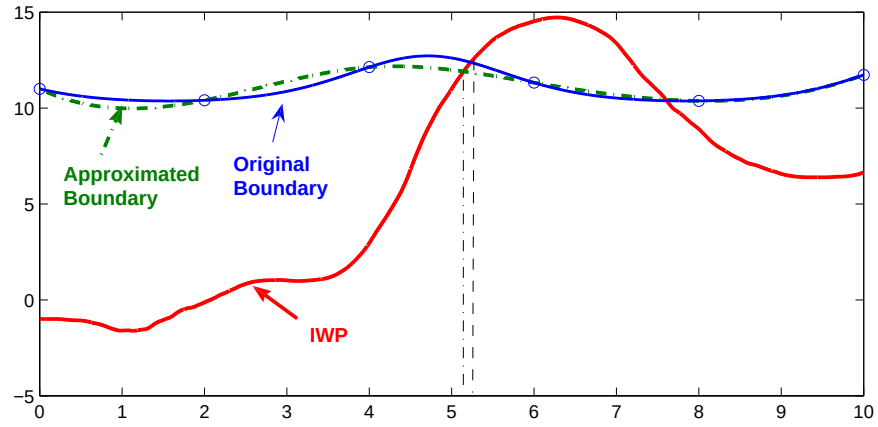

Figure 7.3: Principle of the approximation method: approximating the boundary by a regular piecewise cubic function

The principle of the method is to approximate the first hitting time of the IWP to the boundary f by the first hitting time of the IWP to a smooth piecewise cubic function C_π (see fig. 7.3). The constraints we impose to C_π is to pass through the control points $\{(t_i,\ f(t_i)),\ i = 1 \dots n\}$ and to be at least continuously differentiable. There are several ways for defining it, see, e.g., [245]. We assume for simplicity, but it is not essential here, that f is either C^2 or C^4. One of the most popular interpolation schemes in the second case is provided by the cubic spline that yields a C^2 interpolation of f which is an approximation of order four, i.e.

$$\sup_{t\in[0,T]} |f(t) - C_\pi(t)| \leq K(f)\delta(\pi)^4, \tag{7.26}$$

where $K(f)$ is a function of f only.

$C_\pi(t)$ is therefore given by (7.23), where the coefficients a_i, b_i, α_i, and β_i are functions of f and provided by the particular interpolation scheme one uses, see, e.g., [245].

We first prove the following

Theorem 7.4.2. *The first hitting time of the IWP to a Lipschitz continuous boundary has a density with respect to Lebesgue's measure.*

Proof. We assume that f is Lipschitz continuous. Let L denote the Lipschitz continuity constant of f, we have:

$$f(s+h) - f(s) \geq -Lh \ \ \forall 0 < s < s+h < t$$

For a fixed $t \in [0,T]$, we introduce the boundary $f_t(s) := f(t) + L(t-s)$. Let now

$$\begin{aligned}\tau_t &:= \inf\{s > 0;\ X_s > f_t(s) | X_0 = x_0, W_0 = y_0\} \\ &= \inf\{s > 0;\ X_s + Ls > f(t) + Lt | X_0 = x_0, W_0 = y_0\} \\ &= \inf\{s > 0;\ X_s > f(t) + Lt | X_0 = x_0, W_0 = y_0 + L\}\end{aligned}$$

Obviously, we have:

$$\mathbb{P}(\tau_f \in (t,t+h)) \leq \mathbb{P}(\tau_t \in (t,t+h)) \tag{7.27}$$

and hence the stopping time τ_f has a density $p(t)$ with respect to Lebesgue's measure. From Lachal's formula we have moreover:

$$p(t) \leq \int_{\mathbb{R}} l_{x_0,y_0+L}^{f(t)+Lt}(t,z)dz$$

□

We now relate the first hitting time to the cubic approximation C_π to that to the general boundary f.

Theorem 7.4.3. *The first hitting time of the IWP to the curve C_π before T converges in law to the first hitting time of the IWP to the curve f before T.*

Furthermore, if f is C^2, then this convergence is the same order as the approximation of f by the cubic function C_π. More precisely, for a real function g, if $P(T,g)$ denotes the probability $\mathbb{P}\Big(X_t \geq g(t) \text{ for some } t \in [0,T]\Big)$, there exists a constant $\tilde{K}(f,T)$ depending on the function f and the time T such that:

$$\boxed{|P(T,C_\pi) - P(T,f)| \leq \tilde{K}(f,T)\, \|f - C_\pi\|_{\infty,T}} \tag{7.28}$$

where $\|g\|_{\infty,T} = \sup_{s\in[0,T]} |g(s)|$ is the uniform norm on $[0,T]$.

To prove this theorem, we use the following lemma giving the density of the random variable $\sup_{s\in[0,t]} X_s$.

Lemma 7.4.4. Let $t > 0$ be a fixed real and S_t be the random variable defined by:

$$S_t = \sup_{s\in[0,t]} X_s$$

Then the law of this random variable is characterized by:

$$\begin{aligned}\mathbb{P}_{0,x,y}\Big(S_t \in da\Big) = -da \int_{-\infty}^{\infty}\int_0^t |z|\Big\{ &\frac{\partial p_s(x,y;a,z)}{\partial a} \\ &- \int_0^s \int_0^{+\infty} \mathbb{P}_{(0,-|z|)}\{\tau_0 \in du;\, W_{\tau_0} \in d\mu\} \frac{\partial p_{s-u}(x,y;a,-\varepsilon\mu)}{\partial a}\Big\} \mathbb{1}_A(z)dzdt\end{aligned} \tag{7.29}$$

Proof of lemma 7.4.4. We have:

$$\begin{aligned}\mathbb{P}_{0,x,y}\Big(S_t \geq a\Big) &= \mathbb{P}_{0,x,y}\Big(\tau_a \leq t\Big) \\ &= \int_0^t \int_{-\infty}^{\infty} l_{x,y}^a(t,z)dtdz\end{aligned}$$

where $l_{x,y}^a(t,z)$ is Lachal's density. From the expression of this density and its dependency in a, we can see that the random variable S_t has a density with respect to Lebesgue's measure, and this measure has the expression (7.29) (this formula is obtained using Lebesgue's theorem of derivation under the sum sign). □

Proof of theorem 7.4.3. This result comes directly from the existence of a smooth density of the random variable S_t, the uniform convergence of the curve C_π to f and the smoothness of the function f. Let U_0 be the initial conditions: $(X_0 = x, W_0 = y)$, such that $x < f(0)$.

We have:

$$P(T, f+\varepsilon) \leq P(T, f) \leq P(T, f-\varepsilon)$$

Assume that f_ε is a uniform approximation of f such that

$$\| f_\varepsilon - f \|_{\infty,T} \leq \varepsilon.$$

We have:

$$\begin{aligned}
|P(T, f_\varepsilon) - P(T, f)| &\leq P(T, f-\varepsilon) - P(T, f+\varepsilon) \\
&= P(T, f-\varepsilon) - P(T, f) + P(T, f) - P(T, f+\varepsilon) \\
&= \mathbb{P}\Big(-\varepsilon \leq \sup_{s\in[0,t]} \big(X_s - f(s)\big) \leq 0 \Big) + \mathbb{P}\Big(0 \leq \sup_{s\in[0,t]} \big(X_s - f(s)\big) \leq \varepsilon \Big) \\
&\stackrel{\text{def}}{=} \Delta_{-\varepsilon}(f) + \Delta_\varepsilon(f) \qquad (7.30)
\end{aligned}$$

We have:

$$\begin{aligned}
\Delta_\varepsilon(f) &= \mathbb{P}\Big(0 \leq \sup_{s\in[0,t]} \big(X_s - f(s)\big) \leq \varepsilon \Big| U_0 \Big) \\
&= \int_0^t \int_{\mathbb{R}} \mathbb{P}\left(\tau_f \in ds,\, W_{\tau_f} \in dz \middle| U_0 \right) \mathbb{P}\left(\sup_{v\in[s,t]} (X_v - f(v)) \leq \varepsilon \middle| X_s = f(s),\, W_s = z \right) \\
&= \int_0^t \int_{f'(s)}^{\infty} \mathbb{P}\left(\tau_f \in ds,\, W_{\tau_f} \in dz \middle| U_0 \right) \mathbb{P}\left(\sup_{v\in[s,t]} (X_v - f(v)) \leq \varepsilon \middle| X_s = f(s),\, W_s = z \right)
\end{aligned}$$

The last equality is a consequence of the fact that $\mathbb{P}\left(W_{\tau_f} > f'(\tau_f)\right) = 1$, i.e., $z \geq f'(s)$ almost surely. We can conclude to the convergence of the approximation as an application of Lebesgue's theorem. Indeed, let $s \in [0,t]$ and $z > f'(s)$. Then the process $(X_t - f(t))_{t\geq s}$ conditioned by $\{X_s = f(s), W_s = z\}$ is a differentiable process starting from 0 with a strictly positive derivative at 0 implying that

$$\mathbb{P}\left(\sup_{v\in[s,t]} (X_v - f(v)) \leq \varepsilon \middle| X_s = f(s),\, W_s = z \right) \underset{\varepsilon\to 0}{\longrightarrow} 0$$

Furthermore, $\mathbb{P}\left(\sup_{v\in[s,t]} (X_v - f(v)) \leq \varepsilon \middle| X_s = f(s),\, W_s = z \right) \leq 1$ which is integrable under the measure $\mathbb{P}\left(\tau_f \in ds,\, W_{\tau_f} \in dz \middle| U_0 \right)$ so Lebesgue's theorem applies and we have the expected result:

$$\Delta_\varepsilon(f) \underset{\varepsilon\to 0}{\longrightarrow} 0$$

The same argument applies for the term $\Delta_{-\varepsilon}(f)$ of equation (7.30). Indeed, we can bound this probability for $\varepsilon \leq \frac{f(0)-x}{2}$ by:

$$\begin{aligned}\Delta_{-\varepsilon}(f) &= \mathbb{P}\Big(-\varepsilon \le \sup_{s\in[0,t]} X_s - f(s) \le 0 \Big| X_0 = x, W_0 = y\Big)\\ &= \mathbb{P}\Big(0 \le \sup_{s\in[0,t]} X_s - f(s) \le \varepsilon \Big| X_0 = x+\varepsilon, W_0 = y\Big)\\ &\le \mathbb{P}\Big(0 \le \sup_{s\in[0,t]} X_s - f(s) \le \varepsilon \Big| X_0 = \frac{x+f(0)}{2}, W_0 = y\Big) \qquad (7.31)\\ &\underset{\varepsilon\to 0}{\longrightarrow} 0\end{aligned}$$

We obtain a stronger result if the boundary f is C^2. Lemma 7.4.4 ensures us that the random variable $\sup_{s\in[0,t]} X_s$ has a smooth density with respect to Lebesgue's measure. From Girsanov's theorem, under the probability $\mathbb{Q}$ defined by:

$$\left.\frac{d\mathbb{Q}}{d\mathbb{P}}\right|_{\mathscr{F}_t} = \exp\Big[\int_0^t f''(s)\,dW_s - \frac{1}{2}\int_0^t f''(s)^2\,ds\Big] \overset{\text{def}}{\equiv} L_s$$

the process $\sup_{v\in[s,t]}(X_v - f(v))$ has the law of the sup over $[s,t]$ of an IWP, which is given by (7.29), let us note it $p_L(s)$. For $z > f'(s)$ the probability that appears at the righthand side of (7.31) is equal to

$$\begin{aligned}\int_0^\varepsilon p_L(s)\mathbb{E}_{\mathbb{Q}}(L_s^{-1})\,ds &= \int_0^\varepsilon p_L(s)\mathbb{E}_{\mathbb{Q}}(\tilde{L}_s)\exp\Big[\int_0^s f''(u)^2\,du\Big]\,ds\\ &= \int_0^\varepsilon p_L(s)\exp\Big[\int_0^s f''(u)^2\,du\Big]\,ds,\end{aligned}$$

since $\tilde{L}_s = \exp\Big[-\int_0^t f''(s)\,dW_s - \frac{1}{2}\int_0^t f''(s)^2\,ds\Big]$ is a martingale. The last integral is $O(\varepsilon)$.

So eventually, using again the same bound as (7.31), we have the expected result: there exists a constant $\tilde{\tilde{K}}(f,T)$ such that

$$|P(T,f_\varepsilon) - P(T,f)| \le \tilde{\tilde{K}}(f,T)\varepsilon$$

Finally, if f is C^4 and C_π is a cubic spline interpolation of f we have the convergence estimation (7.26) which yields

$$\begin{aligned}|P(T,C_\pi) - P(T,f)| &\le 2\tilde{\tilde{K}}(f,T)\|C_\pi - f\|_\infty\\ &\le 2\tilde{K}(f,T)\delta(\pi)^4\end{aligned}$$

□

7.5 Approximation of the first hitting time of a general DIP to a general boundary

In this section we derive an approximation formula for the probability density function of the first hitting time of a general double integral process to a general smooth boundary. Here again the idea is to use the formulas we obtained in the section 7.3 to build approximations on a partition of a given time interval $[0,T]$ (see Fig.7.4).

Thanks to lemma 7.2.3, we can restrict ourselves to the first hitting time of a process Y defined by:

$$Y_t = \int_0^t g(s)W_s\,ds \qquad (7.32)$$

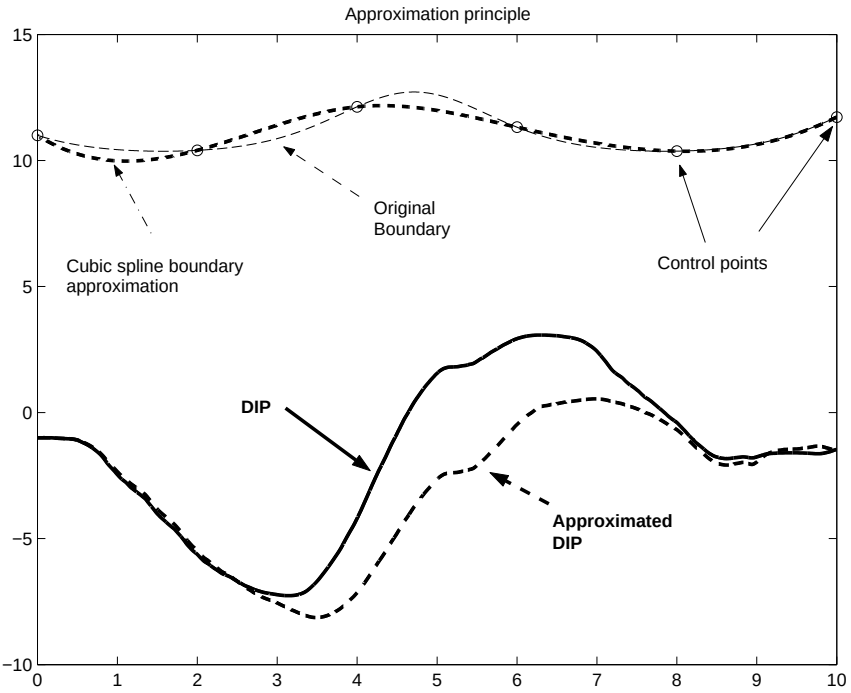

Figure 7.4: Approximation principle for the DIP: The boundary is approximated by a smooth piecewise cubic boundary while the process is approximated by a continuous piecewise IWP process

where $g(\cdot)$ is a continuously differentiable function and W a standard Brownian motion.
Let π be as before a partition of the interval $[0,T]$ with n intervals:

$$0 = t_0 < t_1 < t_2 < \ldots < t_n = T$$

We denote by g^π the piecewise constant approximation of g defined by:

$$g^\pi(t) = \sum_{i=0}^{n-1} g(t_i)\mathbb{1}_{[t_i,t_{i+1})}(t), \tag{7.33}$$

and by Y^π the associated DIP:

$$Y_t^\pi = \int_0^t g^\pi(s)W_s\,ds. \tag{7.34}$$

Proposition 7.5.1. The process Y_t^π converges almost surely to the process Y_t. Furthermore, there exists a real positive process Z_t such that:

$$\sup_{0\le s\le t} |Y_s^\pi - Y_s| \le \delta(\pi)\, Z_t \tag{7.35}$$

Proof.

$$\begin{aligned}\sup_{0\le s\le t}|Y_s^\pi - Y_s| &= \sup_{0\le s\le t}\left|\int_0^s (g^\pi(u)-g(u))W_u\,du\right| \\ &\le \sup_{0\le s\le t}\int_0^s |g^\pi(u)-g(u)||W_u|\,du \\ &\le \left(\sup_{0\le s\le t}|g^\pi(u)-g(u)|\right)\sup_{0\le s\le t}\int_0^s |W_u|\,du\end{aligned}$$

We assumed that g was continuously differentiable on $\mathbb{R}^+$, so it is uniformly Lipschitz on $[0,T]$. We note

$$\|g'\|_{\infty,T} = \sup_{0\le s\le T}|g'(s)|$$

the uniform Lipschitz constant. We eventually have:

$$\sup_{0\le s\le t}|Y_s^\pi - Y_s| \le \delta(\pi)\,\|g'\|_{\infty,T}\sup_{0\le s\le t}\int_0^s |W_u|\,du$$

The process $Z_t := \sup_{0\le s\le t}\int_0^s |W_u|\,du$ is almost surely finite, thus the process Y^π converges almost surely to Y when $\delta(\pi)\to 0$ and we have the upper bound (7.35). □

Let now f be a smooth function (at least two times continuously differentiable) and C^π the approximating function (7.23).

Theorem 7.5.2. *The first hitting time τ^π of the process Y^π to the curve C^π converges in law to the first hitting time τ_f of the process Y to the curve f.*

Proof. A sufficient condition for this convergence is the convergence in law of the process $\sup_{s\in[0,t]}(Y_s^\pi - C_s^\pi)$ to the process $\sup_{s\in[0,t]}\big(Y_s - f(s)\big)$, and this convergence is a direct consequence of the calculations above. Here we only assume that f is continuously differentiable (the corresponding piecewise cubic approximation would be for example the Hermite cubic approximation, see [245]).

In this case, C_t^π converges to f linearly, i.e., there exists a constant $K(f)>0$ depending on f such that:

$$\sup_{t\in[0,T]}|f(t)-C_\pi(t)| \le K(f)\delta(\pi) \tag{7.36}$$

We have:

$$\begin{aligned}\sup_{s\in[0,t]}\left(Y_s^\pi - C_s^\pi\right) &\le \sup_{s\in[0,t]}\left(Y_t^\pi - Y_t\right) + \sup_{s\in[0,t]}\left(f(t)-C_t^\pi\right) + \sup_{s\in[0,t]}\left(Y_t - f(t)\right) \\ &\le \delta(\pi)Z_t + K(f)\delta(\pi) + \sup_{s\in[0,t]}\left(Y_t - f(t)\right)\end{aligned}$$

Writing the same estimation on $\sup_{s\in[0,t]}\left(Y_s - f(s)\right)$ yields:

$$\left|\sup_{s\in[0,t]}\left(Y_s^\pi - C_s^\pi\right) - \sup_{s\in[0,t]}\left(Y_t - f(t)\right)\right| \le \delta(\pi)\left(Z_t + K(f)\right)$$

Hence we have the expected result:

$$\mathbb{P}\Big(\tau^\pi \le t\Big) = \mathbb{P}\Big(\sup_{s\in[0,t]}\big(Y_s^\pi - C_s^\pi\big) > 0\Big)$$
$$\underset{\delta(\pi)\to 0}{\longrightarrow} \mathbb{P}\Big(\sup_{s\in[0,t]}\big(Y_s - f(s)\big) > 0\Big) = \mathbb{P}\Big(\tau_f \le t\Big)$$

□

We now compute the formula of the probability density function of the first crossing time of Y^π to the curve C^π, as we did in the section 7.4.

We consider π a fixed partition of the interval $[0,T]$. We note τ_π^s the first hitting time after time s of the process Y^π to the curve C^π and U^π the two-dimensional process (Y_t^π, W_t). The same proof as in section 7.4 gives us a formula analog to (7.24):

$$\begin{aligned}\mathbb{P}\Big(\tau_\pi^0 \ge t \Big| U_0^\pi\Big) = \int^{(2p)} & \mathbb{P}\Big(\tau_\pi^{t_p} \ge t \Big| U_{t_p}^\pi = u_p\Big) \\ & \times \mathbb{P}\Big(U_{t_p}^\pi \in du_p,\ \tau_\pi^{t_{p-1}} \ge t_p | U_{t_{p-1}}^\pi = u_{p-1}\Big) \\ & \times \mathbb{P}\Big(U_{t_{p-1}}^\pi \in du_{p-1},\ \tau_\pi^{t_{p-2}} \ge t_{p-1} | U_{t_{p-2}}^\pi = u_{p-2}\Big) \\ & \times \dots \\ & \times \mathbb{P}\Big(U_{t_1}^\pi \in du_1 \Big| U_0^\pi\Big) \end{aligned} \tag{7.37}$$

Here again the terms in the recursion formula are of the same kind, and the only quantity we need to calculate are the conditional probabilities $\mathbb{P}\Big(U_{t_k}^\pi \in du_k,\ \tau_\pi^{t_{k-1}} \ge t_k | U_{t_{k-1}}^\pi = u_{k-1}\Big)$ for $k = 1, \cdots, p$.

Note that in the interval $[t_k, t_{k+1})$, the process Y_t^π reads:

$$Y_t^\pi = Y_{t_i}^\pi + g(t_k)(X_t - X_{t_k}), \tag{7.38}$$

and that $(X_t - X_{t_k})_{t\ge t_k}$ is simply an IWP starting from 0. We then have

$$\begin{aligned} & \mathbb{P}\Big(U_{t_k}^\pi \in du_k,\ \tau_\pi^{t_{k-1}} \ge t_k | U_{t_{k-1}}^\pi = u_{k-1}\Big) \qquad (7.39) \\ & = \mathbb{P}\Big(U_{t_k}^\pi \in du_k | U_{t_{k-1}}^\pi = u_{k-1}\Big) - \mathbb{P}\Big(U_{t_k}^\pi \in du_k,\ \tau_\pi^{t_{k-1}} \le t_{p-1} | U_{t_{k-1}}^\pi = u_{k-1}\Big) \\ & = \mathbb{P}\Big(U_{t_k}^\pi \in du_k | U_{t_{k-1}}^\pi = u_{k-1}\Big) - \int_{t_{k-1}}^{t_k} \mathbb{P}\Big(U_{t_k}^\pi \in du_k, \tau_\pi^{t_{k-1}} \in ds | U_{t_{k-1}}^\pi = u_{k-1}\Big) \\ & \qquad \times \mathbb{P}\Big(U_{t_k}^\pi = du_k | U_{t_{k-1}}^\pi = u_{k-1}\Big) \\ & \qquad - \int_{t_{k-1}}^{t_k}\int_{\mathbb{R}} \mathbb{P}\Big(U_{t_k}^\pi \in du_k | \tau_\pi^{t_{k-1}} = s,\ W_s = y,\ U_{t_{k-1}}^\pi = u_{k-1}\Big) \\ & \qquad \times \mathbb{P}\Big(\tau_\pi^{t_{k-1}} \in ds,\ W_s \in dy |\ U_{t_{k-1}}^\pi = u_{k-1}\Big) \\ & = du_k\Big(\tilde{p}(t_k, u_k; t_{k-1}, u_{k-1}) - \int_{t_{k-1}}^{t_k}\int_{\mathbb{R}} \tilde{p}(t_k, u_k; s, (C^\pi(s), y)) \\ & \qquad \times \mathbb{P}\Big(\tau_\pi^{t_{k-1}} \in ds,\ W_s \in dy |\ U_{t_{k-1}}^\pi = u_{k-1}\Big)\Big) \qquad (7.40) \end{aligned}$$

where $\tilde{p}(t,x,y;s,u,v)$ is the transition function of the process U^π (for $t \geq s$). This function can be deduced from (7.11) and (7.38) for s and t in the same bin $[t_k, t_{k+1})$ and reads:

$$\begin{aligned}
\tilde{p}(t,x,y;s,u,v) &= \mathbb{P}\left(Y_t^\pi = x, W_t = y \middle| Y_s^\pi = u, W_s = v\right) \\
&= \mathbb{P}\left(Y_s^\pi + g(t_k)(X_t - X_s) = x, W_t = y \middle| Y_s^\pi = u, W_s = v\right) \\
&= \mathbb{P}\left(X_t - X_s = \frac{x-u}{g(t_k)}, W_t = y \middle| Y_s^\pi = u, W_s = v\right) \\
&= \mathbb{P}\left(X_t - X_s = \frac{x-u}{g(t_k)}, W_t - W_s = y - v \middle| Y_s^\pi = u, W_s = v\right)
\end{aligned} \tag{7.41}$$

We have seen in a remark in section 7.2.2 that conditionally to W_s the increments of the two-dimensional process are independent of $\mathscr{F}_s$, so we have:

$$\begin{aligned}
\tilde{p}(t,x,y;s,u,v) &= \mathbb{P}\left(X_{t-s} = \frac{x-u}{g(t_k)}, W_{t-s} = y - v \middle| X_0 = 0, W_0 = 0\right) \\
&= p_{t-s}\left(\frac{x-u}{g(t_k)}, y - v; 0, 0\right)
\end{aligned} \tag{7.42}$$

Hence the general term (7.40) of the expansion reads:

$$\begin{aligned}
dx_k\, dy_k \Big\{ & p_{t_k - t_{k-1}}\left(\frac{x_k - x_{k-1}}{g(t_{k-1})}, y_k - y_{k-1}; 0, 0\right) - \\
& \int_{t_{k-1}}^{t_k} \int_{\mathbb{R}} p_{t_k - s}\left(\frac{x_k - C^\pi(s)}{g(t_{k-1})}, y_k - y; 0, 0\right) \mathbb{P}\left(\tau^\pi \in ds,\, W_s \in dy \middle|\, U_{t_{k-1}}^\pi = u_{k-1}\right) \Big\}
\end{aligned} \tag{7.43}$$

The last thing to compute is $\mathbb{P}\left(\tau^\pi \in ds,\, W_s \in dy \middle|\, U_{t_{k-1}}^\pi = u_{k-1}\right)$ the law of the hitting time τ^π in a given bin $[t_k, t_{k-1})$, which appears in the expression (7.40). This law can be deduced from that of the first hitting time of the IWP using the formula (7.38).

Indeed, to compute this probability, we use the fact that conditionally on the event $\{U_{t_{k-1}}^\pi = u_{k-1}, t \geq t_{k-1}\}$ we have:

$$\begin{aligned}
\tau^\pi &= \inf\{s > t_{k-1},\, Y_s^\pi = C^\pi(s) | U_{t_{k-1}}^\pi = u_{k-1}\} \\
&= \inf\{s > t_{k-1},\, Y_{t_{k-1}}^\pi + g(t_{k-1})(X_s - X_{t_{k-1}}) = C^\pi(s) | U_{t_{k-1}}^\pi = u_{k-1}\} \\
&= \inf\{s > t_{k-1},\, X_s - X_{t_{k-1}} = \frac{C^\pi(s) - Y_{t_{k-1}}^\pi}{g(t_{k-1})} | U_{t_{k-1}}^\pi = u_{k-1}\} \\
&= \inf\{s > 0,\, \widetilde{X}_s = \frac{C^\pi(s) - Y_{t_{k-1}}^\pi}{g(t_{k-1})} | \widetilde{X}_0 = 0, \widetilde{W}_0 = u_{t_{k-1},2}\}
\end{aligned}$$

where $(\widetilde{X}_t, \widetilde{W}_t)_t$ is a standard IWP and $u_{t_{k-1},2}$ is the second component of $U_{t_{k-1}}^\pi$. Hence we have:

$$\mathbb{P}\left(\tau^\pi \in ds,\, W_s \in dy \middle|\, U_{t_{k-1}}^\pi = u_{k-1}\right) = \mathbb{P}_{s,(0,u_{t_{k-1},2})}\left(\tau_{(C - Y_{t_{k-1}}^\pi)/g(t_{k-1})} \in ds,\, W_s \in dy\right) \tag{7.44}$$

and the last expression is given by (7.21) and (7.22).

We have proved the following

Theorem 7.5.3. *Let g be a Lipschitz continuous real function, $T>0$ and π a partition of the interval $[0,T]$*

$$0=t_0<t_1<\ldots<t_n=T$$

Let f be a continuously differentiable function. The first hitting time τ^π of the approximated process Y^π defined by (7.34) *to a cubic spline approximation of f on the partition π, denoted by f^π, satisfies the equation:*

$$\mathbb{P}(\tau^\pi \geq T|U_0)=\int^{(2n)}\prod_{k=1}^{n}\Bigg\{p_{t_k-t_{k-1}}\Big(\frac{x_k-x_{k-1}}{g(t_{k-1})},y_k-y_{k-1};0,0\Big)-\int_{t_k-1}^{t_k}\int_{\mathbb{R}} p_{t_k-s}\Big(\frac{x_k-f^\pi(s)}{g(t_{k-1})},y_k-y;0,0\Big)\mathbb{P}_{s,(0,y)}(\tau_{(C-x_{k-1})/g(t_{k-1})}\in ds,\ W_s\in dy)\Bigg\}dx_k dy_k \quad (7.45)$$

where $\mathbb{P}(\tau_C\in ds,\ W_s\in dy)$ is given by equations (7.22) *or* (7.21)*.*

7.6 Numerical Evaluation

7.6.1 Algorithm

In this section we propose an algorithm to evaluate the approximation formula we derived in the previous section. The expressions we found for the first hitting time involve integrals on $\mathbb{R}^{2n}$ when there are $n+1$ points in the mesh, which have no closed-form expression. Numerical computation of these integrals can be quite intricate and time consuming, so a numerical approximation is needed and another approximation is done besides (7.28) and theorem 7.5.2. The principle of the numerical approximation we propose is to express this integral as an expectation over a certain probability measure and to use a Monte-Carlo algorithm to compute this expectation. The accuracy of this approximation can be assessed through standard procedures for Monte Carlo simulations [206, 227].

Corollary 7.6.1 (of theorem 7.4.1)**.** Let $(X_t,W_t)_{t\geq 0}$ be a standard IWP-Brownian motion pair and f a smooth boundary function. The law of the first hitting time τ of X to f satisfies for $t\in[t_{p-1},t_p)$:

$$\mathbb{P}\Big(\tau_C\geq t\Big|U_0\Big)=\mathbb{E}\Big[h_p(\pi,t,X_{t_1},W_{t_1},\ldots,X_{t_{p-1}},W_{t_{p-1}},X_t,W_t)\Big|U_0\Big] \quad (7.46)$$

where the function h_p is defined for $t\in[t_{p-1},t_p)$ by:

$$h_p(\pi,t,x_1,y_1,\ldots,x,y) := \prod_{k=1}^{p-1}\left(1-\int_{t_{k-1}}^{t_k}\int_{\mathbb{R}}\frac{p_{t_k-s}(x_k,y_k,C(s),z)}{p_{t_k-t_{k-1}}(x_k,y_k,x_{k-1},y_{k-1})}\right.$$
$$\left.\times\,\mathbb{P}\left(\tau_C\in ds,\,W_{\tau_C}\in dz\middle|X_{t_{k-1}}=x_{k-1},W_{t_{k-1}}=y_{k-1}\right)\right)$$
$$\times\left(1-\int_{t_{p-1}}^{t}\int_{\mathbb{R}}\frac{p_{t_{p-1}-s}(x,y,C(s),z)}{p_{t-t_{p-1}}(x,y,x_{p-1},y_{p-1})}\mathbb{P}\left(\tau_C\in ds,\,W_{\tau_C}\in dz\middle|X_{t_{p-1}}=x_{p-1},W_{t_{p-1}}=y_{p-1}\right)\right) \tag{7.47}$$

The same method can be applied for the DIP for a given function g.

Corollary 7.6.2 (of theorem 7.5.3)**.** Let g be a Lipschitz continuous real function, $(X_t,W_t)_{t\geq 0}$ be a standard IWP-Brownian motion pair, $T>0$ and π a partition of the interval $[0,T]$

$$0=t_0<t_1<\ldots<t_n=T$$

Let f be a continuously differentiable function. The first hitting time τ^π of the approximated process Y^π defined by (7.34) to a cubic spline approximation of f on the partition π, denoted f^π, can be computed as the expectation:

$$\mathbb{P}\left(\tau^\pi\geq t\middle|U_0\right)=\mathbb{E}\left[h_p^{g,\pi}(t,X_{t_1},Wt_1,\ldots,X_t,W_t)\middle|U_0\right] \tag{7.48}$$

where the function $h_p^{g,\pi}$ is defined by:

$$h_p^{g,\pi}(x_1,y_1\ldots,x,y) := \prod_{k=1}^{p-1}\left\{\frac{p_{t_k-t_{k-1}}\left(\frac{x_k-x_{k-1}}{g(t_{k-1})},y_k-y_{k-1};0,0\right)}{p_{t_k-t_{k-1}}(x_k,y_k,x_{k-1},y_{k-1})}-\int_{t_{k-1}}^{t_k}\int_{\mathbb{R}}\right.$$
$$\left.\frac{p_{t_k-s}\left(\frac{x_k-f^\pi(s)}{g(t_{k-1})},y_k-z;0,0\right)}{p_{t_k-t_{k-1}}(x_k,y_k,x_{k-1},y_{k-1})}\mathbb{P}_{s,(0,y_s)}(\tau_{(C-x_{k-1})/g(t_{k-1})}\in ds,\,W_s\in dz)\right\}$$
$$\times\left(\frac{p_{t-t_{p-1}}\left(\frac{x-x_{p-1}}{g(t_{p-1})},y-y_{p-1};0,0\right)}{p_{t-t_{p-1}}(x,y,x_{p-1},y_{p-1})}\right.$$
$$\left.-\int_{t_{p-1}}^{t}\int_{\mathbb{R}}\frac{p_{t-s}\left(\frac{x-f^\pi(s)}{g(t_{p-1})},y-z;0,0\right)}{p_{t-t_{p-1}}(x,y,x_{p-1},y_{p-1})}\mathbb{P}_{s,(0,z)}(\tau_{(C-x_{p-1})/g(t_{p-1})}\in ds,\,W_s\in dz)\right) \tag{7.49}$$

where $\mathbb{P}(\tau_C\in ds,\,W_s\in dy_s)$ is given by equations (7.22) or (7.21).

Hence the problem is now reduced to the computation of the expectation of a certain function of the Gaussian random vector $(X_0,W_0,X_{t_1},W_{t_1},\ldots,X_{t_n},W_{t_n})$. This vector is Gaussian of mean 0 and covariance matrix defined by blocks as:

$$K(t_1,\ldots,t_n)=\left(\begin{array}{cc}\frac{t_j^2}{6}(3t_i-t_j) & \frac{t_j}{2}(2t_i-t_j)\\ \frac{t_j^2}{2} & t_j\end{array}\right)_{(i,j)\in\{0\ldots n\},\,j\leq i}, \tag{7.50}$$

The Monte-Carlo algorithm we use to compute the expected probability is the following:

(i). Compute the square root $K(t_1,\dots,t_n)^{1/2}$ of the covariance matrix (7.50) (using for instance a Cholesky decomposition)

(ii). Generate an i.i.d. sample $u=[u_1,u_2,\dots,u_{2n}]^T$ from the normal standard distribution $\mathcal{N}(0,1)$.

(iii). Compute the transformation $x=K(t_1,\dots,t_n)^{1/2}\cdot u$

(iv). Calculate $h_n(x)$ or $h_n^{g,\pi}(x)$

(v). Repeat steps (ii)-(iv) N times and calculate the frequency

$$P_N=\frac{1}{N}\sum_{\text{over the realizations}} h_n(x)(\text{resp. } h_n^{g,\pi}(x))$$

The probability $\mathbb{P}(\tau\geq T)$ is then estimated by P_N. The standard error of this estimator is given by :

$$\mathscr{E}(N)=\sqrt{\frac{\sum\left[h(x)-P_N\right]^2}{N(N-1)}} \tag{7.51}$$

7.6.2 Numerical Results

Lachal's formula has been implemented using Gauss integration method. This method is very interesting for computing the double integral of Lachal's formula. It allows us to control the precision of the approximation using standard methods (see e.g. [245]). With this method we obtain the two-dimensional joint probability density function of (τ_a,W_{τ_a}) conditioned on the starting point. Figure 7.5 represents the dependence of this law on the starting point. Note that the probability that the hitting time τ_a is strictly less than infinity is always one, as proved by [197]. The process almost surely crosses any given constant. Computation times for a precision set to 10^{-6} are around 0.1ms.

The formula we obtained for a cubic density is simply a transformation of Lachal's density using formulas (7.21) and (7.22). It is clear that now the crossing probability will not always be equal to one, for instance when $\beta>0$. Figure 7.6 illustrates this property and we give a numerical estimation of the probability of crossing the boundary. This probability can be computed using the formulas we obtained, but it is not in the scope of the present work.

Finally, our last formula can be implemented using different Monte-Carlo algorithms. Here we only get the inverse cumulative distribution function of the first hitting time. Computation times are quite large, but the main interest of this technique is not computational. Figure 7.7 present some results obtained for the sinusoidal functions $f(x)=\sin(x)$ and $g(x)=\cos(x)$ functions and a comparison between the results obtained using formula (7.48) and a direct integration of Lachal's formula in the case where f and g are identically equal to 1 and the boundary is constant equal to 1. In these cases, computation times are reasonable since there is no need to have a large number of points in our partition.

Finally, in table 7.1 we present results obtained with formula (7.48) for the first hitting time of the IWP to the sinusoidal function $t\mapsto 1-sin(\frac{2t}{\pi})$ in the interval $[0,1]$. We discretized the interval with 5 points (hence the approximation is of order 10^{-3}). Monte-Carlo calculations are quite long to obtain the same order of approximation

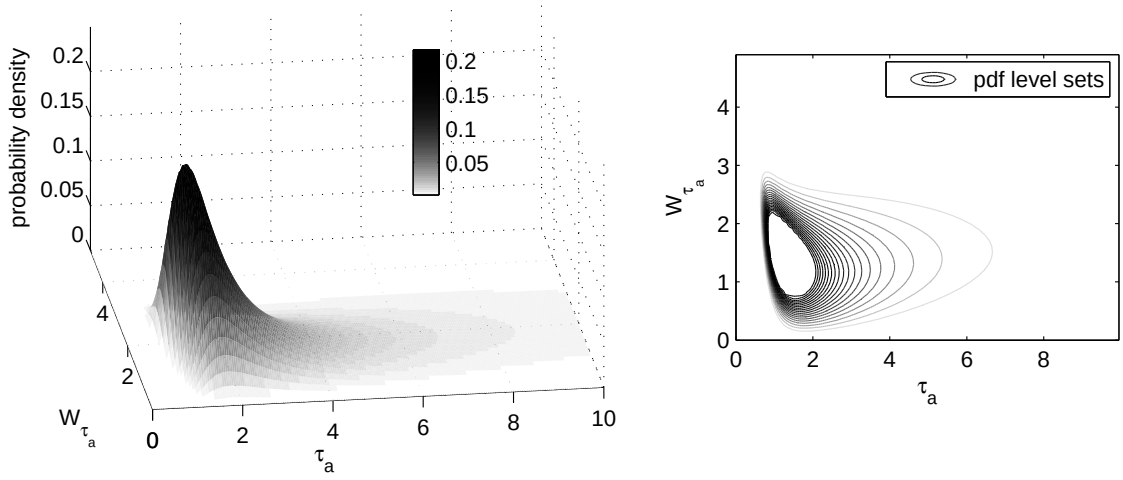

(a) Lachal's probability density function for $X_0 = 0, W_0 = 0, a = 1$

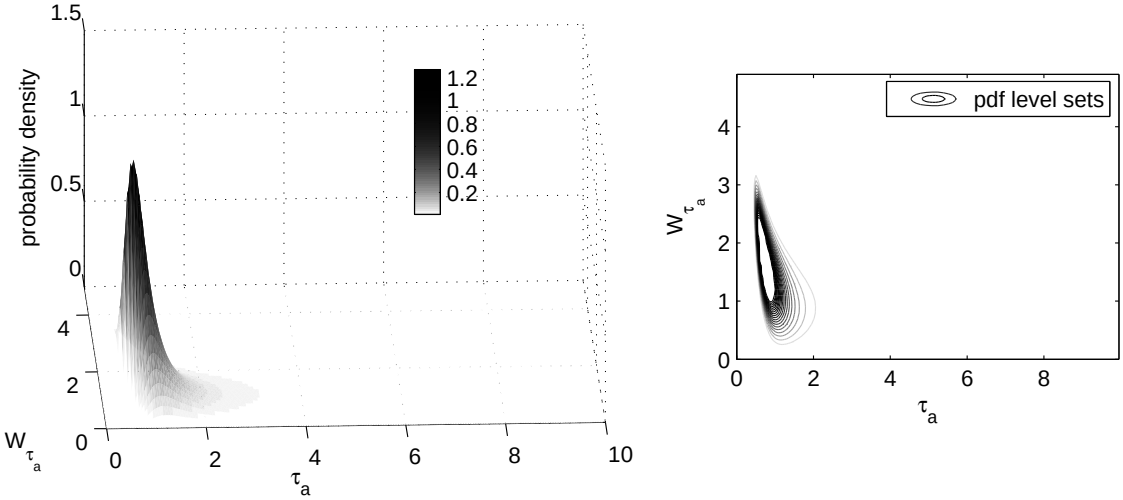

(b) Lachal's probability density function for $X_0 = 0, W_0 = 1, a = 1$

Figure 7.5: Probabilty density function of the first hitting time of the IWP to the constant $a = 1$ for different initial conditions. Level sets show how the pdf is distributed. The uppermost half level sets are not displayed for the sake of visibility.

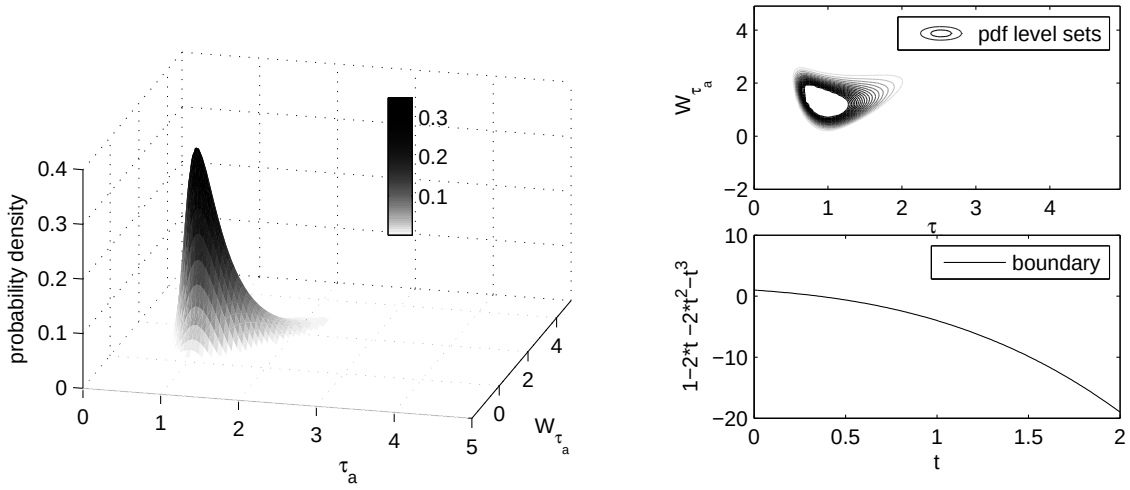

(a) Probability density function of the first hitting time of the IWP to the cubic curve: $t \mapsto 1-2t-2t^2-t^3$ with the initial condition $X_0 = 0, W_0 = 0$. The total mass is 1 in this case.

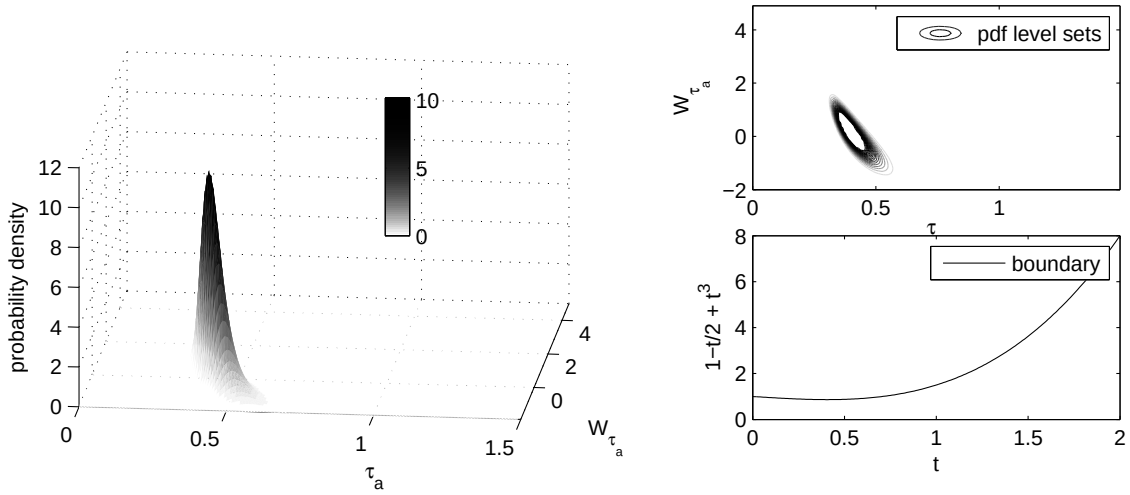

(b) Probability density function of the first hitting time of the IWP to the cubic curve: $t \mapsto 1-\frac{1}{2}t+t^3$ with the initial condition $X_0 = 0, W_0 = 0$. The total mass is ≈ 0.2578 in this case.

Figure 7.6: Probability density function of the first hitting time of the IWP to different cubic boundaries for the same initial conditions.

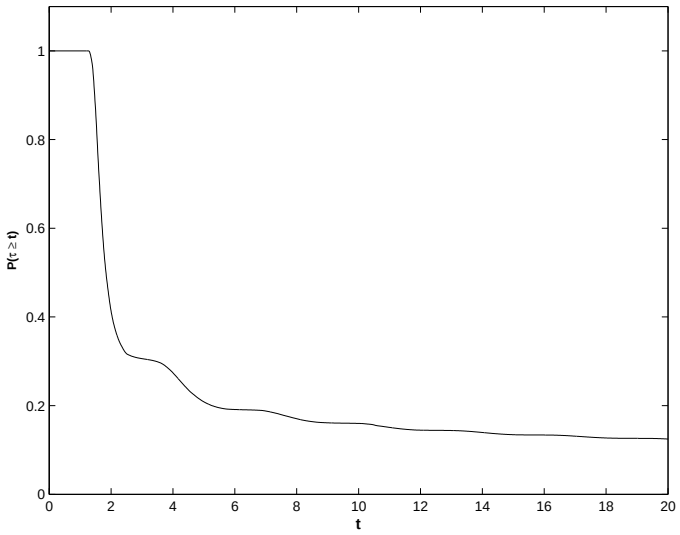

(a) Inverse cumulative distribution of the first hitting time of a linear curve of a DIP defined by the sinusoidal functions $f(x) = sin(x)$ and $g(x) = cos(x)$.

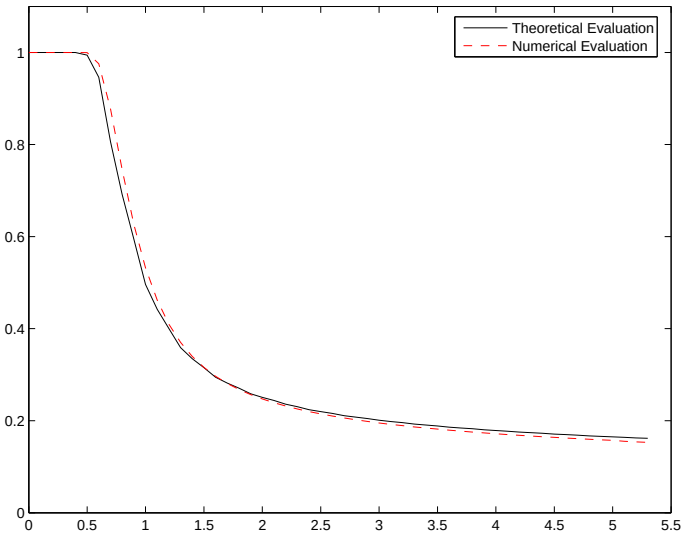

(b) Inverse cumulative distribution function of the IWP to a constant boundary 1 obtained by our method compared with the theoretical evaluation.

Figure 7.7: Inverse cumulative distribution function of the first hitting time of DIPs with different functions to different boundaries.

time	$\mathbb{P}(\tau_\pi \geq t \vert U_0)$
0.1	1.008819
0.2	1.003199
0.3	1.000000
0.4	0.999871
0.5	0.999576
0.6	0.996399
0.7	0.984581

Table 7.1: Table of the probabilities of crossing the sinusoidal function $t \mapsto 1 - sin(\frac{2t}{\pi})$ after time t by an IWP starting at the origin.

(10^6 trials for points in $\mathbb{R}^{10}$ per point of the curve). Indeed, the computation of the function inside the integral on $\mathbb{R}^{2p}$ involves the computation of a fourth order integral which we compute using a Gauss method of the same order of approximation, which takes quite a long computation time. Hence we only show a table of results.

Probably other algorithms would be more efficient, but the corresponding computational issues are outside the scope of the present study.

CONCLUSION

In this chapter, we have provided a method of approximation of the probability distribution of the first hitting time of a Double Integral Process (DIP) to a curved boundary. To our knowledge this is the first result for this problem.

We first obtain a closed-form expression of the probability distribution of the first hitting time of the Integrated Wiener Process (IWP) to a continuous piecewise cubic boundary.

By approximating a general smooth boundary with a piecewise cubic function we use this expression to compute an approximation of the probability distribution of the first hitting time of the IWP to any smooth curved boundary, and prove that it converges (very fast in many cases) towards the probability distribution of the first hitting time of the IWP to the original curved boundary.

We then extend the method to solve the problem of approximating the probability distribution of the first hitting of a DIP to a smooth curved boundary.

Lastly we sketch a numerical procedure based on Monte-Carlo simulation to compute the probability distribution efficiently.

These results have potential applications in many fields of physics and biology.

Part IV

Population Models

So far we investigated models of single neurons. We now turn to population modeling. As discussed in chapter 1, the brain features a great number of neurons interacting in a nonlinear fashion. This system cannot be globally apprehended yet but some structures and functions, emerging at different spatial and temporal scales, can be observed and sometimes modeled.

Realistic networks of neurons are in general untractable. In the first chapter of this part, we introduce an event-based description of neuronal networks based on modelling the times of the spikes in a network. In the other two parts we use a looser, *mesoscopic* scale description of the network, considering homogeneous localized populations of hundreds to thousands of neurons, the neural masses, as elementary building blocks. Chapter 9 discusses the way to get such a mesoscopic description in noisy networks, and chapter 10 studies certain classical mesoscopic models of cortical colums. This mesoscopic scale modeling seems relevant for many reasons. First of all it seems that individual neurons contribute at this scale to the functions of the brain. Moreover, it models MEG and scalp EEG recordings, multi-electrode recordings, in vitro experiments on pharmacologically treated brain slices and new imaging techniques like extrinsic optical imaging corresponding mostly to a bulk signal of a cortical area.

CHAPTER 8

A MARKOVIAN MODEL FOR STOCHASTIC INTEGRATE-AND-FIRE NETWORKS

OVERVIEW

In this chapter we introduce and study a mathematical framework aimed to characterize and simulate networks of noisy integrate-and-fire neurons. This framework is based on a Markovian modelization of the network, similar to the event-based modelization of deterministic networks. In these networks the value of interest at each neuron is not the membrane potential itself but the related *countdown process*, which is defined loosely as the time remaining to the next spike if nothing occurs meanwhile in the network.

We prove that a wide range of integrate-and-fire neuron models and different types of interactions fit into this general mathematical framework and that the resulting dynamics of this countdown process, possibly supplemented with other variables, is an autonomous Markov process (i.e. that does not depend on the membrane's potential). This framework involves renewal processes and has already been studied in the field of random networks in a more restricted setting by Cottrell, Robert, Turova for instance [55, 56, 101, 272, 273], and from a mathematical viewpoint, ergodicity matters have been discussed Fayolle, Menshikov, Malyshev and Borovkov [26, 89].

This modelization provides a very efficient algorithm to simulate large networks of noisy integrate-and-fire neuron models. We discuss different types of implementations, and developed together with Renaud Keriven and Alexandre Chariot a very efficient parallel simulator implemented on GPU. This work was done together with Romain Brette, Olivier Faugeras and Olivier Rochel, and has been presented at the NeuroMath 2006 conference [257] and at the CNS 2007 conference [263], is published as a research report [256].

Contents

INTRODUCTION

Growing experimental evidences tend to establish that spike timings are essential to explain neural computations. This fact has motivated the use of spiking neuron models, rather than the traditional rate-based models. At the same time, a growing number of tools have appeared, allowing the simulation of deterministic spiking neural networks (i.e. in the absence of noise). As discussed in depth in [31], there are two families of algorithms for the simulation of neural networks: synchronous or "clock-driven" algorithms, in which all neurons are updated simultaneously at every tick of a clock, and asynchronous or "event-driven" algorithms, in which neurons are updated only when they receive or emit a spike. Synchronous algorithms can be easily coded and apply to any model. Because spike times are typically bound to a discrete time grid, the precision of the simulation can be an issue. Asynchronous algorithms have been developed mostly for exact simulation, which is possible for simple models. In synchronous algorithms, noise can be added without an excessive increase of complexity, either by adding random external spikes or simulating a stochastic process. The former case can be quite easily applied to asynchronous algorithms, but, as stated in [31], there is no algorithm treating the latter case.

In this chapter we provide an event-based (asynchronous) description of networks of integrate-and-fire neurons with different intrinsic dynamics and different kinds of synaptic integration. This description necessitates the introduction of a special mathematical framework to describe the dynamics of the spikes which is done in section 8.1. We then instantiate neuron models and show how the framework allows to define a Markov variable governing the times of the spikes in the case of inhibitory networks. The case of excitatory networks is slightly more complex, and needs the introduction of one of two biologically plausible elements: the refractory period and /or the synaptic delays. This extension is done in section 8.3. Eventually, we discuss ergodicity matterns on these networks (section 8.4) and possible numerical implementations of these models (section 8.5).

8.1 THEORETICAL FRAMEWORK

8.1.1 Neuron models

In this chapter we build a bridge between a wide range of biological networks models and a general mathematical framework. The type of network we consider is composed of N stochastic integrate-and-fire neurons such as the ones introduced in section 6.2 of chapter 6 (see figure 8.1). Classically, neuron's activity is described by its membrane potential. The membrane potential dynamics we consider in this chapter is stochastic: each neuron receives at his synapses noisy inputs corresponding to the random activity of ion channels and to the external activity of the network, as reviewed in chapter 1. This random spike incoming is here modeled as Brownian motion, using a diffusion approximation (see section 1.4.3). Different types of intrinsic dynamics and of synaptic integration will be considered and can coexist in a given network.

During the time intervals where no spike is emitted in the network, the membrane potential of each neuron evolves independently according to its intrinsic dynamics (see Fig.8.2). When the membrane potential $V^{(i)}(t)$ of the neuron indexed by i reaches its deterministic threshold function $\theta(t)$ at time t_0, the neuron elicits an ac-

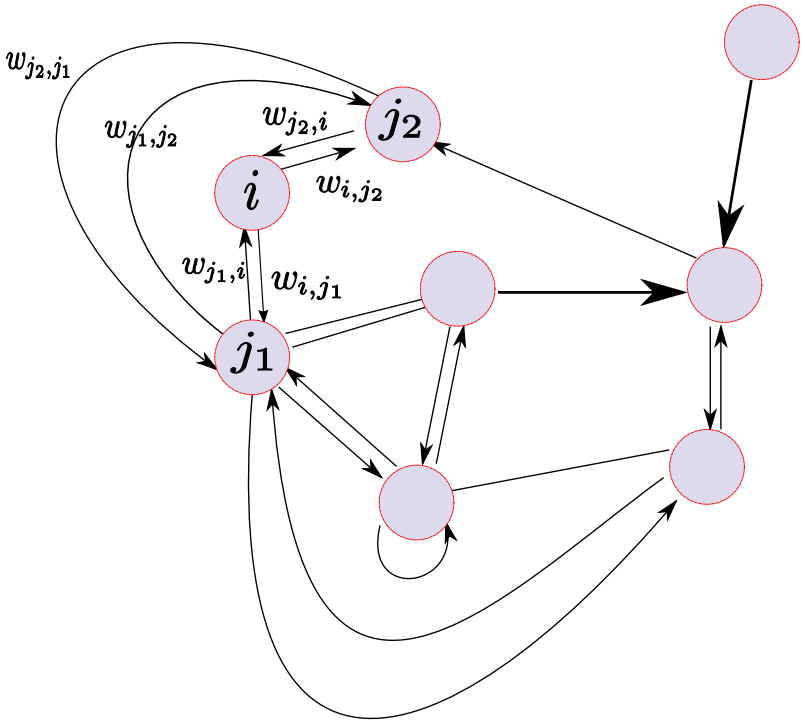

Figure 8.1: A general neural network architecture: the network is composed of neurons (blue circles) connected through a directional connectivity map (black arrow) with synaptic efficiency w_{ij}. The intrinsic dynamics and the effect of an incoming spike on the postsynaptic neuron can be modeled in various fashions.

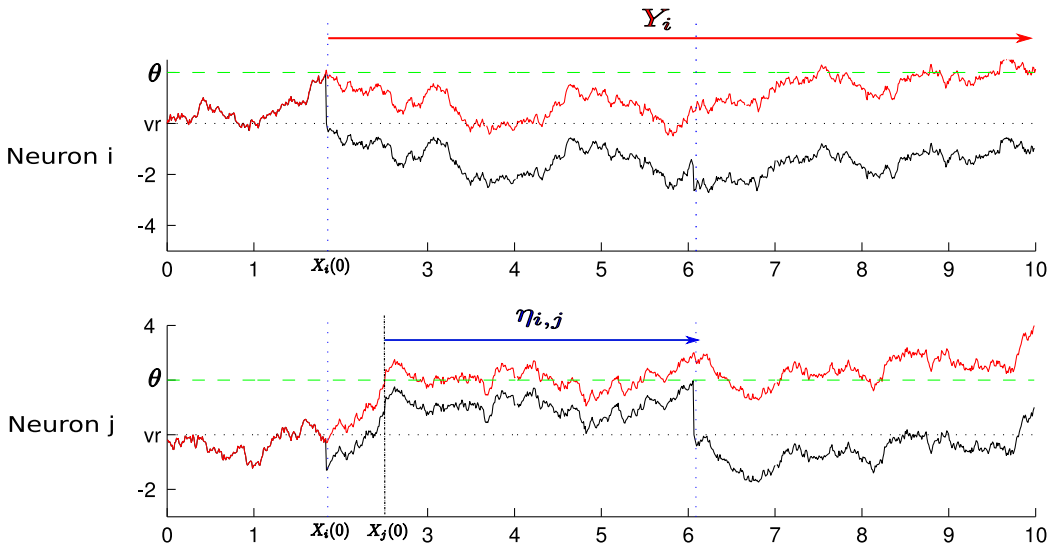

Figure 8.2: A sample trace of the membrane potential for two connected neurons index by i and j. The neuron i is the first to spike in the network: it has the lowest first spike time $X_i(0)$. At this time, the neuron i is reset to $V_r^{(i)} = v_r$ and its next spike time is reset according to Y_i. At this time a spike is sent to its neighboring neurons, among which j, which acts by changing the time of the next spike (in the figure the membrane potential is instantaneously modified) of a random duration η_{ij} which can be positive or negative. This figure was produced in the case of the Perfect Integrate-and-fire model.

tion potential. Subsequently, its membrane potential is reset to a given value $V_r^{(i)}$, and the states of all the postsynaptic neurons j connected to the neuron i is modified. We denote by $\mathscr{V}(i)$ the postsynaptic neighborhood of the neuron i, i.e. the set of neurons that receive the spikes fired by neuron i. The effect of a presynaptic spike received by neuron $j \in \mathscr{V}(i)$ can be modelled in different fashions: it can be considered as having an instantaneous effect on the membrane potential (i.e. $V^{(j)}(t_0) = V^{(j)}(t_0^-) + w_{ij}$ where w_{ij} is the synaptic efficiency of the connection $i \to j$), or more complex, involving for instance synaptic pulses.

This type of model was studied for instance by Brunel and Hakim [36] with the use of the Fokker-Planck equation. Assuming that the network is sparsely connected, they found that in the limit $N \to \infty$ the network exhibited a sharp transition between two regimes: a stationnary regime and a weakly synchronized oscillatory regime. In their model, each neuron is an integrate-and-fire neuron, and is randomly connected to C neurons of the network, and to C_{ext} external neurons. The sparse connectivity assumption corresponds to the limit case $C/N \ll 1$. Interactions between external and internal neurons are delayed by a constant amount of time δ, and the authors show that these delays play a crucial role in the generation of global oscillations. One of the aims of this chapter is to re-express the dynamics of such networks under weaker assumptions and from an event-driven point of view (see for example Reutimann, Giugliano and Fusi [222]).

In details, we are interested in expressing the dynamics of stochastic integrate-and-fire networks in terms of the dynamics of the *hourglass model*, a network model

independently developed in the field of stochastic networks and queuing theory [15, 55, 56, 272, 273]. Let the state of the network be described by a N-dimensional vector $(X_t)_{t\geq 0} = \left((X^{(i)}(t))_{i=1\ldots N}\right)_{t\geq 0}$ having the following dynamics: let $t > 0$,

(i). if $\forall i \in \{1\ldots N\},\ X^{(i)}(t) > 0$ then each component of X decreases linearly with slope -1 in time;

(ii). if $\exists i \in \{1\ldots N\},\ X^{(i)}(t^-) = 0$, then:

- $X^{(i)}(t)$ is reset by drawing from the law of a positive random variable Y_i independent of all the history of the process called the *reset* random variable.
- $\forall j \in \mathscr{V}(i)$, a positive value drawn from the law of the *interaction* random variable η_{ij} is added the state of neuron j is added : $X^{(j)}(t) = X^{(j)}(t^-) + \eta_{ij}$.

This network is of the class of interacting renewal processes, and the interaction variable is always positive. Let us now cast all this in the framework of spiking neurons.

8.1.2 From Biological networks to the Hourglass model

Let us consider a network composed of N stochastic integrate-and-fire neurons with inhibitory interactions. We attach to each neuron at a given time t a positive value called the *countdown value* defined by:

Definition 8.1.1. *[Countdown process]* For each neuron i, let us define $X^{(i)}(t) \geq 0$ to be the remaining time until the next emission of a spike by neuron i if it does not receive any spike meanwhile. We call this stochastic process the *countdown process* of the neuron i.

The dynamics of $X^{(i)}$ is linearly decreasing with slope -1 during the intervals of time where no spike is received or produced:

$$\frac{dX^{(i)}}{dt} = -1 \tag{8.1}$$

At time t, the next spike will occur in neuron $i = \mathrm{Arg\,Min}_{j\in 1\ldots N} X^{(j)}(t)$ at time $t + X^{(i)}(t)$. In most of the cases, for instance in the case where all the random variables have a density with respect to Lebesgue's measure, the probability for two neurons to spike exactly at the same time is null when the network is inhibitory. We therefore assume that only one neuron spikes at a given time. At spike time, $X_t^{(i)}$ is instantaneously reset by drawing from the law of a random variable, noted Y_i, which has the same distribution as the first hitting time of the stochastic process $(V_t^{(i)})_{t\geq 0}$ starting from $V_r^{(i)}$ to the boundary $\theta(t)$ (the distribution of the interspike interval in terms of neural models). The states of all neurons just before the spike are given by: $X^{(j)}\left((t + X^{(i)}(t))^-\right) = X^{(j)}(t) - X^{(i)}(t)$. All the neurons connected to neuron i receive a spike, and the time to the next spike is therefore modified by a random value, which can depend on the value of the postsynaptic membrane potential at the time when it receives the spike (see Fig 8.3). The interaction variable only depends on the postsynaptic dynamics of the membrane potential and on the synaptic efficiency w. When the neuron j receives a spike from the neuron i at time t, the time to the next spike fired by neuron j is modified. For instance in the case of instantaneous interactions, the random variable corresponding to the additional time resulting from

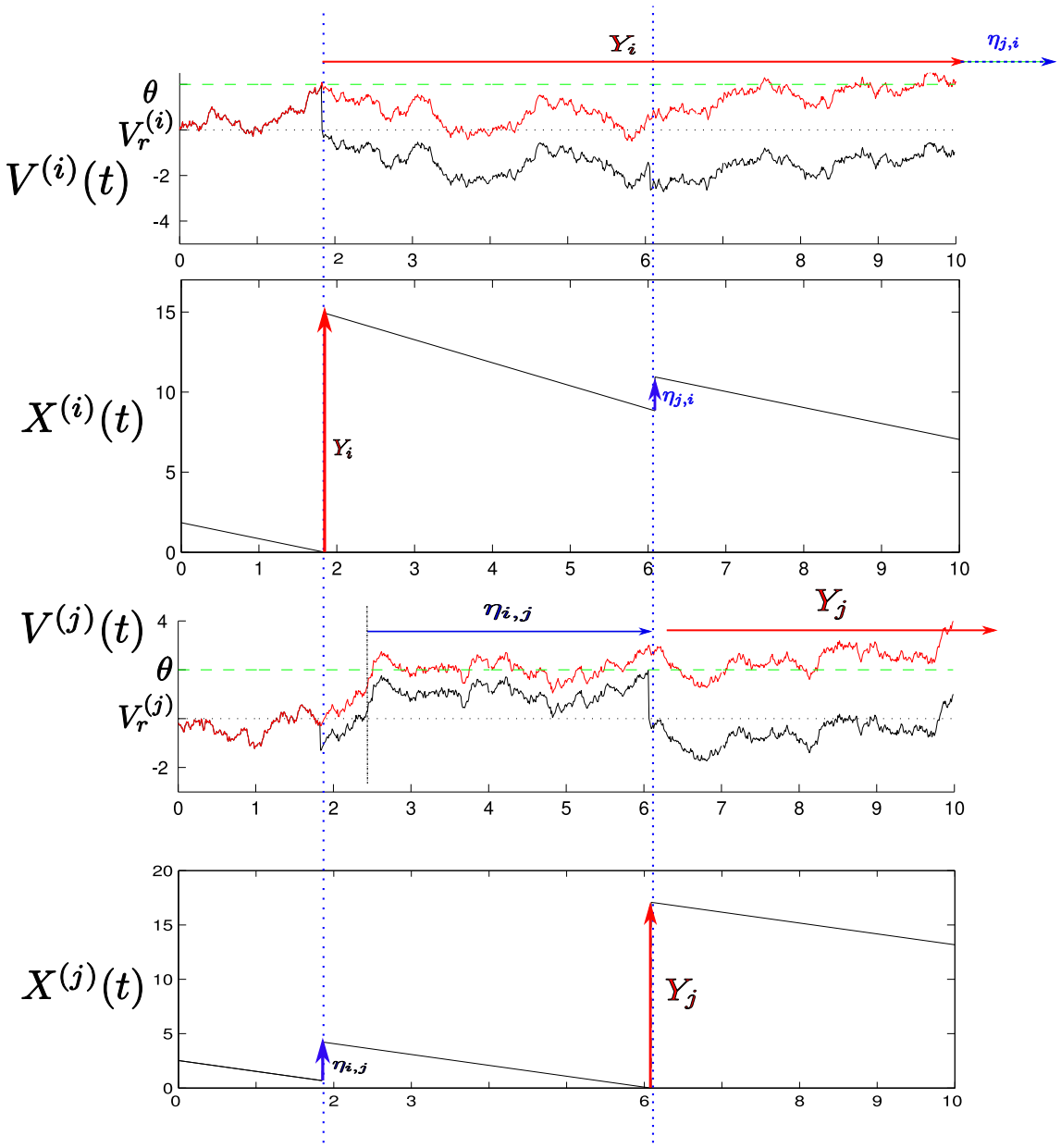

Figure 8.3: A representation of a sample path for the countdown process and the related membrane potential in the case of the perfect integrate-and-fire neuron represented in figure 8.2.

the reception of a new spike is equal to the difference between the time to reach the threshold starting from $V^{(j)}(t)+w_{ij}$ and the time to reach the threshold starting from $V^{(j)}(t)$. Hence in the general case, this random variable depends on the value of the potential at time t. This additional time is denoted η_{ij} and corresponds to the interaction random variable of the hourglass model. But in our case, it is no more a random variable independent of the process. Interestingly, in most of the models considered in section 8.2, we will see that it depends in fact only on $X^{(j)}$, so that the update reads $X^{(j)}(t+X^{(i)}(t)) = X^{(j)}(t) - X^{(i)}(t) + \eta_{ij}(X^{(j)}(t) - X^{(i)}(t))$, where $x \mapsto \eta_{ij}(x)$ is a random function.

Therefore, the dynamics of the spikes can be modeled through the use of the countdown process $X(t) \stackrel{\text{def}}{=} (X^{(i)}(t))_{1\leq i\leq N}$. Up to an additional Markov chain, this model will be a continuous time Markov process, as we will show in section 8.2. The process $(X_t)_t$ defined is piecewise continuous, so the analysis of Davis in [66] can be applied to it. Our case is even simpler since the discontinuities are very simply related to the value of the process. This special property implies that studying the continuous time stochastic process is strictly equivalent to considering a discrete time Markov chain. Indeed, let (t_n) denote the sequence of the spikes times of emission for all the neurons of the network, (Z_n) the sequence of the states just before each spike and (X_n) the vector of states just after each spike. The study of the continuous process $X(t)$ is equivalent to the study of one of the following Markov chains:

$$Z_n = X(t_n^-) \tag{8.2}$$

$$X_n = X(t_n) \tag{8.3}$$

In section 8.2, we study inhibitory networks and show that the spike dynamics can be described as a Markov chain using the countdown process. We then extend in section 8.3 these results to balanced networks (including excitatory and inhibitory connections). We will see that in many cases, these random variables can be related to first hitting times of stochastic processes. Therefore, the study we did in chapters 6 and 7 will be very useful for studying and simulating the processes, as we will see in section 8.5.

8.2 Inhibitory Networks with instantaneous interactions

In this section we consider different types of models of linear integrate-and-fire neurons and different types of inhibitory synaptic interactions, and show that spike dynamics can be described by a simpler Markov chain, similar to the hourglass model, and identify the law of the reset and interaction random variables.

8.2.1 The reset random variable

The reset random variable of the countdown process has the law of the first hitting time of the membrane potential process to the threshold function $\theta(t)$. Indeed, when a neuron elicits a spike, its membrane potential is reset to a certain value[1]. Therefore, if no interaction occurs for neuron i, the time before the next spike it fires has the law of the first hitting time of the membrane potential to the threshold.

[1]The reset value can also be considered as a random variable, with no additional complexity. The results we obtain for a constant reset value can be readily extended to this more general model.

When parameters of the model are not stationary, for instance when the input current or the threshold are deterministic non-constant functions of time, the reset random variable depends on the last spiking time of each neuron. Therefore in that case, in order to define the reset random variable at each spike time, one has to know the absolute time. To this purpose, we add to the dynamics a vector made of the last spike times of the each neuron, in order to be able to define the reset random variable.

8.2.2 Perfect integrate-and-fire models

PIF neuron with instantaneous synapses

We start by considering the Perfect Integrate-and-Fire (PIF) neuron with external inputs and Brownian noise[2]. The membrane potential of the neuron i, denoted $V^{(i)}(t)$, is hence driven by the following equation between two spikes:

$$\tau_i dV^{(i)}(t) = I_e^{(i)}(t)dt + \sigma_i dW_t^{(i)} \tag{8.4}$$

where τ_i is the membrane potential time constant, $I_e^{(i)}(t)$ is the input current, σ_i the standard deviation of the noise and $(W^{(i)})_{1\leq i\leq N}$ are independent Brownian motions, which represent noisy synaptic stimulations[3]. The neuron fires when its membrane potential reaches the threshold $\theta(t)$): the membrane potential is reset to a value $V_r^{(i)}$ and a spike is emitted.

$$V^{(i)}(t^-) = \theta(t)) \Rightarrow V^{(i)}(t) = V_r^{(i)} \tag{8.5}$$

In the absence of interactions, $V^{(i)}(t)$ integrates the entry $I_e^{(i)}$ with an additive noise proportional to a Brownian motion, i.e. :

$$V^{(i)}(t) = V^{(i)}(0) + \int_0^t I_e^{(i)}(s)\,ds + \sigma_i W_t^{(i)} \tag{8.6}$$

In this model, since the synaptic integration is instantaneous, it makes sense to consider instantaneous synaptic interactions. More precisely, when the neuron j receives a spike from a presynaptic neuron i at time t^*, then its membrane potential is instantaneously increased by the synaptic weight:

$$V^{(j)}(t^*) = V^{(j)}(t^{*-}) + w_{ij} \qquad \forall j \in \mathscr{V}(i) \tag{8.7}$$

v If the neuron i fired at time t^*, the reset random variable of the related countdown process has the law of the first hitting time of the Brownian motion starting from $V_r^{(i)}$ to the boundary $\frac{1}{\sigma_i}(\theta(t+t^*) - \int_{t^*}^{t^*+t} I_e^{(i)}(s)\,ds)$ as discussed in section 8.2.1. This law can be computed by Volterra's, Durbin's or Girsanov's method if the input current and/or the threshold are non stationary, or known in a closed form if the input current is constant and the threshold an affine function of time, as reviewed in chapter 6.

[2]This assumption corresponds to the assumption that the time constant of the leak is very large compared to the time scale of the observation, of the inputs, and of the firing rate.

[3]It would be possible to replace the Brownian motions by instantaneous increments ($V^{(i)} \to V^{(i)} + \delta$) triggered according to a Poisson process (the equation (8.4) is the diffusion approximation of this type of excitation). This would change considerably the following study, since the process is no more continuous between two consecutive spikes

The interaction random variable is deduced from the effect of a presynaptic spike incoming at a synapse. If neuron j receives an inhibitory spike from neuron i at time t^*, the membrane potential at time $X^{(j)}(t^*)$ reads:

$$V^{(j)}(X^{(j)}(t^*)) = \theta(X^{(j)}(t^*))v + w_{ij} < \theta(X^{(j)}(t^*))$$

From this value the membrane potential integrates the input and the noise, and the additional time before the next spike time of neuron j is

$$\eta_{ij} \sim \inf\{t>0; \theta(X^{(j)}(t^*)+t^*)+w_{ij}+\int_0^t I_e^{(i)}(s+X^{(j)}(t^*)+t^*)\,ds+\sigma_i W_t^{(i)} = \theta(t+t^*+X^{(j)}(t^*))\}.$$

It has therefore the law of the first hitting time of the standard Brownian motion to the boundary

$$t \mapsto \frac{1}{\sigma_i}\left(\theta(X^{(j)}(t^*)+t^*+t) - \theta(X^{(j)}(t^*)+t^*) - w_{ij} - \int_0^t I_e^{(i)}(s+t^*+X^{(j)}(t^*))\,ds\right).$$

In the case of stationary inputs and threshold, this random variable has the law of the first hitting time of a drifted Brownian motion starting from 0 to the constant barrier $|w_{ij}|$, whose density reads (see chapter 6):

$$p^{(i,j)}(t) = \frac{|w_{ij}|}{\sqrt{2\pi t^3}} e^{-\frac{(w_{ij}-I_e t)^2}{2t}} \mathbb{1}_{\mathbb{R}_+^*}(t) \tag{8.8}$$

In the case of stationary inputs, we can see that the countdown process is an *autonomous Markov process*. Indeed, the sequence $(X_n)_{n\geq 0}$ (or equivalently $(X_t)_{t\geq 0}$) is a Markov chain with transitions given by the law of the reset and interaction random variables, which only depend on the parameters of the model, and therefore fits in the framework of the hourglass model.

If the input current and/or the threshold depend upon time, then the chain $(X_n, t_n)_{n\geq 0}$ where t_n is the time of the last spike fired in the network (or equivalently $(X_t, t)_{t\geq 0}$) is an autonomous Markov chain (resp. process). Indeed, the we have seen that in that case both the reset and the interaction random variables depend on the last spike time, and that the interaction random variable depends on $X^{(j)}(t^*)$. More precisely, let (X_n, t_n) be the state of the Markov chain after $n-1$ spikes. Define $i_n = Argmin_i\{X_n^{(i)}\}$. The neuron i_n fires the n^{th} spike, and is reset by drawing from the law of the first hitting time of the standard Brownian motion starting from $V_r^{(i)}$ to the boundary

$$t \mapsto \frac{1}{\sigma_i}\left(\theta(t+t_n+X^{(i_n)}) - \int_0^t I_e^{(i)}(t_n+X^{(i_n)}+s)\,ds\right),$$

and the state of neurons j connected i_n is updated by adding an independent random variable $\eta_{i_n j}$ having the law of the first hitting time of the standard Brownian motion to the boundary

$$t \mapsto \frac{1}{\sigma_i}\left(\theta(X_n^{(j)}+t_n+t) - \theta(\theta(X_n^{(j)}+t_n) - w_{ij} - \int_0^t I_e^{(i)}(s+\theta(X_n^{(j)}+t_n)\,ds\right),$$

and eventually $t_{n+1} = t_n + X_n^{(i_n)}$.

Perfect integrate-and-fire neuron with synaptic integration

We now extend the results of the perfect integrate-and-fire model by considering that inputs are integrated at the level of the synapse with a characteristic time constant $\tau_s \neq 0$. The membrane potential satisfies the equations:

$$\begin{cases} \frac{dV_t^{(i)}}{dt} & = I_e^{(i)}(t) + I_s^{(i)}(t) \\ \tau_s^{(i)} dI_s^{(i)}(t) & = -I_s^{(i)}(t)dt + \sigma_i dW_t^{(i)} \end{cases} \tag{8.9}$$

whose solution reads:

$$V_t^{(i)} = V^{(i)}(0) + \int_0^t I_e^{(i)}(s)\,ds + \tau_s^{(i)}(1 - e^{-t/\tau_s^{(i)}})I_s^{(i)}(0) + \sigma_i \int_0^t \int_0^s e^{-(s-u)/\tau_s^{(i)}}\, dW_u^{(i)}\, ds,$$

expression that involves a DIP (see chapter 7). A spike is emitted when the membrane potential reaches a threshold θ assume constant here.

If we further consider that $\tau_s^{(i)}$ is very big compared to the time constants of the observation, we obtain the perfect integrate-and-fire model with perfect synaptic currents:

$$V_t^{(i)} = V(i)(0) + \int_0^t I_e^{(i)}(s)\,ds + I_s^{(i)}(0)t + \sigma_i \int_0^t W_s^{(i)}\, ds,$$

which involves an IWP.

We now consider the related countdown process $(X_t)_t$ and compute the random variables necessary to the definition of its dynamics. The related reset random variable in the case of the exponentially decaying synaptic currents has the law the first hitting time of the DIP $\int_0^t \int_0^s e^{-(s-u)/\tau_s^{(i)}}\, dW_u^{(i)}\, ds$ or $\int_0^t W_s^{(i)}\, ds$ to a curved boundary depending on the inputs of the neuron and the initial condition of the synaptic input. These hitting time can be approximated using the framework we developed in chapter 7 and no closed-form solution can be provided.

In the case where the decay time of the synapse is not taken into account, this reset random variable has the law of the first hitting time of an IWP to the curve $V^{(i)}(0) + \int_0^t I_e^{(i)}(s)\,ds + I_s^{(i)}(0)t$. Therefore, we have closed-form expressions for the pdf of the law of this random variable for polynomials input currents of order lower or equal to 2 (see section 7), depending on the initial condition on the input current $I_s^{(i)}(0)$.

Let us now compute the interaction random variable. We first consider instantaneous synaptic integration of the spikes. Using the linearity of the equation, the interaction random variable has the law of the first hitting time of the threshold θ of the membrane potential process starting from $(\theta + w_{ij}, I_s^{(i)}(X_j))$ to reach the threshold θ, and can therefore be computed using the same approximations or formulas depending on the model we choose and the type of input current considered.

The case of integrated inputs makes more sense: it corresponds to the assumption that whatever its origin, the inputs received at the level of the synapse are integrated in the same fashion. In that case the effect of an incoming spike on a postsynaptic neuron is added instantaneously to the synaptic current. Therefore, using the same technique as before, we can obtain the law of the interaction variable. For the perfect integrate and fire neuron with exponentially decaying synaptic current, if neuron j receives an incoming spike from neuron i at time t^*, the law of this random variable is deduced from the law of the first hitting time of the related DIP starting from $(\theta + w_{ij}\tau_s^{(i)}(1 - e^{-t^*/\tau_s^{(i)}}), I_s(X^{(j)}(t^*) + w_{ij}e^{-X^{(j)}(t^*)/\tau_s^{(i)}})$ to reach the threshold θ. In the case

of the perfect integrate-and-fire neuron with perfect synapses, the law of the interaction random variable is given by the law of the first hitting time of the related IWP starting from $(\theta + t^* w_{ij}, I_s(X^{(j)}(t^*)) + w_{ij})$ to reach the threshold θ.

In these cases the countdown process is not a Markov process by itself. But considering in addition the value of the synaptic current at the time of the next spike $I_s(n)$ the time of the last spike fired time t_n constitutes a Markov chain whose modeling the times of the spikes. More precisely, consider $(X_n, I_s(n), t_n)$ the countdown process together with the synaptic current at the next spike time and t_n the last spike time. The first spike will be fired from the neuron i_n having the lowest countdown value. It will fire at time $t_{n+1} = t_n + X_n^{(i_n)}$. Its countdown value and the value of the synaptic current at the next spike time is computed by drawing from the law of the pair composed of next spike time and the relative location of the synaptic currents at this time (see chapter 7). The countdown value and the future synaptic current of each neuron $j \in \mathscr{V}(i)$ is updated by drawing from the law of the first hitting time of the membrane potential of neuron j, and the other neurons' states are unchanged.

8.2.3 Leaky integrate-and-fire models with instantaneous synapses

We now take into account the leak of the membrane potential, but still consider the synaptic integration instantaneous, Therefore this model corresponds to the one we introduced in section 6.2.1. The general Leaky Integrate-and-Fire (LIF) equation with instantaneous synaptic and noisy input currents reads :

$$\left\{ \begin{array}{lcl} \tau_i dV^{(i)} & = & -(V^{(i)} + I_e^{(i)}(t))dt + \sigma_i dW_t^{(i)} \\ V^{(i)}(t^-) & = & \theta \Rightarrow V^{(i)}(t) = V_r^{(i)} \end{array} \right. \tag{8.10}$$

where $(W_t^i)_{1 \leq i \leq N}$ are independent Brownian motions. The reset random variable is the same for all synaptic interactions, and is distributed as the hitting time of the threshold θ starting from $V_r^{(i)}$ of the process defined by (8.10) with time-shifted input current $I_e^{(i)'}(t) = I_e^{(i)}(t + t^*)$.

We consider that the membrane potential follows the equation (8.10), together with the spiking condition:

$$V^{(i)}(t^-) = \theta \Rightarrow \left\{ \begin{array}{lcll} V^{(i)}(t) & = & V_r^{(i)} & \\ V^{(j)}(t) & = & V^{(j)}(t^-) + w_{ij} & \forall j \in \mathscr{V}(i) \end{array} \right. \tag{8.11}$$

Let t^* be the time when the neuron j receives a spike from neuron i. We note $V^{(j)}$ its membrane potential, $V_{(j)}^* := V^{(j)}(t^{*-})$ and $X_{(j)}^* := X^{(j)}(t^{*-})$. We have :

$$V^{(j)}(t^* + t) = (V_{(j)}^* + w_{ij}) e^{-t/\tau_j} + \frac{1}{\tau_j} \int_0^t e^{(s-t)/\tau_j} I_e^{(j)}(s + t^*)\, ds + \frac{1}{\tau_j} \int_0^t e^{(s-t)/\tau_j} \sigma_j\, dW_s^{(j)}$$

Let $\widetilde{V}^{(j)}$ the membrane potential of the neuron j without any interaction with other neurons. It satisfies the equation:

$$\widetilde{V}^{(j)}(t^* + t) = V_{(j)}^* e^{-t/\tau_j} + \frac{1}{\tau_j} \int_0^t e^{(s-t)/\tau_j} I_e^{(j)}(s + t^*)\, ds + \frac{1}{\tau_j} \int_0^t e^{(s-t)/\tau_j} \sigma_j\, dW_s^{(j)}$$

Therefore we have:

$$V^{(j)}(t^* + t) = \widetilde{V}^{(j)}(t^* + t) + w_{ij} e^{-t/\tau_j} \tag{8.12}$$

(note that this property simply comes from the fact that the equation of the LIF neuron is linear). For $t = X^*_{(j)}$ we have $\widetilde{V}^{(j)}(t^* + X^*_{(j)}) = \theta$ and, from (8.12), we have :

$$V^{(j)}(t^* + X^*_{(j)} + t) = (\theta + w_{ij} e^{-X^*_{(j)}/\tau_j}) e^{-t/\tau_j} + \frac{1}{\tau_j} \int_0^t e^{(s-t)/\tau_j} I_e^{(j)}(s + t^* + X^*_{(j)})\, ds + \frac{1}{\tau_j} \int_0^t e^{(s-t)/\tau_j} \sigma_j\, dW_s^{(j)} \quad (8.13)$$

It is clear from equation (8.12) that the hitting time of the barrier θ by the process $V^{(j)}$, conditionally on the random variable $X^*_{(j)}$ is the sum of $X^*_{(j)}$ and an independent random variable whose law is equal to the hitting time to the barrier θ of the process (8.10) with initial condition $V^{(j)}(0) = \theta + w_{ij} e^{-X^*_{(j)}/\tau_j}$ and with the time shifted input current $\tilde{I}_e^{(j)}(t) := I_e^{(j)}(t + t^* + X^*_{(j)})$.

$$\eta_{ij}(u) := \inf \left\{ t > 0;\ U^{(j)}(t) = \theta | U^{(j)}(0) = \theta + w_{ij} e^{-X^*_{(j)}/\tau_j} \right\} \quad (8.14)$$

where $U^{(j)}(t)$ is the solution of equation (8.10) with the time-shifted current specified.

The problem of the first hitting time of the LIF neuron with constant or curved boundaries was addressed in chapter 6, no closed-form solution is available for the pdf of this law, which can be computed numerically using for instance Volterra's, Durbin's and Girsanov's methods.

An important remark is that this random variable only depends on $X^*_{(j)}$. Conditionally to $X^*_{(j)}$, the added random variable is independent of the past of the process, so the sequence $X^{(j)}$ is Markovian. Furthermore, the network countdown process dynamics is autonomous: we do not need to refer to the underlying membrane's potential to describe its evolution. This is very interesting since we can study and simulate this random variable by itself. Therefore, the variable (X_t), possibly completed with the time t if the input current or the threshold are not stationary, is a Markov process, and this process sampled at the times of the spikes is a Markov chain. Furthermore, the law of the zeros of this process is equal to the one of the spikes of the underlying network.

LIF model with general post-synaptic current pulse

In this section we consider a LIF neuron described by (8.10). Following the models presented in [105, section 4.1.3], each presynaptic spike generates a postsynaptic current pulse. More precisely, if the neuron i spikes at time t^* and $j \in \mathscr{V}(i)$ receives the spike, then this neuron feels an additional input current given by:

$$I_{PSP}(t^* + t) = w_{ij}\, \alpha(t) \quad (8.15)$$

We include the integration of the spikes to the the input current $\widetilde{I_e}$

$$\widetilde{I}_e^{(j)}(t) = I_e(t) + \sum_{i \neq j} \sum_{t^j \leq t_i^j \leq t} w_{ij}\, \alpha(t - t_i^j)$$

where t^j denotes the time of the last spike emitted by the neuron j and t_i^j the sequences of spikes transmitted from the neuron i to the neuron j.

The same calculations lead to:

$$V^{(j)}(t^* + X^*_{(j)}) = \theta + w_{ij} e^{-X^*_{(j)}/\tau_j} \int_0^{X^*_{(j)}} \alpha(s) e^{s/\tau_j} ds \tag{8.16}$$

Hence the additional time induced by the reception of a presynaptic spike from neuron i has the law of the first hitting time of the stochastic process $V^{(j)}$ starting from the value (8.16) to the threshold θ, with a new external current.

For general pulses, the countdown process cannot be considered as a Markov process since its dynamics depends on the whole sequence of spikes in the network until time t. Nevertheless this analysis can be simplified if considering postsynaptic current pulses solutions of an ordinary differential equation. This is a very general case, and covers most of the usual models of synaptic coupling (see for instance the works of van Rotterdam and colleagues for the modeling of postsynaptic current pulses [275]). These postsynaptic pulses are in general considered as an exponentially decaying pulse, when taking into account only the decay of the synaptic integration and considering the rise time null. In that case the postsynaptic pulse has the form:

$$\alpha(s) = k e^{-s/\tau_s} \mathbb{1}_{s \geq 0}$$

which is solution of a first order linear differential equation. An even more realistic model taking into account the rise time τ_r of the synapse and its decay τ_s is modelled by the following α function for $\tau_r \neq \tau_s$

$$\alpha(s) = \frac{k}{\tau_s - \tau_r} \left[e^{-s/\tau_s} - e^{-s/\tau_r} \right] \mathbb{1}_{s \geq 0}$$

and for $\tau_r = \tau_s$,

$$\alpha(s) = k s e^{-s/\tau_s} \mathbb{1}_{s \geq 0}$$

In that case the pulse is solution of a second order linear differential equation.

To take into account this synaptic integration of spikes in our framework, we have to extend the phase space of our Markov chain. More precisely, the Markovian model we consider includes a second variable, the spike-induced current $(I^i_a(t))_{i=1\ldots N, t\geq 0}$. If we denote by $\mathscr{L}$ the linear differential operator of the α function, the spike induced current is solution of the equation

$$\mathscr{L} I_a = \delta,$$

where δ is the Dirac distribution.

The new membrane potential equation for a given neuron i in the network is now given by:

$$\begin{cases} \tau_i dV^{(i)}_t & = (-V^{(i)}_t + I_e(t))\, dt + I^{(i)}_a(t)\, dt + \sigma_i dW_t \\ \mathscr{L} I^{(i)}_a(t) & = 0 \end{cases}$$

The Markovian variable we consider is now the process $(X_t, I_a(t))_{t\geq 0}$. When a neuron i elicits a spike, i.e. when its countdown reaches 0 at time t^*, its countdown value is reset by drawing from the law of the first hitting time of the membrane potential with initial condition $(V^{(i)}_r, I^{(i)}_a(t^*))$ to the threshold and for all neuron $j \in \mathscr{V}(i)$, their spike-induced current $I^{(j)}_a(t^*)$ are instantaneously updated by adding the synaptic efficiency w_{ij} : $I^{(j)}_a(t^*) = I^{(j)}_a(t^{*-}) + w_{ij}$. Simulating this Markov process, that can be sampled at the times of the spike emission, is equivalent from the spikes point of view as simulating the whole membrane potential process.

8.2.4 LIF model with exponentially decaying synaptic integration

We now take into account the decay time of synapse at the level of the noise integration itself. In this case the membrane potential and the synaptic noise are coupled via the following differential equation:

$$\begin{cases} \tau_i dV^{(i)} &= (\mu_i - V^{(i)}(t))dt + I_e^{(i)}(t)dt + I_s^{(i)}(t)dt \quad 1 \leq i \leq N \\ \tau_s^{(i)} dI_s^{(i)} &= -I_s^{(i)}(t)dt + \sigma_i dW_t^i \end{cases} \tag{8.17}$$

and the spiking condition reads:

$$V^{(i)}(t^-) = \theta \Rightarrow \begin{cases} V^{(i)}(t) &= V_r^{(i)} \\ I_s^{(j)}(t) &= I_s^{(j)}(t^-) + w_{ij} \mathbb{1}_{j \in \mathscr{V}(i)} \end{cases} \tag{8.18}$$

Qualitatively, when a spike is received by a neuron, the synaptic current I_s integrates the spike and the effect on the membrane potential is smoother. Therefore in this model it is interesting to consider post-synaptic pulses having the same dynamics as the noise integration, i.e. solution of the differential equation:

$$\tau_s^{(i)} \frac{\mathrm{d}I_a^{(i)}}{\mathrm{d}t} = -I_a^{(i)}(t).$$

The very same analysis could be done if we considered an instantaneous spike integration, but we do not present the results here since it seems strange to us to consider two levels of synaptic integration: the noise integration and the spike integration. The calculations can nevertheless be performed exactly as in the case of the perfect integrate-and-fire.

The reset random variable is given by the first hitting time of the membrane potential stochastic process. The same type of calculations as in the previous section yield, for $j \in \mathscr{V}(i)$ and $\tau_j \neq \tau_s^{(j)}$ the relationship :

$$V^{(j)}(t^* + t) = \widetilde{V}^{(j)}(t^* + t) + e^{-t/\tau_j} w_{ij} \frac{1 - e^{-\alpha_j t}}{\alpha_j} \tag{8.19}$$

where $\alpha_j = \frac{1}{\tau_s^{(j)}} - \frac{1}{\tau_j}$ and again $\widetilde{V}^{(j)}(t^* + t)$ the membrane potential of the neuron j without any interaction. We can see that after the time $X^*_{(j)}$, the membrane potential of j is $\theta + w_{ij} e^{-t/\tau_j} \frac{1 - e^{-\alpha_j X^*_{(j)}}}{\alpha_j}$. The evolution of the potential $V^{(j)}$ after $t^* + X^*_{(j)}$ and conditionally on $X^*_{(j)}$ and $I_s(t^*)$ is independent of the past, so we have to wait for the process (8.18) to reach the threshold θ from the initial condition $\theta + w_{ij} e^{-t/\tau_j} \frac{1 - e^{-\alpha_j X^*_{(j)}}}{\alpha_j}$ and with the "time and space" shifted currents $\tilde{I}_e^j(t) := I_e^j(t + t^* + X^*_{(j)}) + w_{ij} e^{-\frac{X^*_{(j)}}{\tau_s^{(j)}}}$.

In the case $\tau_j = \tau_s^{(j)}$ we only have to replace the expression $\frac{1 - e^{-\alpha_j X^*_{(j)}}}{\alpha_j}$ by $X^*_{(j)} w_{ij} e^{-t/\tau_j}$, and the change in the currents is the same.

Therefore, the variable $(X_t, I_s(t))$ is Markovian and we deduce the precise firing times from its study. This Markovian variable requires to evaluate the law of the first hitting time of a DIP to a curved boundary, which can be achieved using the technique provided in chapter 7. As in the case of the perfect integrate-and-fire neuron, we can show that this process, possibly augmented with the time process t, and possibly

sampled at the times of the spikes, satisfy the Markov property and the law of the zeros of the Markov process is the same as the law of the spikes of the underlying network.

Let us precise its dynamics in the case of non-stationary inputs. The dynamics of the countdown process together with the synaptic current at the next firing time and the last spike time can be described as follows: consider that this process after the n^{th} spike is (X^n, I_s^n, t^n). Then the next spike will be fired from the neuron i_n having the lowest countdown value. It will fire at time $t^{n+1} = t^n + X_{i_n}^n$. Its countdown value will be reset to the first hitting time of the related DIP, and as we have seen in chapter 7, the law of the pair composed of next spike time and the relative location of the synaptic currents at this time is known. Therefore, by drawing from the law of this pair, we have the new countdown value and the future synaptic current at the time of the next spike for i_n. Similarly, each neuron $j \in \mathscr{V}(i)$ is updated according to the law of the first hitting time of the related membrane's potential starting with input current given by I_j^n to reach a given threshold, and therefore the new countdown value and the future location of the input current are computed at the same time using the results of chapter 7. The other neurons states are unchanged. It is clear that the law of the spikes is the same as the law of the zeros of the countdown process.

8.2.5 LIF models with noisy conductances

The interactions considered in the last subsection are reasonable models of current interaction. Nevertheless reality it is even more complicated. Indeed, as discussed in chapter 1, the effect of a spike on the postsynaptic cell does not directly results in the generation of currents. It results in changes in the membrane's conductance, and these modifications produce a ionic current. As discussed in section 1.2.6 of chapter 1, this resulting current is approximately proportional to the membrane potential. The modulation of the conductance of the post-synaptic membrane has a certain time course $g(t-t^*)$, which is in general considered as constant, to keep the model tractable. Here again we consider the noise and the spikes integrated in the same fashion, i.e. via the conductances. Therefore the membrane potential when no spike is received is solution of the linear stochastic differential equation:

$$\begin{cases} dV^{(i)} &= (I_e^{(i)}(t) - \lambda_i(V_t^{(i)} - V_{rev}^{(i)}))\,dt + I_s^{(i)}(t)\,dt + \sigma_i g_i\,(V^{(i)} - V_{rev}^{(i)})\,dW_t^i \\ V^{(i)}(t^-) &= \theta \Rightarrow V^{(i)}(t) = V_r^{(i)} \end{cases} \tag{8.20}$$

In this equation the term $I_s^{(i)}$ corresponds to the current generated by the spikes. When neuron j receives a spike from one of its neighbors i, a current is generated, which has the value $w_{ij}g(V^{(j)} - V_{rev})$ (V_{rev} is the reversal potential of the synapse). Note that we artificially introduced V_{rev} in the leak term, which amounts to formally changing the current $I_e^{(i)}$, in order to integrate more simply this equation. We clearly see in this equation the effect of a presynaptic spike on the conductances. More precise models take into account the vanishing of this effect in the time. General time profiles of the postsynaptic conductance pulses are alpha functions as described in the previous section, and hence can be modeled as solution of a linear ordinary differential equation of order one, two or greater. Nevertheless, even in the simpler case, we will see that these models cannot be expressed as a Markovian model in function of the countdown process and possibly other real processes.

We first consider the case where the neuron j receives a spike at time t^* from neuron i and that this increases the conductance by a coefficient $w_{ij}g$. The solution of the membrane potential equation after time t^* reads:

$$V^{(j)}(t+t^*) = V^*_{(j)} Z_t + \int_0^t I_e^{(j)}(s+t^*) Z_{t-s}\, ds \tag{8.21}$$

where $Z_t = \exp\{-(\lambda_j + 1/2\sigma_j^2 - w_{ij}g)(t-t^*) + \sigma_j W_t^{(j)}\}$. The membrane potential if no spike were received at time t^* would read:

$$\widetilde{V}^{(j)}(t+t^*) = V^*_{(j)} \widetilde{Z}_t + \int_0^t I_e^{(j)}(s+t^*) \widetilde{Z}_{t-s}\, ds \tag{8.22}$$

where $\widetilde{Z}_t = \exp\{-(\lambda_j + 1/2\sigma_j^2 - w_{ij}g)(t-t^*) + \sigma_j W_t^{(j)}\} = e^{w_{ij}g(t-t^*)} Z_t$. At time $X^*_{(j)}$ the membrane potential reads:

$$V^{(j)}(X^*_{(j)} + t^*) = \theta e^{w_{ij}gX^*_{(j)}} + \int_0^{X^*_{(j)}} I_e^{(j)}(s+t^*) Z_{t-s}(e^{w_{ij}gs} - 1)\, ds$$

This expression therefore depends on the whole past of the Brownian motion, and cannot be written as a function of $X^*_{(j)}$, even taking into account the conductance as an additional variable. These models are not amenable to the Markovian modelization we propose in this chapter.

8.3 Balanced networks with synaptic delays and refractory period

In the previous section, we only considered inhibitory interactions in order to be closer to classical hourglass models. These inhibitory interactions prevented also from what we will call the spike avalanche phenomenon that can appear in excitatory networks with instantaneous interactions. In that case the following process can occur: if the synaptic efficiencies are big enough, the spike emission of a neuron can induce at the very same time the spike emission of the neurons directly connected to this neuron, which in turn can elicit spikes in their neighborhood. A spike can therefore be transmitted in the whole network, and even make the first neuron spike again, which closes the loop: at a given instant, the neuron fires infinitely many spikes.

In biological network, this issue does not appear because the refractory period of the neuron upperbounds the firing frequency. Furthermore, the synaptic delays in the transmission of the spike also avoids the avalanche process by avoiding the self-excitation, through the network, of a given cell. The refractory period is a transient phase just after the firing during which it is impossible or very difficult to excite the cell. This phenomenon is linked with the dynamics of ion channels and the hyperpolarization phase of the spike emission, lasts few milliseconds, and prevents the neuron from firing spikes at an arbitrary high firing rate. It can be decomposed into two phases: the *absolute* refractory period, which is a constant period of time corresponding loosely to the hyperpolarization of the neuron during which is it impossible to excite the cell no matter how great the stimulating current applied is (see for instance [158, chapter 9] for a further biological discussion of the phenomenon and [13, 105] for a discussion on modelling this refractory period). Immediately after this phase begins the *relative* refractory period during which the initiation of a second action potential is inhibited but still possible. It amounts considering that the synaptic

inputs received at the level of the cell are weighted by a function depending on the time elapsed since the spike emission. This phase also lasts around one millisecond.

To be coherent in our modelization, when we take into account such fast phenomena, we need to consider another fast phenomenon: the axonal spike transmission from the presynaptic cell to the postsynaptic one. The delay induced by the spike transport and its transmission via the synapse depends on the distance between the two cells, the speed of transmission of the signal along the axon and the transmission time at the synapse, and has a typical duration of a few milliseconds.

To model the absolute refractory period, we consider that if the neuron indexed by i fires at time t, it stays at his resting potential $V_r^{(i)}$ until time $t+R_i$ where R_i is the time duration of the absolute refractory period, that only depends on the presynaptic neuron.

We model the relative refractory period only for the spike integration, and not for the noise integration, mainly for technical reasons. This assumption does not affect significantly the dynamics of the network, since the probability that the noisy current integrated during a time period as short as 1 or $2ms$ to be substantial is very small. For the spike integration this remark is no more valid, since a single spike induces substantial changes in the membrane's voltage. During the relative refractory period, we consider that synaptic efficiency are weighted by a function depending on the time elapsed since the last spike has been fired. We denote this function $\kappa(t)$ following the notation of Gerstner and Kistler in [105]. In our case this function is unspecified, is zero at $t=0$ and increases to 1 with a characteristic time of around $2ms$. It can be of bounded support or defined on $\mathbb{R}$.

To model the synaptic delay we consider that spikes emitted by a neuron do not affect instantaneously the target neurons, but only after some delay Δ_{ij} which can depend on both the presynaptic and the postsynaptic neurons (see figure 8.4) since this delay is linked to the duration of the spike transmission and therefore may depend on some measure of distance between the pre- and post-synaptic neurons.

In the present section, we model these three phenomena, and show that in these cases we can also define a Markov chain describing the spike times of the neural network, that will be also based on the countdown process. For inhibitory networks, the modifications with the previous framework is very simple, but it will become slightly more complex, but still tractable, when taking into account excitatory interactions. For the sake of compactness of notations, we define the function $\kappa_j(t)$ for all $t>0$. This function is identically equal to 0 for $t\in[0,R_j]$, and increases to one after time R_j with a characteristic time of the order of a millisecond (see figure 8.5).

If neuron i fires a spike at time t_i, its effect on the postsynaptic neuron j depends on the synaptic delay Δ_{ij}, the countdown value $X^{(j)}(t)$, and the time of the last spike emitted by j:

(i). If $\Delta_{ij}<X^{(j)}(t)$, then the reception of a spike at time t acts on the post-synaptic neuron at time $t+\Delta_{ij}$ in the same fashions as discussed in the different models considered in section 8.2, but in that case the interaction can be either excitatory or inhibitory, with a synaptic efficiency $w_{ij}\kappa_j(t_i+\Delta_{ij}-t_j)$.

(ii). If $\Delta_{ij}>X^{(j)}(t)$, the postsynaptic neuron will fire before receiving the spike from the presynaptic cell i, and it will act on the postsynaptic cell's membrane with an efficiency $w_{ij}\kappa_j(t_i+\Delta_{ij}-X_j)$.

Let us consider the effect of these features from the countdown process viewpoint. The reset variable is only affected by the absolute refractory period, and in a very

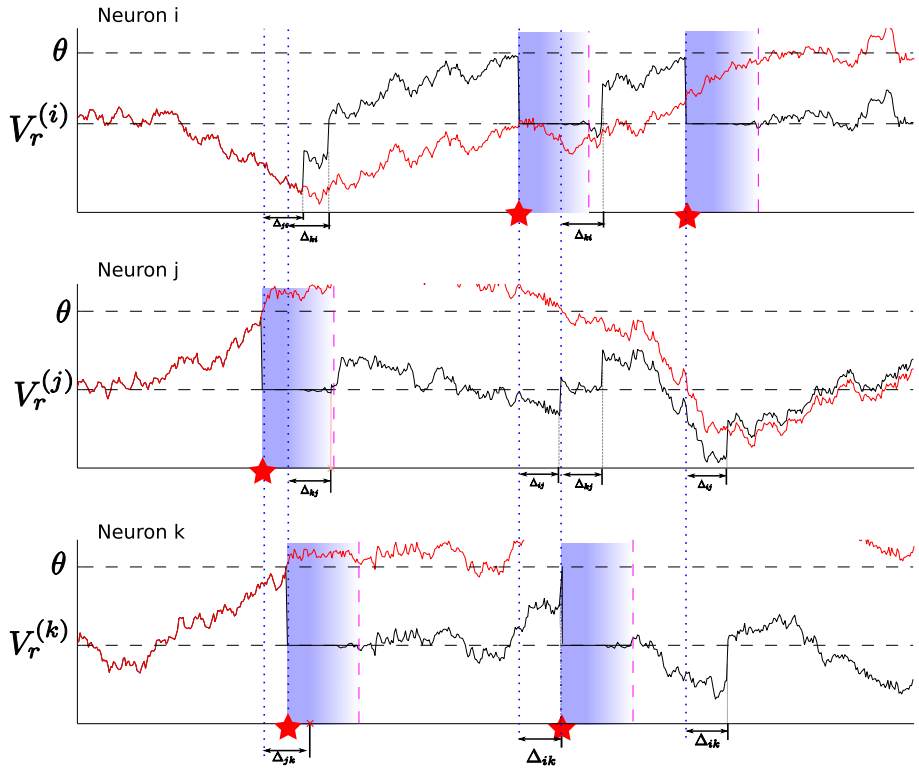

Figure 8.4: Sample path of the membrane potential of a three-neuron excitatory network with synaptic delays and refractory period in the case of the perfect integrate-and-fire neuron. The black curve represents the membrane potential, the red curve the membrane potential process with no reset and no interaction. The spikes are represented by red stars and blue dotted lines. The refractory period is represented by the blue boxes: plain blue for the absolute refractory period, and the intensity is proportional to the attenuation of the spike during the relative refractory period.

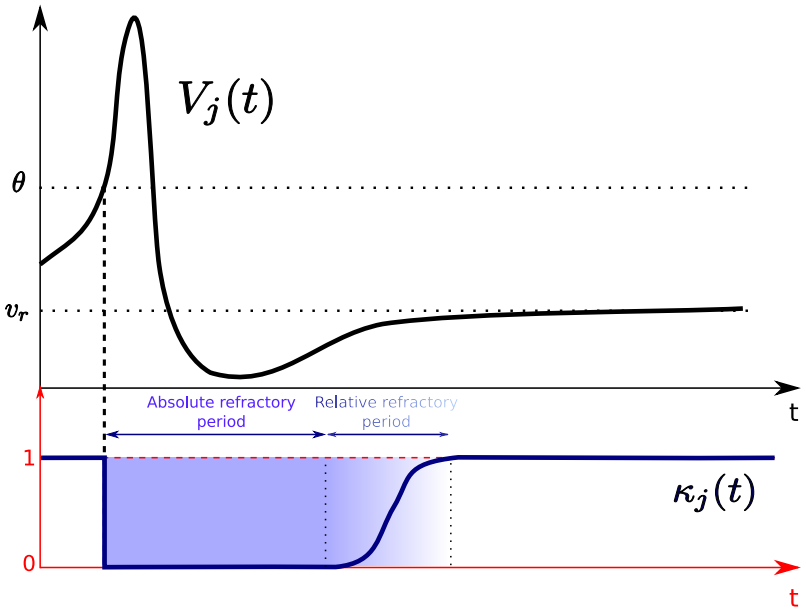

Figure 8.5: The refractory period at a spike emission, and the related κ function weighting the synaptic inputs

simple way. Indeed, we formally consider that the neuron i is stuck at its reset value $V_r^{(i)}$ during a fixed period of time R_i after having fired. After this period, the neuron's membrane potential follows its evolution depending on the model chosen. Therefore, time of the next spike starting from time $t+R_i$ has the law of the reset variable in the case where we did not take into account the refractory period and the synaptic delay, i.e. has the law of the first hitting time of the membrane potential process to the spike threshold, with the time-shifted input $I_e(t+t^*+R_i)$ in the case of non-stationary inputs. If we denote τ_i this random variable, the new reset variable of the related countdown process has simply the law of $Y_i = \tau_i + R_i$.

The case of the interaction variable is a little bit more intricate, and we will deal with it in the following subsections.

8.3.1 Modeling the refractory period

We first consider that the transmission delay is null. In this case the effect of a presynaptic spike on the cell j will be weighted by the function $\kappa_j(t-t_j)$ where t_j is the time of the last spike emitted by the cell j. We show that for the models discussed in section 8.2, the spikes in the network have the same law as the zeros of a simpler Markov process based on the countdown process, and that this dynamics can be reduced to the one of a Markov chain. To this purpose, we identify the random variables needed to define the countdown process. In figure 8.6 we represent a sample path of the countdown process related to the perfect integrate-and-fire neuron when considering an absolute refractory period. Two random variables are necessary to define the dynamics of the countdown process: the reset variable and the interaction variable. We already identified the law of the reset random variable for the countdown process when considering a refractory period. For the interaction variable, the case is readily deduced from the analysis of section 8.2 in the case of inhibitory interactions. Indeed,

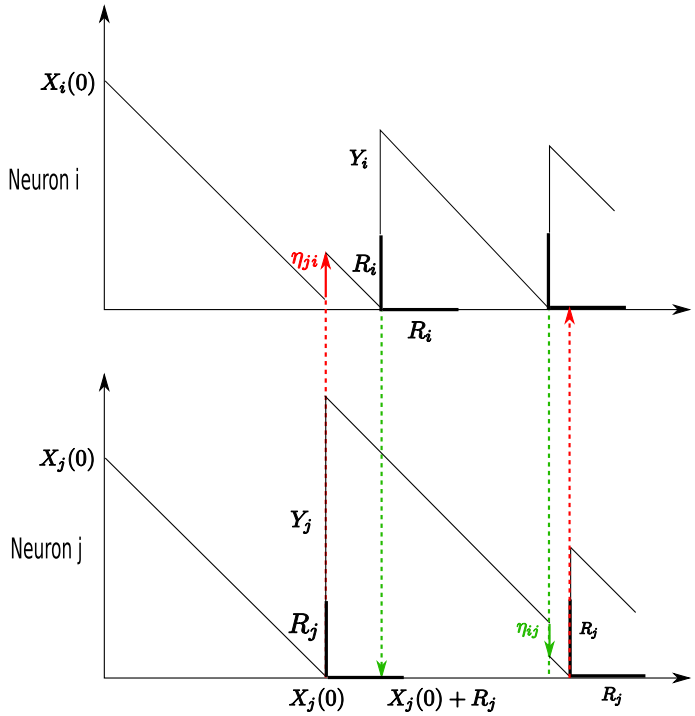

Figure 8.6: A sample path of the countdown process taking into account the refractory period. This figure represent the countdown value for a 2 neurons network. Neuron j fires first at an instant where the cell membrane is excitable, and has an inhibitory effect on neuron i, whose spike is postponed. When neuron i fires for the first time, the neuron j is still in its refractory period and therefore does not integrate the effect of the incoming spike. The second spike emitted from neuron i excites the cell j and advances the spike time. Neuron j then spikes during the refractory period of neuron i.

if neuron i elicits a spike at time t_i, it will affect the postsynaptic neuron j only if it is not during its absolute refractory period, with a weighted synaptic efficiency. Denote by t_j the time of the last spike elicited by j. The presynaptic spike coming from neuron i will affect the neuron j only if $t_j + R_j < t_i$, and if it does, the action of the presynaptic spike on the next spike time has exactly the same effect as treated in the previous section, with a synaptic efficiency $w_{ij}\kappa_j(t_i - t_j)$. Therefore, adding a refractory period makes the random variable depend upon the last firing times of each neuron.

To take into account this fact, we define the *last firing times* variable $H \in \mathbb{R}^N$, that stores the last spike time of each neuron. All its components are set to $R \stackrel{\text{def}}{=} \min_{i=1\ldots N} -R_i$ at the initial time. The j^{th} component is this variable is constant between two spikes of the neuron j. If neuron j spikes at time t_j, this component is instantaneously set to t, and all the other components of this variables are unchanged. This value will remain constant until neuron j spikes again.

If the synapses are inhibitory, the interaction variable η_{ij} of the new countdown process is simply deduced from the law interaction variable $\tilde{\eta}_{ij}(w_{ij})$ by changing the synaptic weight. In the unified case of relative refractory period, we have $\eta_{ij} = \tilde{\eta}_{ij}(w_{ij}\kappa_j(t_i - t_j))$. In the particular case of pure absolute refractory period, this random variable is simply $\eta_{ij} = \tilde{\eta}_{ij}(w_{ij})\mathbb{1}_{X_i > H_j + R_j}$. This new interaction variable depends therefore on the same variables as the one in the case of section 8.2 and on the last firing time variable. The process (X_t, H_t, t, A_t), where A_t are the possible additional variables (typically the value of the synaptic current or the interaction current) is hence a Markov process. Indeed, if all the components of X are strictly positive, the time increases linearly with slope 1, the countdown process decreases linearly with slope -1, the last firing time variable and the possible additional variables remain constant. If the component i of the countdown process reaches 0, this neuron spikes. Almost surely only one neuron realize this infimum at a given time. At this time, say t_i, the following operations occur:

- $X^{(i)}(t_i)$ is reset to an independent copy of Y_i and A_{t_i} is updated according to its dynamics.
- $H_i(t_i) = t_i$ and $H_j(t_i) = H_j(t_i^-)$ for all $j \neq i$ (i.e. theses components are unchanged).
- $\forall j \in \mathscr{V}(i)$, $X^{(j)}(t_i) = X^{(j)}_{t_i^-} + \eta_{ij}\mathbb{1}_{t_i > H_j + R_j}$
- the time is trivially updated.

For excitatory interactions, the case is slightly more complex. Indeed, the calculations we did in section 8.2 are valid only in the inhibitory case, since we used the Markov property of the processes we were studying to compute the interaction variable. More precisely, when an inhibitory interaction occurs, the time of the next spike is increased. The state of the countdown value gave us the time of the next spike, together with the state of possible additional variables. This information was taken into account: using the Markov property of the processes we studied, we stated at the time of the predicted spike if no interaction had taken place meanwhile, and from this point we computed the law of the additional time to wait until the next spike because of the interaction. In the case of excitatory interactions, this trick cannot be applied: indeed, the time to the next spike after the excitatory interaction is smaller than the one predicted by the countdown process. While we conditioned on the past of the process in the case of inhibitory interactions, we will be conditioning on the future in the case of excitatory synapses in order to derive our random variables.

Perfect IF neuron with instantaneous synapses: Assume that the neuron j receives a spike from neuron i at time t_i. The countdown process value of the neuron j just before this interaction is denoted X_j^*. The interaction random variable η_{ij} is the difference of time between the spike time after interaction and the spike time before interaction, conditionally to the fact that this next spike time was predicted to be X_j^*. After some simple calculations, we observe that it has the law of the first hitting time of the membrane potential process to $\theta - w_{ij}$ conditionally to the fact that the first hitting time of this process to θ is X_j^*. Denote by ζ_{ij} this random variable. The law of the update random variable η_{ij} will be defined by $(\zeta_{ij} - X_j)\mathbb{1}_{X_i > H_j + R_j}$ (note that the variable ζ_{ij} is always positive; if the interaction makes the neuron spike instantaneously, its means that $\zeta_{ij} = 0$ and therefore the new countdown value for j is 0). Furthermore in that case, since the Markov's property cannot be used, the random variable will not be independent of the value of the membrane's potential at the time of the spike, which we denote by V_j^*. Let us characterize the law of ζ_{ij}:

$$\begin{aligned}
\mathbb{P}\left[\zeta_{ij} = u\right] &= \mathbb{P}\left[\tau_{\theta - w_{ij}\kappa_j(t_i - H_j)} = u \middle| V_j^*, \tau_\theta = X_j^*\right] \\
&= \mathbb{P}\left[\tau_\theta = X_j^* \middle| V_j^*, \tau_{\theta - w_{ij}\kappa_j(t_i - H_j)} = u\right] \frac{\mathbb{P}\left[\tau_{\theta - w_{ij}\kappa_j(t_i - H_j)} = u \middle| V_j^*\right]}{\mathbb{P}\left[\tau_\theta = X_j^* \middle| V_j^*\right]} \\
&= \mathbb{P}\left[\tau_\theta = X_j^* \middle| W_u = \theta - w_{ij}\kappa_j(t_i - H_j)\right] \frac{\mathbb{P}\left[\tau_{\theta - w_{ij}\kappa_j(t_i - H_j)} = u \middle| V_j^*\right]}{\mathbb{P}\left[\tau_\theta = X_j^* \middle| V_j^*\right]} \qquad (8.23)
\end{aligned}$$

This random variable is null whenever $V_j^* > \theta - w_{ij}$. This gives us the law of the interaction variable in the case of excitatory inputs. Nevertheless, we can see that it involves the value of the membrane potential's process at the times of the spike. Therefore, we need an additional variable in order to define autonomously the countdown process: it is the membrane potential's value at the times of the spike receptions. At each time that a spike is emitted in the network, this variable is updated in the following fashion:

- For the neuron i that elicited a spike, this value is set to $V_r^{(i)}$
- For the other neurons, it is updated by drawing in the law of the membrane potential conditionally to the fact that it will reach the threshold at the time given by the countdown process.

In summary, to simulate the process with a Markovian framework including the countdown process, we simulate a discrete time Markov chain (X, H, V), where H is the last firing time variable, X the countdown process and V the membrane potential at the time of the spike. The transition of this chain from (X^n, H^n, V^n, t^n) is given by:

$$\begin{cases}
V_{i_n}^{n+1} & = V_r \\
V_j^{n+1} & : \text{ drawn from the law of } V_t^{(j)} \text{ conditionally to the fact that it is} \\
 & \quad V_j^n \text{at time } t^n \text{ and } \theta \text{ at time } t^n + X_j^n \text{ for } j \neq i_n \\
t^{n+1} & = t^n + X_{i_n}^n \\
H_{i_n}^{n+1} & = t^{n+1} \\
X_{i_n}^{n+1} & : \text{ drawn from the law of } Y_{i_n} \\
X_j^{n+1} & = X_j^n + \eta_{i_n j}(X_j^n, V_j^{n+1}, H_j^{n+1}) \text{ for } j \neq i_n
\end{cases}$$

Excitatory synapses for PIF neuron with synaptic integration: In the case of the perfect integrate-and-fire neuron with excitatory synapses, the same issue as before appears: the Markov property does not apply, and hence we have to apply the same transformation as we performed in equation (8.23). In that case, the calculations lead to keep in memory both the membrane potential and the synaptic current at the times of the spikes. The same type of expressions and the same type of dynamics of the resulting Markov chain is obtained. Indeed, assume that the countdown process value at the time of the spike is X_j^* and the value of the additional variable (the synaptic current at the time of the next spike) is I_j^*. Then the probability to spike at time $u < X_j^*$ and for an input current $I_s = v$ after the excitation has been received can be computed as the first hitting time of the underlying membrane potential. In the case of instantaneous interactions, it has the law of the first hitting time of the membrane potential process starting at $(V_j(t^*), I_j(t^*))$ the values of the membrane potential and of the synaptic current at the time of the spike considered, to reach the threshold $\theta - w_{ij}\kappa_j(t_i - H_j)$ at time u with the synaptic current v conditionally on reaching the threshold θ at time X_j^* with the input current I_j^*. The law of this random variable can be computed in the same fashion as we did in (8.23). We can see that it depends on the value of the membrane potential and of the input current at the times of the spikes. The law of this random variable is known and can be computed. Therefore, we can provide a Markovian framework to study this type of behaviors. For the other types of perfect integrate-and-fire models, the same reasoning applies.

LIF with instantaneous synapses: In the case of the leaky integrate-and-fire neuron with instantaneous synaptic integration, no further simplification can be provided, and we obtain that the new spike time after interaction has the law of the first hitting time of the membrane potential process to reach the boundary $\theta - w_{ij}\kappa_j(t_i - H_j)e^{-t/\tau}$ (where t_i is the time of the presynaptic spike) conditionally on the fact that the first hitting time of the boundary θ is equal to X_j^*. In that case again, we need an additional variable: the membrane potential at the times of the spikes, in order to define a Markov chain containing the times of the spikes.

The case of postsynaptic current pulses can be treated in the same way. In that case again it will be necessary to know the membrane potential's voltage at the times of the spike in order to be able to simulate the countdown process.

LIF with synaptic integration: The case of the LIF neuron with synaptic integration can be treated in the same fashion as the case of the perfect integrate-and-fire with synaptic integration.

8.3.2 Including synaptic delays

Delays are known to be very important, for instance in shaping spatio-temporal dynamics of neuronal activity [231] or for generating global oscillations [36]. When we take into account this phenomenon in addition to the refractory period, the reset variable of the related countdown process is the same as in the case where we only consider the cell's refractory period: taking into account the axonal delay does not affect the reset variable which, for a given neuron i, has the same law as $R_i + \tau_i$ where τ_i has the law of the first hitting time of the membrane potential process to the threshold starting from $V_r^{(i)}$. The synaptic delay nevertheless affects the interaction variable in a quite intricate fashion (see figure 8.7). Indeed, it adds a non-trivial memory-like

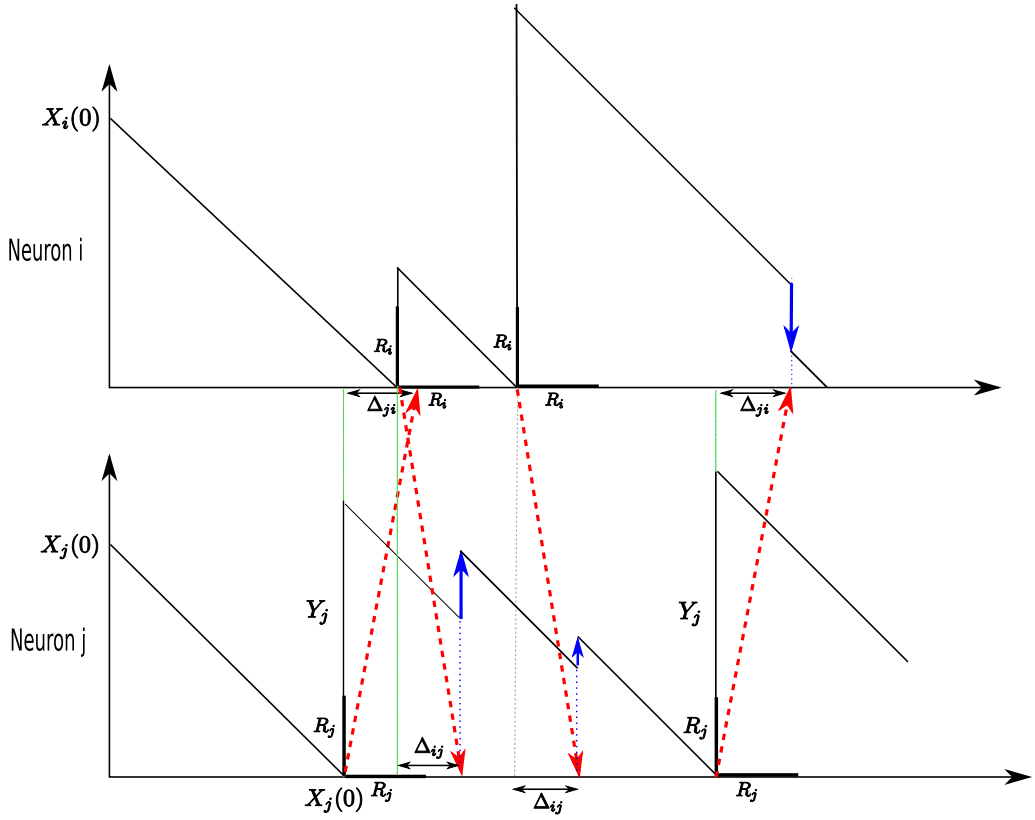

Figure 8.7: A sample path of the countdown process in the case of the perfect integrate-and-fire neuron with instantaneous interactions, when taking into account the synaptic delays and the refractory period. The first spike is emitted by neuron j but arrives at neuron i during its refractory period hence does not affect its evolution. Neuron i sends a spike during the refractory period of neuron j which is received after this period and hence affects the dynamics of the countdown process. The action of neuron i on j is inhibitory and the action of j on i excitatory.

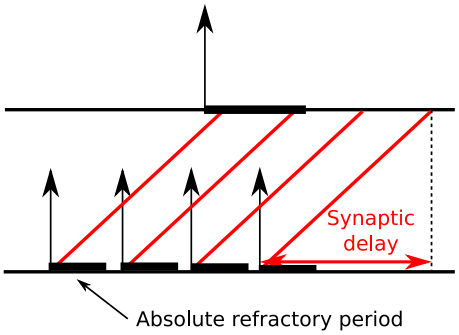

Figure 8.8: Presynaptic spikes emitted before a postsynaptic spike can affect the postsynaptic cell after the firing.

phenomenon in the network. This remark slightly modifies our framework. Indeed, in our previous framework the random variables were updated instantaneously at each spike time, even when the interaction at the level of the membrane potential was not instantaneous. The network memory induced by the transmission delays leads us to keep the memory a certain number of spikes. Fortunately, because of the absolute refractory period, we only have to take into account a finite number of spikes that can possibly affect the postsynaptic potential after it elicits a spike (see figure 8.8). The maximal number of spikes concerned is given by $M \stackrel{\text{def}}{=} \lfloor \frac{\Delta_{ij}}{R_j} \rfloor$ where $\lfloor x \rfloor$ is the floor function, i.e. the largest integer small or equal to x.

In this case, instead of considering the last firing times variable which contained only the last firing time for each neuron of the network, we consider the last M firing times variables. This variable is a matrix $H_M \in \mathbb{R}^{N \times M}$. Each row of the matrix corresponds to the M last firing times of the neuron. Each row i of the matrix is constant between two spike times of the neuron i. At the initial time, the M components of this row are set to the value $\min_{ij}\{-R_i - \Delta_{ij}\}$. If the neuron spikes at time t_i, then each component of the row are modified: for all $k \in \{2, \ldots, N\}$, $H_{i,k-1} = H_{i,k}$ and $H_{i,M} = t_i$. This matrix stores the times of the M last spike times of the neuron i, in the chronological order.

In this case again, we can describe a Markov process and a Markov chain in order to reproduce the times of the spikes. This chain is composed of the same elements as the model with no delay. Let us denote by X^n the countdown chain , by A^n the possible additional variables, H^n the M last firing times variables, t^n the event times, and by $\tilde{V}^n$ the variables containing the membrane potential at the times of the spikes, which is necessary only in the case of excitatory interactions. An event in this chain is either a spike, or the arrival of a spike on a postsynaptic spike, now that these two events are no more simultaneous. The next spike if no delayed interaction occurs will be fired after a time given by $\tau = \min_i X_i^n$, and the first arrival of a possible spike at a cell is given by

$$\nu = \min_{\substack{i,j \in \{1,\ldots,N\} \\ k \in \{1,\ldots,M\}}} \{x = H_{i,k} + \Delta_{ij} - t; x > 0\}$$

If this set is empty, the min is set to $+\infty$. If $\tau < \nu$, a spike will be fired by the neuron i having the lowest countdown value. The state of the countdown variable for this neuron is reset according to the law we already described, and all other variables are updated: the row i of the last M firing times will be updated, the time will be

updated to $t+X_i$, and the additional variables are updated. No interaction is taken into account at this time. If $\nu < \tau$, assume that the minimum is achieved for the value $H_{i,k}+\Delta_{ij}$ for some i,j,k. This means that the k^{th} latest spike of neuron i reaches the cell j. Therefore, the related interaction variable of this connection will be added, and the countdown value of neuron j will be updated, together with the possible additional variables. The time is advanced to $t+\nu$. Note also that many 3-uplets (i,j,k) can achieve this min at the same time. Moreover, it is possible also that an excitatory interaction makes a postsynaptic neuron fire instantaneously at the reception of the spike. All these cases might be treated sequentially, by iterating the mechanism we just described. Nevertheless, we are ensured that no avalanche can occur, because of the absolute refractory period and of the delays.

We finally note that in the case of purely inhibitory networks, the update of this chain can be done only at the times of the spike. Indeed, let us consider that the state of this chain at the iteration n is (X^n,H^n,t^n,A^n) and that neuron i just spiked. We then compute its next spike time if no interaction occurs meanwhile Y_i. But we know through the variable H^n that possibly, before this time Y_i, spikes emitted from other neurons will arrive at the synapses of i. We can therefore at this same time t^n draw in the laws of the interaction variables the additional time that their arrival will provoke on the next spike time for i (this time may depend on the time when the spike will arrive at the synapse of i, which can also be computed with the variables we have). Therefore in that case, the countdown value will be an hourglass chain as defined in section 8.1.

8.4 Ergodicity of the network

The approach we developed in the last sections resulted in providing a simpler framework than the usual one based on the membrane potential for modeling the spikes in a neural network of stochastic integrate-and-fire neurons. This model is equivalent in law from the viewpoint of the spike times, to the usual model. If this modelization gives us a very natural and sometimes very efficient way for simulating the network (see section 8.5), it also provides a good framework for studying its mathematical properties in a more elegant and tractable fashion. Indeed, the models we obtained fit into a class of models studied in the queuing theory in the past ten years. The first analysis of this type of modelled is due to Marie Cottrell [55]. In this article she studied the hourglass model where the interaction random variable is deterministic and inhibitory (i.e. $\forall i,j$, we have $\eta_{ij}(u) \equiv \eta$ where η is a positive constant). In her article, she proves in that case that the related Markov chain is irreducible and aperiodic. Furthermore, she provides a criterion for the positive recurrence of this chain and characterizes the ISI for a two neuron network. In the transient case she shows that some neuron will stop firing in a finite time, and studies the pattern formed by the "dead" neurons (those that will never spike again).

The proof of the irreducibility and aperiodicity of the chain consists in constructing a set of probability in which all the N neurons fire consecutively. The probability of this set is strictly positive, and we can show that every state is accessible after the Nth spike triggered by the last neuron. The same analysis can be done after the next spike, so at spike $N+1$, which proves that the embedded Markov chain X_n is irreducible and aperiodic.

She then proves that if $\mathbb{E}\left[Y_i^2\right] < \infty$ and $\eta < \inf_{i=1,\dots,N} \frac{\mathbb{E}[Y_i]}{|\mathscr{V}(i)|}$ where η is the interaction constant, Y the reset random variable and $|\mathscr{V}(i)|$ the number of neighbors (postsynap-

tic neurons) of the neuron i, then the countdown process $(X_t)_t$ and the related Markov chain (X_n) are ergodic, irreducible, aperiodic and positive recurrent.

This result was then generalized by Fricker, Robert et al [101]. In this paper, the authors find necessary and sufficient conditions of ergodicity for the system when the variables of interaction η_{ij} do not depend on the state of the variable, and are an iid sequence of random variables (not considered deterministic anymore). Assume that the network is fully connected, and that the reset random variables Y_i are exponentially distributed, with parameter λ_i, and that the interactions are the same for all the neighbors of a neuron (i.e. $\eta_{ij} = \eta_i$ for all $j \in \mathscr{V}(i)$).

For the fully connected network, the authors prove that the network is stable if $\rho \stackrel{\text{def}}{=} \max_i \frac{\mathbb{E}[\eta_i]}{\mathbb{E}[Y_i]} < 1$. Under this stability condition, they give an explicit expression for the Laplace transform of the invariant measure of the Markov process associated to this model. They then prove that if $\rho > 1$, the network is not stable, and after a finite time, only one neuron would spike and all the other neurons die (i.e. stop firing).

Then the authors examine also the case of the linear networks. The interaction variables η_i are now considered independent and identically exponentially distributed with the same parameter λ. In this framework they prove that:

(i). if N is odd then the network is stable if $\rho = \frac{\lambda}{\mu} < 1/2$ and not stable if $\rho > 1/2$.

(ii). if N is even, then the network is stable if $\rho < \frac{1}{2cos(\pi/(N+1))}$ and not stable if $\rho > \frac{1}{2cos(\pi/(N+1))}$

Note that the proof of ergodicity is based on an adapted version of the *second vector field* associated to a Markov process. It was introduced by Malyshev and Menshikov in [192].

These results were later generalized by Turova. She also studied the effect of excitatory connections. She proved for instance that in a simple balanced networks with iid interactions, there exists a critical value of the ratio excitation/inhibition below which the network is transient and above which the network is recurrent [56]. She also proved for a purely excitatory network that there almost surely existed a time for which all neurons spike (complete synchronization of the network, see [274]) and in another context that adding one inhibitory connection augmented the probability of synchronization, i.e. stabilizes the oscillations of the total activity [271]. She then studied the effect of plasticity in these networks [273], and the type of patterns observed in the case of transient networks, which she relates with neuronal coding [56]. She also opened the way to more realistic models of neurons.

We are interested in the present section in generalizing these results to the case of stochastic integrate-and-fire networks. We will not go into the details, but the model we propose here are a generalization of the framework of the hourglass model, and therefore could be studied with the same mathematical tools as the ones used in these previous publications. An interesting way for studying these networks would be to use hydrodynamics limits as presented in [60, 61, 62, 173]. Another very interesting way to study mathematically these models would be the dynamical system approach to networks as developed by Malyshev and collaborators in [89, 191, 192].

The usual questions solved in this framework, such as the ergodicity or the transience, are not of great interest from a biological point of view. Indeed, the questions that naturally arise in neuroscience when studying this type of networks are mostly

discriminating between chaos and oscillations and characterizing the temporal features of activity. If we can prove the ergodicity of the network, it will be therefore interesting to study for instance the stationary measures.

We prove in the sequel that the techniques developed do not apply to the case of realistic neurons. In the case of purely excitatory networks, the chain will always be ergodic provided that the reset random variable is almost surely finite. This property depends on the neuron model we consider and the input current. If this random variable is not almost surely finite, the probability to stop firing for a given neuron in the network is simply equally to the probability that its reset variable is infinite, and no network effect has to be taken into account. The problem of balanced networks having both excitatory and inhibitory connections is more complex. To obtain a sufficient condition for their ergodicity, we will transform these balanced networks into a purely inhibitory network by "cutting" the excitatory connections, which amounts to replacing all the original connectivity weights w_{ij} by $\min(w_{ij}, 0)$. The countdown process of the original network is therefore upperbounded in law by the countdown process of the new process where excitation is blocked. If the new process is ergodic, it implies that the original process also is. Therefore, we will be interested in proving ergodicity for purely inhibitory networks.

8.4.1 Ergodicity of the PIF models

For the perfect integrate-and fire neuron, we have seen that the interaction variables η_{ij} that we have to add only depend on w_{ij} possibly weighted by a function depending on the last spike time of the postsynaptic cell j in the case where we take into account the refractory period, and that may be added to the presynaptic neuron in the case where we take into account transmission delays. Note eventually that the ergodicity of the network is not influenced by the delays if taken into account.

Nevertheless in this case, both the expected value of the reset variable and of the interaction variable are infinite whatever the parameters. Indeed, they are expressed as first hitting times of Brownian motion and it is known that the expected values of these random variables are infinite (see e.g. [253]). Therefore, it does not fit in the framework previously used. Nevertheless, in the simulations we did in this type of network, we obtain the same result as in the theoretical cases treated: for small synaptic connectivities, the network is recurrent, and each neuron will spike after any given time, but when the synaptic strength are too big, some neurons stop firing. In the case of a fully connected network, asymptotically only one neuron spikes after a given time, and in a linear or a ring network, one upon two neurons stops firing (see figure 8.10). The same type of behavior can therefore be observed as in the other cases, but has still to be mathematically characterized.

8.4.2 Ergodicity of the LIF models

The cases of leaky integrate-and-fire models neither fit in the previous framework developed. Indeed, the interaction random variable depends on the value of the countdown process at the time when it receives a spike. Nevertheless, both the reset and the interaction random variables have an expected value and are $\mathbb{L}^2$. The interaction variable is bounded by the variable associated with a countdown value equal to 0. Denote by $E_{ij}(x)$ the expected value of the interaction variable, where x is the value of the countdown process when the interaction occurs. In the case where we have $E(0)|\mathscr{V}(i)| < \mathbb{E}[Y_i]$ for all i, the network will be ergodic.

If this is not the case, then we can prove that when $x \to \infty$, we have $E(x) \to 0$ (we even prove that the interaction variable tends to 0 in law, see [253]). Therefore, the countdown value of the neuron will not tend to infinity in this case and always return in the zone where $E(x)|\mathcal{V}(i)| \geq \mathbb{E}Y_i$. We conjecture that in this case, there is another condition on the synaptic weights for the network to be ergodic or not. Simulation results confort us in this conjecture.

8.5 Numerical Simulations

As reviewed by Romain Brette and collaborators in [31], there are two main families of algorithms for the simulation of neural networks: synchronous or "clock-driven" algorithms, in which all neurons are updated simultaneously at every tick of a clock, and asynchronous or "event-driven" algorithms, in which neurons are updated only when they receive or emit a spike. We describe the simple clock-driven strategy to simulate this kind of neural network in section 8.5.1 and then study more precisely the implications of the above analysis to elaborate an event-driven simulator for stochastic networks in section 8.5.2.

8.5.1 Clock-Driven simulation

In the synchronous or "clock-driven" algorithms, the state variables of all neurons are updated simultaneously at every tick of a clock ($X(t) \to X(t+dt)$, see figure 8.9), using a numerical integration algorithm. Then, after updating all the variables, the spiking condition is checked for every neuron (in the case of stochastic differential equations, the refinement presented in section 6.3.7 might be used). Each neuron that satisfies this condition produces a spike which is transmitted with or without delay, and updates their corresponding variables. The membrane potential of every spiking cell is reset.

As reviewed in [31], the cost of the update phase is of order N for each time step. For simulating the network during a time T, the complexity will therefore be $O(NT/dt)$. If F is the average firing rate, an average of $F \times N$ spikes are produced by the neurons and each of these needs to be propagated to p target neurons. Thus, the propagation phase consists in $F \times N \times p$ spike propagations per second. These are essentially additions of weights w_{ij} to state variables, and thus are simple operations whose cost does not grow with the complexity of the models. Summing up, the total mean computational cost per second of biological time is of order $O(N/dt + FNp)$. The cost of taking into account delays is not very high, and does not change the complexity of the algorithm. The obvious drawback of this type of algorithm is that spikes are aligned to a grid (ticks of the clock) thus the simulation is approximate even when the membrane potential is solved exactly. Furthermore, the spiking condition itself is checked at given times and therefore spikes can be missed. Many solutions to fix these issues have been proposed but none is really fully satisfactory.

For simulating a stochastic network with a synchronous algorithm, we used the Brian software [112], for its efficiency to deal with linear models. The code we used for perfect integrate-and-fire neuron is now freely accessible by downloading in the examples provided with the software.

The simulation results in this case are compatible with our conjectures: for small inhibitory connectivities, the network is ergodic and when the absolute value of the connectivities is big, one upon two neurons stop firing in the linear or ring network, or all but one neuron in the case of the fully connected network (see figures 8.10).

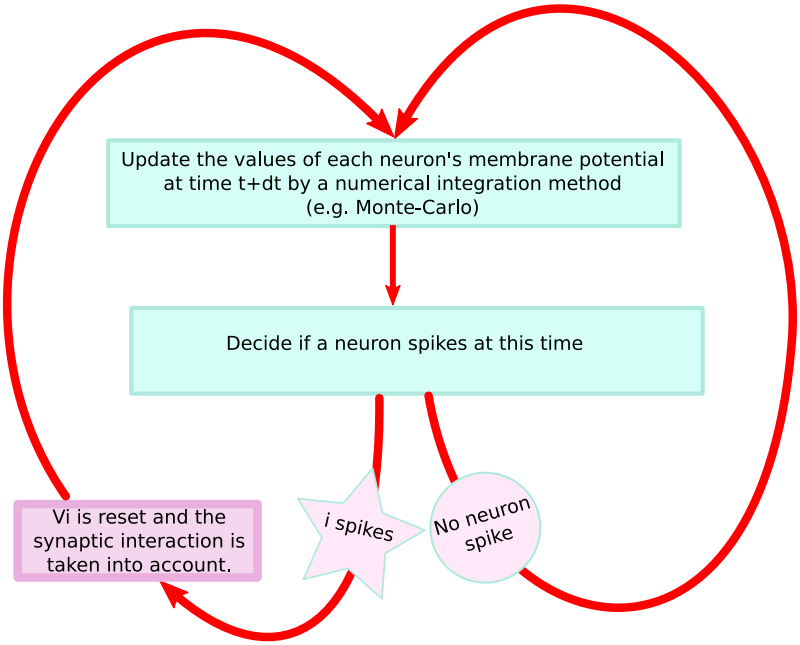

Figure 8.9: Monte-Carlo algorithm for the simulation of the stochastic neural network. The voltage potential is simulated at each time step and a decision is taken wether a spike is emitted or not.

8.5.2 Event-driven simulation

The approach developed in the previous sections provides a very natural way to define an event-based simulation algorithm for stochastic networks. This method consist in building a Markov chain describing the time of the spikes for each neuron. We have seen that simulating the times of the spikes is equivalent in law to simulating the membrane potential, from the spikes viewpoint. The event-based simulation consists in building this Markov chain. Simulating this Markov chain necessitates to draw at each spike time in the law of the reset random and the interaction random variables. We have seen that these random variables can be expressed in most of the cases as first hitting times of random processes, which we have been studying in chapters 6 or 7. In the cases where these laws are known in a closed form, a very efficient simulation procedure can be used. If it is not the case, then we will have to evaluate these random variables. We describe those two simulation ways in the following paragraphs.

Known interaction variables

We consider a network of stochastic integrate-and-fire neurons such that the reset and the interaction variables are known, either analytically, or that computed offline using the techniques of chapter 6 or 7 and tabulated. In that case, simulating the related countdown process will be very efficient and will precisely give the spike times.

To define our event-based algorithm, we explain how to initialize the network and how to compute the spike times recursively. Assume that at the initial time t_0 the values of membrane potential of each neuron and of the additional variables of the model are known. The initial countdown value for a given neuron will be simply

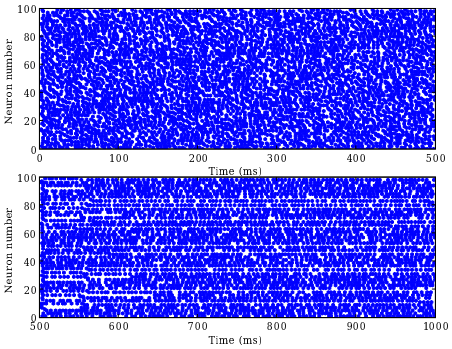

(a) Ring network of PIF

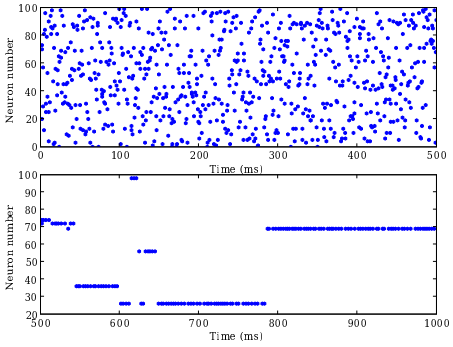

(b) Fully connected network of PIF

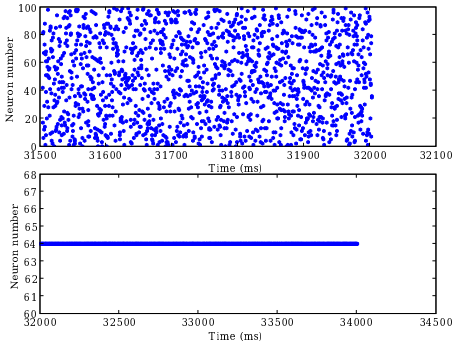

(c) Fully connected network of LIF

Figure 8.10: Clock-driven simulation of a 100 stochastic integrate-and-fire neurons network during $500ms$ using Brian software. (a): ring network of PIF neurons for small (up) and big (down) inhibitory connectivities. (b) same simulations for fully connected networks. (c) Case of the LIF fully connected network.

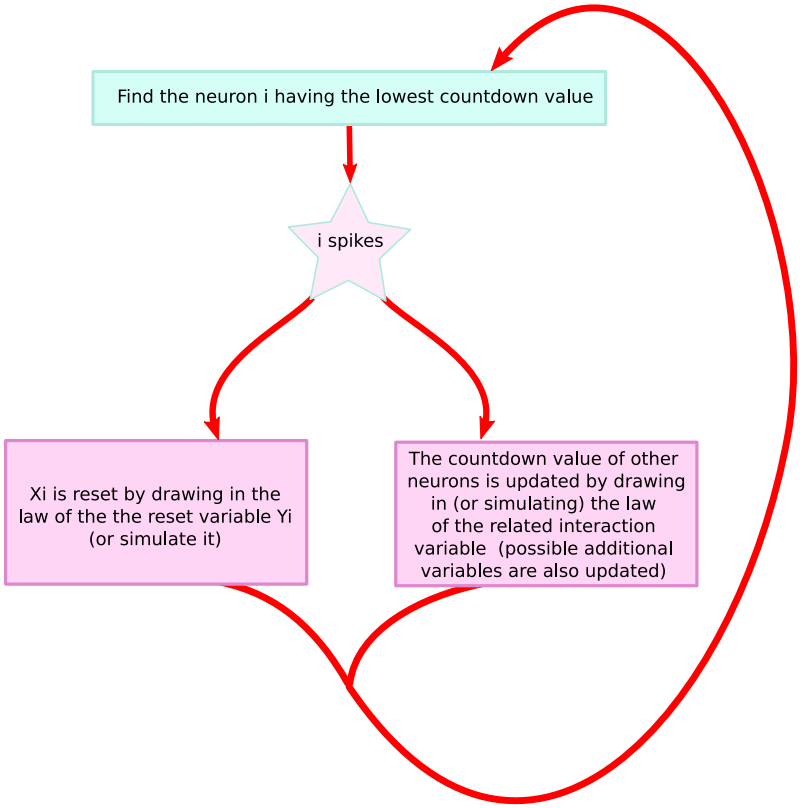

Figure 8.11: Principle of the event-based simulation using the countdown process studied in the previous sections

computed as the first hitting time of its membrane potential process starting from this initial condition to reach the threshold and therefore can be computed in the same way as the reset variable. From this initial time, the principle of the algorithm is to build the discrete-time Markov chain containing as a variable the countdown process that gives the times of the spikes (we have seen that sometimes additional variables were necessary). Then to deduce the state of the chain at time $n+1$ knowing the chain at time n, we use the recursion relation described in sections 8.2 and 8.3 (see figure 8.11):

- We first identify the neuron having the lowest countdown value, which amounts finding the minimal value in a list of N elements, an elementary operation efficiently coded. This neuron is the one that elicits the first spike.

- When this neuron is identified, we directly jump to this time, and draw the new state of the network: the neuron that just fired a spike is reset by drawing in the law of the related reset variable and the other neurons' state is updated by drawing in the law of their respective interaction variables. Once the state of all neurons have been updated, the simulation proceeds.

This method was implemented using the software MVASpike [228, 229, 276]. Simulation results are provided in figure 8.12.

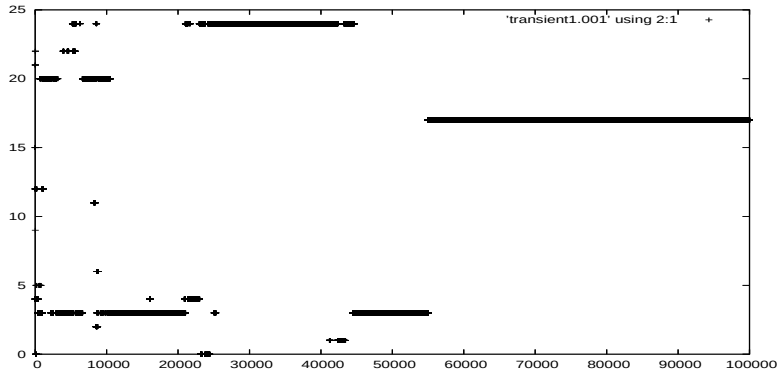

(a) Fully connected network

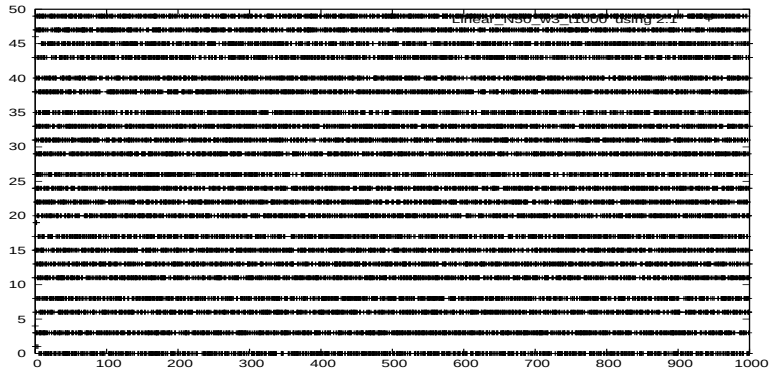

(b) Linear network

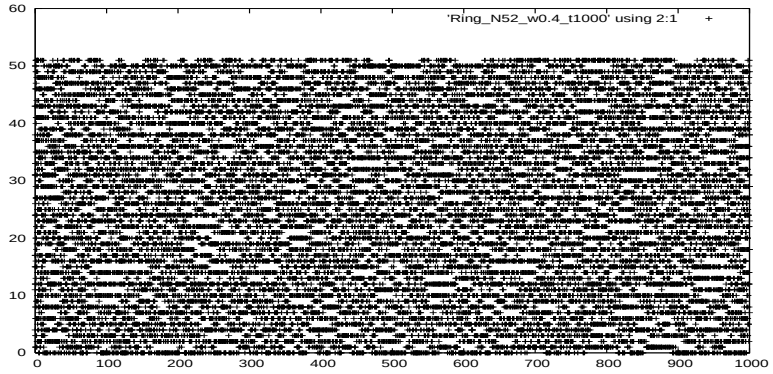

(c) Recurrent network

Figure 8.12: Linear and fully connected networks of perfect integrate-and-fire neuron with constant inputs, simulated with MVASpike. Simulations of 25 to 50 neurons for 10*s* to 1000*s*. We obtain the same results as expected from the mathematical analysis.

Parallel implementation

In the cases where the pdf of the first hitting time of the membrane potential is neither known analytical nor tabulated, the computation of the reset and interaction random variables can be performed by simulating a sample paths of the membrane potential using a Monte-Carlo algorithm. This type of simulation requires that the user defines a clock, i.e. a time step for the simulation of trajectories in order to compute first hitting times of stochastic processes using a Monte-Carlo simulation. As a conclusion of the theoretical analysis driven above, an important remark is that at each spike time, the reset variables and the interaction variables are pairwise independent. Therefore they can be computed independently, and for instance simultaneously using a parallel algorithm.

Therefore we developed, together with Renaud Keriven and Alexandre Chariot, a simulation algorithm of the network on graphics processing unit (GPU), dedicated graphics rendering devices with a highly parallel structure. One of the main issue for this implementation was to develop a random number generator. Indeed, usual graphical cards were not using integers. Very recent cards, starting from the cards NVidia 8xxx, are able to handle integers, and therefore it opened the way random number generators and random simulation. Another issue is the decorrelation between the random number generators on each processor. To this purpose, Keriven and collaborators developed the following algorithm: they generate random seeds on CPU to be used by the random number generation algorithm on each processor. After this common phase, each processor will behave independently. The processor that computes the reset variable by using the Monte-Carlo algorithm described in section 6.3.7. This simulation is based on a pathwise simulation of the membrane potential and the evaluation of the spiking probability between two time steps. When at a given processor the random variable has been evaluated, the neuron is flagged, the simulation on this computer stops, the value of the random variable is recorded, and we wait for all the processors to reach this phase.

This process can be done for a number of neuron lower than or equal to 4096^2 ($\sim 1.6\,10^7$ units) because of the limited memory available on these cards. Nevertheless, we can overcome this difficulty by repeating many times this procedure.

With this algorithm we obtain speed up ratios from 20 to up to 100, by comparing with the same algorithm coded in C++.

CONCLUSION

In this chapter we developed an event-based mathematical framework for the study of stochastic integrate-and-fire neural networks. This model can be studied efficiently using the powerful tools of communication networks theory. With this approach we can address in a more tractable way mathematical questions as ergodicity properties, invariant measures. This framework seems also promising in order to deal with biological issues whatever the connectivity map, the number of connections or on the number of neuron. This study opens the door to the mathematical study of the macroscopic behavior of large networks using the hydrodynamics limits developed to study large queuing processes, to infer and model collective behaviors of such networks.

One of the main advantages of this model is to provide an efficient way to simulate networks. This simulation is exact in law if the probability density function of the first hitting times of the membrane potential is known. But when unknown, the simulation becomes more tricky and probably as efficient as the clock-driven simula-

tion.

CHAPTER 9

A CONSTRUCTIVE MEAN FIELD ANALYSIS OF MULTI POPULATION NEURAL NETWORKS WITH RANDOM SYNAPTIC WEIGHTS AND STOCHASTIC INPUTS

Hâtez-vous lentement, et, sans perdre courage,
Vingt fois sur le métier remettez votre ouvrage :
Polissez-le sans cesse et le repolissez ;
Ajoutez quelquefois, et souvent effacez.
– Nicolas Boileau

ABSTRACT

In this chapter we deal with the problem of bridging the gap between two scales in neuronal modeling. At the first (microscopic) scale, neurons are considered individually and their behavior described by stochastic differential equations that govern the time variations of their membrane potentials. They are coupled by synaptic connections acting on their resulting activity, a nonlinear function of their membrane potential. At the second (mesoscopic) scale, interacting populations of neurons are described individually by similar equations. The equations describing the dynamical and the stationary mean field behaviors are considered as functional equations on a set of stochastic processes. Using this new point of view allows us to prove that these equations are well-posed on any finite time interval and to provide, by a fixed point method, a constructive method for effectively computing their unique solution. This method is proved to converge to the unique solution and we characterize its complexity and convergence rate. We also provide partial results for the stationary problem on infinite time intervals. These results shed some new light on such neural mass models as the one of Jansen and Rit [149]: their dynamics appears as a coarse approximation of the much richer dynamics that emerges from our analysis. Our numerical experiments confirm that the framework we propose and the numerical methods we derive from it provide a new and powerful tool for the exploration of neural behaviors at different scales.

Contents

INTRODUCTION

Modeling neural activity at scales integrating the effect of thousands of neurons is of central importance for several reasons. First, most imaging techniques are not able to measure individual neuron activity ("microscopic" scale), but are instead measuring mesoscopic effects resulting from the activity of several hundreds to several hundreds of thousands of neurons. Second, anatomical data recorded in the cortex reveal the existence of structures, such as the cortical columns, with a diameter of about $50\mu m$ to $1mm$, containing of the order of one hundred to one hundred thousand neurons belonging to a few different species. These columns have specific functions. For example, in the visual cortex V1, they respond to preferential orientations of bar-shaped visual stimuli. In this case, information processing does not occur at the scale of individual neurons but rather corresponds to an activity integrating the collective dynamics of many interacting neurons and resulting in a mesoscopic signal. The description of this collective dynamics requires models which are different from individual neurons models. In particular, if the accurate description of one neuron requires "m" parameters (such as sodium, potassium, calcium conductances, membrane capacitance, etc...), it is not necessarily true that an accurate mesoscopic description of an assembly of N neurons requires Nm parameters. Indeed, when N is large enough averaging effects appear, and the collective dynamics is well described by an effective mean-field, summarizing the effect of the interactions of a neuron with the other neurons, and depending on a few effective control parameters. This vision, inherited from statistical physics requires that the space scale be large enough to include a large number of microscopic components (here neurons) and small enough so that the region considered is homogeneous. This is in effect for instance the case of cortical columns.

However, obtaining the evolution equations of the effective mean-field from microscopic dynamics is far from being evident. In simple physical models this can be achieved via the law of large numbers and the central limit theorem, provided that time correlations decrease sufficiently fast. This type of approach has been generalized to such fields as quantum field theory or non equilibrium statistical mechanics. To the best of our knowledge, the idea of applying mean-field methods to neural networks dates back to Amari [7, 8]. In his approach, the author uses an assumption that he called the "local chaos hypothesis", reminiscent of Boltzmann's "molecular chaos hypothesis", that postulates the vanishing of individual correlations between neurons, when the number N of neurons tends to infinity. Later on, Crisanti, Sompolinsky and coworkers [240] used a dynamic mean-field approach to conjecture the existence of chaos in an homogeneous neural network with random independent synaptic weights. This approach was formerly developed by Sompolinsky and coworkers for spin-glasses [58, 59, 241], where complex effects such as aging or coexistence of a diverging number of metastable states, renders the mean-field analysis delicate in the long time limit [134].

On the opposite, these effects do not appear in the neural network considered in [240] because the synaptic weights are independent [46] (and especially non symmetric, in opposition to spin glasses). In this case, the Amari approach and the dynamic mean-field approach lead to the same mean-field equations. Later on, the mean-field equations derived by Sompolinsky and Zippelius [241] for spin-glasses were rigorously obtained by Ben Arous and Guionnet [20, 21, 122]. The application of their method to a discrete time version of the neural network considered in [240] and in [198] was done by Moynot and Samuelides [201].

Mean-field methods are often used in the neural network community but there are only a few rigorous results using the dynamic mean-field method. The main advantage of dynamic mean-field techniques is that they allow one to consider neural networks where synaptic weights are random (and independent). The mean-field approach allows one to state general and generic results about the dynamics as a function of the statistical parameters controlling the probability distribution of the synaptic weights [233]. It does not only provide the evolution of the mean activity of the network but, because it is an equation on the law of the mean-field, it also provides informations on the fluctuations around the mean and their correlations. These correlations are of crucial importance as revealed in the paper by Sompolinsky and coworkers [240]. Indeed, in their work, the analysis of correlations allows them to discriminate between two distinct regimes: a dynamics with a stable fixed point and a chaotic dynamics, while the mean is identically zero in the two regimes.

However, this approach has also several drawbacks explaining why it is so seldom used. First, this method uses a generating function approach that requires heavy computations and some "art" for obtaining the mean-field equations. Second, it is hard to generalize to models including several populations. Finally, dynamic mean-field equations are usually supposed to characterize *in fine* a stationary process. It is then natural to search for stationary solutions. This considerably simplifies the dynamic mean-field equations by reducing them to a set of differential equations (see section 9.4) but the price to pay is the unavoidable occurrence in the equations of a non free parameter, the initial condition, that can only be characterized through the investigation of the non stationary case.

Hence it is not clear whether such a stationary solution exists, and, if it is the case, how to characterize it. To the best of our knowledge, this difficult question has only been investigated for neural networks in one paper by Crisanti and coworkers [57].

Different alternative approaches have been used to get a mean-field description of a given neural network and to find its solutions. In the neuroscience community, a static mean-field study of multi population network activity was developed by Treves in [268]. This author did not consider external inputs but incorporated dynamical synaptic currents and adaptation effects. His analysis was completed in [2], where the authors considered a unique population of nonlinear oscillators subject to a noisy input current. They proved, using a stationary Fokker-Planck formalism, the stability of an asynchronous state in the network. Later on, Gerstner in [104] built a new approach to characterize the mean-field dynamics for the Spike Response Model, via the introduction of suitable kernels propagating the collective activity of a neural population in time.

Brunel and Hakim considered a network composed of integrate-and-fire neurons connected with constant synaptic weights [36]. In the case of sparse connectivity, stationarity, and considering a regime where individual neurons emit spikes at low rate, they were able to study analytically the dynamics of the network and to show that the network exhibited a sharp transition between a stationary regime and a regime of fast collective oscillations weakly synchronized. Their approach was based on a perturbative analysis of the Fokker-Planck equation. A similar formalism was used in [196] which, when complemented with self-consistency equations, resulted in the dynamical description of the mean-field equations of the network, and was extended to a multi population network.

Finally, Chizhov and Graham [48] have recently proposed a new method based on

a population density approach allowing to characterize the mesoscopic behaviour of neuron populations in conductance-based models. We shortly discuss their approach and compare it to ours in the discussion section 3.5.

In the present chapter, we investigate the problem of deriving the equations of evolution of neural masses at mesoscopic scales from neurons dynamics, using a new and rigorous approach based on stochastic analysis.

The article is organized as follows. In section 9.1 we derive from first principles the equations relating the membrane potential of each of a set of neurons as function of the external injected current and noise and of the shapes and intensities of the postsynaptic potentials in the case where these shapes depend only on the postsynaptic neuron (the so-called voltage-based model). Assuming that the shapes of the postsynaptic potentials can be described by linear (possibly time-dependent) differential equations we express the dynamics of the neurons as a set of stochastic differential equations. Assuming that the synaptic connectivities between neurons satisfy statistical relationship only depending on the population they belong to, we obtain the mean-field equations summarizing the interactions of the P populations in the limit where the number of neurons tend to infinity. These equations can be derived in several ways, either heuristically following the lines of Amari [7, 8], Sompolinsky [57, 240], and Cessac [46, 233], or rigorously as in the work of Benarous and Guionnet [20, 21, 122]. The purpose of this article is not the derivation of these mean-field equations but to prove that they are well-posed and to provide an algorithm for computing their solution. Before we do this we provide the reader with two important examples of such mean-field equations. The first example is what we call the simple model, a straightforward generalization of the case studied by Amari and Sompolinsky. The second example is a neuronal assembly model, or neural mass model, as introduced by Freeman [99] and examplified in Jansen and Rit's cortical column model [149].

In section 9.2 we consider the problem of solutions over a finite time interval $[t_0, T]$. We prove, under some mild assumptions, the existence and uniqueness of a solution of the dynamic mean-field equations given an initial condition at time t_0. The proof consists in showing that a nonlinear equation defined on the set of multidimensional Gaussian random processes defined on $[t_0, T]$ has a fixed point. We extend this proof in section 9.3 to the case of stationary solutions over the time interval $[-\infty, T]$ for the simple model. Both proofs are constructive and provide an algorithm for computing numerically the solutions of the mean-field equations.

We then study in section 9.4 the complexity and the convergence rate of this algorithm and put it to good use: We first compare our numerical results to the theoretical results of Sompolinsky and coworkers [57, 240]. We then provide an example of numerical experiments in the case of two populations of neurons where the role of the mean-field fluctuations is emphasized.

Along the chapter we introduce several constants. To help the reader we have collected in table 9.1 the most important ones and the place where they are defined in the text.

9.1 MEAN FIELD EQUATIONS FOR MULTI-POPULATIONS NEURAL NETWORK MODELS

In this section we introduce the classical neural mass models and compute the re-

lated mean field equations they satisfy in the limit of an infinite number of neurons

9.1.1 The general model

General framework

We consider a network composed of N neurons indexed by $i \in \{1, \dots, N\}$ belonging to P populations indexed by $\alpha \in \{1, \dots, P\}$ such as those shown in figure 9.1. Let N_α be the number of neurons in population α. We have $N = \sum_{\alpha=1}^{P} N_\alpha$. In the following we are interested in the limit $N \to \infty$. We assume that the proportions of neurons in each population are non-trivial, i.e. :

$$\lim_{N\to\infty} \frac{N_\alpha}{N} = n_\alpha \ \in \ (0,1) \ \forall \alpha \in \{1, \dots, P\}.$$

If it were not the case the corresponding population would not affect the global behavior of the system, would not contribute to the mean field equation, and could be neglected.

We introduce the function $p : \{1, \dots, N\} \to \{1, \dots, P\}$ such that $p(i)$ is the index of the population which the neuron i belongs to.

The following derivation is built after Ermentrout's review [81]. We consider that each neuron i is described by its membrane potential $V_i(t)$ or by its instantaneous firing rate $\nu_i(t)$, the relation between the two quantities being of the form $\nu_i(t) = S_i(V_i(t))$ [67, 106], where S_i is sigmoidal.
A single action potential from neuron j is seen as a post-synaptic potential $PSP_{ij}(t-s)$ by neuron i, where s is the time of the spike hitting the synapse and t the time after the spike. We neglect the delays due to the distance travelled down the axon by the spikes.

Assuming that the post-synaptic potentials sum linearly, the average membrane potential of neuron i is

$$V_i(t) = \sum_{j,k} PSP_{ij}(t - t_k),$$

where the sum is taken over the arrival times of the spikes produced by the neurons j. The number of spikes arriving between t and $t + dt$ is $\nu_j(t)dt$. Therefore we have

$$V_i(t) = \sum_j \int_{-\infty}^{t} PSP_{ij}(t-s)\nu_j(s)\,ds = \sum_j \int_{-\infty}^{t} PSP_{ij}(t-s)S_j(V_j(s))\,ds,$$

or, equivalently

$$\nu_i(t) = S_i\left(\sum_j \int_{t_0}^{t} PSP_{ij}(t-s)\nu_j(s)\,ds\right). \tag{9.1}$$

The PSP_{ij}s can depend on several variables in order to account for instance for adaptation or learning.

The voltage-based model

The assumption, made in [132], is that the post-synaptic potential has the same shape no matter which presynaptic population caused it, the sign and amplitude may vary though. This leads to the relation

$$PSP_{ij}(t) = J_{ij}g_i(t).$$

g_i represents the unweighted shape (called a g-shape) of the postsynaptic potentials and J_{ij} is the strength of the postsynaptic potentials elicited by neuron j on neuron i. Thus we have

$$V_i(t) = \int_{t_0}^{t} g_i(t-s)\left(\sum_j J_{ij}\nu_j(s)\right) ds.$$

So far we have only considered the synaptic inputs to the neurons. We also assume that neuron i receives an external current density $I_i(t)$ and some noise $n_i(t)$ so that

$$V_i(t) = \int_{t_0}^{t} g_i(t-s)\left(\sum_j J_{ij}\nu_j(s) + I_i(s) + n_i(s)\right) ds. \tag{9.2}$$

We assume that the external current and the g-shapes satisfy $I_i = I_{p(i)}$, $g_i = g_{p(i)}$, $S_i = S_{p(i)}$, i.e. they only depend upon the neuron population. The noise model is described later. Finally we assume that $g_i = g_\alpha$ (where $\alpha = p(i)$) is the Green function of a linear differential equation of order k, i.e. satisfies

$$\sum_{l=0}^{k} a_\alpha^l(t)\frac{d^l g_\alpha}{dt^l}(t) = \delta(t). \tag{9.3}$$

We assume that the functions $a_\alpha^l(t)$ are continuous for $l = 0,\cdots,k$ and $\alpha = 1,\cdots,P$. We also assume $a_\alpha^k(t) \geq c > 0$ for all $t \in \mathbb{R}$, $\alpha = 1,\cdots,P$.

Known examples of g-shapes, see section 9.1.4 below, are $g_\alpha(t) = Ke^{-t/\tau}Y(t)$ ($k = 1, a_1(t) = \frac{1}{K}, a_0(t) = \frac{1}{K\tau}$)or $g_\alpha(t) = Kte^{-t/\tau}Y(t)$ ($k = 2, a_2(t) = \frac{1}{K}, a_1(t) = \frac{2}{K\tau}, a_0(t) = \frac{1}{K\tau}$), where Y is the Heaviside function.

We note D_α^k the corresponding differential operator, $D_\alpha^k g_\alpha = \delta$, and $\mathbf{D}_N^k$ the N-dimensional differential operator containing N_α copies of D_α^k, $\alpha = 1,\cdots,P$. We write (9.2) in vector form

$$\mathbf{V}^{(N)} = \mathbf{J}^{(N)}\mathrm{diag}(g_\alpha) * S^{(N)}(\mathbf{V}^{(N)}) + \mathrm{diag}(g_\alpha) * \mathbf{I}^{(N)} + \mathrm{diag}(g_\alpha) * \mathbf{n}^{(N)},$$

where $\mathrm{diag}(g_\alpha)$ is the N-dimensional diagonal matrix containing N_α copies of g_α, $\alpha = 1,\cdots,P$ and $*$ indicates the convolution operator. $S^{(N)}$ is the mapping $\mathbb{R}^N \to \mathbb{R}^N$ such that $S^{(N)}(\mathbf{V}^{(N)})_i = S_{p(i)}(\mathbf{V}_i^{(N)})$. We apply the operator $\mathbf{D}_N^k$ to both sides to obtain

$$\mathbf{D}_N^k \mathbf{V}^{(N)} = \mathbf{J}^{(N)} \cdot S^{(N)}(\mathbf{V}^{(N)}) + \mathbf{I}_V^{(N)} + \mathbf{n}_V^{(N)}, \tag{9.4}$$

which is a stochastic differential equation

$$d\left(\frac{d^{k-1}\mathbf{V}^{(N)}}{dt^{k-1}}\right) = \left(-\mathbf{D}_N^{k-1}\mathbf{V}^{(N)} + \mathbf{J}^{(N)} \cdot S^{(N)}(\mathbf{V}^{(N)}) + \mathbf{I}^{(N)}\right) dt + d\mathbf{n}_t^{(N)},$$

where $\mathbf{D}_N^{k-1}$ is obtained from the P differential operators of order $k-1$ $D_\alpha^{k-1} = \sum_{l=0}^{k-2} \frac{a_\alpha^l(t)}{a_\alpha^k(t)} \frac{d^l}{dt^l}$.

The activity-based model If we make the assumption that the shape of a PSP depends only on the nature of the presynaptic cell, that is

$$PSP_{ij} = J_{ij} g_j,$$

and define the activity as

$$A_j(t) = \int_{-\infty}^{t} g_j(t-s)\nu_j(s)\, ds,$$

multiplying both sides of equation (9.1) by $g_i(t-s)$ and integrating with respect to s, we obtain

$$A_i(t) = \int_{-\infty}^{t} g_i(t-s) S_i \left(\sum_j J_{ij} A_j(s) + I_i(s) + n_i(s) \right) ds,$$

where we have added an external current and a noise. If $p(i) = \alpha$, this yields

$$D_\alpha^k A_i = S_i \left(\sum_j J_{ij} A_j(t) + I_i(t) + n_i(t) \right),$$

and in terms of the N-dimensional vector $\mathbf{A}^{(N)}$

$$\mathbf{D}_N^k \mathbf{A}^{(N)} = S^{(N)}(\mathbf{J}^{(N)} \mathbf{A}^{(N)} + \mathbf{I}_A^{(N)} + \mathbf{n}_A^{(N)}). \tag{9.5}$$

Equivalence of the two models As a matter of fact these two equations are equivalent provided that $\mathbf{J}^{(N)}$ is invertible[1]. Indeed, let us use the change of variable $\mathbf{V}^{(N)} = \mathbf{J}^{(N)} \mathbf{A}^{(N)} + \mathbf{I}_A^{(N)} + \mathbf{n}_A^{(N)}$. We have, because $\mathbf{J}^{(N)}$ is not a function of time,

$$\mathbf{D}_N^k \mathbf{V}^{(N)} = \mathbf{J}^{(N)} \mathbf{D}_N^k \mathbf{A}^{(N)} + \mathbf{D}_N^k \mathbf{I}_A^{(N)} + \mathbf{D}_N^k \mathbf{n}_A^{(N)}.$$

Replacing $\mathbf{D}_N^k \mathbf{V}^{(N)}$ by this value in (9.4) we obtain

$$\mathbf{J}^{(N)} \mathbf{D}_N^k \mathbf{A}^{(N)} + \mathbf{D}_N^k \mathbf{I}_A^{(N)} + \mathbf{D}_N^k \mathbf{n}_A^{(N)} = \mathbf{J}^{(N)} \cdot S^{(N)}(\mathbf{J}^{(N)} \mathbf{A}^{(N)} + \mathbf{I}_A^{(N)} + \mathbf{n}_A^{(N)}) + \mathbf{I}_V^{(N)} + \mathbf{n}_V^{(N)}.$$

Assuming that the matrix $\mathbf{J}^{(N)}$ is invertible yields

$$\mathbf{D}_N^k \mathbf{A}^{(N)} = S^{(N)}(\mathbf{J}^{(N)} \mathbf{A}^{(N)} + \mathbf{I}_A^{(N)} + \mathbf{n}_A^{(N)}) + (\mathbf{J}^{(N)})^{-1} \left(\mathbf{I}_V^{(N)} - \mathbf{D}_N^k \mathbf{I}_A^{(N)} + \mathbf{n}_V^{(N)} - \mathbf{D}_N^k \mathbf{n}_A^{(N)} \right).$$

Given the current $\mathbf{I}_V^{(N)}$ (respectively the noise $\mathbf{n}_V^{(N)}$), we can choose the current $\mathbf{I}_A^{(N)}$ (respectively the noise $\mathbf{n}_A^{(N)}$) solution of the linear differential equation $\mathbf{D}_N^k \mathbf{I}_A^{(N)} = \mathbf{I}_V^{(N)}$ (respectively $\mathbf{D}_N^k \mathbf{n}_A^{(N)} = \mathbf{n}_V^{(N)}$). Using the Green functions g_α, $\alpha = 1, \cdots, P$ this is equivalent to $\mathbf{I}_A^{(N)} = \mathrm{diag}(g_\alpha) * \mathbf{I}_V^{(N)}$ (respectively $\mathbf{n}_A^{(N)} = \mathrm{diag}(g_\alpha) * \mathbf{n}_V^{(N)}$).

The dynamics We introduce the $k-1$ N-dimensional vectors $\mathbf{V}^{(l)}(t) = [V_1^{(l)}, \cdots, V_N^{(l)}]^T$, $l = 1, \cdots, k-1$ of the lth-order derivative of $\mathbf{V}^{(N)}(t)$, and the Nk-dimensional vector

$$\widetilde{\mathbf{V}}^{(N)}(t) = \begin{bmatrix} \mathbf{V}^{(N)}(t) \\ \mathbf{V}^{(N)(1)}(t) \\ \vdots \\ \mathbf{V}^{(N)(k-1)}(t) \end{bmatrix}.$$

The N-neurons network is described by the Nk-dimensional vector $\widetilde{\mathbf{V}}^{(N)}(t)$. We consider the direct sum $\mathbb{R}^{Nk} = E^{(0)} \oplus \cdots \oplus E^{(k-1)}$, where each $E^{(l)} = \mathbb{R}^N$, $l = 0, \cdots, k-1$

[1]Note that in the cases we treat in this chapter, the matrix $\mathbf{J}^{(N)}$ is always almost surely invertible since it has non-degenerate Gaussian coefficients, and hence the equivalence in law will always be valid

and introduce the following notation: if $\mathbf{x}$ is a vector of $\mathbb{R}^{Nk}$, $\mathbf{x}_l$ is its component in $E^{(l)}$, $l = 0, \cdots, k-1$, an N-dimensional vector. In particular we have $\widetilde{\mathbf{V}}_l^{(N)}(t) = \mathbf{V}^{(N)(l)}(t)$ for $l = 0, \cdots, k-1$ with the convention that $\mathbf{V}^{(N)(0)} = \mathbf{V}^{(N)}$.

We now write the equations governing the time variation of the first $k-1$ vectors of $\widetilde{\mathbf{V}}^{(N)}(t)$, i.e. the derivatives of order $0, \ldots k-2$ of $\mathbf{V}^{(N)}(t)$. These equation in effect determine the noise model. We write

$$d\widetilde{\mathbf{V}}_l^{(N)}(t) = \widetilde{\mathbf{V}}_{l+1}^{(N)}(t)\, dt + \Lambda_l^{(N)} \cdot d\mathbf{W}_t^{(N)} \quad l = 0, \cdots, k-2, \tag{9.6}$$

where $\Lambda_l^{(N)}$ is the $N \times N$ diagonal matrix $\mathrm{diag}(s_\alpha^l)$, where s_α^l, $\alpha = 1, \cdots, P$ is repeated N_α times, and $\mathbf{W}_t^{(N)}$ an N-dimensional standard Brownian process.

The equation governing the $(k-1)$th differential of the membrane potential has a linear part determined by the differential operator $\mathbf{D}^{k-1}$ and must account for the external inputs (deterministic and stochastic) and the activity of the neighbors, see (9.4). Keeping the same notations as before for the inputs and denoting by $\mathscr{L}^{(N)}$ the $N \times Nk$ matrix describing the action of the neurons membrane potentials and their derivatives on the $(k-1)$th derivative of $\mathbf{V}$, we have:

$$d\widetilde{\mathbf{V}}_{k-1}^{(N)}(t) = \left(\mathscr{L}^{(N)}(t) \cdot \widetilde{\mathbf{V}}^{(N)}(t) + \left(\mathbf{J}^{(N)} \cdot S^{(N)}(\widetilde{\mathbf{V}}_0^{(N)}(t))\right) + \mathbf{I}^{(N)}(t)\right) dt + \Lambda_{k-1}^{(N)}(t) \cdot d\mathbf{W}_t^{(N)}, \tag{9.7}$$

where

$$\mathscr{L}^{(N)} = \left[\ \mathrm{diag}(a_\alpha^0(t)) \quad \cdots \quad \mathrm{diag}(a_\alpha^{k-1}(t))\ \right].$$

We define

$$\mathbf{L}^{(N)}(t) = \begin{bmatrix} 0 & \mathrm{Id}_N & \cdots & 0 \\ 0 & 0 & \ddots & 0 \\ \vdots & \vdots & & \mathrm{Id}_N \\ \mathrm{diag}(a_\alpha^0(t)) & \mathrm{diag}(a_\alpha^1(t)) & \cdots & \mathrm{diag}(a_\alpha^{k-1}(t)) \end{bmatrix},$$

where Id_N is the $N \times N$ identity matrix. We also denote by:

$$\widetilde{\mathbf{U}}_t^{(N)} = \begin{bmatrix} 0 \\ \vdots \\ 0 \\ \mathbf{J}^{(N)} \cdot S^{(N)}(\widetilde{\mathbf{V}}_0(t)) \end{bmatrix} \text{ and } \widetilde{\mathbf{I}}_t^{(N)} = \begin{bmatrix} 0 \\ \vdots \\ 0 \\ \mathbf{I}^{(N)}(t) \end{bmatrix}.$$

The full equation satisfied by $\widetilde{\mathbf{V}}^{(N)}$ can be written:

$$d\widetilde{\mathbf{V}}^{(N)}(t) = \left(\mathbf{L}^{(N)}(t)\widetilde{\mathbf{V}}^{(N)}(t) + \widetilde{\mathbf{U}}_t^{(N)} + \widetilde{\mathbf{I}}_t^{(N)}\right) dt + \Lambda^{(N)}(t) \cdot d\mathbf{W}_t^{(N)}, \tag{9.8}$$

where the $kN \times kN$ matrix $\Lambda^{(N)}(t)$ is equal to $\mathrm{diag}(\Lambda_0^{(N)}, \cdots, \Lambda_{k-1}^{(N)})$.

Note that the kth-order differential equation describing the time variation of the membrane potential of each neuron contains a noise term which is a linear combination of various integrated Brownian processes (up to the order $k-1$) as shown in the

following formula which is derived from (9.6) and (9.7).

$$d\widetilde{\mathbf{V}}_{k-1}^{(N)}(t) = \left(\sum_{l=0}^{k-1} \mathbf{L}_l^{(N)}(t)\widetilde{\mathbf{V}}_l^{(N)}\right) dt + \left(\sum_{l=0}^{k-2} \mathbf{L}_l^{(N)}(t)\left(\sum_{h=0}^{k-l-2}\int_0^t\int_0^{s_1}\cdots\int_0^{s_{h-1}} \Lambda_{l+h}^{(N)}(s_h)d\mathbf{W}_{s_h}d_{s_{h-1}}\cdots ds_0\right)\right) dt + \Lambda_{k-1}^{(N)}(t)d\mathbf{W}_t.$$

Comparing with equation (9.4) we see that the noise $\mathbf{n}^{(N)}dt$ is a weighted sum of Brownian and integrated Brownian processes.

9.1.2 Introduction of the Mean Field equations

General derivation of the mean field equation

The connectivity weight J_{ij} are modeled as independent Gaussian random variables. Their distribution depends only on the population pair $\alpha = p(i), \beta = p(j)$, and on the total number of neurons N_β of population β:

$$J_{ij} \sim \mathcal{N}\left(\frac{\bar{J}_{\alpha\beta}}{N_\beta}, \frac{\sigma_{\alpha\beta}}{\sqrt{N_\beta}}\right).$$

We are interested in the limit law when $N \to \infty$ of the vector $\mathbf{V}^{(N)}$ under the joint law of the connectivities and the Brownian motions, which we call the mean field limit. This law can be described by a set of P equations, the mean field equations. As mentioned in the introduction these equations can be derived in several ways, either heuristically as in the work of Amari [7, 8], Sompolinsky [57, 240], and Cessac [46, 233], or rigorously as in the work of Ben-Arous and Guionnet [20, 21, 122]. We derive them here in a pedestrian way, prove that they are well-posed, and provide an algorithm for computing their solution.

The effective description of the network population by population is possible because the neurons in each population are interchangeable, i.e. have the same probability distribution under the joint law of the multidimensional Brownian motion and the connectivity weights. This is the case because of the form of equation (9.8).

The Mean Field equations We note $C([t_0,T],\mathbb{R}^P)$ (respectively $C((-\infty,T],\mathbb{R}^P)$) the set of continuous functions from the real interval $[t_0,T]$ (respectively $(-\infty,T]$) to $\mathbb{R}^P$. By assigning a probability to subsets of such functions, a continuous stochastic process X defines a positive measure of unit mass on $C([t_0,T],\mathbb{R}^P)$ (respectively $C((-\infty,T],\mathbb{R}^P)$). This set of positive measures of unit mass is noted $\mathscr{M}_1^+(C([t_0,T],\mathbb{R}^P))$ (respectively $\mathscr{M}_1^+(C((-\infty,T],\mathbb{R}^P))$.

We now define a process of particular importance for describing the limit process: the effective interaction process.

Definition 9.1.1 (Effective Interaction Process)**.** Let $X \in \mathscr{M}_1^+(C([t_0,T],\mathbb{R}^P))$ (resp. $\mathscr{M}_1^+(C((-\infty,T],\mathbb{R}^P))$ be a given stochastic process. The effective interaction term is the Gaussian process $\mathbf{U}^X \in \mathscr{M}_1^+(C([t_0,T],\mathbb{R}^{P\times P}))$, (resp. $\mathscr{M}_1^+(C((-\infty,T],\mathbb{R}^{P\times P}))$ statistically independent of the external noise $(\mathbf{W}_t)_{t\geq t_0}$ and of the initial condition X_{t_0} (when $t_0 > -\infty$), defined by:

$$\begin{cases} \mathbb{E}\left[U^X_{\alpha\beta}(t)\right] = \bar{J}_{\alpha\beta} m^X_{\alpha\beta}(t) \text{ where } \quad m^X_{\alpha\beta}(t) \stackrel{\text{def}}{=} \mathbb{E}[S_{\alpha\beta}(X_\beta(t))]; \\ \text{Cov}(U^X_{\alpha\beta}(t), U^X_{\alpha\beta}(s)) = \sigma^2_{\alpha\beta} \Delta^X_{\alpha\beta}(t,s) \text{ where} \\ \qquad\qquad \Delta^X_{\alpha\beta}(t,s) \stackrel{\text{def}}{=} \mathbb{E}\Big[S_{\alpha\beta}(X_\beta(t)) S_{\alpha\beta}(X_\beta(s))\Big]; \\ \text{Cov}(U^X_{\alpha\beta}(t), U^X_{\gamma\delta}(s)) = 0 \text{ if } \alpha \neq \gamma \text{ or } \beta \neq \delta. \end{cases} \tag{9.9}$$

Choose P neurons $i_1, \ldots, i_P$, one in each population (neuron i_α belongs to the population α). Then it can be shown, using either a heuristic argument or large deviations techniques (see section 9.1.3), that the sequence of processes

$$\left(\widetilde{\mathbf{V}}^{(N)}(t) = [\tilde{V}^{(N)}_{i_1}(t), \ldots, \tilde{V}^{(N)}_{i_P}(t)]^T_{t \geq t_0}\right)_{N \geq 1}$$

converges in law to the process $\widetilde{\mathbf{V}}(t) = [\tilde{V}_1(t), \ldots, \tilde{V}_P(t)]^T_{t \geq t_0}$ solution of the following mean field equation:

$$d\widetilde{\mathbf{V}}(t) = \left(\mathbf{L}(t)\widetilde{\mathbf{V}}(t) + \widetilde{\mathbf{U}}^{\mathbf{V}}_t + \widetilde{\mathbf{I}}(t)\right) dt + \Lambda(t) \cdot d\mathbf{W}_t, \tag{9.10}$$

where $\widetilde{\mathbf{V}}$ is a kP-dimensional vector containing the P-dimensional vector $\mathbf{V}$ and its $k-1$ derivatives, and $\mathbf{L}$ is the $Pk \times Pk$ matrix

$$\mathbf{L}(t) = \begin{bmatrix} 0_{P\times P} & \text{Id}_P & \cdots & 0_{P\times P} \\ 0_{P\times P} & 0_{P\times P} & \ddots & 0_{P\times P} \\ \vdots & \vdots & & \text{Id}_P \\ \mathbf{L}_0(t) & \mathbf{L}_1(t) & \cdots & \mathbf{L}_{k-1}(t) \end{bmatrix},$$

where Id_P is the $P \times P$ identity matrix and $0_{P\times P}$ the null $P \times P$ matrix. $(\mathbf{W}_t)$ is a kP-dimensional standard Brownian process and:

$$\widetilde{\mathbf{U}}^{\mathbf{V}}_t = \begin{bmatrix} 0_P \\ \vdots \\ 0_P \\ \mathbf{U}^{\mathbf{V}}_t \cdot \mathbf{1} \end{bmatrix} \quad \widetilde{\mathbf{I}}(t) = \begin{bmatrix} 0_P \\ \vdots \\ 0_P \\ \mathbf{I}(t) \end{bmatrix} \quad \Lambda(t) = \text{diag}(\Lambda_0(t), \cdots, \Lambda_{k-1}(t)).$$

The matrices $\mathbf{L}_0, \cdots, \mathbf{L}_{k-1}$ (respectively $\Lambda_0, \cdots, \Lambda_{k-1}$) are obtained by selecting the same P rows and P columns of the matrices $\mathbf{L}^{(N)}_0, \cdots, \mathbf{L}^{(N)}_{k-1}$ (respectively $\Lambda^{(N)}_0, \cdots, \Lambda^{(N)}_{k-1}$) corresponding to P neurons in different populations, $(\mathbf{U}^{\mathbf{V}}_t)$ is the effective interaction process associated with $\mathbf{V}$, and $\mathbf{I}(\cdot)$ is the P-dimensional external current.

To proceed further we formally integrate the equation using the flow, or resolvent, of the equation, noted $\Phi_L(t, t_0)$ (see appendix E.1), and we obtain, since we assumed $\mathbf{L}$ continuous, an implicit representation of $\mathbf{V}$:

$$\widetilde{\mathbf{V}}(t) = \Phi_L(t,t_0)\widetilde{\mathbf{V}}(t_0) + \int_{t_0}^t \Phi_L(t,s) \cdot \left(\widetilde{\mathbf{U}}^{\mathbf{V}}_s + \widetilde{\mathbf{I}}(s)\right) ds + \int_{t_0}^t \Phi_L(t,s) \cdot \Lambda(s) d\mathbf{W}_s \tag{9.11}$$

9.1.3 Derivation of the Mean Field equations

There have been many attemps in order to rigorously or heuristically prove the Mean-field equations from first principles. The most classical heuristic proof is provided by

the use of the local chaos hypothesis. To our knowledge, the only rigorous proof was provided by Ben-Arous and Guionnet. We provide these two proofs, and prove that the local chaos hypothesis leads to contradictions, whereas the rigorous approach based on large deviation techniques leads to a more complex equation which can be interpreted as our MFE.

The local chaos hypothesis method

The mean field equations can be obtained heuristically under the local chaos hypothesis, assuming that in the limit $N \to \infty$, the neural network behaves as if the $(V_i)_{i\in\{1,\dots,N\}}$ were asymptotically independent and also independent of the synaptic weights J_{ij}. This hypothesis has been widely discussed. For instance the aging phenomenon widely studied (see e.g. [18, 19, 134]. We show also that hypothesis leads very fast a to contradiction. This is why we will turn to more rigorous approaches in the next subsection.

Let us derive under this hypothesis the limit of the microscopic equations (9.15) when the number of neurons tends to infinity. More precisely, we assume that the process converges to a continuous process which has the asymptotic independence property and we characterize the limiting distribution. This proof is based on the theory of the convergence in law of processes [23].

Proposition 9.1.1. Let $i_1^{(N)},\dots,i_P^{(N)}$ be P neurons among the N neurons of the total population, where the neuron $i_\alpha^{(N)}$ belongs to the population α. Assume that the sequence of P-dimensional processes $\mathbf{V}^{(N)} := (V_{i_1^{(N)}}^{(N)}(t),\dots,V_{i_P^{(N)}}^{(N)}(t))_{t\geq 0}^T$ converges in law to a continuous process $(\mathbf{V}(t))_t$ having pairwise independent components and which is independent of the synaptic weights J_{ij}. and that for all $\varepsilon > 0$ and $\eta > 0$ there exists $\delta > 0$ such that

$$\limsup \mathbb{P}\left\{ \sup_{|t-s|<\delta} \|\mathbf{V}(t)-\mathbf{V}(s)\| > \eta \right\} < \varepsilon \tag{9.12}$$

Then the microscopic interaction process

$$U_{\alpha\beta}^N := \sum_{j=1}^{N_\beta} J_{ij} S_{\alpha\beta}\big(V_j(t)\big)$$

converges in law when $N \to \infty$ to the effective interaction process defined in definition 9.1.1

Heuristic proof. We give here a a heuristic argument usually provided to derive the MFE. As we will see, the main approximation done is to consider that the asymptotic independence coming from the local chaos hypothesis is true for N big but finite.

The convergence to a Gaussian process is a direct consequence of the functional central limit theorem, which applies when condition (9.12) is satisfied (see e.g. [216]), under the condition that the finite dimensional distribution converge.

The heuristic proof of this property requires two steps. The first step consists in proving the tightness of the sequence of processes $(U_{\alpha,\beta}^N)_{N\geq 0}$ for given integers α,β, and the second to identify the possible limits of this process.

The tightness can be proved by using Aldous' criterion of tightness in the Skorokhod space (see [23]). Let α and β be fixed integers in $\{1,\dots,P\}$. We denote by V^N

the process of membrane potential for a network of N neurons. This criterion ensures us that it is enough to prove that the sequence of processes satisfies the property:

$$\lim_{|t-s|\to 0}\sup_N \mathbb{E}\left[\left|U^N_{\alpha,\beta}(t)-U^N_{\alpha,\beta}(s)\right|^2\Big|\mathscr{F}_s\right]=0$$

This is true for our process, since we have under local chaos hypothesis:

$$\begin{aligned}\lim_{N\to\infty}\mathbb{E}\left[\left|U^N_{\alpha,\beta}(t)-U^N_{\alpha,\beta}(s)\right|^2\Big|\mathscr{F}_s\right]&=\lim_{N\to\infty}\mathbb{E}\left[\left|\sum_{j=1}^{N_\beta}J_{i,j}\big(S_{\alpha\beta}(V_j(t))-S_{\alpha\beta}(V_j(s))\big)\right|^2\Big|\mathscr{F}_s\right]\\&=\lim_{N\to\infty}\sum_{j=1}^{N_\beta}\sum_{k=1}^{N_\beta}\mathbb{E}\left[J_{i,j}J_{i,k}\big(S_{\alpha\beta}(V_j(t))-S_{\alpha\beta}(V_j(s))\big)\big(S_{\alpha\beta}(V_k(t))-S_{\alpha\beta}(V_k(s))\big)\Big|\mathscr{F}_s\right]\end{aligned}$$

At this point, we assume that the independence property between the membrane potential and the interaction is valid for N big but fixed. Hence we get:

$$\begin{aligned}&=\lim_{N\to\infty}\left\{\sum_{j=1}^{N_\beta}\sum_{\substack{k=1\\k\neq j}}^{N_\beta}\frac{\bar{J}^2_{\alpha\beta}}{N^2_\beta}\mathbb{E}\left[\big(S_{\alpha\beta}(V_j(t))-S_{\alpha\beta}(V_j(s))\big)\big(S_{\alpha\beta}(V_k(t))-S_{\alpha\beta}(V_k(s))\big)\right]\right.\\&\quad\left.+\sum_{j=1}^{N_\beta}\frac{\sigma^2_{\alpha\beta}}{N_\beta}\mathbb{E}\left[\big(S_{\alpha\beta}(V_j(t))-S_{\alpha\beta}(V_j(s))\big)^2\right]\right\}\\&=\lim_{N\to\infty}\left\{\sum_{j=1}^{N_\beta}\sum_{\substack{k=1\\k\neq j}}^{N_\beta}\frac{\bar{J}^2_{\alpha\beta}}{N^2_\beta}\mathbb{E}\left[\big(S_{\alpha\beta}(V_j(t))-S_{\alpha\beta}(V_j(s))\big)\right]\mathbb{E}\left[\big(S_{\alpha\beta}(V_k(t))-S_{\alpha\beta}(V_k(s))\big)\right]\right.\\&\quad\left.+\sum_{j=1}^{N_\beta}\frac{\sigma^2_{\alpha\beta}}{N_\beta}\mathbb{E}\left[\big(S_{\alpha\beta}(V_j(t))-S_{\alpha\beta}(V_j(s))\big)^2\right]\right\}\\&\leq\max_{\alpha,\beta}\bar{J}^2_{\alpha\beta}\mathbb{E}\left[\big(S_{\alpha\beta}(V_j(t))-S_{\alpha\beta}(V_j(s))\big)\right]^2+\max_{\alpha,\beta}\sigma^2_{\alpha\beta}\mathbb{E}\left[\big(S_{\alpha\beta}(V_j(t))-S_{\alpha\beta}(V_j(s))\big)^2\right]\\&\underset{|t-s|\to 0}{\longrightarrow}0\end{aligned}$$

since we assumed that the process V^N converged in law to a continuous process.

Moreover, for a fixed finite N, we have

$$\sup_{n\leq N}\mathbb{E}\left[\left|U^n_{\alpha,\beta}(t)-U^n_{\alpha,\beta}(s)\right|^2\Big|\mathscr{F}_s\right]\underset{|t-s|\to 0}{\longrightarrow}0$$

By the continuity of each process of the sum.

Hence we complete the simple Aldous-like criterion:

$$\sup_{N\in\mathbb{N}}\mathbb{E}\left[\left|U^N_{\alpha,\beta}(t)-U^N_{\alpha,\beta}(s)\right|^2\Big|\mathscr{F}_s\right]\underset{|t-s|\to 0}{\longrightarrow}0$$

Hence by a simplified version of Aldous' theorem [23], we conclude that the sequence is tight. By Prohorov's theorem, we know that the sequence $(U^N_{\alpha,\beta})_{N\geq 0}$ is locally compact, and thus from each subsequence we can extract a converging subsequence.

Identifying the finite dimensional asymptotic process is an application of the law of large numbers and of the central limit theorem. Indeed, let $n\in\mathbb{N}$ and $(t_1,\ldots,t_n)\in$

$\mathbb{R}^n$. We consider the sequence of finite dimensional random variables

$$\left((U^N_{\alpha,\beta}(t_1))_{\alpha,\beta\in\{1,\dots,P\}},\dots,(U^N_{\alpha,\beta}(t_n))_{\alpha,\beta\in\{1,\dots,P\}}\right)_N.$$

It can be considered as a sum of independent identically distributed multi-dimensional random variables when $N\to\infty$ under the approximation that the independence is true for N big (but finite), and hence the central limit theorem applies. We have:

$$\begin{aligned}
\lim_{N\to\infty}\mathbb{E}\Big(U^N_{\alpha,\beta}(t)\Big) &= \lim_{N\to\infty}\mathbb{E}\Big(\sum_{j=1}^{N_\beta}J_{i,j}S_{\alpha\beta}(V_j(t))\Big)\\
&= \lim_{N\to\infty}\sum_{j=1}^{N_\beta}\mathbb{E}\Big(J_{i,j}S_{\alpha\beta}(V_j(t))\Big)\\
&= \lim_{N\to\infty}\frac{1}{N_\beta}\sum_{j=1}^{N_\beta}\bar{J_{\alpha\beta}}m_\beta(t)\\
&= \bar{J_{\alpha\beta}}m_\beta(t)
\end{aligned}$$

The covariance reads, for $\alpha(i)=\alpha$ and $\alpha(l)=\gamma$:

$$\begin{aligned}
&\lim_{N\to\infty}\mathrm{Cov}\Big(U^N_{\alpha,\beta}(t),U^N_{\gamma,\delta}(s)\Big) =\\
&\lim_{N\to\infty}\mathbb{E}\left(\left\{\sum_{j=1}^{N_\beta}J_{i,j}S_{\alpha\beta}(V_j(t))-\frac{\bar{J_{\alpha\beta}}}{N_\beta}m_\beta(t)\right\}\times\left\{\sum_{k=1}^{N_\delta}J_{l,k}S_\delta(V_k(t))-\frac{\bar{J_{\gamma\delta}}}{N_\delta}m_\delta(t)\right\}\right)\\
&=\lim_{N\to\infty}\mathbb{E}\left(\left\{\sum_{j=1}^{N_\beta}(J_{i,j}-\frac{\bar{J_{\alpha\beta}}}{N_\beta})S_{\alpha\beta}(V_j(t))+\frac{\bar{J_{\alpha\beta}}}{N_\beta}(S_{\alpha\beta}(V_j(t))-m_\beta(t))\right\}\right.\\
&\qquad\left.\times\left\{\sum_{k=1}^{N_\delta}(J_{l,k}-\frac{\bar{J_{\gamma\delta}}}{N_\delta})S_\delta(V_k(t))+\frac{\bar{J_{\gamma\delta}}}{N_\delta}(S_\delta(V_k(t))-m_\delta(t))\right\}\right)\\
&=\lim_{N\to\infty}\sum_{j=1}^{N_\beta}\sum_{k=1}^{N_\delta}\left[\mathbb{1}_{\alpha=\gamma,\beta=\delta,j=k}\frac{\sigma^2_{\alpha\beta}}{N_\beta}\mathbb{E}\Big(S_{\alpha\beta}(V_j(t))S_\delta(V_k(s))\Big)+\frac{\bar{J_{\alpha\beta}}}{N_\beta}\frac{\bar{J_{\gamma,\delta}}}{N_\delta}\mathrm{Cov}\left(S_{\alpha\beta}(V_j(t)),S_\delta(V_k(s))\right)\right]
\end{aligned}$$

Under the local chaos hypothesis and since the law of V_j,V_k only depend on their population $\mathrm{Cov}\left(S_{\alpha\beta}(V_j(t)),S_\delta(V_k(s))\right)=\mathrm{Cov}\left(S_{\alpha\beta}(V_j(t)),S_\delta(V_k(s))\right)\mathbb{1}_{\beta=\delta,j=k}$, we obtain:

$$\begin{aligned}
&\lim_{N\to\infty}\mathrm{Cov}\Big(U^N_{\alpha,\beta}(t),U^N_{\gamma,\delta}(s)\Big) =\\
&=\lim_{N\to\infty}\mathbb{1}_{\alpha=\gamma,\beta=\delta}\left[\sigma^2_{\alpha\beta}\mathbb{E}\Big(S_{\alpha\beta}(V_j(t))S_{\alpha\beta}(V_j(s))\Big)+\sum_{j=1}^{N_\beta}\frac{\bar{J^2_{\alpha\beta}}}{N^2_\beta}\mathrm{Cov}(S_{\alpha\beta}(V_j(t)),S_{\alpha\beta}(V_j(s)))\right]\\
&=\mathbb{1}_{\alpha=\gamma,\beta=\delta}\sigma^2_{\alpha\beta}\mathbb{E}\Big(S_{\alpha\beta}(V_\beta(t))S_{\alpha\beta}(V_\beta(s))\Big)
\end{aligned}$$

Eventually, the limit of the interaction term is identified. Using this result, we know, for instance integrating formally the equation (9.15) that the process converges in law to the solution of the equation (9.16), and hence the theorem is proved.

□

This proof is based under the assumption of two limit can be commuted. This property is not always ensured, and even in the present case, this assumption leads to contradictions. Indeed, using the same type of calculations, one can prove that the effective interaction process is statistically independent of the membrane potential V, which is not the case. In details, since both the membrane potential and the effective interaction terms are Gaussian processes, we only have to show that their correlation is null. This is true since, if we take i neuron of class γ and $\alpha,\beta \in \{1,\dots,P\}$. Let k a neuron of population α. We have:

$$\begin{aligned}\mathrm{Cov}(V_i(t),U_{\alpha,\beta}(s)) &= \mathrm{Cov}(V_i(t),\lim_{N\to\infty}\sum_{j=1}^{N_\beta} J_{k,j}S_{\alpha\beta}(V_j(s)))\\ &= \lim_{N\to\infty}\sum_{j=1}^{N_\beta}\mathrm{Cov}(V_i(t),J_{k,j}S_{\alpha\beta}(V_j(s)))\\ &= 0.\end{aligned}$$

In going from the first to the second line we made the approximation that the limit and the expectation commuted. Under the same approximation as before, i.e. independence of the processes and the connectivity weights for N big, the only term that is possibly non-vanishing is the correlation between $V_i(t)$ and $J_{k,i}V_i(s)$ if $\beta=\gamma$. But this term is scaled by $\frac{1}{N_\beta}$ and hence the correlation vanishes.

This assumption and this type of calculations are therefore very slippery, and this is why we now turn to a more rigorous approach.

Large deviations techniques

Gérard Ben-Arous and Alice Guionnet studied from a mathematical point of view the problem of finding a mean-field description of large networks of spin glasses. They obtained using different methods of stochastic analysis a weak limit of the law of a given spin and proved their independence.

Our equations do not directly fit in their study: indeed, the spin intrinsic dynamics is nonlinear while the interaction is linear, and everything in done in dimension one. Nevertheless, their proof extends to our case which is somehow more simple. For instance in the case of the Simple Model with one population, we can readily adapt their proof in our case. More precisely, let $P=1$, the equation of the network reads:

$$\tau dV_t^j = (-V_t^j + \sum_{i=1}^{N} J_{ij}S(V_t^i))\,dt + \sigma dW_t^j$$

In this case, we define for $X \in \mathscr{M}_1^+(C([t_0,T],\mathbb{R})$ the effective interaction term (U_t^X) which is the effective interaction process defined in 9.1.1, i.e. the Gaussian process of mean $\bar{J}_{\alpha\beta}\mathbb{E}[S(X_t)]$ and of covariance: $\mathrm{Cov}\left(U_t^X,U_s^X\right) =: \sigma_{\alpha\beta}^2\mathbb{E}[S(X_t)S(X_s)]$.

Let us note $\mathscr{P}$ the law of the membrane potential when there is no interaction (it is an Ornstein-Ulhenbeck process), and the empirical measure $\hat{V}^N = \frac{1}{N}\sum_{i=1}^N \delta_{V^i}$. We can prove that under the probability distribution averaged over the connectivities, see below, the empirical measure satisfies a large deviation principle with good rate function H defined as in [122]. Using this large deviation result, we can prove annealed and quenched tightness of the empirical measure, and finally its convergence

towards the unique process where the good rate function H achieves its unique minimum, which is defined by the property of having a density with respect to $\mathscr{P}$ and whose density satisfies the implicit equation:

$$Q \ll \mathscr{P} \qquad \frac{dQ}{d\mathscr{P}} = \mathscr{E}\left[\exp\left\{\int_0^T U_t^Q dW_t - \frac{1}{2}\int_0^T (U_t^Q)^2\, dt\right\}\right] \tag{9.13}$$

where $\mathscr{E}$ denotes the expectation over the effective interaction process U^Q.

We can also prove following the steps of Ben-Arous and Guionnet in [21] that there exists a unique solution to this equation, and that this solution satisfies the nonlinear nonmarkovian stochastic differential equation:

$$\begin{cases} \tau dV_t = -V_t\, dt + dB_t \\ dB_t = dW_t + \int_0^t dB_s \mathscr{E}\left[U_s^Q U_t^Q \frac{\exp\{-\frac{1}{2}\int_0^t (U_u^Q)^2 du\}}{\mathscr{E}[\exp\{-\frac{1}{2}\int_0^t (U_u^Q)^2 du\}]}\right] \\ \text{Law of } (V) = Q, \ \text{ law of } (V_0) = Z_0 \end{cases} \tag{9.14}$$

which can also be written as our mean field equation, averaged on the connectivities (see [20]). More precisely, let L^V be the law of the solution of the equation:

$$\begin{cases} \tau dV_t = -V_t dt + dW_t + U_t^V dt \\ \text{Law of } V_0 = Z_0 \end{cases},$$

which is exactly equation (9.16). They prove that V satisfies the nonlinear equation:

$$V \stackrel{\mathscr{L}}{=} \mathscr{E}(L^V)$$

This result also readily extends to the multi-population case. The only difference is that one is lead to make use of the multi-dimensional Girsanov's theorem. The principle of the proof is exactly the same, and the proof that the resulting H function is good rate function is provided by the original proof for spin glasses.

9.1.4 Neural Network Models

We now introduce quite frequently used neural mass models which are one of the motivations of the present chapter.

Example: The Simple Model

In the Simple Model, each neuron membrane potential decreases exponentially to its rest value if it receives no input, with a time constant τ_α depending only on the population. The noise is modeled by an independent Brownian process per neuron whose standard deviation is the same for all neurons belonging to a given population.

Hence the dynamics of a given neuron i from population α of the network reads:

$$dV_i^{(N)}(t) = \Big[-\frac{V_i^{(N)}(t)}{\tau_\alpha} + \sum_{\beta=1}^{P}\sum_{j=1}^{N_\beta} J_{ij} S_{\alpha\beta}\big(V_j^{(N)}(t)\big) + I_\alpha(t)\Big]\, dt + s_\alpha dW_{(i)}(t). \tag{9.15}$$

This is a special case of equation (9.10) where $k=1$ and $\mathbf{L}=-\mathrm{diag}(\frac{1}{\tau_1},\cdots,\frac{1}{\tau_P})$, $\Phi_L(t,t_0)=\mathrm{diag}(e^{-(t-t_0)/\tau_1},\cdots,e^{-(t-t_0)/\tau_P})$, and $\Lambda=\mathrm{diag}(s_1,\cdots,s_P)$. The corresponding mean field equation reads:

$$dV_\alpha(t)=\Big(-\frac{V_\alpha}{\tau_\alpha}(t)+\sum_{\beta=1}^{P}U^V_{\alpha\beta}(t)+I_\alpha(t)\Big)\,dt+s_\alpha dW_\alpha(t),\ \ \forall\alpha\in\{1,\ldots,P\},\tag{9.16}$$

where the processes $(W_\alpha(t))_{t\geq 0}$ are independent standard Brownian motions, $\mathbf{U}^V(t)=(U^V_{\alpha\beta}(t);\ \alpha,\beta\in\{1,\ldots,P\})_t$ is the effective interaction term.

This equation can be integrated implicitly and we obtain the following integral representation of the process $V_\alpha(t)$:

$$V_\alpha(t)=e^{-(t-t_0)/\tau_\alpha}V_\alpha(t_0)+\int_{t_0}^{t}e^{-(t-s)/\tau_\alpha}\Big(\sum_{\beta=1}^{P}U^V_{\alpha\beta}(s)+I_\alpha(s)\Big)\,ds \\ +s_\alpha\int_{t_0}^{t}e^{-(t-s)/\tau_\alpha}dW_\alpha(s)\Big)\tag{9.17}$$

where t_0 is the initial time. It is an implicit equation on the probability distribution of $\mathbf{V}(t)$, a special case of (9.11).

The Jansen and Rit's model

One of the motivations of this study is to characterize the global behavior of an assembly of neurons in particular to get a better understanding of non-invasive cortical signals like EEG or MEG. One of the classical models of neural masses is Jansen and Rit's mass model [149], in short the JR model (see figure 9.1).

The model features a population of pyramidal neurons (central part of figure 9.1.a.) that receives excitatory and inhibitory feedback from local inter-neurons and an excitatory input from neighboring cortical units and sub-cortical structures such as the thalamus. The excitatory input is represented by an arbitrary average firing rate $p(t)$ that can be stochastic (accounting for a non specific background activity) or deterministic, accounting for some specific activity in other cortical units. The transfer functions h_e and h_i of figure 9.1 convert the average firing rate describing the input to a population into an average excitatory or inhibitory post-synaptic potential (EPSP or IPSP). They correspond to the synaptic integration.

In the model introduced originally by Jansen and Rit, the connectivity weights were assumed to be constant, equal to their mean value (it is the constants C_i, $i=1\ldots4$ in figure 9.1). Nevertheless, there exists a variability on these coefficients, and as we will see in the sequel, the effect of the connectivity variability impacts the solution at the level of the neural mass. Statistical properties of the connectivities have been studied in details for instance in [28]. In our model we consider these connectivities as independent Gaussian random variables of mean and standard deviation equal to the ones found in [28].

We now use diagram 9.1 to derive the membrane potential expressions. We consider a network of N neurons belonging to the three populations described. We denote by P (resp E, I) the pyramidal (respectively excitatory, inhibitory) populations. We choose in population P (respectively populations E, I) a particular pyramidal neuron

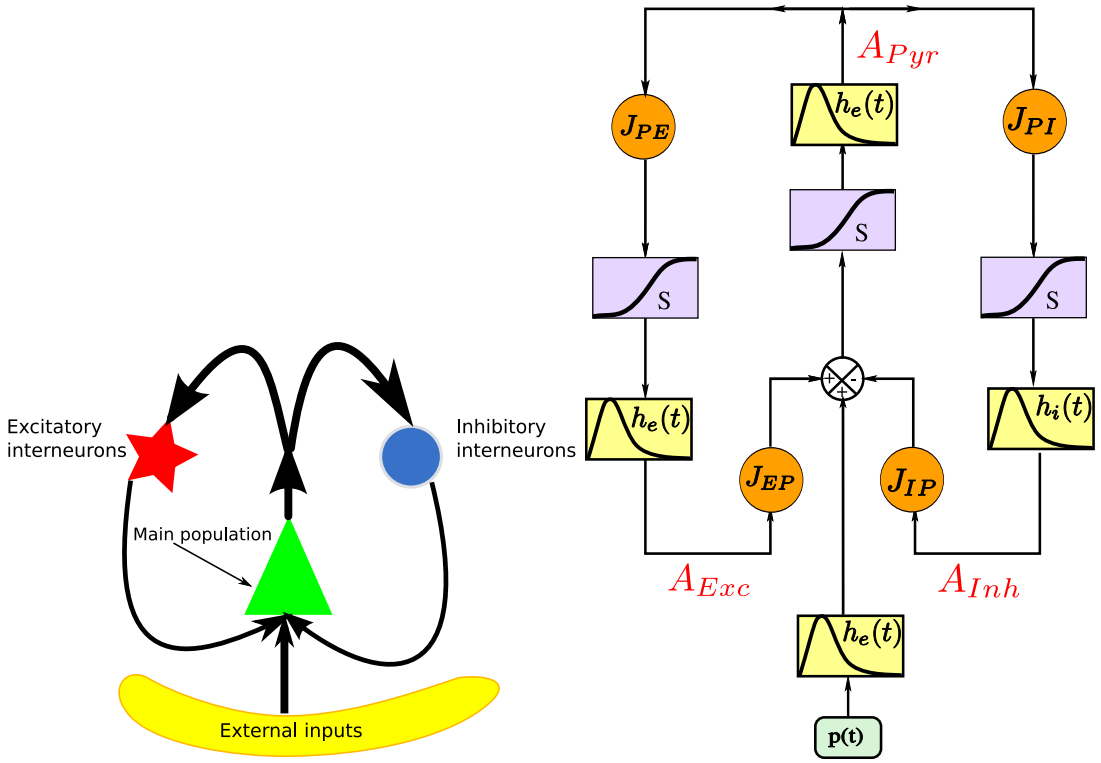

(a) Populations involved in Jansen's model (b) Block diagram

Figure 9.1: a. Neural mass model: a population of pyramidal cells interacts with two populations of inter-neurons: an excitatory one and an inhibitory one. b. Block representation of the model. The h boxes account for the synaptic integration between neuronal populations. S boxes simulate cell bodies of neurons by transforming the membrane potential of a population into an output firing rate. The coefficients $J_{\alpha\beta}$ are the random synaptic efficiency of population β on population α (P is the pyramidal population, E the excitatory and I the inhibitory ones).

(respectively excitatory, inhibitory interneuron) indexed by i_{pyr} (respectively i_{exc}, i_{inh}). The equations of their activity variable read:

$$\begin{cases} A^N_{i_{pyr}} &= h_e * S(\sum_{j\ Exc} J_{ij} A^N_j + h_e * p(\cdot) + \sum_{j\ Inh} J_{ij} A^N_j) \\ A^N_{i_{exc}} &= h_e * S(\sum_{j\ Pyr} J_{ij} A^N_j) \\ A^N_{i_{inh}} &= h_i * S(\sum_{j\ Pyr} J_{ij} A^N_j) \end{cases}$$

This is therefore an activity-based model. As stated before, it is equivalent via a change of variable to a voltage-based model, with the same connectivity matrix, the same intrinsic dynamics, and modified inputs (see section 9.1.1).

In the mean field limit, denoting by A_P (respectively A_E, A_I) the activity of the pyramidal neurons (resp excitatory, inhibitory interneurons), we obtain the following activity equations:

$$\begin{cases} A_P &= h_e * S(U_{PE} + h_e * p + U_{PI}) \\ A_E &= h_e * S(U_{EP}) \\ A_I &= h_e * S(U_{IP}) \end{cases} \tag{9.18}$$

where $\mathbf{U} = (U_{ij})_{i,j\in\{P,E,I\}}$ is the effective interaction process associated with this problem, i.e. a Gaussian process of means:

$$\begin{cases} \mathbb{E}[U_{EP}] &= \bar{J_{EP}}\mathbb{E}[A_E] \\ \mathbb{E}[U_{IP}] &= \bar{J_{IP}}\mathbb{E}[A_I] \\ \mathbb{E}[U_{PI}] &= \bar{J_{PI}}\mathbb{E}[A_P] \\ \mathbb{E}[U_{PE}] &= \bar{J_{PE}}\mathbb{E}[A_P] \end{cases}$$

and whose covariance matrix can be deduced from (9.9). The voltage-based model can be deduced from this activity-based description using a simple change of variable as stated previously. Note that the change of variable is possible since the activity current I_A is equal to $h_e * p$ and, as shown in section 9.1.1, I_A is smooth enough so that we can apply to it the suitable differential operator. p is the corresponding voltage current I_V.

Let us now instantiate the synaptic dynamics and compare the mean field equation with Jansen's population equations (sometimes improperly called also mean field equations).

The simplest model of synaptic integration is a first-order integration, which yields exponential post-synaptic potentials:

$$h(t) = \begin{cases} \alpha e^{-\beta t} & t \geq 0 \\ 0 & t < 0 \end{cases}$$

that satisfies the following differential equations

$$\dot{h}(t) = -\beta h(t) + \alpha\delta(t),$$

In these equations β is the time constant of the synaptic integration and α the synaptic efficiency. The coefficients named α and β are the same for the pyramidal and the excitatory population, and different from the ones of the inhibitory synapse. In the pyramidal or excitatory (respectively the inhibitory) case we have $\alpha = A$, $\beta = a$ (respectively $\alpha = B$, $\beta = b$). Eventually, the sigmoid functions are the same whatever the populations, and is given by

$$S(v) = \frac{\nu_{\max}}{1 + e^{r(v_0 - v)}},$$

$\nu_{\max}$ is the maximum firing rate, and v_0 is a voltage reference.

With this synaptic dynamics we obtain the first-order Jansen and Rit's equation:

$$\begin{cases} \frac{dA_P}{dt}(t) &= -aA_P(t) + AS(U_{PE} + U_{PI} + h_e * p(t)) \\ \frac{dA_E}{dt}(t) &= -aA_E(t) + AS(U_{EP}) \\ \frac{dA_I}{dt}(t) &= -bA_I(t) + BS(U_{IP}) \end{cases}. \tag{9.19}$$

while the "original" Jansen and Rit's equation [114, 149] reads:

$$\begin{cases} \frac{dA_P}{dt}(t) &= -aA_P(t) + AS(C_2A_E(t) - C_4A_I(t) + h_e * p(t)) \\ \frac{dA_E}{dt}(t) &= -aA_E(t) + AS(C_1A_P(t)) \\ \frac{dA_I}{dt}(t) &= -bA_I(t) + BS(C_3A_P(t)) \end{cases}. \tag{9.20}$$

Hence the original JR equation amounts to computing the expectation of the activity in each population and to assume that

$$\mathbb{E}\left[S(U_{PE}+U_{PI}+h_e*p(t))\right]=S(\mathbb{E}\left[U_{PE}+U_{PI}+h_e*p\right]),$$

which is a quite sharp assumption given that the sigmoidal function is nonlinear.

A higher order model was introduced to better account for the synaptic integration and to better reproduce the characteristics of real EPSPs and IPSPs by van Rotterdam and colleagues [275]. In this model the PSP satisfies a second order differential equation:

$$h(t)=\begin{cases}\alpha\beta te^{-\beta t} & t\geq 0\\ 0 & t<0\end{cases},$$

solution of the differential equation $\ddot{y}(t)=\alpha\beta\delta(t)-2\beta\dot{y}(t)-\beta^2y(t)$. With this type of synaptic integration, we obtain the following mean field equations:

$$\begin{cases}\frac{d^2A_P}{dt^2}(t) &= AaS(U_{PE}+U_{PI}+h_e*p(t))-2a\frac{dA_P}{dt}(t)-a^2A_P(t)\\ \frac{d^2A_E}{dt^2}(t) &= AaS(U_{EP})-2a\frac{dA_E}{dt}(t)-a^2A_E(t)\\ \frac{d^2A_I}{dt^2}(t) &= BbS(U_{IP})-2b\frac{dA_I}{dt}(t)-b^2A_I(t)\end{cases}\tag{9.21}$$

while the original system satisfies the equations:

$$\begin{cases}\frac{d^2A_P}{dt^2}(t) &= AaS(C_2A_E(t)-C_4A_I(t)+h_e*p(t))-2a\frac{dA_P}{dt}(t)-a^2A_P(t)\\ \frac{d^2A_E}{dt^2}(t) &= AaS(C_1A_P(t))-2a\frac{dA_E}{dt}(t)-a^2A_E(t)\\ \frac{d^2A_I}{dt^2}(t) &= BbC_4S(C_3A_P(t))-2b\frac{d^2A_I}{dt^2}(t)-b^2A_I(t)\end{cases}\tag{9.22}$$

Here again, going from the mean field equations (9.21) to the neural mass model (9.22) consists in studying the equation of the mean of the process given by (9.21) and commuting the sigmoidal function with the expectation.

Note that the introduction of higher order synaptic integrations results in richer behaviors. For instance, Grimbert and Faugeras [114] showed that some bifurcations can appear in the second-order JR model giving rise to epileptic like oscillations and alpha activity, that do not appear in the first order model.

9.2 Existence and uniqueness of solutions in finite time

The mean field equation (9.11) is an implicit equation of the stochastic process $(V(t))_{t\geq t_0}$. We prove in this section that under some mild assumptions this implicit equation has a unique solution. This solution is a fixed point in the set $\mathscr{M}_1^+(C([t_0,T],\mathbb{R}^{kP}))$ of kP-dimensional processes. We construct a sequence of processes and prove that it converges in distribution toward this fixed point.

We denote by $\mathscr{X}$ the set of random variables (r.v.) with values in $\mathbb{R}^{kP}$. We first recall some results on the convergence of random variables and stochastic processes.

9.2.1 Convergence of Gaussian processes

We recall the following result from [25].

Theorem 9.2.1. *Let $\{X_n\}_{n=1}^{\infty}$ be a sequence of kP-dimensional Gaussian processes defined on $[t_0,T]$ or on an unbounded interval of $\mathbb{R}$[2]. The sequence converges to a Gaussian process X if and only if the following three conditions are satisfied:*

- *The sequence $\{X_n\}_{n=1}^{\infty}$ is uniformly tight.*
- *The sequence $\mu_n(t)$ of the mean functions converges for the uniform norm.*
- *The sequence C_n of the covariance operators converges for the uniform norm.*

We now define such a sequence of Gaussian processes.

Let us fix Z_0, a kP-dimensional Gaussian random variable, independent of the Brownian.

Definition 9.2.1. Let X an element of $\mathscr{M}_1^+(C([t_0,T],\mathbb{R}^{kP}))$. Let F_k be the function such that

$$F_k(X)_t = \Phi_L(t,t_0)\cdot Z_0 + \int_{t_0}^{t} \Phi_L(t,s)\cdot\left(\widetilde{\mathbf{U}}_s^X + \widetilde{\mathbf{I}}(s)\right) ds + \int_{t_0}^{t} \Phi_L(t,s)\cdot\Lambda(s) d\mathbf{W}_s$$

where $\widetilde{\mathbf{U}}_s^X$ and $\widetilde{\mathbf{I}}(s)$ are defined in section 9.1.

Note that, by definition, the random process $(F_k(X))_{t\in[t_0,T]}$, $k\geq 1$ is the sum of a deterministic function (defined by the external current) and three independent random processes defined by the initial condition, the interaction between neurons, and the external noise.

Let X be a given stochastic process of $\mathscr{M}_1^+(C([t_0,T],\mathbb{R}^{kP}))$ such that $X_{t_0}=Z_0$. We define the sequence of processes $\{X_n\}_{n=0}^{\infty}\in\mathscr{M}_1^+(C([t_0,T],\mathbb{R}^{kP})$ by:

$$\begin{cases} X_0 & = X \\ X_{n+1} & = F_k(X_n) = F_k^{(n)}(X_0). \end{cases} \tag{9.23}$$

In the remaining of this section we show that the sequence of processes $\{F_k^{(n)}(X)\}_{n=0}^{\infty}$ converges in distribution toward the unique fixed-point Y of F_k.

9.2.2 Existence and uniqueness of solution for the mean field equations

The following upper and lower bounds are used in the sequel.

Lemma 9.2.2. We consider the Gaussian process $((\mathbf{U}_t^X\cdot\mathbf{1})_t)_{t\in[t_0,T]}$. $\mathbf{U}^X$ is defined in 9.1.1 and $\mathbf{1}$ is the P-dimensional vector with all coordinates equal to 1. We have

$$\left\|\mathbb{E}\left[\mathbf{U}_t^X\cdot\mathbf{1}\right]\right\|_{\infty} \leq \mu \stackrel{\text{def}}{=} \max_{\alpha}\sum_{\beta}|\bar{J}_{\alpha\beta}|\,\|S_{\alpha\beta}\|_{\infty} \tag{9.24}$$

for all $t_0\leq t\leq T$. The maximum eigenvalue of its covariance matrix is upperbounded by $\sigma_{\max}^2 \stackrel{\text{def}}{=} \max_\alpha\sum_\beta \sigma_{\alpha\beta}^2\|S_{\alpha\beta}\|_\infty^2$ where $\|S_{\alpha\beta}\|_\infty$ is the supremum of the absolute value of $S_{\alpha\beta}$.

Proof. The proof is straightforward from definition 9.2.1. □

[2] In [25, Chapter 3.8], the property is stated whenever the mean and covariance are defined on a separable Hilbert space.

We also note $\sigma^2_{\min} \stackrel{\text{def}}{=} \min_{\alpha,\beta} \sigma^2_{\alpha\beta}$.

The proof of existence and uniqueness of solution, and of the convergence of the sequence (9.23) is in two main steps. We first prove that the sequence of Gaussian processes $\{F_k^{(n)}(X)\}_{n=0}^{\infty}, k \geq 1$ is uniformly tight by proving that Kolmogorov's criterion for tightness holds. This takes care of condition 1) in theorem 9.2.1. We next prove that the sequences of the mean functions and covariance operators are Cauchy sequences for the uniform norms, taking care of conditions 2) and 3).

Theorem 9.2.3. *The sequence of processes* $\left\{F_k^{(n)}(X)\right\}_{n=0}^{\infty}$, $k \geq 1$ *is uniformly tight.*

Proof. We use Kolmogorov's criterion for tightness and do the proof for $k = 1$, the case $k > 1$ is similar. If we assume that $n \geq 1$ and $s < t$ we have

$$
\begin{aligned}
F_1^{(n)}(X)_t - F_1^{(n)}(X)_s &= (\Phi_L(t,t_0) - \Phi_L(s,t_0))X_{t_0} \\
&+ \int_{t_0}^{s} (\Phi_L(t,s) - Id)\Phi_L(s,u)\mathbf{U}_u^{F_1^{(n-1)}(X)} \cdot \mathbf{1}\, du + \int_s^t \Phi_L(t,u)\mathbf{U}_u^{F_1^{(n-1)}(X)} \cdot \mathbf{1}\, du \\
&+ \int_{t_0}^{s} (\Phi_L(t,s) - Id)\Phi_L(s,u)\Lambda(u)\, d\mathbf{W}_u + \int_s^t \Phi_L(t,u)\Lambda(u)\, d\mathbf{W}_u \\
&+ \int_{t_0}^{s} (\Phi_L(t,s) - Id)\Phi_L(s,u)\mathbf{I}(u)\, du + \int_s^t \Phi_L(t,u)\mathbf{I}(u)\, du
\end{aligned}
$$

and therefore (Cauchy-Schwarz and Jensen's inequalities):

$$
\begin{aligned}
\frac{1}{7}\|F_1^{(n)}(X)_t - F_1^{(n)}(X)_s\|^2 &\leq \|\Phi_L(t,t_0) - \Phi_L(s,t_0)\|^2 \|\mathbf{X}_{t_0}\|^2 \\
&+ (s - t_0)\|\Phi_L(t,s) - Id\|^2 \int_{t_0}^{s} \|\Phi_L(s,u)\|^2 \|\mathbf{U}_u^{F_1^{(n-1)}(X)} \cdot \mathbf{1}\|^2\, du \\
&+ (t - s)\int_s^t \|\Phi_L(t,u)\|^2 \|\mathbf{U}_u^{F_1^{(n-1)}(X)} \cdot \mathbf{1}\|^2\, du \\
&+ \left\| \int_{t_0}^{s} \Phi_L(s,u)(\Phi_L(t,s) - Id)\Lambda(u)\, d\mathbf{W}_u \right\|^2 + \left\| \int_s^t \Phi_L(t,u)\Lambda(u)\, d\mathbf{W}_u \right\|^2 \\
&+ (s - t_0)^2 \|\Phi_L(t,s) - Id\|^2 I^2_{\max} \sup_{u \in [t_0,s]} \|\Phi_L(s,u)\|^2 \\
&+ (t - s)^2 I^2_{\max} \sup_{u \in [s,t]} \|\Phi_L(t,u)\|^2.
\end{aligned}
$$

Because $\|\Phi_L(t,t_0) - \Phi_L(s,t_0)\| \leq |t - s|\|\mathbf{L}\|$ we see that all terms in the righthand side of the inequality but the two involving the Brownian motion are of the order of $(t - s)^2$. We raise again both sides to the second power, use the Cauchy-Schwarz inequality again, and take the expected value:

$$\begin{aligned}
\frac{1}{7^3}\mathbb{E}\left[\|F_1^{(n)}(X)_t - F_1^{(n)}(X)_s\|^4\right] &\leq \|\Phi_L(t,t_0)-\Phi_L(s,t_0)\|^4\mathbb{E}\left[\|\mathbf{X}_{t_0}\|^4\right] \\
&+ (s-t_0)^3\|\Phi_L(t,s)-Id\|^4\int_{t_0}^{s}\|\Phi_L(s,u)\|^4\mathbb{E}\left[\|\mathbf{U}_u^{F_1^{(n-1)}(X)}\cdot\mathbf{1}\|^4\right]du \\
&+ (t-s)^3\int_{s}^{t}\|\Phi_L(t,u)\|^4\mathbb{E}\left[\|\mathbf{U}_u^{F_1^{(n-1)}(X)}\cdot\mathbf{1}\|^4\right]du \\
&+ \mathbb{E}\left[\left\|\int_{t_0}^{s}\Phi_L(s,u)(\Phi_L(t,s)-Id)\Lambda(u)\,d\mathbf{W}_u\right\|^4\right] \\
&+ \mathbb{E}\left[\left\|\int_{s}^{t}\Phi_L(t,u)\Lambda(u)\,d\mathbf{W}_u\right\|^4\right] \\
&+ (s-t_0)^4\|\Phi_L(t,s)-Id\|^4\sup_{u\in[t_0,s]}\|\Phi_L(s,u)\|^4 I_{\max}^4 \\
&+ (t-s)^4 I_{\max}^4\sup_{u\in[s,t]}\|\Phi_L(t,u)\|^4.
\end{aligned} \tag{9.25}$$

Remember that $\mathbf{U}_u^{F_1^{(n-1)}(X)}\cdot\mathbf{1}$ is a P-dimensional diagonal Gaussian process, noted $\mathbf{Y}_u$, therefore:

$$\mathbb{E}\left[\|\mathbf{Y}_u\|^4\right] = \sum_{\alpha}\mathbb{E}\left[Y_\alpha(u)^4\right] + \sum_{\alpha_1\neq\alpha_2}\mathbb{E}\left[Y_{\alpha_1}^2(u)\right]\mathbb{E}\left[Y_{\alpha_2}^2(u)\right].$$

The second order moments are upperbounded by some regular function of μ and $\sigma_{\max}$ (defined in lemma 9.2.2) and, because of the properties of Gaussian integrals, so are the fourth order moments.

Let us now evaluate $\mathbb{E}\left[\left\|\int_a^b\mathbf{A}(u)\,d\mathbf{W}_u\right\|^4\right]$ for some $P\times P$ matrix $\mathbf{A}$. We have

$$\begin{aligned}
\mathbb{E}\left[\left\|\int_a^b\mathbf{A}(u)\,d\mathbf{W}_u\right\|^4\right] &= \mathbb{E}\left[\left(\left\|\int_a^b\mathbf{A}(u)\,d\mathbf{W}_u\right\|^2\right)^2\right] \\
&= \mathbb{E}\left[\left(\sum_{i=1}^{P}\left(\sum_{j=1}^{P}\int_a^b A_{ij}(u)\,dW_u^j\right)\left(\sum_{k=1}^{P}\int_a^b A_{ik}(u)\,dW_u^k\right)\right)^2\right] \\
&= \sum_{i_1,i_2,j_1,j_2,k_1,k_2}\mathbb{E}\left[\int_a^b A_{i_1j_1}(u)\,dW_u^{j_1}\int_a^b A_{i_1k_1}(u)\,dW_u^{k_1}\int_a^b A_{i_2j_2}(u)\,dW_u^{j_2}\int_a^b A_{i_2k_2}(u)\,dW_u^{k_2}\right].
\end{aligned}$$

Because of the properties of the Brownian process, the last term is the sum of three types of terms:

$$\begin{aligned}
\sum_{i_1,i_2}\mathbb{E}\left[\left(\int_a^b A_{i_1j}(u)\,dW_u^j\right)^2\left(\int_a^b A_{i_2j}(u)\,dW_u^j\right)^2\right] \leq \\
\sum_{i_1,i_2}\mathbb{E}\left[\left(\int_a^b A_{i_1j}(u)\,dW_u^j\right)^4\right]^{1/2}\mathbb{E}\left[\left(\int_a^b A_{i_2j}(u)\,dW_u^j\right)^4\right]^{1/2},
\end{aligned}$$

and

$$\sum_{i_1,i_2,j_1\neq j_2}\mathbb{E}\left[\left(\int_a^b A_{i_1j_1}(u)\,dW_u^{j_1}\right)^2\left(\int_a^b A_{i_2j_2}(u)\,dW_u^{j_2}\right)^2\right]=$$
$$\sum_{i_1,i_2,j_1\neq j_2}\mathbb{E}\left[\left(\int_a^b A_{i_1j_1}(u)\,dW_u^{j_1}\right)^2\right]\mathbb{E}\left[\left(\int_a^b A_{i_2j_2}(u)\,dW_u^{j_2}\right)^2\right],$$

and

$$\sum_{i_1,i_2,j_1\neq j_2}\mathbb{E}\left[\int_a^b A_{i_1j_1}(u)\,dW_u^{j_1}\int_a^b A_{i_2j_1}(u)\,dW_u^{j_1}\int_a^b A_{i_1j_2}(u)\,dW_u^{j_2}\int_a^b A_{i_2j_2}(u)\,dW_u^{j_2}\right]=$$
$$\mathbb{E}\left[\int_a^b A_{i_1j_1}(u)\,dW_u^{j_1}\int_a^b A_{i_2j_1}(u)\,dW_u^{j_1}\right]\mathbb{E}\left[\int_a^b A_{i_1j_2}(u)\,dW_u^{j_2}\int_a^b A_{i_2j_2}(u)\,dW_u^{j_2}\right],$$

Because of the properties of the stochastic integral, $\int_a^b A_{i_1j}(u)\,dW_u^j=\mathcal{N}(0,\left(\int_a^b A_{i_1j}^2(u)\,du\right)^{1/2})$ hence, because of the properties of the Gaussian integrals

$$\mathbb{E}\left[\left(\int_a^b A_{i_1j}(u)\,dW_u^j\right)^4\right]=k\left(\int_a^b A_{i_1j}^2(u)\,du\right)^2,$$

for some positive constant k. Moreover

$$\mathbb{E}\left[\left(\int_a^b A_{i_1j_1}(u)\,dW_u^{j_1}\right)^2\right]=\int_a^b A_{i_1j_1}^2(u)\,du,$$

and

$$\mathbb{E}\left[\int_a^b A_{i_1j_1}(u)\,dW_u^{j_1}\int_a^b A_{i_2j_1}(u)\,dW_u^{j_1}\right]=\int_a^b A_{i_1j_1}(u)A_{i_2j_1}(u)\,du.$$

This shows that the two terms $\mathbb{E}\left[\left\|\int_{t_0}^s(\Phi_L(t,s)-Id)\Phi_L(s,u)\Lambda(u)\,d\mathbf{W}_u\right\|^4\right]$ and $\mathbb{E}\left[\left\|\int_s^t\Phi_L(t,u)\Lambda(u)\,d\mathbf{W}_u\right\|^4\right]$ in (9.25) are of the order of $(t-s)^{1+a}$ where $a\geq 1$. Therefore we have

$$\mathbb{E}\left[\|F_1^{(n)}(X)_t-F_1^{(n)}(X)_s\|^4\right]\leq C|t-s|^{1+a},\quad a\geq 1$$

for all s,t in $[t_0,T]$, where C is a constant independent of t,s. According to Kolmogorov criterion for tightness, the sequence of processes $\left\{F_1^{(n)}(X)\right\}_{n=0}^{\infty}$ is uniformly tight.

The proof for F_k, $k>1$ is similar. □

Let us note $\mu^n(t)$ (respectively $C^n(t,s)$) the mean (respectively the covariance matrix) function of $X_n=F_k(X_{n-1})$, $n\geq 1$. We have:

$$C^{n+1}(t,s)=\Phi_L(t,t_0)\Sigma^{Z_0}\Phi_L(s,t_0)^T+\int_{t_0}^{t\wedge s}\Phi_L(t,u)\Lambda(u)\Lambda(u)^T\Phi_L(s,u)^T\,du+$$
$$\int_{t_0}^t\int_{t_0}^s\Phi_L(t,u)\mathrm{cov}\left(\widetilde{\mathbf{U}}_u^{X_n},\widetilde{\mathbf{U}}_v^{X_n}\right)\Phi_L(s,v)^T\,du\,dv\quad(9.26)$$

Note that the $kP\times kP$ covariance matrix $\mathrm{cov}\left(\widetilde{\mathbf{U}}_u^{X_n},\widetilde{\mathbf{U}}_v^{X_n}\right)$ has only one nonzero $P\times P$ block:

$$\mathrm{cov}\left(\widetilde{\mathbf{U}}_u^{X_n},\widetilde{\mathbf{U}}_v^{X_n}\right)_{kk}=\mathrm{cov}\left(\mathbf{U}_u^{X_n}\cdot\mathbf{1},\mathbf{U}_v^{X_n}\cdot\mathbf{1}\right),$$

We have

$$\mathrm{cov}\left(\mathbf{U}_u^{X_n}\cdot\mathbf{1},\mathbf{U}_v^{X_n}\cdot\mathbf{1}\right)=\mathrm{diag}\left(\sum_\beta\sigma_{\alpha\beta}^2\mathbb{E}\left[S_{\alpha\beta}(X_{n\beta}(u))S_{\alpha\beta}(X_{n\beta}(v))\right]\right),$$

and

$$\mathbb{E}\left[S_{\alpha\beta}(X_n(u))S_{\alpha\beta}(X_n(v))\right]=$$
$$\int_{\mathbb{R}^2}S_{\alpha\beta}\left(\frac{\sqrt{C^n_{\beta\beta}(u,u)C^n_{\beta\beta}(v,v)-C^n_{\beta\beta}(u,v)^2}}{\sqrt{C^n_{\beta\beta}(u,u)}}x+\frac{C^n_{\beta\beta}(u,v)}{\sqrt{C^n_{\beta\beta}(u,u)}}y+\mu^n_\beta(v)\right)$$
$$S_{\alpha\beta}\left(y\sqrt{C^n_{\beta\beta}(u,u)}+\mu^n_\beta(u)\right)DxDy,\quad(9.27)$$

where

$$Dx=\frac{1}{\sqrt{2\pi}}e^{-\frac{x^2}{2}}dx.$$

Similarly we have

$$\mu^n(t)=\Phi_L(t,t_0)\mu^{Z_0}+\int_{t_0}^t\Phi_L(t,u)\left(\mathbb{E}\left[\widetilde{\mathbf{U}}_u^{X_n}\right]+\tilde{\mathbf{I}}(u)\right)du=$$
$$\Phi_L(t,t_0)\mu^{Z_0}+$$
$$\int_{t_0}^t\Phi_L(t,u)\left(\left[0_P^T,\cdots,0_P^T,\left[\sum_\beta\bar{J}_{\alpha\beta}\int_{\mathbb{R}}S_{\alpha\beta}\left(x\sqrt{C^n_{\beta\beta}(u,u)}+\mu^n_\beta(u)\right)\right]_{\alpha=1,\cdots,P}\right]^T+\tilde{\mathbf{I}}(u)\right)Dxdu$$

We require the following four lemmas.

Lemma 9.2.4. For all $\alpha=1,\cdots,P$ and $n\geq1$ the quantity $C^n_{\alpha\alpha}(s,s)C^n_{\alpha\alpha}(t,t)-C^n_{\alpha\alpha}(t,s)^2$ is lowerbounded by the positive symmetric function:

$$\theta(s,t)=|t-s|\lambda^2_{\min}\lambda^{\Sigma^{Z_0}}_{\min}\lambda^{\Gamma}_{\min},$$

where $\lambda_{\min}$ is the smallest singular value of the positive symmetric definite matrix $\Phi_L(t,t_0)\Phi_L(t,t_0)^T$ for $t\in[t_0,T]$, $\lambda^{\Sigma^{Z_0}}_{\min}$ is the smallest eigenvalue of the positive symmetric definite covariance matrix Σ^{Z_0}, and $\lambda^{\Gamma}_{\min}$ is the smallest singular value of the matrix $\Lambda(u)$ for $u\in[t_0,T]$.

Proof. We use equation (9.26) which we rewrite as follows, using the group property of the resolvent Φ_L :

$$C^{n+1}(t,s)=\Phi_L(t,t_0)\left(\Sigma^{Z_0}+\int_{t_0}^{t\wedge s}\Phi_L(t_0,u)\Lambda(u)\Lambda(u)^T\Phi_L(t_0,u)^T\,du+\right.$$
$$\left.\int_{t_0}^t\int_{t_0}^s\Phi_L(t_0,u)\mathrm{cov}\left(\widetilde{\mathbf{U}}_u^{X_n},\widetilde{\mathbf{U}}_v^{X_n}\right)\Phi_L(t_0,v)^T\,du\,dv\right)\Phi_L(t_0,s)^T.$$

We now assume $s<t$ and introduce the following notations, dropping the index n for simplicity:

$$\begin{array}{rcl}A(s)&=&\Sigma^{Z_0}+\int_{t_0}^s\Phi_L(t_0,u)\Lambda(u)\Lambda(u)^T\Phi_L(t_0,u)^T\,du\\B(s,t)&=&\int_s^t\Phi_L(t_0,u)\Lambda(u)\Lambda(u)^T\Phi_L(t_0,u)^T\,du\\a(t,s)&=&\int_{t_0}^t\int_{t_0}^s\Phi_L(t_0,u)\mathrm{cov}\left(\widetilde{\mathbf{U}}_u^{X_n},\widetilde{\mathbf{U}}_v^{X_n}\right)\Phi_L(t_0,v)^T\,du\,dv\end{array}$$

Let e_α, $\alpha = 1, \cdots, kP$, be the unit vector of the canonical basis whose coordinates are all equal to 0 except the αth one which is equal to 1. We note $E_\alpha(t)$ the vector $\Phi_L(t,t_0)^T e_\alpha$. We have

$$\begin{aligned} C_{\alpha\alpha}(t,s) &= E_\alpha(t)^T \left(A(s) + a(t,s)\right) E_\alpha(s) \\ C_{\alpha\alpha}(s,s) &= E_\alpha(s)^T (A(s) + a(s,s)) E_\alpha(s) \\ C_{\alpha\alpha}(t,t) &= E_\alpha(t)^T (A(s) + B(s,t) + a(t,t)) E_\alpha(t). \end{aligned}$$

Note that the last expression does not depend on s, since $A(s) + B(s,t) = A(t)$, which is consistent with the first equality. The reason why we introduce s in this expression is to simplify the following calculations.

The expression $C_{\alpha\alpha}(s,s)C_{\alpha\alpha}(t,t) - C_{\alpha\alpha}(t,s)^2$ is the sum of four sub-expressions:

$$e_1(s,t) = \left(E_\alpha(s)^T A(s) E_\alpha(s)\right) \left(E_\alpha(t)^T A(s) E_\alpha(t)\right) - \left(E_\alpha(t)^T A(s) E_\alpha(s)\right)^2,$$

which is greater than or equal to 0 because $A(s)$ is a covariance matrix,

$$e_2(s,t) = \left(E_\alpha(s)^T a(s,s) E_\alpha(s)\right) \left(E_\alpha(t)^T a(t,t) E_\alpha(t)\right) - \left(E_\alpha(t)^T a(t,s) E_\alpha(s)\right)^2,$$

which is also greater than or equal to 0 because $a(t,s)$ is a covariance matrix function,

$$\begin{aligned} e_3(s,t) = \left(E_\alpha(s)^T A(s) E_\alpha(s)\right) \left(E_\alpha(t)^T a(t,t) E_\alpha(t)\right) + \\ \left(E_\alpha(t)^T A(s) E_\alpha(t)\right) \left(E_\alpha(s)^T a(s,s) E_\alpha(s)\right) - \\ 2 \left(E_\alpha(t)^T A(s) E_\alpha(s)\right) \left(E_\alpha(t)^T a(t,s) E_\alpha(s)\right) \end{aligned}$$

Because $a(t,s)$ is a covariance matrix function we have

$$E_\alpha(t)^T a(t,t) E_\alpha(t) + E_\alpha(s)^T a(s,s) E_\alpha(s) - 2 E_\alpha(t)^T a(t,s) E_\alpha(s) \geq 0,$$

and , as seen above, $e_2(s,t) \geq 0$. Because $e_1(s,t) \geq 0$ we also have

$$\begin{aligned} -\sqrt{E_\alpha(s)^T A(s) E_\alpha(s)} \sqrt{E_\alpha(t)^T A(s) E_\alpha(t)} \leq E_\alpha(t)^T A(s) E_\alpha(s) \leq \\ \sqrt{E_\alpha(s)^T A(s) E_\alpha(s)} \sqrt{E_\alpha(t)^T A(s) E_\alpha(t)}, \end{aligned}$$

and, as it can be readily verified, this implies $e_3(s,t) \geq 0$.

Therefore we can lowerbound $C_{\alpha\alpha}(s,s)C_{\alpha\alpha}(t,t) - C_{\alpha\alpha}(t,s)^2$ by the fourth subexpression:

$$\begin{aligned} C_{\alpha\alpha}(s,s)C_{\alpha\alpha}(t,t) - C_{\alpha\alpha}(t,s)^2 &\geq \left(E_\alpha(s)^T A(s) E_\alpha(s)\right) \left(E_\alpha(t)^T B(s,t) E_\alpha(t)\right) \\ &\quad + \left(E_\alpha(s)^T a(s,s) E_\alpha(s)\right) \left(E_\alpha(t)^T B(s,t) E_\alpha(t)\right) \\ &\geq \left(E_\alpha(s)^T A(s) E_\alpha(s)\right) \left(E_\alpha(t)^T B(s,t) E_\alpha(t)\right), \end{aligned}$$

since $B(s,t)$ and $a(s,s)$ are covariance matrixes. We next have

$$E_\alpha(s)^T A(s) E_\alpha(s) = \frac{E_\alpha(s)^T A(s) E_\alpha(s)}{E_\alpha(s)^T E_\alpha(s)} \frac{e_\alpha^T \Phi_L(s,t_0) \Phi_L(s,t_0)^T e_\alpha}{e_\alpha^T e_\alpha},$$

by definition of $E_\alpha(s)$. Therefore

$$E_\alpha(s)^T A(s) E_\alpha(s) \geq \lambda_{\min}^{A(s)} \lambda_{\min}^{\Phi_L(s,t_0)\Phi_L(s,t_0)^T} \geq \lambda_{\min}^{\Sigma^{Z_0}} \lambda_{\min},$$

where $\lambda_{\min}^{C}$ is the smallest eigenvalue of the symmetric positive matrix C. Similarly we have

$$E_\alpha(t)^T B(s,t) E_\alpha(t) \geq \lambda_{\min}^{B(s,t)} \lambda_{\min}.$$

Let us write $\Gamma(u) = \Lambda(u)\Lambda(u)^T$. We have

$$\begin{aligned}
\lambda_{\min}^{B(s,t)} &= \min_{\|x\|\leq 1} \int_s^t \frac{x^T \Phi_L(t_0,u)\Gamma(u)\Phi_L(t_0,u)^T x}{x^T x}\, du \\
&= \min_{\|x\|\leq 1} \int_s^t \frac{x^T \Phi_L(t_0,u)\Gamma(u)\Phi_L(t_0,u)^T x}{x^T \Phi_L(t_0,u)\Phi_L(t_0,u) x} \frac{x^T \Phi_L(t_0,u)\Phi_L(t_0,u) x}{x^T x}\, du \\
&\geq \int_s^t \min_{\|x\|\leq 1} \left(\frac{x^T \Phi_L(t_0,u)\Gamma(u)\Phi_L(t_0,u)^T x}{x^T \Phi_L(t_0,u)\Phi_L(t_0,u) x} \frac{x^T \Phi_L(t_0,u)\Phi_L(t_0,u) x}{x^T x} \right) du \\
&\geq (t-s)\lambda_{\min}\lambda_{\min}^{\Gamma}.
\end{aligned}$$

Combining these results we have

$$C_{\alpha\alpha}(s,s)C_{\alpha\alpha}(t,t) - C_{\alpha\alpha}(t,s)^2 \geq |t-s|\lambda_{\min}^2 \lambda_{\min}^{\Sigma^{Z_0}} \lambda_{\min}^{\Gamma}$$

□

Lemma 9.2.5. For all $t \in [t_0, T]$ all $\alpha = 1, \cdots, P$, and $n \geq 1$, we have

$$C_{\alpha\alpha}^n(t,t) \geq k_0 > 0.$$

Proof. $C_{\alpha\alpha}^n(t,t)$ is larger than $(\Phi_L(t,t_0)\Sigma^{Z_0}\Phi_L(t,t_0)^T)_{\alpha\alpha}$ which is larger than the smallest eigenvalue of the matrix $\Phi_L(t,t_0)\Sigma^{Z_0}\Phi_L(t,t_0)^T$. This smallest eigenvalue is equal to

$$\begin{aligned}
\min_x \frac{x^T \Phi_L(t,t_0)\Sigma^{Z_0}\Phi_L(t,t_0)^T x}{x^T x} &= \min_x \frac{x^T \Phi_L(t,t_0)\Sigma^{Z_0}\Phi_L(t,t_0)^T x}{x^T \Phi_L(t,t_0)\Phi_L(t,t_0)^T x} \frac{x^T \Phi_L(t,t_0)\Phi_L(t,t_0)^T x}{x^T x} \\
&\geq \min_x \frac{x^T \Phi_L(t,t_0)\Sigma^{Z_0}\Phi_L(t,t_0)^T x}{x^T \Phi_L(t,t_0)\Phi_L(t,t_0)^T x} \min_x \frac{x^T \Phi_L(t,t_0)\Phi_L(t,t_0)^T x}{x^T x}.
\end{aligned}$$

In the last expression the first term is larger than the smallest eigenvalue $\lambda_{\min}^{\Sigma^{Z_0}}$ of the matrix Σ^{Z_0} which is positive definite since we have assumed the Gaussian random variable Z_0 nondegenerate. The second term is equal to the smallest singular value $\lambda_{\min}$ of the matrix $\Phi_L(t,t_0)$ which is also strictly positive for all $t \in [t_0, T]$ by hypothesis, see appendix E.1, equation (E.6).

□

We also use the following lemma.

Lemma 9.2.6. The $2n$-dimensional integral

$$\begin{aligned}
I_n = \int_{[t_0, t\vee s]^2} \rho_1(u_1,v_1) \Bigg(\int_{[t_0,u_1\vee v_1]^2} \cdots \Bigg(\int_{[t_0,u_{n-2}\vee v_{n-2}]^2} \rho_{n-1}(u_{n-1},v_{n-1}) \\
\left(\int_{[t_0,u_{n-1}\vee v_{n-1}]^2} \rho_n(u_n,v_n) du_n dv_n \right) du_{n-1} dv_{n-1} \Bigg) \cdots \Bigg) du_1 dv_1,
\end{aligned}$$

where the functions $\rho_i(u_i,v_i)$, $i = 1, \cdots, n$ are either equal to 1 or to $1/\sqrt{\theta(u_i,v_i)}$, is upperbounded by $k^n/(n-1)!$ for some positive constant k.

Proof. First note that the integral is well-defined because of lemma 9.2.4. Second, note that there exists a constant K such that $K/\sqrt{\theta(u,v)} \geq 1$ for all $(u,v) \in [t_0, t \vee s]^2$, i.e. $K = \lambda_{\min} \sqrt{\lambda_{\min}^{\Sigma^{Z_0}} \lambda_{\min}^{\Gamma} (T - t_0)}$. Therefore the integral is upperbounded by K_0^n, where $K_0 = \max(1, K)$ times the integral obtained when $\rho_i(u_i, v_i) = 1/\sqrt{|u_i - v_i|}$ for all $i = 1, \cdots, n$. Let us then consider this situation. Without loss of generality we assume $t_0 = 0$. The cases $n = 1, 2, 3$ allow one to understand the process.

$$I_1 \leq K_0 \int_{[0, t \vee s]^2} \frac{dudv}{\sqrt{|u - v|}}. \tag{9.28}$$

Let us rotate the axes by $-\frac{\pi}{4}$ by performing the change of variables

$$u = \frac{U + V}{\sqrt{2}},$$
$$v = \frac{V - U}{\sqrt{2}}.$$

Using the symmetry of the integrand in s and t and the change of variable, the integral in the righthand side of (9.28) is equal to (see figure 9.2):

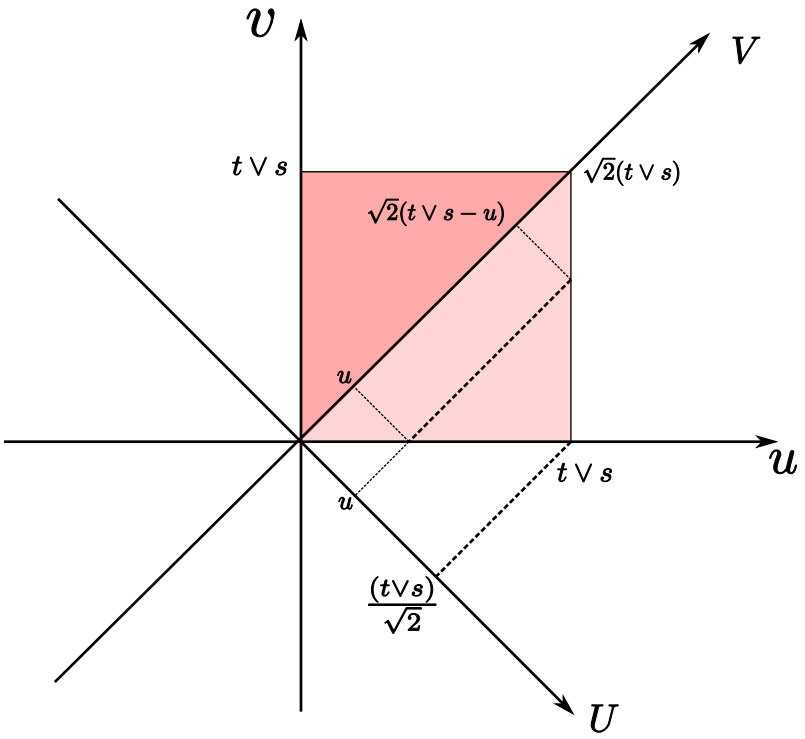

Figure 9.2: The change of coordinates: the integal over the whole square is only computed in the light color triangle, along the axis U and V.

$$2 \frac{1}{2^{1/4}} \int_0^{\frac{t \vee s}{\sqrt{2}}} \int_U^{\sqrt{2}(t \vee s) - U} \frac{dV dU}{\sqrt{U}} = 2^{3/4} \int_0^{a/2} \frac{a - 2U}{\sqrt{U}} dU = 2^{3/4} \alpha_1 a^{3/2},$$

where $a = \sqrt{2}(t \vee s)$ and $\alpha_1 = \frac{2\sqrt{2}}{3}$.

Let us now look at I_2. It is upperbounded by the factor $K_0^2(2^{3/4})^2\alpha_1$ times the integral

$$\int_0^{a/2}\int_U^{a-U}\frac{(\sqrt{2}(u\vee v))^{3/2}}{\sqrt{U}}dUdV.$$

Since in the area of integration $u\vee v = v = \frac{V-U}{\sqrt{2}}$ we are led to the product of $2/5$ by the one-dimensional integral

$$\int_0^{a/2}\frac{(a-2U)^{5/2}}{\sqrt{U}}dUdV = \alpha_2 a^3,$$

where $\alpha_2 = \frac{5\sqrt{2}\pi}{32}$.

Similarly I_3 is upperbounded by the product of $K_0^3(2^{3/4})^3\alpha_1\alpha_2\frac{2}{5}\frac{2}{8}$ times the integral

$$\int_0^{a/2}\frac{(a-2U)^4}{\sqrt{U}}dUdV = \alpha_3 a^{9/2},$$

where $\alpha_3 = \frac{128\sqrt{2}}{315}$. One easily shows then that:

$$I_n \leq K_0^n F(2^{3/4})^n 2^n\left(\prod_{i=1}^n\alpha_i\right)\left(\frac{1}{\prod_{j=1}^n(2+3(j-1))}\right).$$

It can be verified by using a system for symbolic computation that $0<\alpha_i<1$ for all $i\geq 1$. One also notices that

$$\prod_{j=1}^n(2+3(j-1)) \geq \frac{3^{n-1}}{2}(n-1)!,$$

therefore

$$I_n \leq K_0^n(2^{3/4})^n 2^{n-1}3^{-(n-1)}\frac{1}{(n-1)!},$$

and this finishes the proof.

□

We now prove the following proposition.

Proposition 9.2.7. The sequences of covariance matrix functions $C^n(t,s)$ and of mean functions $\mu^n(t)$, s,t in $[t_0,T]$ are Cauchy sequences for the uniform norms.

Proof. We have

$$C^{n+1}(t,s)-C^n(t,s) = \int_{t_0}^t\int_{t_0}^s \Phi_L(t,u)\Big(\mathrm{cov}\left(\widetilde{\mathbf{U}}_u^{X_n},\widetilde{\mathbf{U}}_v^{X_n}\right) - \mathrm{cov}\left(\widetilde{\mathbf{U}}_u^{X_{n-1}},\widetilde{\mathbf{U}}_v^{X_{n-1}}\right)\Big)\Phi_L(s,v)^T\,dudv.$$

We take the infinite matrix norm of both sides of this equality and use the upperbounds $\|\Phi_L(t,u)\|_\infty \leq e^{\|\mathbf{L}\|_\infty(T-t_0)} = k_L$ and $\left\|\Phi_L(t,u)^T\right\|_\infty \leq e^{\left\|\mathbf{L}^T\right\|_\infty(T-t_0)} = k_{L^T}$ (see appendix E.1) to obtain

$$\begin{aligned}\left\|C^{n+1}(t,s)-C^n(t,s)\right\|_\infty &\leq k_L k_{L^T}\int_{t_0}^t\int_{t_0}^s\left\|\mathrm{cov}\left(\widetilde{\mathbf{U}}_u^{X_n},\widetilde{\mathbf{U}}_v^{X_n}\right)-\mathrm{cov}\left(\widetilde{\mathbf{U}}_u^{X_{n-1}},\widetilde{\mathbf{U}}_v^{X_{n-1}}\right)\right\|_\infty^v dudv\\ &= k_L k_{L^T}\int_{t_0}^t\int_{t_0}^s\left\|\mathrm{cov}\left(\mathbf{U}_u^{X_n}\cdot\mathbf{1},\mathbf{U}_v^{X_n}\cdot\mathbf{1}\right)-\mathrm{cov}\left(\mathbf{U}_u^{X_{n-1}}\cdot\mathbf{1},\mathbf{U}_v^{X_{n-1}}\cdot\mathbf{1}\right)\right\|_\infty^v dudv. \qquad (9.29)\end{aligned}$$

According to equations (9.27) we are led to consider the difference $A_n - A_{n-1}$, where:

$$A_n \stackrel{\text{def}}{=}$$
$$S_{\alpha\beta}\Big(\frac{\sqrt{C^n_{\beta\beta}(u,u)C^n_{\beta\beta}(v,v)-C^n_{\beta\beta}(u,v)^2}}{\sqrt{C^n_{\beta\beta}(u,u)}}x+\frac{C^n_{\beta\beta}(u,v)}{\sqrt{C^n_{\beta\beta}(u,u)}}y+\mu^n_\beta(v)\Big)S_{\alpha\beta}\left(y\sqrt{C^n_{\beta\beta}(u,u)}+\mu^n_\beta(u)\right)$$
$$\stackrel{\text{def}}{=} S_{\alpha\beta}\left[f^n_\beta(u,v)x+g^n_\beta(u,v)y+\mu^n_\beta(v)\right]S_{\alpha\beta}\left[h^n_\beta(u)y+\mu^n_\beta(u)\right].$$

We write next:

$$A_n - A_{n-1} = S_{\alpha\beta}\left[f^n_\beta(u,v)x+g^n_\beta(u,v)y+\mu^n_\beta(v)\right]$$
$$\left(S_{\alpha\beta}\left[h^n_\beta(u)y+\mu^n_\beta(u)\right]-S_{\alpha\beta}\left[h^{n-1}_\beta(u)y+\mu^{n-1}_\beta(u)\right]\right)+$$
$$S_{\alpha\beta}\left[h^{n-1}_\beta(u)y+\mu^{n-1}_\beta(u)\right]$$
$$\left(S_{\alpha\beta}\left[f^n_\beta(u,v)x+g^n_\beta(u,v)y+\mu^n_\beta(v)\right]-S_{\alpha\beta}\left[f^{n-1}_\beta(u,v)x+g^{n-1}_\beta(u,v)y+\mu^{n-1}_\beta(v)\right]\right).$$

The mean value theorem yields:

$$|A_n - A_{n-1}| \leq \left\|S_{\alpha\beta}\right\|_\infty \left\|S'_{\alpha\beta}\right\|_\infty \Big(|x|\,|f^n_\beta(u,v)-f^{n-1}_\beta(u,v)| +$$
$$|y|\,|g^n_\beta(u,v)-g^{n-1}_\beta(u,v)| + |\mu^n_\beta(v)-\mu^{n-1}_\beta(v)| + |y|\,|h^n_\beta(u)-h^{n-1}_\beta(u)| +$$
$$|\mu^n_\beta(u)-\mu^{n-1}_\beta(u)|\Big).$$

Using the fact that $\int_{-\infty}^{\infty}|x|\,Dx = \sqrt{\frac{2}{\pi}}$, we obtain:

$$\left\|C^{n+1}(t,s)-C^n(t,s)\right\|_\infty \leq k_L k_{L^T} k_C \Bigg(\sqrt{\frac{2}{\pi}}\int_{t_0}^t\int_{t_0}^s \left\|f^n(u,v)-f^{n-1}(u,v)\right\|_\infty du\,dv$$
$$+\sqrt{\frac{2}{\pi}}\int_{t_0}^t\int_{t_0}^s \left\|g^n(u,v)-g^{n-1}(u,v)\right\|_\infty du\,dv$$
$$+(t-t_0)\int_{t_0}^s \left\|\mu^n(v)-\mu^{n-1}(v)\right\|_\infty dv + (s-t_0)\int_{t_0}^t \left\|\mu^n(u)-\mu^{n-1}(u)\right\|_\infty du$$
$$+\sqrt{\frac{2}{\pi}}(s-t_0)\int_{t_0}^t \left\|h^n(u)-h^{n-1}(u)\right\|_\infty du\Bigg),$$

where

$$k_C = \max_\alpha \sum_\beta \sigma^2_{\alpha\beta}\left\|S_{\alpha\beta}\right\|_\infty \left\|S'_{\alpha\beta}\right\|_\infty. \tag{9.30}$$

A similar process applied to the mean values yields:

$$\left\|\mu^{n+1}(t)-\mu^n(t)\right\|_\infty \leq k_L\mu\Big(\int_{t_0}^t \left\|h^n(u)-h^{n-1}(u)\right\|_\infty du + \int_{t_0}^t \left\|\mu^n(u)-\mu^{n-1}(u)\right\|_\infty du\Big).$$

We now use the mean value theorem and lemmas 9.2.5 and 9.2.4 to find upperbounds for $\left\|f^n(u,v)-f^{n-1}(u,v)\right\|_\infty$, $\left\|g^n(u,v)-g^{n-1}(u,v)\right\|_\infty$ and $\left\|h^n(u)-h^{n-1}(u)\right\|_\infty$. We have

$$|h^n_\beta(u)-h^{n-1}_\beta(u)| = \left|\sqrt{C^n_{\beta\beta}(u,u)}-\sqrt{C^{n-1}_{\beta\beta}(u,u)}\right| \leq \frac{1}{2\sqrt{k_0}}\left|C^n_{\beta\beta}(u,u)-C^{n-1}_{\beta\beta}(u,u)\right|,$$

where k_0 is defined in lemma 9.2.5. Hence:

$$\left\|h^n(u)-h^{n-1}(u)\right\|_\infty \leq \frac{1}{2\sqrt{k_0}}\left\|C^n(u,u)-C^{n-1}(u,u)\right\|_\infty.$$

Along the same lines we can show easily that:

$$\left\|g^n(u,v)-g^{n-1}(u,v)\right\|_\infty \leq k\Big(\left\|C^n(u,v)-C^{n-1}(u,v)\right\|_\infty+\left\|C^n(u,u)-C^{n-1}(u,u)\right\|_\infty\Big),$$

and that:

$$\left\|f^n(u,v)-f^{n-1}(u,v)\right\|_\infty \leq \frac{k}{\sqrt{\theta(u,v)}}\Big(\left\|C^n(u,v)-C^{n-1}(u,v)\right\|_\infty+ \left\|C^n(u,u)-C^{n-1}(u,u)\right\|_\infty+\left\|C^n(v,v)-C^{n-1}(v,v)\right\|_\infty\Big),$$

where $\theta(u,v)$ is defined in lemma 9.2.4. Grouping terms together and using the fact that all integrated functions are positive, we write:

$$\begin{aligned}\left\|C^{n+1}(t,s)-C^n(t,s)\right\|_\infty \leq k\Bigg(&\int_{[t_0,t\vee s]^2}\frac{1}{\sqrt{\theta(u,v)}}\left\|C^n(u,v)-C^{n-1}(u,v)\right\|_\infty du\,dv\\ &+\int_{[t_0,t\vee s]^2}\frac{1}{\sqrt{\theta(u,v)}}\left\|C^n(u,u)-C^{n-1}(u,u)\right\|_\infty du\,dv\\ &+\int_{[t_0,t\vee s]^2}\left\|C^n(u,v)-C^{n-1}(u,v)\right\|_\infty du\,dv\\ &+\int_{[t_0,t\vee s]^2}\left\|C^n(u,u)-C^{n-1}(u,u)\right\|_\infty du\,dv\\ &+\int_{[t_0,t\vee s]^2}\left\|\mu^n(u)-\mu^{n-1}(u)\right\|_\infty dudv\Bigg).\end{aligned} \tag{9.31}$$

Note that, because of lemma 9.2.5, all integrals are well-defined. Regarding the mean functions, we write:

$$\begin{aligned}\left\|\mu^{n+1}(t)-\mu^n(t)\right\|_\infty \leq k\Bigg(&\int_{[t_0,t\vee s]^2}\left\|C^n(u,u)-C^{n-1}(u,u)\right\|_\infty dudv+\\ &\int_{[t_0,t\vee s]^2}\left\|\mu^n(u)-\mu^{n-1}(u)\right\|_\infty dudv\Bigg).\end{aligned} \tag{9.32}$$

Proceeding recursively until we reach C^0 and μ^0 we obtain an upperbound for $\left\|C^{n+1}(t,s)-C^n(t,s)\right\|_\infty$ (respectively for $\left\|\mu^{n+1}(t)-\mu^n(t)\right\|_\infty$) which is the sum of less than 5^n terms each one being the product of k raised to a power less than or equal to n, times 2μ or 2Σ (upperbounds for the norms of the mean vector and the covariance matrix), times a $2n$-dimensional integral I_n given by

$$\begin{aligned}\int_{[t_0,t\vee s]^2}\rho_1(u_1,v_1)\Bigg(\int_{[t_0,u_1\vee v_1]^2}\cdots\Bigg(&\int_{[t_0,u_{n-2}\vee v_{n-2}]^2}\rho_{n-1}(u_{n-1},v_{n-1})\\ &\left(\int_{[t_0,u_{n-1}\vee v_{n-1}]^2}\rho_n(u_n,v_n)du_n dv_n\right)du_{n-1}dv_{n-1}\Bigg)\cdots\Bigg)du_1dv_1,\end{aligned}$$

where the functions $\rho_i(u_i,v_i)$, $i=1,\cdots,n$ are either equal to 1 or to $1/\sqrt{\theta(u_i,v_i)}$. According to lemma 9.2.6, this integral is of the order of some positive constant raised to the power n divided by $(n-1)!$. Hence the sum is less than some positive constant k raised to the power n divided by $(n-1)!$. By taking the supremum with respect to t and s in $[t_0,T]$ we obtain the same result for $\left\|C^{n+1}-C^n\right\|_\infty$ (respectively for $\left\|\mu^{n+1}-\mu^n\right\|_\infty$). Since the series $\sum_{n\geq 1}\frac{k^n}{n!}$ is convergent, this implies that $\|C^{n+p}-C^n\|_\infty$ (respectively $\|\mu^{n+p}-\mu^n\|_\infty$) can be made arbitrarily small for large n and p and the sequence C^n (respectively μ^n) is a Cauchy sequence.

□

We can now prove the following theorem

Theorem 9.2.8. *For any nondegenerate kP-dimensional Gaussian random variable Z_0 and any initial process X such that $X(t_0)=Z_0$, the map F_k has a unique fixed point in $\mathscr{M}_1^+(C([t_0,T],\mathbb{R}^{kP}))$ towards which the sequence $\{F_k^{(n)}(X)\}_{n=0}^\infty$ of Gaussian processes converges in law.*

Proof. Since $C([t_0,T],\mathbb{R}^{kP})$ (respectively $C([t_0,T]^2,\mathbb{R}^{kP\times kP})$) is a Banach space for the uniform norm, the Cauchy sequence μ^n (respectively C^n) of proposition 9.2.7 converges to an element μ of $C([t_0,T],\mathbb{R}^{kP})$ (respectively an element C of $C([t_0,T]^2,\mathbb{R}^{kP\times kP})$). Therefore, according to theorem 9.2.1, the sequence $\{F_k^{(n)}(X)\}_{n=0}^\infty$ of Gaussian processes converges in law toward the Gaussian process Y with mean function μ and covariance function C. This process is clearly a fixed point of F_k.

Hence we know that there there exists at least one fixed point for the map F_k. Assume there exist two distinct fixed points Y_1 and Y_2 of F_k with mean functions μ_i and covariance functions C_i, $i=1,2$, with the same initial condition. Since for all $n\geq 1$ we have $F_k^{(n)}(Y_i)=Y_i$, $i=1,2$, the proof of proposition 9.2.7 shows that $\|\mu_1^n-\mu_2^n\|_\infty$ (respectively $\left\|C_1^n-C_n^2\right\|_\infty$) is upperbounded by the product of a positive number a_n (respectively b_n) with $\|\mu_1-\mu_2\|_\infty$ (respectively with $\|C_1-C_2\|_\infty$). Since $\lim_{n\to\infty}a_n=\lim_{n\to\infty}b_n=0$ and $\mu_i^n=\mu_i$, $i=1,2$ (respectively $C_i^n=C_i$, $i=1,2$), this shows that $\mu_1=\mu_2$ and $C_1=C_2$, hence the two Gaussian processes Y_1 and Y_2 are indistinguishable.

□

Conclusion

We have proved that for any non degenerate initial condition Z_0 there exists a unique solution of the mean field equations. The proof of theorem 9.2.8 is constructive, and hence provides a way for computing the solution of the mean field equations by iterating the map F_k, starting from any initial process X satisfying $X(t_0)=Z_0$, for instance a Gaussian process such as an Ornstein-Uhlenbeck process. We build upon these facts in section 9.4.

Note that the existence and uniqueness is true whatever the initial time t_0 and the final time T.

9.3 Existence and uniqueness of stationary solutions

So far, we have investigated the existence and uniqueness of solutions of the mean field equation for a given initial condition. We are now interested in investigating stationary solutions, which allow for some simplifications of the formalism.

A stationary solution is a solution whose probability distribution does not change under the flow of the equation. These solutions have been already investigated by several authors (see [36, 240]). We propose a new framework to study and simulate these processes. Indeed we show in this section that under a certain contraction condition there exists a unique solution to the stationary problem. As in the previous section our proof is constructive and provides a way to simulate the solutions.

Remark 13. The long-time mean field description of a network is still a great endeavor in mathematics and statistical physics. In this section we formally take the mean field equation we obtained and let $t_0 \to -\infty$. This way we obtain an equation which is the limit of the mean field equation when $t_0 \to -\infty$. It means that we consider first the limit $N \to \infty$ and then $t_0 \to -\infty$. These two limits do not necessarily commute and there are known examples, for instance in spin glasses, where they do not.

It is clear that in order to get stationary solutions, we have to assume that the leak matrix $\mathbf{L}(t)$ does not depend upon t. Therefore, the resolvent $\Phi_L(t,s)$ is equal to $e^{\mathbf{L}(t-s)}$. To ensure stability of the solutions and the existence of a stationary process we also assume that the real parts of its eigenvalues are negative:

$$\mathrm{Re}(\lambda) < -\lambda_L \quad \lambda_L > 0 \tag{9.33}$$

for all eigenvalues λ of $\mathbf{L}$. This implies that we only consider first-order system since otherwise the matrix $\mathbf{L}$ has eigenvalues equal to 0.

For the same reason, we assume that the noise matrix $\Lambda(t)$ and the input currents $\mathbf{I}(t)$ are constant in time. We further assume that the matrix Λ has full rank.

Proposition 9.3.1. Under the previous assumptions we have

$$\begin{cases} \lim_{t_0 \to -\infty} e^{\mathbf{L}(t-t_0)} = 0, \\ \int_{-\infty}^{t} \left\| e^{\mathbf{L}(t-s)} \right\| ds = \int_0^\infty \left\| e^{\mathbf{L}u} \right\|_\infty du \stackrel{\text{def}}{=} M_L < \infty, \\ \int_{-\infty}^{t} \left\| e^{\mathbf{L}^T(t-s)} \right\|_\infty ds = \int_0^\infty \left\| e^{\mathbf{L}^T u} \right\|_\infty du \stackrel{\text{def}}{=} M_{L^T} < \infty, \end{cases}$$

and the process $Y_t^{t_0} = \int_{t_0}^t e^{\mathbf{L}(t-s)} \Lambda \cdot d\mathbf{W}_s$ is well-defined, Gaussian and stationary when $t_0 \to -\infty$.

Proof. The first property follows from the fact that $\mathrm{Re}(\lambda) < -\lambda_L$ for all eigenvalues λ of $\mathbf{L}$. This assumption also implies that there exists a norm on $\mathbb{R}^P$ such that

$$\left\| e^{\mathbf{L}t} \right\| \leq e^{-\lambda_L t} \ \forall t \geq 0,$$

and hence

$$\left\| e^{\mathbf{L}t} \right\|_\infty \leq k e^{-\lambda_L t} \ \forall t \geq 0, \tag{9.34}$$

for some positive constant k. This implies the remaining two properties.

The stochastic integral $\int_{t_0}^t e^{\mathbf{L}(t-s)} \Lambda \cdot d\mathbf{W}_s$ is well-defined $\forall t \leq T$ and is Gaussian with zero-mean. We note $Y_t^{t_0}$ the corresponding process. Its covariance matrix reads:

$$\Sigma^{Y_t^{t_0} Y_{t'}^{t_0}} = \int_{t_0}^{t \wedge t'} e^{\mathbf{L}(t-s)} \Lambda \Lambda^T e^{\mathbf{L}^T (t'-s)} \, ds.$$

Let us assume for instance that $t' < t$ and perform the change of variable $u = t - s$ to obtain

$$\Sigma^{Y_t^{t_0} Y_{t'}^{t_0}} = \left(\int_{t-t'}^{t-t_0} e^{\mathbf{L}u} \Lambda\Lambda^T e^{\mathbf{L}^T u}\, du \right) e^{\mathbf{L}^T (t'-t)}.$$

Under the previous assumptions this matrix integral is defined when $t_0 \to -\infty$ (dominated convergence theorem) and we have

$$\Sigma^{Y_t^{-\infty} Y_{t'}^{-\infty}} = \left(\int_{t-t'}^{+\infty} e^{\mathbf{L}u} \Lambda\Lambda^T e^{\mathbf{L}^T u}\, du \right) e^{\mathbf{L}^T (t'-t)},$$

which is a function of $t'-t$. □

This guarantees that there exists a stationary distribution of the equation:

$$d\mathbf{X}_0(t) = \mathbf{L} \cdot \mathbf{X}_0(t)\, dt + \Lambda \cdot d\mathbf{W}_t, \tag{9.35}$$

such that $\mathbb{E}[\mathbf{X}_0(t)] = 0$. We have

$$\mathbf{X}_0(t) = \int_{-\infty}^{t} e^{\mathbf{L}(t-s)} \Lambda \cdot d\mathbf{W}_s.$$

Its covariance matrix Σ^0 is equal to $\Sigma^{Y_t^{-\infty} Y_t^{-\infty}}$ and is independent of t.

We call *long term mean field equation* (LTMFE) the implicit equation:

$$\mathbf{V}(t) = \int_{-\infty}^{t} e^{\mathbf{L}(t-s)} \left(\mathbf{U}_s^{\mathbf{V}} \cdot \mathbf{1} + \mathbf{I} \right) ds + \mathbf{X}_0(t) \tag{9.36}$$

where $\mathbf{X}_0$ is the stationary process defined by equation (9.35) and where $\mathbf{U}^{\mathbf{V}}(t)$ is the effective interaction process introduced previously.

We next define the long term function $F_{\text{stat}} : \mathscr{M}_1^+(C((-\infty, T], \mathbb{R}^P) \to \mathscr{M}_1^+(C((-\infty, T], \mathbb{R}^P)$:

$$F_{\text{stat}}(\mathbf{X})_t = \int_{-\infty}^{t} e^{\mathbf{L}(t-s)} \left(\mathbf{U}_s^X \cdot \mathbf{1} + \mathbf{I} \right) ds + \mathbf{X}_0(t).$$

Proposition 9.3.2. The function F_{stat} is well defined on $\mathscr{M}_1^+(C((-\infty, T], \mathbb{R}^P)$.

Proof. We have already seen that the process $\mathbf{X}_0$ is well defined. The term $\int_{-\infty}^{t} e^{\mathbf{L}(t-s)} \mathbf{I}\, ds = \left(\int_{-\infty}^{t} e^{\mathbf{L}(t-s)}\, ds \right) \mathbf{I}$ is also well defined because of the assumptions on $\mathbf{L}$.

Let X be a given process in $\mathscr{M}_1^+(C((-\infty, T], \mathbb{R}^P)$. To prove the proposition we just have to ensure that the Gaussian process $\int_{-\infty}^{t} e^{\mathbf{L}(t-s)} \mathbf{U}_s^X \cdot \mathbf{1}\, ds$ is well defined. This results from the contraction assumption on $\mathbf{L}$ and the fact that the functions $S_{\alpha\beta}$ are bounded. We decompose this process into a "long memory" term $\int_{-\infty}^{0} e^{\mathbf{L}(t-s)} \mathbf{U}_s^X \cdot \mathbf{1}\, ds$ and the interaction term from time $t = 0$, namely $\int_0^t e^{\mathbf{L}(t-s)} \mathbf{U}_s^X \cdot \mathbf{1}\, ds$. This latter term is clearly well defined. We show that the memory term is also well defined as a Gaussian random variable.

We write this term $e^{\mathbf{L}t} \int_{-\infty}^{0} e^{-\mathbf{L}s} \mathbf{U}_s^X \cdot \mathbf{1}\, ds$ and consider the second factor. This random variable is Gaussian, its mean reads $\int_0^{\infty} e^{\mathbf{L}s} \mu^{\mathbf{U}_{-s}^X} \cdot \mathbf{1}\, ds$ where

$$\mu^{\mathbf{U}_{-s}^X} = \left(\sum_{\beta=1}^{P} \bar{J}_{\alpha\beta} \mathbb{E}\left[S_{\alpha\beta}(X_\beta(-s)) \right] + I_\alpha \right)_{\alpha = 1 \ldots P}$$

The integral defining the mean is well-defined because of (9.34) and the fact that the functions $S_{\alpha\beta}$ are bounded. A similar reasoning shows that the corresponding covariance matrix is well-defined. Hence the Gaussian process $\int_{-\infty}^{0} e^{-\mathbf{L}s}\mathbf{U}_s^X \cdot \mathbf{1} ds$ is well defined, and hence for any process $X \in \mathscr{M}_1^+(C((-\infty,T],\mathbb{R}^P)$, the process $F_{\text{stat}}(X)$ is well defined. □

We can now prove the following proposition.

Proposition 9.3.3. The mean vectors and the covariance matrices of the processes in the image of F_{stat} are bounded.

Proof. Indeed, since $\mathbb{E}[X_0(t)] = 0$, we have:

$$\|\mathbb{E}[F_{\text{stat}}(\mathbf{X})_t]\|_\infty = \left\| \int_{-\infty}^{t} e^{\mathbf{L}(t-s)} \mu^{\mathbf{U}_s^X} ds \right\|_\infty \leq M_L(\mu + \|I\|_\infty) \stackrel{\text{def}}{=} \mu_{LT}.$$

In a similar fashion the covariance matrices of the processes in the image of F_{stat} are bounded. Indeed we have:

$$\mathbb{E}\left[F_{\text{stat}}(\mathbf{X})_t F_{\text{stat}}(\mathbf{X})_t^T\right] = \Sigma^0 + \int_{-\infty}^{t}\int_{-\infty}^{t} e^{\mathbf{L}(t-s_1)} \text{diag}\left(\sum_\beta \sigma_{\alpha\beta}^2 \mathbb{E}\left[S_{\alpha\beta}(X_\beta(s_1))S_{\alpha\beta}(X_\beta(s_2))\right]\right) e^{\mathbf{L}^T(t-s_2)} ds_1\, ds_2,$$

resulting in

$$\left\|\mathbb{E}\left[F_{\text{stat}}(\mathbf{X})_t F_{\text{stat}}(\mathbf{X})_t^T\right]\right\|_\infty \leq \left\|\Sigma^0\right\|_\infty + k^2\left(\frac{\sigma_{\max}}{\lambda_L}\right)^2 \stackrel{\text{def}}{=} \Sigma_{LT}.$$

□

Lemma 9.3.4. The set of stationary processes is invariant by F_{stat}.

Proof. Since the processes in the image of F_{stat} are Gaussian processes, one just needs to check that the mean of the process is constant in time and that its covariance matrix $C(s,t)$ only depends on $t-s$.

Let Z be a stationary process and $Y = F_{\text{stat}}(Z)$. We denote by μ_α^Z the mean of the process $Z_\alpha(t)$ and by $C_\alpha^Z(t-s)$ its covariance function. The mean of the process $U_{\alpha\beta}^Z$ reads:

$$m_{\alpha,\beta}^Z(t) = \mathbb{E}\left[S_{\alpha\beta}(Z_\beta(t))\right] = \frac{1}{\sqrt{2\pi C_\beta^Z(0)}} \int_{\mathbb{R}} S_{\alpha\beta}(x) e^{\frac{(x-\mu_\beta^Z)^2}{2C_\beta^Z(0)}} dx$$

and hence does not depends on time. We note μ^Z the mean vector of the stationary process $\mathbf{U}^Z \cdot \mathbf{1}$.

Similarly, its covariance function reads:

$$\Delta_{\alpha\beta}^Z(t,s) = \mathbb{E}\left[S_{\alpha\beta}(Z_\beta(t))S_{\alpha\beta}(Z_\beta(s))\right] = \int_{\mathbb{R}^2} S_{\alpha\beta}(x)S_{\alpha\beta}(y) \exp\left(-\frac{1}{2}\begin{pmatrix} x-\mu_\beta^Z \\ y-\mu_\beta^Z \end{pmatrix}^T \begin{pmatrix} C_\beta^Z(0) & C_\beta^Z(t-s) \\ C_\beta^Z(t-s) & C_\beta^Z(0) \end{pmatrix}^{-1} \begin{pmatrix} x-\mu_\beta^Z \\ y-\mu_\beta^Z \end{pmatrix}\right) dx\, dy$$

which is clearly a function, noted $\Delta^Z_{\alpha\beta}(t-s)$, of $t-s$. Hence $\mathbf{U}^Z \cdot \mathbf{1}$ is stationary and we denote by $C^{U^Z}(t-s)$ its covariance function.

It follows that the mean of Y_t reads:

$$\begin{aligned}\mu^Y(t) &= \mathbb{E}\left[F_{\text{stat}}(Z)_t\right] \\ &= \mathbb{E}\left[X_0(t)\right] + \mathbb{E}\left[\int_{-\infty}^t e^{\mathbf{L}(t-s)}\left(\mathbf{I}+\mathbf{U}^Z_s\cdot\mathbf{1}\right)ds\right] \\ &= \int_{-\infty}^t e^{\mathbf{L}(t-s)}\left(\mathbf{I}+\mathbb{E}\left[\mathbf{U}^Z_s\cdot\mathbf{1}\right]\right)ds \\ &= \left(\int_{-\infty}^0 e^{\mathbf{L}u}du\right)\left(\mathbf{I}+\mu^Z\right)\end{aligned}$$

Since we proved that $\mathbb{E}\left[\mathbf{U}^Z_s\cdot\mathbf{1}\right] = \mu^Z$ was not a function of s.

Similarly, we compute the covariance function and check that it can be written as a function of $(t-s)$. Indeed, it reads:

$$\begin{aligned}C^Y(t,s) &= \int_{-\infty}^t\int_{-\infty}^s e^{\mathbf{L}(t-u)}Cov(\mathbf{U}^Z_u\cdot\mathbf{1},\mathbf{U}^Z_v\cdot\mathbf{1})e^{\mathbf{L}^T(s-v)}du\,dv + Cov(X_0(t),X_0(s)) \\ &= \int_{-\infty}^0\int_{-\infty}^0 e^{\mathbf{L}u}C^{U^Z}(t-s+(u-v))e^{\mathbf{L}^Tv}du\,dv + C^{X_0}(t-s)\end{aligned}$$

since the process X_0 is stationary. $C^Y(t,s)$ is clearly a function of $t-s$. Hence Y is a stationary process, and the proposition is proved.

□

Theorem 9.3.5. *The sequence of processes $\{F^{(n)}_{stat}(X)\}_{n=0}^\infty$ is uniformly tight.*

Proof. The proof is essentially the same as the proof of theorem 9.2.3, since we can write

$$F_{\text{stat}}(X)_t = e^{\mathbf{L}t}F_{\text{stat}}(X)_0 + \int_0^t e^{\mathbf{L}(t-s)}(\mathbf{U}^X_s\cdot\mathbf{1}+\mathbf{I})\,ds + \int_0^t e^{\mathbf{L}(t-u)}\Lambda d\mathbf{W}_s$$

$F_{\text{stat}}(X)_t$ appears as the sum of the random variable $F_{\text{stat}}(X)_0$ and the Gaussian process defined by $\int_0^t e^{\mathbf{L}(t-s)}(\mathbf{U}^X_s\cdot\mathbf{1}+\mathbf{I})\,ds + \int_0^t e^{\mathbf{L}(t-u)}\Lambda d\mathbf{W}_s$ which is equal to $F_k(X)_t$ defined in section 9.2 for $t_0 = 0$. Therefore $F^{(n)}_{\text{stat}}(X)_t = F^{(n)}_k(X)_t$ for $t > 0$. We have proved the uniform tightness of the sequence of processes $\{F^{(n)}_k(X)\}_{n=0}^\infty$ in theorem 9.2.3. Hence, according to Kolmogorov's criterion for tightness, we just have to prove that the sequence of Gaussian random variables:

$$F^{(n)}_{\text{stat}}(X)_0 = \left\{\int_{-\infty}^0 \Phi_L(-u)(\mathbf{U}_u^{F^{(n)}_{\text{stat}}(X)}\cdot\mathbf{1}+\mathbf{I})du + \mathbf{X}_0(0)\right\}_{n\geq 0}$$

is uniformly tight. Since it is a sequence of Gaussian random variables, it is sufficient to prove that their means and covariance matrices are upperbounded to obtain that for any $\varepsilon > 0$ there exists a compact K_ε such that for any $n \in \mathbb{N}$, we have $\mathbb{P}(F^{(n)}_{\text{stat}}(X)_0 \in K_\varepsilon) \geq 1-\varepsilon$. This is a consequence of proposition 9.3.3 for the first random variable and of the definition of $\mathbf{X}_0$ for the second. By Kolmogorov's criterion the sequence of processes $\{F^{(n)}_{\text{stat}}(X)\}_{n=0}^\infty$ is uniformly tight

□

In order to apply theorem 9.2.1 we need to prove that the sequences of covariance and mean functions are convergent. Unlike the case of t_0 finite, this is not always true. Indeed, to ensure existence and uniqueness of solutions in the stationary case, the parameters of the system have to satisfy a contraction condition, and proposition 9.2.7 extends as follows.

Proposition 9.3.6. If λ_L defined in (9.33) satisfies the conditions (9.37) defined in the proof, depending upon k_C (defined in (9.30)), k_0, μ_{LT} and Σ_{LT} (defined in proposition 9.3.3)then the sequences of covariance matrix functions $C^n(t,s)$ and of mean functions $\mu^n(t)$, s,t in $[t_0,T]$ are Cauchy sequences for the uniform norms.

Proof. The proof follows that of proposition 9.2.7 with a few modifications that we indicate. In establishing the equation corresponding to (9.29) we use the fact that $\|\Phi_L(t,u)\|_\infty \leq ke^{-\lambda_L(t-u)}$ for some positive constant k and all u, t, $u \leq t$. We therefore have:

$$\left\|C^{n+1}(t,s)-C^n(t,s)\right\|_\infty \leq k^2e^{-\lambda_L(t+s)}\int_{-\infty}^{t}\int_{-\infty}^{s}e^{\lambda_L(u+v)}\left\|Cov\left(\mathbf{U}_u^{X_n},\mathbf{U}_v^{X_n}\right)-Cov\left(\mathbf{U}_u^{X_{n-1}},\mathbf{U}_v^{X_{n-1}}\right)\right\|_\infty^v dudv$$

The rest of the proof proceeds the same way as in proposition 9.2.7. Equations (9.31) and (9.32) become:

$$\begin{aligned}\left\|C^{n+1}(t,s)-C^n(t,s)\right\|_\infty \leq Ke^{-\lambda_L(t+s)}\Bigg(&\int_{[-\infty,t\vee s]^2}\frac{e^{\lambda_L(u+v)}}{\sqrt{f(u,v)}}\left\|C^n(u,v)-C^{n-1}(u,v)\right\|_\infty dudv\\ &+\int_{[-\infty,t\vee s]^2}\frac{e^{\lambda_L(u+v)}}{\sqrt{f(u,v)}}\left\|C^n(u,u)-C^{n-1}(u,u)\right\|_\infty dudv\\ &+\int_{[-\infty,t\vee s]^2}e^{\lambda_L(u+v)}\left\|C^n(u,v)-C^{n-1}(u,v)\right\|_\infty dudv\\ &+\int_{[-\infty,t\vee s]^2}e^{\lambda_L(u+v)}\left\|C^n(u,u)-C^{n-1}(u,u)\right\|_\infty dudv\\ &+\int_{[-\infty,t\vee s]^2}e^{\lambda_L(u+v)}\left\|\mu^n(u)-\mu^{n-1}(u)\right\|_\infty dudv\Bigg),\end{aligned}$$

and

$$\begin{aligned}\left\|\mu^{n+1}(t)-\mu^n(t)\right\|_\infty \leq Ke^{-\lambda_L(t+s)}\Bigg(&\int_{[-\infty,t\vee s]^2}e^{\lambda_L(u+v)}\left\|C^n(u,u)-C^{n-1}(u,u)\right\|_\infty dudv+\\ &\int_{[-\infty,t\vee s]^2}e^{\lambda_L(u+v)}\left\|\mu^n(u)-\mu^{n-1}(u)\right\|_\infty dudv\Bigg),\end{aligned}$$

for some positive constant K, function of k, k_C (defined in (9.30)), and k_0.

Proceeding recursively until we reach C^0 and μ^0 we obtain an upperbound for $\left\|C^{n+1}(t,s)-C^n(t,s)\right\|_\infty$ (respectively for $\left\|\mu^{n+1}(t)-\mu^n(t)\right\|_\infty$) which is the sum of less than 5^n terms each one being the product of K^n, times $2\mu_{LT}$ or $2\Sigma_{LT}$, times a $2n$-dimensional

integral I_n given by:

$$\int_{[-\infty,t\vee s]^2}\rho_1(u_1,v_1)\left(\int_{[-\infty,u_1\vee v_1]^2}\cdots\left(\int_{[-\infty,u_{n-2}\vee v_{n-2}]^2}\rho_{n-1}(u_{n-1},v_{n-1})\right.\right.$$
$$\left.\left.\left(\int_{[-\infty,u_{n-1}\vee v_{n-1}]^2}e^{\lambda_L(u_n+v_n)}\rho_n(u_n,v_n)du_ndv_n\right)du_{n-1}dv_{n-1}\right)\cdots\right)du_1dv_1,$$

where the functions $\rho_i(u_i,v_i)$, $i=1,\cdots,n$ are either equal to 1 or to $1/\sqrt{\theta(u_i,v_i)}$.

It can be shown by straightforward calculation that each sub-integral contributes at most either

$$\frac{K_0}{\lambda_L^2}\quad\text{if}\quad\rho_i=1\quad\text{or}\quad\sqrt{\frac{\pi}{2}}\frac{K_0}{\lambda_L^{3/2}},$$

in the other case. Hence we obtain factors of the type

$$K_0^n\left(\frac{1}{\lambda_L^2}\right)^p\left(\sqrt{\frac{\pi}{2}}\frac{1}{\lambda_L^{3/2}}\right)^{n-p}=\left(\sqrt{\frac{\pi}{2}}\right)^{n-p}\left(\frac{1}{\lambda_L}\right)^{(3n+p)/2}K_0^n,$$

where $0\le p\le n$. If $\lambda_L<1$, $(\lambda_L)^{(3n+p)/2}\ge\lambda_L^{2n}$ and else $(\lambda_L)^{(3n+p)/2}\ge\lambda_L^{3n/2}$. Since $\left(\sqrt{\frac{\pi}{2}}\right)^{n-p}\le\left(\sqrt{\frac{\pi}{2}}\right)^n$ we obtain the two conditions

$$1>\lambda_L^2\ge 5\sqrt{\frac{\pi}{2}}KK_0\quad\text{or}\quad\left\{\lambda_L^{3/2}>5\sqrt{\frac{\pi}{2}}KK_0\quad\text{and}\quad\lambda_L\ge 1\right\}\tag{9.37}$$

□

Putting all these results together we obtain the following theorem of existence and uniqueness of solutions for the long term mean field equations:

Theorem 9.3.7. *Under the contraction conditions* (9.37)*, the function F_{stat} has a unique solution in $\mathscr{M}_1^+(C((-\infty,T],\mathbb{R}^P)$ which is stationary, and for any process X, the sequence $\{F_{stat}^{(n)}(X)\}_{n=0}^{\infty}$ of Gaussian processes converges in law toward the unique fixed point of the function F_{stat}.*

Proof. The proof is essentially similar to the one of theorem 9.2.8. Indeed, the mean and the covariance matrixes converge since they are Cauchy sequences in the complete space of continuous functions equipped with the uniform norm. Using theorem 9.2.1, we obtain that the sequence converges to a process Y which is necessarily a fixed point of F_{stat}. Hence we have existence of a fixed point for F_{stat}. The uniqueness comes from the results obtained in the proof of proposition 9.3.6. The limiting process is necessarily stationary. Indeed, let X be a stationary process. Then for any $n\in\mathbb{N}$, the process $F_{\text{stat}}^{(n)}(X)$ will be stationary by the virtue of lemma 9.3.4, and hence so will be the limiting process which is the only fixed point of F_{stat}.

□

Hence in the stationary case, the existence and uniqueness of a solution is not always ensured. For instance if the leaks are too small (i.e. when the time constants of the decay of the membrane potentials are too long) then the sequence can diverge or have multiple fixed points.

9.4 NUMERICAL EXPERIMENTS

9.4.1 Simulation algorithm

Beyond the mathematical results, the framework that we introduced in the previous sections gives us a strategy to compute numerically the solutions of the dynamic mean-field equations. Indeed, we proved in section 9.2 that under very moderate assumptions on the covariance matrix of the noise, the iterations of the map F_k starting from any initial condition converge to the solution of the mean field equations.

This convergence result gives us a direct way to compute numerically the solution of the mean field equations. Since we are dealing with Gaussian processes, determining the law of the iterates of the map F_k amounts to computing its mean and covariance functions. In this section we describe our numerical algorithm in the case of the Simple Model of section 9.1.4.

Computing F_k.

Let X be a P-dimensional Gaussian process of mean $\mu^X = (\mu^X_\alpha(t))_{\alpha=1\dots P}$ and covariance $C^X = (C^X_{\alpha\beta}(s,t))_{\alpha,\beta\in\{1\dots P\}}$. We fix a time interval $[t_0 = 0, T]$ and denote by Y the image of the process X under F_1. In the case of the simple model, the covariance of Y is diagonal. Hence in this case the expressions we obtain in section 9.2 simply read:

$$\begin{aligned}\mu^Y_\alpha(t) &= \mu^X_\alpha(0)e^{-t/\tau_\alpha} + \int_0^t e^{-(t-s)/\tau_\alpha}\left(\sum_{\beta=1}^P \bar{J}_{\alpha\beta}\,\mathbb{E}\left[S_{\alpha,\beta}(X_\beta(s))\right] + I_\alpha(s)\right)ds \\ &= \mu^X_\alpha(0)e^{-t/\tau_\alpha} + \int_0^t e^{-(t-s)/\tau_\alpha} I_\alpha(s)ds \\ &\quad + \sum_{\beta=1}^P \bar{J}_{\alpha\beta}\int_0^t e^{-(t-s)/\tau_\alpha}\int_{-\infty}^{+\infty} S_{\alpha\beta}\left(x\sqrt{v^X_\beta(s)} + \mu^X_\beta(s)\right)Dxds.\end{aligned}$$

where we denoted $v^X_\alpha(s)$ the standard deviation of X_α at time s, instead of $C^X_{\alpha\alpha}(s,s)$. Thus, knowing $v^X_\alpha(s), s\in[0,t]$ we can compute $\mu^Y_\alpha(t)$ using a standard discretization scheme of the integral, with a small time step compared with τ_α and the characteristic time of variation of the input current I_α. Alternatively, we can use the fact that μ^Y_α satisfies the differential equation:

$$\frac{d\mu^Y_\alpha}{dt} = -\frac{\mu^Y_\alpha}{\tau_\alpha} + \sum_{\beta=1}^P \bar{J}_{\alpha\beta}\int_{-\infty}^{+\infty} S_{\alpha\beta}\left(x\sqrt{v^X_\beta(t)} + \mu^X_\beta(t)\right)Dx + I_\alpha(t),$$

and compute the solution using a Runge-Kutta algorithm (which is faster and more accurate). Note that, when all the standard deviations of the process X are null for all time $t\in[0,T]$, we obtain a standard dynamical system. Nevertheless, in the general case, $v^X_\beta(t) > 0$ for some βs, and the dynamical evolution of μ^Y_α depends on the Gaussian fluctuations of the field X. These fluctuations must be computed via the complete equation of the covariance diagonal coefficient $C^Y_{\alpha\alpha}(t,s)$, which reads:

$$C^Y_{\alpha\alpha}(t,s) = e^{-(t+s)/\tau_\alpha}\left[v^X_\alpha(0) + \frac{\tau_\alpha s^2_\alpha}{2}\left(e^{\frac{2s}{\tau_\alpha}} - 1\right) + \sum_{\beta=1}^P \sigma^2_{\alpha\beta}\int_0^t\int_0^s e^{(u+v)/\tau_\alpha}\Delta^X_{\alpha\beta}(u,v)dudv\right],$$

where:

$$\Delta^X_{\alpha\beta}(u,v) = \int_{\mathbb{R}^2} S_{\alpha\beta}\left(x\frac{\sqrt{v^X_\beta(u)v^X_\beta(v) - C^X_{\beta\beta}(u,v)^2}}{\sqrt{v^X_\beta(v)}} + y\frac{C^X_{\beta\beta}(u,v)}{\sqrt{v^X_\beta(v)}} + \mu^X_\beta(u)\right) \times S_{\alpha\beta}\left(y\sqrt{v^X_\beta(v)} + \mu^X_\beta(v)\right) Dx Dy.$$

Unless if we assume the stationarity of the process (see e.g. section 9.4.2), this equation cannot be written as an ordinary differential equation. We clearly observe here the non-Markovian nature of the problem: $C^X_{\alpha\alpha}(t,s)$ depends on the whole past of the process until time $t \vee s$.

This covariance can be split into the sum of two terms: the external noise contribution $C^{OU}_{\alpha\alpha}(t,s) = e^{-(t+s)/\tau_\alpha}\left[v^X_\alpha(0) + \frac{\tau_\alpha s^2_\alpha}{2}\left(e^{\frac{2s}{\tau_\alpha}} - 1\right)\right]$ and the interaction between the neurons. The external noise contribution is a simple function and can be computed directly. To compute the interactions contribution to the standard deviation we have to compute the symmetric two-variables function:

$$H^X_{\alpha\beta}(t,s) = e^{-(t+s)/\tau_\alpha}\int_0^t\int_0^s e^{(u+v)/\tau_\alpha}\Delta^X_{\alpha\beta}(u,v)dudv,$$

from which one obtains the standard deviation using the formula

$$C^Y_{\alpha\alpha}(t,s) = C^{OU}_{\alpha\alpha}(t,s) + \sum_{\beta=1}^P \sigma^2_{\alpha\beta}H^X_{\alpha\beta}(t,s).$$

To compute the function $H^X_{\alpha\beta}(t,s)$, we start from $t=0$ and $s=0$, where $H^X_{\alpha\beta}(0,0)=0$. We only compute $H^X_{\alpha\beta}(t,s)$ for $t>s$ because of the symmetry. It is straightforward to see that:

$$H^X_{\alpha\beta}(t+dt,s) = H^X_{\alpha\beta}(t,s)\left[1 - \frac{dt}{\tau_\alpha}\right] + D^X_{\alpha\beta}(t,s)dt + o(dt),$$

with

$$D^X_{\alpha\beta}(t,s) = e^{-s/\tau_\alpha}\int_0^s e^{v/\tau_\alpha}\Delta^X_{\alpha\beta}(t,v)dv.$$

Hence computing $H^X_{\alpha\beta}(t+dt,s)$ knowing $H^X_{\alpha\beta}(t,s)$ amounts to computing $D_{\alpha\beta}(t,s)$. Fix $t \geq 0$. We have $D_{\alpha\beta}(t,0) = 0$ and

$$D^X_{\alpha\beta}(t,s+ds) = D^X_{\alpha\beta}(t,s)(1 - \frac{ds}{\tau_\alpha}) + \Delta^X_{\alpha\beta}(t,s)ds + o(ds).$$

This algorithm enables us to compute $H^X_{\alpha\beta}(t,s)$ for $t>s$. We deduce $H^X_{\alpha\beta}(t,s)$ for $t<s$ using the symmetry of this function. Finally, to get the values of $H^X_{\alpha\beta}(t,s)$ for $t=s$, we use the symmetry property of this function and get:

$$H^X_{\alpha\beta}(t+dt,t+dt) = H^X_{\alpha\beta}(t,t)\left[1 - \frac{2dt}{\tau_\alpha}\right] + 2D^X_{\alpha\beta}(t,t)dt + o(dt).$$

These numerical schemes provide an efficient way for computing the mean and the covariance functions of the Gaussian process $F_1(X)$ (hence its probability distribution) knowing the law of the Gaussian process X. The algorithm used to compute the solution of the mean field equations for the general models GM1 and GMk is a straightforward generalization.

Analysis of the algorithm

Convergence rate As proved in theorem 9.2.8, given Z_0 a nondegenerate kP-dimensional Gaussian random variable and X a Gaussian process such that $X(0) = Z_0$, the sequences of means and covariance functions computed theoretically converge uniformly towards those of the unique fixed point of the map F_k. It is clear that our algorithm converges uniformly towards the real function it emulates. Hence for a finite N, the algorithm will converge uniformly towards the mean and covariance matrix of the process $F_k^N(X)$.

Denote by X_f the fixed point of F_k in $\mathscr{M}_1^+(C([t_0,T],\mathbb{R}^{kP}))$, of mean $\mu^{X_f}(t)$ and covariance matrix $C^{X_f}(t,s)$, and by $\widehat{F_k^N}(X)$ the numerical approximation of $F_k^N(X)$ computed using the algorithm previously described, whose mean is noted $\mu^{\widehat{F_k^N}(X)}(t)$ and whose covariance matrix is noted $C^{\widehat{F_k^N}(X)}(t,s)$. The uniform error between the simulated mean after N iterations with a time step dt and the fixed point's mean and covariance is the sum of the numerical error of the algorithm and the distance between the simulated process and the fixed point, is controlled by:

$$\|\mu^{\widehat{F_k^N}(X)} - \mu^{X_f}\|_\infty + \|C^{\widehat{F_k^N}(X)} - C^{X_f}\|_\infty = O(\ (N+T)\,dt + R_N(k_{\max})\ ) \tag{9.38}$$

where $k_{\max} = \max(k,\tilde{k})$ and k and $\tilde{k}$) are the constants that appear in the proof of proposition 9.2.7 for the mean and covariance functions, and $R_N(x)$ is the exponential remainder, i.e. $R_N(x) = \sum_{n=N}^{\infty} x^n/n!$.

Indeed, we have:

$$\|\mu^{\widehat{F_k^N}(X)} - \mu^{X_f}\|_\infty \leq \|\mu^{\widehat{F_k^N}(X)} - \mu^{F_k^N(X)}\|_\infty + \|\mu^{F_k^N(X)} - \mu^{X_f}\|_\infty \tag{9.39}$$

The discretization algorithm used converges in $O(dt)$. Let us denote by C_1 the convergence constant, which depends on the sharpness of the function we approximate, which can be uniformly controlled over the iterations. Iterating the numerical algorithm has the effect of propagating the errors. Using these simple remarks we can bound the first term of the righthand side of (9.39), i.e. the approximation error at the Nth iteration:

$$\|\mu^{\widehat{F_k^N}(X)} - \mu^{F_k^N(X)}\|_\infty \leq C_1 N\,dt$$

Because the sequence of means is a Cauchy sequence, we can also bound the second term of the righthand side of (9.39):

$$\begin{aligned}\|\mu^{F_k^N(X)} - \mu^{X_f}\|_\infty &\leq \sum_{n=N}^{\infty} \|\mu^{F_k^{n+1}(X)} - \mu^{F_k^n(X)}\|_\infty \\ &\leq \sum_{n=N}^{\infty} \frac{k^n}{n!} =: R_N(k)\end{aligned}$$

for some positive constant k introduced in the proof of proposition 9.2.7. The remainders sequence $(R_n(k))_{n\geq 0}$ converges fast towards 0 (an estimation of its convergence can be obtained using the fact that $\limsup_{k\to\infty}(1/k!)^{1/k} = 0$ by Stirling's formula).

Hence we have:

$$\|\mu^{\widehat{F_k^N}(X)} - \mu^{X_f}\|_\infty \leq C_1 N\,dt + R_N(k) \tag{9.40}$$

For the covariance, the principle of the approximation is exactly the same:

$$\|C^{\widehat{F_k^N}(X)} - C^{X_f}\|_\infty \leq \|C^{\widehat{F_k^N}(X)} - C^{F_k^N(X)}\|_\infty + \|C^{F_k^N(X)} - C^{X_f}\|_\infty$$

The second term of the righthand side can be controlled using the same evaluation by $R_N(\tilde{k})$ where $\tilde{k}$ is the constant introduced in the proof of proposition 9.2.7, and the first term is controlled by the rate of convergence of the approximation of the double integral, which is bounded by $C_2(N+T)\,dt$ where C_2 depends on the parameters of the system and the discretization algorithm used.

Hence we have:

$$\|C^{\widehat{F_k^N}(X)} - C^{X_f}\|_\infty \leq C_2\,(N+T-t_0)\,dt + R_N(\tilde{k}) \tag{9.41}$$

The expressions (9.40) and (9.41) are the sum of two terms, one of which is increasing with N and T and decreasing with dt and the other one decreasing in N. If we want to obtain an estimation with an error bounded by some $\varepsilon > 0$, we can for instance fix N such that $\max(R_N(k), R_N(\tilde{k})) < \varepsilon/2$ and then fix the time step dt smaller than $\min(\,\varepsilon/(2C_1N), \varepsilon/(2C_2(N+T-t_0))\,)$.

Complexity The complexity of the algorithm depends on the complexity of the computations of the integrals. The algorithm described hence has the complexity $O(N(\frac{T}{dt})^2)$.

9.4.2 The importance of the covariance: Simple Model, one population.

As a first example and a benchmark for our numerical scheme we revisit the work of Sompolinsky and coworkers [240]. These authors studied the case of the simple model with one population ($P = 1$), with the centered sigmoidal function $S(x) = \tanh(gx)$, centered connectivity weights $\bar{J} = 0$ of standard deviation $\sigma = 1$ and no input ($I = 0, \Lambda = 0$). Note therefore that there is no "noise" in the system, which therefore does not match the non degeneracy conditions of proposition 9.2.4 and of theorem 9.2.8 . This issue is discussed below. In this case, the mean equals 0 for all t. Nevertheless, the Gaussian process is non trivial as revealed by the study of the covariance $C(t,s)$.

Stationary solutions

Assuming that the solution of the mean field equation is a stationary solution with $C(t,s) \equiv C(t-s) = C(\tau)$, Sompolinsky and his collaborators found that the covariance obeyed a second order differential equation :

$$\frac{d^2C}{d\tau^2} = -\frac{\partial V_q}{\partial C}. \tag{9.42}$$

This form corresponds to the motion of a particle in a potential well and it is easy to draw the phase portrait of the corresponding dynamical system. However, there is a difficulty. The potential V_q depends on a parameter q which is in fact precisely the covariance at $\tau = 0$ ($q = C(0)$). In the stationary case, this covariance depends on the whole solution, and hence cannot be really considered as a parameter of the system. This is one of the main difficulties in this approach: mean field equations in the stationary regime are self-consistent.

Nevertheless, the study of the shape of V_q, considering q as a free parameter gives us some informations. Indeed, V_q has the following Taylor expansion (V_q is even because S is odd):

$$V_q(C) = \frac{\lambda}{2}C^2 + \frac{\gamma}{4}C^4 + O(C^6)$$

where $\lambda = (1 - g^2J^2\langle S'\rangle_q^2)$ and $\gamma = \frac{1}{6}J^2g^6\langle S^{(3)}\rangle_q^2)$, $\langle\phi\rangle_q$ being the average value of ϕ under the Gaussian distribution with mean zero and variance $q = C(0)$.

If $\lambda > 0$, i.e. when $g^2J^2\langle S'\rangle_q^2 < 1$, then the dynamical system (9.42) has a unique solution $C(t) = 0, \forall t \geq 0$. This corresponds to a stable fixed point (i.e. a deterministic trajectory, $\mu = 0$ with no fluctuations) for the neural network dynamics. On the other hand, if $g^2J^2\langle S'\rangle_q^2 \geq 1$ there is a homoclinic trajectory in (9.42) connecting the point $q = C^* > 0$ where V_q vanishes to the point $C = 0$. This solution is interpreted by the authors as a chaotic solution in the neural network. A stability analysis shows that this is the only stable[3] stationary solution [240].

The equation for the homoclinic solution is easily found using energy conservation and the fact that $V_q(q) = 0$ and $\frac{dV_q}{dC}(q) = 0$. One finds:

$$u = \frac{dC}{dx} = -\sqrt{-V_q(C)}.$$

At the fourth order in the Taylor expansion of V_q this gives

$$C(\tau) = \frac{\sqrt{\frac{-2\lambda}{\gamma}}}{\cosh(\sqrt{-\frac{\lambda}{2}}\tau)}.$$

Though λ depends on q it can be used as a free parameter for interpolating the curve of $C(\tau)$ obtained from numerical data.

Numerical experiments

This case is a good benchmark for our numerical procedure since we know analytically the solutions we are searching for. We expect to find two regimes. In one case the correlation function is identically zero in the stationary regime, for sufficiently small g values or for a sufficiently small q (trivial case). The other case corresponds to a regime where $C(\tau) > 0$ and $C(\tau) \to 0$ has $\tau \to +\infty$ ("chaotic" case). This regime requires that g be sufficiently large and that q be large too. We took $\tau_\alpha = 0.25, \sigma_{\alpha\alpha} = 1$. For these values, the change in dynamics predicted by Sompolinsky and collaborators is $g_c = 4$.

In sections 9.2 and 9.3 we have introduced the assumption of non-degeneracy of the noise, in order to ensure that the mean field process was non degenerate. However, in the present example, there is no external noise in the evolution, so we can observe the effects of relaxing this hypothesis in a situation where the results of proposition 9.2.4 and of theorem 9.2.8 cannot be applied. First, we observed numerically that, without external noise, the process could become degenerate (namely some eigenvalues of the covariance matrix $C_\alpha(t,s)$ become very small and even vanish.). This has also an incidence on the convergence of the method which presents numerical instabilities, though the iterations leads to a curve which is well fitted by

[3] More precisely, this is the only minimum for the large deviation functional.

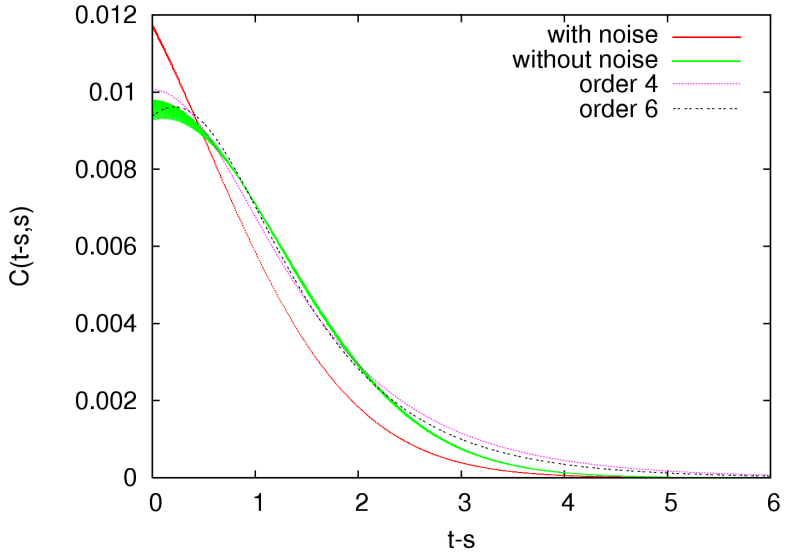

Figure 9.3: Numerical solution of the mean field equation after 14 iterations in the chaotic case ($g = 5$). We clearly see the numerical instabilities in the no-noise case, which do not exist in the low-noise case.

the theoretical results of Sompolinsky et al. (see Fig. 9.3) . The instability essentially disappears if one adds a small noise. But, note that in this case, the solution does not match with Sompolinsky et al. theoretical calculation (see Fig. 9.3).

Modulo this remark, we have first considered the trivial case corresponding to small g values. We took $g = 0.5$ and $T = 5$. We choose as initial process the stationary Ornstein-Uhlenbeck process corresponding to the uncoupled system with $\Lambda = 0.1$. We drew $\mu_\alpha(0)$ randomly from the uniform distribution in $[-1,1]$ and $v_\alpha(0)$ randomly from the uniform distribution in $[0,1]$.

Starting from this initial stationary process, we iterated the function F_1. Then, during the iterations, we set $s_\alpha = 0$ in order to match the conditions imposed by Sompolinsky and coworkers. We observe that the method converges towards the expected solution: the mean function converges to zero, while the variance $v(t)$ decreases exponentially fast in time towards a constant value corresponding to the stationary regime. This asymptotic value decreases between two consecutive iterations, which is consistent with the theoretical expectation that $v(t) = 0$ in the stationary regime of the trivial case. Finally, we observe that the covariance $C(t-s,s)$ stabilizes to a curve that does not depend on s and the stationary value (large $t-s$) converges to zero.

We applied the same procedure for $g = 5$ corresponding to the "chaotic" regime. The behavior was the same for $\mu(t)$ but was quite different for the covariance function $C(t,s)$. Indeed, while in the first case the stationary value of $v(t)$ tends to zero with the number of iterations, in the chaotic case it stabilizes to a finite value. In the same way, the covariance $C(t-s,s)$ stabilizes to a curve that does not depend on s. The shape of this curve can be extrapolated thanks to Sompolinsky et al. results. We observe a very good agreement with the theoretical predictions with a fit $f_4(x) = \frac{a}{\cosh(b(x-\delta))}$, corresponding to the fourth expansion of V_q. Using a 6-th order expansion of $V_q(x) = \frac{a}{2}x^2 + \frac{b}{4}x^4 + \frac{c}{6}x^2$ gives a fit $f_6(x) = \frac{\rho}{\cosh(\lambda(x-\delta))} \frac{1}{\sqrt{1+K^2 - \frac{1}{\cosh^2(\lambda(x-\delta))}}}$, where ρ, K, λ are

explicit functions of a,b,c, we obtain a slightly better approximation.

9.4.3 s

Mean field equations for two populations with a negative feedback loop.

Let us now present a case where the fluctuations of the Gaussian field act on the dynamics of $\mu_\alpha(t)$ in a non trivial way, with a behavior strongly departing from the naive mean field picture. We consider two interacting populations where the connectivity weights are Gaussian random variables $J_{\alpha\beta} \equiv \mathcal{N}(\bar{J}_{\alpha\beta}, \sigma_{\alpha\beta} = 1)$ for $(\alpha,\beta) \in \{1,2\}^2$. We set $S_{\alpha\beta}(x) = \tanh(gx)$ and $I_\alpha = 0, s_\alpha = 0, \alpha = 1,2$.

Theoretical framework.

The dynamic mean field equation for $\mu_\alpha(t)$ is given, in differential form, by:

$$\frac{d\mu_\alpha}{dt} = -\frac{\mu_\alpha}{\tau_\alpha} + \sum_{\beta=1}^{2} \bar{J}_{\alpha\beta} \int_{-\infty}^{\infty} S\left(\sqrt{v_\beta(t)}x + \mu_\beta(t)\right) Dx, \ \alpha = 1,2.$$

Let us denote by $G_\alpha(\mu, v(t))$ the function in the righthand side of the equality. Since S is odd, $\int_{-\infty}^{\infty} S(\sqrt{v_\beta(t)}x) Dx = 0$. Therefore, we have $G_\alpha(0, v(t)) = 0$ whatever $v(t)$, and hence the point $\mu_1 = 0, \mu_2 = 0$ is always a fixed point of this equation.

Let us study the stability of this fixed point. To this purpose, we compute the partial derivatives of $G_\alpha(\mu, v(t))$ with respect to μ_β for $(\alpha,\beta) \in \{1,2\}^2$. We have:

$$\frac{\partial G_\alpha}{\partial \mu_\beta}(\mu, v(t)) = -\frac{\delta_{\alpha\beta}}{\tau_\alpha} + g\bar{J}_{\alpha\beta} \int_{-\infty}^{\infty} \left(1 - \tanh^2\left(\sqrt{v_\beta(t)}x + \mu_\beta(t)\right)\right) Dx,$$

and hence at the point $\mu_1 = 0, \mu_2 = 0$, these derivatives read:

$$\frac{\partial G_\alpha}{\partial \mu_\beta}(0, v(t)) = -\frac{\delta_{\alpha\beta}}{\tau_\alpha} + g\bar{J}_{\alpha\beta} h(v_\beta(t)),$$

where $h(v_\beta(t)) = 1 - \int_{-\infty}^{\infty} \tanh^2(\sqrt{v_\beta(t)}x) Dx$.

In the case $v_\alpha(0) = 0, J = 0, s_\alpha = 0$, implying $v_\alpha(t) = 0, t \geq 0$, the equation for μ_α reduces to:

$$\frac{d\mu_\alpha}{dt} = -\frac{\mu_\alpha}{\tau_\alpha} + \sum_{\beta=1}^{2} \bar{J}_{\alpha\beta} S(\mu_\beta(t))$$

which is the standard Amari-Cohen-Grossberg-Hopfield system. This corresponds to the naive mean field approach where Gaussian fluctuations are neglected. In this case the stability of the fixed point $\mu = 0$ is given by the sign of the largest eigenvalue of the Jacobian matrix of the system that reads:

$$\begin{pmatrix} -\frac{1}{\tau_1} & 0 \\ 0 & -\frac{1}{\tau_2} \end{pmatrix} + g \begin{pmatrix} \bar{J}_{11} & \bar{J}_{12} \\ \bar{J}_{21} & \bar{J}_{22} \end{pmatrix}.$$

For the sake of simplicity we assume that the two time constants τ_α are equal and we denote this value τ. The eigenvalues are in this case $-\frac{1}{\tau} + g\lambda$, where λ are the eigenvalues of $\bar{\mathcal{J}}$ and have the form:

$$\lambda_{1,2} = \frac{\bar{J}_{11} + \bar{J}_{22} \pm \sqrt{(J_{11} - J_{22})^2 + 4J_{12}J_{21}}}{2}.$$

Hence, they are complex whenever $\bar{J}_{12}\bar{J}_{21} < -(\bar{J}_{11}-\bar{J}_{22})^2/4$, corresponding to a negative feedback loop between population 1 and 2. Moreover, they have a real part only if $\bar{J}_{11}+\bar{J}_{22}$ is non zero (self interaction).

This opens up the possibility to have an instability of the fixed point ($\mu = 0$) leading to a regime where the average value of the membrane potential oscillates. This occurs if $\bar{J}_{11}+\bar{J}_{22} > 0$ and if g is larger than:

$$g_c = \frac{2}{\tau(\bar{J}_{11}+J_{22})}.$$

The corresponding bifurcation is a Hopf bifurcation.

The situation is different if one takes into account the fluctuations of the Gaussian field. Indeed, in this case the stability of the fixed point $\mu = 0$ depends on $v(t)$. More precisely, the real and imaginary part of the eigenvalues of $DG(0, v(t))$ depend on $v(t)$. Therefore, the variations of $v(t)$ act on the stability and oscillations period of $v(t)$. Though the evolution of $\mu(t), v(t)$ are coupled we cannot consider this evolution as a coupled dynamical system, since $v(t) = C(t,t)$ is determined by the mean field equation for $C(t,s)$ which cannot be written as an ordinary differential equation. Note that we cannot assume stationarity here, as in the previous case, since $\mu(t)$ depends on time for sufficiently large g. This opens up the possibility of having complex dynamical regimes when g is large.

Numerical experiments

We have considered the case $\bar{J}_{11} = \bar{J}_{22} = 5, \tau = 0.1$ giving a Hopf bifurcation for $g_c = 2$ when $J = 0$ (fig. 9.4). The trajectory of $\mu_1(t)$ and $v_1(t)$ is represented in Figure 9.4 in the case $g = 3$. When $J = 0$, $\mu_1(t)$ presents regular oscillations (with non linear effects since $g = 3$ is larger than the critical value for the Hopf bifurcation, $g_c = 2$). In this case, the solution $v_1(t) = 0$ is stable as seen on the figure. When $J \neq 0$ the Gaussian field has (small) fluctuations which nevertheless strongly interact with the dynamics of $\mu_1(t)$, leading to a regime where $\mu_1(t)$ and $v_1(t)$ oscillate periodically

CONCLUSION

The problem of bridging scales is overwhelming in general when studying complex systems and in particular in neuroscience. After many others we look at this difficult problem from the theoretical and numerical viewpoints, hoping to get closer to its solution from relatively simple and physically/biologically plausible first principles and assumptions. One of our motivations is to better understand such phenomenological neural mass models as that of Jansen and Rit [149].

We consider several populations of neurons and start from a microscopic, i.e. individual, description of the dynamics of the membrane potential of each neuron that contains four terms. The first one controls the intrinsic dynamics of the neuron. It is linear in this article but this assumption is not essential and could probably be safely removed if necessary. The second term is a stochastic input current, correlated or uncorrelated. The third one is a deterministic input current, and the fourth one describes the interaction between the neurons through random connectivity coefficients that weigh the contributions of other neurons through a set of functions that are applied to their membranes potentials. The only hypothesis on these functions is that they are smooth and bounded. The obvious choice of sigmoids is motivated by

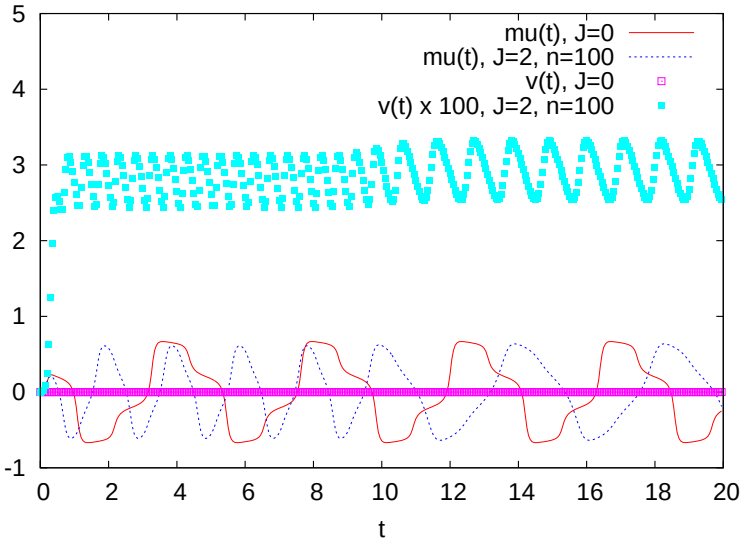

Figure 9.4: Evolution of the mean $\mu_1(t)$ and variance $v_1(t)$ for the mean field of population 1, for $J = 0$ and $J = 2$, over a time window $[0,20]$. n is the number of iterations of F_1 defined in section 9.2. This corresponds to a number of iterations for which the method has essentially converged (up to some precision). Note that $v_1(t)$ has been magnified by a factor of 100. Though Gaussian fluctuations are small, they have a strong influence on $\mu_1(t)$.

standard rate models ideas. Another appealing choice is a smooth approximation to a Dirac delta function thereby opening a window on the world of spiking neurons.

We then derive the mean field equations and provide a constructive and new proof, under some mild assumptions, of the existence and uniqueness of a solution of these equations over finite and infinite time intervals. The key idea is to look at this mean field description as a *global problem* on the probability distribution of the membranes potentials, unlike previous studies. Our proof provides an efficient way of computing this solution and our numerical experiments show a good agreement with previous studies.

In the case where the nonlinearities are chosen to be sigmoidal our results shed a new and fascinating light on existing neural mass models. Indeed these appear as approximations of the mean field equations where the intricate but fundamental coupling between the time variations of the mean membrane potentials and their fluctuations, as represented by the covariance functions, is neglected. This article is just a small step toward answering from the theoretical and numerical standpoints the questions raised by this coupling but we are convinced that a host of interesting results can be found there.

IMPORTANT QUANTITIES

Table 9.1 summarizes some notations which are introduced in the article and used in several places.

Constant	Defined in
μ	lemma 9.2.2 equation (9.24)
$\sigma_{\max}$	lemma 9.2.2
$\sigma_{\min}$	lemma 9.2.2
k_0	lemma 9.2.5
K	proof of lemma 9.2.6
k_C	proposition 9.2.7 equation (9.30)
λ_L	equation (9.33)

Table 9.1: Some important quantities defined in the article.

CHAPTER 10

DYNAMICS OF DETERMINISTIC NONLINEAR NEURAL MASS MODELS

OVERVIEW

Temporal lobe epilepsy is one of the most common chronic neurological disorder characterized by the occurrence of spontaneous recurrent seizures which can be observed at the level of populations through electroencephalogram (EEG) recordings. This chapter summarizes some preliminary works aimed to understand from a theoretical viewpoint the occurrence of this type of seizures and the origin of the oscillatory activity in some classical cortical column models. We relate these rhythmic activities to the structure of the set of periodic orbits in the models, and therefore to their bifurcations. We will be mainly interested Jansen and Rit model, and study the codimension one, two and a codimension three bifurcations of equilibria and cycles of this model. We can therefore understand the effect of the different biological parameters of the system of the apparition of epileptiform activity and observe the emergence of alpha, delta and theta sleep waves in a certain range of parameter. We then present a very quick study of Wendling and Chauvel's model which takes into account $GABA_A$ inhibitory postsynaptic currents.

Contents

10.1 Introduction

Epilepsy is a common chronic neurological disorder affecting 1% of the world population. It is characterized by the occurence of spontaneous recurrent seizures. These seizures are transient signs or symptoms due to abnormal, excessive or synchronous neuronal activity in the brain. It can manifest as an alteration in mental state, tonic or clonic[1] movements, convulsions, and various other psychic symptoms. Different types of seizures are distinguished according to whether the source of the seizure within the brain is localized (*partial* or *focal* onset seizures) or distributed (*generalized* seizures) further divided according to the possible loss of conciousness and to the possible effect on the body.

Since neuron are excitable cells as we have already widely discussed in this manuscript, it makes sense to assume that seizure result from a change in the excitability of single neurons or groups of neurons (see [158]). This is corroborated by electrical recordings at the level of the cell (intracellular or extracellular recordings) and at a mesoscopic level via electroencephalogram (EEG) recordings. Seizures are characterized by single electrical transients called *spikes* at a slow time resolution (hundreds of milliseconds to seconds), macroscopic events which have to be distinguished from spikes of single nerve cells, that last only 1 or 2ms.

The EEG represents a set of potential recorded by multiple electrodes on the surface of the scalp. The electrical signal recorded is a measure of the extracellular current flow from the summated activity of many neurons, distorted by the filtering, attenuated by layers of tissues and bone, representing the activity of neural population of the brain. EEG patterns are characterized by the frequency and the amplitude of electrical activity in the range of $1-30$Hz (sometimes larger) with amplitudes of $20-100\mu$V, and the frequencies observed are divided into four groups: delta (0.5-4 Hz), theta (4-7Hz), alpha (8-13 Hz) and beta (13-30 Hz). As neuronal aggregates become synchronized, the amplitude of the summated current becomes larger.

Computational models developed in the field of epilepsy integrate new and detailed knowledge coming from neurobiological research, and is not only aimed to reproduce experimental findings but also to generate experimentally testable hypotheses. Two main complementary approaches have been developed over the past few decades: the *detailed* approach in which single neurons are accurately modeled (dendrites, soma, axon, passive or active ion channels), and the *macroscopic* or *lumped* modelization taking into featuring a higher level of organization (the neuronal population).

Detailed models are based on the definition of neuronal networks from the interconnection of several thousands of principal neurons and different types of interneurons with appropriate synaptic interactions. The summated postsynaptic potentials of pyramidal cell is interpreted as the field activity can be studied as a function of various parameters (types of neurons, network size, connectivity patterns, conduction delays, ...). This approach has been extensively developed by Traub and collaborators since the early 1980s [264, 265, 266, 267] who studied some spatial and temporal properties of the activity in simulated patch of neuronal tissue. The use of such models has explained some basic mechanisms by which synchronized activity emerges. In particular, these models are able to generate activity patterns, in realistic networks, that closely mimic epileptic activity recorded in vitro as well as different types of EEG activity seen in patients.

[1] rapid muscular contraction and decontraction.

Detailed approach are in general too complex to be mathematically tractable, and mean-field limits as treated in chapter 9 can be useful. The mean-field equation obtained by the techniques given in that chapter provides a phenomenological description of the whole aggregate of neurons, and bridges the gap between the detailed and the macroscopic approach.

The macroscopic approach is built upon the fact that neurons are organized in different populations and that the EEG is a reflection of global activity rising from macroscopic statistical interactions between interconnected neuronal subpopulations (pyramidal cells and interneurons). It conceptually differs from the detailed approach in the sense that it emphasizes the properties of neural populations instead of those of individual cells. Based on these assumptions, population models represent the temporal dynamics of the aggregates while the spatial interactions between cells are neglected. The relevant variable of these models is no more individual spikes but rather the firing-rate.

Seminal works on models of localized neural populations date back to the 1970s with Wilson and Cowan [285] who laid the theoretical theoretical foundations of these modelizations, using the results obtained by Mountcastle [199], and Hubel and Wiesel [136, 137] who brought physiological evidence for the existence of such populations (high redundancy within relatively small volumes of cortical tissue, many cells have nearly identical responses to an identical stimulus, see chapter 1). They considered a population as being composed of two subpopulations, one excitatory and the other one inhibitory and proposed an approach based on two variables, representing the proportion of excitatory and inhibitory cells firing per unit time. They modelled the dynamics of these variables as the solution of a non-linear differential equations governing the population temporal dynamics using a sigmoid function for each subpopulation response. Simple and multiple hysteresis phenomena and limit cycle activities represented in the model were then studied from phase plane analysis and the results provided a physiological basis for oscillatory characteristics observed in particular EEG rhythms. Following the same approach, Freeman and colleagues developed a comprehensive model of the olfactory system from the early 1960s [96, 97, 98]. Based on histological and physiological analytic methods conducted in animal models (cat), their model reproduces the global organization of the olfactory system. Freeman's model key feature is that these subsets represent aggregates of strongly interconnected neurons having similar averaged properties. Each subset is referred to as *neural mass* or *neural population*. The second key feature is that the dynamics of each subset are simply described by a second order non-linear ordinary differential equation (ODE) representing conversion operations between the population average postsynaptic potential and the density of action potentials fired by local neurons. Freeman and colleagues empirically showed that the model produces realistic EEG signals that approximate those experimentally recorded in the same structures [100]. Similar ideas developed at the same time by Lopes da Silva and collaborators [189, 190] led to the development of a lumped-parameter population model able to explain the alpha rhythm of the EEG observed in dogs. The model was based on two interacting populations of neurons representing a subset of excitatory thalamocortical relay cells and a subset of inhibitory interneurons connected to the former subset through a negative feedback loop. In each population, the conversion between the mean membrane potential and the average density of action potentials fired by the population is represented by a non-linear sigmoidal function, whereas conversion from presynaptic density of spikes into mean postsynaptic potential is described by a

linear transfer function. Interaction between the two populations is adjusted by coupling constants representing the average number of synaptic contacts between the two cell types. This model was shown to generate oscillations ranging from 8 to 11 Hz and closely resembling cortical alpha rhythm for physiologically-relevant model parameters.

These studies constitute the first formalizations of neurophysiological observations into computational models, and revealed the close relationships between postsynaptic potentials generated from neuronal populations and oscillatory dynamics reflected in EEG signals. The general concept they introduced make these approach very flexible, and it constitutes the base of many successive studies dealing with regular or pathological neural mass and EEG activity models. Recently, a spatially extended version of these models was studied to model bumps and waves in spatially extended non-pathological neural fields, which provides a model for voltage-sensitive dyes optical imaging [85, 87, 115].

In the field of epilepsy, we refer to Zetterberg and colleagues [288] who concluded that epileptic spikes are generated by populations of neurons close to instability. Lopes da Silva and colleagues used a thalamocortical model to understand the mechanisms of transition from regular EEG activity and epileptiform paroxysmal activity[248, 249].

Among these models, a sort of minimal model for EEG signal was introduced by Jansen and Rit in the mid 1990s [149, 150], which was extended by Wendling and collaborators [280, 281, 283] in the context of model-based interpretation of intracerebral EEG signals in epilepsy. These models will be studied in detailed in this chapter, in order to understand the different rhythms observed and the origin of epileptiform activity.

10.2 Neural mass models

Jansen's neural mass model was first introduced by Lopes Da Silva and colleagues in 1974, and studied further by Van Rotterdam *et al.* in 1982 [189, 190, 275]. These authors developed a biologically inspired mathematical framework to simulate spontaneous electrical activities of neuronal assemblies measured for instance by EEG, with a particular interest for alpha activity. In their model, three neuronal populations interact with both excitatory and inhibitory connections. Jansen *et al.* [149, 150] discovered that besides alpha activity, this model was also able to simulate evoked potentials, i.e. EEG-like activity observed after a sensory stimulation. More recently, Wendling and colleagues used this model to synthesize activities very similar to those observed in epileptic patients [281], and David and Friston studied connectivity between cortical areas with a similar framework [64, 65]. Nevertheless, one of the main issue of Jansen's model is that it is not able to produce all the rhythms in play in epileptic activity or observed in EEG recordings. This limitation of the model lead Wendling, Chauvel and their colleagues [282, 283] to develop an extended Jansen model to better reproduce EEG signals. This model is based on neurological studies [151] revealing that gamma-frequency oscillations were linked with the inhibitory interneurons in the hippocampal networks, and that two types of $GABA_A$ inhibitory postsynaptic currents may play a crucial role in the formation of the nested theta/gamma rhythms in the hippocampal pyramidal cells. For these reasons, we will also study the 5-populations extended Wendling and Chauvel's model.

10.2.1 Jansen and Rit's model

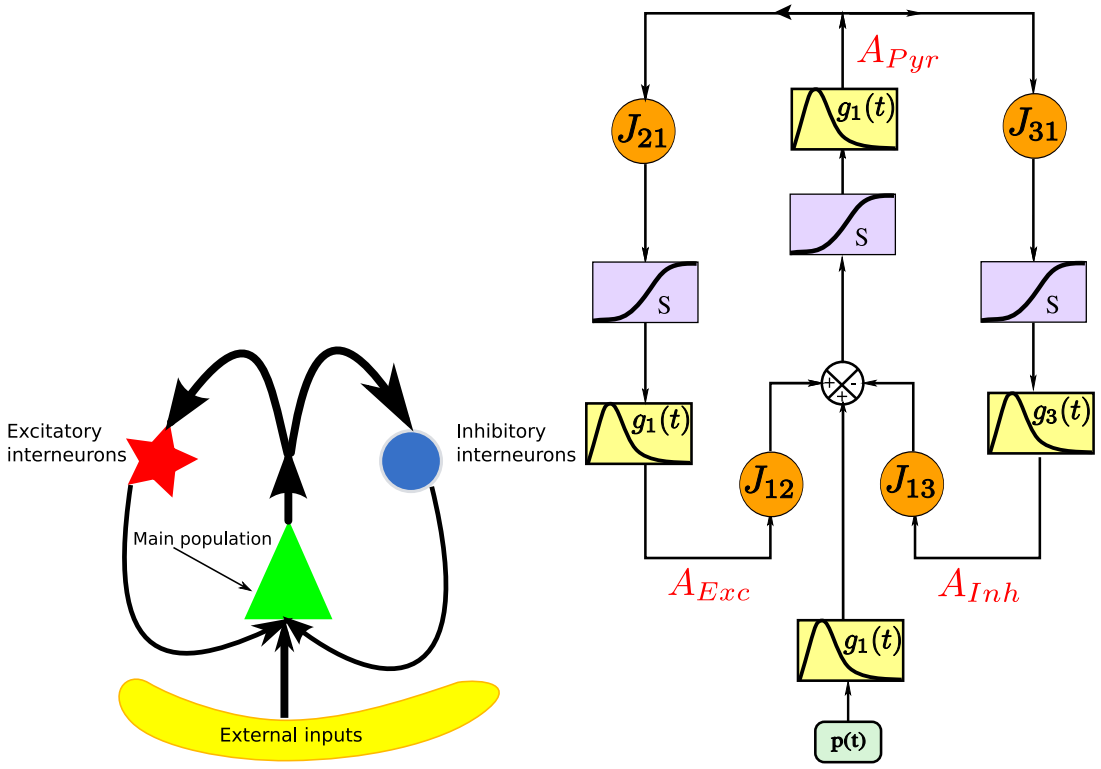

(a) Populations involved in Jansen's model

(b) Block diagram

Figure 10.1: (10.1(a))Neural mass model of a cortical unit: a pyramidal cells population interacts with an excitatory and an inhibitory population of interneurons. (10.1(b)) Block representation of a unit. h boxes are synaptic transformations, S boxes simulate cell bodies of neurons and is the sigmoidal transform of the membrane potential into an output firing rate. The constants J_i account for the strength of the synaptic connections between populations.

Description of the model The initial Jansen and Rit's model features a population of pyramidal neurons (central part of figure 10.1(a)) that receive excitatory and inhibitory feedback from local inter-neurons and an excitatory input from neighboring cortical units and sub-cortical structures like the thalamus. Actually the excitatory feedback must be considered as coming from both local pyramidal neurons and genuine excitatory interneurons like spiny stellate cells.

Figure 10.1(b) is a block diagram representation of figure 10.1(a) representing the mathematical operations performed inside such a cortical unit. The excitatory input is represented by an arbitrary average firing rate $p(t)$ which can be random (accounting for a non specific background activity) or deterministic, accounting for some specific activity in other cortical units.

The postsynaptic system The functions $h_e(t)$ and $h_i(t)$ of figure 10.1(b) are the average EPSP and IPSP. They convert the average input firing rate into an average excitatory or inhibitory post-synaptic potential. Following the works of van Rotter-

dam et al [275] these transfer function are of type:

$$h(t) = \begin{cases} \alpha\beta t e^{-\beta t} & t \geq 0 \\ 0 & t < 0 \end{cases}.$$

In other words, if $x(t)$ is the input to the system, its output $y(t)$ is the convolution product $h \star x(t)$. The parameters α determines the maximal amplitude of the post-synaptic potentials and β corresponds to the characteristic time of integration, which is mainly linked with the kinetics of synaptic transmission and with the averaged distributed delays in the dendritic tree.

These transfer functions are solutions of the second-order differential equation:

$$\ddot{y}(t) = \alpha\beta x(t) - 2\beta\dot{y}(t) - \beta^2 y(t),$$

which can be conveniently rewritten as a system of two first-order equations

$$\begin{cases} \dot{y}(t) & = z(t) \\ \dot{z}(t) & = \alpha\beta x(t) - 2\alpha z(t) - \alpha^2 y(t) \end{cases}$$

These two constants are different for the excitatory and inhibitory populations to fit the experimentally recorded EPSP and IPSP functions. The parameters α and β have been adjusted by van Rotterdam [275] to reproduce some basic properties of real post-synaptic potentials. Following their works, parameters can be set as follows:

$$\begin{cases} \text{Excitatory population} & \alpha =: A = 3.25\,mV & \beta =: a = 100\,s^{-1} \\ \text{Inhibitory population} & \alpha =: B = 22\,mV & \beta =: b = 50\,s^{-1} \end{cases}$$

Firing rates The activity of the population is considered to be the related mean firing rate. This mean firing rate is modelled as a sigmoidal transformation of the average membrane potential (see, e.g. [105]). The function Sigm we chose in this model approximates the functions proposed by Freeman [99], and has the form:

$$\text{Sigm}(v) = \frac{v_{max}}{2}(1 + \tanh\frac{r}{2}(v - v_0)) = \frac{v_{max}}{1 + e^{r(v_0 - v)}},$$

where v_{max} is the maximum firing rate of the families of neurons, v_0 is the value of the potential for which a 50% firing rate is achieved and r is the slope of the sigmoid at v_0.

The excitability of cortical neurons can vary as a function of the action of several substances and v_0 could potentially take different values. In our model, we nevertheless consider a fixed value $v_0 = 6mV$ as suggested by Jansen on the basis of experimental studies due to Freeman [100]. The works of the latter also suggest that $v_{max} = 5s^{-1}$ and $r = 0.56mV^{-1}$, the values used by Jansen and Rit.

Interconnections The three neural populations defined interact through excitatory and inhibitory synapses. The number of synapses established between two neuronal populations i and j is denoted by J_i for $i = 1 \ldots 4$ as in diagram 10.1(b). They are considered to be constant and proportional to the average number of synapses between populations, and we denote by α_i the related coefficient (i.e. $J_i = \alpha_i J$). On the basis of several neuroanatomical studies (see for instance [28]) these quantities have been estimated by counting synapses, and their numerical values is given in table 10.1.

Parameter	Interpretation	Value
A	Average excitatory synaptic gain	$3.25mV$
B	Average inhibitory synaptic gain	$22mV$
$1/a$	Time constant of excitatory PSP	$10ms$
$1/b$	Time constant of inhibitory PSP	$20ms$
α_1, α_2	Average number of synaptic contacts in the feedback excitatory loop	$\alpha_1 = 1$, $\alpha_2 = 0.8$
α_3, α_4	Average number of synaptic contacts in the slow feedback inhibitory loop	$\alpha_3 = \alpha_4 = 0.25$
v_0, v_{max}, r	Parameters of the Sigmoid S	$v_0 = 6mV$, $v_{max} = 5s^{-1}$ $r = 0.56mV^{-1}$

Table 10.1: Numerical values used in Jansen's original model

Note that we consider here constant synaptic weights. The variability in the connectivity weights can be taken into account as we do in chapter 9, and the resulting equation is way more complex than the equation we deal with in the present chapter.

Equations of the model As proved in section 9.1.4, this model is an activity based model. Following Jansen and Rit's initial work, we consider the three variables y_0, y_1 and y_2 of figure 10.1(b). To write the system into a set of first-order ordinary differential equation we introduce the derivatives of these variables, $\dot{y}_0, \dot{y}_1, \dot{y}_2$, noted y_3, y_4 and y_5, respectively. We therefore obtain a system of 6 first-order differential equations that describes Jansen's neural mass model:

$$\begin{cases} \dot{y_0}(t) = y_3(t) & \dot{y_3}(t) = Aa\text{Sigm}[y_1(t) - y_2(t)] - 2ay_3(t) - a^2 y_0(t) \\ \dot{y_1}(t) = y_4(t) & \dot{y_4}(t) = Aa\{p(t) + J_2\text{Sigm}[J_1 y_0(t)]\} - 2ay_4(t) - a^2 y_1(t) \\ \dot{y_2}(t) = y_5(t) & \dot{y_5}(t) = BbJ_4\text{Sigm}[J_3 y_0(t)] - 2by_5(t) - b^2 y_2(t). \end{cases} \tag{10.1}$$

Our study will focus on the variable $y = y_1 - y_2$ which models the membrane potential of the pyramidal cells since their electrical activity corresponds to the EEG signal: pyramidal neurons throw their apical dendrites to the superficial layers of the cortex where the post-synaptic potentials are summed, and therefore account for the essential part of the EEG activity [158]. Table 10.1 summarizes the different numerical values of the original Jansen and Rit's model.

Dimensionless reduction of Jansen's model We now change variables in order to reduce the number of parameters in the system. First of all, we chose the time scale of the excitatory population as our new unit time and define $\tau = at$. Therefore the new characteristic scale of the inhibitory variable will be given by the ratio $d = \frac{b}{a}$, G the ratio of postsynaptic amplitudes B/A. The dimensionless sigmoidal transform we define is

$$S(x) = \frac{1}{1 + k_0 e^{-x}}$$

where $k_0 = e^{rv_0}$. We eventually introduce the dimensionless scaled input parameter $P = (rA)\frac{p}{a}$ and and the dimensionless scaled connectivity strength $j = (rA)\frac{v_{max}}{a} J$. The

new state variables $(Y_0, X, Y_1, Y_2, Y_3, Y_4, Y_5)$ defined by

$$\begin{aligned} Y_0(\tau) &= Jry_0(\tau/a) \\ Y_i(\tau) &= ry_i(\tau/a) \quad i = 1, 2 \\ X &= Y_1 - Y_2. \end{aligned}$$

satisfy the equations

$$\begin{cases} \dot{Y_0} &= Y_3 \\ \dot{X} &= Y_4 - Y_5 \\ \dot{Y_2} &= Y_5 \\ \dot{Y_3} &= jS(X) - 2Y_3 - Y_0 \\ \dot{Y_4} &= P + \alpha_2\, jS(\alpha_1 Y_0) - 2Y_4 - (Y_2 + X) \\ \dot{Y_5} &= d\,\alpha_4\, G\, jS(\alpha_3 Y_0) - 2d\,Y_5 - d^2 Y_2 \end{cases} \tag{10.2}$$

They depend upon the nine dimensionless parameters α_i, $i = 1, \cdots, 4$, k_0, d, G, j, and P as opposed to the 11 parameters of the original model (see table 10.1). The numerical values these parameters corresponding to table 10.1 are given by:

$$\begin{cases} G &= \frac{B}{A} = 6.7692 & & \\ d &= \frac{b}{a} = 0.5 & & \\ \alpha_1 &= 1 & \alpha_2 &= 0.8 \\ \alpha_3 &= 0.25 & \alpha_4 &= 0.25 \\ \log(k_0) &= rv_0 = 3.36 & & \\ j &= (rA)\,\frac{v_{max}}{a}\,J = 12.285 & & \end{cases}$$

10.2.2 Wendling and Chauvel's extended model

One of the main drawbacks of Jansen's model is that it is unable to generate certain types of cortical activity, for instance seen in epileptic activity. As an example, it cannot reproduce the type of fast activity observed at the onset of seizures in limbic structures. In order to propose a better cortical mass model, Wendling, Chauvel and colleagues [282, 283] revisited the organization of subsets of neurons and interneurons, focusing on the hippocampus activity. Based on these considerations, they proposed a new neural mass model whose parameters were estimated using real EEG signals. Their model is shown as a block diagram in figure Fig. 10.2. The main difference with Jansen's initial model is the addition of somatic-projecting inhibitory neurons ($\text{GABA}_{\text{A,fast}}$ receptors).

In this block diagram representation, the PSP functions are given by:

$$\begin{cases} h_e(t) &= Aate^{-at} \\ h_i(t) &= Bbte^{-bt} \\ h_f(t) &= Ccte^{-ct} \end{cases}$$

The equations of the extended model hence read:

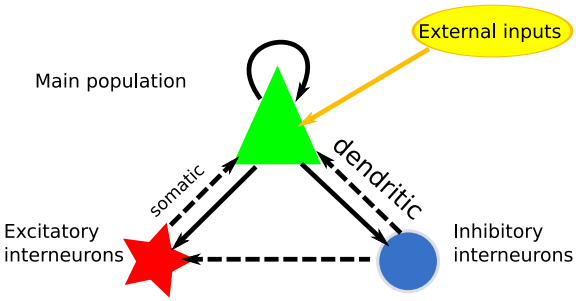

(a) Populations and connectivities

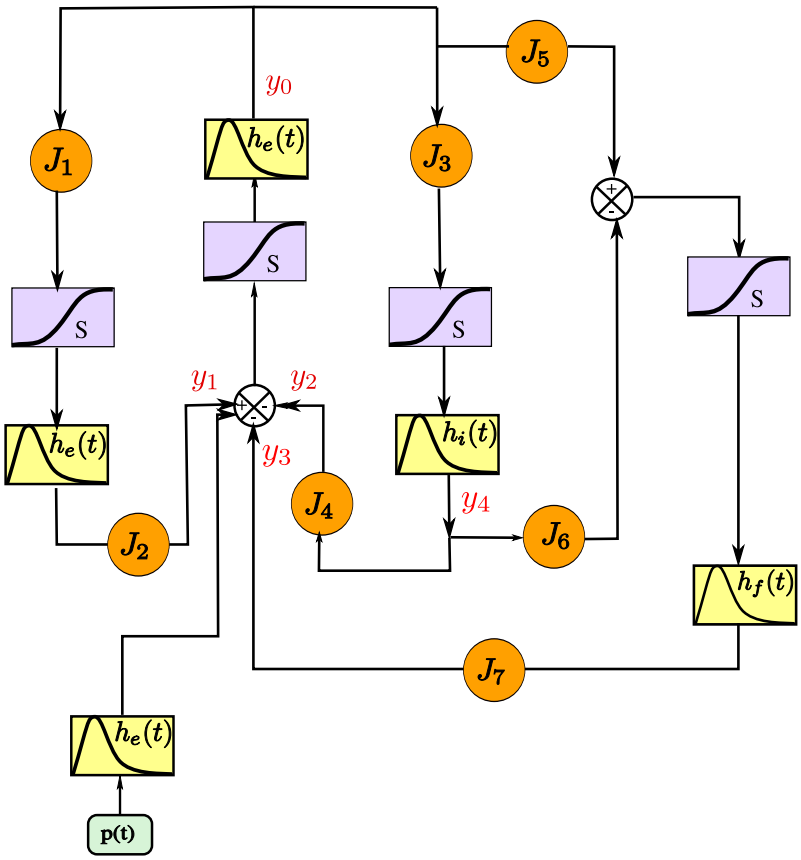

(b) Block diagram

Figure 10.2: Neuronal population model based on the cellular organization of the hippocampus. 10.2(a): Schematic representation of the model. The pyramidal cells population projects to and receives feedback excitatory and inhibitory interneurons, and has a recurrent excitation. 10.2(b) : Related block diagram.

Parameter	Interpretation	Value
A	Average excitatory synaptic gain	$3.25mV$
B	Average inhibitory synaptic gain, slow dendritic inhibition loop	$22mV$
C	Average inhibitory synaptic gain, fast somatic inhibition loop	$20mV$
$\frac{1}{a}$	Time constant of average excitatory postsynaptic potentials	$10ms$
$\frac{1}{b}$	Time constant of average inhibitory postsynaptic potentials	$35ms$
$\frac{1}{c}$	Time constant of the filter time delay	$5ms$
α_5, α_6	probability of synaptic contacts in the fast feedback inhibitory loop	0.1
α_7	connection probability between slow and fast inhibitory neuron	0.8

Table 10.2: Parameters interpretations and values of the extended model proposed by Wendling and Chauvel (see [282]). The parameters $\alpha_1,\ldots,\alpha_4$, J, v_0, r and v_{max} have the same interpretations and values as in Jansen's original model, see table 10.1

$$\begin{cases} \dot{y_0} &= y_5 \\ \dot{y_5} &= AaS(y_1-y_2-y_3)-2ay_5-a^2y_0 \\ \dot{y_1} &= y_6 \\ \dot{y_6} &= Aa\{p(t)+J_2S(J_1y_0)\}-2ay_6-a^2y_1 \\ \dot{y_2} &= y_7 \\ \dot{y_7} &= BbJ_4S(J_3y_0)-2by_7-b^2y_2 \\ \dot{y_3} &= y_8 \\ \dot{y_8} &= CcJ_7S(J_5y_0-J_6y_4)-2cy_8-c^2y_3 \\ \dot{y_4} &= y_9 \\ \dot{y_9} &= BbS(J_3y_0)-2by_9-b^2y_4 \end{cases} \tag{10.3}$$

Numerical values of the parameters This model has been fitted using SEEG data, and the authors obtained the values given in the table 10.2.

Reduced Wendling-Chauvel's model First of all, one of the most straightforward reduction of the model consists in removing the variables y_4 and y_9 since they are deduced of y_2 and y_7 by the simple formulas: $y_2 = J_4y_4$ and $y_7 = J_4y_9$. To reduce further the model we proceed in the same way as in Jansen and Rit's case. We make the system dimensionless by introducing the new time $\tau = at$ and proceeding to the change of variables:

$$\begin{cases} Y_i(\tau) = Jry_i(\tau/a) & i\in\{0,4\} \\ Y_i(\tau) = ry_i(\tau/a) & i\in\{1,2,3\} \\ Y_i(\tau) = \frac{Jr}{a}y_i(\tau/a) & i\in\{5,9\} \\ Y_i(\tau) = \frac{r}{a}y_i(\tau/a) & i\in\{6,7,8\} \end{cases}$$

We denote by X the interesting signal related to the EEG signal: $X = Y_1 - Y_2 - Y_3$ feeding the pyramidal population and by $Z = \alpha_5Y_0 - \alpha_6Y_4 = \alpha_5Y_0 - \alpha_6/\alpha_4Y_2$ the action of the dendritic inhibitory interneuron population on the somatic inhibitory interneuron population. We consider now the variables $(Y_0, X, Z, Y_3, Y_5, Y_6, Y_7, Y_8)$.

These new variables satisfies the following set of differential equations, where we denote for the sake of compactness of notations by a dot the derivative with respect to τ:

$$\begin{cases} \dot{Y_0} &= Y_5 \\ \dot{X} &= Y_6 - Y_7 - Y_8 \\ \dot{Z} &= \alpha_5 Y_5 - \frac{\alpha_6}{\alpha_4} Y_7 \\ \dot{Y_3} &= Y_8 \\ \dot{Y_5} &= jS(X) - 2Y_5 - Y_0 \\ \dot{Y_6} &= j\alpha_2 S(\alpha_1 Y_0) - 2Y_6 - (X + Y_2 + Y_3) + P(t) \\ \dot{Y_7} &= jd_1 G_1 \alpha_4 S(\alpha_3 Y_0) - 2d_1 Y_7 - d_1^2 \frac{\alpha_4}{\alpha_6}(\alpha_5 Y_0 - Z) \\ \dot{Y_8} &= jd_2 G_2 \alpha_7 S(Z) - 2d_2 Y_8 - d_2^2 Y_3 \end{cases} \tag{10.4}$$

where j, P and $S(x)$ are the same as the one introduced for Jansen and Rit's model. We used the notations:

$$\begin{cases} G_1 = \frac{B}{A} & G_2 = \frac{C}{A} \\ d_1 = \frac{b}{a} & d_2 = \frac{c}{a} \end{cases} \tag{10.5}$$

Using the numerical values in table 10.2 we obtain

$$\begin{cases} G_1 = 6.76923 & G_2 = 6.15385 \\ d_1 = 0.2857 & d_2 = 2 \end{cases}$$

In this chapter we are interested in the influence of the other parameters of the model together with the input on the fixed points. More precisely, we are interested in the codimension two bifurcations of this model with respect to 3 pairs of parameters:

(i). The input P and the coupling strength j.

(ii). The input P and the delays ratio d.

(iii). The input P and the PSP amplitude ratio G.

For this preliminary study we present an in depth study of the influence of the coupling strength in Jansen's model. For the effects of the other parameters and the study of Wendling's model, we will only provide the bifurcation diagrams. The study of the computational behavior is the subject of future studies.

10.3 Influence of the total connectivity parameter in Jansen and Rit's model

We first study the dynamical properties of Jansen and Rit's model. We recall in the first subsection the main features described by Grimbert and Faugeras in [114], and extend their study to codimension two and three bifurcations.

10.3.1 Fixed points and stability

An interesting property of the system (10.2) is that the equilibria can be parametrized as a function of the state variable $X = Y_1 - Y_2$:

$$
\begin{aligned}
Y_0 &= jS(X) \\
Y_2 &= \alpha_4 \frac{G}{d}\, jS(\alpha_3 jS(X)) \\
P &= X + jS(X) - \alpha_2 jS(\alpha_1 jS(X))
\end{aligned}
$$

The Jacobian matrix at the fixed point is also parametrized by X and reads:

$$
J(X) = \begin{pmatrix}
0 & 0 & 0 & 1 & 0 & 0 \\
0 & 0 & 0 & 0 & 1 & -1 \\
0 & 0 & 0 & 0 & 0 & 1 \\
-1 & jS'(X) & 0 & -2 & 0 & 0 \\
\alpha_1\alpha_2 jS'(j\alpha_1 S(X)) & -1 & -1 & 0 & -2 & 0 \\
\alpha_3\alpha_4 jdS'(j\alpha_3 S(X)) & 0 & -d^2 & 0 & 0 & -2d
\end{pmatrix}
$$

Although all the dynamics can be parametrized with the variable X, because of the complexity of the sigmoidal function, the analytical bifurcation study is untractable, and one has to make use of a numerical software in order to solve the problem[2].

In the present case, almost all the calculations can be performed analytically in function of the variable X. For this reason, for computing accurately the bifurcations of equilibria, we developed our own software implemented using Maple® in order to identify our codimension two bifurcations. For simple models, the programs we developed give closed-form expressions for the bifurcations points. For the continuation of periodic orbits, the analytical study is no more possible, and we used both the Matlab® toolbox MatCont [72] and XPPAut continuation softwares to study the global bifurcations. The algorithms we use and the results we obtain are presented in appendix B.

10.3.2 Codimension 1 bifurcations

The dependency of the dynamics to the input firing rate has already been studied Grimbert and Faugeras in [114] when parameters are set as in table 10.1. They describe a very rich bifurcation diagram, with the coexistence of two limit cycle, one coming from a Hopf bifurcation, and the other collapsing on the fixed points manifold, as we show in figure 10.3.

The system features two saddle-node and three Hopf bifurcations. One of the Hopf bifurcations is subcritical, the other two supercritical. The branch of unstable limit cycles originating from this point undergoes a fold bifurcation and connects to a family of stable limit cycles of large amplitude that eventually collide with a saddle-node bifurcation point and disappear via saddle-node homoclinic bifurcation. The periods of these cycles correspond to frequencies in the dimensioned model ranging from 0 to 5Hz which is consistent with the frequencies of recorded epileptic spikes. It corresponds to what was interpreted as epileptic oscillatory activity.

The other two Hopf bifurcation share the same family of periodic orbits. The period of these cycles is almost constant, ranging from 9 to 9.6 in the dimensionless model, which corresponds in the original model to frequencies in the alpha band.

The system undergoes a saddle-node homoclinic bifurcation (SNIC) at the saddle-node bifurcation point, corresponding to a transition between a periodic orbit and an heteroclinic orbit (see figure 10.4), and after this bifurcation, the system presents a

[2]Grimbert and Faugeras used the XPPAut software [79]

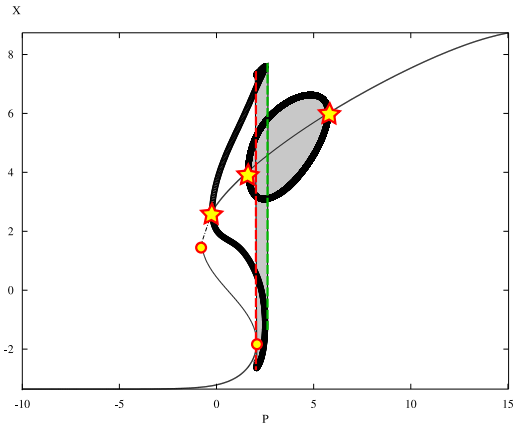

(a) Codimension 1 bifurcations

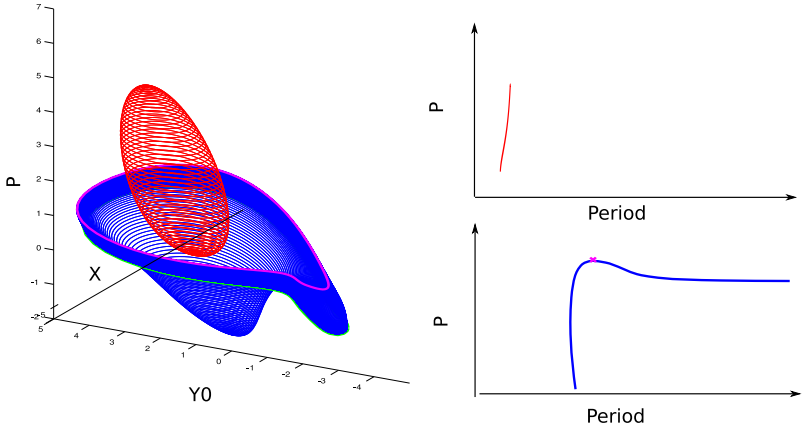

(b) Cycles

Figure 10.3: (a): Bifurcations in the reduced Jansen's model with respect to the input firing rate parameter P. Circles represent the two saddle-node bifurcations and the stars the three Hopfs bifurcations. The bold lines and the grayed zones represent the extension of the limit cycles, the red dashed line a saddle homoclinic bifurcation and the green dashed line a fold of limit cycle bifurcation (figure generated using XPPAut). (b): (Left) Limit cycles and related period. The eggcup-like family of limit cycles in blue are originated from the subcritical Hopf bifurcation. Cycles are unstable from the Hopf bifurcation until the fold of limit cycle (purple cycle) (cup of the eggcup) and stable on the handle of the eggcup. Red cycles (the egg) are stable and correspond to the supercritical Hopf bifurcations.

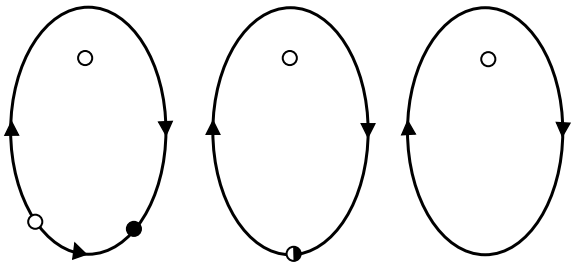

Figure 10.4: Projection of a SNIC bifurcation in a subplane of the phase space. Three invariant circles are represented: Left. An heteroclinic orbit. Center. The two fixed points belonging to the invariant circle merge into a saddle-node fixed point. The resulting homoclinic orbit has an infinite period. Right. The invariant circle turns into a periodic orbit as the fixed points disappear.

family of heteroclinic orbits, which are not linked with oscillations, since the cycle contains a stable fixed point.

It had been suggested by Grimbert and Faugeras [114] that this picture was quite sensitive to changes in the parameters. They observed that varying any parameter by more than 5% resulted in drastic changes in the bifurcation diagram and the behaviors. This is why we were interested in understanding better the appearance of these features and its sensitivity in function of different parameters.

In this section, we will be particularly interested in the influence of the coupling strength j.

10.3.3 Effect of the coupling strength and of the input current

Let us first study the bifurcations of the system with respect to the pair of parameters (j,P). We first study the bifurcations of equilibria of the system, before studying global bifurcations of cycles and the resulting rhythms generated.

We numerically observe that the system undergoes the following bifurcations of equilibria (See appendix B and figure 10.5):

(i). A saddle-node bifurcation manifold,

(ii). An Andronov-Hopf bifurcation manifold,

(iii). A Cusp bifurcation C,

(iv). A Bogdanov-Takens bifurcation BT,

(v). A Bautin bifurcation GH.

The periodic orbits are also explored using a continuation algorithm. We are especially interested in stable cycles which correspond to observable activity in the presence of noise. We chose MatCont continuation package developed by Kuznetsov, Govaerts and colleagues [71, 72] and which is very efficient for identifying bifurcations of periodic orbits.

First of all, at the Bogdanov-Takens bifurcation point, a curve of saddle-homoclinic bifurcations is generated. This curve can be locally computed using the normal form of the system at this point, and continued using a continuation algorithm. Along this

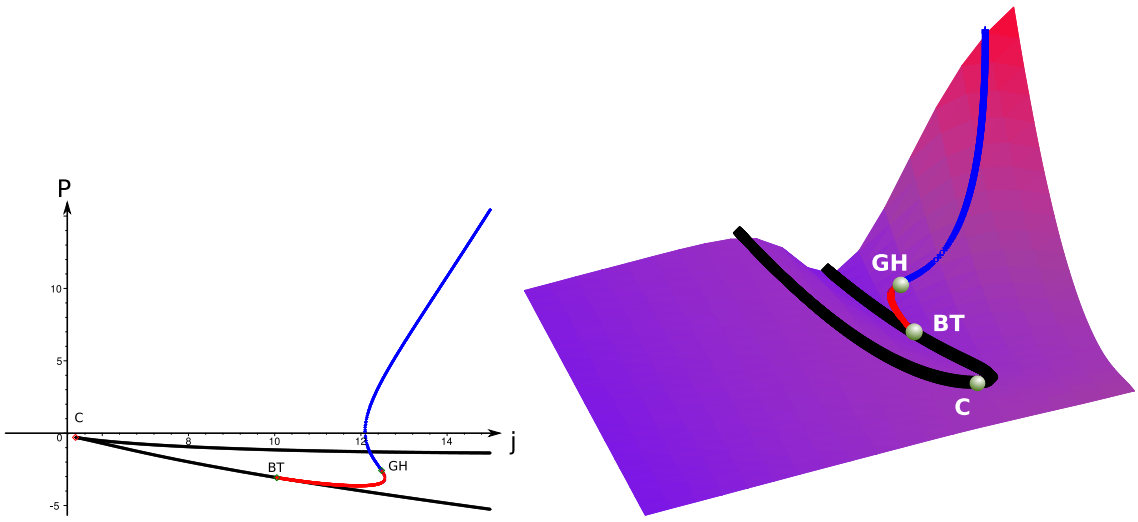

(a) Bifurcations of equilibria (b) Bifurcations of equilibria in 3D

Figure 10.5: Full bifurcation diagram represented on the fixed points manifold (see text for the description)

curve, a branch of limit cycles collapse with the saddle fixed points manifold, and the period of the related cycles tends to infinity when approaching this curve. When numerically continuing this curve we observe that that at the value of parameter j related to the Bautin bifurcation, this saddle-homoclinic bifurcation curve collapses with the saddle-node bifurcation manifold and the saddle homoclinic loop becomes a saddle-node homoclinic loop, and connects to a saddle-node limit cycle at a point we denote S.

From the Bautin bifurcation point, a family of stable limit cycles and a family of unstable limit cycles collapse and disappear along a nondegenerate fold bifurcation of cycles (FIC) (see figure 10.6). From the Bautin bifurcation, the manifold of FIC is continued and we numerically observe that cycles undergo a cusp bifurcation (See figure 10.7). The upper branch of limit cycles corresponds to the branch of folds of limit cycles generated at the Bautin bifurcation the cycles shrink to a single point GH. The lower branch connects to the homoclinic saddle-node manifold. At this point, the cycle corresponding to the FIC bifurcation is a saddle-node homoclinic cycle (point S). Note that the curve of folds of limit cycles originating from the Bautin point can be seen as a function of $j(P)$ which is first decreasing then increasing. The point where it changes monotony is named E.

The full bifurcation diagram is provided in figure 10.8. The analysis of the bifurcation diagram leads to classify the system into 8 classes depending on the coupling strength. In each class the system has the same dynamical features and the same qualitative behaviors.

Neuro-Computational features

The different classes of parameters respresented in color in figure 10.8 correspond to different responses to varying inputs. Eight classes can be distinguishes. We observe that the original Jansen's model is in zone labelled (D) which is of very small

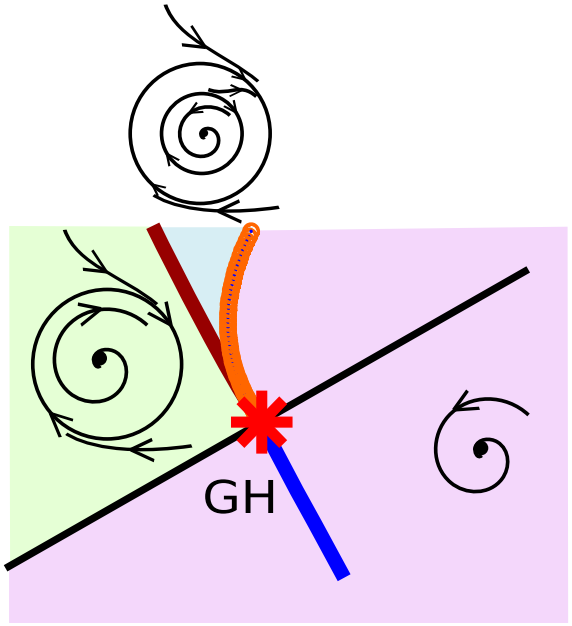

Figure 10.6: Bautin bifurcation: in region 1 the system has a single stable equilibrium an no cycle. Crossing the Hopf bifurcation boundary H_- to region 2 implies the appearance of a stable limit cycle which survives when we enter region 3. Crossing the Hopf boundary H_+ creates an extra unstable limit cycle inside the first one, while the equilibrium regains its stability. Two cycles of opposite stability exist in region 3 and collapse at the curve T through a fold bifurcation that leaves a single equilibrium. The curves are computed in the case of Jansen's model.

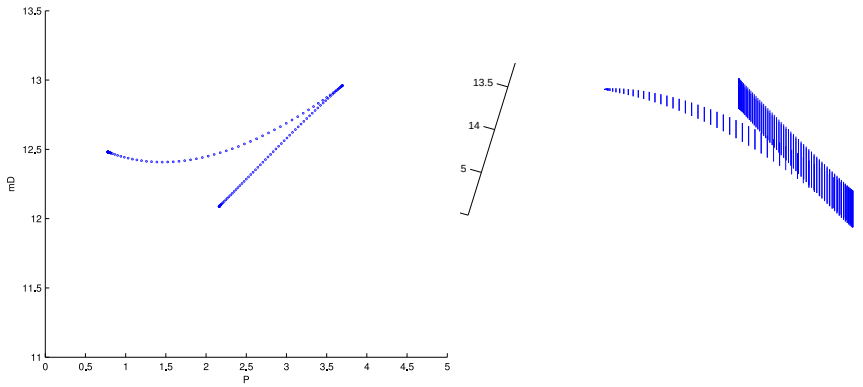

(a) Fold of limit cycles in (j,P) (b) Fold of limit cycles in (j,P,Y)

Figure 10.7: Fold of limit cycles in the plane j and P. We can see that a cusp of limit cycle exist, hence two folds of limit cycles exist for a given j, and these two branches collapse.

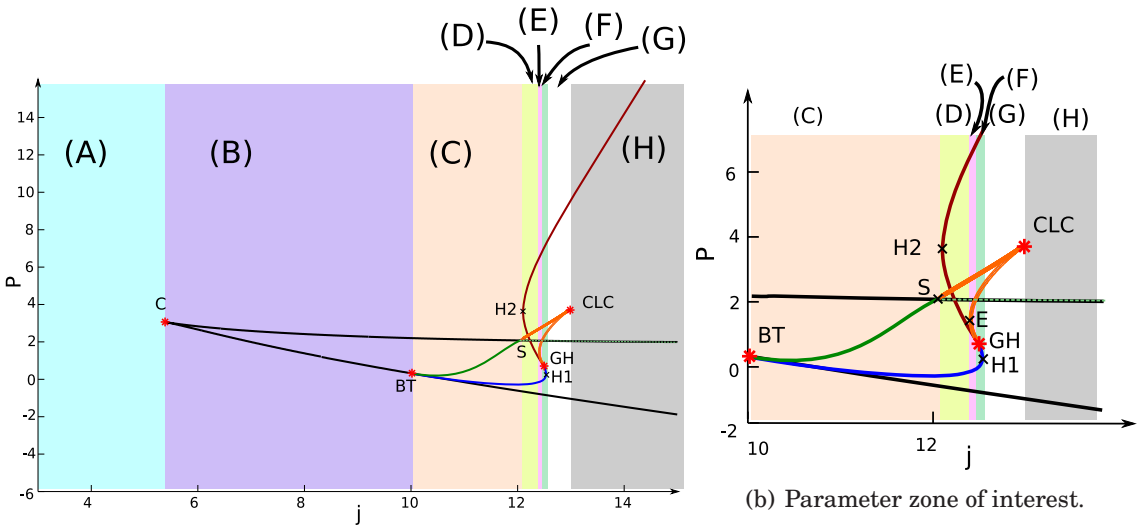

(a) Full Diagram

(b) Parameter zone of interest.

Figure 10.8: Full bifurcation diagram of Jansen's model in function of the parameters P and j. The behaviors can be classified in height zones $(A)\dots(H)$ described in the text. The black curve corresponds to the saddle-node bifurcations manifold, the point C the cusp bifurcation point, the blue curve corresponds to the subcritical Hopf bifurcations. It is connected to the saddle-node manifold via subcritical Boganov-Takens bifurcation t the point BT. At this point, the saddle-homoclinic bifurcations curve is plotted in green. It exists while j is inferior to the value related to the Bautin bifurcation. At this point, the saddle-homoclinic bifurcation connects to the saddle-node manifold and generates a curve of saddle-node homoclinic bifurcations (dashed green line). The subcritical Hopf bifurcation manifold is connected to the supercritical Hopf bifurcation manifold (red curve) through a Bautin bifurcation (point GH). From this bifurcation point there is a manifold of folds of limit cycles represented in orange. Cycles undergoes a cusp bifurcation at the CLC point and a saddle-node homoclinic bifurcation at the point S.

Point	j	P
C	5.38	-0.29
BT	10.05	-3.07
H2	12.10	0.10
E	12.38	1.21
GH	12.48	-2.58
H1	12.55	-3.10
CLC	12.93	3.75

Table 10.3: Numerical parameters of the different special points of the system

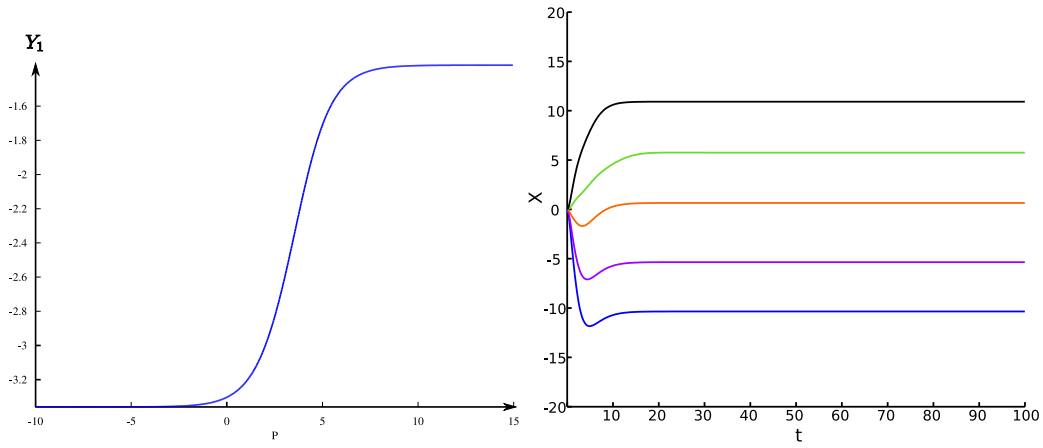

(a) Equilibria (b) Behaviors

Figure 10.9: Case (A): $j = 4$. (a) equilibria (coordinate Y_1 as a function of the input current P). For each value of P there exists a unique stable equilibrium. (b) behavior of the system. Coordinate X, for different values of P: the system always converge to the unique equilibrium.

extension.

Non-oscillating behaviors For $j < j_{H2}$, the system does not present any stable oscillation (zones (A), (B) and (C)), and therefore the cortical column will not present oscillations.

A. For $j < j_C$, the system has a unique fixed point and no cycle for any input firing rate P. Therefore, when the current is fixes, for any initial condition, the activity of the column will converge towards this unique equilibrium. In that case the cortical column has a quite trivial behavior: it has no oscillatory activity and converges to rest whatever the input.

B. For $j_C < j < j_{BT}$, the system undergoes two saddle-node bifurcations when varying the parameter P. Depending P, the system has one, two or three fixed points and no cycle (see figure 10.10). For $P \notin [P_1, P_2]$ (i.e. not between the values of the the two saddle-node bifurcations), there is a unique fixed point which is stable and the system converges to this fixed point. When $P \in (P_1, P_2)$, there are three fixed point, one is unstable and the other two stable. The system is therefore bistable: depending on the initial condition, the activity will converge towards one or the other stable fixed point, corresponding to an up-state and down-state activity. The system also presents hysteresis when continuously varying the input in this zone of inputs. Eventually, it can switch between the two stable fixed point if perturbed.

C. For $j_{BT} < j < j_{H1}$: The system has two saddle-node bifurcations and a subcritical Hopf bifurcation (see figure 10.11). Therefore, the system has a unique stable fixed point when the input P is not between the two saddle-node bifurcation points (i.e. $P \notin [P_1, P_2]$), and the system converges towards this fixed point. For P between the first saddle-node bifurcation value and the Hopf bifurcation (i.e.

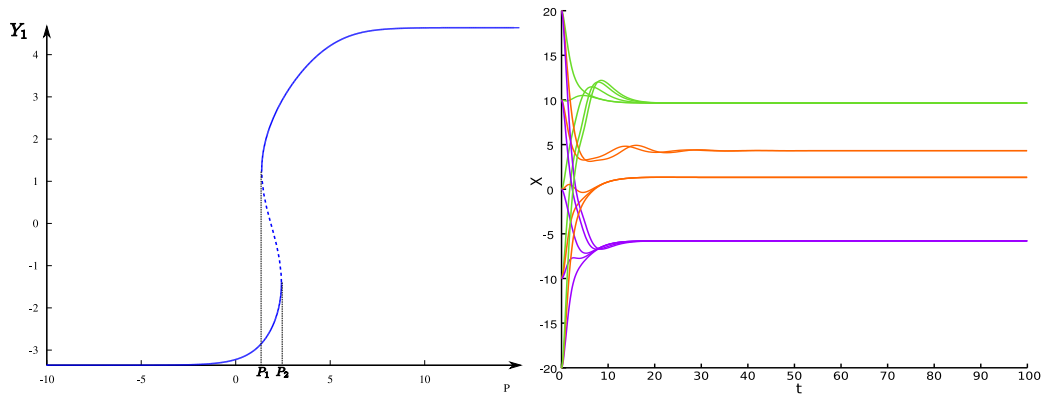

(a) Equilibria (b) Behaviors

Figure 10.10: Case (B): $j = 8$. (a) equilibria (coordinate Y_1 as a function of the input current P), and stability. Plain line: stable equilibrium, dashed line: unstable. For $P \notin [P_1, P_2]$ there exists a unique stable equilibrium, and for $P \in (P_1, P_2)$ there exist three equilibria, two stable and one unstable. (b): Behavior of the system for different input and initial conditions. Purple: $P = -10$ and green: $P = 10$: the system always converge to the unique equilibrium. Orange: $P = 2$: bistability. We observe that the activity resemble real evoked potential.

$P \in (P_1, P_H)$), the system has 2 unstable fixed points and a stable fixed point, and generically converges towards the stable fixed point. In the zone between the Hopf bifurcation and saddle homoclinic point ($P \in (P_H, P_{Sh})$) , the system presents two stable fixed points, an unstable fixed point and an unstable limit cycle. Depending on the initial condition, the system will either converge to one or the other fixed point. When P is greater the saddle-homoclinic bifurcation value and below the greatest saddle-node value ($P \in (P_{Sh}, P_2)$), the system has two stable fixed points and an unstable fixed point, and its behavior is similar to the behavior in the previous case. We can see that the system returns to equilibrium via oscillations. Hence in the presence of noise, the system will present oscillations at a certain frequency superimposed to its noisy behavior.

Rhythmic activity For values of the connectivity greater than j_{H_2}, the system will always present a supercritical Hopf bifurcation and therefore a stable periodic orbit, corresponding to a rhythmic activity of the column.

D. For $j \in [j_{H_2}, j_E]$, the system undergoes two saddle-node bifurcations, two supercritical and a subcritical Hopf bifurcations, and one fold of limit cycles. It is the case of Jansen's model with original parameters 10.1. We label the bifurcation points as in figure 10.12. For $P < P_1$, the system has a unique stable fixed point and for any initial condition, it converges towards this point. For $P_1 < P < P_{H_1}$, the system has three fixed points, one of which is stable and the other two unstable, and the system still converges towards the unique fixed point. For $P_{H_1} < P < P_{H_2}$, the greatest fixed point becomes stable and an unstable limit cycle exists. In this region, the system converges towards one of the two stable fixed point depending on the initial condition of the system. For $P_{H_2} < P < P_2$, the greatest fixed point loses stability via subcritical Hopf bifur-

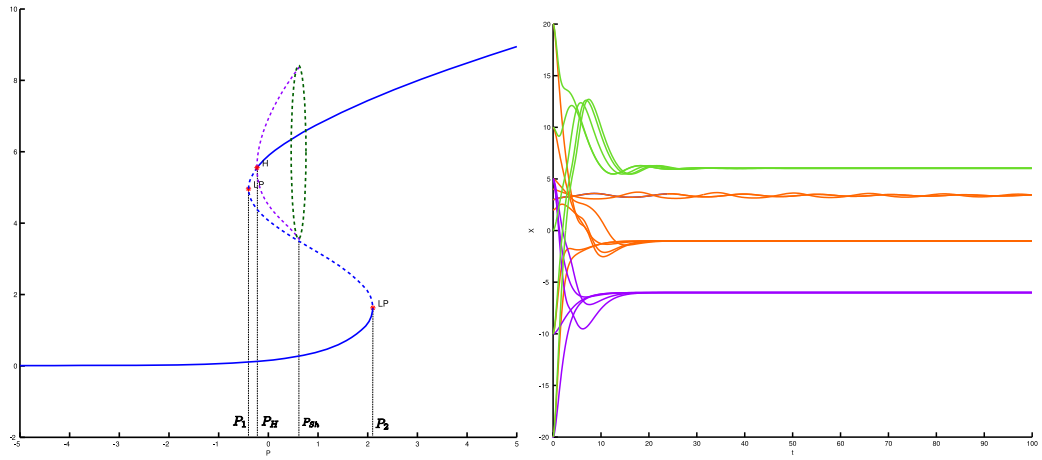

(a) Equilibria (b) Behaviors

Figure 10.11: Case (C): $j = 11$. (a): Equilibria and bifurcations (coordinate Y_1 as a function of the input current P), and stability. Blue lines: Plain : stable equilibrium, dashed : unstable. Dashed purple line: unstable cycles. Green cycle: saddle homoclinic orbit. For $P \notin [P_1, P_2]$ there exists a unique stable equilibrium, and for $P \in (P_1, P_2)$ there exist three equilibria: for $P \in (P_1, P_H)$ two unstable and one stable, and no limit cycle. For $P \in (P_H, P_2)$, two stable and one unstable. For $P \in [P_H, P_{Sh}]$, there exists an unstable limit cycle. (b): Behavior of the system for different input and initial conditions. Purple: $P = -10$ and green: $P = 10$: the system always converge to the unique equilibrium. Orange: $P = 0$: bistability and damped oscillations. We observe that the activity resemble real evoked potential.

cation and a stable periodic exists with frequency of about 10Hz corresponding to purely alpha activity. In this region, the system either oscillates around the periodic orbit and presents alpha-activity, or converges to the stable fixed point. For $P_2 < P < P_{FLC}$, the system has no fixed point and two stable limit cycles: the cycle corresponding to the continuation of the subcritical Hopf bifurcation and which corresponds to alpha activity, and a large amplitude cycle with a frequency ranging from 0 to 5 Hz and which corresponds to an epileptiform activity. The system selects one of these cycles depending on the initial condition, and can switch from one to another activity when the system is perturbed. Assume that we slowly increase the input P. If the system was in the down equilibrium state, it will converge to the epileptic cycle when crossing the bifurcation, and if it was in the up state to the alpha cycle. For $P_{FLC} < P < P_{H_3}$, the system has a unique stable trajectory which is a periodic orbit with frequency close to 10Hz, and for any initial condition the system will converge towards this cycle. Eventually, for $P > P_{H_3}$ the system has a unique fixed point and for any initial condition, the solutions of the differential equation converges towards this fixed point.

E. For $J \in [j_E, j_{GH}]$, the number and stability of the fixed points are the same as in the previous case. But in this case, the structure of the cycles is more complex. The family of unstable periodic orbits originating from the subcritical Hopf bifurcation is connected to the family of limit cycles of the supercritical Hopf bifurcation H_2 associated with the smaller j value, and the branch of limit cycles of the supercritical Hopf bifurcation H_3 associated with the greatest j value undergoes two fold bifurcations of cycles and disappears via saddle-node homoclinic bifurcation (see figure 10.13 and labels herein). For $P < P_{FLC_1}$ the behavior of the system is exactly the same as in case (D): the system generically converges to the unique stable fixed point for $P < P_{H_2}$, and either converges to the stable fixed point or to the stable cycle depending on the initial condition. For $P_{FLC_1} < P < P_{FLC_2}$, the system return to the down-state equilibrium. For $P_{FLC_2} < P < P_2$, the system has a stable fixed point (down-state equilibrium), a stable limit cycle corresponding to alpha-like activity and an unstable limit cycle. In this zone of input with have bistability between alpha-activity and rest. For $P_2 < P < P_{FLC_3}$, the system has no stable fixed points and three cycles, one of which is unstable, another one corresponding to alpha activity and the third one to epileptiform activity. For $P > P_{FLC_3}$ the behavior is the same as in the case (D) for $P > P_{FLC}$: while $P < P_{H_3}$ the system presents purely alpha oscillations, and for $P > P_{H_3}$ the system converges to the unique up-state equilibrium.

F. For $j_{GH} < j < j_{H_1}$, the system has two subcritical Hopf bifurcations whose family of limit cycle are connected, and a supercritical Hopf bifurcation whose limit cycle undergo two saddle-node bifurcations and collapse on the saddle-node manifold via saddle-node homoclinic bifurcation (see figure 10.14). For $P < P_{H_1}$ the system converges to the down-state equilibrium. For $P_{H_1} < P < P_{H_2}$, the system is bistable and either converges to the upstate equilibrium or to the downstate equilibrium depending on the initial condition. For $P_{H_2} < P < P_2$ the system converges to the downstate equilibrium. Therefore for $P < P_{H_2}$, the system only presents damped subthreshold oscillation and no real rhythmic activity. For $P_2 < P < P_{FLC_1}$ the system is in a pure epileptic activity, for $P_{FLC_1} < P < P_{FLC_2}$ the system presents both epileptic activity and alpha activity, and for $P_{FLC_2} < P < P_{H_3}$

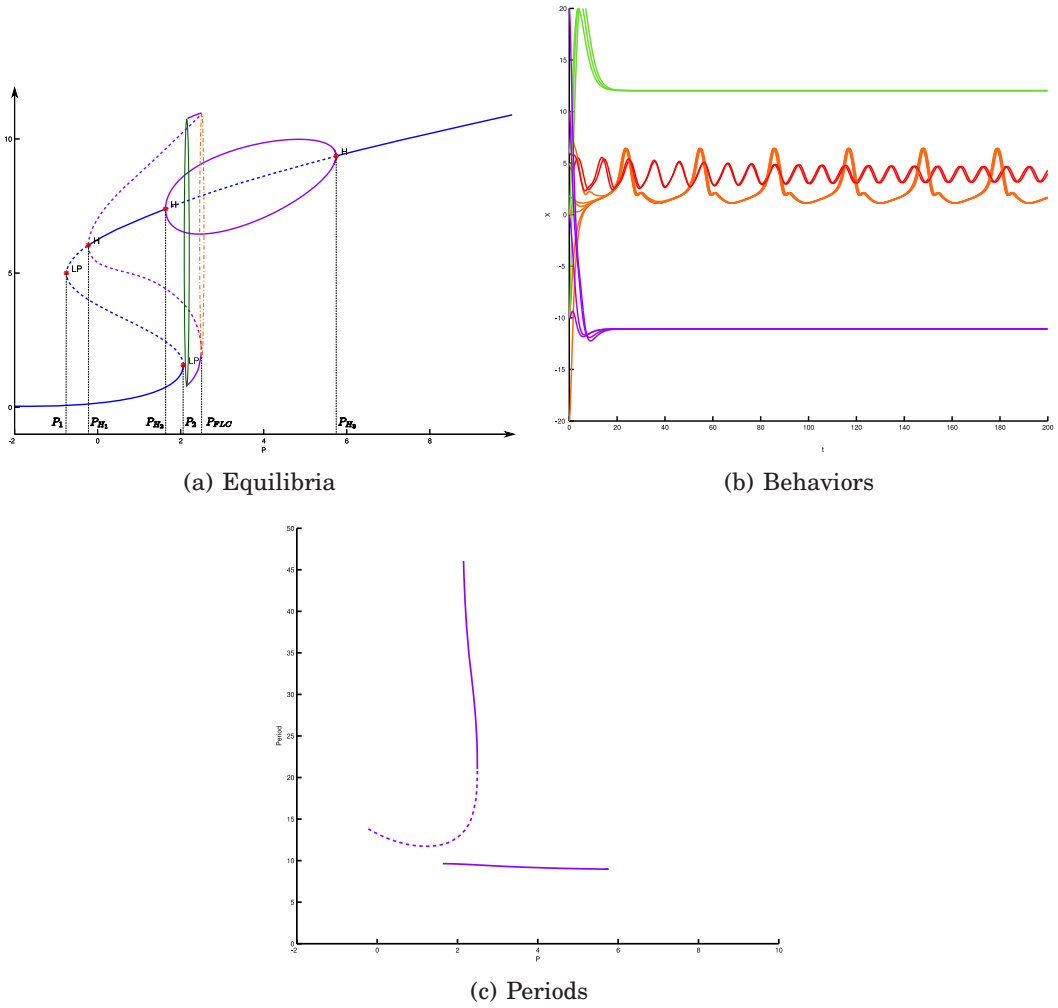

(a) Equilibria

(b) Behaviors

(c) Periods

Figure 10.12: Case (D): $j = 12.285$. (a): Equilibria and bifurcations (coordinate Y_1 as a function of the input current P), and stability. Blue lines: Plain : stable equilibrium, dashed : unstable. Purple line: dashed:unstable cycles, plain: stable. Green cycle: saddle homoclinic orbit, orange cycle: fold of limit cycles (see text) (b): Behavior of the system for different input and initial conditions. Purple: $P = -10$ and green: $P = 10$: the system always converge to the unique equilibrium. Red and orange: $P = 2.3$: bistability of cycles: orange: epileptic spikes, red: alpha activity. (c):period of the limit cycles.

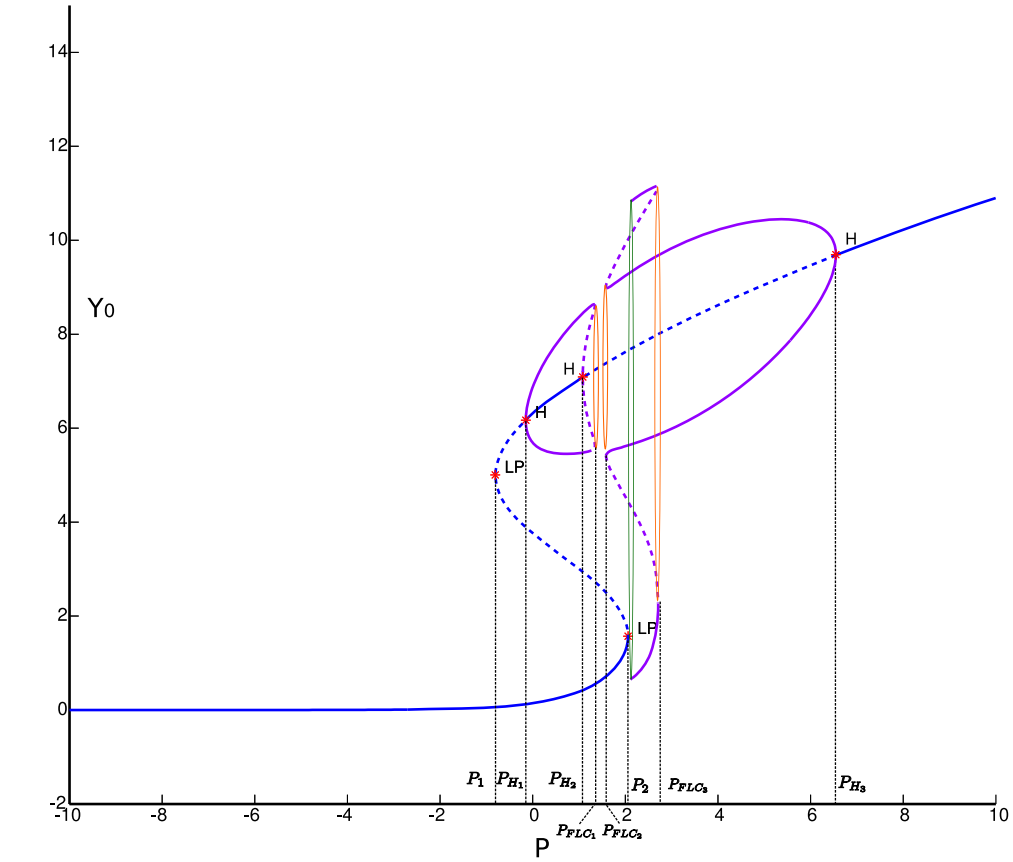

(a) Equilibria

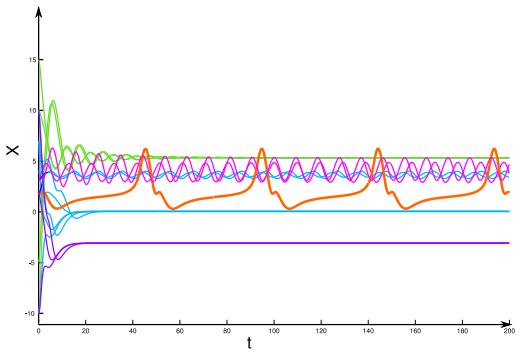

(b) Behaviors

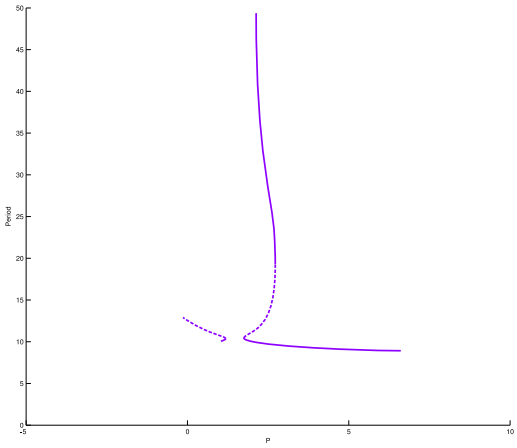

(c) Periods

Figure 10.13: Case (E): $j = 12.42$. (a): Equilibria and bifurcations (coordinate Y_1 as a function of the input current P), and stability. Blue lines: Plain : stable equilibrium, dashed : unstable. Purple line: dashed:unstable cycles, plain: stable. Green cycle: saddle homoclinic orbit, orange cycles: folds of limit cycles (see text). (b): Behavior of the system for different inputs and initial conditions. Purple: $P = -4$ and green: $P = 10$: the system always converge to the unique equilibrium. Red and orange: $P = 2.4$: alpha and epileptic activity, light blue: $P = 1.1$: rest and alpha oscillations, pink: $P = 4$: purely alpha activity.

the system only presents alpha activity. In this case, when slowly varying the input P, the system will always present epileptic activity: indeed, it is the only stable activity in a certain range of parameters.

G. For $j_{H_1} < j < j_{CLC}$, the system has two saddle-node bifurcations and a supercritical Hopf bifurcation, whose limit cycles undergo two saddle-node bifurcations and disappear via saddle-node homoclinic bifurcation. For all $P < P_2$, the system always converges to the downstate equilibrium. For $P_2 < P < P_{FLC_1}$ the system presents epileptic spikes, and for $P_{FLC_1} < P < P_{FLC_2}$ bistability with epileptic spikes and alpha activity. For $P_{FLC_2} < P < P_{H_1}$ the system presents only a stable alpha activity and for $P > P_{H_1}$ the system always returns to an upstate equilibrium whatever the initial condition (see figure 10.15)

H. For $j > j_{CLC}$ the system has two saddle-node bifurcations and a supercritical Hopf bifurcation whose family of limit cycle is regular and disappears via saddle-node homoclinic bifurcation (see figure 10.16). For $P < P_2$ or $P > P_{H_1}$ the system converges to the unique fixed point, and for $P_2 < P < P_{H_1}$ the system presents oscillations. This case is very interesting from a neuro-computational point of view. Indeed, the family of limit cycles created presents a stable region of oscillations around 10Hz corresponding to alpha activity as in the previous case, for a quite large set of inputs $P_\alpha < P < P_{H_1}$. At $P = P_\alpha$ it abruptly switches from alpha activity to theta activity where it stay for $P_\theta < P < P_\alpha$ and eventually switches regularly to delta activity for $P_2 < P < P_\theta$. In this region of parameter therefore the system presents the rhythm of the normal sleep activity.

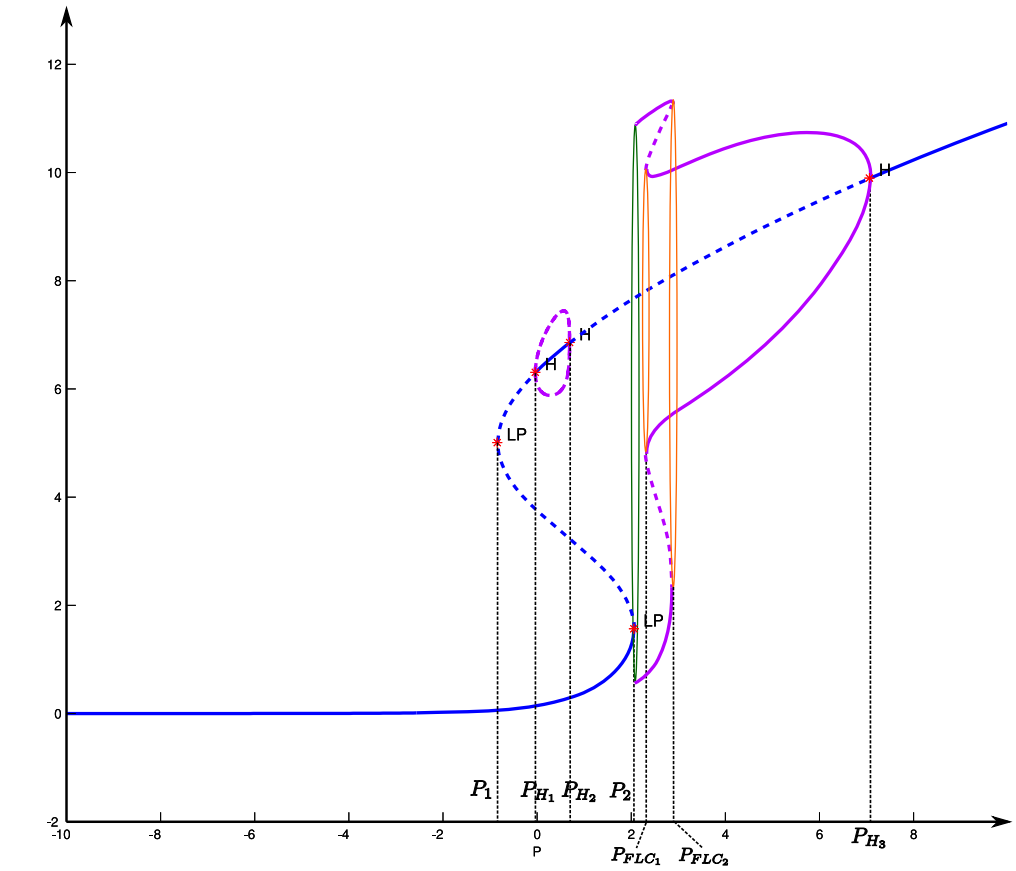

(a) Equilibria

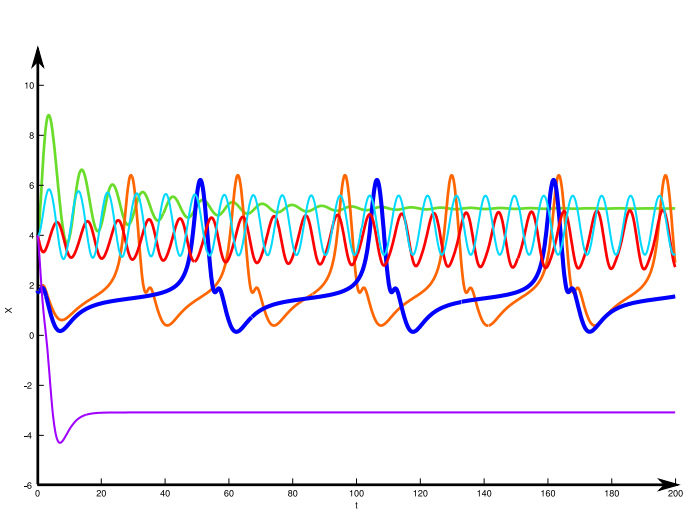

(b) Behaviors

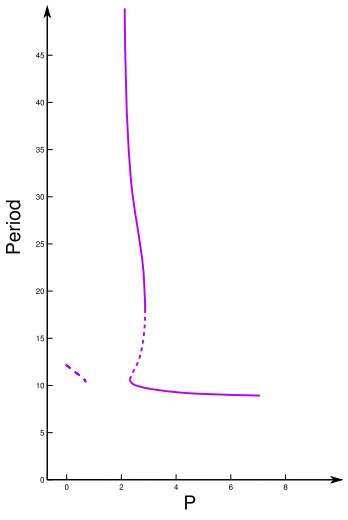

(c) Periods

Figure 10.14: Case (F): $j = 12.5$. (a): Equilibria and bifurcations (coordinate Y_1 as a function of the input current P), and stability. Blue lines: Plain : stable equilibrium, dashed : unstable. Purple line: dashed:unstable cycles, plain: stable. Green cycle: saddle homoclinic orbit, orange cycles: folds of limit cycles (see text). (b): Behavior of the system for different inputs and initial conditions. Purple: $P = -2$ and green: $P = 9$: the system always converge to the unique equilibrium. Dark blue: $P = 2.05$: purely epileptic activity: slow waves of high amplitude. Red and orange: $P = 2.3$: alpha and epileptic activity coexist, light blue: $P = 5$: only alpha oscillations.

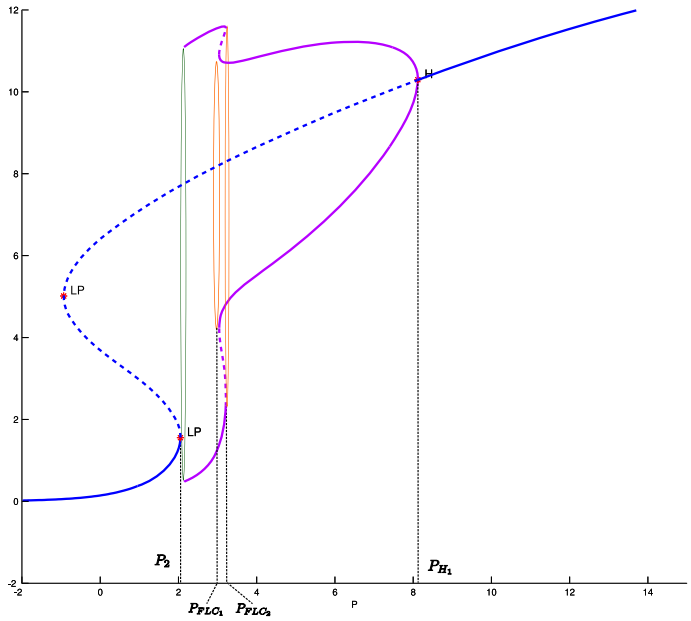

(a) Equilibria

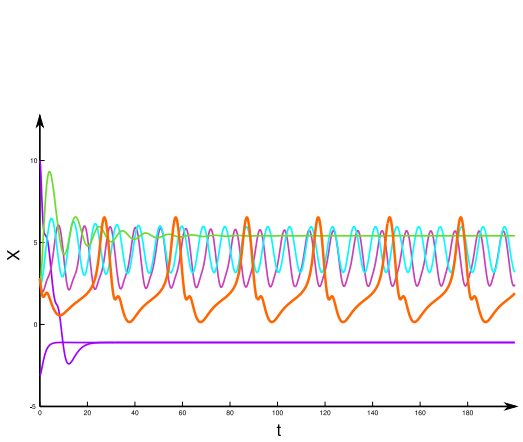

(b) Behaviors

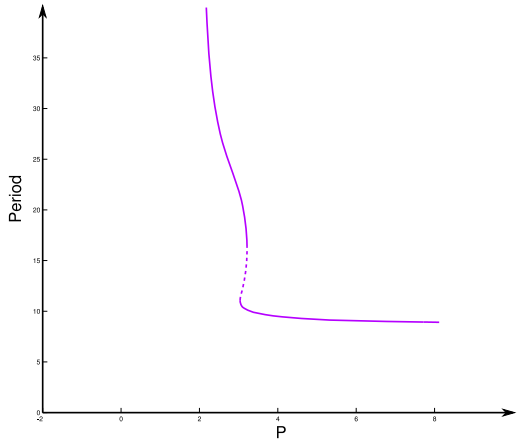

(c) Periods

Figure 10.15: Case (G): $j = 12.7$. (a): Equilibria and bifurcations (coordinate Y_1 as a function of the input current P), and stability. Blue lines: Plain : stable equilibrium, dashed : unstable. Purple line: dashed:unstable cycles, plain: stable. Green cycle: saddle homoclinic orbit, orange cycles: folds of limit cycles (see text). (b): Behavior of the system for different inputs and initial conditions. Purple: $P = 0$ and green: $P = 11$: the system always converge to the unique equilibrium. Orange: $P = 2.3$: purely epileptic activity: slow waves of high amplitude. Pink: $P = 3.1$: alpha and epileptic activity coexist, light blue: $P = 5$: only alpha oscillations.

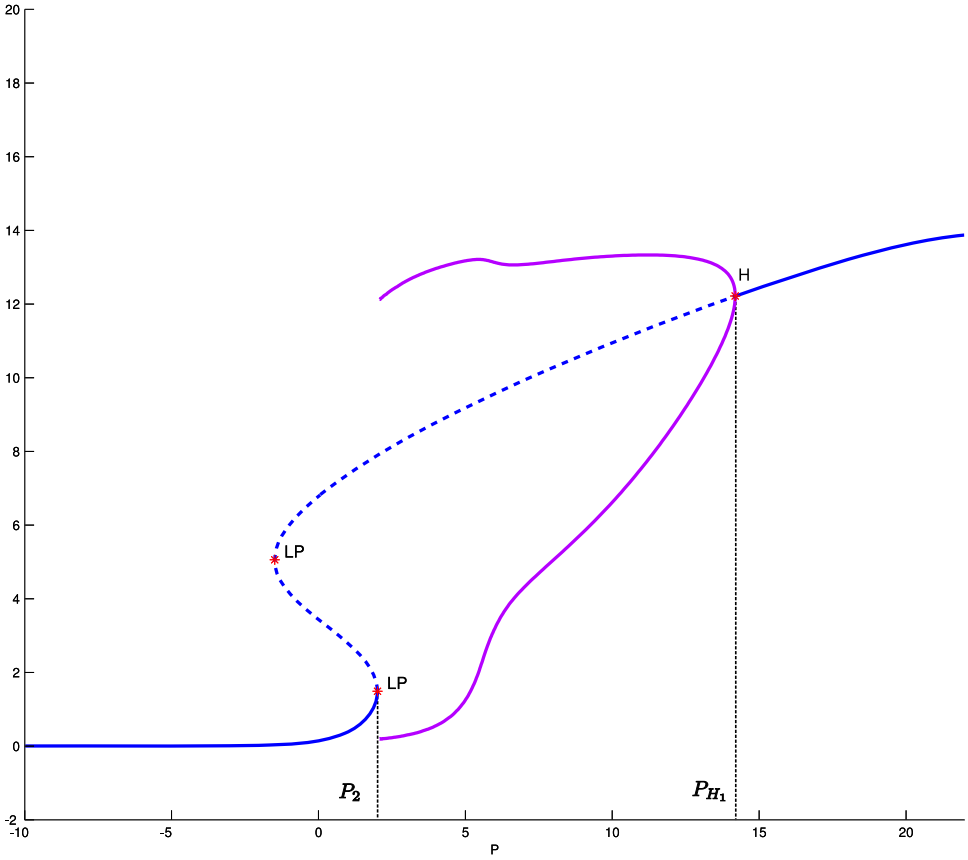

(a) Equilibria

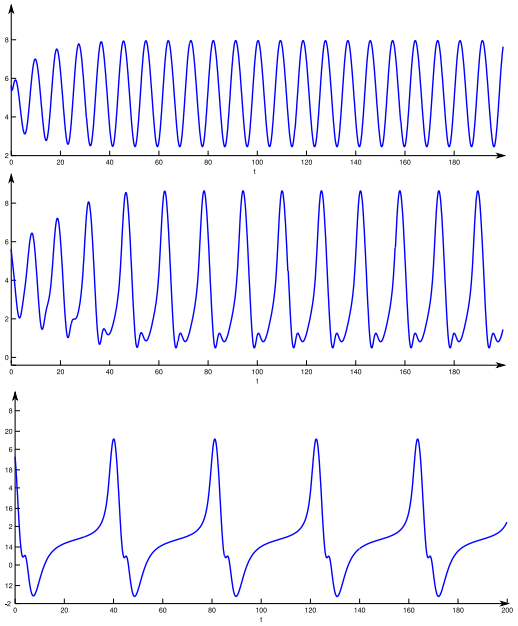

(b) Behaviors

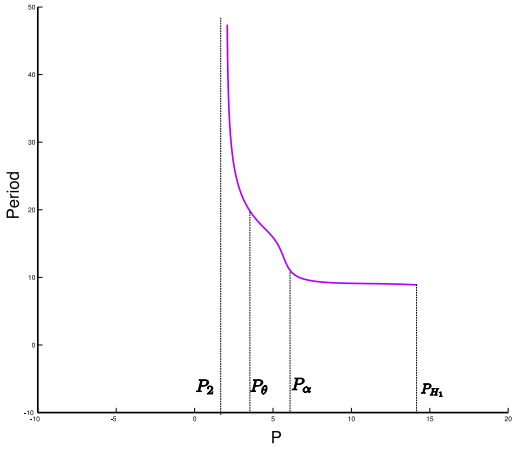

(c) Periods

Figure 10.16: Case (H): $j = 14$. (a): Equilibria and bifurcations (coordinate Y_1 as a function of the input current P), and stability. Blue lines: Plain : stable equilibrium, dashed : unstable. Purple line: dashed:unstable cycles, plain: stable (see text). (b): Behavior of the system for different inputs and initial conditions. Up: $P = 10$: alpha activity, Middle: $P = 5$ theta activity. Down $P = 2.3$: delta activity.

10.4 Influence of other parameter in Jansen's model

10.4.1 Effect of the PSP amplitude ratio

The bifurcation structure in function of the PSP amplitude ratio G is very similar to the one corresponding to the coupling strength G. The system also presents a cusp, a Bogdanov-Takens and a Bautin bifurcation, two branches of saddle-node of limit cycles collapsing at a cusp of limit cycles. The same types of behaviors will be observed. We decompose here again the bifurcation diagram into zones depending of G, and use the same notations as in the previous case. The bifurcation diagram and the decomposition in zones is given in figure 10.17.

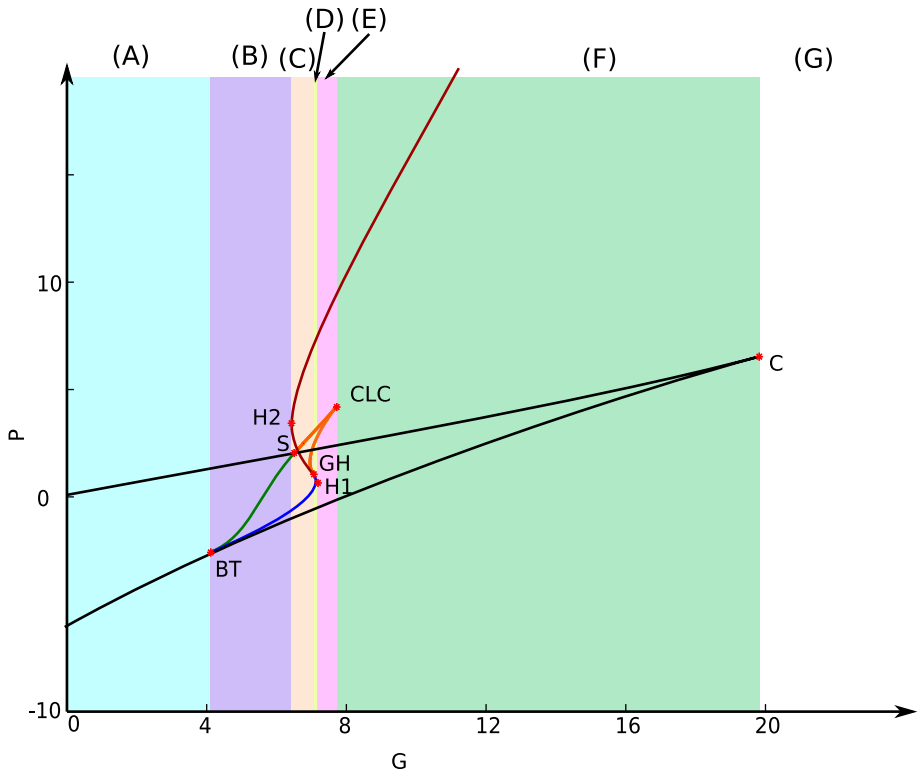

Figure 10.17: Codimention 2 bifurcations in Jansen and Rit's models with respect to the PSP amplitude ratio G and P.

10.4.2 Effect of the delay ratio

The delay ratio also presents the same bifurcation structure with a cusp , a Bogdanov-Takens, a Bautin and a cusp of limit cycles bifurcations, together with saddle-homoclinic and saddle-node homoclinic bifurcations. The bifurcation diagram is provided in 10.18.

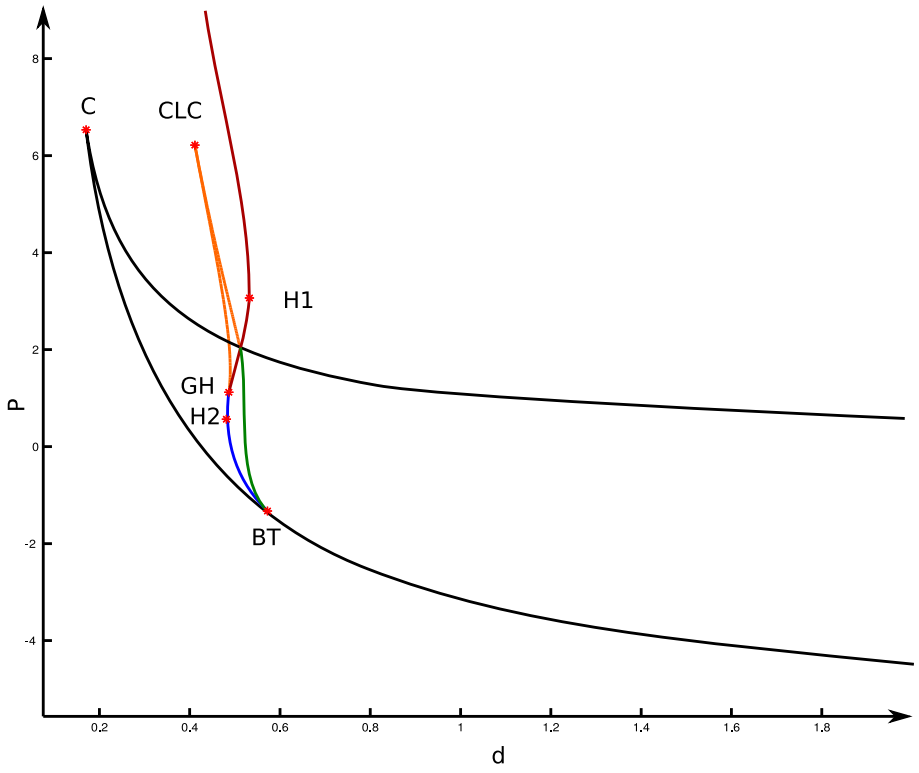

Figure 10.18: Codimention 2 bifurcations in Jansen and Rit's models with respect to the delay ratio ratio d and P.

10.4.3 Sensitivity to the connection probability parameters

The structure of cycles we studied is unaffected by changes in α_1, α_3 and α_4. For the parameter α_2, the picture is not exactly the same. Indeed, the bifurcation diagram presents a codimension three bifurcation corresponding to the cusp case of the degenerate Bogdanov-Takens bifurcation. With respect to these parameters, the cusp bifurcation point is also a point of the Andronov-Hopf bifurcation. Note that at this precise point, the bifurcation diagram is very close to the one of Wendling and Chauvel's models (see below) and therefore will locally generate the same behaviors as this more complex model.

This codimension three bifurcation corresponds to the values $DBT : \{P = 3.236,\ \alpha_2 = 0.365\}$.

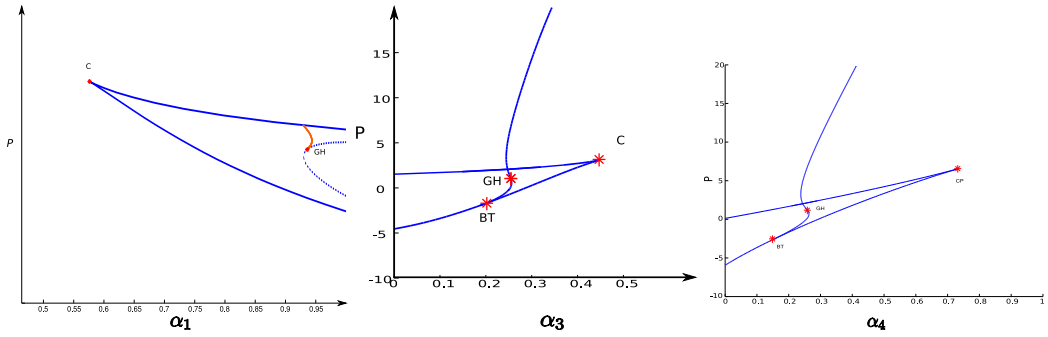

(a) Codim. 2 bifurcations in α_1 and P (b) Codim. 2 bifurcations in α_3 and P (c) Codim. 2 bifurcations in α_4 and P

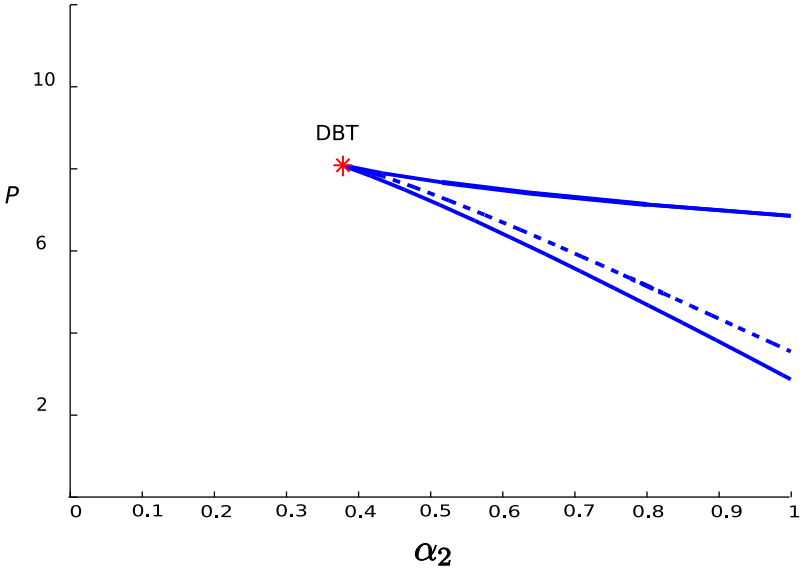

(d) Codim. 2 bifurcations in α_2 and P

Figure 10.19: Codimension 2 bifurcations of Jansen's model with respect to the connection probability parameters. In the three first cases no new bifurcations appear, and there are only a saddle-node and a Hopf bifurcation manifold, with possibly Bogdanov-Takens and Bautin bifurcation points. In case (d) we observe the apparition of a codimension three degenerate Bogdanov Takens bifurcation point.

10.5 Bifurcations Wendling and Chauvel's model

10.5.1 Fixed points of the model

Wendling and Chauvel's dynamical system is even more intricate than Jansen's model, since it has ten dimensions, sigmoidal nonlinearities and component mixing. Nevertheless in this case again, the fixed points of the system can be parametrized as a function of the state variable $X = Y_1 - Y_2$. This manifold has the equation:

$$\begin{cases} Y_0 &= jS(X) \\ Y_2 &= \frac{jG_1\alpha_4}{d_1} S(\alpha_3 jS(X)) \\ Z &= -\frac{jG_1\alpha_6}{d_1} S(\alpha_3 jS(X)) + \alpha_5 jS(X) \\ Y_3 &= \frac{jG_2\alpha_7}{d_2} S(-\frac{jG_1\alpha_6}{d_1} S(\alpha_3 jS(X)) + \alpha_5 jS(X)) \\ P &= X + Y_2(X) + Y_3(X) - \alpha_2 jS(\alpha_1 jS(X)) \\ Y_i &= 0 \qquad \forall i \in \{5 \dots 9\} \end{cases}$$

The input current P will always be an important parameter in our study. We first provide a description of codimension 1 bifurcations in Wendling's model with respect to this parameter fixing the values of the other parameters to the values found by Wendling and colleagues in their papers, and then consider the evolution of this diagram when changing the relevant parameters of the model.

As a preliminary result, we state that the system globally presents the same codimension 1 and 2 bifurcations: a saddle-node and a Hopf bifurcation manifolds, a cusp, Bautin and Bogdanov-Takens bifurcation manifolds, and a codimension three degenerate Bogdanov-Takens bifurcation. The precise study of the cycles generated and their bifurcations is the subject of forthcoming works.

10.6 Conclusion

We presented in this chapter some preliminary results of the study of the bifurcations in neural mass models in order to understand the origin of rhythms and epileptic seizures. The study of the different cycles of the system is of great interest. The effect of the different parameters can be understood with the lights of these bifurcations. The effect of noise in such a system, and the relations between the dynamics of these deterministic models and the related mean field equation is a great endeavor which will probably provide great insights on the effect of noise in the apparition of seizures and in the rhythms of the brain. This work has been done together with Olivier Faugeras.

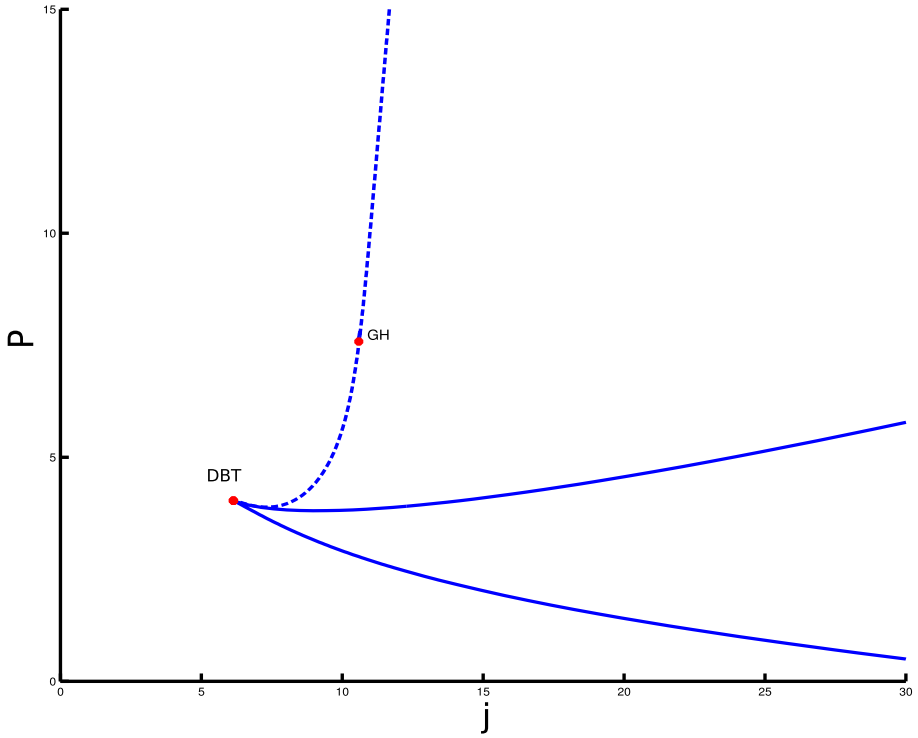

Figure 10.20: Bifurcations of Wendling and Chauvel's model with the original parameters of table 10.2 with respect to the parameters P and j. We observe a saddle-node bifurcation manifold (plain blue curve), a Hopf bifurcation manifold (dashed blue curve), a Bautin bifurcation, and a codimension three degenerate Bogdanov-Takens bifurcation (DBT)

Conclusion and perspectives

Conclusion

Most people think I count fish, but I don't.
I look at them. I look at their souls and read their dreams
and then I let them into my dreams.
– Emir Kusturica, Arizona Dream.

In this thesis, we intended to bring together advanced mathematical tools and biological problems of interest. Neuroscience gathered so far a huge amount of data and computational models, which raises new and interesting mathematical questions.

First of all, the nonlinear excitabilty of nerve cells and the fact that they exchange stereotyped signals lead us in part II to study hybrid dynamical systems featuring both a nonlinear ordinary differential accounting for the dynamics of the excitable membrane voltage and a discrete dynamical system accounting for the spike emission. These hybrid dynamical systems are very interesting from a mathematical point of view, since they put together the capabilities of both type of dynamics. From a neuro-computational point of view, the precise mathematical study provides a better understanding of the influence of the different parameters, the sensitivity with respect to these parameters, and the ranges of parameters for obtaining a given behavior and therefore simulating a given type of cell. Furthermore, this study provided a new model having the largest class of behaviors possible and keeping as simple as the others, the quartic model.

The effect of noise in the neurons influences also the way signals are processed. It is generally agreed that the variability of spike trains has important effects in terms of neural coding. Studying this problem in part III lead us to review in depth first hitting times of stochastic processes. The simplest problems were tractable using existing mathematical material, but as soon as de description of the neural activity becomes more precise, usual mathematical analysis fails. Therefore unsolved mathematical problems are raised by these biologically inspired questions with more acuity than the pure theoretical interest. We adressed the question of generalizing available mathematical results to take into account synaptic integration for a simple neuron model, and this study quite theoretical would probably have applications in the fields of mathematics, physics, and in other domains of mathematical and computational biology. Other problems involving first hitting times of nonlinear processes to curved boundary are still open problems whose resolution are of great interest in mathematics and biology.

Eventually, the brain is a highly complex system, since it is composed of a huge number of neurons which are complex entities, interacting in a nonlinear and complex fashion through a very specific and intricate connectivity map. This complexity raises the question of the reduction of this complexity in order to determine and study the essential aspects accounting for the population's function. The question of modeling and studying neural population models, reduce their complexity, pro-

vide and study tractable models is discussed in part IV. A first idea to get efficient computational models is to consider that the neurons communicate by exchanging action potentials which are stereotyped binary signals. This idea lead us to discuss an event-based modelization for stochastic spiking neuron networks. But taking into account each neuron's dynamics and their precise interaction in a huge bunch of cells having a global function is probably not the suitable level of description. We then turn to mesoscopic and macroscopic models. First, we studied the way one can get a global *mean-field* description of the network. We studied these equation from a theoretical point of view and show that they are well-posed in the mathematical sense, i.e. that there exists a unique solution to these equations. Simplifying these equations lead to more classical deterministic neural mass models. These are nonlinear ordinary differential equations in high dimensional spaces and with a large number of parameters. We reduce and study these models, and the particular study of the periodic solutions provides a better understanding of the rhythmic activity observed in electroencephalogram recordings and of the occurance of epileptiform activity.

Perspectives

These studies shed some light on new modeling problems, unsolved mathematical issues, and open the way to more neuroscientific issues.

Our work on nonlinear planar neuron models and the relation between the bifurcation structure of these models and electrophysiological properties we provide in chapter 4 can be useful to quantitative and compuational further studies of such systems. The description of the spike activity we provide in chapter 3 could be used in order to study small networks of such neurons when interconnected. This precise study lead us also to prove that a usual model used in some very large scale simulation was of slippery use, and the study of the results obtained by simulating this model have to been carefully look at considering this fact.

The study of spike statistics opens the way to new and interesting studies, both in the field of mathematics by adressing the problems that keep unsolved such as the first hitting time problems for nonlinear neuron models, as in the neuroscience community in order to validate models, compute spike statistics and simulate event-based networks. A collaboration with Christophe Pouzat, neuroscientist at Paris V university in on tracks in order to compare the spikes statistic of *in-vivo* spike recordings in insects and the models we developped in this thesis. This study could lead to fit our model if possible, and to disqualify some models if the spike trains they produce present qualitative differences with the intracellular recordings. Applications of the result of the first hitting times of DIPs to general boundaries may also be developped in many scientific fields.

Eventually, the study of population models of the last part of this dissertation is to our point of view very promising. First of all, the event-based model opens the way to efficient simulations of stochastic integrate-and-fire models. The mean-field study provides an efficient way to compute the stationary and dynamic mean-field solution for stochastic neurons, and is likely to be applied to compute the solutions of large networks in a more tractable way. The study of these solutions will be particularly interesting in comparition with the results obtained in the last section which is a study of a deterministic approximation of these systems. These comparitions will be of particular interest to understand the effect of noise in a bifurcating system. The codimension three bifurcation observed in the two neural mass models is also a very

interesting aspect of this work, since it seems to be the origin of biologically plausible behaviors. The links between these mean field and deterministic models and EEG recordings will be one of our focus in the next few months, and will probably lead to new understandings of the collective activity of nerve cells, and possibly to some new predictions.

Other effects of the noise on cortical systems might also be taken into account, such as the high conductance states, in which the noise acts as a facilitating effect for the signal transmission. Models of these effects include partial differential equations with random coefficients, which have been studied intensively studied since the beginning of this century and which are still an active field of research.

Conclusion (version française)

Dans cette thèse, nous avons tenté d'allier des outils avancés d'analyse mathématique et des problèmes biologiques intéressants. La neuroscience a accumulé jusqu'à aujourd'hui une importante quantité de données et de modèles, qui soulèvent des questions mathématiques nouvelles et très intéressantes.

Tout d'abord, l'excitabilité des cellules nerveuses et le fait qu'elles communiquent entre elles en s'échangeant des impulsions stéréotypées nous a conduit à étudier des systèmes dynamiques hybrides décrits à la fois une équation différentielle non-linéaire ordinaire reproduisant la dynamique du potentiel de membrane de la cellule et un système dynamique discret modélisant l'émission d'un potentiel d'action. Ces systèmes dynamiques hybrides sont très intéressants d'un point de vue mathématique puisqu'ils allient les capacités des deux types de dynamiques. D'un point de vue neuro-computationnel, l'étude mathématique précise nous fournit une meilleure compréhension de l'influence de différents paramètres, la sensibilité du système à ceux-ci, et les zones de paramètres associées à un comportement donné et donc à un certain type de cellule. Par ailleurs, cette étude a aboutit à l'introduction d'un nouveau modèle de neurone possédant la plus grande variété de comportements possibles et restant aussi simple à étudier et à simuler que les autres modèles de la classe: le modèle quartique.

L'effet du bruit sur les neurones influence la façon dont les signaux sont traités. Il est généralement admis que la variabilité des trains de spikes a des implications importantes en termes de codage neuronal. L'étude de ce problème nous a mené à étudier en profondeur le problème des premiers temps d'atteinte de processus stochastiques. Les problèmes les plus simples peuvent être traités en utilisant les outils mathématiques existants, mais dès que la description du neurone et de son activité devient un peu plus précise, l'analyse mathématique usuelle échoue. Des problèmes mathématiques non résolus sont soulevés par ces questions inspirées de problèmes biologiques, avec plus d'acuité que le simple intérêt théorique. Nous avons généralisé les resultats mathématiques existants afin de prendre en compte l'intégration synaptique pour un modèle simple de neurone et de synapse, et cette étude théorique pourrait avoir de nouvelles applications dans le domaine des mathématiques, de la physique et de la biologie mathématique. D'autres problèmes incluant les premiers temps d'atteinte de processus non-linéaires à des frontières générales sont toujours des problèmes ouverts dont la résolution serait d'un grand intérêt tant en mathématiques qu'en biologie.

Enfin, le cerveau est un système très complexe, puisqu'il est composé d'un trés grand nombre de neurones qui sont eux-même des entités complexes, interagissant de façon non-linéaire et compliquée à travers un réseau à la connectivité très spécifique et labyrinthique. Cette complexité pose la question de sa réduction, afin de déterminer et d'étudier les aspects essentiels en jeu dans la fonction d'une aire corticale. La ques-

tion de la modélisation d'une population de neurones, de la réduction de leur complexité, de fournir et d'étudier des modèles accessibles à l'analyse mathématique est discutée dans ma thèse. Une première idée afin d'obtenir un modèle efficace à simuler consiste à prendre en compte la nature binaire des potentiels d'action. Cette observation nous a mené a proposer une modélisation événementielle de réseaux de neurones à spikes stochastiques. La prise de compte de la dynamique de chaque neurone et de leurs interactions précises au sein d'un immense groupe de cellules présentant une fonction spécifique n'est probablement pas un niveau de description adapté. Nous nous intéressons donc à des modèles mésoscopiques et macroscopiques. Tout d'abord, nous avons étudié une méthode afin de passer d'une description microscopique à une description mésoscopique de type champ-moyen du réseau. Nous avons étudié ces équations théoriquement et avons prouvé qu'elles étaient mathématiquement bien posées, c'est-à-dire qu'elles admettent une unique solution. Une simplification de ces équations nous a mené à étudier des modèles déterministes plus classiques de masses neuronales. Il s'agit d'équations différentielles ordinaires dans des espaces de grande dimension avec un grand nombre de paramètres. Nous avons réduit et étudié ces modèles et l'étude des solutions périodiques nous fournit une meilleure compréhension de l'activité rythmique observée dans des enregistrements d'electroencephalogrammes et de l'apparition d'une activité épileptique.

Perspectives

Ces études ont mis en lumière de nouveaux problèmes de modélisation et des questions mathématiques non résolues, et ouvre la voie à des applications plus proches des questions biologiques.

Nos travaux sur les modèles de neurones planaires et les relations entre les bifurcations et les propriétés électrophysiologiques que nous obtenons dans le chapitre 4 peuvent être utiles pour de futures études quantitatives et computationelles de tels systèmes. La description de la dynamique des spikes que nous obtenons au chapitre 3 peut être utilisée afin d'étudier de petits réseaux de neurones de ce type interconnectés. Cette étude précise nous a aussi mené à réaliser qu'un des modèles les plus utilisés dans ce cadre, notamment dans des simulations à très grande échelle, présentait une forte dépendence à un paramètre non biologique, et les résultats qui ont été obtenus dans d'autres études utilisant ce modèle doivent être étudiés précisément afin de prendre en compte ces aspects.

L'étude des statistiques de trains de spikes ouvre la voie à de nouvelles études intéressantes, tant dans le domaine des mathématiques en traitant les problèmes non encore résolus comme les premiers temps d'atteintes pour des modèles de neurones non-linéaires, que dans le domaine des neurosciences afin de valider des modèles et de simuler des grands réseaux de neurones bruités avec une modélisation événementielle. Une collaboration avec Christophe Pouzat, neuroscientifique à l'université de Paris V est actuellement en cours, et le but est de comparer les statistiques d'enregistrements de trains de spikes *in-vivo* chez l'insecte aux modèles que nous avons traités dans cette thèse. Cette étude pourrait nous mener à valider ou invalider des modèles et les calibrer. Le résultat que nous avons obtenu sur la distribution de probabilité des premiers temps d'atteintes de processus doublement intégrés a lui aussi des applications possibles dans de multiples domaines scientifiques.

Enfin, l'étude des modèles de populations de neurones développée dans la dernière partie de cette thèse nous semble prometteuse. Tout d'abord, la modélisation événe-

mentielle de réseaux de neurones à spikes ouvre la voie à la simulation efficace et rapide de modèles de neurones à impulsion bruités. L'étude champ moyen des réseaux fournit une méthode efficace afin de calculer la solution stationaire et dynamique des équations de champ moyen pour des neurones stochastiques et permet de resoudre ces equations d'une façon plus efficace. L'étude de ces solutions sera particulièrement intéressante. Les liens entre ces résultats et les conclusions du dernier chapitre de la thèse qui consiste à étudier des approximations déterministes de ces équations constitue un sujet d'étude très intéressant que nous développons actuellement. Cette comparaison nous permettra de mieux comprendre les effets du bruit sur un système présentant des bifurcations. La bifurcation de codimension trois observée dans les modèles de masse neuronales est elle-même très intéressante et semble être à l'origine de comportements biologiquement plausibles. Les liens entre les équations de champ moyen, les équations de masses neuronales et des enregistrements EEG sera mon principal sujet de recherche dans les mois à venir, et nous permettra probablement de mieux comprendre l'activité collective des cellules nerveuses, l'apparition de crises d'épilepsie.

D'autres effets du bruit sur les systèmes corticaux pourraient également être pris en compte, tels que les états de haute conductance, dans lesquels le bruit apparaît comme un élément facilitant la transmission des signaux. Les modèles prenant en compte ces effets sont des équations aux dérivées partielles à coefficients aléatoires, qui ont été étudiés intensivement depuis le début du siècle et qui restent un domaine de recherches très actif.

Part V

Mathematical Tools

APPENDIX **A**

A CRASH COURSE ON DYNAMICAL SYSTEMS

This appendix is aimed to define and provide the reader with the basic definitions and theorems we used in the manuscript in the field of dynamical system. The theory of dynamical systems has been widely studied in the field of mathematics and theoretical physics. For a comprehensive basic introduction of notions and tools, the reader is referred to [246]. The elementary tools of bifurcations of equilibria and cycles are studied in depth in [118, 167], extensions in Banach spaces mainly for applications to partial differential equations and to systems with symetries in [49, 111, 125, 139]. For in depth studies of discrete-time dynamical systems the reader is referred to the excellent book of [70].

This domain has been applied successfuly in such fields as physics, biology, chemistry and economics. For biological applications and especially to neuroscience the reader is referred to [145, 202, 225].

In this chapter we quickly review the different concepts and the main theorems of dynamical systems used in the manuscript. But let us first ask a fundamental question: what is a dynamical system?

A.1 WHAT IS A DYNAMICAL SYSTEM?

A dynamical system is a mathematical formalization for processes evolving in time. A *system* evolving in *time* having the property that its present state governs the whole subsequent evolution is called a *dynamical system*. The state of the systems we consider here are defined by a point in an open set Ω of a Banach space E. We review the different types of spaces, times and the basic concepts we will deal in this chapter.

A.1.1 Phase space

From a mathematical point of view, a dynamical system is the action of a group on a given space. The space we consider is called the *phase (or state) space* H. This set is composed of all possible states of a systems, and is in general assumed to be a Banach space. It can be of different types : open set of $\mathbb{R}^d$, $\mathbb{C}^d$, infinite or semi-infinite sequences of symbols (symbolic dynamics), ... The dynamical system property implies that the specification of a point $x \in H$ must be sufficient not only to describe the current "position" of the system but also to determine its evolution

A.1.2 Time

The *evolution* of a dynamical system implies a notion of time. Time is considered to be indexed by a number set T. We will consider two types of dynamical systems: those with continuous (real) time $T = \mathbb{R}$ or an open subset of $\mathbb{R}$, and those with discrete (integer) time $T = \mathbb{Z}$. Systems of the first type are called continuous-time dynamical systems, while those of the second are termed discrete-time dynamical systems. Discrete-time systems appear naturally in ecology and economics when the state of a system at a certain moment of time t completely determines its state after a given time (a year for instance), say at $t+1$.

A.1.3 Evolution operator

The main component of a dynamical system is an evolution law that determines the state x_t of the system at time t, provided the initial state x_0 is known. The most general way to specify the evolution is to assume that for any given $t \in T$ a map φ^t is defined in the state space H,

$$\varphi^t : H \mapsto H,$$

which transforms an initial state $x_0 \in H$ into some state $x_t \in H$ at time t:

$$x_t = \varphi^t x_0.$$

The map φ^t is often called the evolution operator of the dynamical system. It might be known explicitly; however, in most cases, it is defined indirectly and can be computed only approximately. In the continuous-time case, the family $\{\varphi^t \, ; \, t \in T\}$ of evolution operators is called a flow. Note that $\varphi^t x$ may not be defined for all pairs $(x,t) \in H \times T$. Dynamical systems with evolution operator φ^t defined for both $t \geq 0$ and $t < 0$ are called invertible. In such systems the initial state x_0 completely defines not only the future states of the system, but its past behavior as well. However, it is useful to consider also dynamical systems whose future behavior for $t > 0$ is completely determined by their initial state x_0 at $t = 0$, but the history for $t < 0$ can not be unambigously reconstructed. Such (noninvertible) dynamical systems are described by evolution operators defined only for $t \geq 0$ (i.e., for $t \in R^+$ or $\mathbb{Z}^+$). In the continuous-time case, they are called semiflows.

It is also possible that $\varphi^t x_0$ is defined only locally in time, for example, for $0 \leq t < t_0$, where t_0 depends on $x_0 \in H$. An important example of such a behavior is a "blow-up", when a continuous-time system in $H = \mathbb{R}^n$ approaches infinity within a finite time, i.e., $\varphi^t x_0 \to \infty$ for $t \to t_0$.

The evolution operators have two natural properties that reflect the deterministic character of the behavior of dynamical systems. First of all,

(DS.1). $\varphi^0 = id$ where id is the identity map on H.

(DS.2). $\varphi^{t+s} = \varphi^t \circ \varphi^s$ i.e $\varphi^{t+s}x = \varphi^t(\varphi^s x)$ for all $x \in H$ and $t,s \in T$. This property means that the law governing the behavior of the system does not change in time: the system is "autonomous".

For invertible systems, the evolution operator φ^t satisfies the property (DS.2) for t and s both negative and nonnegative. In such systems, the operator φ^{-t} is the inverse of φ^t ($(\varphi^t)^{-1} = \varphi^{-t}$) because of properties (DS.2) and (DS.1).

A discrete-time dynamical system with integer t is fully specified by defining only one map $f = \varphi^1$, called "time-one map", using recursively (DS.2)

A.1.4 Definition of a dynamical system

Now we are able to give a formal definition of a dynamical system.

Definition A.1.1. A dynamical system is a triple $\{T, H, \varphi^t\}$, where T is a time set, H is a state space, and $\varphi^t : H \mapsto H$ is a family of evolution operators parametrized by $t \in T$ and satisfying the properties (DS.1) and (DS.2).

A.1.5 Orbits and phase portraits

Throughout the manuscript we discussed a geometrical point of view on dynamical systems. The basic geometrical objects associated with a dynamical system $\{T, H, \varphi^t\}$ are its orbits in the state space and the phase portrait composed of these orbits.

Definition A.1.2. An orbit starting at x_0 is an ordered subset of the state space H,

$$Or(x_0) = \{x \in H : x = \varphi^t x_0, \text{ for all } t \in T \text{ such that } \varphi^t x_0 \text{is defined}\}.$$

Orbits of a continuous-time system with a continuous evolution operator are curves in the state space H parametrized by the time t and oriented by its direction of increase (see Figure 1.3). Orbits of a discrete-time system are sequences of points in the state space H enumerated by increasing integers. Orbits are often also called trajectories. If $y_0 = \varphi^{t_0} x_0$ for some t_0, the sets $Or(x_0)$ and $Or(y_0)$ coincide.

Definition A.1.3. A point $x_0 \in H$ is called an equilibrium (fixed point) if $\varphi^t x_0 = x_0$ for all $t \in T$.

The evolution operator maps an equilibrium onto itself. Equivalently, a system placed at an equilibrium remains there forever. Thus, equilibria represent the simplest mode of behavior of the system.

Another relatively simple type of orbit is a cycle.

Definition A.1.4. A cycle is a periodic orbit, namely a nonequilibrium orbit L_0, such that each point $x_0 \in L_0$ satisfies $\varphi^{t+T_0} x_0 = \varphi^t x_0$ with some $T0 > 0$, for all $t \in T$. The minimal T_0 with this property is called the period of the cycle L_0.

If a system starts its evolution at a point x_0 on the cycle, it will return exactly to this point after every T_0 units of time. The system exhibits periodic oscillations. In the continuous-time case a cycle L_0 is a closed curve

Definition A.1.5. A cycle of a continuous-time dynamical system, in a neighborhood of which there are no other cycles, is called a limit cycle.

In the discrete-time case a cycle is a (finite) set of points $x_0, f(x_0), f^2(x_0), ..., f^{N_0}(x_0) = x_0$, where $f = \varphi^1$ and the period $T_0 = N_0$ is obviously an integer. Notice that each point of this set is a fixed point of the N_0^{th} iterate f^{N_0} of the map f. We can roughly classify all possible orbits in dynamical systems into fixed points, cycles, and "the rest".

Definition A.1.6. The phase portrait of a dynamical system is a partitioning of the state space into orbits.

The phase portrait contains a lot of information on the behavior of a dynamical system. By looking at the phase portrait, we can determine the number and types of asymptotic states to which the system tends as $t \to \infty$ (and as $t \to -\infty$ if the system is invertible).

A.1.6 Invariant sets

Definition and types

To further classify elements of a phase portrait - in particular, possible asymptotic states of the system - the following definition is useful.

Definition A.1.7. An invariant set of a dynamical system $\{T,H,\varphi^t\}$ is a subset $S \subset H$ such that $x_0 \in S$ implies $\varphi^t x_0 \in S$ for all $t \in T$.

The definition means that $\varphi^t S \subseteq S$ for all $t \in T$. Clearly, an invariant set S consists of orbits of the dynamical system. Any individual orbit $Or(x_0)$ is obviously an invariant set. We always can restrict the evolution operator φ^t of the system to its invariant set S. If the state space H is endowed with a metric ρ, we could consider closed invariant sets in H. Equilibria (fixed points) and cycles are clearly the simplest examples of closed invariant sets. There are other types of closed invariant sets. The next more complex are invariant manifolds, that is, finite-dimensional hypersurfaces in some space $\mathbb{R}^K$.

Stability of invariant sets

Let $\{T,H,\varphi^t\}$ be a dynamical system on a complete metric space H, and S_0 a closed invariant set.

Definition A.1.8. An invariant set S_0 is called stable if

i. for any sufficiently small neighborhood $U \supset S_0$ there exists a neighborhood $V \supset S_0$ such that $\varphi^t x \in U$ for all $x \in V$ and all $t > 0$;

ii. there exists a neighborhood $U_0 \supset S_0$ such that $\varphi^t x \to S_0$ for all $x \in U_0$, as $t \to \infty$.

If S_0 is an equilibrium or a cycle, this definition turns into the standard definition of stable equilibria or cycles. Property (i) of the definition is called Lyapunov stability. If a set S_0 is Lyapunov stable, nearby orbits do not leave its neighborhood. Property (ii) is sometimes called asymptotic stability.

There are invariant sets that are Lyapunov stable but not asymptotically stable. In contrast, there are invariant sets that are attracting but not Lyapunov stable, since some orbits starting near S_0 eventually approach S_0, but only after an excursion outside a small but fixed neighborhood of this set.

If x_0 is a fixed point of a finite-dimensional, smooth, discrete-time dynamical system, then sufficient conditions for its stability can be formulated in terms of the Jacobian matrix evaluated at x_0.

Theorem A.1.1. *Consider a discrete-time dynamical system*

$$x \mapsto f(x),\ x \in \mathbb{R}^n,$$

where f is a smooth map. Suppose it has a fixed point x_0, namely $f(x_0) = x_0$, and denote by A the Jacobian matrix of $f(x)$ evaluated at x_0. Then the fixed point is stable if all eigenvalues $\mu_1, \mu_2, \ldots, \mu_n$ of A satisfy $|\mu| < 1$.

The eigenvalues of a fixed point are usually called multipliers. Theorem A.1.1 applied to the N_0^{th} iterate f^{N_0} of the map f at any point of the periodic orbit, also gives a sufficient condition for the stability of an N_0-cycle.

Another important case where we can establish the stability of a fixed point of a discrete-time dynamical system is provided by the following theorem.

Theorem A.1.2 (Contraction Mapping Principle)**.** *Let H be a complete metric space with distance defined by ρ. Assume that there is a map $f : H \mapsto H$ that is continuous and that satisfies, for all $x,y \in H$,*

$$\rho(f(x), f(y)) \leq \lambda \rho(x,y),$$

with some $0 < \lambda < 1$. Then the discrete-time dynamical system $\{\mathbb{Z}^+, H, f\}$ has a stable fixed point $x_0 \in H$. Moreover, $f^k(x) \to x_0$ as $k \to \infty$, starting from any point $x \in H$.

Notice that there is no restriction on the dimension of the state space. It can be, for example, an infinite dimensional function space. Another important difference from Theorem A.1.1 is that Theorem A.1.2 guarantees the existence and uniqueness of the fixed point x_0, whereas this has to be assumed in Theorem A.1.1. Actually, the map f from Theorem A.1.1 is locally contracting near x_0, provided an appropriate metric in R^n is introduced. The Contraction Mapping Principle is a powerful tool. Using this principle, we can prove the Implicit Function Theorem, the Inverse Function Theorem, as well as Theorem A.2.1 ahead.

A.2 Ordinary differential equations

In this section we recall the main definitions and theorems in ordinary differential equations (ODE) we used in the manuscript. We consider H a Banach space, $\Omega \subset H$ an open set, $I \subset \mathbb{R}$ an open set and Λ a set (the parameter set). We denote the *vector field* of the equation $X_\lambda(t,x)$. It is an application defined on $\Lambda \times I \times \Omega$ taking its values in H.

A.2.1 General results

One of the first question to adress is the existence and uniqueness of solutions of a dynamical system.

Theorem A.2.1 (Cauchy-Lipchitz theorem)**.** *Assume that $X_\lambda(t,x)$ a vector field k times continuously differentiable with $k \geq 0$, locally lipchitz continuous in x, and let $x_\lambda(t;t_0,x_0)$ the solution of:*

$$\begin{cases} \frac{dx}{dt} & = X_\lambda(t,x) \\ x(t_0) & = x_0 \end{cases} \tag{A.1}$$

For all (λ_0, τ, u_0), there exists $\delta > 0$ and $\alpha > 0$ such that x_λ is defined on $(t_0 - \alpha, t_0 + \alpha)$ for any $(\lambda, t_0, x_0) \in B(\lambda_0, \delta) \times (\tau - \delta, \tau + \delta) \times B(u_0, \delta)$.

Furthermore, the application $(t, \lambda, t_0, u_0) \mapsto x_\lambda(t;t_0,u_0)$ is k times continuously differentiable on its definition domain.

The proof of this theorem is essentially based on Picard's theorem and the implicit functions theorem. The function $x = x_\lambda(t;t_0x_0)$, considered as a function of time t, is called a solution starting at x_0. It defines, for each $x_0 \in U$, two objects: a solution curve

$$Cr(t_0,x_0) = (t,x) : x = x_\lambda(t;t_0,x_0), t \in J \subset \mathbb{R} \times H$$

and an orbit, which is the projection of $Cr(t_0,x_0)$ onto the state space,

$$Or(t_0,x_0) = x : x = x(t;t_0,x_0), t \in J \subset H.$$

Both curves are parametrized by time t and oriented by the direction of time advance.

Lemma A.2.2 (Gronwall's lemma)**.** Let $g(t,z)$ an application lipchitz continuous in z and ρ the solution of:

$$\begin{cases} \frac{d\rho}{dt} = g(t,\rho) \\ \rho(t_0) = |x(t_0)| \end{cases}$$

then if $x : I \mapsto \mathbb{R}^n$ satisfies $|\frac{dx}{dt}| \leq g(t,|x(t)|)$, we have for $t \geq t_0$ in I

$$|x(t)| \leq \rho(t)$$

Even when $X(t,x)$ is defined for all t and all x, the solutions are not defined for all time. A classical example is $X(t,x) = x^2$.

A.2.2 Maximality and Explosion

Proposition A.2.3. Let J be the union of all intervals containing t_0 on which a solution of (A.1) is defined. There exists a solution x defined on J and any other solution of (A.1) is a restriction of x to its definition interval. x is called maximal solution of (A.1).

According to Cauchy-Lipschitz theorem, J is an open set.

Proposition A.2.4. Let $X : (t_-,t_+) \times \Omega \mapsto E$ satisfying the Cauchy-Lipschitz hypothesis and x be a maximal solution, defined on $J = (\tau_-,\tau_+)$. If $\tau_+ < t_+$, then x exits any compact for $t \to \tau_+$ (i.e. blows up at time τ_+).

Proposition A.2.5. Let f a continuously differentiable function and $F = \{x | f(x) \leq 0\}$, and X a vector field defined in the neighborhood of F, and such that $df(x) \cdot X(t,x) < 0$ on $\{x \mid f(x) = 0\}$. Then any solution of the differential equation defined by X inside F at $t = t_0$ stay in F for any $t \geq t_0$. In particular if F is compact, the solutions are defined on a right semi-infinite interval.

Applications of Gronwall's lemma A.2.2 help controlling the explosion time of the solutions.

A.2.3 ODE as Dynamical Systems

We now consider $H = \mathbb{R}^n$.

Definition A.2.1 (Flow of the equation)**.** The flow of the equation $\dot{x}(t) = X(t,x(t))$ is the map:

$$\varphi : \mathbb{R} \times \mathbb{R} \times \mathbb{R}^n \mapsto \mathbb{R}^n$$

such that $\Phi(t,t_0,x_0) = x(t)$ where x is solution of (A.1). We will denote this application $f_{t_0}^t(x_0)$.

When the vector field does not depend on time (autonomous vector field), the solution $x_\lambda(t;t_0,x_0)$ is a function of $t - t_0$, which we denote $x_\lambda(t - t_0,x_0)$. We can define the evolution operator $\varphi^t : E \mapsto E$ by the formula

$$\varphi^t x_0 = \varphi_{t_0,t+t_0}(x_0)$$

which assigns to x_0 a point on the orbit through x_0 that is passed t time units later and which is independent of the choice of t_0. It is easy to check that $\{\mathbb{R},H,\varphi^t\}$ is a continuous-time dynamical system.

Definition A.2.2. Let h be a diffeomorphism, and $X(t,x)$ a vector field. We denote by $h\star X$ the vector field defined by:

$$h\star X(t,x) = dh(h^{-1}(x))X(t,h^{-1}(x))$$

Proposition A.2.6. Let $\varphi_{t_0}^t$ be the flow of X and ψ^t the flow of $Y = h\star X$. We have:

$$\psi^t = h\circ\varphi^t\circ h^{-1}.$$

In particular, if X is autonomous (i.e. does not depend on time), h maps the orbits of X on the ones of Y.

We now consider autonomous flows.

A.2.4 Topology and Poincaré applications

Proposition A.2.7 (theoreme du redressement)**.** Let X a vector field such that $X(x_0)\neq 0$. Then there exists a diffeomorphism h defined in the neighborhood of x_0 such that $h\star X$ is constant.

This proposition allows us to define a Poincaré section of the flow as a hypersurface Σ transversal to the flow. Let $x(t)$ be a periodic solution of period T and Σ a Poincaré section at the point $x(0)$. Consider now orbits in the neighborhood of the cycle. The cycle itself is an orbit that starts at a point on Σ and returns to Σ at the same point $x(0)$. Since the solutions of (A.1) depend smoothly on their initial condition (theorem A.2.1), an orbit starting at a point $x\in\Sigma$ sufficiently close to $x(0)$ also returns to Σ at some point $\tilde{x}\in\Sigma$ near $x(0)$. Moreover, nearby orbits will also intersect Σ transversally because of proposition A.2.7. which defines a map

$$\Big\{P:\Sigma\mapsto\Sigma, x\mapsto\tilde{x}=P(x),$$

called the Poincaré map.

Definition A.2.3 (Poincaré map)**.** The map P is called a Poincaré map associated with the cycle x.

The Poincaré map P is locally defined, is as smooth as the vector field, and is invertible near $x(0)$. The intersection point $x(0)$ is a fixed point of the Poincaré map. Theorem A.2.7 gives us a system of local coordinates $\xi=(\xi_1,\xi_2,...,\xi_{n-1})$ on Σ such that $\xi=0$ corresponds to x_0. Then the Poincaré map will be characterized by a locally defined map $P:\mathbb{R}^{n-1}\mapsto\mathbb{R}^{n-1}$, which transforms ξ corresponding to x into $\tilde{\xi}$ corresponding to $\tilde{x}$, $P(\xi)=\tilde{\xi}$. The origin $\xi=0$ of $\mathbb{R}^{n-1}$ is a fixed point of the map P : $P(0)=0$. The stability of the cycle L_0 is equivalent to the stability of the fixed point $\xi_0=0$ of the Poincaré map. Thus, the cycle is stable if all eigenvalues (multipliers) $\mu_1,\mu_2,\ldots,\mu_{n-1}$ of the $(n-1)\times(n-1)$ Jacobian matrix of P, are located inside the unit circle $|\mu|=1$ (see Theorem A.1.1).

One may ask whether the multipliers depend on the choice of the point x_0 on L_0, the cross-section Σ, or the coordinates ξ on it. If this were the case, determining stability using multipliers would be confusing or even impossible.

Lemma A.2.8. The multipliers $\mu_1,\mu_2,\ldots,\mu_{n-1}$ of the Jacobian matrix A of the Poincaré map P associated with a cycle L_0 are independent of the point x_0 on L_0, the cross-section Σ, and local coordinates on it.

Furthermore, proposition A.2.7 implies that the Poincaré map is a diffeomorphism on a neighborhood of $x(0)$.

We call ω-limit set of x the adherence values of $\varphi^t(x)$ when $t \to \infty$, and denote it by $L_\omega(x)$. Similarly, we denote $L_\alpha(x)$ the set of adhence values of $\varphi^t(x)$ when $t \to -\infty$. Eventually, for $Z \subset \mathbb{R}^n$, we denote $L_\omega(Z) = \cup_{z\in Z} L_\omega(z)$ and $L_\alpha(Z) = \cup_{z\in Z} L_\alpha(z)$.

Proposition A.2.9. i. If $Z \subset Y$ and Y closed and invariant by the positive flow ($\varphi^t(Y) \subset Y$ for all $t > 0$), then $L_\omega(Z) \subset Y$.

ii. $L_\omega(Z)$ is closed

iii. $L_\omega(Z)$ is flow-invariant

iv. If Z is connect, so is $L_\omega(Z)$.

Theorem A.2.10 (Jordan)**.** *Let $\gamma : S^1 \mapsto \mathbb{R}^2$ a one-to-one continuous map of the circle a subset of the real plane. Then $\mathbb{R}^2 \setminus \gamma(S^1)$ has two connected components, one is bounded, and the other unbouded, and $\gamma(S^1)$ is their common boundary.*

This theorem is quite intuitive, but its proof is rather intricate. A proof can be found in [74, Appendix of chapter 9 p.246]. For C^1 curves the proof is simpler. Modern proofs exist, involving homology theory, have the interest to generalize to dimensions greater than 2.

Lemma A.2.11. Let $x(t_1), x(t_2), x(t_3)$ three points on Σ. The orders of the points on the trajectory and on Σ coincide.

This lemma implies that the orders are inverted after application of the Poincaré map. Futhermore, it is useful to prove the following theorem:

Theorem A.2.12 (Poincaré-Bendixon)**.** *Let $x(t)$ be the solution of a planar dynamical system defined by the vector field $X(x)$. If $x(t)$ stays bounded when $t \to \infty$, then the adherence of $x(t)$ either contains a fixed point or a periodic orbit. In the latter case, if $x(t)$ is not periodic itself, the periodic orbit is named* limit cycle*.*

A.3 MAPS DYNAMICS

In this section we study the dynamics of iterated maps. Fixed points of iterated map are solutions of the equation $f(x) = x$. A point x is periodic of period n if $f^n(x) = x$. The least positive n satisfying this property is called the prime period of x. The set of all iterates of a periodic point form a periodic orbit. A point is *eventually periodic* of period n if x is not periodic but there exists $m > 0$ such that $f^{n+i}(x) = f^i(x)$ for $i \geq m$ (i.e. $f^m(x)$ is periodic).

Let p a periodic point of period n. A point x is forward asymptotic to p if $\lim_{i\to\infty} f^{in}(x) = p$. The stable set of p we already defined, is composed of all points forward asymptotic to p.

Definition A.3.1 (Sarkovskii's order)**.** We define the following ordering in natural numbers:

$$
\begin{aligned}
&3 \rhd 5 \rhd 7 \rhd 9 \rhd 11 \rhd \dots \\
&2\cdot 3 \rhd 2\cdot 5 \rhd 2\cdot 7 \rhd 2\cdot 9 \rhd 2\cdot 11 \rhd \dots \\
&2^2\cdot 3 \rhd 2^2\cdot 5 \rhd 2^2\cdot 7 \rhd 2^2\cdot 9 \rhd 2^2\cdot 11 \rhd \dots \\
&2^3\cdot 3 \rhd 2^3\cdot 5 \rhd 2^3\cdot 7 \rhd 2^3\cdot 9 \rhd 2^3\cdot 11 \rhd \dots \\
&2^4 \rhd 2^3 \rhd 2^2 \rhd 2 \rhd 1.
\end{aligned}
$$

This ordering first lists all odd numbers except one, followed by 2 times the odds, 2^2 times the odd, etc. This exhausts all natural numbers except the powers of two which are listed last in decreasing order.

Theorem A.3.1 (Sarkovskii)**.** *Let $f : \mathbb{R} \mapsto \mathbb{R}$ be continuous. Suppose that f has a periodic point of prime period k. Then f has periodic points of periods l for any $l \lhd k$ in Sarkovskii's order.*

As a consequence, if the map has a periodic point of period three, it has periodic points of any period.

We note that whenever f has a periodic point whose period is not a power of two, then it has infinitely many periodic points. Sharkovskii's theorem does not state that there are stable cycles of those periods, just that such cycles exist. For instance a system such as the logistic map or the adaptation map we studied in chapter 3 present a stable period three cycle which apparently attracts all the orbits. In fact, there must be cycles of all periods there, but they are not stable and therefore not visible on the computer generated picture.

We eventually note that the converse of Sarkovskii's theorem is also true.

Lee and Yorke [180] proved that there is an uncountable subset of points which are not even asymptotically periodic.

I provide here the proof of this theorem for period three which I find very elegant and simple, for such a strong result under so loose assumptions. An elementary proof due to Block, Guckenheimer, Misiurwicz and Young [24] based on the same elementary observations can be provided, but is slightly more complex.

Proof. The proof is based on two simple observations: if I and J are closed intervals with $I \subset J$ and $f(I) \supset J$, then f has a fixed point in I (consequence of the intermediate values theorem) and if $A_0, A_1, \ldots, A_n$ are closed intervals such that $f(A_i) \supset A_{i+1}$ for $i \in \{0, \ldots, n-1\}$, then there exists at least one subinterval J_0 of A_0 which is mapped onto A_1, a subinterval $J_1 \subset J_0$ mapped onto A_2, and continuing this construction, a nested sequence of intervals which are mapped into the various A_i. Therefore for each i there exists $x \in A_0$ such that $f^i(x) \in A_i$. We say that $f(A_i)$ covers A_{i+1}. If we find a sequence of intervals $I_1 \to I_2 \to \ldots \to I_n \to I_1$ then the previous observation implies that there exists a fixed point of f^n in I_1.

To prove the theorem, let $a, b, c \in \mathbb{R}$ and suppose $f(a) = b, f(b) = c$ and $f(c) = a$, and that $a < b < c$. The only non-equivalent possibility would be $f(a) = c$ and is handled similarly. Therefore f has a fixed point in $[b,c]$, and f^2 has fixed points in $[a,b]$, and one of them must have period two. Let now $n \geq 2$, and let us produce a periodic point of period $n > 3$. We note $I_0 = [a,b]$ and $I_1 = [b,c]$. The assumption implies that $f(I_0) \supset I_1$ and $f(I_1) \supset I_0 \cup I_1$. Inductively, we define a sequence of nested intervals $A_0, A_1, \ldots, A_{n-2} \subset I_1$ as follows. Set $A_0 = I_1$. Since $f(I_1) \supset I_1$, there is a subinterval $A_1 \subset A_0$ such that $f(A_1) = A_0 = I_1$. Then there is a subinterval $A_2 \subset A_1$ such that $f(A_2) = A_1$ and $f^2(A_2) = A_0 = I_1$. Continuing in the same fashion, we build a subinterval $A_{n-2} \subset A_{n-3}$ such that $f(A_{n-2}) = A_{n-3}$. Therefore there exists $x \in A_{n-2}$ such that $f(x), f^2(x), \ldots, f^{n-2}(x) \in A_0$ and $f^{n-2}(A_{n-2}) = A_0 = I_1$.

Since $F(i_1) \supset I_0$, there exists a subinterval $A_{n-1} \subset A_{n-2}$ such that $f^{n-1}(A_{n-1}) = I_0$. Finally since $f(I_0) \supset I_1$ we have $f^n(A_{n-1}) \supset I_1$ so that $f^n(A_{n-1})$ covers A_{n-1}. It follows from the first observation that f^n has a fixed point p in A_{n-1}. This point has prime period n since the first $n-2$ iterations lie in I_1, the $(n-1)^{th}$ in I_0 and the n^{th} is p. If $f^{n-1}(p)$ lies in the interior of I_0 then it follows easily that it has prime period n. If it

lies on the boundary, then $n=2$ or $n=3$ which is false by assumption, which concludes the proof. □

A.4 TOPOLOGICAL EQUIVALENCE, BIFURCATIONS AND STRUCTURAL STABILITY OF DYNAMICAL SYSTEMS

In this section we introduce and discuss the following fundamental notions that will be used throughout the book: topological equivalence of dynamical systems and their classification, bifurcations and bifurcation diagrams, and topological normal forms for bifurcations. The last section is devoted to the more abstract notion of structural stability. In this chapter we will be dealing only with dynamical systems in the state space $X = R^n$.

A.4.1 Equivalence of dynamical systems

We would like to study general (qualitative) features of the behavior of dynamical systems, in particular, to classify possible types of their behavior and compare the behavior of different dynamical systems. The comparison of any objects is based on an equivalence relation allowing us to define classes of equivalent objects and to study transitions between these classes. Thus, we have to specify when we define two dynamical systems as being "qualitatively similar" or equivalent. Such a definition must meet some general intuitive criteria. For instance, it is natural to expect that two equivalent systems have the same number of equilibria and cycles of the same stability types. The "relative position" of these invariant sets and the shape of their regions of attraction should also be similar for equivalent systems. In other words, we consider two dynamical systems as equivalent if their phase portraits are "qualitatively similar", namely, if one portrait can be obtained from another by a continuous transformation.

Definition A.4.1 (Topological equivalence)**.** A dynamical system $\{T, \mathbb{R}^n, \varphi^t\}$ is called *topologically equivalent* to a dynamical system $\{T, \mathbb{R}^n, \psi^t\}$ if there is a homeomorphism $h : \mathbb{R}^n \mapsto \mathbb{R}^n$ mapping orbits of the first system onto orbits of the second system, preserving the direction of time.

We recall that a homeomorphism (diffeomorphism) is an invertible map such that both the map and its inverse are continuous (continuously differentiable).

For discrete time dynamical systems, the topological equivalence between the dynamical system defined f and the one defined by g is given by the *conjugacy relation*:

$$f = h^{-1} \circ g \circ h,$$

for h a homeomorphims. If h is a C^k-diffeomorphism, the corresponding systems are called smoothly conjugate or diffeomorphic. Two diffeomorphic maps can be considered as the same map written in two different coordinate systems x and $y = h(x)$. Consequently, two diffeormorphic discrete time dynamical systems are practically indistinguishable.

To continuous-time dynamical systems defined by the vector fields X and Y are topologically equivalent if there exists a homeomorphism h such that $Y = h \star X$. Two diffeomorphic systems are practically identical and can be viewed as the same system written using different coordinates. For example, the eigenvalues corresponding to equilibria are the same.

Suppose that $\mu(x) > 0$ is a smooth scalar positive function and that the two vector fields X and Y are related by

$$X(x) = \mu(x)Y(x) \tag{A.2}$$

for all $x \in \mathbb{R}^n$. Then, obviously, the two dynamical systems are topologically equivalent since their orbits are identical and it is the velocity of the motion that makes them different (the ratio of the velocities at a point x is exactly $\mu(x)$.) Thus, the homeomorphism h is the identity map $h(x) = x$. In other words, the systems are distinguished only by the time parametrization along the orbits.

Definition A.4.2. Two dynamical systems X and Y satisfying (A.2) for a smooth positive function μ are called orbitally equivalent.

Clearly, two orbitally equivalent systems can be nondiffeomorphic, having cycles that look like the same closed curve in the phase space but have different periods. Very often we study system dynamics locally, e.g., not in the whole state space $\mathbb{R}^n$ but in some region $U \subset \mathbb{R}^n$. Such a region may be, for example, a neighborhood of an equilibrium (fixed point) or a cycle. The above definitions of topological, smooth, and orbital equivalences can be easily "localized" by introducing appropriate regions. For example, in the topological classification of the phase portraits near equilibrium points, the following modification of Definition A.4.1 is useful.

Definition A.4.3. A dynamical system $\{T, \mathbb{R}^n, \varphi^t\}$ is called locally topologically equivalent near an equilibrium x_0 to a dynamical system $\{T, \mathbb{R}^n, \psi^t\}$ near an equilibrium y_0 if there exists a homeomorphism $h : \mathbb{R}^n \mapsto \mathbb{R}^n$ that is

i. defined in a small neighborhood $U \subset \mathbb{R}^n$ of x_0;

ii. satisfies $y_0 = h(x_0)$;

iii. maps orbits of the first system in U onto orbits of the second system in $V = f(U) \subset \mathbb{R}^n$, preserving the direction of time.

Definition A.4.4. Two dynamical systems X and Y are called *smoothly orbitally equivalent* if Y is smoothly equivalent to a system orbitally equivalent to X.

According to this definition, two systems are equivalent (in $\mathbb{R}^n$ or in some region $U \subset \mathbb{R}^n$) if we can transform one of them into the other by a smooth invertible change of coordinates and multiplication by a positive smooth function of the coordinates. Clearly, two smoothly orbitally equivalent systems are topologically equivalent, while the converse is not true.

A.4.2 Topological classification of generic equilibria

In this section we study the geometry of the phase portrait near generic, namely hyperbolic, equilibrium points in continuous- and discrete-time dynamical systems and present their topological classification.

Hyperbolic equilibria in continuous-time systems

Consider a continuous-time dynamical system defined by

$$\dot{x} = f(x), x \in \mathbb{R}^n \tag{A.3}$$

where f is smooth. Let $x_0 = 0$ be an equilibrium of the system (i.e., $f(x_0) = 0$) and let A denote the Jacobian matrix evaluated at x_0. Let n_-, n_0, and n_+ be the numbers of eigenvalues of A (counting multiplicities) with negative, zero, and positive real part, respectively.

Definition A.4.5. An equilibrium is called hyperbolic if $n_0 = 0$, that is, if there are no eigenvalues on the imaginary axis. A hyperbolic equilibrium is called a hyperbolic saddle if $n_- n_+ \neq 0$.

Using measure theory and transversality argument, we can ground the intuitive observation that *generically*, a matrix has no eigenvalues on the imaginary axis, and hyperbolicity is a typical property and an equilibrium in a generic system is hyperbolic.

Theorem A.4.1 (Hartman-Grobman)**.** *If $n_0 = 0$, there exists a homeomorphism the dynamical system* (A.3) *is topologically equivalent to its linearization.*

For an equilibrium (not necessarily a hyperbolic one), we introduce two invariant sets:

$$W^s(x_0) = \{x : \varphi^t x \to x_0, t \to \infty\},\ W^u(x_0) = \{x : \varphi^t x \to x_0, t \to -\infty\},$$

where φ^t is the flow associated with (A.3).

Definition A.4.6. $W^s(x_0)$ is called the stable set of x_0, while $W^u(x_0)$ is called the unstable set of x_0.

Theorem A.4.2 (Local Stable Manifold)**.** *Let x_0 be a hyperbolic equilibrium (i.e., $n_0 = 0$, $n_- + n_+ = n$). Then the intersections of $W^s(x_0)$ and $W^u(x_0)$ with a sufficiently small neighborhood of x_0 contain smooth submanifolds $W^s_{loc}(x_0)$ and $W^u_{loc}(x_0)$ of dimension n_- and n_+, respectively. Moreover, $W^s_{loc}(x_0)$ (resp $W^u_{loc}(x_0)$) is tangeant at x_0 to T^s (resp. T^u), where T^s (resp. T^u) is the generalized eigenspace corresponding to the union of all eigenvalues of A with of strictly negative (resp. positive) real part.*

The invariant sets W^s and W^u are immersed manifold of dimensions n_+ and n_- having the same smoothness properties as f.

Theorem A.4.3. *The phase portraits of system A.3 near two hyperbolic equilibria x_0 and y_0 are locally topologically equivalent if and only if these equilibria have the same numbers n_- and n_+.*

Hyperbilic fixed points in discrete time systems

We consider a discrete-time dynamical system $x \mapsto f(x)$. for $x \in \mathbb{R}^n$ where f is a diffeomorphism. We consider x_0 a fixed point of the system and A the Jacobian matrix evaluated at x_0. Because of the invertibility of the map, there is no zero multiplier. Let n_-, n_0 and n_+ be the numbers of multipliers of x_0 lying inside, on, and outside the unit circle respectively. A fixed point is called hyperbolic if $n_0 = 0$ (i.e. if there is no multiplier on the unit disc). It is called hyperbolic saddle if $n_- n_+ \neq 0$.

Theorem A.4.4 (Hartman–Grobman)**.** *The system is locally topologically equivalent around x_0 to the linearized dynamical system.*

(n_+, n_-)	Eigenvalues	Phase portrait	Stability
(0, 2)	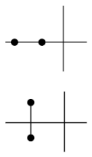	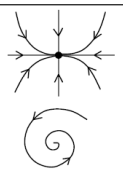 node focus	stable
(1, 1)		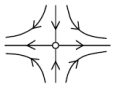 saddle	unstable
(2, 0)	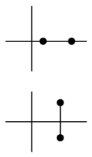	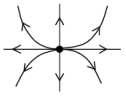 node  focus	unstable

Figure A.1: Topological classification of generic hyperbolic equilibria in the plane

As in the continuous-time case, we can introduce stable and unstable invariant sets for a fixed point x_0 (not necessarily a hyperbolic one):

$$W^s(x_0) = \{x : f^k(x) \to x_0, k \to \infty\},$$

$$W^u(x_0) = \{x : f^k(x) \to x_0, k \to -\infty\},$$

where k is integer "time" and $f^k(x)$ denotes the k^{th} iterate of x under f.

Theorem A.4.5 (Local Stable Manifold)**.** *Let x_0 be a hyperbolic fixed point. The intersections of $W^s(x_0)$ and $W^u(x_0)$ with a sufficiently small neighborhood of x_0 contain smooth submanifolds $W^s_l oc(x_0)$ and $W^u_l oc(x_0)$ of dimension n_- and n_+, respectively. Moreover, $W^s_l oc(x_0)(W^u_l oc(x_0))$ is tangent at x_0 to $T^s(T^u)$, where $T^s(T^u)$ is the generalized eigenspace corresponding to the union of all eigenvalues of A with of modulus strictly inferior (superior) to* 1.

Theorem A.4.6. *The phase portraits of (2.12) near two hyperbolic fixed points, x_0 and y_0, are locally topologically equivalent if and only if these fixed points have the same number n_- and n_+ of multipliers with $|\mu| < 1$ and $|\mu| > 1$, respectively, and the signs of the products of all the multipliers with $|\mu| < 1$ and with $|\mu| > 1$ are the same for both fixed points.*

The additional conditions on the products are due to the fact that the dynamical system can define either an orientation preserving or orientation-reversing map on the stable or unstable manifold near the fixed point. Recall that a diffeomorphism on $\mathbb{R}$ preserves orientation $detJ > 0$, where J is its Jacobian matrix, and reverses it otherwise.

Hyperbolic limit cycles

The same construction can be performed using the Poincaré map construction. The definitions and the vocabulary of the previous section extend to the case of limit cycles on the Poincaré section.

A.4.3 Bifurcations

We now consider a dynamical system depending on parameters:

$$\dot{x} = f(x, \alpha) \tag{A.4}$$

in the continuous time case, and

$$x \mapsto f(x, \alpha) \tag{A.5}$$

in the discrete-time case, where $x \in \mathbb{R}^n$ and $\alpha \in \mathbb{R}^m$ represent the phase variable and the parameters. As the parameters vary, the system either remains topologically equivalent to the original one, or its topology changes. The appearance of a topologically nonequivalent phase portrait under variation of parameters is called a *bifurcation*.

Thus, a bifurcation is a change of the topological type of the system as its parameters pass through a bifurcation (critical) value.

A *bifurcation diagram* of the dynamical system is a partition of the parameter space induced by the topological equivalence relation. The *codimension* of a bifurcation is the difference between the dimension of the parameter space and the dimension of the corresponding bifurcation boundary.

We now discuss the topological normal form for bifurcations. To this end, we consider two continuous time dynamical systems

$$\dot{x} = f(x, \alpha) \tag{A.6}$$

and

$$\dot{x} = g(x, \alpha) \tag{A.7}$$

smooth with the same number of parameters and variables.

Definition A.4.7. The two dynamical systems are called *topologically equivalent* if

i. there exists a homeomorphism of the parameter space $p : \mathbb{R}^m \mapsto \mathbb{R}^m$ such that $\beta = p(\alpha)$.

ii. there exists a parameter-dependent homeomorphism of the phase space $h_\alpha : \mathbb{R}^n \mapsto \mathbb{R}^n$, mapping the orbits of the system (A.6) at parameter value α onto the orbits of (A.7) at parameter value $p(\alpha)$ preserving the direction of time.

The homeomorphism p transforms the parametric portrait of system f into the parametric portrait of system g, while the homeomorphism h_α maps corresponding phase portraits. By definition, topologically equivalent parameter-dependent systems have (topologically) equivalent bifurcation diagrams.

A similar notion of local topological equivalence can be introduced. For local bifurcations of equilibria and fixed points, universal bifurcation diagrams are provided by *topological normal forms*, which is a central notion in bifurcation theory. Sometimes, it is possible to construct a simple (polynomial) system

$$\dot{\xi} = g(\xi, \beta; \sigma), \qquad \xi \in \mathbb{R}^n,\ \beta \in \mathbb{R}^m,\ \sigma \in \mathbb{R}^l \tag{A.8}$$

which has at $\beta = 0$ and equilibrium $\xi = 0$ satsifying k bifurcation conditions determining a codimension k bifurcation of this equilibrium. σ is a vector of coefficients σ_i of the polynomial of (A.8).

Definition A.4.8 (Topological normal form)**.** System (A.8) is called a topological normal form for the bifurcation if any generic system (A.4) with equilibrium x_0 satisfying the same bifurcations at α_0 is locally topologically equivalent to (A.8) for some values of the coefficients σ_i.

Generic means that the system satisfies a finite number of *genericity conditions* having the form of inequalities $N_i[f] \neq 0$ where N_i are some algebraic functions of certain partial derivatives of f with respect to x and α evaluated at (x_0, α_0) (these conditions determine the coefficients σ_i). It is usefull to distinguish the nondegeneracy conditions (depending only on derivatives of f with respect to x) and the other called transversality conditions.

The system $\dot{y} = g(y, \beta)$ is said to be induced by system (A.4) if $g(y, \beta) = f(y, p(\beta))$ where $\beta : \mathbb{R}^m \mapsto \mathbb{R}^m$ is a continuous map (p is not assumed to be invertible).

Definition A.4.9 (Universal unfolding)**.** System (A.8) is a universal unfolding for the corresponding local bifurcation if any system (A.4) satisfying the same bifurcations and genericity conditions at an equilibrium (x_0, α_0) is locally topologically equivalent near the origin to a system induced by (A.8) for certain values of the coefficients σ_i.

A.4.4 Structural stability

There are dynamical systems whose phase portrait (in some domain) does not change qualitatively under sufficiently small perturbations. This property is call *structural stability*.

System $\dot{x} = f(x)$ is *strictly structurally stable* in the region U if any system $\dot{x} = g(x)$ that is sufficiently C^1-close in U is topologicaly equivalent in U. A more locallized defintion was proposed by Andronov.

Definition A.4.10 (Andronov's structural stability)**.** A dynamical system f defined in a region $D \subset \mathbb{R}^n$ is called *structurally stable* in a region $D_0 \subset D$ if for any sufficiently C^1-close in D system g there are regions $U, V \subset D$, $D_0 \subset U$ such that f is topologically equivalent in U to g in V.

A.4.5 Center Manifold

We consider a continuous time dynamical system $\dot{x} = f(x)$ for $x \in \mathbb{R}$ where f is smooth and $f(0) = 0$. Let $\lambda_1, \ldots, \lambda_n$ the eigenvalues of the Jacobian matrix A at the equilibrium point 0. We assume that the equilibrium is not hyperbolic (therefore there are $n_0 \neq 0$ eigenvalues with zero real part). Let T^c denote the (generalized) eigenspace of A corresponding to the *critical* eigenvalues (with zero real part).

Theorem A.4.7 (Center Manifold Theorem)**.** *There exists a locally defined smooth n_0-dimensional invariant manifold $W^c_{loc}(0)$ tangent to T^c at 0. Moreover there is a neighborhood U of $x_0 = 0$ such that if $\varphi^t x \in U$ for all $t \geq 0$ ($t \leq 0$) then $\varphi^t x \to W^c_{loc}(0)$ for $t \to \infty$ ($t \to -\infty$).*

The manifold W^c_{loc} is called the center manifold. It is not necesarily unique. In the eigenbasis of A, the system can be written as:

$$\begin{cases} \dot{u} = Bu + g(u, v) \\ \dot{v} = Cv + h(u, v) \end{cases} \tag{A.9}$$

where $u \in \mathbb{R}^{n_0}$ and $v \in \mathbb{R}n_+ + n_-$, B is a $n_0 \times n_0$ matrix with all eigenvalues on the imaginary axis and C an $(n_+ + n_-) \times (n_+ + n_-)$ matrix with no eigenvalue on the imaginary axis, and h and g functions with Taylor expansions starting with at least quadratic terms. Because of the implicit function theorem, the center manifold of system (A.9) can be locally represented as the graph of a smooth function

$$W^c = \{(u,v) : v = V(u)\}$$

with $V : \mathbb{R}^{n_0} \mapsto \mathbb{R}n_+ + n_-$ and due to the tangency property, $V(u) = O(\|u\|^2)$.

Theorem A.4.8 (Reduction principle)**.** *System A.9 is locally topologically equivalent near the origin to the system:*

$$\begin{cases} \dot{u} = Bu + g(u, V(u)) \\ \dot{v} = Cv. \end{cases} \tag{A.10}$$

These two equations are uncoupled and the dynamics of the structurally instable system (A.9) is essentially determined by the reduction. If there are more than one center manifold, all resulting systems (A.10) are topologically equivalent.

Similar theorems can be provided for discrete-time systems and parameter-dependent systems. In the latter case, the center manifold depends on the parameter value.

A.5 BIFURCATIONS OF EQUILIBRIA IN CONTINUOUS TIME DYNAMICAL SYSTEMS

Bifurcations appear at non-hyperbolic points, and because of the center manifold theorem, the study of these bifurcations in the lowest possible dimension can be extended to higher dimensional systems.

A.5.1 Codimension one bifurcation

We consider the system (A.4) with $\alpha \in \mathbb{R}$ and f smooth with respect to both x and y. Generically, there are two ways in which the hyperbolicity of an equilibrium can be lost. Either a simple real eigenvalue approaches zero ($\lambda_1 = 0$ for some value of the parameter) or a pair of simple complex eigenvalues reaches the imaginary axis ($\lambda_{1,2} = \pm \mathbf{i} w_0$ for some value of the parameter) . It can be rigorously proved that one needs more parameters to allocate extra eigenvalues on the imaginary axis, but this might not be true for non-generic systems such as the ones having symmetries (see e.g. [167, Chapter 7]).

Saddle-node bifurcation

The saddle-node (or fold or tangent) bifurcation is the case linked with the appearance of a null eigenvalue.

Theorem A.5.1 (Genericity conditions of the saddle-node bifurcation)**.** *Suppose that we have a one-dimensional system* (A.4) *with smooth f having at $\alpha = 0$ the equilibrium $x = 0$ and let $\lambda = f_x(0,0) = 0$. Assume that the following conditions are satisfied:*

SN.1. $f_{xx}(0,0) \neq 0$*;*

SN.2. $f_\alpha(0,0) \neq 0$.

Then there are invertible changes of coordinate and parameter transforming the system into:

$$\dot{\eta} = \beta \pm \eta^2 + O(\eta^3)$$

Therefore unde these two genericity conditions the scalar system is locally topologically equivalent near the origin to the topological normal form:

$$\dot{\eta} = \beta \pm \eta^2$$

Andronov-Hopf bifurcation

The case where two purely imaginary eigenvalues appear when varying the parameters is called the Andronov-Hopf bifurcation.

Theorem A.5.2. *We consider a planar system* (A.4) *with* $\alpha \in \mathbb{R}$ *and* $x \in \mathbb{R}^2$ *with smooth* f*, having at* $\alpha = 0$ *a non-hyperbolic equilibrium with eigenvalues* $\mathbf{i}w_0$ *with* $w_0 > 0$*. For sufficiently small* $|\alpha|$ *the equilibrium* $x = 0$ *has eigenvalues*

$$\lambda_{1,2} = \mu(\alpha) \pm \mathbf{i}w(\alpha)$$

with $\mu(0) = 0$ *and* $w(0) = w_0 > 0$*. Let the following conditions be satisfied:*

AH.1. $l_1(0) \neq 0$ *where* l_1 *is the first Lyapunov coefficient (see [167, definition 3.3]*

AH.2. $\mu'(0) \neq 0$.

Then there exists an invertible change of parameter, coordinates and time transforming the system into

$$\frac{d}{d\tau}\begin{pmatrix} y_1 \\ y_2 \end{pmatrix} = \begin{pmatrix} \beta & -1 \\ 1 & \beta \end{pmatrix}\begin{pmatrix} y_1 \\ y_2 \end{pmatrix} + \sigma(y_1^2 + y_2^2)\begin{pmatrix} y_1 \\ y_2 \end{pmatrix} + O(\|y\|^4)$$

where $\sigma = sign(l_1(0))$.

Furthermore, any such system satisfying these genericity conditions is locally topologically equivalent near the origin to one of the following normal forms:

$$\frac{d}{d\tau}\begin{pmatrix} y_1 \\ y_2 \end{pmatrix} = \begin{pmatrix} \beta & -1 \\ 1 & \beta \end{pmatrix}\begin{pmatrix} y_1 \\ y_2 \end{pmatrix} + \sigma(y_1^2 + y_2^2)\begin{pmatrix} y_1 \\ y_2 \end{pmatrix}.$$

The normal form can be studied using a polar representation $z = \rho e^{\mathbf{i}\theta}$. In this system of coordinates it is simple to prove that two types of behaviors occur depending on the sign of the first Lyapunov exponent (see figure A.2):

- if $l_1(0) < 0$ the normal form has an equilibrium at the origin, which is asymptotically stable for $\beta \leq 0$ (weakly at $\beta = 0$) and unstable for $\beta > 0$. Moreover, there is a unique and stable circular limit cycle that exists for $\beta > 0$ and has radius $\sqrt{\beta}$. This is named a *supercritical* Andronov-Hopf bifurcation.
- if $l_1(0) > 0$, the origin in the normal form is asymptotically stable for $\beta < 0$ and unstable for $\beta \geq 0$ (weakly at $\beta = 0$), while a unique and unstable limit cycle exists for $\beta < 0$. This is called a *subcritical* Andronov-Hopf bifurcation

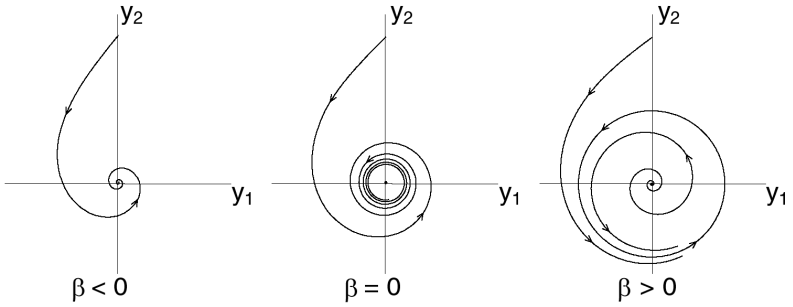

(a) Supercritical AH

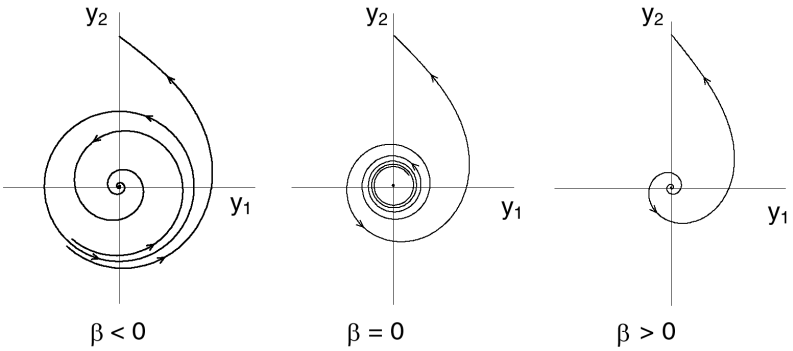

(b) Subcritical AH

Figure A.2: Sub and Supercritical Andronov-Hopf bifurcations

A.5.2 Codimension two bifurcations of equilibria

In this section we quickly review generic bifurcations of equilibria in continuous-time dynamical systems. Here again generically there is a quite restricted number of such bifurcations: either extra eigenvalues reach the the imaginary axis, changing the dimension of the center manifold, or genericity conditions for codim. 1 bifurcation fail.

Cusp bifurcation

Consider a dynamical system (A.4) with $x \in \mathbb{R}$ and $\alpha \in \mathbb{R}^2$ having at $\alpha = 0$ the equilibrium $x = 0$ such that $f_x(0,0) = f_{xx}(0,0) = 0$. Assume that:

C.1. $f_{xxx}(0,0) \neq 0$

C.2. $(f_{\alpha_1} f_{x\alpha_2} - f_{\alpha_2} f_{x\alpha_1})(0,0) \neq 0$

Then there are smooth invertible changes of coordinates and parameter changing the system into:

$$eta = \beta_1 + \beta_2 \eta \pm \eta^3 + O(\eta^4)$$

Under the genericity conditions the system is locally topologically equivalent to this last formula with $O(\eta^4) = 0$.

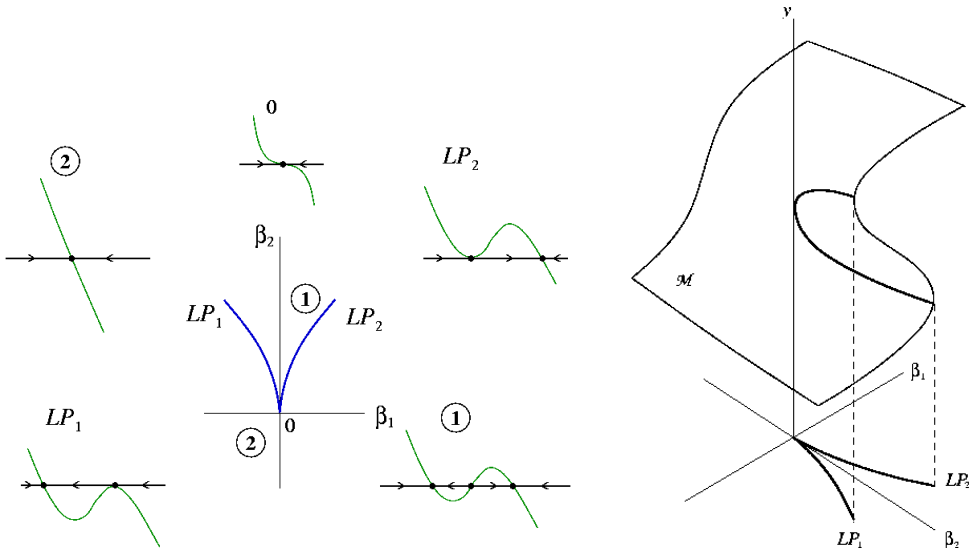

(a) Bifurcation diagram (b) Equilibria vs parameters

Figure A.3: Cusp bifurcation in one-dimensional system: local bifurcation diagram of the normal form with $\sigma = -1$. (Left) The point $\beta = 0$ is the origin of two branches of the saddle-node bifurcation curve: $LP_{1,2} = \{(\beta_1, \beta_2) : \beta_1 = \mp \frac{2}{3\sqrt{3}} \beta_2^{3/2},\ \beta_2 > 0\}$, which divide the parameter plane into two regions. Inside the wedge between LP_1 and LP_2, there are three equilibria, two stable and one unstable. Outside the wedge, there is a single equilibrium, which is stable. If we approach the cusp point from inside the wedge, all three equilibria merge together. (Right) The equilibrium manifold of the normal form is reprensented by $\mathscr{M}$. The projection of this manifold onto the parameter plane has fold singularities along $LP_{1,2}$, while the cusp singularity shows up at the origin. Here we have hysteresis: A jump to a different stable equilibrium happens at either LP_1 or LP_2, depending on whether the traced under variation of β_1 equilibrium belongs initially to the upper or lower sheet of $\mathscr{M}$.

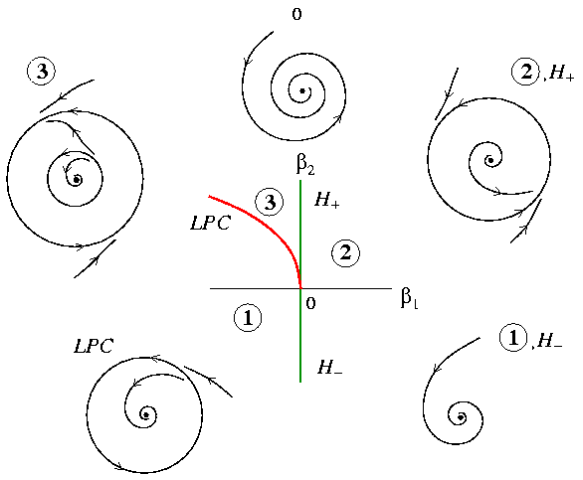

Figure A.4: Crossing the Hopf bifurcation boundary H_- to region 2 implies the appearance of a stable limit cycle which survives when we enter region 3. Crossing the Hopf boundary H_+ creates an extra unstable limit cycle inside the first one, while the equilibrium regains its stability. Two cycles of opposite stability exist in region 3 and collapse at the curve T through a fold bifurcation that leaves a single equilibrium.

Bautin (Generalized Hopf) bifurcation

Consider system (A.4) with $x \in \mathbb{R}^2$ and $\alpha \in \mathbb{R}^2$ with f smooth having at $\alpha = 0$ the equilibrium $x = 0$. Assume that at this point the Jacobian matrix has two purely imaginary eigenvalues and a null Lyapunov coefficient. If the second Lyapunov exponent does not vanish ($l_2(0) \neq 0$) at this point and the map $\alpha \mapsto (\mu(\alpha), l_1(\alpha))$ is regular at 0, then the system is locally topologically equivalent to the normal form in complex coordinates:

$$\dot{z} = (\beta_1 + \mathbf{i})z + \beta_2 z|z|^2 \pm z|z|^4.$$

Bogdanov-Takens bifurcation

Consider a planar system (A.4) with two parameters and suppose that it has at $\alpha = 0$ the equilibrium $x = 0$ with two zero eigenvalues, a non-null Jacobian matrix, and three other genericity conditions (quite complex to summarize, the interested reader is referred to [167, Chapter 8.4]), then the system is locally topologically equivalent to the normal form:

$$\begin{cases} \dot{\eta}_1 = \eta_2 \\ \dot{\eta}_2 = \beta_1 + \beta_2\eta_1 + \eta_1^2 + s\eta_1\eta_2. \end{cases}$$

Any equilibria of the system are located on the horizontal axis $\eta_2 = 0$, and satisfy the equation

$$\beta_1 + \beta_2\eta_1 + \eta_2 = 0.$$

The discriminant parabola:

$$T = \{(\beta_1, \beta_2) : 4\beta_1 - \beta_2 = 0\}$$

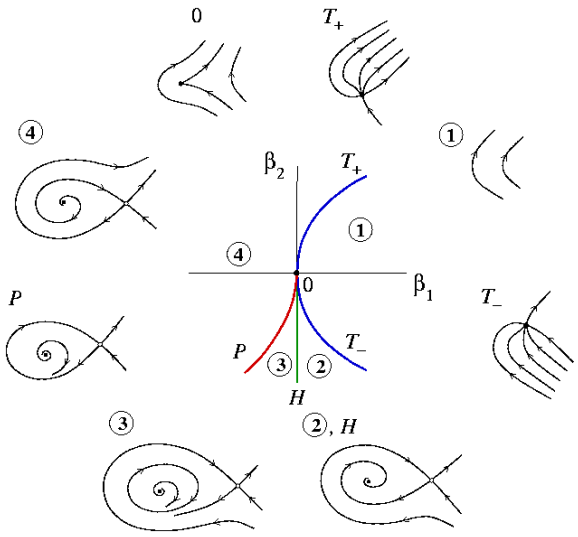

Figure A.5: Bogdanov-Takens bifurcation. Make a roundtrip near the Bogdanov-Takens point $\beta = 0$, starting from region 1 where there are no equilibria (and thus no limit cycles are possible). Entering from region 1 into region 2 through the component T_- of the fold curve yields two equilibria: a saddle and a stable node. Then the node turns into a focus and loses stability as we cross the Hopf bifurcation boundary H. A stable limit cycle is present for close parameter values to the left of H. If we continue the journey clockwise and finally return to region 1, cycles disappear via saddle homoclinic bifurcation along E_2.

corresponds to a fold bifurcation: Along this curve the normal system has an equilibrium with a zero eigenvalue. If $\beta_2 \neq 0$, then the fold bifurcation is nondegenerate and crossing T from right to left implies the appearance of two equilibria. Let us denote the left one by E_1 and the right one by E_2:

$$E_{1,2} = (\eta^0_{1,2}, 0) = \left(-\beta_2 \pm \frac{\sqrt{\beta_2^2 - 4\beta_1}}{2}, 0 \right).$$

The point $\beta = 0$ separates two branches T_- and T_+ of the fold curve corresponding to $\beta_2 < 0$ and $\beta_2 > 0$, respectively. We can check that passage through T_- implies the coalescence of a stable node E_1 and a saddle point E_2, while crossing T_+ generates an unstable node E_1 and a saddle E_2. There is a nonbifurcation curve (not shown in the figure) located at $\beta_1 > 0$ and passing through the origin at which the equilibrium E_1 undergoes a node to focus transition. The vertical axis $\beta_1 = 0$ is a line on which the equilibrium E_1 has a pair of eigenvalues with zero sum: $\lambda_1 + \lambda_2 = 0$. The lower part,

$$H = \{(\beta_1, \beta_2) : \beta_1 = 0, \beta_2 < 0\},$$

corresponds to a nondegenerate Andronov-Hopf bifurcation ($\lambda_{1,2} = \pm \mathbf{i}w$), while the upper half-axis is a nonbifurcation line corresponding to a neutral saddle. The Hopf bifurcation gives rise to a stable limit cycle, since $l_1 < 0$. The cycle exists near H for $\beta_1 < 0$. The equilibrium E_2 remains a saddle for all parameter values to the left of the curve T and does not bifurcate. There are no other local bifurcations.

There is a unique smooth curve P corresponding to a saddle homoclinic bifurcation in normal form of the Bogdanov-Takens bifurcation originating at $\beta = 0$ and having the following local representation:

$$P = \{(\beta_1, \beta_2) : \beta_1 = -\frac{6}{25}\beta_2^2 + o(\beta_2^2), \beta_2 < 0\}.$$

Moreover, for $|\beta|$ small, the normal system has a unique and hyperbolic stable cycle for parameter values inside the region bounded by the Hopf bifurcation curve H and the homoclinic bifurcation curve P, and no cycles outside this region.

A.5.3 Other bifurcations

Two other codimension two bifurcations appear in higher dimensional systems: fold-Hopf in at least three-dimensional systems and Hopf-Hopf in spaces of dimension greater than 4. They will not appear in our manuscript hence we do not discuss then and refer the interested reader to the books of Kuznetsov [167, chapters 8.5 and 8.6] and [118].

Bifurcations of codimension superior can also appear.

A.6 BIFURCATIONS OF FIXED POINT IN DISCRETE-TIME DYNAMICAL SYSTEMS

Here again we introduce and study the generic bifurcations of fixed points in the lowest dimensional system, this study beeing as general as possible because of the center manifold theorem. In all the study we consider a parameter-dependent system:

$$x \mapsto f(x, \alpha) \qquad x \in \mathbb{R}^n, \alpha \in \mathbb{R}^m. \tag{A.11}$$

A.6.1 Codimension 1 bifurcations

There are three ways in which an hyperbolic equilibrium can loose hyperbolicity: either a simple positive multiplier reaches the unit circle ($\mu_1 = 1$), or a simple negative multiplier ($\mu_1 = -1$), or a pair of simple complex multipliers reaches the unit circle ($\mu_{1,2} = e^{\pm \mathbf{i}w}$, $w \in (0, \pi)$).

Fold bifurcation

The case where a simple positive multiplier reaches 1 is called the *fold* (or saddle-node) bifurcation. Assume that $n = m = 1$ and f has at $\alpha = 0$ the equilibrium $x = 0$ and $f_x(0,0) = 1$. If furthermore we have $f_{xx}(0,0) \neq 0$ and $f_\alpha(0,0) \neq 0$, then the system is locally topologically equivalent to the normal form:

$$\eta \mapsto \beta + \eta \pm \eta^2.$$

Period doubling bifurcation

The case where a simple negative multiplier reaches -1 is named the *period doubling* (or flip) bifurcation. Assume that $n = m = 1$ and f has at $\alpha = 0$ the equilibrium $x = 0$ and

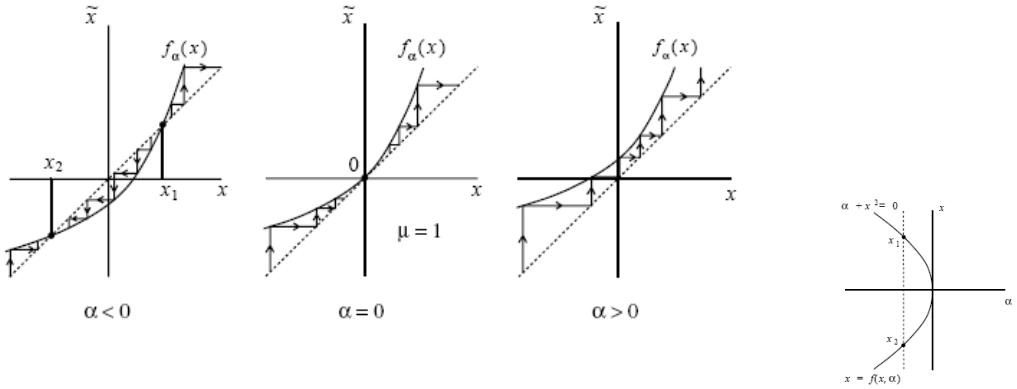

(a) Fold bifurcation

(b) Fixed point manifold

Figure A.6: Representation of the fold bifurcation and the fixed points manifold

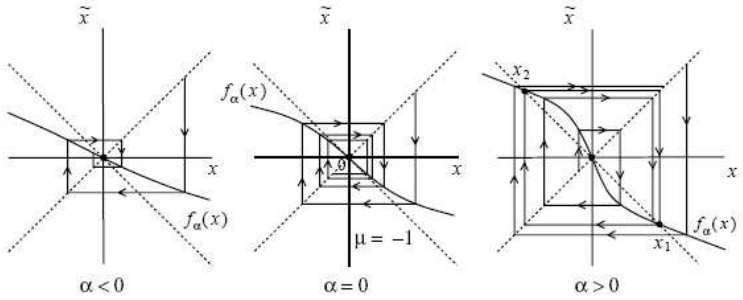

Figure A.7: Flip bifurcation

$f_x(0,0) = -1$. If furthermore we have $1/2(f_{xx}(0,0))^2 + 1/2 f_{xxx}(0,0) \neq 0$ and $f_{x\alpha}(0,0) \neq 0$, then the system is locally topologically equivalent at the origin to the normal form:

$$\eta \mapsto -(1+\beta)\eta + \sigma\eta^3,$$

where $\sigma = \pm 1$.

When the bifurcation occurs, a stable fixed point loses stability, and a two new fixed point appear for the second iterate of f (via pitchfork bifurcation). In the case where $\sigma = 1$ (*supercritical* case), the equilibrium for $\beta < 0$ is stable, non-hyperbolic for $\beta = 0$ nonlinearly stable and unstable for $\beta > 0$. There are no other fixed point for small $|\beta|$ near the origin. The second iterate $f^2(x,\alpha) = f(f(x,\alpha),\alpha)$ has two nontrivial stable fixed points for small $\beta > 0$ which constitute a cycle of period two for the original map f. In the case $\sigma = -1$ (*subcritical* case), the equilibrium $x = 0$ has the same stability as in the previous case. At the parameter value $\beta = 0$ the fixed point is nonlinearly unstable and the analysis of the second iterate of f reveals an unstable cycle of period two for $\beta < 0$ which disappears at $\beta = 0$.

Neimark-Sacker bifurcation

The case where a pair of simple complex multipliers reaches the unit circle corresponds generically to the case of a Neimark-Sacker (or Hopf) bifurcation. The bifur-

cation can be supercritical or subcritical, resulting in a stable or unstable (within an invariant two-dimensional manifold) closed invariant curve, respectively. When it happens in the Poincare map of a limit cycle, the bifurcation generates an invariant two-dimensional torus in the corresponding ODE. The normal form derivation is quite intricate, and behaviors are very rich in the neighborhood of this bifurcation. Nevertheless, we will not use it in the manuscript and for this reason the reader is referred to [167, chapters 4.6 and 4.7].

A.6.2 Codimension two bifurcations

Here again, codimension two bifurcations appear when varying simultaneously two parameters. At some parameter values, extra multipliers can approach the unit circle, changing the dimension of the center manifold, and some of the nondegeneracy conditions for codim 1 bifurcations can fail. New phenomena can appear in two parameters systems called *strong resonnances*. Eleven types of generic codimension two bifurcations are distinguished. We refer to the great chapter 9 of the book of Kuznetsov [167] that describe all these bifurcations, but since they are not useful in the text, we do not present them is this appendix. Note nevertheless that similar bifurcations as in continuous-time systems can appear, as the cusp bifurcation, the generalized flip and Chenciner (generalized Neimark-Sacker) bifurcations (which resemble more or less to the Bautin bifurcation).

A.7 BIFURCATIONS OF PERIODIC ORBITS

A combination of the Poincaré map and the center manifold allows us to apply results of discrete-time dynamical systems bifurcations to limit cycle bifurcations in n-dimensional continuous-time dynamical systems.

Let L_0 be a limit cycle of system (A.4) at $\alpha = 0$ and P_α the associated Poincaré map for nearby α, $P_\alpha : \Sigma \mapsto \Sigma$ where Σ is a local cross-section to L_0. The map P_α is smooth and locally invertible. Suppose that L_0 is non-hyperbolic, having n_0 multipliers on the unit circle. The center manifold theorems then gives a parameter-dependent invariant manifold $W^c_\alpha \subset \Sigma$ of P_α on which the essential events takes place.

A.7.1 Fold bifurcation of cycles

Fix $n = 3$ and assume that at $\alpha = 0$ the cycle has a simple multiplier $\mu_1 = 1$ and its other multiplier satisfies $0 < \mu_2 < 1$. The restriction of P_α to the invariant manifold W^c_α is a one-dimensional map, having a fixed point with $\mu_1 = 1$ at $\alpha = 0$. It implies the collision and disappearance of two fixed points of P_α as α passes through zero. Under our assumption on μ_2, this happens on a one-dimensional attracting invariant manifold of P_α; thus, a stable and a saddle fixed point are involved in the bifurcation (see figure A.8. Each fixed point of the Poincaré map corresponds to a limit cycle of the continuous-time system. Therefore, two limit cycles (stable and saddle) collide and disappear at this bifurcation.

A.7.2 Period doubling of limit cycles

Suppose that at $\alpha = 0$ the cycle has a simple multiplier $\mu_1 = -1$, while $-1 < \mu_2 < 0$. Then, the restriction of P_α to the invariant manifold will demonstrate generically the

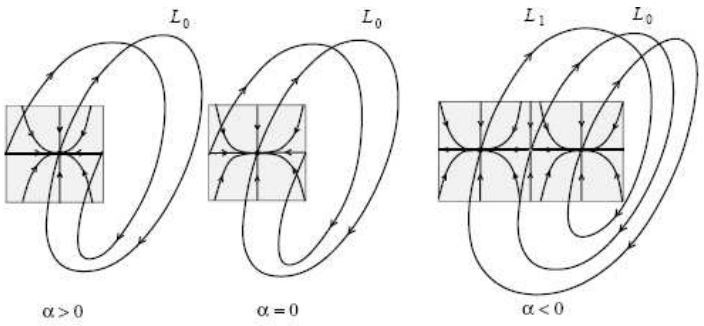

Figure A.8: Fold bifurcation of limit cycles

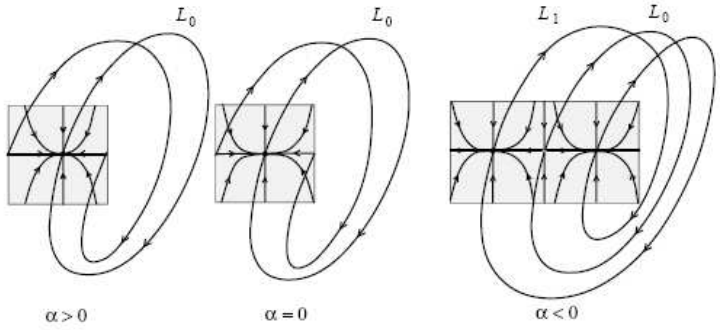

Figure A.9: Period doubling bifurcation of limit cycles

period-doubling (flip) bifurcation: A cycle of period two appears for the map, while the fixed point changes its stability (see Figure A.9). Since the manifold is attracting, the stable fixed point, for example, loses stability and becomes a saddle point, while a stable cycle of period two appears. The fixed points correspond to limit cycles of the relevant stability. The cycle of period-two points for the map corresponds to a unique stable limit cycle with approximately twice the period of the original cycle L_0. The double-period cycle makes two big excursions near L_0 before the closure. The exact bifurcation scenario is determined by the normal form coefficient of the restricted Poincaré map evaluated at $\alpha = 0$.

A.7.3 Neimark-Sacker bifurcation of cycles

The last codim 1 bifurcation corresponds to the case when the multipliers are complex and simple and lie on the unit circle: $\mu_{1,2} = e^{\pm \mathbf{i}\theta_0}$. The Poincaré map then has a parameter-dependent, two-dimensional, invariant manifold on which a closed invariant curve generically bifurcates from the fixed point (see Figure A.10). This closed curve corresponds to a twodimensional invariant torus $\mathbb{T}^2$. The bifurcation is determined by the normal form coefficient of the restricted Poincaré map at the critical parameter value. The orbit structure on the torus $\mathbb{T}^2$ is determined by the restriction of the Poincaré map to this closed invariant curve. Thus, generically, there are long-period cycles of different stability types located on the torus.

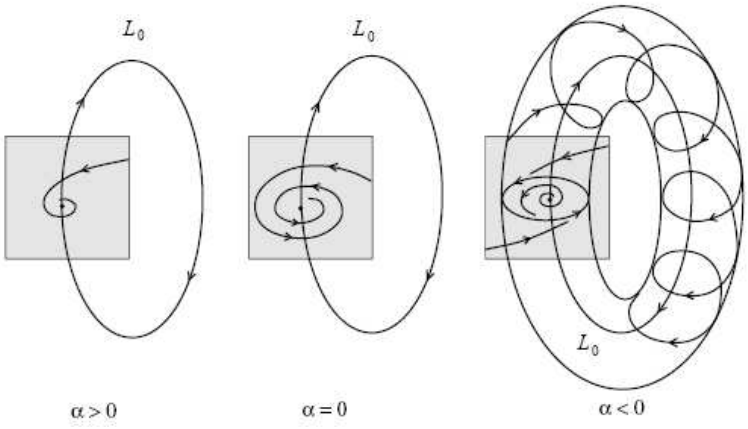

Figure A.10: Neimark-Sacker bifurcation of limit cycles

A.8 Bifurcations of Homoclinic and Heteroclinic orbits

A very interesting topic in bifurcation theory and dynamical systems is the study of homoclinic and heteroclinic orbits. These orbits connect fixed points or limit cycles. They present a very rich dynamics, and can lead to chaotic dynamics as in the blue sky catastrophe. Results are not summarized here since they would need large developments in order to be rigorously studied. The interested reader is referred to the excellent books of Shil'nikov [236].

Aknowledgement of debt

This text is mainly inspired from the excellent book of Yuri A. Kuznetsov [167] from which I borrowed most of the figures.

APPENDIX **B**

A NUMERICAL BIFURCATION ALGORITHM

In this appendix we present a numerical algorithm to compute formally or numerically local bifurcations for vector fields implemented in Maple®. This algorithm is based on the closed form formulations for genericity and transversality conditions given in textbooks such as [118, 167]. We present the main features of the algorithm in the first section, and then apply this algorithm to compute codimension two bifurcations for Jansen and Rit's neural mass model we introduce and study in chapter 10.

B.1 NUMERICAL ALGORITHM

B.1.1 Solver of equations

For our numerical analysis, we implemented a precise and efficient solver of equations based on dichotomy. This algorithm controls the precision of the solution we are searching for, and is way faster than the native `fsolve` Maple application.

B.1.2 Saddle-node bifurcation manifold

We recall that given a dynamical system of the type $\dot{x} = f(\mu, x)$ for $x \in \mathbb{R}^n$ and $\mu \in \mathbb{R}$, the systems undergoes a saddle-node bifurcation at the equilibrium $x = x_0, \mu = \mu_0$ if and only if (see e.g. [118, Theorem 3.4.1.]):

(SN1). $D_x f(\mu_0, x_0)$ has a simple 0 eigenvalue. Denote by v (resp w) the right (resp. left) eigenvector.

(SN2). $\langle w, \partial f/\partial \mu)(x_0, \mu_0)\rangle \neq 0$

(SN3). $\langle w, (D_x^2 f(\mu_0, x_0))(v, v)\rangle \neq 0$

The algorithm we use to identify the saddle-node bifurcation manifold is a straightforward application of this theorem, and consists in:

- solving the implicit equation $\det(D_x f(\mu_0, x_0)) = 0$ on the fixed-points manifold. We obtain the equilibria where Jacobian determinant vanishes, i.e. where there is a null eigenvalue.

- We then (2) compute the left and right eigenvectors of the Jacobian matrix at these points:
  - check that the dimension of the eigenspace related to the eigenvalue 0 is 1
  - check conditions (SN2) and (SN3).

On the line where the determinant of the Jacobian matrix vanishes and the conditions are not satisfied, we will consider two cases: the cusp and the Bogdanov-Takens bifurcations

B.1.3 Cusp bifurcation

At a cusp bifurcation point, the Jacobian matrix of the system has a null eigenvalue and the first coefficient of the normal form (given by condition (SN3)) vanishes. In that case, under the differential transversality and genericity conditions of [167, lemma 8.1], a smooth change of coordinates puts locally the system in the normal form of the cusp bifurcation. Our algorithm numerically checks the two conditions on these singular points.

B.1.4 Bogdanov-Takens bifurcation

If along the saddle node manifold a second eigenvalue vanishes, under the genericity and transversality conditions of [118, chapter 7.3], a smooth change of coordinates puts locally the system in the normal form of the Bogdanov-Takens bifurcation. These conditions are also numerically checked by our algorithm.

B.1.5 Andronov-Hopf bifurcation manifold

Changes in the stability of fixed points can also occur via Andronov-Hopf bifurcations. In this case, the real part of an eigenvalue crosses 0 but not its imaginary part. Theoretically, the dynamical system $\dot{x} = f(x,\mu)$ undergoes a Hopf bifurcation at the point $x = x_0, \mu = \mu_0$ if and only if (see [118, Theorem 3.4.2]):

- $D_x f(x_0,\mu_0)$ has a simple pair of pure imaginary eigenvalues and no other eigenvalues with zero real part. Denote by $\lambda(\mu)$ the eigenvalue which is purely imaginary at μ_0.
- $l_1(x_0,\mu_0) \neq 0$ where l_1 is the first Lyapunov exponent.
- $\frac{d}{d\mu}(Re(\lambda(\mu)))|_{\mu=\mu_0} = d \neq 0$

In this case, checking condition B.1.5 is not as easy as condition (SN1). Different methods are available in order to compute Hopf bifurcation points (see [119, 120]). Our algorithm is based on computing the bialternate product of the Jacobian matrix of the system $2J(j,P) \odot Id$ where Id is the identity matrix. It is known that the determinant of this matrix vanishes if and only if the Jacobian matrix has two opposed eigenvalues (its eigenvalues are $\lambda_i + \lambda_j$ where λ_i and λ_j are eigenvalues of the initial matrix $J(j,P)$). Therefore this points where the bialternate product vanishes we have to check that there exists a purely imaginary eigenvalue to avoid cases where the system has two real opposed eigenvalues. Even with this step, bialternate product method is way more efficient than other methods based on the characteristic polynomial such as Kubicek's method [166].

B.1.6 Bautin bifurcation

If along the line of the Hopf bifurcations the first Lyapunov coefficient vanishes and a subcritical Hopf bifurcation becomes supercritical when changing the parameters, under the differential conditions of [167, theorem 8.2], the system undergoes a Bautin bifurcation. At the points where the first Lyapunov coefficient vanish, the algorithm numerically checks these conditions.

B.1.7 Application to Jansen and Rit's model

Saddle-node bifurcation manifold

In the case of Jansen and Rit's model (see chapter 10, the possible saddle-node bifurcations points are located on a curve in the parameter space depending on the variable X, and whose expression is:

$$d = jS'(X)(\alpha_1\alpha_2 d S'(\alpha_1 jS(X)) - \alpha_3\alpha_4 G S'(\alpha_3 jS(X))) \tag{B.1}$$

In the case of Wendling and Chauvel's model,

$$\begin{aligned} 1 = j^2 S'(X)\Bigg\{ & \alpha_1\alpha_2 S'(\alpha_1 jS(X)) - \frac{\alpha_3\alpha_4}{d_1} G_1 S'(\alpha_3 jS(X)) \\ & + S'(-\frac{jG_1\alpha_6}{d_1} S(\alpha_3 jS(X)) + \alpha_5 jS(X))\Big(\frac{\alpha_3\alpha_6\alpha_7}{d_1 d_2} G_2 S'(\alpha_3 jS(X)) - \frac{\alpha_5\alpha_6}{d_2} G_2 S'(X)\Big)\Bigg\} \end{aligned} \tag{B.2}$$

On these curve we have to check the genericity and the transversality conditions. For this step we have to resign to purely numerical simulation, since the computations are too heavy to be performed analytically.

We obtain that condition (SN2) is always satisfied. For each point of the curve, the dimension of the eigenspace associated with the eigenvalue 0 is equal to 1, except for the point BT of coordinates $j_{BT} = 10.05$, $P_{BT} = -3.0742$, $X_{BT} = 3.2956$. We will specifically study this point below and prove that at this point the system undergoes a Bogdanov-Takens bifurcation.

Eventually, condition (SN3) is satisfied everywhere except at a point C of coordinates $j_C = 5.38$, $P_C = -0.29$, $Y_C = 3.63$ (Figure B.1(c) represents the cubic coefficient of the Taylor's expansion on the center manifold involved in condition (SN3)). We will also specifically study this point and show that at this point the system undergoes a *cusp bifurcation*.

The curves we obtain are represented in figure B.1. The curve displayed in the space (j, P, Y) is smooth but its projection in the (j, P) plane presents a singularity at the point C.

Andronov-Hopf bifurcation manifold

We obtain using our symbolic computation algorithm the parameter manifold where the system possibly undergo Hopf bifurcations. We fixing all the parameters but 2, this manifold is a curve in a two dimensional space parametrized by the variable X, and at each point of this line we check the transversality B.1.5 and the genericity B.1.5 conditions. This line can be computed in a closed form but the expression is very involved.

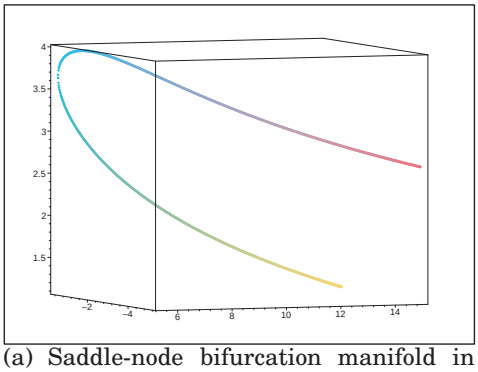

(a) Saddle-node bifurcation manifold in (Y, j, P)

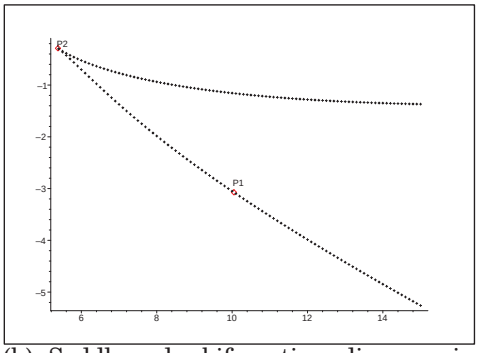

(b) Saddle-node bifurcation diagram in (j, P)

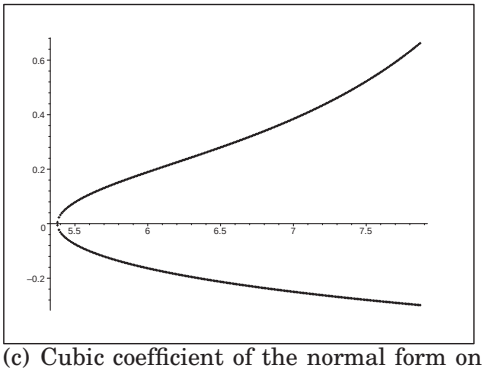

(c) Cubic coefficient of the normal form on the center manifold.

Figure B.1: Saddle-node bifurcation manifold and bifurcation diagram in (j, P).

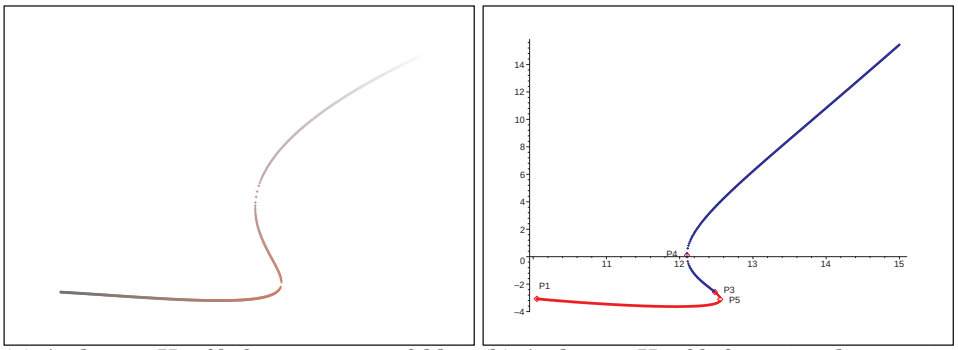

(a) Andronov-Hopf bifurcation manifold in (Y, j, P) (b) Andronov-Hopf bifurcation diagram in (j, P)

Figure B.2: Andronov-Hopf bifurcation manifold and bifurcation diagram in (j, P, Y) and (j, P). The red part corresponds to subcritical Hopf bifurcation (i.e. generating unstable limit cycles) and the blue one to supercritical Hopf bifurcations (stable limit cycles). The green curve represents the saddle node bifurcation of periodic orbits (LPC).

We compute the eigenvalues and eigenvectors using Maple's algorithm, and compute numerically the derivative of the real part of the eigenvalue at this point and the first Lyapunov exponent which is given in a closed form in function of the eigenvectors (see [167]). The points we obtain where the system undergoes an Andronov-Hopf bifurcation are plotted in figure Fig.B.2 in the space (Y, j, P) and the bifurcation diagram (j, P) together with the sub- or supercritical type.

We observe that there is no Hopf bifurcation for $j < j_{BT}$. When increasing j, a branch of subcritical Hopf bifurcations appears. When we reach the point H_2 defined by $j_{H_2} = 12.099480, P_{H_2} = 0.095382, Y_{H_2} = 4.150820$, two additional Hopf bifurcation points appear. This point H_2 is a regular Hopf bifurcation point (the Jacobian matrix has two purely imaginary eigenvalue and the dependence in the parameters is regular). After this point, when increasing further the parameter j, the system has three Hopf bifurcations, one of them beeing subcritical and the other two subcritical. We then reach a singular point GH of coordinates $j_{GH} = 12.48, P_{GH} = -2.58, Y_{GH} = 3.58$ where the first Lyapunov exponent vanishes. At this point, one of the supercritical Hopf bifurcation becomes subcritical. Finally, the two subcritical Hopf bifurcations collapse at the regular Hopf bifurcation point H_1 of coordinates $j_{H_1} = 12.55375000, P_{H_1} = -3.104094843, Y_{H_1} = 3.450451048$. For values of j greater than j_{H_1}, the system has a unique Hopf supercritical Hopf bifurcation.

Cusp bifurcation We now study the point C. At this point, the Jacobian matrix has a unique 0 eigenvalue and the cubic coefficient of Taylor's expansion in the center manifold vanishes, hence lead us to check wether if it corresponds to a cusp bifurcation.

Indeed, we have at this point first and second derivatives of the normal form vanishing and :

(C1). The cubic coefficient of the normal form in the center manifold does not vanishes (its numerical value is $c = -3.032\,10^{-2}$).

(C2). The transversality condition is satified: the dependence in the parameters and the variables is regular at this point. Indeed, in the center manifold we have check that a certain determinant does not vanishes. We change variables to be on the center manifold and compute numerically this value. We obtain the value -0.061 hence the system satisfies the transversality condition.

Bogdanov-Takens bifurcation As noticed, at the point BT, the Jacobian of the system has two 0 eigenvalues.

(BT1). condition (BT1): we compute the quadratic coefficients of Taylor's expansion in the center manifold and obtain using Kuznetsov's notations $a = 0.005342$ and $b = 0.009434$, hence at the point BT we have $ab > 0$ and $\sigma = sign(ab) = 1$.

(BT2). the transversality condition is checked by computing the determinant of the Jacobian matrix of a certain application.

Hence the point BT corresponds to a supercritical Bogdanov-Takens bifurcation (i.e. generating unstable limit cycles). Hence from this point there is a saddle-homoclinic bifurcation curve we will study further on in the global bifurcations section.

Bautin (Generalized Hopf) bifurcation As noticed, at the point GH the system undergoes an Hopf bifurcation and the first Lyapunov exponent vanishes. At this point, the second Lyapunov exponent and to check a transversality condition. Heavy but yet straightforward differential computations yield to get the second Lyapunov coefficient. We obtain $l_2 = 2.235\,10^{-3}$, and the transversality condition is checked by computing the determinant of a Jacobian matrix, and this determinant does not vanish. Hence the system undergoes a Bautin bifurcation.

Conclusion Figure Fig.B.3 summarizes the different local bifurcations we have found in our study. The black curve represents the saddle-node bifurcation curve, the red curve the subcritical Hopf bifurcations and the blue one the supercritical Hopf bifurcations. The cusp point is denoted by a C, the Bogdanov-Takens point, denoted by a BT, is at the intersection of saddle-nodes and Hopf curves and the Generalized Hopf bifurcation point is the point where subcritical Hopf bifurcations becomes supercritical.

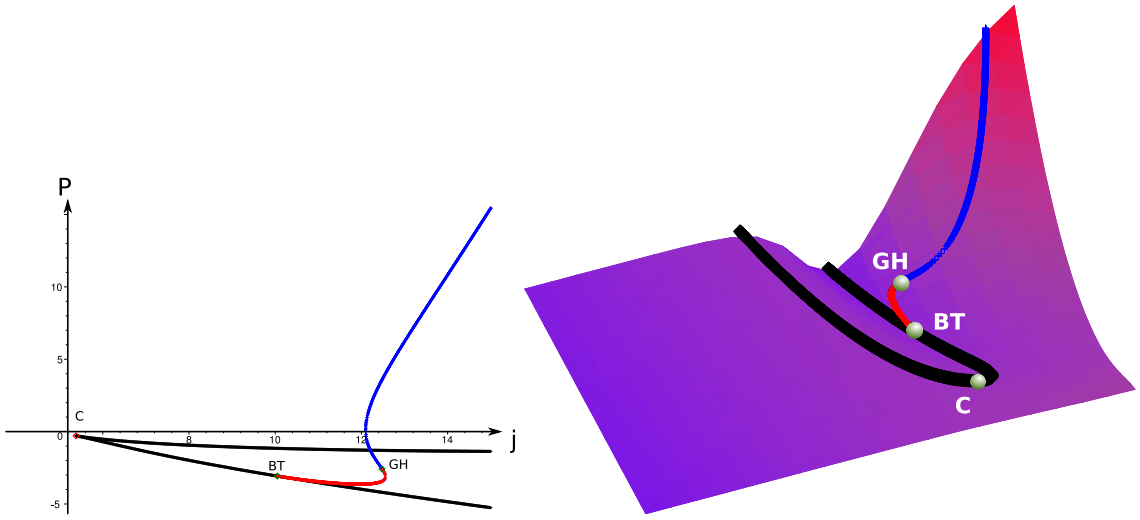

(a) Local Bifurcations

(b) Local Bifurcations 3D

Figure B.3: Full bifurcation diagram represented on the fixed points manifold (see text for the description)

APPENDIX C

A CRASH COURSE ON STOCHASTIC CALCULUS

C.1 A CRASH COURSE ON PROBABILITIES AND STOCHASTIC CALCULUS

We recall some of the basic definitions and results on stochastic processes. The aim of this section is not to be complete but to serve as a quick reference for readers with little background in stochastic calculus. Most of the proofs are omitted. The interested reader can find details in the extensive literature on the subject and follow the reading suggestions given within each section.

C.1.1 Probability Basics

This section heavily relies on Karatzas and Shreve's book [160] and on lecture notes by Jean-François Le Gall [176], where the interested reader can find all the theoretical material. We assume that the reader is familiar with elementary measure theory [232].

Probability theory is a branch of mathematics concerned with the analysis of random phenomena. The randomness is captured by the introduction of a measurable space $(\Omega, \mathscr{F})$, called the *sample space*, on which probability measures can be placed. Elements of Ω are denoted in general by ω. Subsets of Ω are called *events*. $\mathscr{F}$ is a σ-algebra of subsets of Ω.

Definition C.1.1. A probability measure $\mathbb{P}$ on $(\Omega, \mathscr{F})$ is a positive measure such that

$$\mathbb{P}(\Omega) = 1$$

. $(\Omega, \mathscr{F}, \mathbb{P})$ is called a probability space.

Definition C.1.2. A *random variable* is a measurable function from Ω to a measurable set $(X, \mathscr{X})$ called the state space.

Definition C.1.3. A *stochastic process* is a collection of random variables $X = \{X_t, t \in \mathbb{T}\}$ on $(\Omega, \mathscr{F})$ taking values in a state space $(X, \mathscr{X})$. The set $\mathbb{T}$ is called the *time set*. In the present paper, $\mathbb{T}$ is simply $\mathbb{R}^+$ and is referred to as the time of the process. The state space considered is the d-dimensional Euclidian space equiped with the σ-fields of Borel sets $(\mathbb{R}^d, \mathscr{B}(\mathbb{R}^d))$.

The temporal feature of a stochastic process suggests a flow of time, in which at every moment $t \geq 0$ we can talk about the past, present and future of the process. To quantify the *information flow* of the process, we can equip the sample space $(\Omega, \mathscr{F})$ with a *filtration*, i.e. a nondecreasing family $\{\mathscr{F}_t;\, t \geq 0\}$ of sub-σ-fields of $\mathscr{F}$:

$$\forall s \leq t;\ \ \mathscr{F}_s \subset \mathscr{F}_t \subset \mathscr{F}.$$

Given a stochastic process, the simplest choice of filtration is that generated by the process itself, i.e.,

$$\mathscr{F}_t^X := \sigma(X_s;\, 0 \leq s \leq t),$$

the smallest σ-field with respect to which X_s is measurable for every $s \in [0,t]$.

We interpret $A \in \mathscr{F}_t^X$ to mean that by time t, an observer of X knows wether or not A has occured. Hence $\mathscr{F}_t$ can be seen as the accumulated information up to time t.

A stochastic process X is said adapted to a filtration $(\mathscr{F}_t)_{t\geq 0}$ iff for all $t \geq 0$ the random variable X_t is $\mathscr{F}_t$-measurable.

A stochastic process X is said to be right-continuous (resp. left-continuous) iff almost every sample path is right- (resp. left-) continous.

Definition C.1.4 (Brownian Motion/Wiener process)**.** A standard one dimensional Brownian motion (also called a Wiener process) is a continuous adapted process $W = \{W_t, \mathscr{F}_t\, t \geq 0\}$ defined on some probability space $(\Omega, \mathscr{F}, \mathbb{P})$, with the properties that:

(BT1). $W_0 = 0$ a.s.

(BT2). for all $0 \leq s \leq t$ the increment $W_t - W_s$ is independent of $\mathscr{F}_s$ and is normally distributed with mean 0 and variance $t - s$.

Let us now imagine that we are interested in the occurence of a certain phenomenon (e.g. a spike modeled as a threshold crossing of a given process in the present paper). We are thus forced to pay a particular attention to the random instant $\tau(\omega)$ at which the phenomenon manifests at the first time. Interesting models should be such that the event $\{\omega;\, \tau(\omega) \leq t\}$ is part of the information accumulated by that time. Random variables τ satifying this property are called *stopping times*:

$$\forall t \geq 0;\ \ \{\tau \leq t\} \in \mathscr{F}_t$$

Example. For instance, the first hitting time of a continuous stochastic process X to a given deterministic boundary g defined by:

$$\tau := \inf\{t \geq 0;\ \ X_t = g(t)\}$$

is is a stopping time with respect to the natural filtration of X. Indeed, the event $\{\tau \leq t\}$ is the same as $\{\exists s \in [0,t] X_s \geq f(s)\}$. From the continuity property, this last set is equal to $\{\exists s \in [0,t] \cap \mathbb{Q},\, X_s \geq f(s)\}$ which is a coutable union of sets of $\mathscr{F}_t^X$ and hence is contained in $\mathscr{F}_t^X$.

Definition C.1.5 (Conditional Expectation)**.** Let Y be a $\mathbb{L}^1$ random variable of $(\Omega, \mathscr{F}, \mathbb{P})$ and let $\mathscr{G}$ be a sub-σ-field of $\mathscr{F}$. There exists a unique element $\mathbb{E}(Y|\mathscr{G})$ of $\mathbb{L}^1(\Omega, \mathscr{G}, \mathbb{P})$ called conditionnal expectation of Y knowing $\mathscr{G}$, such that for all X bounded and $\mathscr{G}$-measurable:

$$\mathbb{E}(XY) = \mathbb{E}(\mathbb{E}(Y|\mathscr{G})X)$$

A process $\{X_t, \mathscr{F}_t,\ t \geq 0\}$ is called a *submartingale* (resp *supermartingale, martingale*) if for every $0 \leq s < t < \infty$ we have $\mathbb{P}$-almost surely $\mathbb{E}(X_t|\mathscr{F}_s) \geq X_s$ (resp $\mathbb{E}(X_t|\mathscr{F}_s) \leq X_s$, $\mathbb{E}(X_t|\mathscr{F}_s) = X_s$).

Theorem C.1.1 (Optional Sampling Theorem)**.** *Let $\{X_t,\ \mathscr{F}_t, t \geq 0\}$ be a right-continuous submartingale, S and T be two stopping times almost surely bounded (i.e. $\mathbb{P}(T < \infty) = 1$ and $\mathbb{P}(S < \infty) = 1$). Let X_T be the random variable defined by $X_T(\omega) = X_{T(\omega)}(\omega)$. Let $\mathscr{F}_S := \{A \in \mathscr{F}\ ;\ A \cap \{T \leq t\} \in \mathscr{F}_t\}$. Assume that $S \leq T$ amost surely. Then we have:*

$$\mathbb{E}(X_T|\mathscr{F}_S) \geq X_S \ \ a.s.\ \mathbb{P}.$$

Definition C.1.6. Let X be a stochastic process on a probability space $(\Omega, \mathscr{F}, \mathbb{P})$. Let $(\mathscr{F}_t)_{t\geq 0}$ be the natural filtration of the process X. The process X is a *Markov process* iff $\forall t \leq t_1 \leq \ldots \leq t_n < \infty$, for all $\Gamma_1, \ldots, \Gamma_n \in \mathscr{X}$,

$$\mathbb{P}\Big(X_{t_1} \in \Gamma_1, \ldots, X_{t_n} \in \Gamma_n \Big| \mathscr{F}_t\Big) = \mathbb{P}\Big(X_{t_1} \in \Gamma_1, \ldots, X_{t_n} \in \Gamma_n \Big| \sigma(X_t)\Big).$$

It is strongly Markovian if for all T stopping time for the $(\mathscr{F}_t)_t$, for all $\eta_1, \ldots \eta_n$ positive random variable $\mathscr{F}_\tau$-measurable, we have:

$$\mathbb{P}\Big(X_{\tau+\eta_1} \in \Gamma_1, \ldots, X_{\tau+\eta_n} \in \Gamma_n \Big| \mathscr{F}_\tau\Big) = \mathbb{P}\Big(X_{\tau+\eta_1} \in \Gamma_1, \ldots, X_{\tau+\eta_n} \in \Gamma_n \Big| \sigma(X_\tau)\Big).$$

Proposition C.1.2. The Brownian motion is strongly Markovian

Definition C.1.7. A process $(M_t, t \geq 0)$ is a continuous local martingale iff it is a continuous adapted process such that there exists an increasing sequence of stopping times $(T_n)_{n\in\mathbb{N}}$ such that $T_n \to_{n\to\infty} \infty$ and that for each $n \in \mathbb{N}$ $(M_{t\wedge T_n} - M_0)_t$ is a uniformly integrable martingale.

Theorem C.1.3. *Let M be a local martingale. There exists a unique non-decreasing process $\langle M\rangle_t$ such that $(M_t^2 - \langle M\rangle_t)_{t\geq 0}$ is a continuous local martingale. For M and N two continuous local martingales, there exists a unique finite variation process such that $(M_t N_t - \langle M, N\rangle_t)_t$ is a local martingale. Moreover, the application $(M, N) \mapsto \langle M, N\rangle$ is bilinear symetrical.*

Theorem C.1.4 (Stochastic Integral)**.** *Let M be a continuous local martingale and H a measurable process such that for all $t > 0$, $\int_0^t H_s^2 d\langle M\rangle_s < \infty$ (the set of such processes is denoted by $\mathbb{L}^2_{loc}(M)$).*

There exists a unique continuous local martingale $H \cdot M$ starting from 0 such that for all local martingale N we have:

$$\langle H \cdot M, N\rangle = H \cdot \langle M, N\rangle$$

This martingale is denoted $(H \cdot M)_t =: \int_0^t H_s dM_s$ and is called the stochastic integral of H with respect to the local martingale M.

Moreover, we have for all $t > 0$ and $0 =: t_0^n < t_1^n < \ldots < t_{p_n}^n := t$ sequence of nested mesh whose step tends to 0, we have in the sense of probability:

$$\int_0^t H_s dM_s = \lim_{n\to\infty} \sum_{i=1}^{p_n} H_{t_{i-1}^n}(X_{t_i^n} - X_{t_{i-1}^n})$$

Theorem C.1.5 (Itô formula)**.** *Let $X = (X^1, \dots, X^n)$ be n continuous semi-martingales and $F : \mathbb{R}^n \mapsto \mathbb{R}$ a C^2 map. Then we have:*

$$F(X_t) = F(X_0) + \sum_{j=1}^{n} \int_0^t \frac{\partial F}{\partial x^j}(X_s) dX_s^j + \frac{1}{2} \sum_{j=1}^{n} \sum_{k=1}^{n} \int_0^t \frac{\partial^2 F}{\partial x^j \partial x^k}(X_s) d\langle X^j, X^k \rangle_s$$

Theorem C.1.6 (Dubins-Schwarz)**.** *Let M be a continuous local martingale such that $\langle M \rangle_\infty = \infty$ a.s. Then there exists a Brownian motion B such that*

$$M_t = B_{\langle M \rangle_t}$$

Theorem C.1.7 (Girsanov)**.** *Assume that $\mathbb{Q} \sim \mathbb{P}$ on $\mathscr{F}$. Let $D_t = \frac{d\mathbb{Q}}{d\mathbb{P}}\Big|_t$ and L be the unique local martingale such that $D = exp(L - \frac{1}{2}\langle L \rangle)$. Then for all M $\mathbb{P}$-local martingale continuous, the process $M - \langle M, L \rangle$ is a $\mathbb{Q}$-local martingale continuous.*

In particular if M is a $\mathbb{P}$-Brownian motion, then $M - \langle M, L \rangle$ is a $\mathbb{Q}$-Brownian motion.

Definition C.1.8 (Stochastic Differential Equation)**.** Let B be a d-dimensional Brownian motion, $\sigma : \mathbb{R}_+ \times \mathbb{R}^d \mapsto \mathbb{R}^{d \times m}$ and $b : \mathbb{R}_+ \times \mathbb{R}^d \mapsto \mathbb{R}^d$ two measurable locally bounded functions. The Stochastic Differential Equation (SDE) associated to σ and b is defined by:

$$dX_t = \sigma(t, X_t)\, dB_t + b(t, X_t)\, dt$$

This expression is a notation and means:

$$X_t = X_0 + \int_0^t \sigma(s, X_s)\, dB_s + \int_0^t b(s, X_s)\, ds$$

Under suitable conditions on the coefficients σ and b (for instance if both are continuous and (locally) Lipschitz), we have existence and (pathwise) uniqueness of a solution. In the Lipschitz case, then the solution is strongly Markovian.

C.1.2 Stochastic processes and Partial Differential Equations

The aim of this section is to show the link between some functionals of a diffusion process X and PDEs. For more details on diffusion processes we refer to the excellent book of Bass [17]. Interested readers are also refered to [140, 247]. The diffusion process studied here satisfies the equation:

$$dX_t = b(X_t)dt + \sigma(X_t)dB_t \tag{C.1}$$

where $B := ((B_t^{(i)})_{t \geq 0})_{i=1,\dots,d}$ is a d-dimensionnal Brownian motion. This process (X) is called a multi-dimensional *diffusion process*.

We assume that b and σ are bounded and at least $\mathscr{C}^1$. We define $\mathscr{L}$ to be the diffusion operator associated to the diffusion process (C.1)

$$\mathscr{L} f(x) := \frac{1}{2} \sum_{i,j=1}^{d} a_{ij}(x) \frac{\partial^2}{\partial x_i \partial x_j} f(x) + (b(x) \cdot \nabla) f(x) \tag{C.2}$$

where $a(x) = (a_{ij}(x))_{i,j} \in \mathscr{M}_d$ is the symmetrical matrix defined by $a(x) = \sigma(x)\sigma^T(x)$.

Let us now define a real function q, called potential, in reference with Schrödinger's theory.

We consider the operator, called *Schrödinger's operator*, defined by:

$$\mathscr{G}u(x) := \mathscr{L}u(x) + q(x)u(x) \tag{C.3}$$

We have the

Theorem C.1.8. *Let D be a smooth bounded domain, q a $\mathscr{C}^2$ function on $\bar{D}$, f a continuous function on ∂D. Let τ_D be the first hitting time of the border ∂D of D by the process X :*

$$\tau_D := \inf\{t > 0; X_t \in \partial D\} = \inf\{t > 0; X_t \in \partial D\}$$

Let u be the solution of the PDE equation with Dirichlet condition :

$$\begin{cases} \mathscr{L}u(x) + q(x)u(x) = 0 & \forall x \in D \\ u(x) = f(x) & \forall x \in \partial D \end{cases} \tag{C.4}$$

If q is such that :

$$\mathbb{E}_x\left[e^{\int_0^{\tau_D} q^+(X_s)ds}\right] < \infty \tag{C.5}$$

where $q^+(x) := max(q(x), 0)$, then u, solution of (C.4)*, can be written:*

$$u(x) = \mathbb{E}_x\left[f(X_{\tau_D})e^{\int_0^{\tau_D} q(X_s)ds}\right] \tag{C.6}$$

We provide the proof of this theorem because it is simple and because it is a good example of the use of the notions we introduced in section C.1.1.

Proof. Let $Y_t := \int_0^t q(X_s)ds$ and consider the stochastic process $e^{Y_t}u(X_t)$. Itô's formula gives the following expression for this process:

$$\begin{aligned} e^{Y_t}u(X_t) &= u(X_0) + \int_0^t e^{Y_s}u(X_s)dY_s + M_t + \int_0^t e^{Y_s}\mathscr{L}u(X_s)ds \\ &= u(X_0) + M_t + \int_0^t e^{Y_s}(\mathscr{L}u(X_s) + q(X_s)u(X_s))ds \\ &= u(X_0) + M_t + \int_0^t e^{Y_s}\mathscr{G}u(X_s)ds \end{aligned} \tag{C.7}$$

$$\tag{C.8}$$

where M_t denotes an associated local martingale:

$$M_t = \sum_{i=1}^{d}\int_0^t e^{Y_s}b_i(X_s)\frac{\partial u}{\partial x_i}(X_s)ds$$

Let us stop the process under consideration at the stopping time τ_D. Let $S_n := \inf\{t; \text{dist}(X_t, \partial D) < 1/n\}$. We clearly have $S_n \underset{n\to\infty}{\nearrow} \tau_D$. Then since $u \in \mathscr{C}^2(\bar{D})$ we have the property that $M_{t\wedge S_n}$ is a martingale for all $n \in \mathbb{N}$. Let us take the expectation and apply the optimal stopping theorem to (C.7). Stopping the process at time S_n ensures us that $\mathscr{G}u(X_s)$ is 0 because X_s is always inside the domain D. We then have

$$e^{Y_{t\wedge S_n}}u(X_{t\wedge S_n}) = u(X_0) + M_{t\wedge S_n} \quad \text{, and taking the expectation}$$
$$\mathbb{E}_x\left[e^{Y_{t\wedge S_n}}u(X_{t\wedge S_n})\right] = u(x)$$

Finally, letting $n \to \infty$ and using Lebesgue's theorem (the function u is bounded inside the domain D and the hypothesis (C.5) ensures us to have a $\mathbb{L}^1$ bound) we get :

$$\mathbb{E}_x \left[e^{Y_{t\wedge\tau_D}} u(X_{t\wedge\tau_D}) \right] = u(x) \quad \forall t > 0$$

We can conclude letting $t \to \infty$, since the expectation converges by Lebesgue's theorem. □

There is also an interesting connection between the Laplace transform and the diffusion operator associated to a one-dimensional diffusion process. Let $X = (X_t;\, t > 0)$ be a one-dimensional diffusion process given by the equation :

$$dX_t = b(X_t)dt + \sigma(X_t)dB_t \tag{C.9}$$

where $B = (B_t)_{t\geq 0}$ is a standard one-dimensional Brownian motion.

Let $\tau_a(X)$ be the first passage-time of X to the fixed barrier a and let $u_\lambda(x)$ be the Laplace transform of $\tau_a(X)$ conditionally on the fact that $X_0 = x$.

$$\tau_a(X) := \inf\{t > 0; X_t = a\}$$

$$u_\lambda(x) := \mathbb{E}_x \left[e^{-\lambda \tau_a(X)} \right] \quad , \lambda \geq 0 \tag{C.10}$$

Theorem C.1.9. *Assume that $x < a$. The Laplace transform $u_\lambda(x)$ is solution of the following PDE together with limit conditions :*

$$\begin{cases} \mathscr{L} u_\lambda(x) - \lambda u_\lambda(x) = 0 \\ u_\lambda(a) = 1 \\ \lim\limits_{x\to-\infty} u_\lambda(x) = 0 \end{cases} \tag{C.11}$$

Remark 14. The case $x > a$ can be treated in the same way with only a few changes as stated in the beginning of the section.

Theorem C.1.10. *The Laplace transform of the hitting time of a diffusion with generator $\mathscr{L}$ can be written:*

$$\mathbb{E}_x \left[e^{-\lambda \tau_a(X)} \right] = \frac{\Psi_\lambda(x)}{\Psi_\lambda(a)} \tag{C.12}$$

where $\Psi_\lambda(\cdot)$ is proportional to the unique increasing positive solution of

$$\mathscr{L}\Psi_\lambda = \lambda \Psi_\lambda$$

(i.e. the eigenfunction of the diffusion operator $\mathscr{L}$ associated to the eigenvalue λ).

Let us now consider section a one-dimensional diffusion process $X = (X_t;\, t > 0)$ given by the equation :

$$X_t = b(X_t)dt + \sigma(X_t)dB_t \tag{C.13}$$

where $B = (B_t)_{t\geq 0}$ is a standard one-dimensional Brownian motion.

Let $a(t)$ be the boundary, and $\tau_a(X)$ the first passage time of X to the boundary.

We denote $u_\lambda(x)$ be the Laplace transform of $\tau_a(X)$ conditionally on the fact that $X_0 = x$.

$$\tau_a(X) := \inf\{t > 0; X_t = a(t)\}$$

$$u_\lambda(x) := \mathbb{E}_x\left[e^{-\lambda\tau_a(X)}\right] \quad , \lambda \geq 0 \tag{C.14}$$

Theorem C.1.11. *Assume that $x < a(0)$. Then the Laplace transform $u_\lambda(x) = v_\lambda(0,x)$ where $v_\lambda(t,x)$ is solution of the following PDE together with limit conditions :*

$$\begin{cases} \partial_t v_\lambda(t,x) + \mathscr{L} v_\lambda(t,x) - \lambda v_\lambda(t,x) = 0 \\ v_\lambda(t,a(t)) = 1 \\ \lim\limits_{x\to-\infty} v_\lambda(t,x) = 0 \end{cases} \tag{C.15}$$

Proof. The proof of the necessary condition, i.e. assuming that a regular solution ($C^{1,2}$), the proof is very similar to the one of theorem C.1.9.

To prove this theorem we only have to use Itô's formula to the (assumed) $C^{1,2}$ function $e^{-\lambda t}v(t,X_t)$. The local martingale will be a real martingale (it is necessary to bound the process X also to get a martingale, as we did in the last proof), and the optimal stopping theorem will apply and we will eventually get:

$$\mathbb{E}_x\left[e^{-\lambda\tau_a(X)}\right] = v_\lambda(0,x)$$

□

In the present paper we also use several times the Fokker-Planck partial differential equation. This equation which governs the transition probability density of a given process can be deduced straightforwardly form the previous theory.

Theorem C.1.12 (Fokker-Planck equation)**.** *Let X be a diffusion process solution of the stochastic differential equation:*

$$dX_t = b(X_t)\,dt + \sigma(X_t)\,dW_t. \tag{C.16}$$

Under suitable conditions on b and σ, the process X is uniquely defined by (C.16)*, strongly Markovian with stationnaty increments. Its transition function is:*

$$P(t,x,\Gamma) := \mathbb{P}\left(X_{t+s} \in \Gamma \middle| X_s = x\right)$$

We assume that this probability has a density with respect to Lebesgue's measure $P(t,x,\Gamma) = \int_\Gamma p(t,x,y)\,dy$ and that this density satisfies regularity conditions on $\frac{\partial p}{\partial t}$, $\frac{\partial p}{\partial x^i}$ and $\frac{\partial^2 p}{\partial x^i \partial x^j}$. In this case, the transition density probability is the fundamental solution (Green's function) of the equation:

$$\frac{\partial p(t,x,y)}{\partial t} = \frac{1}{2}\sum_{i,j} a^d_{i,j=1}(x)\frac{\partial^2 p(t,x,y)}{\partial x^i \partial x^j} + \sum_{j=1}^{d} b_j(x)\frac{\partial p(t,x,y)}{\partial x^j}. \tag{C.17}$$

i.e. $\frac{\partial p(t,x,y)}{\partial t} = \mathscr{L}_x p(t,x,y)$. This equation is called forward Kolmogorov equation.

Under regularity conditions on $\frac{\partial p}{\partial t}$, $\frac{\partial p}{\partial y^i}$ *and* $\frac{\partial^2 p}{\partial y^i \partial y^j}$, *the transition probability density is the fundamental solution (Green's function) of the backward Kolmogorov equation, or* Fokker-Planck equation*:*

$$\frac{\partial p}{\partial t} = \frac{1}{2} \sum_{i,j=1}^{d} \frac{\partial^2 a_i, j(y) p(t,x,y)}{\partial y^i \partial y^j} - \sum_{j=1}^{d} \frac{\partial b^i(y) p(t,x,y)}{\partial y^i} \tag{C.18}$$

or:

$$\frac{\partial p(t,x,y)}{\partial t} = \mathscr{L}_y^* p(t,x,y)$$

.

Part VI

General Appendix

APPENDIX D

CAUCHY PROBLEM

The Cauchy problem consists in proving that there exists a unique solution to the problem (3.1) and (3.2) defined for all $t \in \mathbb{R}$ for a given initial condition (v_0, w_0) at time t_0. It was adressed by Romain Brette in [33] in the case of spiking models defined by a one dimensional ODE with a finite spiking threshold and a reset condition. He found that the reset introduced a countable and ordered set of backward solutions for a given initial condition, and this that this structure of solutions had important implications in terms of neural coding.

The case of the system given by (3.1) and (3.2) is slightly more complex, but can be treated in the same fashion as done in [33]. We have seen in section 3.2.6 that there exists a unique solution to the forward problem. Therefore in this appendix we are interested only in the backward solutions. The backward problem of equations (3.1) and (3.2) with initial conditions (v_0, w_0) at time t_0 corresponds to the forward solutions $v_b(t) = v(t_0 - t)$ and $w_b(t) = w(t_0 - t)$. of the system:

$$\begin{cases} \frac{\mathrm{d}v_b}{\mathrm{d}t} = -F(v) + w - I \\ \frac{\mathrm{d}w_b}{\mathrm{d}t} = -a(bv - w) \\ v_b(0) = v_0 \\ w_b(0) = w_0 \end{cases} \tag{D.1}$$

The nullclines for this system are the same as the nullclines of the forward problem, but the direction of the vector field changes. A new issue appears here: the membrane potential can may to $-\infty$ in finite time. In this case, the solution is not admissible. In the case of the adaptive exponential model, the backward membrane potential and the backward adaptation value will never blow up in finite time. Therefore, this solution is always an admissible solution. But in the case of the quartic model for instance, the membrane potential will always blow up in finite time when the backward solution do not cross the v-nullcline, and such solutions will exist, for instance in the case where there is no fixed point: in the proof of theorem 3.3.1, we show that there exist a spiking solution for which the backward solution tends to infinity. For initial conditions of the backward problem below this orbit, because of Gronwall's theorem, the membrane potential will tend to $-\infty$ in finite time.

- If the backward solution does not blow up in finite time and does not cross the line $\{v_b = v_r\}$, then the solution of the backward equation is unique, and there exists a unique solution of the problem which is defined on $\mathbb{R}$.
- If the backward membrane potential blows up at time t_1 and its orbit does not intersect the line $\{v_b = v_r\}$ there is no solution to the Cauchy problem for $t \leq t_1$.

- If the backward orbit intersects the line $\{v_b = v_r\}$ then the problem splits in two solutions, one of which corresponding to a reset, and the other corresponding to the solution of the system (D.1). The branch of solution corresponding to a regular subthreshold backward problem is treated as described above. For the solution corresponding to a reset, we check if the value of the membrane potential at this point is inside the image of the Poincaré application. If it is the case, the admissible solutions correspond to the different reciprocal images of this value under Φ. There can exist two possible values: one that is inferior or equal to w^* and another one greater than w^*, and these two possible points are on the same orbit (the orbit starting above w^* crosses the line $v = v_r$ at the point below w^*). To avoid the difficulty or resetting at an infinite value of the membrane potential, we directly jump to the reciprocal image of this point by Φ, and compute the same way the possible branches of backward solutions.

Interestingly, in the case of the exponential model, since the backward solutions do not blow up in finite time, the backward solution is always an admissible solution. Therefore, we have a countable number of backward solution in this case.

In the case of the quartic model, the number admissible solutions is smaller. Indeed, the reciprocal images of Φ decrease, and when they are below the spiking trajectory diverging when $v \to -\infty$, the backward equation blows up in finite time. Therefore the only admissible solution is a spiking solution. Figure D.1 illustrates the construction of a backward solution and of the Cauchy problem. From a given initial condition (v_0, w_0), if the backward solution never crosses the reset line $\{v = v_r\}$ there is only one admissible solution provided it does not blow up in finite time. If the backward solution crosses the reset line (star (1) and (2) of figure D.1), the solution splits into two solutions, one of which corresponds to a spike when it exists (star (1)) and the other one corresponding to the regular solution of the backward equation (for star (2) no spiking solution correspond to the related adaptation value). Below the bold line corresponding to a diverging solution of the backward equation, in the case of models such as the quartic one, the only admissible solution is a spiking solution (star (3)).

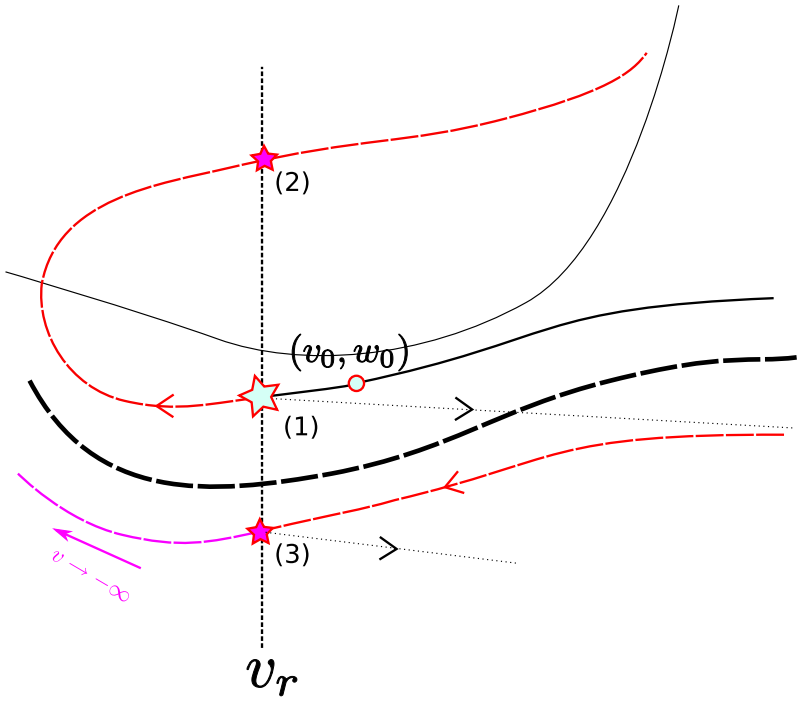

Figure D.1: Construction of the backward set of solutions. Description in the text.

APPENDIX **E**

MEAN FIELD ANALYSIS

E.1 THE RESOLVENT

In this appendix we introduce and give some useful properties of the resolvent Φ_L of a homogeneous differential equation

$$\frac{\mathrm{d}x}{\mathrm{d}t} = \mathbf{L}(t)x(t) \quad x(t_0) = x_0 \in \mathbb{R}^P, \tag{E.1}$$

where $\mathbf{L} : [t_0, T] \to \mathscr{M}_{P\times P}$ (or $(-\infty, T] \to \mathscr{M}_{P\times P}$) is C^0.

Definition E.1.1. The resolvent of (E.1) is defined as the unique solution of the linear equation:

$$\begin{cases} \frac{\mathrm{d}\Phi_L(t,t_0)}{\mathrm{d}t} & = \mathbf{L}(t)\Phi_L(t,t_0) \\ \Phi_L(t_0,t_0) & = \mathrm{Id}_P \end{cases} \tag{E.2}$$

where Id_P is the $P \times P$ identity matrix.

Proposition E.1.1. The resolvent satisfies the following properties:

(i). $\Phi_L(t+s,t_0) = \Phi_L(t+s,t) \cdot \Phi_L(t,t_0)$

(ii). $\Phi_L(t,t_0)$ is invertible of inverse $\Phi_L(t_0,t)$ which satisfies:

$$\begin{cases} \frac{\mathrm{d}\Phi_L(t_0,t)}{\mathrm{d}t} & = -\Phi_L(t_0,t)\mathbf{L}(t) \\ \Phi_L(t_0,t_0) & = \mathrm{Id}_{P\times P} \end{cases} \tag{E.3}$$

(iii). Let $\|\ \|$ be a norm on $\mathscr{M}_{P\times P}$ and assume that $\|\mathbf{L}(t)\| \leq k_L$ on $[t_0, T]$. Then we have:

$$\|\Phi_L(t,t_0)\| \leq e^{k_L|t-t_0|} \quad \forall t \in [t_0, T] \tag{E.4}$$

Similarly, if $\left\|\mathbf{L}^T(t)\right\| \leq k_{L^T}$ on $[t_0, T]$ we have:

$$\left\|\Phi_L^T(t,t_0)\right\| \leq e^{k_{L^T}|t-t_0|} \quad \forall t \in [t_0, T] \tag{E.5}$$

(iv). We have

$$\det\Phi_L(t,t_0) = \exp \int_{t_0}^{t} \mathrm{Tr}\mathbf{L}(s)\, ds$$

Proof. The properties (i) and (ii) are directly linked with the property of group of the flow of a reversible ODE. (iii) is an application of Gronwald's lemma. (iv) is obtained by a first order Taylor series expansion. □

We also need in the article a lower bound on $\|\Phi_L(t,t_0)\|$ for all $t \in [t_0,T]$ in the general case where $\mathbf{L}$ is not constant. This can be achieved for example using Floquet's theory. Consider the interval $[t_0, 2T-t_0]$ and define the continuous periodic function $\widetilde{\mathbf{L}}(t)$ of period $2(T-t_0)$ defined by

$$\widetilde{\mathbf{L}}(t) = \begin{cases} \mathbf{L}(t) & t_0 \le t \le T \\ \mathbf{L}(2T-t) & T \le t \le 2T-t_0 \end{cases}$$

The corresponding resolvent $\Phi_{\tilde{L}}(t,t_0)$ is equal to $\Phi_L(t,t_0)$ for $t_0 \le t \le T$. $\Phi_{\tilde{L}}(2T-t_0,t_0)$ is invertible and hence there exists $a \in \mathbb{R}$ such that

$$e^{2a(T-t_0)} < |\lambda|$$

for all eigenvalues λ of $\Phi_{\tilde{L}}(2T-t_0,t_0)$. One of Floquet's theorems states that there exists a norm on $\mathbb{R}^P$ and $\gamma > 0$ such that

$$\gamma e^{a(t-t_0)} < \|\Phi_{\tilde{L}}(t,t_0)\| \quad t \ge t_0,$$

and in particular

$$\gamma e^{a(t-t_0)} < \|\Phi_L(t,t_0)\| \quad t_0 \le t \le T \tag{E.6}$$

Theorem E.1.2 (Solution of an inhomogeneous linear SDE)**.** *The solution of the inhomogeneous linear Stochastic Differential Equation:*

$$\begin{cases} dX_t &= (\mathbf{L}(t)X(t) + \mathbf{I}(t))\,dt + \Lambda(s)d\mathbf{W}_s \\ X_{t_0} &= X_0 \end{cases} \tag{E.7}$$

can be written using the resolvent:

$$X_t = \Phi_L(t,t_0)X_0 + \int_{t_0}^t \Phi_L(t,s)\mathbf{I}(s)\,ds + \int_{t_0}^t \Phi_L(s,t)\Lambda(s)d\mathbf{W}_s \tag{E.8}$$

Proof. Pathwise (strong) uniqueness of solution directly comes from the results on the SDE with Lipschitz coefficients (see e.g. [161, Theorem 2.5 of Chapter 5]). It is clear that $X_{t_0} = X_0$. We use Itô's formula for the product of two stochastic processes to prove that the process (E.8) is solution of equation (E.7):

$$\begin{aligned} dX_t &= \left(\mathbf{L}(t)\Phi_L(t,t_0)X_0 + \Phi_L(t,t)\mathbf{I}(t) + \int_{t_0}^t \mathbf{L}(t)\Phi_L(t,s)\mathbf{I}(s)\,ds\right)dt \\ &\quad + \Phi_L(t,t)\Lambda(t)d\mathbf{W}_t + \int_{t_0}^t \mathbf{L}(t)\Phi_L(s,t)\Lambda(s)d\mathbf{W}_s\,dt \\ &= \left(\mathbf{L}(t)\left[\Phi_L(t,t_0)X_0 + \int_{t_0}^t \Phi_L(s,t)I(s)\,ds + \int_{t_0}^t \Phi_L(s,t)\Lambda(s)d\mathbf{W}_s\right] + \mathbf{I}(t)\right)dt \\ &\quad + \Lambda(t)d\mathbf{W}_t \\ &= (\mathbf{L}(t)X(t) + \mathbf{I}(t))\,dt + \Lambda(t)d\mathbf{W}_t \end{aligned}$$

Hence the theorem is proved. □

E.2 MATRIX NORMS

In this section we recall some definitions on matrix and vector norms. Let $\mathscr{M}_{n\times n}$ be the set of $n\times n$ real matrices. It is a vector space of dimension n^2 and the usual L^p norms $1 \leq p \leq \infty$ can be defined. Given $\mathbf{L} \in \mathscr{M}_{n\times n}$, we note $\|\mathbf{L}\|_p^v$ the corresponding norm. Given a vector norm, noted $\|\ \|$, on $\mathbb{R}^n$ the induced norm, noted $\|\ \|$, on $\mathscr{M}_{n\times n}$ is defined as

$$\|\mathbf{L}\| = \sup_{x\in\mathbb{R}^n,\, \|x\|\leq 1} \frac{\|\mathbf{L}x\|}{\|x\|}$$

Since $\mathscr{M}_{n\times n}$ is finite dimensional all norms are equivalent. In this article we use the following norms

(i). $\|\mathbf{L}\|_\infty = \max_i \sum_{j=1}^n |L_{ij}|$.

(ii). $\|\mathbf{L}\|_\infty^v = \max_{i,j} |L_{ij}|$

(iii). $\|\mathbf{L}\|_2 = \sup_{x\in\mathbb{R}^n,\, \|x\|_2\leq 1} \frac{\|\mathbf{L}x\|_2}{\|x\|_2}$. This so-called *spectral* norm is equal to the square root of the largest singular value of $\mathbf{L}$ which is the largest eigenvalue of the positive matrix $\mathbf{L}^T\mathbf{L}$. If $\mathbf{L}$ is positive definite this is its largest eigenvalue which is also called its spectral radius, noted $\rho(\mathbf{L})$.

APPENDIX **F**

PUBLICATIONS

Journal Papers

1. *Jonathan Touboul, Romain Brette* **Spiking dynamics of bidimensional integrate-and-fire neurons** , 2008, *(in preparation)*
2. *Jonathan Touboul* **Sensitivity to the cutoff value in the quadratic adaptive integrate-and-fire model**, 2008 *(submitted)*
3. *Olivier Faugeras, Jonathan Touboul and Bruno Cessac* **A constructive mean field analysis of multi population neural networks with random synaptic weights and stochastic inputs**, 2008 (submitted)
4. *Jonathan Touboul, Romain Brette* **Dynamics and bifurcations of the adaptive exponential integrate-and-fire model**, 2008, Biological Cybernetics (accepted)
5. *Jonathan Touboul, Olivier Faugeras* **First hitting times of Double Integral Process to curved boundaries.** Advances in Applied Probability, vol. 40, number 2, pp 501–528
6. *Jonathan Touboul* **Bifurcation analysis of a general class of non-linear integrate and fire neurons.** SIAM Applied Math, 2008, vol.68, number 4, pp.1045–1079
7. *Jonathan Touboul, Olivier Faugeras* **The statistics of spikes trains: a stochastic calculus approach.** (2007) Journal of Physiology, Paris vol. 101 number 1–3, pp. 78-98.

Preprints

8. *Jonathan Touboul, Romain Brette, Olivier Faugeras* **An event based description of stochastic neural networks**
9. *Jonathan Touboul, Olivier Faugeras* **Codimension two bifurcations and rhythms in neural mass models**.
10. *Jonathan Touboul, Bruno Cessac* **Symbolic dynamics of a discrete time neuronal network with random synaptic weights.**

Talks

11. **A constructive approach for multipopulation Mean-Field equations**, invited for the 4th computational neuroscience day, Gif sur Yvette, April 2008

12. **The statistics of spikes trains: a stochastic calculus approach.** *Seminar Probability and Biology, Universtity Pierre et Marie Curie (Paris VI)*, December 2007.

13. **Nonlinear neuron models and their bifurcations**, (LCN, EPFL, Lausanne: invited by Wulfram Gerstner for the weekly seminar of the group, October 2007)

14. **Stochastic and Nonlinear approaches of neuronal activity**, *East Coast summer tour, July 2007!* (NYU, Courant Institute, Columbia, NJIT, Princeton seminars)

15. **Nonlinear neuron models and their bifurcations**, presented at the Workshop on Biomathematics and Dynamical Systems (CIRM, june 2007) and at the Nonlinear Physics school (Peyresq 2007)

16. **Statistics of spike train: the point of view of the continuous stochastic calculus**, First Computational Neuroscience Day, Gif-Sur-Yvette (January 2007).

17. *Olivier Faugeras, Theodore Papadopoulo, Jonathan Touboul, Denis Talay, Etienne Tanre and Mireille Bossy*, **The statistics of spike trains for some simple types of neuron models**, NeuroComp Conference (Pont-à-Mousson, 2006)

Posters

18. *Jonathan Touboul, Romain Brette* **Dynamics and chaos in bidimensional nonlinear integrate-and-fire neurons**, presented at the workshop Chas and Dynamics in Biological Networks (Cargese 2008)

19. *Jonathan Touboul, Olivier Faugeras, Olivier Rochel*, **Event-driven mathematical framework for noisy integrate-and-fire neuron networks** CNS 2007 (Toronto)

20. *Jonathan Touboul, Romain Brette* **Dynamics of noisy inhibitory networks of integrate-and-fire neurons: a stochastic network theory approach**, NeuroMath 2006 (Andorra)

Miscellaneous:

Popularization Papers

21. *Jonathan Touboul* **Nombres premiers et cryptologie : l'algorithme RSA**, (Dec. 2007) published in)i(nterstice

Patents

22. *Jonathan Touboul (inventor), Pierre Sabatier (owned by Sagem Inc)* **"Dispositif pour detecter des yeux rouges sur une image et dispositif d'impression d'image mettant en oeuvre ce procédé"**: French patent number FR0550181 (publication number FR2880969)) (published 2006-07-21 (BOPI 2006-29)).

23. *Jonathan Touboul (inventor), Pierre Sabatier (owned by Sagem Inc)* : **"Procdé pour détecter des yeux rouges basé sur détection d'une zone de peau" (Red eyes detection process based on skin detection)** : European patent EP06300026 (publication number EP1684210) (published 2006-07-26 (Bulletin 2006-30))

Research Reports

24. *Jonathan Touboul* **Controllability of parabolic and hyperbolic partial differential equations, and of their finite difference approximations, with respect to the shape of the domain** (2007), arXiv:0705.4221v1

Bibliography

[1] LF Abbott and C. van Vreeswijk. Asynchronous states in networks of pulse-coupled oscillators. *Physical Review E*, 48(2):1483–1490, 1993.

[2] L.F Abbott and C.A. Van Vreeswijk. Asynchronous states in networks of pulse-coupled neuron. *Phys. Rev*, 48:1483–1490, 1993.

[3] Milton Abramowitz and Irene A. Stegun. *Handbook of mathematical functions*. Dover, 1970.

[4] L. Alili, P. Patie, and J. L. Pedersen. Representations of the first hitting time density of an ornstein-uhlenbeck process. *Stochastic Models*, 21:967–980, 2005.

[5] A. Alonso and R. Klink. Differential electroresponsiveness of stellate and pyramidal-like cells of medial entorhinal cortex layer II. *Journal of Neurophysiology*, 70:128–143, 1993.

[6] A. Alonso and R. Llinás. Subthreshold Na+-dependent theta-like rhythmicity in stellate cells of entorhinal cortex layer II. *Nature*, 342:175–177, 1989.

[7] S. Amari. Characteristics of random nets of analog neuron-like elements. *Syst. Man Cybernet. SMC-2*, 1972.

[8] Shun-Ichi Amari, Kiyonori Yoshida, and Ken-Ichi Kanatani. A mathematical foundation for statistical neurodynamics. *Siam J. Appl. Math.*, 33(1):95–126, 1977.

[9] A. Ames. CNS energy metabolism as related to function. *Brain Research Reviews*, 34(1-2):42–68, 2000.

[10] R Amir, M. Michaelis, and M. Devor. Membrane potential oscillations in dorsal root ganglion neurons: Role in normal electrogenesis and neuropathic pain. *The Journal of Neuroscience*, 19:8589–8596, 1999.

[11] R. S. Anderssen, F. R. De Hood, and R. Weiss. On the numerical solution of brownian motion processes. *Journal of Applied Probability*, 10:409–418, 1973.

[12] Elaine Angelino and Michael P Brenner. Excitability constraints on voltage-gated sodium channels. *PLoS Comput Biol*, 3(9):e177, Sep 2007.

[13] Arbib. *The Handbook of Brain Theory and Neural Networks*. MIT Press, 1998.

[14] C.M. Armstrong and B. Hille. Voltage-Gated Ion Channels and Electrical Excitability. *Neuron(Cambridge, Mass.)*, 20(3):371–380, 1998.

[15] Soren Asmussen and Tatyana S. Turova. Stationarity properties of neural networks. *Journal of Applied Probabilities*, 35:783–794, 1998.

[16] Laurent Badel, Sandrine Lefort, Romain Brette, Carl C. H. Petersen, Wulfram Gerstner, and Magnus J. E. Richardson. Dynamic i-v curves are reliable predictors of naturalistic pyramidal-neuron voltage traces. *Journal of Neurophysiology*, 99:656–66, feb 2008. PMID: 18057107 doi: 01107.2007.

[17] Richard F. Bass. *Diffusions and Elliptic Operators*. Springer, 1998.

[18] G. Ben Arous. Aging and spin-glass dynamics. *Proceedings of the International Congress of Mathematicians*, 3:3–14, 2002.

[19] G. BEN AROUS, A. DEMBO, and A. GUIONNET. Aging of spherical spin glasses. *Probability theory and related fields*, 120(1):1–67, 2001.

[20] G Ben-Arous and A. Guionnet. Large deviations for Langevin spin glass dynamics. *Probability Theory and Related Fields*, 102(4):455–509, 1995.

[21] G. Ben-Arous and A. Guionnet. Symmetric Langevin Spin Glass Dynamics. *The Annals of Probability*, 25(3):1367–1422, 1997.

[22] L.S. Bernardo and R.E. Foster. Oscillatory behavior in inferior olive neurons: mechanism, modulation, cell agregates. *Brain research Bulletin*, 17:773–784, 1986.

[23] Patrick Billingsley. *Convergence of Probability Measures*. Wiley series in probability and statistics, 1999.

[24] L. Block, J. Guckenheimer, M. Misiurewicz, and L.S. Young. Periodic points and topological entropy of one dimensional maps. *Global theory of dynamical systems, Proc. int. Conf., Evanston/Ill.*, 1979.

[25] V.I. Bogachev. *Gaussian Measures*. American Mathematical Society, 1998.

[26] A.A. Borovkov. *Ergodicity and stability of stochastic processes*. Wiley, Chichester, 1998.

[27] K. Borovkov and Alexander Novikov. Explicit bounds for approximation rates for boundary crossing probabilities for the wiener process. *Journal of Applied Probability*, 42:82–92, 2005.

[28] Valentino Braitenberg and Almut Schüz. *Cortex: Statistics and Geometry of Neuronal Connectivity*. Springer, 2nd edition, 1998.

[29] L. Breiman. First exit times from a square root boundary. *Fifth Berkeley Symposium*, 2:9–16, 1967.

[30] R. Brette and W. Gerstner. Adaptive exponential integrate-and-fire model as an effective description of neuronal activity. *Journal of Neurophysiology*, 94:3637–3642, 2005.

[31] R. Brette, M. Rudolph, T. Carnevale, M. Hines, D. Beeman, J. M. Bower, M. Diesmann, A. Morrison, P. H. Goodman, F. C. Harris Jr., M. Zirpe, T. Natschläger, D. Pecevski, B. Ermentrout, M. Djurfeldt, A. Lansner, O. Rochel,

T. Vieville, E. Muller, A. P. Davison, S. El Boustani, and A. Destexhe. Simulation of networks of spiking neurons: a review of tools and strategies. *Journal of Computational Neuroscience*, 23(3):349–398, 2007.

[32] Romain Brette. Dynamics of one-dimensional spiking neuron models. *Journal of Mathematical Biology*, 48:38–56, 2004.

[33] Romain Brette. The cauchy problem for one-dimensional spiking neuron models. *Cognitive Neurodynamics*, 2(1):21–27, 2007.

[34] K. Brodmann. *Vergleichende Lokalisationslehre der Grobhirnrinde*. J.A.Barth, Leipzig, 1909.

[35] N. Brunel. Dynamics of sparsely connected networks of excitatory and inhibitory spiking neurons. *Journal of Computational Neuroscience*, 8:183–208, 2000.

[36] N. Brunel and V. Hakim. Fast global oscillations in networks of integrate-and-fire neurons with low firing rates. *Neural Computation*, 11:1621–1671, 1999.

[37] N Brunel and P Latham. Firing rate of noisy quadratic integrate-and-fire neurons. *Neural Computation*, 15:2281–2306, 2003.

[38] Nicolas Brunel and Simone Sergi. Firing frequency of leaky integrate and fire neurons with synaptic current dynamics. *J. Theor. Biol.*, 195(87–95), 1998.

[39] H. Brunner and PJ van der Houwen. *The Numerical Solution of Volterra Equations*. Amsterdam, 1986.

[40] HL Bryant and JP Segundo. Spike initiation by transmembrane current: a white-noise analysis. *The Journal of Physiology*, 260(2):279–314, 1976.

[41] Guido Bugmann, Chris Christodoulou, and John G. Taylor. Role of temporal integration and fluctuation detection in the highly irregular firing of a leaky integrator neuron model with partial reset. *Neural Computation*, 9(5):985–1000, 1997.

[42] A. Buonocore, A. G. Nobile, and L. M. Ricciardi. A new integral equation for the evaluation of first-passage-time probability densities. *Advances in Applied Probability*, 19(4):784–800, December 1987.

[43] B. Delisle Burns and A. C. Webb. The spontaneous activity of neurones in the cat's cerebral cortex. *Proceedings of the Royal Society of London. Series B, Biological Sciences*, 194:211–223, 1976.

[44] D.P. Buxhoeveden and M.F. Casanova. The minicolumn hypothesis in neuroscience. *Brain*, 125:935–951, 2002.

[45] WH Calvin and CF Stevens. Synaptic noise and other sources of randomness in motoneuron interspike intervals. *Journal of Neurophysiology*, 31(4):574–587, 1968.

[46] B. Cessac. Increase in complexity in random neural networks. *Journal de Physique I (France)*, 5:409–432, 1995.

[47] B. Cessac and M. Samuelides. From neuron to neural networks dynamics. *EPJ Special topics: Topics in Dynamical Neural Networks*, 142(1):7–88, 2007.

[48] Anton V. Chizhov and Lyle J. Graham. Population model of hippocampal pyramidal neurons, linking to refractory density approach to conductance-based neurons. *Phys. rev. E*, 75(011924):114, 2007.

[49] P. Chossat and R. Lauterbach. *Methods in Equivariant Bifurcations and Dynamical Systems*. World Scientific Publishing Company, 2000.

[50] C.C. Chow and J.A. White. Spontaneous action potentials due to channel fluctuations. *Biophysical Journal*, 71:3013–3021, 1996.

[51] C. Clopath, R. Jolivet, A. Rauch, H.R. Lüscher, and W. Gerstner. Predicting neuronal activity with simple models of the threshold type: Adaptive Exponential Integrate-and-Fire model with two compartments. *Neurocomputing*, 70(10-12):1668–1673, 2007.

[52] KS Cole. Membranes, Ions and Impulses. *A Chapter of Classical Biophysics*, 1, 1968.

[53] K.S. Cole and H.J. Curtis. Electric impedance of nerve and muscle. *Cold Spring Harbor symposia on quantitative biology, Cold Spring Harbor, Long Island Biological Association*, 4(73), 1936.

[54] K.S. Cole and H.J. Curtis. Electric impedance of the squid giant axon during activity. *The Journal of General Physiology*, 22(5):649–670, 1939.

[55] M. Cottrell. Mathematical analysis of a neural network with inhibitory coupling. *Stochastic Processes and their Applications*, 40:103–127, 1992.

[56] M. Cottrell and T.S. Turova. Use of an hourglass model in neuronal coding. *Journal of applied probability*, 37:168–186, 2000.

[57] A. Crisanti, HJ. Sommers, and H. Sompolinsky. chaos in neural networks : chaotic solutions. 1990.

[58] A. Crisanti and H. Sompolinsky. Dynamics of spin systems with randomly asymmetric bonds: Langevin dynamics and a spherical model. *Physical Review A*, 36(10):4922–4939, 1987.

[59] A. Crisanti and H. Sompolinsky. Dynamics of spin systems with randomly asymmetric bounds: Ising spins and glauber dynamics. *Phys. Review A*, 37(12):4865, 1987.

[60] J. G. Dai. On positive harris recurrence of multiclass queueing networks: A unified approach via fluid limit models. *The Annals of Applied Probability*, 5:49–77, 1995.

[61] J. G. Dai. A fluid limit model criterion for instability of multiclass queueing networks. *Annals of Applied Probability*, 6:751–757, 1996.

[62] JG Dai and SP Meyer. Stability and convergence of moments for multiclass queuing networks via fluid limits models. *IEEE trans. on automatic control*, 40:1889–1904, 1995.

[63] Henry E. Daniels. Approximating the first crossing-time density for a curved boundary. *Bernoulli*, 2:133–143, 1996.

[64] Olivier David, Diego Cosmelli, and Karl J. Friston. Evaluation of different measures of functional connectivity using a neural mass model. *NeuroImage*, 21:659–673, 2004.

[65] Olivier David and Karl J. Friston. A neural mass model for meg/eeg: coupling and neuronal dynamics. *NeuroImage*, 20:1743–1755, 2003.

[66] M.H.A. Davis. Piecewise-deterministic markov processes: A general class of non-diffusion stochastic models. *Journal of the Royal Society, Series B (Methodological)*, 46:353–388, 1984.

[67] P. Dayan and L. F. Abbott. *Theoretical Neuroscience : Computational and Mathematical Modeling of Neural Systems*. MIT Press, 2001.

[68] Alain Destexhe, Zachary F. Mainen, and Terrence J. Sejnowski. *Methods in Neuronal Modeling*, chapter Kinetic models of synaptic transmission, pages 1–25. In Koch and Segev [165], 1998.

[69] Alain Destexhe and Denis Paré. Impact of network activity on the integrative properties of neocortical pyramidal neurons in vivo. *Journal of Neurophysiology*, 81:1531–1547, 1999.

[70] R.L. Devaney. *An Introduction to Chaotic Dynamical Systems*. Westview Press, 2003.

[71] A. Dhooge, W. Govaerts, and Y.A. Kuznetsov. Numerical Continuation of Fold Bifurcations of Limit Cycles in MATCONT. *Proceedings of the ICCS*, pages 701–710, 2003.

[72] A. Dhooge, W. Govaerts, and Yu. A. Kuznetsov. Matcont: A matlab package for numerical bifurcation analysis of odes. *ACM Trans. Math. Softw.*, 29(2):141–164, 2003.

[73] E. Di Nardo, A. G. Nobile, E. Pirozzi, and L. M. Ricciardi. A computational approach to first passage time problems for Gauss-Markov processes. *Advances in Applied Probability*, 33:453–482, 2001.

[74] Jean Dieudonné. *Éléments d'analyse - Tome I : Fondements de l'analyse moderne*. Gauthier-Villars, 1963.

[75] J.L. Doob. Heuristic approach to the kolmogorov-smirnov theorems. *Ann. Math. Statist.*, 20:393–403, 1949.

[76] J. Durbin. The first-passage-density of a continuous Gaussian process to a general boundary. *J. Appl. Prob.*, 22:99–122, 1985. Correction in volume 25 (1988), 840.

[77] J. Durbin. The first-passage density of the Brownian motion process to a curved boundary. *J. Appl. Prob.*, 29:291–304, 1992.

[78] J. Durbin and D. Williams. The first-passage density of the brownian motion process to a curved boundary. *Journal of applied probability*, 29(2):291–304, 1992.

[79] B. Ermentrout. *Simulating, Analyzing, and Animating Dynamical Systems: A Guide to XPPAUT for Researchers and Students*. Society for Industrial Mathematics, 2002.

[80] B. Ermentrout, M. Pascal, and B. Gutkin. The effects of spike frequency adaptation and negative feedback on the synchronization of neural oscillators. *Neural Comput*, 13(6):1285–1310, Jun 2001.

[81] Bard Ermentrout. Neural networks as spatio-temporal pattern-forming systems. *Reports on Progress in Physics*, 61:353–430, 1998.

[82] G B Ermentrout and N Kopell. Parabolic bursting in an excitable system coupled with a slow oscillation. *SIAM J. Appl. Math.*, 46(2):233–253, 1986.

[83] Y. Etzion and Y. Grossman. Potassium currents modulation of calcium spike firing in dendrites of cerebellar Purkinje cells. *Experimental Brain Research*, 122(3):283–294, 1998.

[84] L.C. Evans. *Partial Differential Equations*, volume 19 of *Graduate Studies in Mathematics*. Proceedings of the American Mathematical Society, 1998.

[85] O. Faugeras, F. Grimbert, and J.-J. Slotine. Abolute stability and complete synchronization in a class of neural fields models. 61(1):205–250, sep 2008.

[86] Olivier Faugeras, Theo Papadopoulo, Jonathan Touboul, Etienne Tanré, Mireille Bossy, and Denis Talay. The statistics of spikes trains for some simple types of neuron models. In *1ère conférence francophone de Neurosciences Computationelles*, 2006.

[87] Olivier Faugeras, Romain Veltz, and François Grimbert. Persistent neural states: stationary localized activity patterns in nonlinear continuous n-population, q-dimensional neural networks. Technical report, INRIA, 2007.

[88] L. Favella, M.T. Reineri, L.M. Ricciardi, and L. Sacerdote. First passage time problems and related computational methods. *Cybernetics and Systems*, 13:95–128, 1982.

[89] G. Fayolle, V.A. Malyshev, and MV Menshikov. *Topics in the Constructive Theory of Countable Markov Chains*. Cambridge University Press, 1995.

[90] B. Ferebee. The tangent approximation to one-sided brownian exit densities. *Probability Theory and Related Fields*, 61(3):309–326, 1982.

[91] U. Feudel, A. Neiman, X. Pei, W. Wojtenek, H. Braun, M. Huber, and F. Moss. Homoclinic bifurcation in a Hodgkin–Huxley model of thermally sensitive neurons. *Chaos: An Interdisciplinary Journal of Nonlinear Science*, 10:231, 2000.

[92] R. FitzHugh. *Mathematical models of excitation and propagation in nerve*, chapter 1.

[93] R. Fitzhugh. Theoretical Effect of Temperature on Threshold in the Hodgkin-Huxley Nerve Model. *The Journal of General Physiology*, 49(5):989–1005, 1966.

[94] Nicolas Fourcaud and Nicolas Brunel. Dynamics of the firing probability of noisy integrate-and-fire neurons. *Neural Computation*, 14:2057–2110, 2002.

[95] N. Fourcaud-Trocme, D. Hansel, C. van Vreeswijk, and N. Brunel. How Spike Generation Mechanisms Determine the Neuronal Response to Fluctuating Inputs. *Journal of Neuroscience*, 23(37):11628, 2003.

[96] W.J. Freeman. The Electrical Activity of a Primary Sensory Cortex: Analysis of EEG waves. *International Reviews of Neurobiology*, 5(10):53–119, 1963.

[97] WJ Freeman. Patterns of variation in waveform of averaged evoked potentials from prepyriform cortex of cats. *Journal of Neurophysiology*, 31(1):1–13, 1968.

[98] WJ Freeman. A model of the olfactory system. *Neural Modeling*, pages 41–62, 1973.

[99] W.J. Freeman. Mass action in the nervous system. *Academic Press, New York*, 1975.

[100] W.J. Freeman. Simulation of chaotic eeg patterns with a dynamic model of the olfactory system. *Biological Cybernetics*, 56:139–150, 1987.

[101] Christine Fricker, Philippe Robert, Ellen Saada, and Danielle Tibi. Analysis of some networks with interaction. *Annals of Applied Probability*, 4:1112–1128, 1994.

[102] EJ Furshpan and DD Potter. Transmission at the giant motor synapses of the crayfish. *The Journal of Physiology*, 145(2):289, 1959.

[103] Georges L. Gerstein and Benoit Mandelbrot. Random walk models for the spike activity of a single neuron. *Biophysical Journal*, 4:41–68, 1964.

[104] W. Gerstner. Time structure of the activity in neural network models. *Physical Review E*, 51(1):738–758, 1995.

[105] W. Gerstner and W. Kistler. *Spiking Neuron Models*. Cambridge University Press, 2002.

[106] W. Gerstner and W. M. Kistler. Mathematical formulations of hebbian learning. *Biological Cybernetics*, 87:404–415, 2002.

[107] M.T. Giraudo, L. Sacerdote, and C. Zucca. A monte-carlo method for the simulation of first passage time diffusion processes. *Methodology and computing in applied probability*, 3:215–231, 2001.

[108] E. Gobet. Weak approximation of killed diffusion using Euler schemes. *Stochastic Processes and their Applications*, 87(2):167–197, 2000.

[109] D.E. Goldman. Potential, Impedance, and Rectification in Membranes. *The Journal of General Physiology*, 27(1):37–60, 1943.

[110] Malcolm Goldman. On the first passage of the integrated Wiener process. *Ann. Mat. Statist.*, 42:2150–2155, 1971.

[111] M. Golubitsky, I. Stewart, and D.G. Schaeffer. *Singularities and Groups in Bifurcation Theory*. Springer, 1988.

[112] D Goodman and R Brette. Brian: a simulator for spiking neural networks in python. *Frontiers in Neuroinformatics (in preparation)*, 2008.

[113] F. Grimbert. *Mesoscopic models of cortical structures*. PhD thesis, University of Nice Sophia-Antipolis, feb 2008.

[114] F. Grimbert and O. Faugeras. Bifurcation analysis of Jansen's neural mass model. *Neural Computation*, 18(12):3052–3068, December 2006.

[115] F. Grimbert, O. Faugeras, and F. Chavane. From neural fields to VSD optical imaging. In Holmes et al. [131]. Cette référence est inexacte, elle l'apparaît pas dans les proceedings de la conférence.

[116] Piet Groeneboom. Brownian motion with parabolic drift and airy functions. *Probability Theory and Related Fields*, 81:79–109, 1989.

[117] T. H. Gronwall. Note on the derivative with respect to a parameter of the solutions of a system of differential equations. *Annals of Mathematics*, 20:292–296, 1919.

[118] J. Guckenheimer and P. J. Holmes. *Nonlinear Oscillations, Dynamical Systems and Bifurcations of Vector Fields*, volume 42 of *Applied mathematical sciences*. Springer, 1983.

[119] J. Guckenheimer and M. Myers. Computing Hopf bifurcations II: Three examples from neurophysiology. *SIAM J. Sci. Comput*, 17(6):1275–1301, 1996.

[120] J. Guckenheimer, M. Myers, and B. Sturmfels. Computing Hopf Bifurcations I. *SIAM J. Num. Anal.*, 33, 1996.

[121] J. Guckenheimer and R.A. Oliva. Chaos in the hodgkin–huxley model. *SIAM Journal on Applied Dynamical Systems*, 1:105, 2002.

[122] A. Guionnet. Averaged and quenched propagation of chaos for spin glass dynamics. *Probability Theory and Related Fields*, 109(2):183–215, 1997.

[123] B. Gutkin, B. Ermentrout, and A. Reyes. Phase-response curves give the responses of neurons to transient inputs. *J Neurophysiol*, 94(2):1623–1635, Aug 2005.

[124] B. Hille. *Ion channels of excitable membranes*. Sinauer Sunderland, Mass, 2001.

[125] H.Kielhöfer. *Bifurcation Theory: An Introduction with Applications to PDEs*. Springer, 2003.

[126] AL Hodgkin. The local electric changes associated with repetitive action in a non-medullated axon. *The Journal of Physiology*, 107(2):165, 1948.

[127] A.L. Hodgkin and A.F. Huxley. Action potentials recorded from inside a nerve fibre. *Nature*, 144:710–711, 1939.

[128] A.L. Hodgkin and A.F. Huxley. A quantitative description of membrane current and its application to conduction and excitation in nerve. *Journal of Physiology*, 117:500–544, 1952.

[129] AL Hodgkin and B. Katz. The effect of sodium ions on the electrical activity of the giant axon of the squid. *The Journal of Physiology*, 108(1):37, 1949.

[130] A.V. Holden. Models of the Stochastic Activity of Neurones. *Lecture Notes in Biomathematics*, 12:1–368, 1976.

[131] W. R. Holmes, R. Jung, and F. Skinner, editors. volume 8, Suppl 2 of *BMC Neuroscience*, jul 2007.

[132] J. J. Hopfield. Neurons with graded response have collective computational properties like those of two-state neurons. *Proceedings of the National Academy of Sciences, USA*, 81(10):3088–3092, 1984.

[133] F. Hoppensteadt and E.M. Izhikevich. *Weakly connected neural networks*. Springer-Verlag New York, Inc., 1997.

[134] A. Houghton, S. Jain, and A. P. Young. Role of initial conditions in the mean-field theory of spin-glass dynamics. *Phys. Rev. B*, 28(5):2630–2637, Sep 1983.

[135] J. Hounsgaard and J. Midtgaard. Synaptic control of excitability in turtle cerebellar Purkinje cells. *The Journal of Physiology*, 409:157, 1989.

[136] DH Hubel and TN Wiesel. Shape and arrangement of columns in cat's striate cortex. *The Journal of Physiology*, 165(3):559, 1963.

[137] D.H. Hubel and T.N. Wiesel. Receptive fields and functional architecture in two nonstriate visual areas (18 and 19) of the cat. *Journal of Neurophysiology*, 28:229–289, 1965.

[138] AF Huxley and R. Stämpfli. Evidence for saltatory conduction in peripheral myelinated nerve fibres. *The Journal of Physiology*, 108(3):315, 1949.

[139] Gérard Ioos and Moritz Adelmeyer. *Topics in Bifurcation Theory and Applications*. Advanced Series in Nonlinear Dynamics. World Scientific, 2nd edition, 1999.

[140] Kiyosi Ito and Henry P. MacKean. *Diffusion processes and their sample paths*. Springer, 1996.

[141] E. Izhikevich. Simple model of spiking neurons. *IEEE Transactions on Neural Networks*, 14(6):1569–1572, 2003.

[142] E.M. Izhikevich. Neural excitability, spiking, and bursting. *International Journal of Bifurcation and Chaos*, 10:1171–1266, 2000.

[143] E.M. Izhikevich. Resonance and selective communication via bursts in neurons having subthreshold oscillations. *BioSystems*, 67(1-3):95–102, 2002.

[144] E.M. Izhikevich. Which model to use for cortical spiking neurons? *IEEE Trans Neural Netw*, 15(5):1063–1070, September 2004.

[145] E.M. Izhikevich. *Dynamical Systems in Neuroscience: The Geometry of Excitability And Bursting*. MIT Press, 2007.

[146] Eugene M. Izhikevich. *Dynamical Systems in Neuroscience: The Geometry of Excitability and Bursting*. The MIT Press, 2006. To appear.

[147] Eugene M Izhikevich and Gerald M Edelman. Large-scale model of mammalian thalamocortical systems. *Proc Natl Acad Sci U S A*, 105(9):3593–3598, Mar 2008.

[148] J.J.B. Jack, D. Noble, and R.W. Tsien. *Electric Current Flow in Excitable Cells*. Oxford University Press, USA, 1975.

[149] Ben H. Jansen and Vincent G. Rit. Electroencephalogram and visual evoked potential generation in a mathematical model of coupled cortical columns. *Biological Cybernetics*, 73:357–366, 1995.

[150] Ben H. Jansen, George Zouridakis, and Michael E. Brandt. A neurophysiologically-based mathematical model of flash visual evoked potentials. *Biological Cybernetics*, 68:275–283, 1993.

[151] JG Jefferys and MA Whittington. Review of the role of inhibitory neurons in chronic epileptic foci induced by intracerebral tetanus toxin. *Epilepsy Res*, 26(1):59–66, 1996.

[152] C. Jennen and H.R. Lerche. First exit densities of brownian motion through one-sided moving boundaries. *Probability Theory and Related Fields*, 55(2):133–148, 1981.

[153] C. Jennen and HR Lerche. Asymptotic densities of stopping times associated with tests of power one. *Probability Theory and Related Fields*, 61(4):501–511, 1982.

[154] D. Johnston and S.M. Wu. *Foundations of cellular neurophysiology*. MIT Press Cambridge, Mass, 1995.

[155] R. Jolivet, R. Kobayashi, A. Rauch, R. Naud, S. Shinomoto, and W. Gerstner. A benchmark test for a quantitative assessment of simple neuron models. *Journal of Neuroscience Methods*, 169(2):417–424, 2008.

[156] E.G. Jones and A. Peters, editors. *Cerebral cortex, functional properties of cortical cells*, volume 2. Plenum, New York, 1984.

[157] RSG Jones. Synaptic and intrinsic properties of neurones of origin of the perforant path in layer II of the rat entorhinal cortex in vitro. *Hippocampus '*, 4:335–353, 1994.

[158] E.R. Kandel, J.H. Schwartz, and T.M. Jessel. *Principles of Neural Science*. McGraw-Hill, 4th edition, 2000.

[159] P. Kara, P. Reinagel, and R. C. Reid. Low response variability in simultaneously recorded retinal, thalamic, and cortical neurons. *Neuron*, 27(3):635–646, 2000. Poisson, retina, spike variability.

[160] I. Karatzas and S. Shreve. *Brownian motion and stochatic calculus*. Springer, 1987.

[161] Ioannis Karatzas and Steven E. Shreve. *Brownian motion and stochastic calculus*, volume 113 of *Graduate Texts in Mathematics*. Springer-Verlag, New York, second edition, 1991.

[162] Peter Kloeden and Eckhard Platen. *Numerical solution of stochastic differential equations*. Springer-Verlag, 1992.

[163] B. W. Knight. Dynamics of encoding in a population of neurons. *J. Gen. Physiol.*, 59:734–766, 1972.

[164] C. Koch. *Biophysics of Computation: Information Processing in Single Neurons*. Oxford University Press: New York, New York., 1999.

[165] C. Koch and I. Segev, editors. *Methods in Neuronal Modeling: From Ions to Networks*. The MIT Press, 1998.

[166] M. Kubicek. Algorithm for Evaluation of Complex Bifurcation Points in Ordinary Differential Equations. *SIAM Journal on Applied Mathematics*, 38(1):103–107, 1980.

[167] Yuri A. Kuznetsov. *Elements of Applied Bifurcation Theory*. Applied Mathematical Sciences. Springer, 2nd edition, 1998.

[168] A. Lachal. Sur la distribution de certaines fonctionnelles de l'intégrale du mouvement brownien avec dérives parabolique et cubique. *Communications on Pure and Applied Mathematics*, 49:1299–1338, 1996.

[169] Aimé Lachal. Sur le premier instant de passage de l'intégrale du mouvement brownien. *Annales de l'IHP, section B*, 27:385–405, 1991.

[170] Aimé Lachal. Les temps de passages successifs de l'intégrale du mouvement brownien. *Ann. I. H. P. Sect. B*, 33:1–36, 1997.

[171] L Lapicque. Recherches quantitatifs sur l'excitation des nerfs traitee comme une polarisation. *J. Physiol. Paris*, 9:620–635, 1907.

[172] L. Lapicque. L'excitabilite en fonction du temps. *Presses Universitaires de France, Paris*, 1926.

[173] G. Last and H. Stamer. Recurrence and transience properties of some neural networks: an approach via fluid limit models. *Queueing Systems*, 32:99–130, 1999.

[174] P.E. Latham, B.J. Richmond, P.G. Nelson, and S. Nirenberg. Intrinsic dynamics in neuronal networks. I. Theory. *J. Neurophysiol.*, 83:828–835, 2000.

[175] P.E. Latham, B.J. Richmond, P.G. Nelson, and S. Nirenberg. Intrinsic dynamics in neuronal networks. II. Experiment. *J. Neurophysiol.*, 83:808–827, 2000.

[176] Jean-François Le Gall. Mouvement Brownien et Calcul Stochastique. Lecture notes, January 1997.

[177] N.N. Lebedev. *Special functions and their applications*. Dover publications, 1972.

[178] Mario Lefebvre. First-passage densities of a two-dimensional process. *SIAM Journal on Applied Mathematics*, 49:1514–1523, 1989.

[179] H.R. Lerche. *Boundary crossing of Brownian motion*. Springer-Verlag, 1986.

[180] T.Y. Li and J. Yorke. Period three implies chaos. *American Mathematical Monthly*, 82:985–992, 1975.

[181] R.S. Lillie. Factors affecting transmission and recovery in the passive iron nerve model. *The Journal of General Physiology*, 7(4):473–507, 1925.

[182] Peter Linz. *Analytical and Numerical Methods for Volterra Equations*. SIAM studies in applied mathematics, 1985.

[183] C. Liu, M. Michaelis, R. Amir, and M. Devor. Spinal nerve injury enhances subthreshold membrane potential oscillations in drg neurons: Relation to neuropathic pain. *Journal of Neurophysiology*, 84:205–215, 2000.

[184] R. Llinás. The intrinsic electrophysiological properties of mammalian neurons: insights into central nervous system function. *Science*, 242:1654–1664, 1988.

[185] R. Llinas and M. Sugimori. Electrophysiological properties of in vitro Purkinje cell somata in mammalian cerebellar slices. *The Journal of Physiology*, 305(1):171–195, 1980.

[186] R Llinás and Y Yarom. Electrophysiology of mammalian inferior olivary neurones in vitro. different types of voltage-dependent ionic conductances. *J Physiol.*, 315:549–567., 1981.

[187] R Llinás and Y. Yarom. Oscillatory properties of guinea-pig inferior olivary neurones and their pharmacological modulation: an in vitro study. *Journal of physiology*, 376:163–182, 1986.

[188] RR Llinas, AA Grace, and Y. Yarom. In vitro neurons in mammalian cortical layer 4 exhibit intrinsic oscillatory activity in the 10-to 50-hz frequency range. *Proceedings of the National Academy of Sciences*, 88(3):897–901, 1991.

[189] F.H. Lopes da Silva, A. Hoeks, and L.H. Zetterberg. Model of brain rhythmic activity. *Kybernetik*, 15:27–37, 1974.

[190] F.H. Lopes da Silva, A. van Rotterdam, P. Barts, E. van Heusden, and W. Burr. Model of neuronal populations. the basic mechanism of rhythmicity. *M.A. Corner, D.F. Swaab (eds) Progress in brain research, Elsevier, Amsterdam*, 45:281–308, 1976.

[191] VA Malyshev. Networks and dynamical systems. *Advances in applied probability*, 25(1):140–175, 1993.

[192] V.A. Malyshev and M.V. Menshikov. Ergodicity, continuity, and analyticity of countable markov chains. *Trans. Moscow Math. Soc.*, 1:1–47, 1981.

[193] Y. Mandelblat, Y. Etzion, Y. Grossman, and D. Golomb. Period Doubling of Calcium Spike Firing in a Model of a Purkinje Cell Dendrite. *Journal of Computational Neuroscience*, 11(1):43–62, 2001.

[194] H. Markram, M. Toledo-Rodriguez, Y. Wang, A. Gupta, G. Silberberg, and C. Wu. Interneurons of the neocortical inhibitory system. *Nature Reviews Neuroscience*, 5:793–804, 2004.

[195] P. Marsalek, C. Koch, and J. Maunsell. On the relationship between synaptic input and spike output jitter in individual neurons. *PNAS*, 94:735–740, 1997.

[196] M. Mattia and P. Del Giudice. Population dynamics of interacting spiking neurons. *Physical Review E*, 66(5):51917, 2002.

[197] H. P. McKean. A winding problem for a resonator driven by a white noise. *J. Math. Kyoto Univ.*, 2:227–235, 1963.

[198] L. Molgedey, J. Schuchardt, and H.G. Schuster. Supressing chaos in neural networks by noise. *Physical Review Letters*, 69(26):3717–3719, 1992.

[199] V.B. Mountcastle. Modality and topographic properties of single neurons of cat's somatosensory cortex. *Journal of Neurophysiology*, 20:408–434, 1957.

[200] V.B. Mountcastle. The columnar organization of the neocortex. *Brain*, 120:701–722, 1997.

[201] O. Moynot and M. Samuelides. Large deviations and mean-field theory for asymmetric random recurrent neural networks. *Probability Theory and Related Fields*, 123(1):41–75, 2002.

[202] J.D. Murray. *Mathematical Biology*. Springer, 2003.

[203] R Naud, N Macille, C Clopath, and W Gerstner. Firing patterns in the adaptive exponential integrate-and-fire model. *Biological Cybernetics*, 99(4–5):335–347, nov 2008.

[204] R Naud, N Macille, C Clopath, and W Gerstner. Firing patterns in the adaptive exponential integrate-and-fire model. *Biological Cybernetics (submitted)*, 2008.

[205] E.A. Newman. Glial cell inhibition of neurons by release of ATP. *J Neurosci*, 23(5):1659–1666, 2003.

[206] Harald Niederreiter. *Random number generation and quasi-Monte Carlo methods*. Society for Industrial and Applied Mathematics, 1992.

[207] A. G. Nobile, L. M. Ricciardi, and L. Sacerdote. Exponential trends of first-passage-time densities for a class of diffusion processes with steady-state distribution. *Journal of Applied Probability*, 22:611–618, 1985.

[208] A. G. Nobile, L. M. Ricciardi, and L. Sacerdote. Exponential trends of ornstein-uhlenbeck first-passage-time densities. *Journal of Applied Probability*, 22:360–369, 1985.

[209] John Nolte. *The Human Brain*. Mosby, 5th edition, 2001.

[210] Alex Novikov, Volf Frishling, and Nino Kordzakhia. Approximations of boundary crossing probabilities for a brownian motion. *Journal of Applied Probability*, 36:1019–1030, 1999.

[211] C. Park and FJ Schuurmann. Evaluations of barrier-crossing probabilities of wiener paths. *J. Appl. Probab*, 13(267-275), 1976.

[212] WJ Park. The law of the iterated logarithm for brownian sheets. *J. Appl. Probability*, 12(4):840–844, 1975.

[213] Pierre Patie. *On some first passage time problem motivated by financial applications*. PhD thesis, ETH Zurich, 2004.

[214] A. Peters and E.G. Jones, editors. *Cerebral cortex, cellular components of the cerebral cortex*, volume 1. Plenum, New York, 1984.

[215] H. E. Plesser. *Aspects of signal processing in noisy neurons*. PhD thesis, Georg-August-Universität, 1999.

[216] D. Pollard. *Empirical Processes: Theory and Applications*. Ims, 1990.

[217] Klaus Pötzelberger and Liqun Wang. Boundary crossing probability for brownian motion. *Journal of Applied Probability*, 38:152–164, 2001.

[218] Dale Purves, George J. Augustine, David Fitzpatrick, Lawrence C. Katz, Anthony-Samuel LaMantia, James O. McNamara, and S. Mark Williams. *Neuroscience*. Sinauer Associates, Inc., 2nd edition, 2001.

[219] S. Ramon y Cajal. *A new concept of the histology of the central nervous system*, pages 7—29.

[220] s. Ramon y Cajal. *The stucture and connexions of neurons*, pages 220–253.

[221] D.S. Reich, J.D. Victor, and B.W. Knight. The power ratio and the interval map: Spiking models and extracellular recordings. *Journal of Neuroscience*, 18(23):10090, 1998.

[222] Jan Reutimann, Michele Giugliano, and Stefano Fusi. Event-driven simulation of spiking neurons with stochastic dynamics. *Neural Computation*, 15:811–830, 2003.

[223] L.M. Ricciardi, L. Sacerdote, and S. Sato. On an integral equation for first passage time probability density function. *Journal of Applied Probability*, 21:302–314, 1984.

[224] Luigi M. Ricciardi and Shunsuke Sato. First-passage time density and moments of the ornstein-uhlenbeck process. *Journal of Applied Probability*, 25(1):43–57, March 1988.

[225] J. Rinzel and B. Ermentrout. *Analysis of neural excitability and oscillations*. MIT Press, 1989.

[226] J. Rinzel and R.N. Miller. Numerical calculation of stable and unstable periodic solutions to the Hodgkin-Huxley equations. *Math. Biosci*, 49:27–59, 1980.

[227] Brian D. Ripley. *Stochastic simulation*. John Wiley and Sons, Inc., 1987.

[228] O. Rochel. *Une approche événementielle pour la modélisation et la simulation de neurones impulsionnels*. PhD thesis, Université Henri Poincaré - Nancy 1, 2004.

[229] O. Rochel and D. Martinez. An event-driven framework for the simulation of networks of spiking neurons. In *Proc. 11th European Symposium on Artificial Neural Networks*, pages 295–300, 2003.

[230] A. Ronveaux, editor. *Heun's Differential Equations*. Oxford University Press, 1995.

[231] A. Roxin, N. Brunel, and D. Hansel. Role of Delays in Shaping Spatiotemporal Dynamics of Neuronal Activity in Large Networks. *Physical Review Letters*, 94(23):238103, 2005.

[232] W. Rudin. *Principles of Mathematical Analysis. 3rd ed.* International Series in Pure and Applied Mathematics. McGraw-Hill, 1976.

[233] M. Samuelides and B. Cessac. Random recurrent neural networks. *European Physical Journal - Special Topics*, 142:7–88, 2007.

[234] M. Shadlen and W. Newsome. The variable discharge of cortical neurons: Implications for connectivity. *J. Neurosci*, 18:3870–3896, 1998.

[235] M. N. Shadlen and W. T. Newsome. Noise, neural codes and cortical organization. *Curr Opin Neurobiol*, 4(4):569–579, August 1994.

[236] L.P. Shilnikov. *Methods of Qualitative Theory in Nonlinear Dynamics*. World Scientific, 2001.

[237] A.J.F. Siegert. On the first passage time probability problem. *Physical Review*, 81:617–623, 1951.

[238] D. Siegmund and Y.S. Yuh. Brownian approximations to first passage probabilities. *Probability Theory and Related Fields*, 59(2):239–248, 1982.

[239] William R. Softky and Christof Koch. The highly irregular firing of cortical cells is inconsistent with temporal integration of random epsps. *Journal of Neuroscience*, 13:334–350, 1993.

[240] H. Sompolinsky, A. Crisanti, and HJ Sommers. Chaos in Random Neural Networks. *Physical Review Letters*, 61(3):259–262, 1988.

[241] H. Sompolinsky and A. Zippelius. Relaxational dynamics of the Edwards-Anderson model and the mean-field theory of spin-glasses. *Physical Review B*, 25(11):6860–6875, 1982.

[242] R. B. Stein. A theoretical analysis of neuronal variability. *Biophysics Journal*, 5:173–194, 1965.

[243] R. B. Stein. Some models of neuronal variability. *Biophysical Journal*, 7:37–68, 1967.

[244] RB Stein. The Frequency of Nerve Action Potentials Generated by Applied Currents. *Proceedings of the Royal Society of London. Series B, Biological Sciences (1934-1990)*, 167(1006):64–86, 1967.

[245] J. Stoer and R. Bulirsch. *Introduction to Numerical Analysis*. Springer-Verlag, 1972.

[246] S.H. Strogatz. *Nonlinear dynamics and chaos*. Addison-Wesley Reading, MA, 1994.

[247] Daniel W. Stroock and S.R.S. Varadhan. *Multidimensional diffusion processes*. Springer, 1979.

[248] P. Suffczynski, S. Kalitzin, G. Pfurtscheller, and FH Lopes da Silva. Computational model of thalamo-cortical networks: dynamical control of alpha rhythms in relation to focal attention. *International Journal of Psychophysiology*, 43(1):25–40, 2001.

[249] P. Suffczynski, FH Lopes da Silva, J. Parra, DN Velis, BM Bouwman, CM van Rijn, P. van Hese, P. Boon, H. Khosravani, M. Derchansky, et al. Dynamics of Epileptic Phenomena Determined From Statistics of Ictal Transitions. *Biomedical Engineering, IEEE Transactions on*, 53(3):524–532, 2006.

[250] I. Tasaki. The Electro-Saltatory Transmission of the Nerve Impulse and the Effect of Narcosis upoon the Nerve Fiber. *American Journal of Physiology*, 127(2):211–227, 1939.

[251] I. Tasaki and T. Takeuchi. Der am Ranvierschen Knoten entstehende Aktionsstrom und seine Bedeutung für die Erregungsleitung. *Pflügers Archiv European Journal of Physiology*, 244(6):696–711, 1941.

[252] I. Tasaki and T. Takeuchi. Weitere Studien über den Aktionsstrom der markhaltigen Nervenfaser und über die elektrosaltatorische Übertragung des Nervenimpulses. *Pflügers Archiv European Journal of Physiology*, 245(5):764–782, 1942.

[253] Jonathan Touboul. Stochastic processes and hitting times in mathematical neuroscience. Master's thesis, Universit'e Pierre et Marie Curie, 2006.

[254] Jonathan Touboul. Bifurcation analysis of a general class of nonlinear integrate-and-fire neurons. *SIAM Journal on Applied Mathematics*, 68(4):1045–1079, 2008.

[255] Jonathan Touboul. *Nonlinear and stochastic models in Neuroscience*. PhD thesis, Ecole Polytechnique, dec 2008.

[256] Jonathan Touboul. Sensitivity to the cutoff value in the quadratic adaptive integrate-and-fire model. Research Report 6634, INRIA, aug 2008.

[257] Jonathan Touboul and Romain Brette. Dynamics of noisy inhibitory networks of integrate-and-fire neurons: a stochastic network theory approach. 2006.

[258] Jonathan Touboul and Romain Brette. Dynamics and bifurcations of the adaptive exponential integrate-and-fire model. *Biological Cybernetics*, 99(4–5):319–334, nov 2008. PMID: 19011921 DOI: 10.1007/s00422-008-0267-4.

[259] Jonathan Touboul and Romain Brette. Spiking dynamics of bidimensional integrate-and-fire neurons. Research Report 6531, INRIA, 05 2008.

[260] Jonathan Touboul and Olivier Faugeras. The spikes trains probability distributions: a stochastic calculus approach. *Journal of Physiology, Paris*, 2007. To appear.

[261] Jonathan Touboul and Olivier Faugeras. The spikes trains probability distributions: a stochastic calculus approach. *Journal of Physiology, Paris*, 101/1-3:78–98, dec 2007.

[262] Jonathan Touboul and Olivier Faugeras. First hitting time of double integral processes to curved boundaries. *Advances in Applied Probability*, 40(2):501–528, 2008.

[263] Jonathan Touboul, Olivier Faugeras, and Olivier Rochel. Event-driven mathematical framework for noisy integrate-and-fire neuron networks. In Holmes et al. [131], page 30.

[264] RD Traub. Neocortical pyramidal cells: a model with dendritic calcium conductance reproduces repetitive firing and epileptic behavior. *Brain Res*, 173(2):243–57, 1979.

[265] RD Traub. Simulation of intrinsic bursting in CA3 hippocampal neurons. *Neuroscience*, 7(5):1233–42, 1982.

[266] RD Traub and R. Llinas. Hippocampal pyramidal cells: significance of dendritic ionic conductances for neuronal function and epileptogenesis. *Journal of Neurophysiology*, 42(2):476–496, 1979.

[267] R.D. Traub, M.A. Whittington, E.H. Buhl, F.E.N. LeBeau, A. Bibbig, S. Boyd, H. Cross, and T. Baldeweg. A Possible Role for Gap Junctions in Generation of Very Fast EEG Oscillations Preceding the Onset of, and Perhaps Initiating, Seizures. *Epilepsia*, 42(2):153–170, 2001.

[268] A. Treves. Mean-field analysis of neuronal spike dynamics. *Network: Computation in Neural Systems*, 4(3):259–284, 1993.

[269] Todd Troyer and Kenneth D. Miller. Physiological gain leads to high ISI variability in a simple model of a cortical regular spiking cell. *Neural Computation*, 9(5):971–983, 1997.

[270] H. C. Tuckwell. *Introduction to theoretical neurobiology*. Cambridge University Press, 1988.

[271] T. Turova. Stochastic dynamics of a neural network with inhibitory and excitatory connections. *BioSystems*, 40(1-2):197–202, 1997.

[272] Tatiana S. Turova. Analysis of a biological plausible neural network via an hourglass model. *Markov Processes and related fields*, 2:487–510, 1996.

[273] Tatyana Turova. Neural networks through the hourglass. *BioSystems*, 58:159–165, 2000.

[274] TS Turova, W. Mommaerts, and EC Van Der Meulen. Synchronization of firing times in a stochastic neural network model with excitatory connections. *Stochastic processes and their applications*, 50(1):173–186, 1994.

[275] A. van Rotterdam, F.H. Lopes da Silva, J. van den Ende, M.A. Viergever, and A.J. Hermans. A model of the spatial-temporal characteristics of the alpha rhythm. *Bulletin of Mathematical Biology*, 44(2):283–305, 1982.

[276] T. Viéville and O. Rochel. One step towards an abstract view of computation in spiking neural-networks. In *International Conf. on Cognitive and Neural Systems*, 2006.

[277] L. Wang and K. Pötzelberger. Crossing Probabilities for Diffusion Processes with Piecewise Continuous Boundaries. *Methodology and Computing in Applied Probability*, 9(1):21–40, 2007.

[278] Liqun Wang and Klaus Pötzelberger. Boundary crossing probability for brownian motion and general boundaries. *Journal of Applied Probability*, 34:54–65, 1997.

[279] U. Wehmeier, D. Dong, C. Koch, and D. Van Essen. Modeling the visual system. *Methods in neuronal modeling (C. Koch, and I. Segev, Eds.)*, pages 335–359, 1989.

[280] F. Wendling, F. Bartolomei, JJ Bellanger, and P. Chauvel. Epileptic fast activity can be explained by a model of impaired GABAergic dendritic inhibition. *European Journal of Neuroscience*, 15(9):1499–1508, 2002.

[281] F. Wendling, J.J. Bellanger, F. Bartolomei, and P. Chauvel. Relevance of nonlinear lumped-parameter models in the analysis of depth-eeg epileptic signals. *Biological Cybernetics*, 83:367–378, 2000.

[282] F. Wendling and P. Chauvel. *Computational Neuroscience in Epilepsy*, chapter Transition to Ictal Activity in Temporal Lobe Epilepsy: Insights from Macroscopic Models, pages 356–386.

[283] Fabrice Wendling, Alfredo Hernandez, Jean-Jacques Bellanger, Patrick Chauvel, and Fabrice Bartolomei. Interictal to ictal transition in human temporal lobe epilepsy: insights from a computational model of intracerebral EEG. *J Clin Neurophysiol*, 22(5):343–356, Oct 2005.

[284] J. A. White, T. Budde, and A. R. Kay. A bifurcation analysis of neuronal subthreshold oscillations. *Biophys J*, 69(4):1203–1217, Oct 1995.

[285] H.R. Wilson and J.D. Cowan. Excitatory and inhibitory interactions in localized populations of model neurons. *Biophys. J.*, 12:1–24, 1972.

[286] Adrien Wohrer. *Model and large-scale simulator of a biological retina with contrast gain control*. PhD thesis, University of Nice Sophia-Antipolis, 2008.

[287] G. Young. Note on excitation theories. *Psychometrika*, 2(2):103–106, 1937.

[288] LH Zetterberg, L. Kristiansson, and K. Mossberg. Performance of a model for a local neuron population. *Biological Cybernetics*, 31(1):15–26, 1978.